

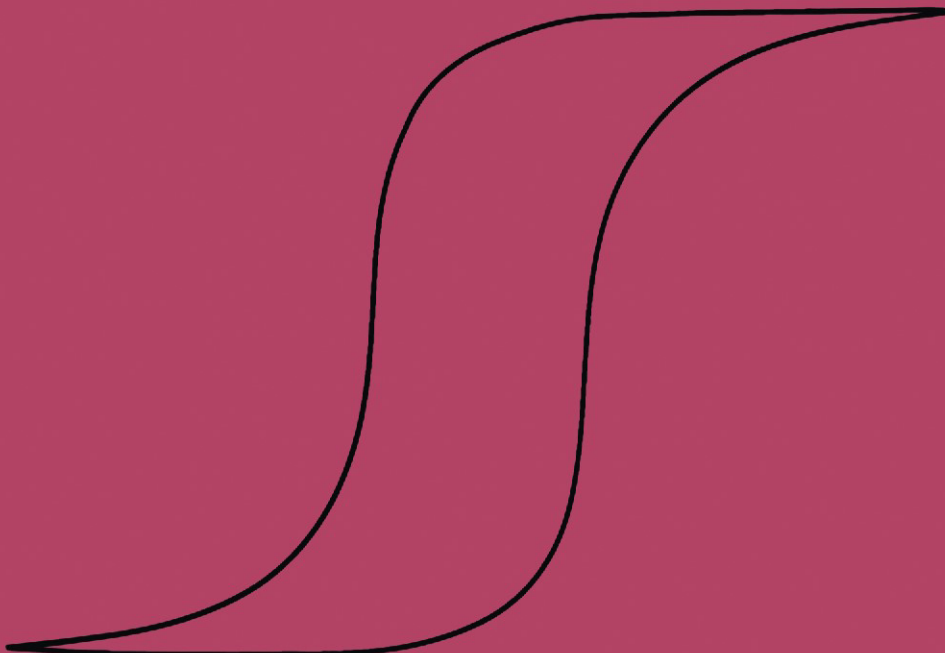
Introduction to

MAGNETISM

and

MAGNETIC MATERIALS

David Jiles



SPRINGER-SCIENCE+BUSINESS MEDIA, B.V.

Introduction to Magnetism and Magnetic Materials

Introduction to Magnetism and Magnetic Materials

David Jiles

*Ames Laboratory,
US Department of Energy
and*

*Department of Materials Science
and Engineering, Iowa State University,
Ames, Iowa, USA*



SPRINGER-SCIENCE+BUSINESS MEDIA, B.V.

First edition 1991

© 1991 David Jiles

Originally published by Chapman and Hall in 1991

Typeset in 10/12 pt Times by
Thomson Press (India) Ltd, New Delhi

All rights reserved. No part of this publication may be reproduced or transmitted, in any form or by any means, electronic, mechanical, photocopying, recording or otherwise, or stored in any retrieval system of any nature, without the written permission of the copyright holder and the publisher, application for which shall be made to the publisher.

British Library Cataloguing in Publication Data

Jiles, David

Introduction to magnetism and magnetic materials.

1. Magnetic materials. Properties

I. Title

538.3

ISBN 978-0-412-38640-4 ISBN 978-1-4615-3868-4 (eBook)

DOI 10.1007/978-1-4615-3868-4

Library of Congress Cataloging-in-Publication Data

Jiles, David.

Introduction to magnetism and magnetic materials / David Jiles.—

1st ed.

p. cm.

Includes bibliographical references and index.

1. Magnetism. 2. Magnetic materials. I. Title.

QC753.2.J55 1990

90-41506

538--dc20

CIP

Few subjects in science are more difficult to understand than magnetism.

Encyclopedia Britannica, Fifteenth Edition 1989.

Preface

Over the years there have been a number of excellent textbooks on the subject of magnetism. Among these we must include Bozorth's *Ferromagnetism* (1950), Chikazumi's *Physics of Magnetism* (1964) and Cullity's *Introduction to Magnetic Materials* (1972). However at present there is no up to date general textbook on magnetism. This book will, I hope, satisfy this need. It is a book for the newcomer to magnetism, and so I anticipate it will be useful as a text for final-year undergraduate courses in magnetism and magnetic materials or for graduate courses. I would also hope that it will be useful to the researcher who, for one reason or another, is beginning a study of magnetism and needs an introductory general text. In this case the extensive references to the literature of magnetism given in the text should prove useful in enabling the reader to gain rapid access to the most important papers on the subject. For the expert there are of course already numerous excellent specialist works, of which the most significant is Wohlfarth's four-volume series *Ferromagnetic Materials*.

The book was conceived as a whole and deals with the fundamentals of magnetism in Chapters 1 to 11, and the principal applications in Chapters 12 to 16. The approach which I have taken is to consider magnetic phenomena first on an everyday macroscopic scale, which should be familiar to most readers, and then gradually to progress to smaller-scale phenomena in the search for explanations of observations on the larger scale. In this way I hope that the book will be of interest to a wider audience consisting of physicists, materials scientists and electrical engineers. One advantage of this approach is that it is possible to introduce the subject from an appeal to the reader's experience rather than through abstract concepts. It is also easier to maintain the reader's interest if he does not find himself immediately confronted with difficult concepts when he first opens the book at chapter one.

Whereas physicists are likely to be mainly interested in the microscopic phenomena discussed in Chapters 9, 10 and 11, the materials scientists and metallurgists are more interested in the domain processes and how these are affected by microstructure, as described in Chapters 6, 7 and 8. Electrical engineers are probably more familiar with field calculations and modelling of magnetic properties in Chapters 1, 2 and 5. Each of these groups should be interested in the applications of our subject since it is the applications which sustain it. There

is a strong demand today for scientists and engineers with skills in magnetism because of applications in magnetic recording, permanent magnets, electrical steels, soft magnetic materials and materials evaluation and measurements; not because it is a deeply interesting and difficult subject – which it undoubtedly is.

The choice of units in magnetism presents a continual problem which those not experienced in the subject will find difficult to comprehend. In research journals papers are primarily written in CGS (Gaussian) units. This system has the advantage that the permeability of free space is unity and that the unit of magnetic field, the oersted, has a very convenient size for practical applications. In electromagnetism the Sommerfeld system of units has been adopted widely. This has the advantage of being completely compatible with the SI unit system but suffers from a serious disadvantage because the permeability of free space, which has the cumbersome value of 12.56×10^{-7} henry/metre, enters into many of the equations. This value has no real significance, being merely the result of the choice of our definition of units, specifically the ampere. In this book I have nevertheless chosen the Sommerfeld unit convention because it is the unit system recommended by the International Union of Pure and Applied Physics, and because this is the unit system for the future. However it was not practicable to convert every diagram taken from research journals and monographs into this unit system. Nor was it desirable since the practitioner of magnetism must learn to be adept in both unit systems. Therefore many of the figures given later in the book remain in their original units. Conversion factors are given in section 1.2.6. so that the reader becomes immediately familiar with these alternative units.

Finally I would like to take this opportunity to acknowledge the advice and assistance given to me by many friends and colleagues while writing this book. In particular thanks go to D. L. Atherton who persuaded me to write it, S. B. Palmer, F. J. Friedlaender and C. D. Graham Jr for reading the entire text, and D. K. Finnemore, R. D. Greenough, K. A. Gschneidner Jr, W. Lord, B. Lograsso, K. J. Overshott, J. Mallinson, R. W. McCallum, A. J. Moses and E. Williams for advice on particular chapters.

D.J.
Ames, Iowa

Foreword

As you study the intricate subject of magnetism in this book you will find that the journey begins at a familiar level with electric currents passing through wires, compass needles rotating in magnetic fields and bar magnets attracting or repelling each other. As the journey progresses though, in order to understand our observations, we must soon peel back the surface and begin to delve into the materials, to look at ever increasing magnification at smaller and smaller details to explain what is happening. This process takes us from bulk magnets (10^{23} – 10^{26} atoms) down to the domain scale (10^{12} – 10^{18} atoms) and then down to the scale of a domain wall (10^3 – 10^2 atoms). In critical phenomena one is often concerned with the behaviour of even smaller numbers (10 atoms or less) in a localized array. Then comes the question of how the magnetic moment of a single atom arises. We must go inside the atom to find the answer by looking at the behaviour of a single electron orbiting a nucleus. The next question is why the magnetic moments of neighbouring atoms are aligned. In order to answer this we must go even further and consider the quantum mechanical exchange interaction between two electrons on neighbouring atoms. This then marks the limit of our journey into the fundamentals of our subject. Subsequently we must ask how can this knowledge be used to our benefit. In Chapters 12 through 16 we look at the most significant applications of magnetism. It is no surprise that apart from superconductors these applications deal exclusively with ferromagnetism. Ferromagnetism is easily the most important technological branch of magnetism and most scientific studies, even of other forms of magnetism, are ultimately designed to help further our understanding of ferromagnetism so that we can both fabricate new magnetic materials with improved properties and make better use of existing materials.

Finally I have adopted an unusual format for the book in which each section is introduced by a question, which the following discussion attempts to answer. Many have said they found this useful in focusing attention on the subject matter at hand since it is then clear what is the objective of each section. I have decided therefore to retain this format from my original notes, realizing that it is unusual in a textbook but hoping that it proves helpful to the reader.

Contents

Preface	vii
Foreword	ix
1 Magnetic Fields	1
1.1 The Magnetic Field	1
1.2 Magnetic Induction	6
1.3 Magnetic Field Calculations	12
Examples and Exercises	26
2 Magnetization and Magnetic Moment	27
2.1 Magnetic Moment and Magnetization	27
2.2 Permeability and Susceptibility of Various Materials	32
2.3 Magnetic Circuits and Demagnetizing Field	36
Examples and Exercises	44
3 Magnetic Measurements	47
3.1 Induction Methods	47
3.2 Methods Depending on Changes in Material Properties	53
3.3 Other Methods	60
Examples and Exercises	67
4 Magnetic Materials	69
4.1 Important Magnetic Properties of Ferromagnets	69
4.2 Different Types of Ferromagnets Materials for Applications	74
4.3 Paramagnetism and Diamagnetism	81
Examples and Exercises	86
5 Magnetic Properties	89
5.1 Hysteresis and Related Properties	89
5.2 The Barkhausen Effect and Related Phenomena	97
5.3 Magnetostriction	98
Examples and Exercises	105

xii *Contents*

6 Magnetic Domains	107
6.1 Development of Domain Theory	107
6.2 Energy Considerations and Domain Patterns	118
Examples and Exercises	125
7 Domain Walls	127
7.1 Properties of Domain Boundaries	127
7.2 Domain-Wall Motion	137
Examples and Exercises	144
8 Domain Processes	147
8.1 Reversible and Irreversible Domain Processes	147
8.2 Determination of Magnetization Curves from Pinning Models	156
8.3 Theory of Ferromagnetic Hysteresis	165
Examples and Exercises	174
9 Magnetic Order and Critical Phenomena	177
9.1 Theories of Diamagnetism and Paramagnetism	177
9.2 Theories of Ordered Magnetism	188
9.3 Magnetic Structure	197
Examples and Exercises	217
10 Electronic Magnetic Moments	219
10.1 The Classical Model of Electronic Magnetic Moments	219
10.2 The Quantum Mechanical Model of Electronic Magnetic Moments	221
10.3 Magnetic Properties of Free Atoms	237
Examples and Exercises	245
11 Quantum Theory of Magnetism	247
11.1 Electron–Electron Interactions	247
11.2 The Localized Electron Theory	254
11.3 The Itinerant Electron Theory	261
Examples and Exercises	268
12 Soft Magnetic Materials	269
12.1 Properties and Uses of Soft Magnetic Materials	269
12.2 Materials for a.c. Applications	272
12.3 Materials for d.c. Applications	290
13 Hard Magnetic Materials	299
13.1 Properties and Applications	299
13.2 Permanent Magnet Materials	311

14 Magnetic Recording	323
14.1 Magnetic Recording Media	323
14.2 The Recording Process and Applications of Magnetic Recording	334
15 Superconductivity	345
15.1 Basic Properties of Superconductors	345
15.2 Applications of Superconductors	358
16 Magnetic Methods for Materials Evaluation	365
16.1 Methods for Evaluation of Intrinsic Properties	365
16.2 Methods for Detection of Flaws and other Inhomogeneities	377
16.3 Conclusions	394
Solutions	399
Index	425

Acknowledgements

I am grateful to the authors and publishers for permission to reproduce the following figures which appear in this book.

- 1.2 P. Ruth (1969) *Introduction to Field and Particle*, Butterworths, London.
- 1.7 G. V. Brown and L. Flax (1964) *Journal of Applied Physics*, **35**, 1764.
- 2.3 F. W. Sears (1951) *Electricity and Magnetism*, Addison Wesley, Reading, Mass.
- 2.5 J. A. Osborne (1945) *Physical Review*, **67**, 351.
- 3.1 D. O. Smith (1956) *Review of Scientific Instruments*, **27**, 261.
- 3.2, 3.6, 3.7 T. R. McGuire and P. J. Flanders (1969) in *Magnetism and Metallurgy* (eds A. E. Berkowitz and E. Kneller), Academic Press, New York.
- 3.5 S. Chikazumi (1964) *Physics of Magnetism*, John Wiley, New York.
- 3.9 B. I. Bleaney and B. Bleaney (1976) *Electricity and Magnetism*, Oxford University Press, Oxford.
- 4.4 J. Fidler, J. Bernardi and P. Skalicky (1987) *High Performance Permanent Magnet Materials*, (eds S. G. Sankar, J. F. Herbst and N. C. Koon), Materials Research Society.
- 4.5 C. Kittel (1986) *Introduction to Solid State Physics*, 6th edn, Wiley, New York. R. J. Elliott and A. F. Gibson (1974), *An Introduction to Solid State Physics and its Applications*, MacMillan, London.
- 4.7, 5.1 A. E. E. McKenzie (1971) *A Second Course of Electricity*, 2nd edn, Cambridge University Press.

xvi Acknowledgements

5.7

E. W. Lee (1955) *Rep. Prog. Phys.* **18**, 184. A. E. Clark and H. T. Savage (1983) *Journal of Magnetism and Magnetics Materials*, **31**, 849.

6.4

H. J. Williams, R. J. Bozorth and W. Shockley (1940) *Physical Review*, **75**, 155.

6.6

C. Kittel (1986) *Introduction to Solid State Physics*, 6th edn, Wiley, New York.

6.7

R. M. Bozorth (1951) *Ferromagnetism*, Van Nostrand, New York.

6.8

C. Kittel and J. K. Galt (1956) *Solid State Physics*, **3**, 437.

7.1

C. Kittel (1949) *Reviews of Modern Physics*, **21**, 541.

7.4

R. W. Deblois and C. D. Graham (1958) *Journal of Applied Physics*, **29**, 931.

7.6

S. Chikazumi (1964) *Physics of Magnetism*, Wiley, New York.

8.2

M. Kersten (1938) *Probleme der Technische Magnetisierungs Kurve*, Springer-Verlag, Berlin.

8.5

K. Hosclitz (1951) *Ferromagnetic Properties of Metals and Alloys*, Oxford University Press, Oxford.

8.8, 8.9

J. Degaugue, B. Astie, J. L. Porteseil and R. Vergne (1982) *Journal of Magnetism and Magnetic Material*, **26**, 261.

8.10

A Globus, P. Duplex and M. Guyot (1971) *IEEE Transactions on Magnetics*, **7**, 617. A. Globus and P. Duplex (1966) *IEEE Transactions on Magnetics*, **2**, 441.

8.12

S. Chikazumi (1964) *Physics of Magnetism*, Wiley, New York.

9.2, 9.3

C. Kittel (1986) *Introduction to Solid State Physics*, 6th edn, Wiley, New York.

9.5

P. Weiss and R. Forrer (1929) *Annalen der Physik*, **12**, 279.

9.6

D. H. Martin (1967) *Magnetism in Solids*, Illife Books, London.

9.7, 9.9, 9.10

G. E. Bacon (1975) *Neutron Diffraction*, 3rd edn, Clarendon Press, Oxford.

- 9.8 J. Crangle (1977) *The Magnetic Properties of Solids*, Edward Arnold, London.
- 9.11 G. L. Squires (1954) *Proceedings of the Physical Society of London*, **A67**, 248.
- 9.12 D. Cribier, B. Jacrot and G. Parette (1962) *Journal of the Physical Society of Japan*, **17-BIII**, 67.
- 9.14, 9.15, 9.16 B. D. Cullity (1972) *Introduction to Magnetic Materials*, Addison-Wesley, Reading, Mass.
- 9.17 C. Kittel (1986) *Introduction to Solid State Physics*, 6th edn, Wiley, New York.
- 9.19 J. A. Hofman, A. Pashkin, K. J. Tauer and R. J. Weiss (1956) *Journal of Physics and Chemistry of Solids*, **1**, 45.
- 9.20 D. H. Martin (1967) *Magnetism in Solids*, Illife Books, London.
- 9.21 S.B. Palmer and C. Isci (1978) *Journal of Physics F. Metal Physics*, **8**, 247.
D. C. Jiles and S. B. Palmer (1980) *Journal of Physics F. Metal Physics*, **10**, 2857.
- 9.22 R. D. Greenough and C. Isci (1978) *Journal of Magnetism and Magnetic Materials*, **8**, 43.
- 10.7, 10.8 H. Semat (1972) *Introduction to Atomic and Nuclear Physics*, 5th edn, Holt, Rinehart and Winston, New York.
- 11.1 D. H. Martin (1967) *Magnetism in Solids*, Illife Books, London.
- 11.3 J. Crangle (1977) *The Magnetic Properties of Solids*, Edwards Arnold, London.
- 11.4 W. E. Henry (1952) *Physical Review*, **88**, 559.
- 11.8 B. D. Cullity (1972) *Introduction to Magnetic Materials*, Addison-Wesley, Reading, Mass.
- 11.9, 12.1 R. M. Bozorth (1951) *Ferromagnetism*, Van Nostrand, New York.
- 12.2, 12.3, 12.13, 12.19 G. Y. Chin and J. H. Wernick (1980) in *Ferromagnetic Materials*, Vol. 2, (ed. E. P. Wohlfarth), North Holland.

xviii Acknowledgements

12.4

M. F. Litmann (1971) *IEEE Transactions on Magnetics*, **7**, 48.

12.5, 12.6

M. F. Litmann (1967) *Journal of Applied Physics*, **38**, 1104.

12.7

E. Adams (1962) *Journal of Applied Physics*, **33**, 1214.

12.8, 12.9, 12.10, 12.11

C. Heck (1972) *Magnetic Materials and their Applications*, Crane, Russak and Company, New York.

12.14, 12.16, 12.1

F. E. Luborsky (1980) in *Ferromagnetic Materials*, Vol. 1, (ed. E. P. Wohlfarth), North Holland.

12.15, 12.17

Reproduced by permission of Allied Signal Company, Morristown, New Jersey.

12.20, 12.21

J. H. Swisher and E. O. Fuchs (1970) *Journal of the Iron and Steel Institute*, August.

12.24

G. W. Elman (1935) *Electrical Engineering*, **54**, 1292.

13.5, 13.6, 13.7, 13.8, 13.9

D. J. Craik (1971) *Structure and Properties of Magnetic Materials*, Pion, London.

13.10, 13.11

R. J. Parker and R. J. Studders (1962) *Permanent Magnets and their Applications*, Wiley, New York.

13.12, 13.13, 13.14

R. A. McCurrie (1982) in *Ferromagnetic Materials*, Vol. 3 (ed. E. P. Wohlfarth), North Holland.

13.16, 13.17

M. McCaig and A. G. Clegg (1987) *Permanent Magnets in Theory and Practice*, 2nd edn, Pentech Press, London.

14.1, 14.2, 14.3, 14.4, 14.8

R. M. White (1985) *Introduction to Magnetic Recording*, IEEE Press, New York.

14.5

C. D. Mee (1964) *The Physics of Magnetic Recording*, North Holland.

15.2

H. Kamerlingh-Onnes Akad (1911) *Wertenschappen*, **14**, 113.

15.3

C. Kittel (1986) *Introduction to Solid State Physics*, 6th edn, Wiley, New York.

15.4

U. Essmann and H. Trauble (1968) *Journal of Applied Physics*, **39**, 4052.

- 15.7 *IEEE Spectrum*, May 1988.
- 15.8, 15.9 J. Clarke, *Physics Today*, March 1986.
- 16.2 R. S. Tebble, I. C. Skidmore and W. D. Corner (1950) *Proceedings of the Physical Society*, **A63**, 739.
- 16.3 G. A. Matzkanin, R. E. Beissner and C. M. Teller, Southwest Research Institute, Report No. NTIAC-79-2.
- 16.6 R. A. Langman (1981) *NDT International*, **14**, 255.
- 16.9, 16.10 H. Kwun (1986) *Materials Evaluation*, **44**, 1560.
- 16.15 R. E. Beissner, G A. Matzkanin and C. M. Teller, Southwest Research Institute, Report No. NTIAC-80-1.
- 16.18 W. E. Lord and J. H. Hwang (1975) *Journal of Testing and Evaluation*, **3**, 21.
- 16.20 T. R. Schmidt (1984) *Materials Evaluation*, **42**, 225.
- 16.21 D. L. Atherton and S. Sullivan (1986) *Materials Evaluation*, **44**, 1544.

Glossary of Symbols

A	Magnetic vector potential
A	Area
H	Helmholz energy
a	Distance
b	Lattice spacing
R	Radius of coil or solenoid
α	Mean field constant
$\alpha_1, \alpha_2, \alpha_3$	Direction cosines of magnetic vector with respect to the applied field
B	Magnetic induction
B_g	Magnetic induction in air gap
B_j(x)	Brillouin function of x
B_R	Remanent magnetic induction
B_s	Saturation magnetic induction
$\beta_1, \beta_2, \beta_3$	Direction cosines of direction of measurement with respect to the applied field
C	Capacitance
C	Curie constant
c	Velocity of light
χ	Susceptibility
D	Electric displacement
D	Diameter of solenoid
d	Diameter
E	Electric field strength
E	Energy
e	Electronic charge
ϵ	Spontaneous strain within a domain
E_a	Anisotropy energy
E_{ex}	Exchange energy
E_f	Fermi energy

xxii *Glossary of symbols*

E_H	Magnetic field energy (Zeeman energy)
E_{Hall}	Hall field
E_{loss}	Energy loss
E_p	Potential energy
E_σ	Stress energy
ϵ	Permittivity
ϵ_0	Permittivity of free space
ϵ_{pin}	Domain wall pinning energy
η	Magnetomotive force
F	Field factor
F	Force
F	Force
F	Magnetomotive force
f	Frequency
	Current factor
G	Gibbs free energy
g	Spectroscopic splitting factor
	Lande splitting factor
γ	Gyromagnetic ratio
	Domain wall energy per unit area
H	Magnetic field strength
h	Planck's constant
H_c	Coercivity
	Critical field
H_{cr}	Remanent coercivity
H_d	Demagnetizing field
H_e	Weiss mean field
H_{eff}	Effective magnetic field
H_g	Magnetic field in air gap
I	Magnetic polarization
	Intensity of magnetization
i	Current
J	Current density
	Total atomic angular momentum quantum number
J	Exchange constant
j	Total electronic angular momentum quantum number
\mathcal{J}	Coupling between nearest-neighbour magnetic moments
J_{atom}	Exchange integral for an electron on an atom with electrons on several nearest neighbours
J_{ex}	Exchange integral; exchange interaction between two electrons

K	Anisotropy constant
	Kundt's constant
k	Pinning coefficient in hysteresis equation
k_B	Boltzmann's constant
K_{u1}	First anisotropy constant for uniaxial system
K_{u2}	Second anisotropy constant for uniaxial system
K_1	First anisotropy constant for cubic system
K_2	Second anisotropy constant for cubic system
L	Inductance
	Length
	Length of solenoid
	Atomic orbital angular momentum
	Electronic orbit length
l	Length
	Orbital angular momentum quantum number
l_d	Domain wall thickness
$\mathcal{L}(x)$	Langevin function of x
λ	Wavelength
	Magnetostriction
	Filling factor for solenoid
	Penetration depth in superconductor
λ_d	Penetration depth
λ_t	Transverse magnetostriction
λ_s	Saturation magnetostriction
λ_0	Spontaneous bulk magnetostriction
M	Magnetization
m	Magnetic moment
m	Mass
	Momentum
M_{an}	Anhysteretic magnetization
m_e	Electronic mass
m_1	Orbital magnetic quantum number
m_0	Orbital magnetic moment of electron
M_R	Remanent magnetization
M_0	Saturation magnetization (spontaneous magnetization at 0 K)
M_s	Spontaneous magnetization within a domain
m_s	Spin magnetic moment of electron
m_s	Spin magnetic quantum number
m_{tot}	Total magnetic moment of atom
μ	Permeability
μ, v	Rayleigh coefficients
μ_B	Bohr magneton

xxiv *Glossary of symbols*

μ_0	Permeability of free space
N	Number of turns of solenoid Number of atoms per unit volume
n	Number of turns per unit length on solenoid Principal quantum number
N_d	Demagnetizing factor
N_0	Avogadro's number
n_s	Number density of paired electrons
ν	Frequency
ω	Angular frequency
P	Pressure
p	Magnetic pole strength Angular momentum operator
P_0	Orbital angular momentum
P_s	Spin angular momentum of electron
P_{tot}	Total angular momentum of electron
Φ	Magnetic flux
ϕ	Angle
Ψ	Spin wavefunction
ψ	Total wavefunction Electron wavefunction
Q	Electric charge
R	Resistance
r	Radius vector Radius
	Electronic orbit radius
R_m	Magnetic reluctance
ρ	Density Resistivity
S	Atomic spin angular momentum
S	Entropy
s	Electronic spin angular momentum quantum number
σ	Conductivity
	Stress
T	Temperature
t	Time
	Thickness
T_c	Curie temperature Critical temperature

t_0	Orbital period of electron
θ	Angle
τ	Torque
	Orbital period
τ_{\max}	Maximum torque
U	Internal energy
u	Unit vector
V	Potential difference
	Volume
	Verdet's constant
v	Velocity
W	Power
W_a	Atomic weight
W_H	Hysteresis loss
x	Distance along x -axis
y	Distance along y -axis
Z	Impedance
	Atomic number
z	Distance along z -axis
	Number of nearest-neighbour atoms

Convention for crystallographic directions and planes:

[100] denotes specific directions;

$\langle 100 \rangle$ denotes family of equivalent directions;

(100) denotes specific planes;

{100} denotes family of equivalent directions.

Abbreviations for SI Units

<i>Quantity</i>	<i>Symbol</i>	<i>Units</i>
Length	m	metre
Mass	kg	kilogram
Time	s	second
Frequency	Hz	hertz
Force	N	newton
Pressure	Pa	pascal
Energy	J	joule
Power	W	watt
Electric charge	C	coulomb
Electric current	A	ampere
Electric potential	V	volt
Resistance	Ω	ohm
Capacitance	F	farad
Inductance	H	henry
Magnetic flux	Wb	weber
Magnetic induction	T	tesla

Values of Selected Physical Constants

Avogadro's number	$N_0 = 6.022 \times 10^{26}$ atoms/kgmole
Boltzmann's constant	$k_B = 1.381 \times 10^{-23}$ J/K
Gas constant	$R = 8.314$ J/mole K
Planck's constant	$\hbar = 6.626 \times 10^{-34}$ J s $\hbar/2\pi = 1.054 \times 10^{-34}$ J s
Velocity of light in empty space	$c = 2.998 \times 10^8$ m/s
Permittivity of empty space	$\epsilon_0 = 8.854 \times 10^{-12}$ F/m
Permeability of empty space	$\mu_0 = 1.257 \times 10^{-6}$ H/m
Atomic mass unit	a.m.u. = 1.661×10^{-27} kg
Properties of electrons	
Electronic charge	$e = -1.602 \times 10^{-19}$ C
Electronic rest mass	$m_e = 9.109 \times 10^{-31}$ kg
Charge to mass ratio	$e/m_e = 1.759 \times 10^{-11}$ C/kg
Electron volt	$eV = 1.602 \times 10^{-19}$ J
Properties of protons	
Proton charge	$e_p = 1.602 \times 10^{-19}$ C
Rest mass	$m_p = 1.673 \times 10^{-27}$ kg
Gyromagnetic ratio of proton	$\gamma_p = 2.675 \times 10^8$ Hz/T
Magnetic constants	
Bohr magneton	$\mu_B = 9.274 \times 10^{-24}$ A m ² (= J/T) = 1.165×10^{-29} J m/A
Nuclear magneton	$\mu_N = 5.051 \times 10^{-27}$ A m ² (= J/T)
Magnetic flux quantum	$\Phi_0 = 2.067 \times 10^{-15}$ Wb (= (V s))

1

Magnetic Fields

In this chapter we will clarify our ideas about what is meant by a ‘magnetic field’ and then show that it is always the result of electrical charge in motion. This will be followed by a discussion of the concept of magnetic induction or ‘flux density’ and its relation to the magnetic field. We will look at the various unit conventions currently in use in magnetism and finally discuss methods for calculating magnetic fields.

1.1 THE MAGNETIC FIELD

What do we mean by ‘magnetic field’?

One of the most fundamental ideas in magnetism is the concept of the magnetic field. When a field is generated in a volume of space it means that there is a change in energy of that volume, and furthermore that there is an energy gradient so that a force is produced which can be detected by the acceleration of an electric charge moving in the field, by the force on a current-carrying conductor, by the torque on a magnetic dipole such as a bar magnet or even by a reorientation of spins on electrons within certain types of atoms. The torque on a compass needle, which is an example of a magnetic dipole, is probably the most familiar property of a magnetic field.

1.1.1 Generation of a magnetic field

What causes magnetic fields in the first place?

A magnetic field is produced whenever there is electrical charge in motion. This can be due to an electrical current flowing in a conductor for example, as was first discovered by Oersted in 1819 [1]. A magnetic field is also produced by a permanent magnet. In this case there is no conventional electric current, but there are the orbital motions and spins of electrons (the so called ‘Ampèrean currents’) within the permanent magnet material which lead to a magnetization within the material and a magnetic field outside. The magnetic field exerts a force on both current-carrying conductors and permanent magnets.

2 Magnetic fields

1.1.2 Definition of magnetic field strength H

What is the unit of magnetic field strength?

There are a number of ways in which the magnetic field strength H can be defined. In accordance with the ideas developed here we wish to emphasize the connection between the magnetic field H and the generating electrical current. We shall therefore define the unit of magnetic field strength, the ampere per metre, in terms of the generating current. The simplest definition is as follows.

The ampere per metre

The ampere per metre is the field strength produced by an infinitely long solenoid containing n turns per metre of coil and carrying a current of $1/n$ amperes.

Since infinitely long solenoids are hypothetical a more practical alternative definition is to define the magnetic field strength in terms of the current passing through unit length of a conductor. A current of 1 ampere passing through a straight 1 metre length of conductor generates a tangential field strength of $1/4\pi$ amperes per metre at a radial distance of 1 metre. These two definitions are equivalent provided the Biot–Savart law holds.

For the time being we will take the viewpoint that the magnetic field H is solely determined by the size and distribution of currents producing it and is independent of the material medium. This will allow us to draw a distinction between magnetic field and induction. However we shall see in section 2.3.3 that this assumption needs to be modified under certain circumstances, particularly when demagnetizing fields are encountered in magnetic materials.

1.1.3 The Biot–Savart law

Is there any way we can calculate the magnetic field strength generated by an electric current?

The Biot–Savart law, which enables us to calculate the magnetic field H generated by an electrical current, is one of the fundamental laws of electromagnetism. It is a statement of experimental observation rather than a theoretical prediction. In its usual form the law gives the field contribution generated by a current flowing in an elementary length of conductor,

$$\delta\mathbf{H} = \frac{1}{4\pi r^2} i \delta\mathbf{l} \times \mathbf{u},$$

where i is the current flowing in an elemental length δl of a conductor, r is the radial distance, \mathbf{u} is a unit vector along the radial direction and $\delta\mathbf{H}$ is the contribution to the magnetic field at r due to the current element $i \delta l$.

This form is known as the Biot–Savart Law (1820) although it was also

discovered independently in a different form by Ampère in the same year. For steady currents it is equivalent to Ampère's circuital law. It is not really capable of direct proof, but is justified by experimental measurements. Notice in particular that it is an inverse square law.

Example 1.1 Field due to a long conductor. Determine the magnetic field \mathbf{H} at some point P distant a metres from an infinitely long conductor carrying a current of i amps. Calculate therefore the field at a distance of 10 cm from the conductor when it carries a current of 0.1 A.

Using the Biot-Savart law the contribution $\delta\mathbf{H}$ to the field at the point P, as shown in Fig. 1.1, due to a current element $i\delta l$ at an angle α is given by

$$\delta\mathbf{H} = \frac{1}{4\pi r^2} i \delta l \sin(90 - \alpha).$$

We can write $\delta l = r d\alpha / \cos \alpha = a d\alpha / \cos^2 \alpha$

$$\delta\mathbf{H} = \frac{i \cos \alpha \delta \alpha}{4\pi a}.$$

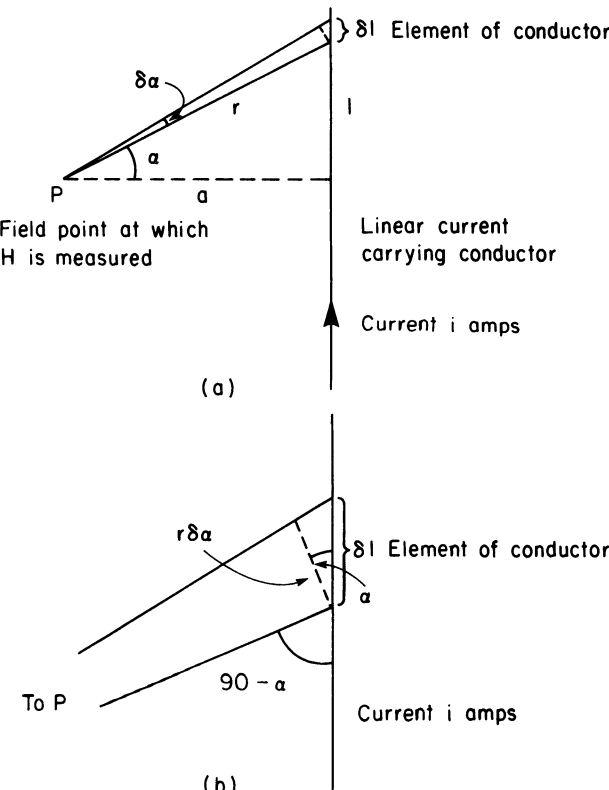


Fig. 1.1 Magnetic field due to a long conductor carrying electric current.

4 Magnetic fields

Now integrating the expression from $\alpha = -\pi/2$ to $\alpha = \pi/2$ to obtain the total H

$$H = \int_{-\pi/2}^{\pi/2} \frac{i}{4\pi a} \cos \alpha d\alpha$$

$$H = \frac{i}{2\pi a} \text{ amps/metre.}$$

Therefore if $a = 0.1$ m and $i = 0.1$ A the field is $1/2\pi$ amps/metre, or

$$H = 0.159 \text{ amps/metre.}$$

The direction of this magnetic field is such that it circulates the conductor obeying the right-hand rule. That is if we look along the conductor in the direction of the conventional current the magnetic field circulates in a clockwise direction.

1.1.4 Field patterns around current-carrying conductors

What do these 'fields' look like?

The magnetic field patterns, detected by magnetic powder, around a bar magnet (magnetic dipole), a straight conductor, a single circular loop and a solenoid are shown in Figs. 1.2 (a–e). The field circulates around a single current-carrying conductor in a direction given by the right-hand corkscrew rule. The fields around a single current loop and a solenoid are similar to those around a bar magnet.

In a bar magnet the field emerges from one end of the magnet, conventionally known as the 'north pole' and passes through the air making a return path to the other end of the bar magnet, known conventionally as the 'south pole'. We can think of the 'north pole' of a magnet as a source of magnetic field H while a 'south pole' behaves as a field sink. Whether such poles have any real existence is debatable. At present the convention is to assume that such poles are fictitious, although the concept of the magnetic pole is very useful to those working with magnetic materials. The matter is discussed again in section 2.1.1.

Notice that the magnetic field produced by a bar magnet is not identical to that of a solenoid. In particular the magnetic field lines within the bar magnet run in the opposite direction to the field lines within the solenoid. We shall look at this again in sections 2.3.1 and 2.3.2. It can be explained because the bar magnet has a magnetization M while the solenoid does not, and this magnetization leads to the generation of a magnetic dipole which acts as a source and sink for magnetic field.

1.1.5 Ampère's circuital law

How can we calculate the strength of a magnetic field generated by an electrical current?

Ampère deduced that a magnetic field is produced by electrical charge in motion when he read of Oersted's discovery of the effect of an electric current on a compass

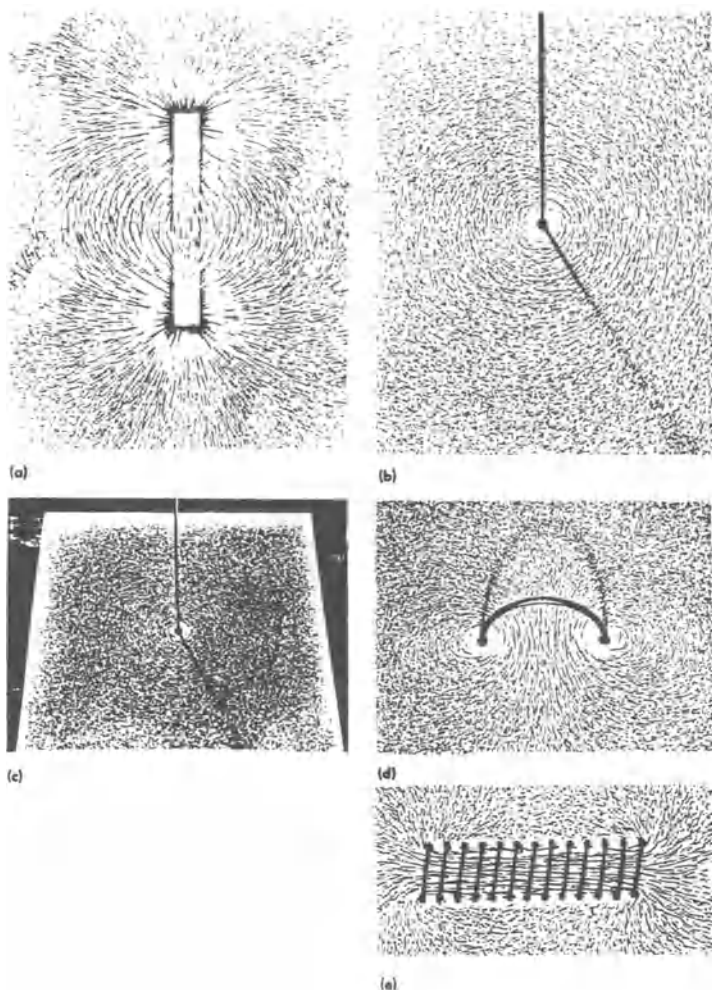


Fig. 1.2 Magnetic field patterns in various situations obtained by using iron filings; (a) a bar magnet; (b) a straight conductor carrying an electric current; (c) a perspective view of (b); (d) a single circular loop of conductor carrying a current; and (e) a solenoid with an air core.

needle. This was a rather remarkable conclusion considering that until then magnetic fields were known to be generated only by permanent magnets and the earth and in neither case was the presence of electrical charge in motion obvious.

According to Ampère the magnetic field generated by an electrical circuit depended on the shape of the circuit (i.e. the conduction path) and the current carried. By assuming that each circuit is made up of an infinite number of current elements each contributing to the field, and by summing or integrating these

6 Magnetic fields

contributions at a point to determine the field, Ampère arrived at the result [2]

$$Ni = \int_{\text{closed path}} \mathbf{H} \cdot d\mathbf{l},$$

where N is the number of current-carrying conductors, each carrying a current i amps. This is the source of the magnetic field \mathbf{H} . $d\mathbf{l}$ is simply a line vector. The total current Ni equals the line integral of \mathbf{H} around a closed path containing the current. We should note that this equation is only true for steady currents.

Ampère's law and the Biot–Savart law can be shown to be equivalent. Consider the field due to a steady current flowing in a long current-carrying conductor. By the Biot–Savart rule the field at a radial distance r from the conductor is

$$\mathbf{H} = \frac{i}{2\pi r},$$

while from Ampère's circuital theorem

$$\int \mathbf{H} \cdot d\mathbf{l} = i$$

and integrating along a closed path around the conductor at a distance r leads to

$$\int \mathbf{H} \cdot d\mathbf{l} = 2\pi r \mathbf{H} = i$$
$$\mathbf{H} = \frac{i}{2\pi r}.$$

(Furthermore Ampère's law, which we have really used to define \mathbf{H} above, can be shown to be equivalent to one of Maxwell's equations of electromagnetism, specifically $\nabla \times \mathbf{H} = \mathbf{J}_f$, where \mathbf{J}_f is the current density of conventional electrical currents.)

1.2 MAGNETIC INDUCTION

How does a medium respond to a magnetic field?

When a magnetic field \mathbf{H} has been generated in a medium by a current, in accordance with Ampère's law, the response of the medium is its magnetic induction \mathbf{B} , also sometimes called the flux density. All media will respond with some induction and, as we shall see, the relation between magnetic induction and magnetic field is a property called the permeability of the medium. For our purposes we shall also consider free space to be a medium since a magnetic induction is produced by the presence of a magnetic field in free space.

1.2.1 Magnetic flux Φ

How can we demonstrate the presence of a magnetic field?

Whenever a magnetic field is present in free space there will be a magnetic flux Φ . This magnetic flux is measured in units of webers and its rate of change can be measured since it generates an e.m.f. in a closed circuit of conductor through which the flux passes. Small magnetic particles such as iron filings align themselves along the direction of the magnetic flux as shown in Fig. 1.2. We can consider the magnetic flux to be caused by the presence of a magnetic field in a medium. We shall see in the next chapter that the amount of flux generated by a given field strength depends on the properties of the medium and varies from one medium to another.

The weber

The weber is the amount of magnetic flux which when reduced uniformly to zero in one second produces an e.m.f. of one volt in a one-turn coil of conductor through which the flux passes.

1.2.2 Definition of magnetic induction B

What is the unit of magnetic induction?

The flux density in webers/metre² is also known as the magnetic induction B and consequently a flux density of one weber per square metre is identical to a magnetic induction of one tesla. The magnetic induction is most usefully described in terms of the force on a moving electric charge or electric current. If the induction is constant then we can define the tesla as follows.

The tesla

A magnetic induction B of 1 tesla generates a force of 1 newton per metre on a conductor carrying a current of 1 ampere perpendicular to the direction of the induction.

This definition can be shown to be equivalent to the older definition of the tesla as the couple exerted in newtons per metre on a small current loop when its axis is normal to the field, divided by the product of the loop current and surface area. We shall see in the next chapter that there are two contributions to the magnetic induction, one from the magnetic field H and one from the magnetization M of the medium.

There is often some confusion between the concept of the magnetic field H and the magnetic induction B , and since a clear idea of the important difference between these two is essential to the development of the subject presented here a discussion of the difference is called for. In many media B is a linear function of H .

8 Magnetic fields

In particular in free space we can write

$$\mathbf{B} = \mu_0 \mathbf{H},$$

where μ_0 is the permeability of free space which is a universal constant. In the unit convention adopted in this book \mathbf{H} is measured in amps/metre and \mathbf{B} is measured in tesla ($= \text{Vs}/\text{m}^2$), the units of μ_0 are therefore (volt second)/(amp metre), also known as henries/metre, and its value is $\mu_0 = 4\pi \times 10^{-7} \text{ H/m}$. If the value of \mathbf{B} in free space is known, then \mathbf{H} in free space is immediately known from this relationship.

However in other media, particularly ferromagnets and ferrimagnets, \mathbf{B} is no longer a linear function of \mathbf{H} , nor is it even a single-valued function of \mathbf{H} . In these materials the distinction becomes readily apparent and important. A simple measurement of the \mathbf{BH} loop of a ferromagnet should be all that is necessary to convince anyone of this. Finally \mathbf{H} and \mathbf{B} are still related by the permeability of the medium μ through the equation,

$$\mathbf{B} = \mu \mathbf{H}$$

but now of course μ is not necessarily a constant. We shall see shortly that in paramagnets and diamagnets μ is constant over a considerable range of values of \mathbf{H} . However in ferromagnets μ varies rapidly with \mathbf{H} .

All of this means that a field \mathbf{H} in amps per metre gives rise to a magnetic induction or flux density \mathbf{B} in tesla in a medium with permeability μ measured in henries per metre.

1.2.3 Force per unit length on a current-carrying conductor in a magnetic field

How does the presence of a magnetic induction affect the passage of an electric current?

The unit of magnetic induction has been defined in terms of the force exerted on a current carrying conductor. This will now be generalized to obtain the force \mathbf{F} on a current-carrying conductor in a magnetic induction \mathbf{B} . The force per metre on a conductor carrying a current i in the direction of the unit vector \mathbf{l} caused by a magnetic induction \mathbf{B} is

$$\mathbf{F} = il \times \mathbf{B}$$

and hence in free space

$$\mathbf{F} = \mu_0 il \times \mathbf{H}.$$

Therefore if two long wires are arranged parallel at a distance of a metres apart and carry currents of i_1 and i_2 amps, the force per metre exerted by one wire on the other is

$$F = \frac{\mu_0}{2\pi a} i_1 i_2.$$

1.2.4 Lines of magnetic induction

How can we visualize the magnetic induction?

The lines of magnetic induction are a geometrical abstraction which help us to visualize the direction and strength of a magnetic field. The direction of the induction can be examined by using a small compass needle (magnetic dipole) or a fine magnetic powder such as iron filings. These show that the magnetic induction around a single linear current-carrying conductor are coaxial with the conductor and follow the right-hand, or corkscrew, rule. While in a solenoid the lines are uniform within the solenoid but form a closed return path outside the solenoid. The lines of induction around a bar magnet are very similar to those around a solenoid since both act as magnetic dipoles.

The lines of induction always form a closed path since we have no direct evidence that isolated magnetic poles exist. This means that through any closed surface the amount of flux entering is equal to the amount of flux leaving. That is the divergence of \mathbf{B} is always zero.

$$\int_{\text{closed surface}} \mathbf{B} \cdot d\mathbf{A} = 0.$$

We sometimes say that \mathbf{B} is ‘solenoidal’ which is the same as saying that the lines of \mathbf{B} form closed paths. (The above equation is equivalent to another of Maxwell’s equations of electromagnetism, specifically $\nabla \cdot \mathbf{B} = 0$.)

1.2.5 Electromagnetic induction

Can the magnetic field generate an electrical current or voltage in return?

When the magnetic flux linking an electric circuit changes an e.m.f. is induced and this phenomenon is called electromagnetic induction. Faraday and Lenz were two of the early investigators of this effect and from their work we have the two laws of induction.

Faraday’s law

The voltage induced in an electrical circuit is proportional to the rate of change of magnetic flux linking the circuit.

Lenz’s law

The induced voltage is in a direction which opposes the flux change producing it.

The phenomenon of electromagnetic induction can be used to determine the magnetic flux Φ . The unit of magnetic flux is the weber which has been chosen so

10 Magnetic fields

that the rate of change of flux linking a circuit is equal to the induced e.m.f. in volts.

$$V = -N \frac{d\Phi}{dt},$$

where Φ is the magnetic flux passing through a coil of N turns and $d\Phi/dt$ the rate of change of flux.

Since the magnetic induction is the flux density,

$$\mathbf{B} = \frac{\Phi}{A}$$

we can rewrite the law of electromagnetic induction as

$$V = -NA \frac{dB}{dt}.$$

This is an important result since it tells us that an electrical current can be generated by a time-dependent magnetic induction.

Example 1.2. Electromagnetic Induction. What is the voltage induced in a 50 turn coil of area 1 cm^2 when the magnetic induction linking it changes uniformly from 3 tesla to zero in 0.01 seconds?

$$\begin{aligned} V &= -NA \frac{dB}{dt} \\ &= -\frac{(50)(1 \times 10^{-4})(3)}{0.01} \\ &= 1.5 \text{ volts.} \end{aligned}$$

1.2.6 The magnetic dipole

What is the most elementary unit of magnetism?

As shown above in Ampère's theorem a current in an electrical circuit generates a field. A circular loop of a conductor carrying an electric current is the simplest circuit which can generate a magnetic field. Such a current loop can be considered the most elementary unit of magnetism.

If a current loop has area A and carries a current i , then its magnetic dipole moment is $\mathbf{m} = i\mathbf{A}$. The units of magnetic moment in the convention which we are adopting are amp metre².

The torque on a magnetic dipole of moment \mathbf{m} in a magnetic induction \mathbf{B} is then simply

$$\tau = \mathbf{m} \times \mathbf{B}$$

and hence in free space

$$\tau = \mu_0 \mathbf{m} \times \mathbf{H}.$$

This means that the magnetic induction \mathbf{B} tries to align the dipole so that the moment \mathbf{m} lies parallel to the induction. Alternatively we can consider that \mathbf{B} tries to align the current loop such that the field produced by the current loop is parallel to it.

If no frictional forces are operating the work done by the turning force will be conserved. This gives rise to the following expression for the energy of the dipole moment \mathbf{m} in the presence of a magnetic induction \mathbf{B}

$$E = -\mathbf{m} \cdot \mathbf{B}$$

and hence in free space

$$E = -\mu_0 \mathbf{m} \cdot \mathbf{H}.$$

The current loop is known as the magnetic dipole for historical reasons, since the field produced by such a loop is identical in form to the field produced by calculation from two hypothetical magnetic poles of strength p separated by a distance l , the dipole moment of such an arrangement being

$$\mathbf{m} = pl.$$

We will see in a later chapter how important the concept of magnetic dipole moment is in the case of magnetic materials. For in that case the electrical ‘current’ is caused by the motion of electrons within the solid, particularly the spins of unpaired electrons, which generate a magnetic moment even in the absence of a conventional current.

1.2.7 Unit systems in magnetism

What unit systems are currently used to measure the various magnetic quantities?

There are currently three systems of units in widespread use in magnetism and several other systems of units which are variants of these. The three unit systems are the Gaussian or CGS system and two MKS unit systems, the Sommerfeld convention and the Kennelly convention. Each of these unit systems has certain advantages and disadvantages. The SI system of units was adopted at the 11th General Congress on Weights and Measures (1960). The Sommerfeld convention was subsequently the one accepted for magnetic measurements by the International Union for Pure and Applied Physics (IUPAP), and therefore this system has slowly been adopted by the magnetism community. This is the system of units used in this book.

Conversion Factors

$$1 \text{ oersted} = (1000/4\pi) \text{ A/m} = 79.58 \text{ A/m}$$

$$1 \text{ gauss} = 10^{-4} \text{ tesla}$$

$$1 \text{ emu/cm}^{-3} = 1000 \text{ A/m}.$$

To give some idea of the sizes of these units, the Earth’s magnetic field is typically

12 Magnetic fields

Table 1.1 Principal unit systems currently used in magnetism

Quantity		SI (Sommerfeld)	SI (Kennelly)	EMU (Gaussian)
Field	H	A/m	A/m	oersteds
Induction	B	tesla	tesla	gauss
Magnetization	M	A/m	—	emu/cc
Intensity of magnetization	I	—	tesla	—
Flux	Φ	weber	weber	maxwell
Moment	m	$A\ m^2$	weber metre	emu
Pole strength	p	A m	weber	emu/cm
Field equation		$B = \mu_0(H + M)$	$B = \mu_0H + I$	$B = H + 4\pi M$
Energy of moment (in free space)		$E = -\mu_0m \cdot H$	$E = -m \cdot H$	$E = -m \cdot H$
Torque on moment (in free space)		$\tau = \mu_0m \times H$	$\tau = m \times H$	$\tau = m \times H$

Note: The intensity of magnetization I used in the Kennelly system of units is merely an alternative measure of the magnetization M , in which tesla is used instead of A/m. Under all circumstances therefore $I = \mu_0M$.

$H = 56\text{ A/m}$ (0.7 Oe), $B = 0.7 \times 10^{-4}$ tesla. The saturation magnetization of iron is $M_0 = 1.7 \times 10^6\text{ A/m}$. Remanence of iron is typically $0.8 \times 10^6\text{ A/m}$. The magnetic field generated by a large laboratory electromagnet is $H = 1.6 \times 10^6\text{ A/m}$, $B = 2$ tesla.

1.3 MAGNETIC FIELD CALCULATIONS

How are magnetic fields of known strength usually produced?

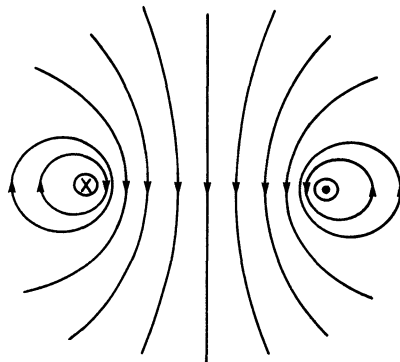
Magnetic fields are usually produced by solenoids or electromagnets. A solenoid is made by winding a large number of turns of insulated copper wire, or a similar electrical conductor, in a helical fashion on an insulated tube known as a ‘former’. Solenoids are often cylindrical in shape. An electromagnet is made in a similar way except that the windings are made on a soft ferromagnetic material, such as soft iron. The ferromagnetic core of an electromagnet generates a higher magnetic induction B than a solenoid for the same magnetic field H .

In view of the widespread use of solenoids of various forms to produce magnetic fields we shall take some time to examine the field strengths produced by a number of different configurations.

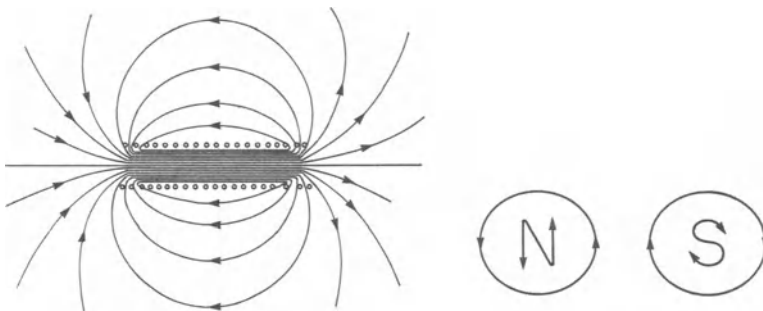
1.3.1 Field at the centre of a long thin solenoid

What is the simplest way to produce a uniform magnetic field?

The simplest way to produce a uniform magnetic field is in a long thin solenoid. If the solenoid has N turns wound on a former of length L and carries a current i



Magnetic field lines around a single loop
of current carrying conductor



Magnetic field lines
around a solenoid

Convention for finding which
end of a solenoid acts as a
north pole (field source) and
south pole (field sink)

Fig. 1.3 Magnetic field lines around a solenoid.

amperes the field inside it will be

$$\mathbf{H} = \frac{Ni}{L} = ni,$$

where n is defined as the number of turns per unit length.

The magnetic field lines in and around a solenoid are shown in Fig. 1.3. A practical method of making an ‘infinite’ solenoid is to make the solenoid toroidal in shape. This ensures that the field is uniform throughout the length of the solenoid. The magnetic field is then

$$\mathbf{H} = \frac{N}{2\pi r} i,$$

where N is the total number of turns, r is the radius of the toroid and i is the current flowing in the windings in amperes.

14 Magnetic fields

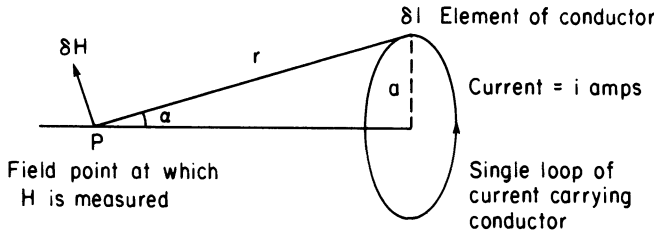


Fig. 1.4 The magnetic field due to a single circular coil carrying an electric current.

1.3.2 Field due to a circular coil

What is the field strength produced by the simplest form of coil geometry the single-turn circular coil?

Field at the centre of a circular coil

The Biot–Savart law can be used to determine the magnetic field \mathbf{H} at the centre of a circular coil of one turn with radius a metres, carrying a current of i amperes as shown in Fig. 1.4. We divide the coil into elements of arc length δl each of which contributes $\delta \mathbf{H}$ to the field at the centre of the coil. Since by Biot–Savart $\delta \mathbf{H} = (1/4\pi r^2)i \delta l \times \mathbf{u}$

$$\mathbf{H} = \sum \frac{1}{4\pi r^2} i \delta l \sin \theta$$

and $\sum \delta l = 2\pi a$, while $d\mathbf{l}$ is perpendicular to \mathbf{u} , so $\theta = 90^\circ$, and hence $\sin \theta = 1$, and $r = a$

$$\mathbf{H} = \frac{i}{2a} \text{ amps/metre.}$$

Field on the axis of a circular coil

The previous calculation of the field at the centre of a circular coil can be generalized to obtain an exact expression for the magnetic field on the axis of a circular coil. Using the situation depicted in Fig. 1.4 and applying the Biot–Savart rule, the field at the general point P is

$$d\mathbf{H} = \frac{1}{4\pi r^2} i d\mathbf{l} \times \mathbf{u}$$

where \mathbf{u} is a unit vector along the r direction. We can make the substitution

$$r = \frac{a}{\sin \alpha},$$

which gives

$$d\mathbf{H} = \frac{1}{4\pi a^2} (\sin^2 \alpha) i d\mathbf{l} \times \mathbf{u}.$$

The component of the field along the axis, which by symmetry will be the only resultant, is $d\mathbf{H}_{\text{axial}} = d\mathbf{H} \sin \alpha$

$$d\mathbf{H}_{\text{axial}} = \frac{1}{4\pi a^2} (\sin^3 \alpha) i dl \times \mathbf{u}.$$

Integrating round the coil, $\int dl = 2\pi a$ and remembering dl is perpendicular to \mathbf{u}

$$\mathbf{H} = \frac{i}{2a} \sin^3 \alpha$$

or, equivalently,

$$\mathbf{H} = \frac{ia^2}{2(a^2 + x^2)^{3/2}}.$$

This can be expressed in the form of a series in x and by symmetry all terms of odd order must have zero coefficients so the form of the dipole field becomes

$$\mathbf{H} = \mathbf{H}_0(1 + c_2x^2 + c_4x^4 + c_6x^6 + \dots),$$

where $\mathbf{H}_0 = i/2a$ is the field at the centre of the coil, and the coefficients have the values $c_2 = -3/2a^2$, $c_4 = 15/8a^4$, and $c_6 = -105/48a^6$.

Example 1.3 If a coil of 100 turns and diameter 10 cm carries a current of 0.1 A, calculate the magnetic field at a distance of 50 cm along the axis of the coil.

When $i = 0.1$ A, $a = 5$ cm, $x = 50$ cm and the coil has 100 turns

$$\begin{aligned}\mathbf{H} &= \frac{(100)(0.05)^2(0.1)}{2[(0.05)^2 + (0.5)^2]^{3/2}} \\ &= \frac{0.025}{2(0.253)^{3/2}} \\ &= \frac{0.025}{0.254}\end{aligned}$$

$$\mathbf{H} = 0.098 \text{ amps per metre.}$$

Off-axis field of a circular coil

As shown in the above derivations a simple analytical expression can be obtained for the magnetic field along the axis of a single loop of conductor carrying a current by using the Biot–Savart law. However, in the vast majority of cases there is no closed-form analytic solution for the field generated by a current-carrying conductor. Those that can produce closed-form analytic solutions are only the very simplest types of situation.

To give an example, there is no closed-form analytic solution for the off-axis field of a single circular loop of conductor carrying a steady current, except for the far-field dipole field which varies with $1/r^3$. This comes at first as somewhat of a

16 Magnetic fields

surprise given the extreme simplicity of the situation. However the example does show how very limited are the situations which yield analytical solutions.

In the case of the off-axis field of the single circular loop the analysis leads to an elliptic integral which has no exact solution. From the Biot–Savart law the magnetic field contribution at any point $d\mathbf{H}$ due to a current element $i dl$ is

$$d\mathbf{H} = \frac{i dl \times u}{4\pi r^2},$$

where r is the distance from the coil.

$$d\mathbf{H} = \frac{i dl \sin \theta}{4\pi(x^2 + a^2)},$$

where now a is also a function of θ instead of being a constant. In the case of the off-axis field the field strength can be calculated from this equation by computer using numerical techniques.

1.3.3 Field due to two coaxial coils

Which simple coil configurations produce: (i) a constant magnetic field, or (ii) a constant field gradient?

In superposition

Often when it is necessary to produce a uniform field over a large volume of space a pair of Helmholtz coils is used. This consists of two flat coaxial coils, each

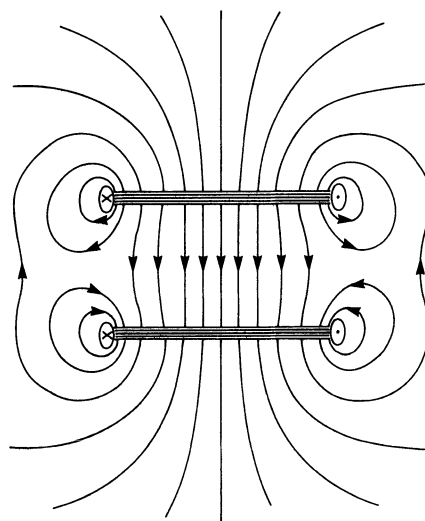


Fig. 1.5 Two coaxial coils configured as a Helmholtz pair with the separation between the coils equal to their common radius.

containing N turns, with the current flowing in the same sense in each coil as shown in Fig. 1.5. The separation d of the coils in a Helmholtz pair is equal to their common radius a .

The axial component of the magnetic field on the axis of the two coils can be calculated from the Biot–Savart law. Since the field on the axis of a single coil of N turns and radius a carrying a current i at a distance x from the plane of the coil is

$$\mathbf{H} = \left(\frac{Ni}{2a} \right) \left(1 + \frac{x^2}{a^2} \right)^{-1.5}.$$

If we define one coil at location $x = 0$ and the other at location $x = a$ the field at the centre of two such coils wound in superposition is

$$\mathbf{H} = \left(\frac{Ni}{2a} \right) \left[\left(1 + \frac{x^2}{a^2} \right)^{-1.5} + \left(1 + \frac{(a-x)^2}{a^2} \right)^{-1.5} \right]$$

and since for the Helmholtz coils $x = a/2$ at the point on the axis midway between the coils, this gives the axial component of the magnetic field at the midpoint as

$$\begin{aligned} \mathbf{H} &= \left(\frac{Ni}{2a} \right) [(1.25)^{-1.5} + (1.25)^{-1.5}] \\ &= \frac{(0.8)^{2/3} Ni}{a} \\ &= \frac{0.7155 Ni}{a}, \end{aligned}$$

and by symmetry the radial component on the axis must be zero.

In fact if a series expansion is made for the axial component of \mathbf{H} in terms of the distance x along the axis from the centre of the coils, as was given for the single coil in section 1.3.2 it is found that the term in x^2 disappears when the coil separation d equals the coil radius a , so that the fourth-order correction term becomes the most significant. The series expansion for the field in terms of x is then,

$$\mathbf{H} = \mathbf{H}_0(1 + c_4x^4 + c_6x^6 + \dots).$$

This results in a small value of $d\mathbf{H}/dx$ at the centre of the coils, and consequently a very uniform field along the axis as x is varied close to zero, which is shown in Fig. 1.6 for three different values of coil radius a . In addition, the axial component of the magnetic field close to the centre of a pair of Helmholtz coils is only very weakly dependent on the radial distance z from the axis. This means that the magnetic field strength \mathbf{H} is maintained fairly constant over a large volume of space between the Helmholtz coils.

The useful region of uniform field between a Helmholtz pair can be increased by making the coil spacing slightly larger than $a/2$, although this leads to a slight reduction in field strength over this region.

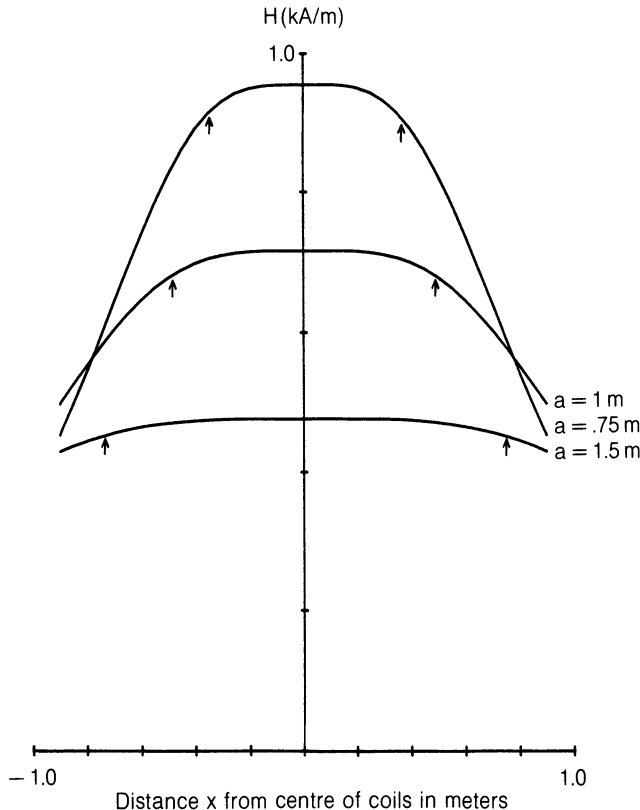


Fig. 1.6 Axial component of the magnetic field H as a function of position along the axis of a pair of Helmholtz coils for various coil radii. The calculation is for an $N = 100$ turn coil carrying a current $i = 10$ A with coil radii $a = 0.5$ m, 0.75 m, 1 m and 1.5 m. The arrows mark the location of the coils in each case.

In opposition

If the current in one of the the two coaxial coils described above is reversed then the magnetic fields generated by the two coils will be in opposition. This is a specific example of a quadrupole field, so called because the form of the field obtained is similar to that obtained from two magnetic dipoles aligned coaxially and antiparallel.

Under these conditions the magnetic field along the axis of the pair of coils is given by

$$\mathbf{H} = \left(\frac{Ni}{2a} \right) \left[\left(1 + \frac{x^2}{a^2} \right)^{-1.5} - \left(1 + \frac{(a-x)^2}{a^2} \right)^{-1.5} \right].$$

Such a configuration generates a uniform field gradient which can be useful for applying a constant force to a sample. See, for example, section 3.3.2.

1.3.4 Field due to a thin solenoid of finite length

What field strength is produced in the more practical case of a solenoid of limited length?

So far the field of an infinite solenoid has been considered. Now solenoids of finite length will be considered. A thin solenoid is one in which the inner and outer diameters of the coil windings are equal. So for example a solenoid consisting of one layer of windings would be considered a thin solenoid.

The field of a long thin solenoid has already been calculated in section 1.3.1. The field on the axis of a thin solenoid of finite length has an analytical solution. If L is the length of the solenoid, D the diameter, i the current in the windings and x the distance from the centre of the solenoid, then the field at x is given by

$$\mathbf{H} = \left(\frac{Ni}{L} \right) \left[\frac{(L+2x)}{2[D^2 + (L+2x)^2]^{1/2}} + \frac{(L-2x)}{2[D^2 + (L-2x)^2]^{1/2}} \right].$$

At the centre of the solenoid $x = 0$ and hence

$$\mathbf{H} = \left(\frac{Ni}{L} \right) \left[\frac{L}{(L^2 + D^2)^{1/2}} \right].$$

Finally, for a long solenoid, $L \gg D$ and $(L^2 + D^2)^{1/2} = L$ so that the result from section 1.3.1 is a limiting case

$$\mathbf{H} = \frac{Ni}{L} = ni.$$

The fields generated by solenoids are of course dipole fields.

The field calculations for thin solenoids, that is solenoids with $L \gg D$, at least along the axis, are relatively straightforward and yield analytical solutions as shown. A useful result to remember is that the field at the end of a solenoid is half the value of the field at the centre. The field in the middle 50% of a solenoid is also known to be very uniform.

1.3.5 Field due to a thick solenoid of finite length

What coil configurations are used to produce higher field strengths?

In order to produce higher field strengths from a solenoid it eventually becomes more effective to increase the number of windings per unit length N/L than to increase the coil current. This is because the Joule heating is proportional to i^2 whereas the field is proportional to i . Consequently if the current is doubled in a coil of fixed resistance the Joule heating is quadrupled while if the number of windings is doubled the Joule heating is only doubled. Both methods will result in a doubling of the \mathbf{H} field. Therefore solenoids are often wound with several layers of windings and hence are no longer ‘thin’. That is the radii of the inner and the outer

20 Magnetic fields

windings are no longer equal or even close to being equal. In the case of these thick solenoids the calculation of the magnetic field is more complicated than for the thin solenoids.

Let L be the length of the solenoid, a_1 the radius of the inner windings and a_2 the radius of the outer windings. Two parameters α and β can then be defined which describe the geometrical properties of the solenoid

$$\alpha = \frac{a_2}{a_1}$$

and

$$\beta = \frac{L}{2a_1}.$$

The field generated by such a solenoid is then a function of α and β and the coil current i . If H_0 is the field at the centre of such a coil then as shown by Montgomery [3]

$$H_0 = F(\alpha, \beta) f(i, a_1, a_2),$$

where $F(\alpha, \beta)$, known as the field factor, is

$$F(\alpha, \beta) = \beta [\operatorname{arcsinh}(\alpha/\beta) - \operatorname{arcsinh}(1/\beta)]$$

and the current factor $f(i, a_1, a_2)$ is

$$f(i, a_1, a_2) = \frac{Ni}{L} \frac{a_1}{(a_2 - a_1)}.$$

The expression for the field can also be written in the slightly different but equivalent form

$$H_0 = \frac{Ni}{a_1} \frac{F(\alpha, \beta)}{2\beta(\alpha - 1)}.$$

The above equations for the field at the centre of a thick solenoid are totally general and can be shown to reduce to the simpler more familiar expression in the limiting case $a_2 = a_1$ when

$$H_0 = Ni \frac{1}{(4a^2 + L^2)^{1/2}}$$

so that as $L \rightarrow 0$, $H_0 \rightarrow Ni/2a$ and as $L \rightarrow \infty$, $H_0 \rightarrow Ni/L$.

1.3.6 Optimization of solenoid geometry for a given power rating

How can the maximum field be produced for a given power consumption?

Often it is necessary to consider the limitations imposed by available power supplies when designing a solenoid coil which will give maximum field. Clearly the

impedance or resistance of the solenoid should be chosen to operate as close to the current and voltage limitations of the supply as possible. That is the optimum resistance R_{opt} should be

$$R_{\text{opt}} = \frac{V_{\text{lim}}}{i_{\text{lim}}}.$$

A formula has been given originally by Fabry [4] and later by Cockcroft [5] which shows the maximum field attainable by a solenoid operated at a given power rating. The equation of the field at the centre of such a solenoid is

$$H = G(\alpha, \beta)(W\lambda/\rho a_1)^{0.5}$$

where once again all the geometrical terms have been collected together in a single expression $G(\alpha, \beta)$ known as the 'geometrical factor'. This equation indicates the geometry of the windings needed to obtain the maximum field for a given power supplied W . Here λ is the filling factor which is defined as

$$\lambda = \frac{V_a}{V_{\text{tot}}}$$

where V_a is the active volume of windings and V_{tot} is the total volume of windings, ρ is the specific resistivity of the material used for the coil in ohm metres, and a_1 is the radius of the inner windings.

The value of $G(\alpha, \beta)$ varies from zero up to 0.179. Since this is dependent solely on geometry it is possible to define an optimum shape of solenoid which is independent of power considerations. The maximum value of $G(\alpha, \beta)$ occurs at $\alpha = 3, \beta = 2$, which indicates that a solenoid of this geometry produces the highest field for a given power consumption. The exact expression for $G(\alpha, \beta)$ is

$$G(\alpha, \beta) = [\beta/2\pi(\alpha^2 - 1)]^{0.5} [\operatorname{arcsinh}(\alpha/\beta) - \operatorname{arcsinh}(1/\beta)].$$

From the above equations it is clear that the relationship between the geometry factor and the field factor is,

$$F(\alpha, \beta) = G(\alpha, \beta)[2\pi(\alpha^2 - 1)\beta]^{0.5}$$

$$F(\alpha, \beta) = G(\alpha, \beta)[\pi L(a_2^2 - a_1^2/a_1^3)]^{0.5}$$

The general equation for the field of a solenoid given above can be rewritten in terms of the available power $W = Vi$, assuming that the filling factor λ , the resistivity of the coil material ρ , and internal radius a_1 remain constant.

$$H_0 = G(\alpha, \beta)(W\lambda/\rho a_1)^{0.5},$$

As $W = i^2 R = V^2/R$

$$H_0 = G(\alpha, \beta)i(R\lambda/\rho a_1)^{0.5}$$

$$H_0 = G(\alpha, \beta)V(\lambda/R\rho a_1)^{0.5}$$

22 Magnetic fields

1.3.7 General formula for the field of a solenoid

How can the field strength generated by a solenoid be determined in more general cases?

Not surprisingly there is no general analytic formula for the magnetic field from a solenoid at a general point in space. However there are some methods of calculation available. The most obvious method is by the straight-forward procedure of using either Ampère's law or the Biot–Savart law, as in section 1.3.2. This leads to a solution containing an elliptic integral which can then be solved numerically.

However there are also some quicker methods which can be used such as that developed by Brown and Flax [6] and by Hart [7]. In the former method any desired solenoid of finite dimensions can be treated as the superposition of four semi-infinite solenoids as shown in Fig. 1.7. The field at any point is the vector sum of the contributions of the four component solenoids.

The advantage of considering four semi-infinite solenoids with no cylindrical hole is that the field contribution of such a solenoid can be expressed in terms of only two variables: the axial distance beyond the end of the solenoid and the radial distance from the unique axis. Therefore one table can be provided for the field at these two reduced coordinates for all semi-infinite

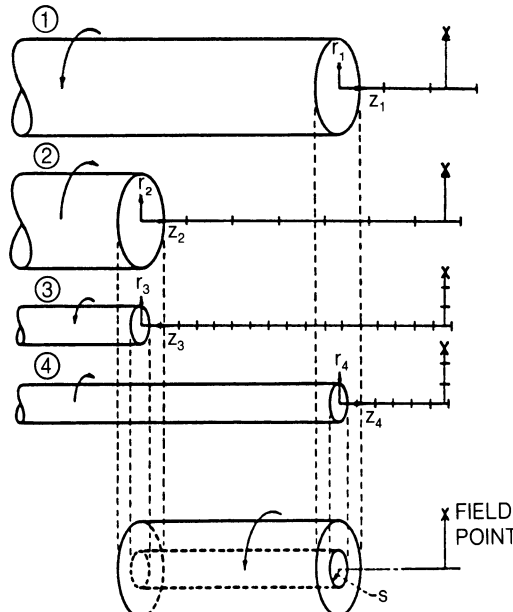


Fig. 1.7 Method of superposing four semi-infinite solenoids to obtain the mathematical equivalent of one finite solenoid, after Brown and Flax [6]. Curved arrows indicate the direction of current flow, z_1, \dots, z_4 represent the distances along the axis, r_1, \dots, r_4 indicate the radii of the solenoids.

solenoids. The field can then be calculated by vector summation of the four contributions.

This method allows rapid and simple calculation of the field of any finite solenoid. Further details of the application of this method can be obtained from the original paper [6].

1.3.8 Field calculations using numerical methods

How can magnetic field strengths be calculated in more complicated situations, for example over an entire volume?

Although it has been shown above how the Biot–Savart law can be applied to determine the magnetic field \mathbf{H} in various simple situations it has also been demonstrated that there is not always an analytic solution (e.g. the off-axis field of a single circular current loop). In more general cases therefore it is necessary to resort to numerical techniques in order to obtain a solution.

In most cases the problem amounts to solving either Laplace's or Poisson's equation over a finite region of space, known as the spatial domain, which may be three dimensional or two dimensional. In most cases the calculation is made over a two-dimensional spatial domain, the third domain being assumed to be effectively infinite in extent in comparison with the other two dimensions. The Laplace's or Poisson's equations cannot be solved without an appropriate set of boundary conditions, even though the current density \mathbf{J} is known over the entire spatial domain.

These numerical methods for calculating the magnetic field are often used to determine the magnetic field in the air gap of an electrical machine. In this case there are no field sources in the gap and so Laplace's equation applies.

$$\nabla^2 \mathbf{A} = 0$$

where \mathbf{A} is the magnetic potential. In cases where field sources occur within the region of interest then the source distributions must be known and included in the calculation. The problem then becomes solving Poisson's equation with the appropriate boundary conditions.

$$\nabla^2 \mathbf{A} = -\mu_0 \mathbf{J},$$

the only difference between this and the previous case being the presence of field sources, in the form of the current density \mathbf{J} . In two-dimensional problems the vector potential \mathbf{A} given here reduces to a scalar equivalent which simplifies the equations and enables a more rapid solution to be obtained.

There are a number of general numerical methods which can be used to solve the equation for the magnetic field \mathbf{H} . Here we shall consider finite-difference, finite-element and boundary-element techniques. At present much research effort is being devoted to the boundary-element method, although the finite-element method which has been in use for over twenty years is well established and a

24 Magnetic fields

number of software packages are available. The finite-difference method which has been in use since the 1940s, and actually traces its origins back to Gauss, is the oldest method, and has largely been superseded by the finite-element method since about 1970.

It should also be realized that there are a number of analytical methods which have been developed for calculation of magnetic fields. Some examples of these are series solutions, conformal mappings and variational formulations. The problem is that these methods suffer from a lack of generality which restricts their use to only the simplest situations. Often they are restricted to steady-state conditions and many are applicable to two dimensions only.

A review of progress in electromagnetic field computation by Trowbridge [8] covers the period 1962–88. This discusses all three main methods and gives a selection of the most important references during the period. The finite-difference method of calculating magnetic fields was the principal numerical tool from the early days of the digital computer in the 1940s until about 1970. The method has been described by Adey and Brebbia [9] and by Chari and Silvester [10]. It is a technique for the solution of differential equations in which each derivative appearing in the differential equation is replaced by its finite-difference approximation at regularly spaced intervals over the volume of space of interest. This means that a continuous region of space must be replaced by a regular grid of discrete points at which the field values are calculated. The process is known as discretization.

In order to ease the computation a regularly spaced orthogonal or polar grid is used for discretization, although in principle the use of curvilinear grids is possible. However as a result of the practical restriction of grids the use of finite differences in the case of complicated geometries has encountered difficulties. Also in situations with large field gradients in order to obtain sufficient accuracy the number of nodes needs to be increased over the whole volume in order to maintain a regular grid (not just over the region of high gradient) and this results in a rapid increase in computation time and memory requirements. Despite these difficulties the finite-difference method has been successfully implemented for field calculations and some excellent examples of its use have been reported [11].

In the finite-element method the spatial domain is divided into triangle-shaped elements and the field values are computed at the three nodes of each element. The sizes of the elements can be varied over the region of interest (unlike the grid in the finite-difference calculations) so that more elements can be included in regions where the field gradient is large. Furthermore the elements used to discretize the spatial domain need not be triangular, they can be of any polygonal shape, however triangles remain the most popular form of element.

An introductory survey of the finite-element technique for the non-specialist has been given by Owen and Hinton [12], while an excellent and more detailed review has been given by Silvester and Ferrari [13]. The method first came to attention in 1965 in the work of Winslow [14] and began to be used on a regular basis for field calculations from about 1968. From this time onwards it gradually supplanted the older finite-difference method.

The advantages of numerical techniques such as the finite-element method over analytical methods of field computation were demonstrated in the case of leakage fields by Hwang and Lord [15]. This was the first successful attempt to use numerical field calculations for the determination of fields in the vicinity of defects in materials. The implementation of both finite-difference and finite-element methods to two-dimensional nonlinear magnetic problems have been compared by Demerdash and Nehl [16]. They concluded that the finite-element technique was superior in that it required less computation time and less memory. However although this conclusion that finite elements seem to be preferable is on the whole true, the relative performance of various numerical methods is highly dependent on the nature of the specific problem under consideration.

Boundary-element techniques for field calculations are the most recent development. The general method has been discussed by Brebbia and Walker [17] and its application to the problem of magnetic field calculations in particular by Lean and Wexler [18]. A comparison of integral and differential equation methods has been made by Simkin [19]. A comprehensive survey of these techniques is given in the book by Hoole [20], which provides an up-to-date guide to the whole subject of numerical methods of field calculation.

REFERENCES

1. Oersted, H. C. (1820) Experiment on the effects of a current on the magnetic needle, *Annals of Philosophy*, **16**.
2. Ampère, A. M. (1958) *Theorie Mathematique des Phenomenes Electrodydnamiques Uniquement Diduite de l'Experience*, reprinted by Blanchard, Paris.
3. Montgomery, D. B. (1980) *Solenoid Magnet Design*, Robert Krieger, New York.
4. Fabry, M. P. A. (1898) *Eclairage Electrique*, **17**, 133.
5. Cockcroft, J. D. (1928) *Phil. Trans. Roy. Soc.*, **227**, 317.
6. Brown, G. V. and Flax, L. (1964) *J. Appl. Phys.*, **35**, 1764.
7. Hart, P. J. (1967) *Universal Tables for Magnetic Fields of Filamentary and Distributed Circular Currents*, Elsevier, New York.
8. Trowbridge, C. W. (1988) *IEEE Trans. Mag.*, **24**, 13.
9. Adey, R. A. and Brebbia, C. A. (1983) *Basic Computational Techniques for Engineers*, Pentech Press, London.
10. Chari, M. V. K. and Silvester, P. P. (1980) *Finite Elements in Electrical and Magnetic Field Problems*, Wiley, New York.
11. Fuchs, E. F. and Erdelyi, E. A. (1973) *IEEE Trans. PAS*, **92**, 583.
12. Owen, D. R. J. and Hinton, E. (1980) *A Simple Guide to Finite Elements*, Pineridge Press.
13. Silvester, P. P. and Ferrari, R. L. (1983) *Finite Elements for Electrical Engineers*, Cambridge University Press, Cambridge.
14. Winslow, A. M. (1965) *Magnetic Field Calculation in an Irregular Mesh*, Lawrence Radiation Laboratory, Report UCRL-7784-T.
15. Hwang, J. H. and Lord, W. (1975) *J. Test and Eval.*, **3**, 21.
16. Demerdash, N. A. and Nehl, T. W. (1976) *IEEE Trans. Mag.*, **12**, 1036.
17. Brebbia, C. A. and Walker, S. (1980) *Boundary Element Techniques in Engineering*, Newnes-Butterworths, London.
18. Lean, M. H. and Wexler, A. (1982) *IEEE Trans. Mag.*, **18**, 331.
19. Simkin, J. (1982) *IEEE Trans. Mag.*, **18**, 401.
20. Hoole, S. R. H. (1989) *Computer Aided Analysis and Design of Electromagnetic Devices*, Elsevier, New York.

26 Magnetic fields

FURTHER READING

- Bennet, G. A. (1968) *Electricity and Modern Physics*, Arnold, Cambridge, London, Ch. 5.
- Cendes, Z. (ed.) (1986) *Computational Electromagnetics*, North Holland Publishing, Amsterdam.
- Chari, M. V. K. and Silvester, P. P. (eds) (1980) *Finite Elements in Electrical and Magnetic Field Problems*, Wiley, New York.
- Grover, F. W. (1946) *Inductance Calculations*, Dover, New York.
- Hoole, S. R. H. (1989) *Computer Aided Analysis and Design of Electromagnetic Devices*, Elsevier, New York.
- Lorrain, P. and Corson, D. R. (1978) *Electromagnetism*, W. H. Freeman, San Francisco.
- McKenzie, A. E. E. (1961) *A Second Course of Electricity*, 2nd edn, Cambridge University Press, Ch 3 and 4, Cambridge.
- Reitz, J. R. and Milford, F. J. (1980) *Foundations of Electromagnetic Theory*, 3rd edn, Addison-Wesley, Ch. 8, Reading, Mass.

EXAMPLES AND EXERCISES

Example 1.4 Magnetic field at the centre of a long solenoid. Prove that the magnetic field \mathbf{H} at the centre of a 'long' solenoid is $\mathbf{H} = ni$, where n is the number of turns per metre and i is the current flowing in the coils in amps.

Example 1.5 Force on a current-carrying conductor

- Calculate the force per unit length between two parallel current-carrying conductors 1 metre apart when each carries a current of 1 amp.
- Find the force exerted on a straight current-carrying conductor of length 3.5 cm carrying a current of 5 amps and situated at right angles to a magnetic field of 160 kA/m.

Example 1.6 Torque on a current-loop dipole. Find the torque on a circular coil of area 4 cm² containing 100 turns when a current of 1 milliampere flows through it and the coil is in a field of magnetic induction 0.2 tesla.

2

Magnetization and Magnetic Moment

We now consider the effect that a magnetic material has on the magnetic induction \mathbf{B} when a field passes through it. This is represented by the magnetization. Materials can alter the magnetic induction either by making it larger, as in the case of paramagnets and ferromagnets, or by making it smaller as in diamagnets. The relative permeability of the material indicates how it changes the magnetic induction compared with the induction that would be observed in free space.

2.1 MAGNETIC MOMENT AND MAGNETIZATION

How do we measure the response of a material to a magnetic field?

When going on to consider magnetic materials it is first necessary to define quantities which represent the response of these materials to the field. These quantities are magnetic moment and magnetization. Once that has been done we can consider another property, the susceptibility, which is closely related to the permeability.

2.1.1 Magnetic moment

Can we use the torque on a specimen in a field of known strength to define its magnetic properties?

In the previous chapter we have defined the magnetic moment \mathbf{m} of a current loop dipole and shown that the torque on the dipole in the presence of a magnetic field in free space is given by $\tau = \mathbf{m} \times \mathbf{B}$. Therefore the magnetic moment can be expressed as the maximum torque on a magnetic dipole τ_{\max} divided by \mathbf{B} .

$$\mathbf{m} = \frac{\tau_{\max}}{\mathbf{B}}$$

and hence in free space

$$\mathbf{m} = \frac{\tau_{\max}}{\mu_0 \mathbf{H}}$$

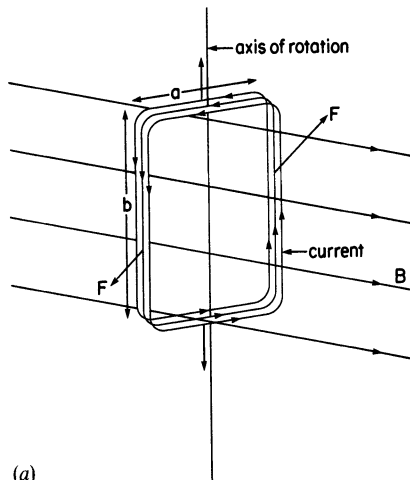
28 Magnetization and magnetic moment

where the magnetic moment \mathbf{m} in the convention we are using is measured in amp metre². This formula applies equally to a current loop or to a bar magnet.

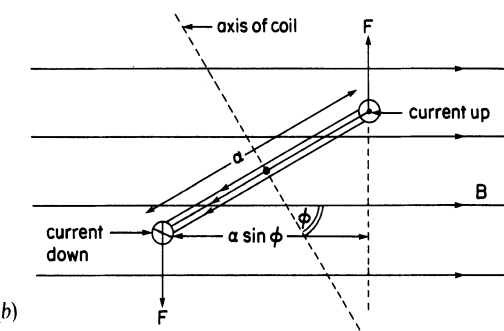
The unit of magnetic moment

A magnetic moment of 1 ampere metre² experiences a maximum torque of 1 newton metre when oriented perpendicular to a magnetic induction of 1 tesla.

In the case of a current loop, as in Fig. 2.1, $\mathbf{m} = iA$, where i is the current flowing and A is the cross-sectional area of the loop. In the case of a bar magnet, as in Fig. 2.2, $\mathbf{m} = pl$ where p is the pole strength in amp metres and l is the dipole length in metres. The ‘pole strength’ is an archaic term arising from the more traditional CGS treatment of magnetism, in which pole strength was defined in terms of the



(a)



(b)

Fig. 2.1 The torque on a current loop in an external magnetic field; (a) side view, and (b) top view. If the loop is free to rotate the torque turns the loop until its plane is normal to the field direction.

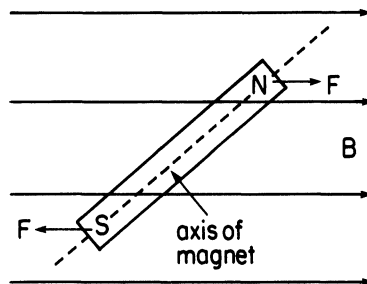


Fig. 2.2 The torque on a bar magnet in an external magnetic field. If the bar is free to rotate the torque turns the bar until its plane is parallel to the field direction.

magnetic flux Φ emanating from a single magnetic pole [1]. In the Sommerfeld convention this is given by $p = \Phi/\mu_0$ so that

$$\mathbf{m} = \frac{\Phi l}{\mu_0},$$

where Φ is the flux in webers passing through the current loop or bar magnet dipole and l is the dipole length.

The magnetic moment vector \mathbf{m} in a bar magnet tends to align itself with \mathbf{B} under the action of the torque as shown in Fig. 2.2. For this reason a bar magnet in the field generated by a second bar magnet experiences a torque which aligns it parallel to the local direction \mathbf{B} . It is this force which gives rise to the most widely recognized phenomenon in magnetism that unlike magnetic poles attract each other while like magnetic poles repel each other. However our difficulty in explaining the exact meaning of magnetic ‘poles’ remains.

As discussed in section 1.2.3 the basic unit of magnetism is the magnetic dipole. The basic unit of electricity is the electric charge. There have been searches for the magnetic monopole which has a theoretical value, according to some authors [2], of $p = 3.29 \times 10^{-9} \text{ A m}$ ($\mu_0 p = 4.136 \times 10^{-15} \text{ Wb}$) and, if it exists, would be the magnetic analogue of electric charge. The discovery of the monopole would have important consequences but the search has so far been inconclusive [3,4].

However if the magnetic monopole is discovered this will lead to fundamental changes in our understanding of magnetism. In particular the much maligned concept of the magnetic pole, which is a useful concept for those working in magnetic materials, would become more acceptable. Maxwell’s equations of electromagnetism would also need to be altered to allow the divergence of \mathbf{B} to be non-zero. A recent work on the subject has been written by Carrigan and Trower [5].

2.1.2 Magnetization M

How are the magnetic properties of the material and the magnetic induction \mathbf{B} related?

30 Magnetization and magnetic moment

We can define a new quantity \mathbf{M} , the magnetization, as the magnetic moment per unit volume of a solid.

$$\mathbf{M} = \frac{\mathbf{m}}{V}.$$

From the relationship between magnetic moment \mathbf{m} and flux given in section 2.1.1 a simple relationship between \mathbf{M} and \mathbf{B} can be found. A bar magnet with flux density Φ at the centre, dipole length l and with cross-sectional area A has a magnetic moment \mathbf{m} given by $\mathbf{m} = \Phi l / \mu_0$. The magnetization \mathbf{M} is therefore given by $\mathbf{M} = m/Al$. Hence,

$$\begin{aligned}\mathbf{M} &= \frac{\Phi}{\mu_0 A} \\ &= \frac{\mathbf{B}}{\mu_0}.\end{aligned}$$

In this case there are no conventional external electric currents present to generate an external magnetic field and so $\mathbf{B} = \mu_0 \mathbf{M}$. We see therefore that the magnetization \mathbf{M} and magnetic field \mathbf{H} contribute to the magnetic induction in a similar way. If both magnetization and magnetic field are present then their contributions can be summed.

2.1.3 Relation between \mathbf{H} , \mathbf{M} and \mathbf{B}

Can we define a universal equation relating these three magnetic quantities, field, induction and magnetization?

We have seen that the magnetic induction \mathbf{B} consists of two contributions: one from the magnetic field, the other from the magnetization. The magnetic induction in free space is $\mu_0 \mathbf{H}$, while in the convention which we are following the contribution to the induction from the magnetization of a material is $\mu_0 \mathbf{M}$. The magnetic induction is then simply the vector sum of these,

$$\mathbf{B} = \mu_0(\mathbf{H} + \mathbf{M}),$$

where \mathbf{B} is in tesla, and \mathbf{H} and \mathbf{M} are in amps per metre. The above equation which relates these three basic magnetic quantities is true under all circumstances.

The magnetic field \mathbf{H} is generated by electrical currents outside the material either from a solenoid or electromagnet, or from a permanent magnet. The magnetization is generated by the resultant (uncompensated) spin and orbital angular momentum of electrons within the solid. The origin of the net angular momentum of the electrons requires further development of ideas before it can be explained. Discussion is therefore deferred until Chapters 9, 10 and 11.

A related quantity, the magnetic polarization or intensity of magnetization I is used in the Kennelly convention. This is defined by

$$I = \mu_0 M.$$

Although it is not often employed when the Sommerfeld system is used, it is a useful unit. Measuring the magnetic polarization I of a material in tesla is often more convenient than measuring the magnetization M in A/m. Crangle [6] has remarked that since the Sommerfeld and Kennelly systems are not mutually exclusive this unit can easily be incorporated into the IUPAP system without contradictions.

In the SI system of units [7,8] M is usually measured in amps per metre (the Sommerfeld convention, which we are using) but you will sometimes find it measured, as indicated above, in tesla (the Kennelly convention). This means that the torque equation in free space is different in the two conventions by a factor of μ_0 , being $\tau = m \times H$ in the Kennelly convention but $\tau = m \times B = \mu_0 m \times H$ in the Sommerfeld convention. Similarly, the magnetic moment in the Sommerfeld convention is measured in amp metre², whereas in the Kennelly convention it is measured in weber metre. The relative merits of the two conventions have been discussed at length [9, 10, 11], and each has its own advantages and disadvantages. In the Sommerfeld convention the definition of susceptibility is useful, but in the Kennelly system the susceptibility is an awkward unit. However, in the Kennelly system the unit of magnetic polarization is more convenient than the unit of magnetization in the Sommerfeld convention. Also the energy of a magnetic moment in a field and the torque on a magnetic moment in a field are simpler in the Kennelly system because μ_0 does not enter the equations.

2.1.4 Saturation magnetization

Is there a limit to the magnetization that a given material can reach?

If a material has n elementary atomic magnetic dipoles per unit volume each of magnetic moment m then the magnetic moment per unit volume of the material when all these moments are aligned parallel is termed the saturation magnetization M_0 . This is equal to the product of n and m .

A distinction can be made between technical saturation M_s and complete saturation M_0 . In order to fully understand this distinction a discussion of domain processes must first be presented. At this stage we shall merely note that technical saturation magnetization is achieved when a material is converted to a single magnetic domain, but at higher fields the magnetization increases very slowly beyond technical saturation. This slow increase of magnetization at high fields is due to an increase in the spontaneous magnetization within a single domain, as discussed in section 6.2.5 and is known as forced magnetization.

32 Magnetization and magnetic moment

2.2 PERMEABILITY AND SUSCEPTIBILITY OF VARIOUS MATERIALS

Can the various types of magnetic materials be classified from their bulk magnetic properties?

The different types of magnetic materials are usually classified on the basis of their susceptibility or permeability. Therefore we must define these related properties precisely before going on to describe the differences between ferromagnetic, paramagnetic and diamagnetic materials.

2.2.1 Permeability and susceptibility

How can we represent the response of a magnetic material to a magnetic field?

We can now make a general statement for the permeability μ and susceptibility χ . The permeability is defined as

$$\mu = \frac{\mathbf{B}}{\mathbf{H}}$$

and the susceptibility is defined as

$$\chi = \frac{\mathbf{M}}{\mathbf{H}}$$

and the differential permeability and susceptibility are defined as,

$$\mu' = \frac{d\mathbf{B}}{d\mathbf{H}}$$

$$\chi' = \frac{d\mathbf{M}}{d\mathbf{H}}.$$

Since \mathbf{B} and \mathbf{M} may or may not be linear functions of \mathbf{H} , depending on the type of material or medium, it should be noted here that permeability and susceptibility may or may not be constant.

Sometimes you will find the term relative permeability used, particularly in SI units. The relative permeability of a medium, denoted μ_r , is given by

$$\mu_r = \frac{\mu}{\mu_0},$$

where μ_0 is of course the permeability of free space $\mu_0 = 4\pi \times 10^{-7}$ henry/metre. The relative permeability of free space is 1. The relative permeability is closely related to the susceptibility and the following equation is always true

$$\mu_r = \chi + 1.$$

Other commonly encountered properties are the initial permeability μ_{in} and the initial susceptibility χ_{in} . These are the values of the respective quantities at the

origin of the initial magnetization curve

$$\mu_{\text{in}} = \left(\frac{d\mathbf{B}}{d\mathbf{H}} \right)_{\mathbf{B}=0, \mathbf{H}=0} = \left(\frac{\mathbf{B}}{\mathbf{H}} \right)_{\mathbf{B}=0, \mathbf{H}=0}$$

$$\chi_{\text{in}} = \left(\frac{d\mathbf{M}}{d\mathbf{H}} \right)_{\mathbf{M}=0, \mathbf{H}=0} = \left(\frac{\mathbf{M}}{\mathbf{H}} \right)_{\mathbf{M}=0, \mathbf{H}=0}$$

In general physicists and materials scientists are more interested in magnetization and susceptibility, while engineers who work mainly with ferromagnets are usually more concerned with magnetic induction and permeability.

Example 2.1 Permeability of and magnetic induction in iron. In a magnetic field of 400 amp/metre the relative permeability of a piece of soft iron is 3000. Calculate the magnetic induction in the iron at this field strength.

$$\begin{aligned}\mathbf{B} &= \mu_0(\mathbf{H} + \mathbf{M}) \\ &= \mu_0 \mu_r \mathbf{H} \\ &= (4\pi \times 10^{-7})(3000)400 \\ &= 0.48\pi \text{ tesla.}\end{aligned}$$

2.2.2 Diamagnets, paramagnets and ferromagnets

How are the different types of magnetic materials classified?

These various different type of magnetic materials are classified according to their bulk susceptibility. The first group are materials for which χ is small and negative $\chi \approx -10^{-5}$. These materials are called diamagnetic, their magnetic response opposes the applied magnetic field. Examples of diamagnets are copper, silver, gold, bismuth and beryllium. Superconductors form another group of diamagnets for which $\chi \approx -1$.

A second group of materials for which χ is small and positive and typically $\chi \approx 10^{-3}$ to 10^{-5} are the paramagnets. The magnetization of paramagnets is weak but aligned parallel with the direction of the magnetic field. Examples of paramagnets are aluminum, platinum and manganese.

The most widely recognized magnetic materials are the ferromagnetic solids for which the susceptibility is positive, much greater than 1, and typically can have values $\chi \approx 50$ to 10 000. Examples of these materials are iron, cobalt and nickel and several rare earth metals and their alloys.

2.2.3 Susceptibilities of diamagnetic and paramagnetic materials

What are typical values of μ and χ in diamagnets and paramagnets?

At constant temperature and for relatively low values of magnetic field \mathbf{H} , the magnetic susceptibilities of diamagnets and paramagnets are constant. Under

34 Magnetization and magnetic moment

these conditions the materials are called ‘linear’, that is \mathbf{M} is proportional to \mathbf{H} . Consequently, it is possible to write

$$\begin{aligned}\mathbf{M} &= \chi \mathbf{H} \\ \mathbf{B} &= \mu_0(1 + \chi) \mathbf{H} \\ &= \mu_0 \mu_r \mathbf{H} \\ &= \mu \mathbf{H}.\end{aligned}$$

Clearly then μ_r is slightly greater than one in the paramagnets and slightly less than one in the diamagnets. At the same time χ is slightly more than zero in the paramagnets and slightly less than zero in the diamagnets.

The linear result is a useful one in that it allows us to write a proportional relation between \mathbf{B} and \mathbf{H} in these materials at low fields. However we shall see later in the classical Langevin theories of diamagnetism and paramagnetism that the linear approximation no longer holds at higher fields and in fact paramagnets exhibits saturation of magnetization at very high fields.

2.2.4 Values of μ_r and χ for various materials

What values of permeability and susceptibility do various metals have?

Table 2.1 Susceptibilities and permeabilities of various elements

		χ	μ_r
<i>Diamagnets</i>	Bi	-1.31×10^{-6}	0.999 83
	Be	-1.85×10^{-6}	0.999 98
	Ag	-2.02×10^{-6}	0.999 97
	Au	-2.74×10^{-6}	0.999 96
	Ge	-0.56×10^{-6}	0.999 99
	Cu	-0.77×10^{-6}	0.999 99
<i>Paramagnets</i>	β -Sn	0.19×10^{-6}	1.000 00
	W	6.18×10^{-6}	1.000 08
	Al	1.65×10^{-6}	1.000 02
	Pt	21.04×10^{-6}	1.000 26
	Mn	66.10×10^{-6}	1.000 83

In ferromagnets neither χ nor μ_r have a constant value. Both permeability and susceptibility in ferromagnets are strongly affected by the prevailing magnetic field \mathbf{H} and the previous history of the material. For example the change in permeability of annealed iron along its initial magnetization curve is shown in Fig. 2.3.

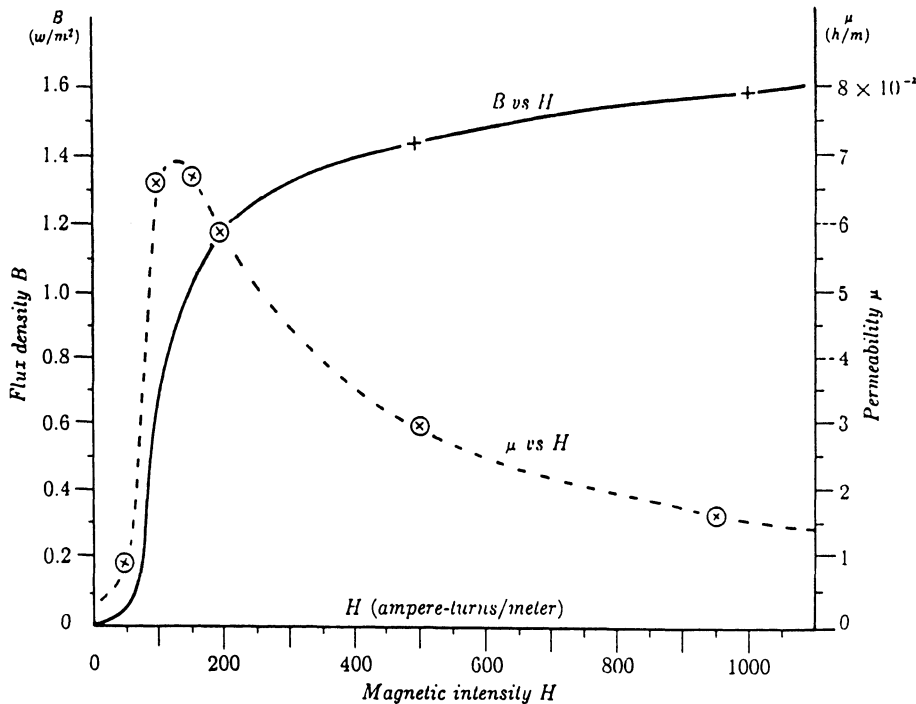


Fig. 2.3 Initial magnetization curve and permeability along the same curve for annealed iron.

2.2.5 Other types of magnetic materials

Are there other types of magnetic materials which the above classification fails to identify?

There are some other types of magnetic materials apart from the three classes of diamagnets, paramagnets and ferromagnets given above. These other materials are all very closely related to ferromagnets because they are magnetically ordered, as explained in Chapter 6. They are ferrimagnets, antiferromagnets, helimagnets and superparamagnets. All were discovered many years after the three classical groups of magnetic materials discussed above. From bulk magnetic measurements the ferrimagnets are indistinguishable from ferromagnets, while the antiferromagnets and helimagnets were for many years mistaken for paramagnets. These magnetic types will be discussed in chapter 9.

Example 2.2 Flux differences between air core and iron core. Calculate the magnetic induction B and flux Φ at the centre of a toroidal solenoid with mean circumference of 50 cm and cross-sectional area of 2.0 cm^2 , wound with 800 turns

36 Magnetization and magnetic moment

of wire carrying 1.0 amp, (a) when the solenoid has an air core and (b) when the solenoid has a soft iron core of relative permeability 1000.

The magnetic field \mathbf{H} will be given by

$$\begin{aligned}\mathbf{H} &= ni \\ &= 1600 \text{ amp/metre.}\end{aligned}$$

(a) In air $\mathbf{B} = \mu_0 \mathbf{H}$

$$\begin{aligned}\mathbf{B} &= (4\pi \times 10^{-7}) 1600 \\ &= 2.0 \times 10^{-3} \text{ tesla.}\end{aligned}$$

$$\Phi = \mathbf{B} \cdot \mathbf{A}$$

$$\begin{aligned}\Phi &= (2.0 \times 10^{-3}) (2.0 \times 10^{-4}) \\ &= 4.0 \times 10^{-7} \text{ webers.}\end{aligned}$$

(b) In iron with $\mu_r = 1000$

$$\begin{aligned}\mathbf{B} &= \mu_r \mu_0 \mathbf{H} \\ &= (1000) (2.0 \times 10^{-3}) \text{ tesla} \\ &= 2.0 \text{ tesla.}\end{aligned}$$

$$\Phi = \mathbf{B} \cdot \mathbf{A}$$

$$\begin{aligned}\Phi &= (2.0) (2.0 \times 10^{-4}) \\ &= 4.0 \times 10^{-4} \text{ webers.}\end{aligned}$$

2.3 MAGNETIC CIRCUITS AND DEMAGNETIZING FIELD

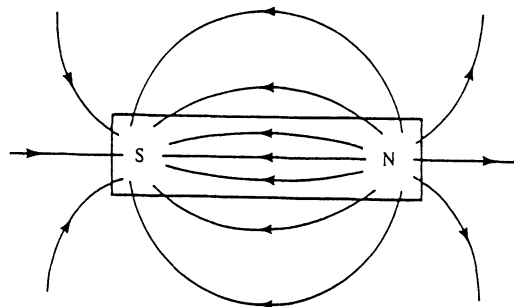
How does a magnetic material alter the field and flux density in its vicinity?

In a given magnetic field \mathbf{H} the presence of a magnetic material affects the magnetic induction \mathbf{B} due to its permeability μ as indicated in the previous chapter. For determining the magnetic flux in magnetic circuits a useful concept is the reluctance R which is the magnetic analogue of electrical resistance. Furthermore, if the magnetic material has finite length the generation of 'magnetic poles' near its ends gives rise to a magnetic field opposing the applied field. This opposing field is called the demagnetization field and its strength is dependent on the geometry and magnetization \mathbf{M} of the material.

2.3.1 Flux lines around a bar magnet

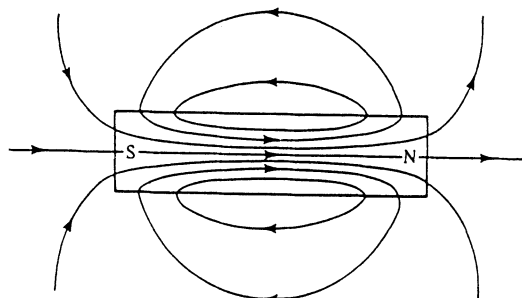
How does the presence of a magnetic material alter the flux lines in its vicinity?

The magnetic flux lines around a bar magnet can be mapped using a small dipole such as a compass needle or iron filings. The flux lines are continuous throughout the material and have the form shown in Fig. 2.4. The flux lines have a similar form



(a)

$$\begin{array}{c} B \longrightarrow \\ H_d \longleftarrow \\ M \longrightarrow \end{array} \quad \left. \right\} \text{Inside the magnet}$$



(b)

Fig. 2.4 (a) Magnetic field H both inside and outside a bar magnet, (b) Magnetic induction B both inside and outside a bar magnet. Notice in particular that the magnetic field and induction lines are identical outside the material, but inside they are quite different (they even point in opposite directions).

to the flux lines in and around a current loop dipole such as a single turn of current-carrying conductor or short solenoid.

2.3.2 Field lines around a bar magnet

Are the magnetic field lines identical to the magnetic flux lines?

The field lines around a bar magnet are the same as the flux lines outside the material as shown in Fig. 2.4, since $B = \mu_0 H$ in free space. However inside the

38 Magnetization and magnetic moment

material they are different and in fact \mathbf{B} and \mathbf{H} point in different directions because of the magnetization of the material \mathbf{M} . This can be proved using Ampère's circuital law. We can view the magnetization as being the effect of aligning the magnetic dipoles within the material which creates magnetic 'poles' near the ends of a finite specimen.

The magnetization vector \mathbf{M} inside a magnetized ferromagnet points from the 'south pole' to the 'north pole' since this is the convention adopted for the definition of magnetic moment for a magnetic dipole. The magnetic field \mathbf{H} always points from a 'north pole' to a 'south pole'.

2.3.3 Demagnetizing fields

Does the shape of a specimen have any effect on the \mathbf{H} field?

In view of the fact that the magnetization \mathbf{M} and the magnetic field \mathbf{H} point in opposite directions inside a magnetized material of finite dimensions, due to the presence of the magnetic dipole moment, it is possible to define a demagnetizing field \mathbf{H}_d which is present whenever magnetic poles are created in a material. This demagnetizing field can be detected during hysteresis measurements on finite-length samples when the applied field is reduced to zero but the measured field is negative due to the remanent magnetization.

The demagnetizing field depends on two factors only. These are the magnetization in the material (i.e. the pole strength) and the shape of the specimen (i.e. the pole separation which is determined by sample geometry). The demagnetizing field is proportional to the magnetization and is given by the expression

$$\mathbf{H}_d = N_d \mathbf{M},$$

where N_d is a demagnetizing factor which is calculated solely from the sample geometry. It should be remembered that the numerical value of N_d depends on the units used for \mathbf{M} and \mathbf{H}_d . In the unit convention used in this book both \mathbf{M} and \mathbf{H}_d are measured in amps/metre so that N_d is simply a dimensionless number.

2.3.4 Demagnetizing factors

What value does the demagnetizing factor have in different cases?

Exact analytic solutions for N_d can only be obtained in the case of second-order shapes, that is spheres and ellipsoids [12]. However tables or charts of approximate calculated demagnetizing factors are available for solids of various shapes, as shown in Fig. 2.5.

Fig. 2.5 Calculated demagnetizing factors for ellipsoids and cylinders. Note that the values of the demagnetizing factor are dependent on the permeability as well as on the shape.

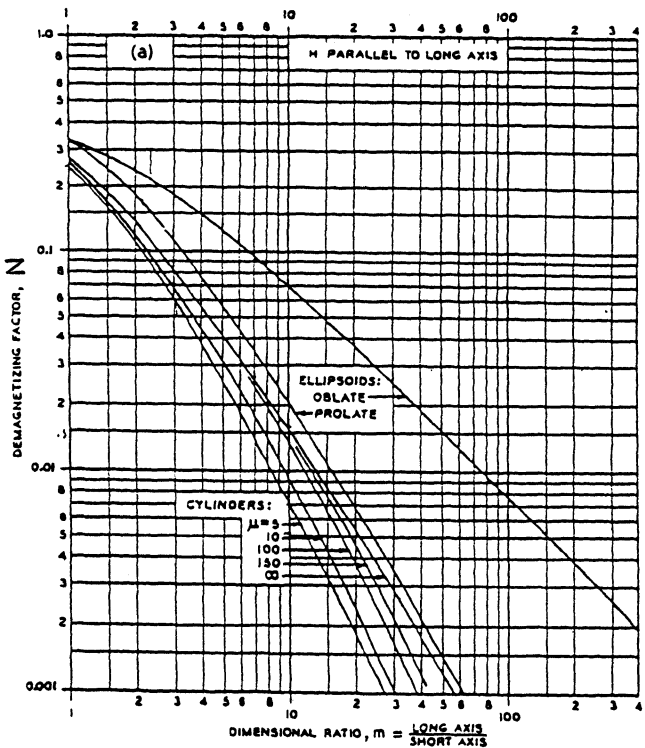
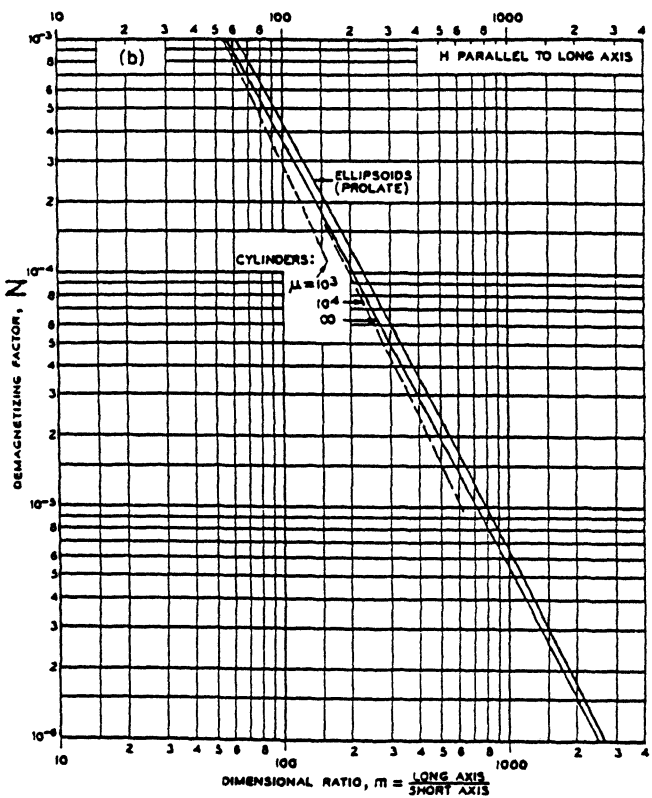


Table 2.2 Demagnetizing factors for various simple geometries

<i>Geometry</i>		N_d
Toroid		0
Long cylinder		0
Cylinder	$l/d = 20$	0.00617
Cylinder	$l/d = 10$	0.0172
Cylinder	$l/d = 8$	0.02
Cylinder	$l/d = 5$	0.040
Cylinder	$l/d = 1$	0.27
Sphere		0.333

2.3.5 Field correction due to demagnetizing field

How do we make a correction to the field if we have specimens of finite dimensions?

We have shown above how the demagnetizing field arises in a sample of given shape with magnetization \mathbf{M} in zero field. When dealing with samples of finite dimensions in an applied magnetic field \mathbf{H}_{app} it is necessary to make some demagnetizing field correction to determine the exact internal field in the solid \mathbf{H}_{in} .

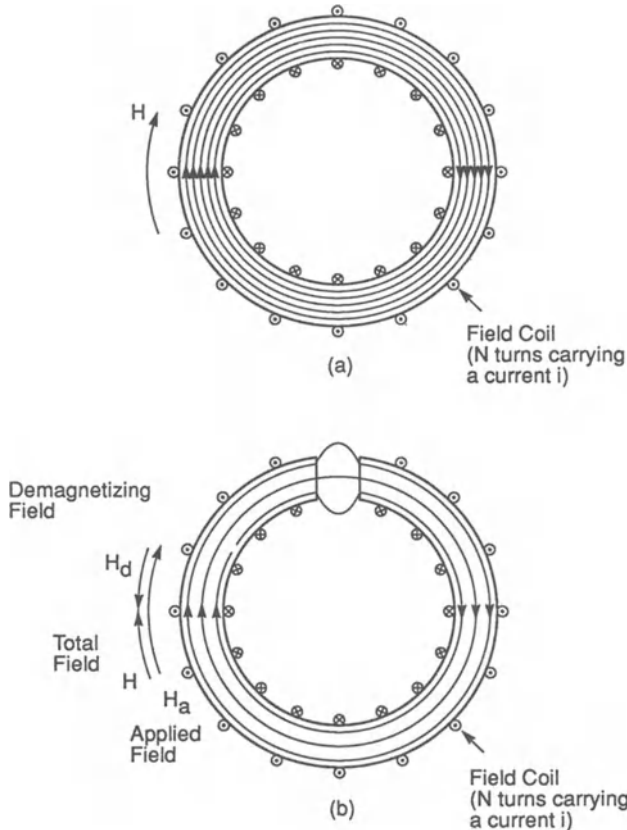
$$\mathbf{H}_{\text{in}} = \mathbf{H}_{\text{app}} - N_d \mathbf{M}.$$

2.3.6 Magnetic circuits and reluctance

How do we calculate magnetic field or flux in situations where we have an air gap or two materials with different magnetic properties?

Situations in which a magnetic flux path is interrupted by an air gap are of practical importance because they occur in engineering applications of permanent magnets, electric motors and generators and in materials testing. The problems encountered here are more complicated than in calculating the flux in a single material, however the ideas of demagnetizing fields together with some generalizations of the equations relating magnetic flux to magnetic field can be employed to provide solutions.

The magnet engineer is often in the situation of calculating the magnetic flux in magnetic circuits [13,14] with a combination of an iron and air core. Consider for example the situation where a ring of iron is wound with N turns of a solenoid which carries a current i as shown in Fig. 2.6 (a). In this case the magnetic field will be Ni/L where L is the average length of the ring and from this, and a knowledge of the permeability, the magnetic flux or flux density passing in the ring can be



Magnetic Circuits: (a) closed, and (b) open.

Fig. 2.6 Magnetic flux path in (a) an iron toroid forming a closed magnetic path, and (b) an iron toroid with an air gap. The flux lines are shown as concentric circles within the iron. The air gap increases the reluctance of the magnetic circuit and reduces the flux density in the iron as well as in the gap.

calculated.

$$\mathbf{B} = \mu_0(\mathbf{H} + \mathbf{M})$$

and from Ampère's law, in this simple situation $\mathbf{H} = Ni/L$, and therefore

$$\mathbf{B} = \mu_0 \left(\frac{Ni}{L} + \mathbf{M} \right)$$

42 Magnetization and magnetic moment

and consequently

$$\begin{aligned} Ni &= \left(\frac{\mathbf{B}}{\mu_0} - \mathbf{M} \right) L \\ &= \frac{\mathbf{BL}}{\mu}. \end{aligned}$$

We can define here the magnetomotive force η which for a solenoid is Ni where N is the number of turns and i is the current flowing in the solenoid. From this we can formulate a general equation relating the magnetic flux Φ , the magnetic reluctance R_m and the magnetomotive force η as follows,

$$\Phi = \frac{\eta}{R_m}$$

which may be considered as a magnetic analogue of Ohm's law. If the iron ring has cross-sectional area A metre² and permeability μ with N turns of solenoid on a length L we can derive an expression for the reluctance. Starting from the relationship between flux, magnetic induction and magnetic field

$$\begin{aligned} \Phi &= \mathbf{BA} = \mu \mathbf{HA} \\ &= \mu \left(\frac{Ni}{L} \right) A \\ &= \frac{Ni}{(L/\mu A)}. \end{aligned}$$

From our definitions above it follows that the term $L/\mu A$ is the magnetic reluctance of the path. This is analogous to electrical resistance in an electrical circuit, which means that magnetic reluctances in series in a magnetic circuit may be added.

A saw slot can be introduced in the ring as shown in Fig. 2.6 (b) to provide an air gap. If the air gap is small there will be little leakage of the flux at the gap, but a single equation $\mathbf{B} = \mu \mathbf{H}$ can no longer apply since the permeability of air and the iron ring are very different.

Ignoring demagnetizing effects for the present calculation and starting from Ampère's circuital law

$$Ni = \int_{\text{closed path}} \mathbf{H} dl$$

and for a two-component magnetic circuit consisting of an iron ring and an air gap

$$Ni = H_i L_i + H_a L_a,$$

where L_i is the path length in the iron and L_a is the path length in the air and H_i and H_a are correspondingly the respective fields in the iron and in the air.

For the ring with the air gap the flux density in the gap equals the flux density in the iron, but the magnetization in the air gap is necessarily zero. Therefore we can write a similar equation for the magnetic induction.

$$\begin{aligned} Ni &= \left(\frac{\mathbf{B}}{\mu_0} - M \right) L_i + \frac{\mathbf{B} L_a}{\mu_a} \\ &= \mathbf{B} \left(\frac{L_i}{\mu_i} + \frac{L_a}{\mu_a} \right). \end{aligned}$$

It is clear from this that there is a discontinuity in \mathbf{H} across the air gap while at the same time there is continuity in \mathbf{B} . Rewriting the equation in terms of flux Φ leads to

$$Ni = \Phi \left(\frac{L_i}{A_i \mu_i} + \frac{L_a}{A_a \mu_a} \right).$$

Therefore from the above definition of magnetic reluctance as the ratio of flux to magnetomotive force, the reluctance of this magnetic circuit with an air gap is

$$R_m = \frac{L_i}{\mu_i A_i} + \frac{L_a}{\mu_a A_a}.$$

The equation for the flux passing through the toroid with an air gap is then

$$\Phi = \frac{Ni}{\left(\frac{L_i}{\mu_i A_i} + \frac{L_a}{\mu_a A_a} \right)}.$$

The magnetic flux in the ring is reduced when the air gap is introduced because it requires more energy to drive the same flux across the air gap than through an equal volume of the iron due to the much lower permeability of the air.

2.3.7 Magnetic field calculations in magnetic materials

How can the magnetic field be calculated in more complex situations such as those with both magnetic materials and air gaps of different shapes?

At the end of Chapter 1 we showed how a variety of numerical techniques could be used to calculate the magnetic field in free space. This was a particularly simple situation. In the presence of magnetic materials the situation becomes more difficult because the magnetization of the material needs to be taken into account. Nevertheless the same general techniques, such as finite-element analysis [15] can be used successfully.

44 Magnetization and magnetic moment

The effect of hysteresis adds a further complication to the problem since the magnetization M of the material then depends not only on magnetic field H , but also on the field history. Even in the cases where hysteresis occurs methods have been devised for calculation of magnetic fields in devices [16] which take hysteresis into account.

REFERENCES

1. Cullity, B. D. (1972) *Introduction to Magnetic Materials*, Addison-Wesley, Reading Mass., p. 5.
2. Dirac, P. A. M. (1931) *Proc. Roy. Soc. Lond.*, **A133**, 60.
3. Fleischer, R. L., Hart, H. R., Jacobs, I. S., Price, P. B., Schwarz, W. M. and Woods, R. T. (1970) *J. Appl. Phys.*, **41**, 958.
4. Trower, W. P. (1983) *IEEE Trans. Mag.*, **19**, 2061.
5. Carrigan, R. A. and Trower, W. P. (1983) *Magnetic Monopoles*, Plenum, New York.
6. Crangle, J. (1977) *The Magnetic Properties of Solids*, Edward Arnold, London, Ch. 1, pp. 13–15.
7. Vigoureux, P. (1971) *Units and Standards in Electromagnetism*, Wykeham Press, London.
8. Hopkins, R. A. (1975) *The International (SI) Metric System*, 3rd edn, AMJ Publishers Tarzana, California.
9. Giacolletto, L. J. (1974) *IEEE Trans. Mag.*, **10**, 1134.
10. Graham, C. D. (1976) *IEEE Trans. Mag.*, **12**, 822.
11. Brown, W. F. (1984) *IEEE Trans. Mag.*, **20**, 112.
12. Osborne, J. A. (1945) *Phys. Rev.*, **67**, 351.
13. Proceedings of the IEEE Workshop on applied magnetics (1972) Washington DC. Published by IEEE, New York.
14. Proceedings of the IEEE Workshop on applied magnetics (1975) Milwaukee, Wisconsin. Published by IEEE, New York.
15. Preis, K., Stogner, H. and Richter, K. R. (1981) *IEEE Trans. Mag.*, **17**, 3396.
16. Saito, Y. (1982) *IEEE Trans. Mag.*, **18**, 546.

FURTHER READING

- Bennet, G. A. (1968) *Electricity and Modern Physics*, Arnold, London, Ch. 6.
Bradley, F. N. (1971) *Materials for Magnetic Functions*, Hayden, New York.
Lorrain, P. and Corson, D. R. (1978) *Electromagnetism*, W. H. Freeman, San Francisco.
McKenzie, A. E. E. (1961) *A Second Course of Electricity*, 2nd edn, Cambridge University Press. Cambridge, Ch. 5 and 6.
Reitz, J. R. and Milford, F. J. (1980) *Foundations of Electromagnetic Theory*, 3rd edn, Addison-Wesley, Reading, Mass., Ch. 9.
Rieger, H. (1978) *The Magnetic Circuit*, Heyden and Son, London, Siemens Aktiengesellschaft, Berlin and Munich.

EXAMPLES AND EXERCISES

Example 2.3 Demagnetizing field calculation. How strong is the magnetic field needed to magnetize an iron sphere to its saturation magnetization ($M_s = 1.69$

$\times 10^6$ amps/metre) assuming that the field needed to overcome the demagnetizing field is much greater than the field needed to saturate the material in toroidal form.

Example 2.4 Demagnetizing effects at different field strengths. A specimen of Terfenol has a length to diameter ratio of 8:1. At a field strength of $H = 80$ kA/m the magnetic induction is 0.9 tesla, while at a field strength of $H = 160$ kA/m the induction is 1.1 tesla. Calculate the internal magnetic field H_{in} in each case and compare with the applied field.

If we consider the fractional error in the observation of the uncorrected field what do you conclude about this error at higher fields? Do demagnetizing effects become more or less of a problem as the applied field increases?

Example 2.5 Flux density in an iron ring with and without an air gap. An iron toroid has a mean path length of 0.5 m with a cross-sectional area of 2×10^{-4} m². The number of turns on the coil wound on the toroid is $N = 800$ and this carries a current of 1 A. If the relative permeability of the iron is 1500 estimate the flux in the iron ring. An air gap of length 0.0005 m is then cut in the ring. Estimate the flux under these conditions. Calculate the current needed to restore the flux to its original value in the uncut toroid.

3

Magnetic Measurements

This chapter is concerned with the various means of measuring the magnetic field, magnetic induction or magnetization. There are several methods available and these divide broadly into two categories of field measurement: those which depend on magnetic induction using coils and those which depend on measuring changes in various properties of materials caused by the presence of a magnetic field. Finally, the measurements of magnetization are either force measurements such as in the torque magnetometer or gradiometer measurements which measure the difference in magnetic induction with and without the sample present.

3.1 INDUCTION METHODS

How can the strength of an external field be measured from the e.m.f. generated in an electrical circuit due to a change in flux linking the circuit?

The induction methods of measuring magnetic flux are all dependent on Faraday's law of electromagnetic induction which has been discussed in section 1.2.2. This states that the e.m.f. induced in a circuit is equal to the rate of change of flux linking the circuit.

$$V = -N \frac{d\Phi}{dt}.$$

If A is the cross-sectional area of the coil and N is the number of turns the magnetic induction is then $\mathbf{B} = \Phi/A$

$$V = -NA \frac{d\mathbf{B}}{dt}.$$

Note that these coil methods measure the magnetic flux passing through the coil Φ , and from a knowledge of the cross-sectional area A the magnetic induction \mathbf{B} can be found. The induced voltage is increased if \mathbf{B} is increased while \mathbf{H} is maintained constant by inserting a high-permeability core into the coil. In free space, of course, $\mathbf{B} = \mu_0 \mathbf{H}$ and so

$$V = -\mu_0 N A \frac{d\mathbf{H}}{dt}.$$

48 Magnetic measurements

3.1.1 Stationary-coil methods

How can the rate of change of field be found using the e.m.f. generated in a stationary coil?

A stationary-coil method can only measure the rate of change of magnetic induction by measuring the induced voltage. Such devices do have applications but if magnetic-induction measurements are required it is necessary to include some form of time integration [1]. A number of integrating voltmeter/fluxmeter devices are now commercially available. These measure the magnetic induction from the relation

$$\mathbf{B} = -\frac{1}{NA} \int V dt.$$

These instruments can be highly sensitive and are used extensively in hysteresis graphs for the measurement of the magnetic properties of soft magnetic materials [2]. These instruments work well but in setting them up it is necessary to pay attention to the problem of drift, which can be adjusted using an offset voltage control. If this is not done the fluxmeter will continue to integrate a small out-of-balance voltage with time, giving the impression of a linearly varying magnetic induction. Under present capabilities this can be a problem for high-sensitivity measurement when the magnetic flux needs to be measured to better than about 10^{-10} webers (0.01 maxwell).

3.1.2 Moving-coil (extraction) method

How is the magnetic induction measured when a search coil is placed in a magnetic field and rapidly removed?

As we know from the Faraday law of electromagnetic induction (section 1.2.2) the induced e.m.f. in a coil resulting from a change in flux linking the coil is given by

$$V = -NA \frac{d\mathbf{B}}{dt}.$$

Integrating this gives

$$\int V dt = -NA(\mathbf{B}_f - \mathbf{B}_i)$$

where \mathbf{B}_i is the initial magnetic induction and \mathbf{B}_f is the final magnetic induction. Therefore if a search coil is moved from the location where the field strength needs to be measured (e.g. between the poles of an electromagnet) to a region of 'zero' field (e.g. outside the electromagnet) $\int V dt$ will be proportional to the magnetic induction.

A ballistic (moving-coil) galvanometer can be used to measure the induction

since, providing the time of oscillation of the ballistic galvanometer is long compared with the voltage pulse from the search coil, the angular deflection ϕ is proportional to $\int V dt$. The device needs calibrating in order to determine the coefficient of proportionality.

$$\begin{aligned}\phi &= \text{constant} \times \int V dt \\ &= \text{constant} \times NA(\mathbf{B}_f - \mathbf{B}_i).\end{aligned}$$

The deflection of the galvanometer is therefore proportional to the change in magnetic induction. After calibration this method is accurate to better than 1%.

3.1.3 Rotating-coil method

Can we make use of a rotating coil to generate the necessary induced e.m.f. in a static field?

In order to obtain a measurement of the magnetic induction it is also possible to use various moving-coil instruments. The simplest of these is the rotating coil which rotates at a fixed angular velocity ω . Under these conditions the flux linking the coil is

$$\mathbf{B}(t) = \mathbf{B} \cos \omega t$$

and the voltage generated is

$$\begin{aligned}V &= -NA \frac{d\mathbf{B}}{dt} \\ &= -\mu_0 NA \frac{d\mathbf{H}}{dt} \\ &= -\mu_0 NA \omega \mathbf{H} \sin \omega t.\end{aligned}$$

Therefore the amplitude of the voltage generated by the rotating coil is proportional to the magnetic induction and therefore the amplitude can be used to measure \mathbf{B} or \mathbf{H} in free space. The signal can be read directly as an a.c. voltage or converted to a d.c. voltage which is proportional to the amplitude. Typical inductions for this instrument range from 10 tesla down to 10^{-7} tesla. The electrical connections to the rotating coil include slip rings which are a source of error in dealing with small voltages. The precision is of the order of one part in 10^4 .

3.1.4 Vibrating-coil magnetometer

How can the linear displacement of a coil in a magnetic field be used to measure the strength of the field?

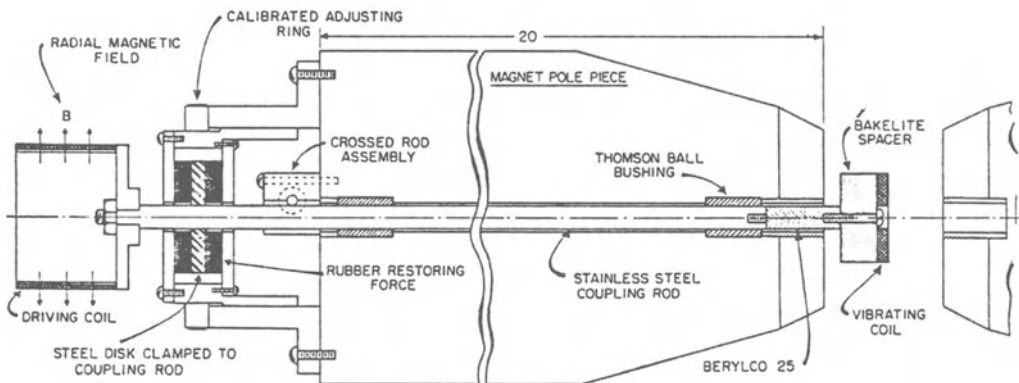
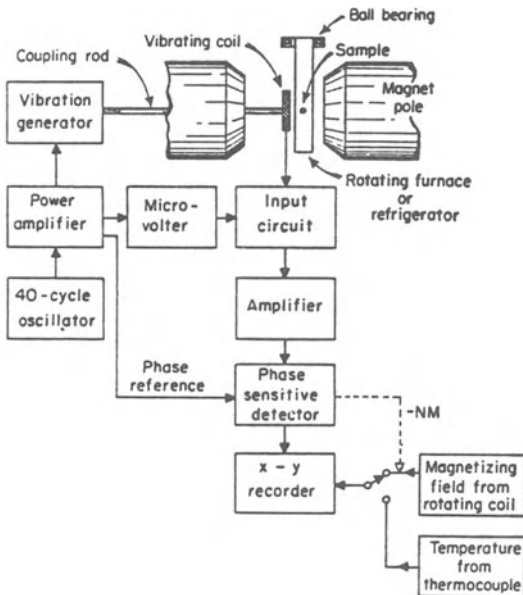


Fig. 3.1 Schematic diagram of a vibrating-coil magnetometer.

The vibrating-coil magnetometer [3,4] is based on the same principles as the previous technique, but is used primarily as a method of determining the magnetization M . The arrangement is shown in Fig. 3.1. The coil vibrates between the sample and a region of free space and thereby acts as a gradiometer by measuring the difference in induction in the two positions. While surrounding the sample the magnetic induction is

$$\mathbf{B}_m = \mu_0(\mathbf{H} + \mathbf{M}),$$

whereas the induction linking the coil when it has moved away from the sample is

$$\mathbf{B}_0 = \mu_0 \mathbf{H}.$$

The change in induction is then simply

$$\Delta \mathbf{B} = \mu_0 \mathbf{M}.$$

The method therefore depends on the flux change caused when the coil is removed from the specimen

$$\int V dt = -NA\mu_0 \mathbf{M}$$

and consequently the output of the vibrating coil magnetometer is independent of \mathbf{H} , but is dependent on \mathbf{M} . This device is subject to noise caused by variation of the magnetic field \mathbf{H} with time and is rarely used in situations in which it is possible to vibrate the sample instead of the coil as in the vibrating-sample magnetometer (section 3.1.5).

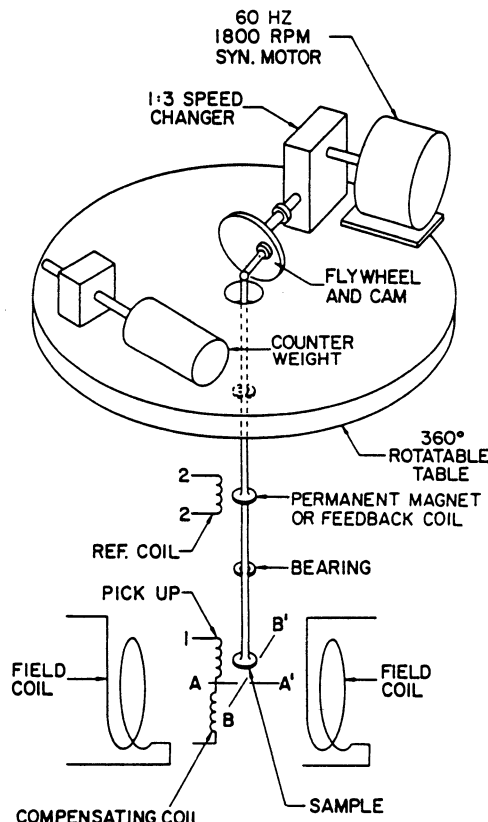


Fig. 3.2 Schematic diagram of a vibrating-sample magnetometer.

52 Magnetic measurements

3.1.5 Vibrating-sample magnetometer (VSM)

If the specimen is moved instead of the coil how can the induced voltage be used to determine the magnetization of the specimen?

The vibrating-sample magnetometer (VSM) is identical in principle to the vibrating-coil magnetometer except that the sample is moved instead of the coil. The VSM was first described by Foner [5] and has now almost completely superseded the vibrating-coil device.

A VSM is really a gradiometer measuring the difference in magnetic induction between a region of space with and without the specimen. It therefore gives a direct measure of the magnetization M .

A schematic of a typical VSM is shown in Fig.3.2. The specimen in general has to be rather short to fit between poles of the electromagnet. The method is therefore in most cases not well suited to the determination of the magnetization curve or hysteresis loop because of the demagnetizing effects associated with the short specimen. However it is well suited for the determination of the saturation magnetization M_s .

The detected signal, being an a.c. signal of fixed frequency, is measured using a lock-in amplifier. A reference signal is provided for the lock-in amplifier as shown in Fig.3.2 by using a permanent magnet and a reference pick-up coil. Magnetic moments as small as $5 \times 10^4 \text{ A m}^2$ (5×10^{-5} emu) are measurable with a VSM. Its accuracy is better than 2%.

3.1.6 Fluxgate magnetometers

How can the nonlinear magnetization characteristics of ferromagnets be used to determine external field strength?

Fluxgate magnetometers, also known as saturable-core magnetometers, were first developed in the 1930s for measurement of the Earth's magnetic field. There are several different modes of operation of fluxgates; we consider here the simplest type. The simple fluxgate consists of one or two cores of high-permeability material, surrounded by a drive coil and one or two sense coils as shown in Fig.3.3

Reviews of fluxgate magnetometry have been given by Primdahl [6] and by Gordon and Brown [7]. The range of field strengths measurable by fluxgates is down to 10^{-4} A/m (10^{-6} Oe). They are mainly used for measuring inductions in the range 10^{-10} to 10^{-7} tesla, corresponding to magnetic fields in the range 10^{-4} to 10^{-1} A/m in free space.

The drive coil is excited with a periodic waveform which saturates the magnetization. The measured field is a d.c. or quasi-d.c. field by comparison. When the measured field is zero therefore the voltage induced in the pick-up coil is necessarily symmetrical, but if there is an external field component along the axis of the core, then the voltage in the secondary coil becomes asymmetric. The degree of

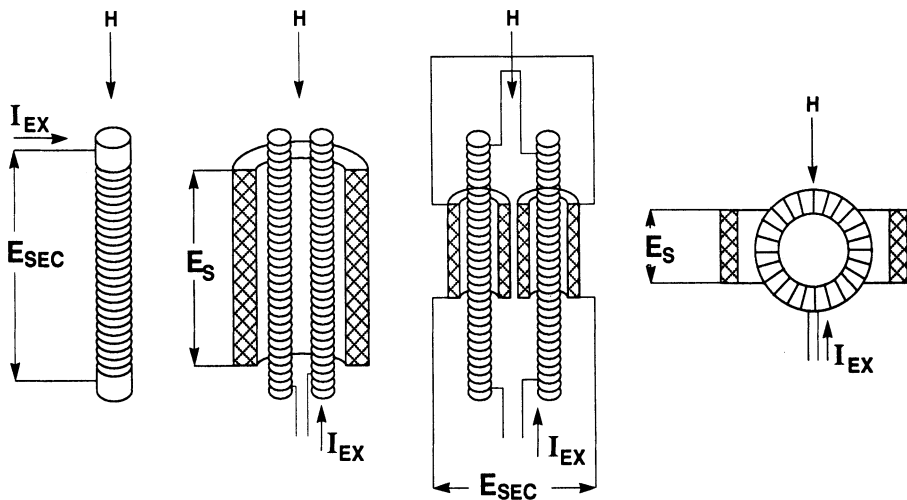


Fig. 3.3 Diagram of various forms of fluxgate magnetometer. These include the single-core configuration, the Vacquier gradiometer configuration with a single secondary coil, the Forster gradiometer configuration with separate secondary coils and the Aschenbrenner and Goubaud configuration with a toroidal core.

asymmetry of this voltage, as measured by the second harmonic component of the induced signal, can then be used to measure the strength of the external field.

The most usual configuration used for fluxgates is the two-core arrangement with the coils wound in opposition (the gradiometer configuration). In this case the voltage in the sense coils is by virtue of symmetry identically zero when the external field is zero. When the external field is non-zero this will lead to an apparent asymmetry in the magnetization curves of the two cores and hence a net voltage observed at twice the drive frequency.

Fluxgates can only measure the component of field strength parallel to the coils, since any field perpendicular to this direction does not affect symmetry.

3.2 METHODS DEPENDING ON CHANGES IN MATERIAL PROPERTIES

How can magnetic field strengths be determined from changes in material properties?

Whereas in the previous sections the measurement of magnetic field was dependent on the change in flux linking a circuit, in the following sections the measurement depends on changes in the properties of materials under the action of a magnetic field.

3.2.1 Hall effect magnetometers

How does the presence of a magnetic field alter the motion of charge carriers?

54 Magnetic measurements

The Hall effect magnetometers are perhaps the most versatile and widely used form of magnetometer. The range of fields measurable by these devices is typically 0.4 A/m up to 4×10^6 A/m (equivalently 5×10^{-3} Oe up to 5×10^4 Oe). Accuracy of measurements is typically 1%.

When a magnetic field is applied to a conducting material carrying an electric current, there is a transverse Lorentz force on the charge carriers given by

$$\mathbf{F} = \mu_0 e \mathbf{v} \times \mathbf{H},$$

as discussed in section 1.2.3. The expression here is for the force on a single charge e with velocity \mathbf{v} in a field of strength \mathbf{H} . Since the force on a charge e can be expressed as,

$$\mathbf{F} = e \mathbf{E}$$

where \mathbf{E} is the electric field we can consider that the force is due to an equivalent electric field \mathbf{E}_{Hall} , known as the Hall field.

$$\mathbf{E}_{\text{Hall}} = \mu_0 \mathbf{v} \times \mathbf{H}$$

and hence to a Hall e.m.f. V_{Hall} which is in the direction perpendicular to the plane containing i and \mathbf{H} . The Hall e.m.f. therefore depends linearly on the magnetic field \mathbf{H} if the current is kept constant and this provides a very convenient measure of magnetic field \mathbf{H} , as the following analysis shows.

If the electric current passes in the x direction and the magnetic field passes in the y direction of a slab of semiconductor of dimensions l_x, l_y, l_z , the Hall e.m.f. will be along the z -axis as shown in Fig. 3.4.

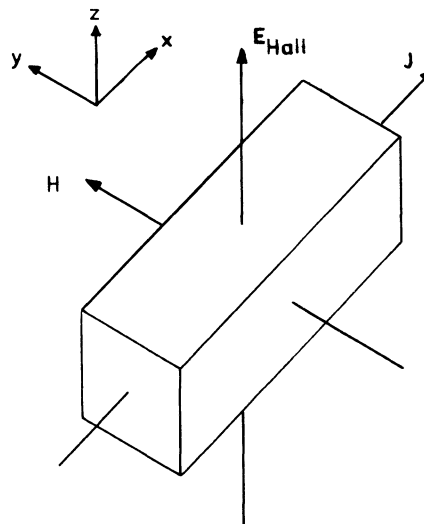


Fig. 3.4 Generation of a Hall e.m.f. in a slab of conducting material. The electric current density J passes along the x -axis, the magnetic field \mathbf{H} lies along the y -axis, and the Hall field \mathbf{E}_{Hall} is generated along the z -axis. The sign of the Hall e.m.f. depends on the sign of the charge carriers.

If n is the number of charge carriers per unit volume, then the current density will be

$$\mathbf{J} = ne\mathbf{v}$$

$$\mathbf{v} = \frac{\mathbf{J}}{ne},$$

and so the Hall field is

$$\mathbf{E}_{\text{Hall}} = \mu_0 \mathbf{J} \times \frac{\mathbf{H}}{ne}$$

and by replacing $1/ne$ by the term R_H , which is called the Hall constant

$$\mathbf{E}_{\text{Hall}} = \mu_0 R_H \mathbf{J} \times \mathbf{H}$$

and since the electric field \mathbf{E} in volts/metre can be expressed by the form $\mathbf{E} = V/l_x$ where V is the potential difference over a distance l_x ,

$$V_{\text{Hall}} = \mu_0 R_H \mathbf{J} \times \frac{\mathbf{H}}{l_x}.$$

Since the current density $\mathbf{J} = i/l_y l_z$

$$V_{\text{Hall}} = \mu_0 R_H i \times \frac{\mathbf{H}}{l_x l_y l_z}.$$

The value of the Hall coefficient R_H is typically 10^{-11} m^3 per coulomb.

The Hall effect magnetometers can be fabricated with very small active areas, down to $1.0 \times 10^{-2} \text{ cm}^2$ which can therefore be used to measure the magnetic field with high spatial resolution. Another important factor is that unlike coils, which measure the flux linkage and therefore need to be scaled appropriately for their cross-sectional area in order to determine the magnetic induction, the Hall magnetometers measure the field strength directly.

The only difficulties with Hall probes arise from deviations from linearity at higher fields and from the temperature dependence of the response. Most commercial Hall probes are made of InSb.

Table 3.1 Values of the Hall coefficient for various materials

Material	R_H (m^3/C)
Li	-1.7×10^{-12}
In	$+1.59 \times 10^{-12}$
Sb	-1.98×10^{-11}
Bi	-5.4×10^{-9}

56 Magnetic measurements

3.2.2 Magnetoresistors

How does the presence of a magnetic field alter the resistance of a material?

Magnetoresistance is the change in electrical resistance of a material when subjected to a magnetic field. Once the variation of resistance with field is known then resistance measurements can be made in order to determine the field strength. Generally the resistance increases when a field is applied but is nonlinear. The main advantage of this method is that very small probes can be fabricated to measure the field at a point. Magnetoresistive probes are particularly useful for field measurements at low temperatures.

In all materials the effect of magnetic field on resistance is greater when the field is perpendicular to the direction of current flow. In ferromagnetic materials the change in resistance can be quite large, typically $\Delta R/R = 2\%$ at saturation in nickel and 0.3% at saturation in iron.

The earliest application of this effect as a field-measuring device was the use of bismuth in which the magnetoresistance increases by 150% in a field of 9.5×10^5 A/m (1.2 T). More recently materials which are rather more sensitive have been found such as the eutectic compound of InSb–NiSb which undergoes a 300% change in magnetoresistance in a field of 2.3×10^5 A/m (0.3 T). Unfortunately the effects of temperature on the resistance of this material are also large and this limits its applications.

Despite these drawbacks the measurement of resistance is fairly simple and hence the method does have great merit in situations where the temperature can be well controlled (e.g. cryogenic applications) and where the range of flux density is limited to less than 16 T but greater than 2 T. The accuracy of field measurements made with this method is about 1%.

There are a number of thin-film magnetoresistive devices available commercially which are capable of a resolution of 10^{-5} A/m (10^{-7} Oe). These devices look very much like strain gauges being flat plates of typically 5 mm \times 5 mm with two terminals attached.

3.2.3 Magnetostrictive devices

Can the change in length of a ferromagnet in the presence of a field be used to measure that field?

When a specimen of magnetic material is subjected to a magnetic field changes in shape of the specimen occur [8]. This phenomenon is known as magnetostriction and it is most often demonstrated by measuring the fractional change in length $\Delta l/l$ of a specimen as it is magnetized. The effect is quite small in most materials but in ferromagnets it is typically of the order of $\Delta l/l = 10^{-6}$ which is measurable by resistive strain gauges or by optical techniques. Recent materials with much higher magnetostrictions have been discovered [9], with $\Delta l/l$ up to 2500×10^{-6} .

The magnetostriction and magnetoresistance are closely related, both being generated by the spin orbit coupling so that the electron distribution at each ionic site is rotated. This change in electron distribution alters the scattering undergone by the conduction electrons (magnetoresistance). The rotation of the moments also leads to a change in the ionic spacing (magnetostriction).

If the magnetostriction of a material as a function of field is known this can be used as a measurement of the magnetic field. High-resolution measurements of magnetostriction down to $dl/l \approx 10^{-10}$ can now be made with magnetostrictive amorphous ferromagnetic materials [10]. The drawback with this is that the magnetostriction is nonlinear, and furthermore exhibits hysteresis.

3.2.4 Magneto-optic methods

How can the changes in optical properties of media under the action of an external field be used to determine field strength or magnetization?

The two principal magneto-optic effects are the Faraday effect, which occurs when light is transmitted through a transparent medium in the presence of a magnetic field along the direction of propagation of the light, and the Kerr effect, which occurs when light is reflected from a ferromagnetic medium. Both involve rotation of the angle of polarization of linearly polarized light [11]. Another phenomenon, the Cotton–Mouton effect, is related to the Faraday effect, and occurs when the magnetic field is perpendicular to the direction of propagation of light transmitted in a medium. However the magnitude of the rotation observed in the Cotton–Mouton effect is much smaller than in the Faraday effect.

The Faraday effect is easily adapted as a technique for measurement of field strength since the rotation of polarization of light passing through a transparent paramagnetic material (such as $\text{MgCe}(\text{PO}_4)_2$) can give a measure of the local magnetic field. The rotation of the plane of polarization is given by

$$\theta = VHt,$$

where V is the Verdet constant ($V = 0.001$ to 0.1 minute/A, or equivalently 0.1 to 10 minute/Oe cm), H is the field strength and t is the thickness of the specimen or more precisely the path length of light in the material.

In ferromagnetic or ferrimagnetic materials the angle of rotation θ can also be related to the magnetization M by

$$\theta = KMt,$$

where K is Kundt's constant, M is the magnetization of the material and t is the path length. K is typically up to 350×10^6 degrees/tesla m (equal to 350 degrees/gauss cm.). Both the Faraday effect and the Cotton–Mouton effect can be used for domain observation. However these techniques are limited to thin sections of ferromagnetic materials in order that sufficient light is transmitted.

The Kerr effect is used to observe domain patterns in ferromagnetic materials

58 Magnetic measurements

and is discussed in more detail in Chapter 6. A beam of linearly polarized light is incident on the surface of the specimen. It is important that the beam is not normal to the surface of the ferromagnet or ferrimagnet since there must be a component of the magnetization in the surface of the specimen parallel to the direction of propagation of the light and it is well known that surface domains are oriented with their magnetizations in the plane of the surface. The magnetization within a domain rotates the plane of polarization of the beam that is reflected from the surface through an angle θ which is related to the magnetization M by

$$\theta = K_r M.$$

Typical rotations are 9 minutes of arc from saturated nickel and 20 minutes of arc from saturated iron and cobalt. This technique can only be used for the determination of field strength in situations where the magnetization can be directly related to the field.

3.2.5 Thin-film magnetometers

Can the presence of magnetic anisotropy be used to measure external field strength?

Magnetic fields can be measured using thin-film magnetometers [12]. Thin films which are in the range 200–5000 ångströms thick are usually fabricated for these purposes from a non-magnetostrictive alloy such as Ni-20%Fe. They have uniaxial anisotropy with the easy axis parallel to the direction of applied field during deposition.

Magnetization measurements are made along the hard axis while the field being measured is applied along the easy axis. Since the applied field effectively alters the anisotropy this leads to changes in the magnetization characteristics. The film is used as the inductor in the frequency-controlling circuit of an oscillator. The output frequency is then a function of the external field. The field ranges over which the thin-film devices are useful are typically from 10^{-7} tesla to 10^{-3} tesla [13].

3.2.6 Magnetic resonance methods

How can we utilize the magnetic properties of elementary particles to determine field strength?

Resonance magnetometers include all magnetic field measurement techniques based on electron spin resonance, nuclear magnetic resonance and proton precession. A review of these has been given by Seiden [14]. The sensitivities of these instruments can be of the order of 10^{-14} tesla (10^{-10} gauss). These methods have the advantage of measuring the total magnetic field in a region of space. That is they are not dependent on the orientation of the field for measurement, as are most other techniques which can only measure the component of magnetization along a given direction.

The discrete energy levels of electrons in materials are changed by the presence of

a magnetic field. This was first discovered by Zeeman [15, 16]. In electron spin resonance (ESR) electrons can be excited from one state to another by high-frequency radiation and hence will exhibit absorption or resonance at those characteristic frequencies.

The resonance frequency v_0 can be used as a measure of the magnetic field strength since it is related to the field by the expression

$$\begin{aligned}\omega_0 &= 2\pi v_0 = \gamma B \\ &= \gamma \mu_0 H,\end{aligned}$$

where γ is a constant known as the gyromagnetic ratio. The value of γ for a free electron (electron paramagnetic spin resonance) is $1.76 \times 10^{11} \text{ Hz/T}$ and so by this method very weak fields may be measured. (The value of γ is related to the fundamental properties of the electron as we shall discuss in Chapter 10, in particular $\gamma = -\mu_B g(2\pi/h)$ where μ_B is the Bohr magneton, g is the Lande splitting factor of the electron and h is Planck's constant.)

The nuclear magnetic resonance (NMR) technique depends on resonance of the magnetic moment of the nucleus in an r.f. field in a similar way to ESR. The energy levels of the nucleus are quantized and are altered by the presence of a magnetic field as in ESR. Therefore resonant absorption is observed when the r.f. energy equals the difference in energy level between these quantized states. The resonant frequency is therefore a measure of the field strength.

Once again, as in ESR, the resonant frequency is proportional to the field, however the gyromagnetic ratio of the particular nucleus γ_n must be used in the equation

$$\omega_0 = \gamma_n \mu_0 H.$$

The material used as the medium in this method need not be very special, in fact water is often used. In this case the nuclei are protons for which $\gamma_n = 2.68 \times 10^8 \text{ Hz/T}$. Values of γ for various nuclei and for free electrons are given in Table 3.2.

The experimental set-up for these techniques for field measurement involves two mutually orthogonal pairs of coils: the r.f. coils which emit the resonant radio frequency and the receiver coils which indicate when resonance occurs. The

Table 3.2 Values of the gyromagnetic ratio γ for various nuclei and free electrons

Particle	γ (rads. sec. $^{-1}$ T $^{-1}$)	$\gamma/2\pi$ (Hz. T $^{-1}$)
^1H (proton)	2.6753×10^8	42.579
^2D (deuteron)	4.1064×10^7	6.536
^7Li	1.0396×10^8	16.546
Free electron	1.762×10^{11}	28.043

60 Magnetic measurements

resonance methods typically have a precision of 1 part in 10^6 . This means that highly accurate field measurements can be made under the right conditions, but because of the high precision there is a need for a highly homogeneous field throughout the specimen being used.

In practice, when these methods are used for field measurement, as distinct from materials property measurements, there are two ways of deducing the field. In one method the field is calculated from the resonance frequency with γ already known; in the other method the field is determined from an amplitude measurement with ω fixed and γ known. Under small-amplitude field modulations $\Delta\mathbf{H}$ of the quasi-d.c. ('static') field close to the resonance \mathbf{H}_0 the voltage response of the pick-up coil ΔV is

$$\Delta V = K\Delta\mathbf{H},$$

where K is a constant of the material, which must be known. In this way $\Delta\mathbf{H}$ can be measured to a high degree of accuracy [17].

A closely related technique based on proton precession is widely used by geophysicists for precise measurements of the local strength of the Earth's field. Proton precession magnetometers are used for flux densities in the range 10^{-9} to 10^{-4} tesla. A container of water is placed in a coil perpendicular to the field to be measured. This coil is then pulsed to align the magnetic moments of the protons. When it is switched off the nuclear moments of the protons precess about the field being measured. This precession generates an e.m.f. in the coil at the precession frequency. Measurement of this frequency enables the field strength to be calculated.

3.3 OTHER METHODS

In this section we look at three additional techniques: two older methods which depend on the force on a magnetic dipole in a field and one much more recent method which depends on the quantization of flux in a superconducting circuit containing a weak link.

3.3.1 Torque magnetometers

How can the magnetic moment or magnetization be found from the torque exerted by a known external field?

The torque magnetometer is used mainly for anisotropy measurements on short specimens. It is based on the fact that a magnetic dipole \mathbf{m} in an external magnetic field \mathbf{H} in free space experiences a torque τ

$$\tau = \mu_0 \mathbf{m} \times \mathbf{H}$$

as described in section 1.2.3. The torque must be measured in a uniform magnetic field. The specimen is aligned so that its magnetization lies in the plane of rotation

of the field (if the field is to be rotated) or the sample is rotated in the plane defined by the magnetic field \mathbf{H} and the magnetization \mathbf{M} .

A restoring torque is used to maintain the specimen in position. In some instruments, notably the earlier ones, this restoring torque was provided by twisting a torsion fibre. The angle ϕ through which the torsion fibre is twisted is dependent on the length of the fibre and its shear modulus as well as the torque. ϕ is therefore proportional to the turning force on the specimen.

$$\begin{aligned}\phi &= \text{constant} \times \tau \\ &= \text{constant} \times \mu_0 \mathbf{m} \times \mathbf{H}.\end{aligned}$$

If α is the angle between \mathbf{m} and \mathbf{H}

$$\phi = \text{constant} \times \mu_0 m H \sin \alpha.$$

The instrument is calibrated using a specimen of known anisotropy, and consequently since μ_0 , \mathbf{H} and the constant are known, the angle α can be measured and the magnetic moment \mathbf{m} can be calculated.

A schematic diagram of a torque magnetometer is shown in Fig. 3.5. In this

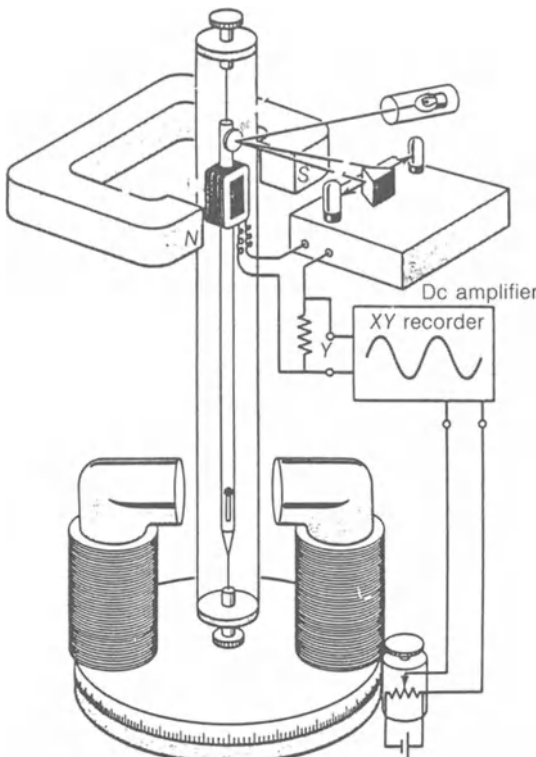


Fig. 3.5 Schematic diagram of a torque magnetometer.

62 Magnetic measurements

instrument the restoring torque is provided by the torque coil in the presence of a field from the permanent magnet, and the torque is proportional to the current in the torque coil.

3.3.2 Susceptibility balances

How can the magnetization be found from the force exerted on a specimen by a known field?

Two types of force-balance methods have been devised for determining the magnetization M or equivalently the susceptibility χ . These are the analytical balance and the torsion balance. Both depend on measuring the linear force on a sample suspended in a magnetic field gradient.

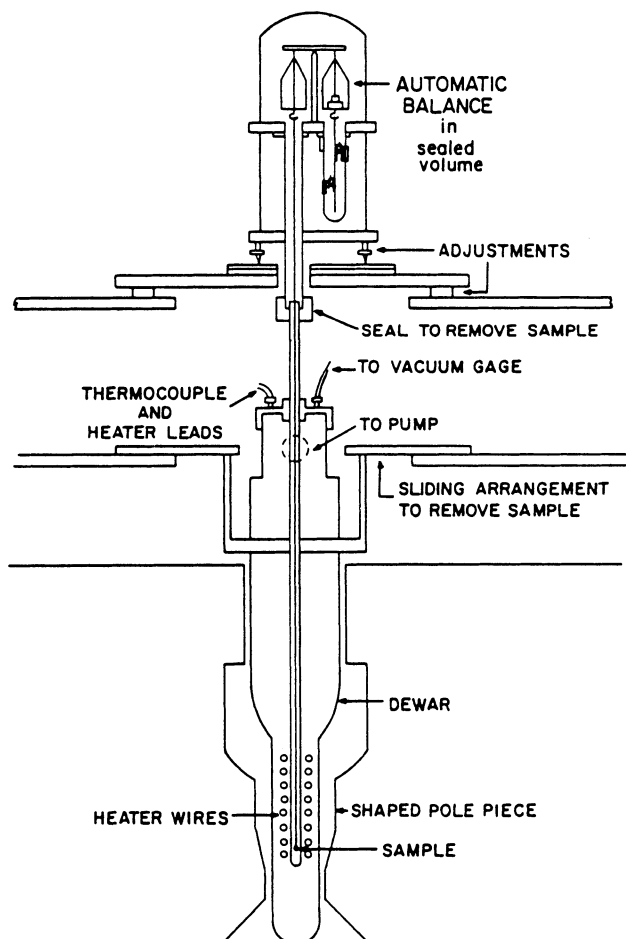


Fig. 3.6 Schematic diagram of an analytical balance.

The specimen is suspended using a long string in a magnetic field with a constant field gradient. The force on the specimen of volume V and magnetization \mathbf{M} is then

$$\mathbf{F}_x = \mu_0 \mathbf{m} \frac{d\mathbf{H}}{dx}$$

$$= -\mu_0 V \mathbf{M} \frac{d\mathbf{H}}{dx}$$

which is obtained by differentiating the equation in section 1.2.3. Since we can write the susceptibility as

$$\chi = \mathbf{M}/\mathbf{H}$$

this leads to

$$\mathbf{F}_x = -\mu_0 \chi V \mathbf{H} \frac{d\mathbf{H}}{dx}.$$

The force on the specimen is therefore proportional to its susceptibility.

This method can usually only be used on a short specimen, so that the whole specimen can be located between the pole pieces of an electromagnet. In addition since the field must have a constant field gradient, the spatial extent of the specimen perpendicular to the field must also be small.

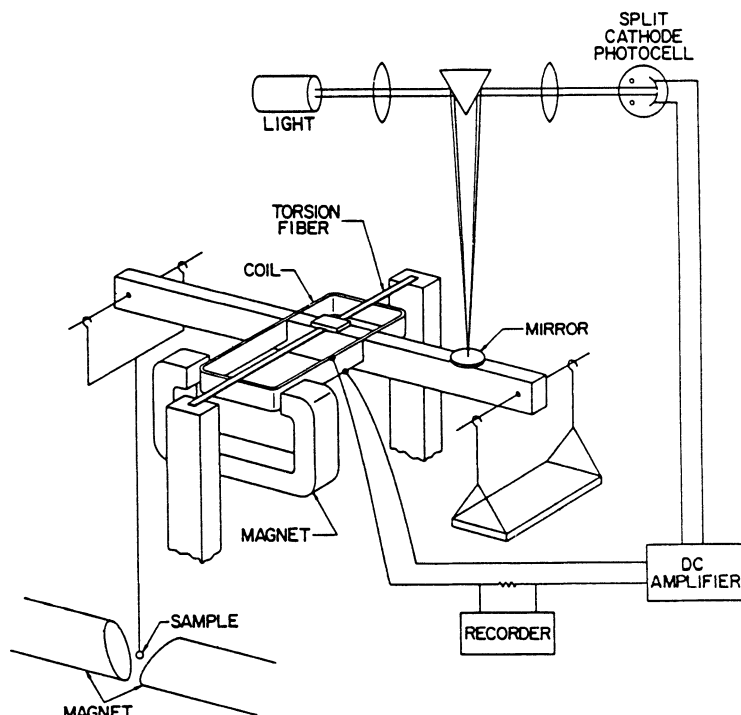


Fig. 3.7 Schematic diagram of a torsion balance.

64 Magnetic measurements

In the analytical balance method in order to measure the force the specimen is suspended by a string from one arm of an analytical balance (hence the name of the method). In zero field the weight of the specimen is counterbalanced and when the field is switched on the force on the specimen can be measured directly. A diagram of the experimental arrangement for this method is shown in Fig. 3.6. The origin of the method is attributed to Faraday.

The torsion balance is shown in Fig. 3.7 and is a variation on the same linear force method. It can be designed to have a very small restoring torque and therefore a high sensitivity, however it cannot support as large a mass as the analytical balance, and therefore is limited to specimens of a few grams.

3.3.3 SQUIDS

What is a SQUID and how can it be used to measure a magnetic field?

At present, SQUIDS (superconducting quantum interference devices) provide the ultimate in resolution for field measurements. The SQUID consists of a superconducting ring with a small insulating layer known as the ‘weak link’, as shown in Fig. 3.8. The weak link is also known as a Josephson junction. The resolution of these devices is down to 10^{-14} tesla (10^{-10} gauss) [18]. The flux passing through the ring is quantized once the ring has gone superconducting but the weak link enables the flux trapped in the ring to change by discrete amounts. Changes in the pick-up voltage occur as the flux is incremented in amounts of $\Delta\Phi = 2.067 \times 10^{-15}$ Wb. The device can thereby be used to measure very small changes in flux. In fact it can be used to count the changes in flux quanta in the ring.

With no weak link flux cannot enter the ring, as we know from superconductivity, and so the field passing through the ring remains at the value it was at when the ring became superconducting. If the link is very thick, so that no

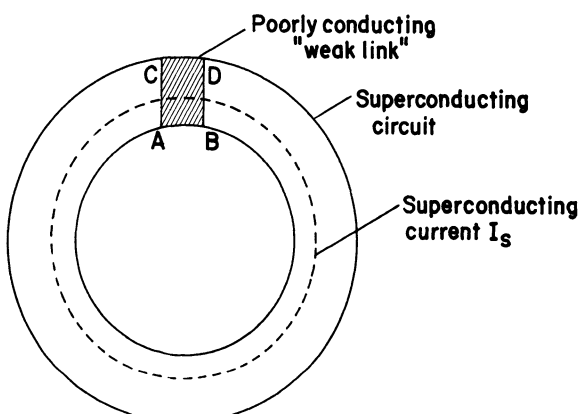


Fig. 3.8 A Josephson junction device, which consists of a superconductor with a poorly conducting ‘weak link’, ABCD.

supercurrent can flow, then the flux in the ring will be exactly that which is expected from the applied field. The presence of the weakly superconducting link typically restricts the value of the supercurrent flowing in the ring to less than 10^{-5} A. Therefore with a weak link magnetic flux can enter the ring. The supercurrent in the weak link tries to oppose the entry of flux but because it is limited by the weak link it cannot achieve this entirely as the flux is increased. It therefore becomes a periodic function of the flux threading the superconducting ring.

The relation between the flux density in the ring and the flux density due to the applied field is

$$\Phi = \Phi_a + LI_s$$

where Φ is the flux density in the ring, Φ_a is the flux due to the applied field, L is the inductance of the ring and I_s is the supercurrent which produces a flux of $\Phi_s = LI_s$. In the Josephson junction the supercurrent I_s in the ring is related to the critical current I_c determined by the properties of the weak link.

$$I_s = I_c \sin \theta,$$

where θ is the phase difference of the electron wavefunctions across the weak link. Therefore

$$\Phi = \Phi_a + LI_c \sin \theta.$$

In a completely superconducting ring the flux is an integral number of flux quanta.

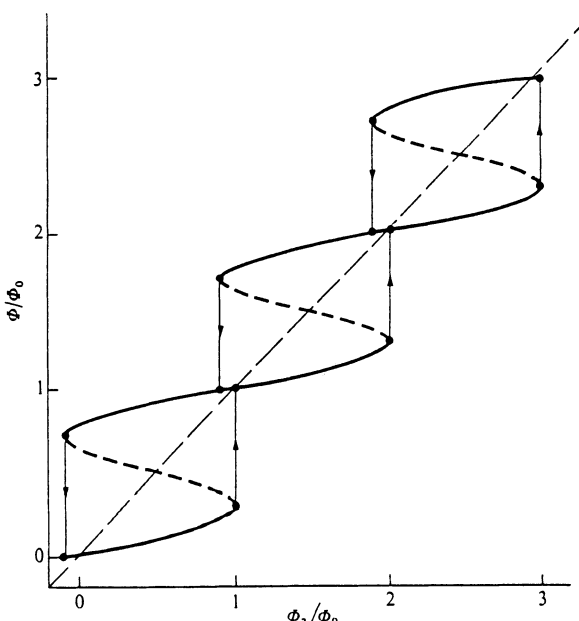


Fig. 3.9 The relation between ϕ , the flux in the ring, and ϕ_a , the flux due to the applied field, in a SQUID magnetometer. (See also section 15.2.4).

66 Magnetic measurements

Therefore if Φ_0 is the flux quantum of 2.067×10^{-15} Wb

$$\Phi = N\Phi_0$$

with the weak link the phase angle θ across the link depends on the flux in the following way

$$\theta = 2\pi N - 2\pi(\Phi/\Phi_0).$$

Since N is an integer

$$\begin{aligned}\sin \theta &= \sin(-2\pi\Phi/\Phi_0) \\ &= -\sin(2\pi\Phi/\Phi_0)\end{aligned}$$

and therefore

$$\Phi = \Phi_a - LI_c \sin(2\pi\Phi/\Phi_0)$$

and the relation between Φ and Φ_a is given in Fig. 3.9. From this graph we see that the SQUID counts flux quanta of the applied field in units of 2.067×10^{-15} Wb. Each time $\sin(2\pi\Phi/\Phi_0) = \theta$ then Φ/Φ_0 and Φ_a/Φ become equal, however at values in between when the flux is not an integral multiple of 2.067×10^{-15} Wb, they are not identical. If a loop of wire or a coil is placed around the superconducting ring then a voltage pulse is induced in the coil at each quantum jump, and this pulse can be used to measure the applied field.

The SQUID is clearly a very highly sensitive device and is therefore really best suited to measuring very small changes in magnetic field.

REFERENCES

1. DeMott, E. G. (1970) *IEEE Trans. Mag.*, **6**, 269.
2. Gordon, D. I., Brown, R. E. and Haben, J. F. (1972) *IEEE Trans. Mag.*, **8**, 48.
3. Smith, D. O. (1956) *Rev. Sci. Inst.*, **27**, 261.
4. Fert, C. and Gautier, P. (1951) *C.R. Acad. Sci., Paris*, **233**, 148.
5. Foner, S. (1959) *Rev. Sci. Inst.*, **30**, 548.
6. Primdahl, H. (1970) *IEEE Trans. Mag.*, **6**, 376.
7. Gordon, D. I. and Brown, R. E. (1972) *IEEE Trans. Mag.*, **8**, 76.
8. Cullity, B. D. (1971) *J. Metals*, **23**, 35.
9. Clark, A. E. and Abbundi, R. (1977) *IEEE Trans. Mag.*, **13**, 1519.
10. Wun Fogle, M., Savage, H. T. and Clark, A. E. (1987) *Sensors and actuators* **12**, 323.
11. Craik, D. J. and Tebble, R. S. (1965) *Ferromagnetism and Ferromagnetic Domains*, North Holland, Amsterdam.
12. Irons, H. R. and Schwei, L. J. (1972) *IEEE Trans. Mag.*, **8**, 61.
13. Bader, C. J. and Fussel, R. L. (1965) Proceedings 1965 Intermag Conference, New York.
14. Seiden, P. E. (1969) in *Magnetism and Metallurgy*, Vol. 1 (eds. A. E. Berkowitz and E. Kneller); Academic Press, New York.
15. Zeeman, P. (1897) *Phil. Mag.*, **43**, 226.
16. Hertzberg, G. (1944) *Atomic Spectra and Atomic Structure*, 2nd ed, Dover, New York, p. 96.
17. Hartman, F. (1972) *IEEE Trans. Mag.*, **8**, 66.
18. Webb, W. (1972) *IEEE Trans. Mag.*, **8**, 51.

FURTHER READING

- Berkowitz, A. E. and Kneller, E. (1969) *Magnetism and Metallurgy*, Vol. 1, Academic Press, Ch. 4.
- Crangle, J. (1977) *The Magnetic Properties of Solids*, Edward Arnold, London.
- Cullity, B. D. (1972) *Introduction to Magnetic Materials*, Addison-Wesley, Reading, Mass.
- Janicke, J. (1975) Magnetic measurements in *IEEE Workshop on Applied Magnetics*, Milwaukee, Wisconsin, IEEE, New York.

EXAMPLES AND EXERCISES

Example 3.1 Torque magnetometer. Explain how to measure the strength of a magnetic field \mathbf{H} using a magnetic dipole of known strength. Define the magnetic moment of a coil and a bar magnet and show that $\mathbf{m} = \phi l / \mu_0$. A magnetized rod of magnetic moment 0.318 A m^2 is suspended horizontally in a magnetic field of 14 A/m . What is the torque required to keep it at an angle of (a) 90° (b) 30° to the field direction?

Example 3.2 Magnetic resonance. Describe the phenomenon of electron spin resonance and explain briefly why it occurs. Explain what is meant by:

- Bohr magneton;
- Gyromagnetic ratio;
- Lande splitting factor.

A dilute paramagnetic material has a ground state $S = \frac{1}{2}$. Calculate the gyromagnetic ratio γ and hence determine the expected resonance frequency in a field of $0.796 \times 10^5 \text{ A/m}$ (equivalent to a free-space magnetic induction of 0.1 tesla).

Example 3.3 Induction coil method. The initial magnetization curve of a specimen of iron of length 20 cm and diameter 0.5 cm is measured using a ballistic galvanometer. The galvanometer has a sensitivity of 0.17×10^{-4} weber turns per mm, and the solenoid used to generate the field gives an \mathbf{H} field of 400 A/m for each ampere flowing in the coil.

Table 3.3

i (Amp)	d (mm)
1.5	24.0
3.1	49.2
4.9	77.6
8.5	103.7
11.0	107.5
12.7	109.1

68 Magnetic measurements

A 40-turn induction coil is wound on the specimen to measure the flux passing through it. The current reversed in the solenoid i and the deflection d were as in Table 3.3.

- (a) Find the demagnetization factor N_d .
- (b) Plot the initial magnetizing curves B against H_{applied} and B against H .
- (c) Find the true and apparent permeability at $B = 1.0$ tesla.

4

Magnetic Materials

The macroscopic behaviour of magnetic materials can be classified using a few magnetic parameters. We look at the most significant of these, give some definitions and show how the most important class of magnetic materials, the ferromagnets, can be classified on this basis. We then survey the main uses of ferromagnets and indicate how the macroscopic properties determine the suitability of a material for a given application.

4.1 IMPORTANT MAGNETIC PROPERTIES OF FERROMAGNETS

Which magnetic materials are the most significant for applications?

By far the most important class of magnetic materials is the ferromagnets. We can make this statement unreservedly both from the practical and the theoretical viewpoints. The applications which these materials find are very diverse and have been discussed in the two most significant ferromagnetic materials reference texts by Heck [1] and Wohlfarth [2]. In engineering applications the ferromagnets are used because of their high permeabilities which enable high magnetic inductions to be obtained with only modest magnetic fields, their ability to retain magnetization and thereby act as a source of field and of course the torque on a magnetic dipole in a field can be used in electric motors. It is perhaps somewhat surprising that the few ferromagnetic elements in the periodic table, iron, cobalt, nickel and several of the lanthanides are so technologically vital.

At this stage we are still considering the materials on a macroscopic scale and consequently all that we have really discussed so far is the definition that ferromagnets have in general very large values of relative permeability μ_r and susceptibility χ . These are important quantities, and later we shall go on to consider what the special factors are that cause such high permeabilities. However we will now pause to consider some of the more characteristic features of ferromagnets which are noticeable on the everyday, macroscopic scale.

4.1.1 Permeability

What is the most important single property of ferromagnets for applications?

70 Magnetic materials

By far the most important single property of ferromagnets is their high relative permeabilities. The permeability of a ferromagnet is not constant as a function of magnetic field in the way that the permeability of a paramagnet is. Instead, in order to characterize the properties of a given ferromagnetic material it is necessary to measure the magnetic induction \mathbf{B} as a function of \mathbf{H} over a continuous range of \mathbf{H} to obtain a hysteresis curve.

We can still make some comments about permeabilities, however. For ferromagnets the initial relative permeabilities usually lie in the range 10 to 10^5 . The highest values occur for special alloys such as permalloy and supermalloy, which are nickel-iron alloys. These materials are useful as flux concentrators. Permanent magnet materials do not have such high permeabilities, but their applications depend on their retentivity which is the next most important property.

4.1.2 Retentivity

What is the most characteristic property of ferromagnets?

It is well known that ferromagnets can be magnetized. That is to say that once exposed to a magnetic field they retain their magnetization even when the field is removed. Probably this is the most widely recognized property of ferromagnets since we have all spent time magnetizing pieces of iron using a permanent magnet. The retention of magnetization distinguishes ferromagnets from paramagnets which although they acquire a magnetic moment in an applied field \mathbf{H} , cannot maintain the magnetization after the field is removed.

4.1.3 Hysteresis

How can we best represent the magnetic properties of ferromagnets?

The most common way to represent the bulk magnetic properties of a ferromagnetic material is by a plot of magnetic induction \mathbf{B} for various field strengths \mathbf{H} . Alternatively plots of magnetization \mathbf{M} against \mathbf{H} are used, but these contain the same information since $\mathbf{B} = \mu_0(\mathbf{H} + \mathbf{M})$. Hysteresis in iron was first observed by Warburg [3]. The term hysteresis, meaning to lag behind, was introduced by Ewing [4] who was the first to systematically investigate it. A typical hysteresis loop is shown in Fig. 4.1.

The suitability of ferromagnetic materials for applications is determined principally from characteristics shown by their hysteresis loops. Therefore materials for transformer applications need to have high permeability and low hysteresis losses because of the need for efficient conversion of electrical energy. Materials for electromagnets need to have low remanence and coercivity in order to ensure that the magnetization can easily be reduced to zero as needed. Permanent magnet materials need high remanence and coercivity in order to retain the magnetization as much as possible.

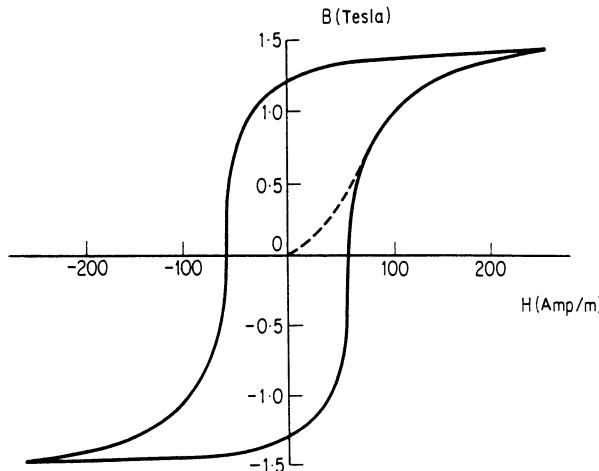


Fig. 4.1 A typical hysteresis loop of a ferromagnetic material.

4.1.4 Saturation magnetization

Is there an upper limit to the magnetization of a ferromagnet?

From the hysteresis plot it can be seen that the ferromagnet in its initial state is not magnetized. Application of a field H causes the magnetic induction to increase in the field direction. If H is increased indefinitely the magnetization eventually reaches saturation at a value which we shall designate M_0 . This represents a condition where all the magnetic dipoles within the material are aligned in the direction of the magnetic field H . The saturation magnetization is dependent only on the magnitude of the atomic magnetic moments m and the number of atoms per unit volume n .

$$M_0 = nm.$$

Table 4.1 Saturation magnetization of various ferromagnets

Material	(10^6 A/m)
Iron	1.71
Cobalt	1.42
Nickel	0.48
78 Permalloy (78% Ni, 22% Fe)	0.86
Supermalloy (80% Ni, 15% Fe, 5% Mo)	0.63
Metglas 2605 ($\text{Fe}_{80}\text{B}_{20}$)	1.27
Metglas 2615 ($\text{Fe}_{80}\text{P}_{16}\text{C}_3\text{B}_1$)	1.36
Permendur (50% Co, 50% Fe)	1.91

72 Magnetic materials

M_0 is therefore dependent only on the materials present in a specimen, it is not structure sensitive. Some typical values of saturation magnetization for different materials are shown in Table 4.1.

4.1.5 Remanence

What happens to the magnetic induction of a ferromagnet when the magnetic field is switched off?

When the field is reduced to zero after magnetizing a magnetic material the remaining magnetic induction is called the remanent induction B_R and the remaining magnetization is called the remanent magnetization M_R .

$$B_R = \mu_0 M_R$$

A convention seems to be emerging in which a distinction is drawn between the remanence and the remanent induction or magnetization. The remanence is used to describe the value of either the remaining induction or magnetization when the field has been removed after the magnetic material has been magnetized to saturation. The remanent induction or magnetization is used to describe the remaining induction or magnetization when the field has been removed after magnetizing to an arbitrary level. The remanence therefore becomes the upper limit for all remanent inductions or magnetizations.

4.1.6 Coercivity

How is the magnetic induction reduced to zero?

The magnetic induction can be reduced to zero by applying a reverse magnetic field of strength H_c . This field strength is known as the coercivity. It is strongly dependent on the condition of the sample, being affected by such factors as heat treatment or deformation.

As with the remanence a distinction is drawn by some authors between the coercive field (or coercive force), which is the magnetic field needed to reduce the magnetization to zero from an arbitrary level, and the coercivity which is the magnetic field needed to reduce the magnetization to zero from saturation [5]. In this nomenclature the coercivity becomes an upper limit for all values of coercive force.

The intrinsic coercivity, denoted H_{ci} , is defined as the field strength at which the magnetization M is reduced to zero. In soft magnetic materials H_c and H_{ci} are so close in value that usually no distinction is made. However in hard magnetic materials there is a clear difference between them, with H_{ci} always being larger than H_c .

4.1.7 Differential permeability

How useful is permeability when considering ferromagnets?

We should note in passing that the permeability μ is not a particularly useful parameter for characterization of ferromagnets, since by virtue of the hysteresis loop almost any value of μ can be obtained including $\mu = \infty$ at the remanence $\mathbf{B} = \mathbf{B}_R$, $\mathbf{H} = 0$ and $\mu = 0$ at the coercivity $\mathbf{B} = 0$, $\mathbf{H} = \mathbf{H}_c$.

The differential permeability $\mu' = dB/dH$ is a more useful quantity although we should remember that this also varies with field. The maximum differential permeability μ'_{\max} , which usually occurs at the coercive point $\mathbf{H} = \mathbf{H}_c$, $\mathbf{B} = 0$, and the initial differential permeability μ'_{in} which is the slope of the initial magnetization curve at the origin, are much more useful since it is possible to relate them to other material properties such as the number and strength of pinning sites [6] and applied stress [7].

4.1.8 Curie temperature

What happens if a ferromagnet is heated?

All ferromagnets when heated to sufficiently high temperatures become paramagnetic. The transition temperature from ferromagnetic to paramagnetic behaviour is called the Curie temperature. At this temperature the permeability of the material drops suddenly and both coercivity and remanence become zero. This property of ferromagnets was known long before the work of Curie. In fact the existence of a transition temperature was first reported by Gilbert [8] who was the author of the first treatise on magnetism.

Table 4.2 Curie temperatures of various materials

Material	Curie temperature
Iron	770 °C
Nickel	358 °C
Cobalt	1130 °C
Gadolinium	20 °C
Terfenol	380–430 °C
$\text{Nd}_2\text{Fe}_{14}\text{B}$	312 °C
Alnico	850 °C
SmCo_5	720 °C
Hard ferrites	400–700 °C
Barium ferrite	450 °C

74 Magnetic materials

The reasons for the sudden transition from ferromagnetism to paramagnetism will be discussed in detail in a later chapter. At this stage however we are interested in this merely as an empirical observation based on the macroscopic magnetic properties that the permeability suddenly decreases at a characteristic temperature.

4.2 DIFFERENT TYPES OF FERROMAGNETIC MATERIALS FOR APPLICATIONS

Where do ferromagnetic materials find their main uses?

We now consider the different applications of ferromagnets such as in permanent magnets, electrical motors, magnetic recording, power generation and inductors. The objective of this section is to give a concise summary of the types of magnetic materials and their uses before treating the subject in detail in Chapters 12, 13 and 14 and before discussing the underlying mechanisms behind the observed macroscopic magnetic properties of these materials in the following chapters. A review of the development and role of magnetic materials in science and technology has been given by Enz [9].

4.2.1 Classification of hard and soft magnetic materials

Is there a simple method of classification of the various ferromagnetic materials?

We can make a simple classification of ferromagnetic materials on the basis of their coercivity. Coercivity is a structure-sensitive magnetic property, which is to say that it can be altered by subjecting the specimen to different thermal and mechanical treatments, in a way that for example saturation magnetization cannot.

It has been noticed in the past that iron and steel specimens that were mechanically hard also had high coercivity, while those that were soft had low coercivity. Therefore the terms 'hard' and 'soft' were used to distinguish ferromagnets on the basis of their coercivity. Broadly 'hard' magnetic materials were those with coercivities above 10 kA/m (125 Oe) while 'soft' magnetic materials were those with coercivities of below 1 kA/m (12.5 Oe).

Some values of relative permeability and coercive force for various materials are given in Fig. 4.2.

4.2.2 Electromagnets

Where do soft magnetic materials find uses?

Soft magnetic materials find applications in electromagnets, motors, transformers and relays. The properties of various soft magnetic materials in use at present have been discussed by Chin and Wernick [10]. The criteria for consideration of

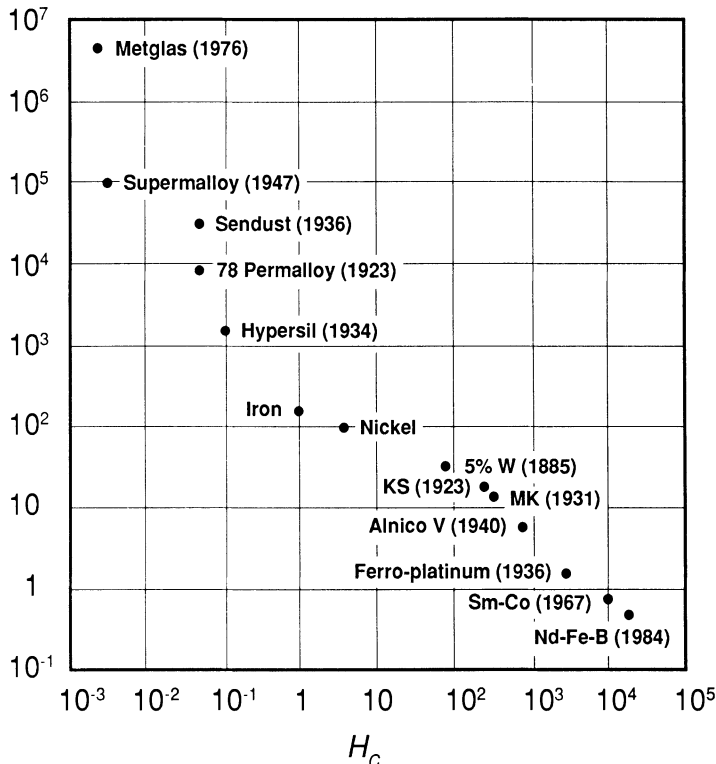


Fig. 4.2 Relative permeabilities and coercive forces (in Oe) of various ferromagnetic materials.

materials for electromagnets are that the core material should have high permeability, to enable high magnetic induction to be achieved, while having a low coercivity so that the induction can easily be reversed.

In electromagnets soft iron is used almost exclusively. Its coercivity is typically 80 A/m (1 Oe), as can be seen from Fig. 4.2, and this when coupled with its high saturation magnetization of $1.7 \times 10^6 \text{ A/m}$ make it the ideal material.

Electromagnets are used in the laboratory for generating high magnetic fields. A typical laboratory electromagnet is capable of generating fields of up to 2.0 tesla without any special configuration and, with small air gaps, fields of up to 2.5 tesla can be produced. Sometimes the pole tips of the electromagnet are made from a cobalt–iron alloy which has a higher saturation magnetization in order to achieve slightly higher fields in the air gap ($M_s = 1.95 \times 10^6 \text{ A/m}$ for an alloy of 35% Co, 65% Fe, compared with $M_s = 1.7 \times 10^6 \text{ A/m}$ for iron.) The material most often used for these pole tips is an alloy containing 49% Fe, 49% Co, 2% V. For magnetic inductions above 3 tesla electromagnets are not very useful because the iron cannot contribute much additional field. Therefore for higher field strengths either water-cooled iron-free magnets, known as Bitter magnets, or superconducting magnets are used.

76 Magnetic materials

4.2.3 Transformers

What are the characteristics of ferromagnetic materials needed in power generation?

At first sight it would appear that the requirements for transformer materials were identical to those for electromagnets. However this is not quite true. Transformers operate under a.c. conditions and therefore although high permeability of the core material is desirable it is also necessary to reduce the eddy current losses by employing as low a conductivity material as possible.

The material that is used exclusively for transformer cores is grain-oriented silicon–iron. This contains about 3–4% by weight silicon to reduce conductivity. The material is usually hot-rolled then cold-worked twice followed by an anneal to improve the grain orientation, increasing permeability along the rolling direction.

One of the most important parameters for transformer steels is the total core loss at line frequency of 50 or 60 Hz. Engineers usually measure this in watts per kilogram. Losses decrease with increasing silicon content but the material also becomes more brittle.

Table 4.3 below shows the electrical core losses in watts per kilogram at a frequency of 60 Hz for sheets of the various materials of thickness 0.3–0.5 mm. These thicknesses are equal to or less than the skin depth δ in the materials, which at 60 Hz is typically $\delta = 0.3\text{--}0.7$ mm.

In recent years there has been an attempt to develop amorphous metals [11] for use in electromagnetic devices. These alloys such as Metglas, have found applications in some smaller devices, but have not been successful in replacing silicon–iron in transformers except in some cases where distribution transformers have been required in locations where fuel costs are high. Several thousand of these Metglas transformers have been built and sold, however this remains a very small fraction of the market for transformers. There does not seem to be any real likelihood of large-scale adoption of Metglas as a transformer core material either in view of recent Japanese efforts which have continued to improve the properties of silicon–iron [12].

Table 4.3 Core losses of selected soft magnetic materials

Material	Core loss at 1.5 T and 60 Hz (W/kg)
Low-carbon steel	2.8
Non-oriented silicon–iron	0.9
Grain-oriented silicon–iron	0.3
80-Permalloy (80% Ni, 20% Fe)	$\approx 2^+$
Metglas	0.2–0.3*

* At 1.4 tesla since loss increases rapidly above this.

+ At saturation magnetization of 0.86 MA/m (1.1 tesla).

4.2.4 Electromagnetic relays

What magnetic properties are useful in magnetic switches and control devices?

A relay is a form of electromagnet which can be used as a switch for opening or closing an electrical circuit. The control circuit which opens and closes the switch and the operating circuit are electrically isolated from each other. Consequently a very weak current in the control circuit can be used to control a much larger current in the operating circuit.

The control circuit of the relay consists of a coil with a magnetizable core and a movable component called the armature, which is used to make or break the circuit. The yoke and core materials of relays have much the same requirements as electromagnets, that is low coercivity, low remanence and high magnetic induction. This leads in addition to low core loss and high permeability. Relay materials are almost always iron or iron-based alloys such as Fe–Si or Fe–Ni. Unalloyed iron is the most frequently used material for relays. The addition of silicon to iron reduces the coercivity from typically 100 amps per metre to a few amps per metre. The addition of nickel to iron can reduce the coercivity to as low as 1 amp per metre.

4.2.5 Magnetic recording materials

What are the desirable characteristics of recording media?

Magnetic recording materials have some characteristics in common with permanent magnets in that to be useful they need to have a relatively high remanence and a sufficiently high coercivity to prevent unanticipated demagnetization resulting in the loss of information stored on the magnetic tape or disk. Magnetic recording can either be analog, as in audio recording of signals on magnetic tape or digital recording, as used in the storage of information of data on magnetic disks and tapes for computer applications. A review of magnetic recording media has been given by Bate [13].

The most widely used magnetic recording material is $\gamma\text{-Fe}_2\text{O}_3$ (gamma ferric oxide) although both chromium dioxide and cobalt-doped $\gamma\text{-Fe}_2\text{O}_3$ are also used. Gamma ferric oxide is used in both equiaxed and acicular form. Equiaxed gamma ferric oxide particles used for magnetic recording have diameters of 0.05–0.3 μm . Magnetic recording tapes contain small needle-shaped particles of one of these oxides. The particles are embedded in a flexible binding material and at present the needles lie in the plane of the tape.

The needle-shaped particles are aligned by a magnetic field during the fabrication process. The final tapes of $\gamma\text{-Fe}_2\text{O}_3$ have coercivities typically of 20–24 kA/m, and the acicular particles have lengths ranging from 0.1–0.7 μm [13], with length-to-diameter ratios from 3:1 to 10:1. Tapes made from CrO_2 have coercivities of 36–44 kA/m. The chromium dioxide particles have dimensions ranging from $0.5 \times 0.03 \mu\text{m}$ to $0.2 \times 0.02 \mu\text{m}$ which are significantly smaller than

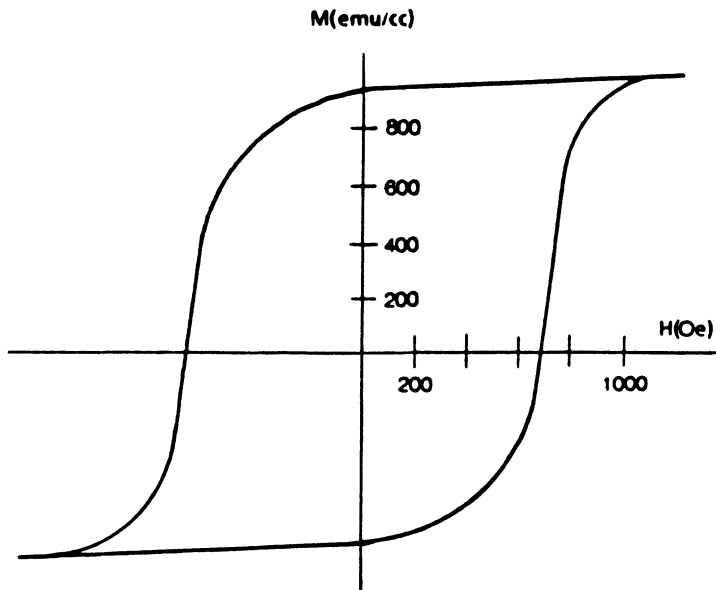


Fig. 4.3 Hysteresis loop for a typical metallic magnetic recording material.

the typical sizes of gamma iron oxide particles used in recording tapes. In all cases the ferromagnetic particles used in magnetic recording are too small to contain a domain wall and we therefore have single-domain particles.

Attempts are being made to develop ‘perpendicular recording’ media in which the needles lie perpendicular to the plane. The advantages of this are that it may be possible to increase the information storage density. Research into perpendicular recording media is continuing [14], in particular much attention is being directed towards CoCr layers for this purpose. However so far the development of these media has encountered difficulties, among which is the fact that the material does not perform as well as was expected.

The hysteresis loops which are desirable for magnetic recording materials are generally square loops, with high remanence, moderately high coercivity and rapid switching from one state to the other, as shown in Fig. 4.3, which is the hysteresis loop of a metallic magnetic recording medium. In this case the coercivity 56 kA/m and remanence $0.9 \times 10^6 \text{ A/m}$ are substantially higher than for $\gamma\text{-Fe}_2\text{O}_3$ particles.

4.2.6 Permanent magnets

Where do we use ferromagnetic materials that remain permanently magnetized such as alnico, neodymium–iron–boron or samarium–cobalt?

Permanent magnets are one of the three most important classes of magnetic materials, the others being electrical steels and magnetic recording media.

Permanent magnets find applications in electrical motors and generators, loudspeakers, television tubes, moving-coil meters, magnetic suspension devices and clamps [15, 16].

Clearly the application determines the choice of the magnetic material based on its hysteresis characteristics. The properties of these materials are usually represented by the 'demagnetization curve' which is the portion of the hysteresis curve in the second quadrant as the magnetization is reduced from saturation. The demagnetization curves for some permanent magnet materials are shown in Fig. 4.4. It is important to realize that the final magnetic properties depend as much on the metallurgical treatment and processing of the material as on its chemical composition.

In recent years a permanent magnet material based on neodymium–iron–boron has been discovered [17]. This has superior magnetic properties for many applications when compared with its predecessor samarium–cobalt [18]. For example its coercivity can be as high as 1.12×10^6 A/m (14 000 Oe) compared with 0.72×10^6 A/m (9000 Oe) for samarium–cobalt.

In addition to the coercivity another parameter of prime importance to permanent magnet users is the maximum energy product BH_{\max} . This is obtained by finding the maximum value of the product $|BH|$ in the second, or demagnetizing, quadrant of the hysteresis loop. It represents the magnetic energy stored in a permanent magnet material. We will discuss its significance to permanent magnet users in detail in Chapter 14. Generally the maximum energy product by itself does not give sufficient information for permanent magnet users to decide on the suitability of a material for a particular application, but it is one parameter which is widely quoted when comparing various permanent magnet materials.

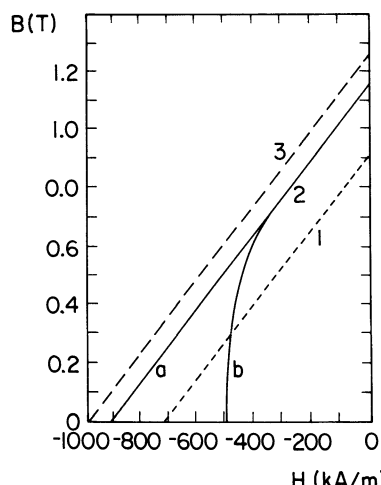


Fig. 4.4 Second quadrant magnetization curves of specimens of samarium–cobalt (1 and 2) and neodymium–iron–boron (3).

For many years the maximum energy product was in the range of $50 \times 10^3 \text{ J m}^{-3}$ (a few megagauss-oersted). Development of samarium–cobalt permanent magnets raised this to about $160 \times 10^3 \text{ J m}^{-3}$ (20 megagauss-oersted) and lately in the neodymium–iron–boron magnets energy products of typically $320 \times 10^3 \text{ J m}^{-3}$ (40 megagauss-oersted) have been achieved.

In most applications the stability of the permanent magnet is an important consideration and therefore the material must be operated sufficiently far from its Curie point since the spontaneous magnetization decreases rapidly with temperature above about 75% of the Curie temperature. This is one of the problems that has arisen with neodymium–iron–boron magnets for higher temperature applications.

4.2.7 Inductance cores: soft ferrites

What additional properties are needed for high-frequency applications of ferromagnets?

Soft magnetic materials are also used as cores for induction coils. They enhance the flux density inside the coil and thereby improve inductance. When inductors are required to operate at high frequencies then, due to the skin depth, only non-conducting or finely laminated magnetic materials can be used. This usually means soft ferrites which are magnetic materials with high electrical resistivity and high permeability which for many years were thought to be ferromagnets. This was because their bulk magnetic properties are very similarly to ferromagnets. It is now known that these materials are different from ferromagnets and this difference is discussed in Chapter 9. Ferrite-cored inductors are used extensively in frequency-selective circuits, so that the resonant frequency of the circuit ensures that it only responds to the given frequency.

Another application of soft ferrites is in antennae for radio receivers. These have an internal ferrite-cored antenna consisting of a short solenoidal coil of N turns enclosing an area A . When this is oriented with its axis parallel to the magnetic field vector of the radio wave signal being received the induced e.m.f. in the coil is

$$E = E_0 \mu_r (2\pi AN)/\lambda,$$

where μ_r is the relative permeability of the ferrite rod, λ the wavelength of the radio waves and E_0 is the strength of the electric field of the received signal in free space. Typical values of μ_r for these applications are $\mu_r \approx 100$ to 1000.

Soft ferrites came into commercial production in 1948. They consist of a compound oxide consisting of iron oxide (Fe_2O_3) together with other oxides such as manganese, nickel or magnesium which have a complicated chemical composition. For example nickel ferrite has the composition $\text{NiO} \cdot \text{Fe}_2\text{O}_3$. In their final form they are usually a brown-coloured ceramic. Their saturation magnetization is typically $M_s = 0.2 \times 10^6 \text{ A/m}$ ($B_s = 0.25 \text{ tesla}$), with coercivities of the order of 8 A/m (0.1 Oe) and maximum permeability $\mu_r = 1500$.

4.2.8 Ceramic magnets: hard ferrites

Which permanent magnet materials should be used where the demagnetizing effects are large?

The hard ferrites, also known as ceramic magnets, are in widespread use in motors, generators and other rotating machines, loudspeakers and various holding or clamping devices. According to Heck [1] half the West German magnet production in 1963 was in the form of barium ferrite ceramic magnets.

They are usually made from barium or strontium ferrite. They are very cheap to produce and can be powdered and included in a plastic binder to form the so called ‘plastic magnets’ which can be formed easily into any desirable shape. They have very high coercivity, typically 200 kA/m so that they can be usefully used in the form of short magnets even though the demagnetizing effects are large.

4.3 PARAMAGNETISM AND DIAMAGNETISM

What uses do paramagnets and diamagnets find?

Paramagnets do not find nearly as many applications as ferromagnets and therefore our discussion at this stage will be somewhat limited. The description of paramagnetism is however of vital importance in the understanding of magnetism. The reason for this is that paramagnetism is a much simpler phenomenon to describe than ferromagnetism and quite reasonable theories of paramagnetism have been developed on the basis of very simple models and these simple theories give good agreement with experimental observation. In the limiting case the atomic magnetic moments of paramagnets can be treated as non-interacting (i.e. ‘dilute paramagnetism’), an approximation which simplifies the modelling greatly.

Diamagnets generally do not find many applications which depend on their magnetic properties either, except for the special case of the superconductors, which are perfect diamagnets with $\chi = -1$.

4.3.1 Paramagnets

How do paramagnets differ fundamentally from ferromagnets?

The study of paramagnetism allows us to investigate the atomic magnetic moments of atoms almost in isolation, since unlike ferromagnetism paramagnetism is not a cooperative phenomenon. Solid-state physicists are therefore more familiar with the underlying theories of paramagnetism such as the temperature dependence of paramagnetic susceptibility, and its description using the classical expression the Langevin function (see Section 9.1.5) or its quantum mechanical analog the Brillouin function (see Section 11.2.2). Materials exhibiting paramagnetism are usually atoms and molecules with an odd number of

82 Magnetic materials

electrons so that there is an unpaired electron spin, giving rise to a net magnetic moment. These include atoms and ions with partially filled inner shells, such as transition elements. Some elements with even numbers of electrons are paramagnetic.

Examples of paramagnetic materials are platinum, aluminum, oxygen, various salts of the transition metals such as chlorides, sulphates and carbonates of manganese, chromium, iron and copper, in which the paramagnetic moments reside on the Cr^{3+} , Mn^{2+} , Fe^{2+} and Cu^{2+} respectively, and hydrated salts such as potassium-chromium alum $\text{KCr}(\text{SO}_4)_2 \cdot 12\text{H}_2\text{O}$. These salts obey the Curie law, which states that the susceptibility χ is inversely proportional to the temperature T , because the magnetic moments are localized on the metal ions, while the presence of the water molecules in the hydrated salts ensures that the interactions between these electrons on neighbouring metal ions are weak.

Salts and oxides of rare earth (lanthanide) elements are strongly paramagnetic. In these solids the magnetic properties are determined by highly localized 4f electrons. These are closely bound to the nucleus, and are effectively shielded by the outer electrons from the magnetic field at the ionic site caused by the other atoms in the crystal lattice, that is the crystal field. Rare earth metals are also paramagnetic for the same reasons, however if the temperature is reduced many of them exhibit ordered states such as ferromagnetism.

All ferromagnetic metals such as cobalt, iron and nickel become paramagnetic above their Curie points, as do the antiferromagnetic metals chromium and manganese above their transition temperatures of 35°C and -173°C , respectively. Paramagnetic metals which do not exhibit a ferromagnetic state include all the alkali metals (sodium series), and the alkaline earth metals (calcium series) with the exception of beryllium. The 3d, 4d and 5d transition metals are all paramagnetic with the exception of copper, zinc, silver, cadmium, aluminum and mercury which are diamagnetic. The elements oxygen, aluminum and tin are also paramagnetic.

4.3.2 Temperature dependence of paramagnetic susceptibility

How does the susceptibility vary with environmental factors such as temperature?

In many paramagnets the susceptibility is inversely proportional to temperature. This dependence is known as the Curie law

$$\chi = \frac{C}{T}$$

where T is the temperature in kelvin and C is a constant known as the Curie constant. In other paramagnets the susceptibility is independent of temperature. Two theories have evolved to deal with these two types of paramagnetism: the localized moment model which leads to the Curie law, and the conduction band electron model due to Pauli which leads to temperature independent and rather weaker susceptibility. The dependence of the susceptibility on temperature of some paramagnetic solids is shown in Fig. 4.5.

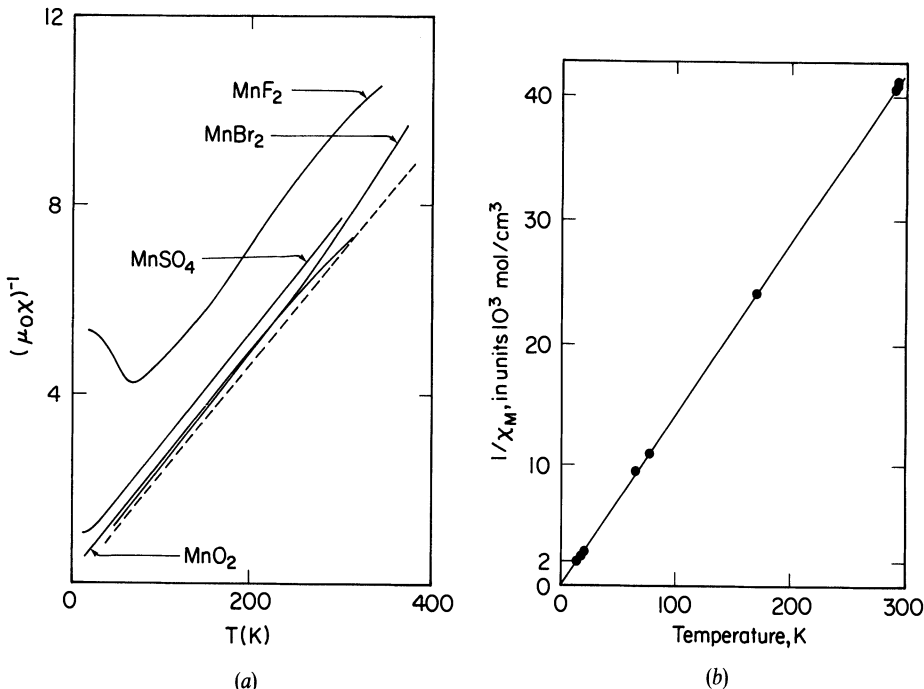


Fig. 4.5 Temperature dependence of the reciprocal magnetic susceptibility of some magnetic materials; (a) manganese compounds after de Haas *et al.*; and (b) $\text{Gd}(\text{C}_2\text{H}_5\text{SO}_4)_3 \cdot 9\text{H}_2\text{O}$ after Jackson and Kamerlingh Onnes.

4.3.3 Field dependence of paramagnetic susceptibility

What effect does a magnetic field have on the susceptibility of a paramagnet?

In paramagnets subjected to magnetic fields other than very high fields the magnetization M is proportional to the field H . That is the susceptibility is virtually constant and lies in the range 10^{-3} to 10^{-5} . In most cases the spins are not coupled or are only weakly coupled so that they can be considered independent to a good approximation. The reason for this is the thermal energy is sufficiently great to cause random alignment of the moments in zero field. When a field is applied the atomic moments begin to align, but the fraction deflected into the field direction remains small for all practical field strengths.

The variation of the magnetization of a typical paramagnet with temperature and field is shown in Fig. 4.6. At moderate to strong fields the susceptibility is still constant and saturation only occurs at very high field strengths. The dependence can be expressed classically using the Langevin function

$$M/nm = \coth\left(\frac{\mu_0 mH}{k_B T}\right) - \left(\frac{k_B T}{\mu_0 mH}\right),$$

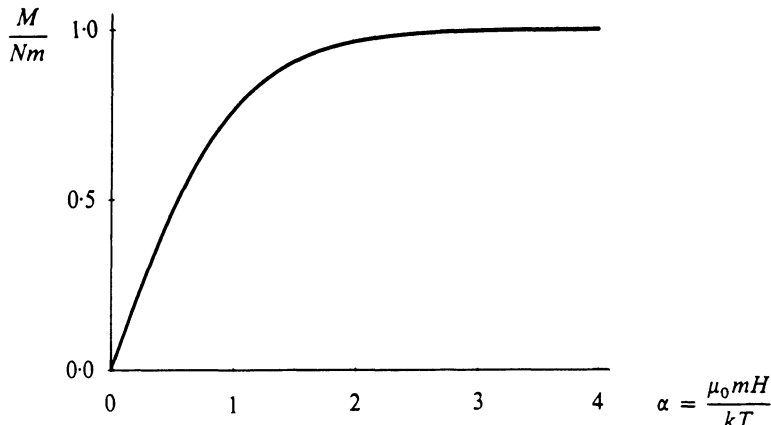


Fig. 4.6 Variation of magnetization of a typical paramagnet with temperature and magnetic field using the classical Langevin equation.

where n is the number of atoms per unit volume, m is the magnetic moment per atom, k_B is Boltzmann's constant and T is the temperature in kelvin. This leads to the following approximate expression for susceptibility, which works well at high temperatures

$$\chi = \frac{\mu_0 n m^2}{3 k_B T}$$

as described in Chapter 9, where $\mu_0 n m^2 / 3 k_B$ is the Curie constant C . A more accurate expression is obtained using the Brillouin function as described in Chapter 11.

4.3.4 Applications of paramagnets

Where do paramagnets find uses?

There are very few applications of paramagnetic materials on the basis of their magnetic properties. Their use occurs primarily in the scientific study of magnetism since they help in our understanding of the much more important phenomenon of ferromagnetism by allowing us to study the electronic properties of materials with net atomic magnetic moments in the absence of strong cooperative effects.

There is an increasing use of paramagnetic materials in electron spin resonance (ESR) for the purpose of measuring magnetic fields in which the magnetic properties of the material are already well characterized (rather than studying the resonance of the material to determine its electronic energy states).

One other application is in the production of very low temperatures. The use of paramagnetic salts to achieve ultra-low temperatures was first suggested by Debye [19] and Giauque [20]. A paramagnetic salt is magnetized isothermally and then cooled to as low a temperature as possible by conventional cryogenic means, for

example by using liquid helium at reduced pressure. It is then thermally isolated and adiabatically demagnetized whereupon the temperature drops even further. By this means temperatures down to the millikelvin range can be achieved.

4.3.5 Diamagnets

How do diamagnets differ fundamentally from paramagnets and ferromagnets?

Elements without permanent atomic electronic magnetic moments are unable to exhibit paramagnetism or ferromagnetism. These atoms have filled electron shells and therefore no net magnetic moment. When subjected to a magnetic field their induced magnetization opposes the applied field, in the manner described by Lenz's law, and so they have negative susceptibility.

The dependence of the magnetization on applied field in diamagnets, that is the susceptibility, is according to the classical Langevin theory of diamagnetism (Section 9.1.2) given by

$$\chi = -\frac{\mu_0 Z e^2 n \langle r^2 \rangle}{6m_e},$$

where n is the number of atoms per unit volume, Z is the number of electrons per atom, e is the electronic charge, m_e is the electronic mass and $\langle r^2 \rangle$ is the root mean square atomic radius, which is typically 10^{-21} m^2 . Diamagnetic susceptibility is substantially independent of temperature.

4.3.6 Superconductors

How are superconductors classified among magnetic materials?

Superconductors are diamagnets which find many applications, however they are a unique class of diamagnet in which the susceptibility is caused by macroscopic currents circulating in the material which oppose the applied field rather than changes in the orbital motion of closely bound electrons. They therefore represent a very special case. Clearly their susceptibility is temperature dependent since above their critical temperature they are no longer perfect diamagnets. These materials will be dealt with separately in Chapter 12.

REFERENCES

1. Heck, C. (1974) *Magnetic Materials and their Applications*, Crane and Russak & Co., New York.
2. Wohlfarth, E. P. (ed.) (1980 and 1982) *Ferromagnetic Materials*, Three-volume series, North Holland, Amsterdam.
3. Warburg, E. (1981) *Ann. Physik*, **13**, 141.
4. Ewing, J. A. (1900) *Magnetic Induction in Iron and other Metals*, 3rd edn, The Electrician Publishing Co., London, 1900, and (1882) *Proc. Roy. Soc.*, **220**, 39.

86 Magnetic materials

5. Chen, C. W. (1977) *Magnetism and Metallurgy of Soft Magnetic Materials*, North Holland, Amsterdam.
6. Hilzinger, H. R. and Kronmuller, H. (1977) *Physica*, **86–88B**, 1365.
7. Jiles, D. C., Garikapati, P. and Chang, T. T. (1988) *IEEE Trans. Mag.*, **24**, 2922.
8. Gilbert, W. (1958), *De Magnete* (Trans. *On the magnet*) (1600) Republished by Dover, New York.
9. Enz, U. (1982) Magnetism and magnetic materials: Historical developments and present role in industry and technology, in *Ferromagnetic Materials*, Vol. 3, (ed. E. P. Wohlfarth), North Holland, Amsterdam.
10. Chin, G. Y. and Wernick, J. H. (1980) Soft magnetic metallic materials, in *Ferromagnetic Materials*, Vol. 2 (ed. E. P. Wohlfarth), North Holland, Amsterdam.
11. Luborsky, F. E. (1980) Amorphous ferromagnets, in *Ferromagnetic Materials*, Vol. 1 (ed. E. P. Wohlfarth), North Holland, Amsterdam.
12. Shiozaki, M. (1987) Recent trends in non oriented and grain oriented electrical steel sheets in Japan. *Proceedings of the Sixth Annual Conference on Properties and Applications of Magnetic Materials*, Illinois Institute of Technology, Chicago.
13. Bate, G. (1980) Recording materials, in *Ferromagnetic Materials*, Vol. 2 (ed. E. P. Wohlfarth), North Holland, Amsterdam.
14. Bernards, J. P. C., Schrauwen, C. P. G., Luitjens, S. B., Zieren, V. and de Bie, R. W. (1987) *IEEE Trans. Mag.*, **23**, 125.
15. McCaig, M. (1977) *Permanent Magnets in Theory and Practice*, Wiley, New York.
16. Moskowitz, L. R. (1976) *Permanent Magnet Design and Application Handbook*, Cahner, Boston.
17. Croat, J. J., Herbst, J. F., Lee, R. W. and Pinkerton, F. E. (1984) *J. Appl. Phys.*, **55**, 2078.
18. Strnat, K., Hoffer, G., Olson, J., Ostertag, W. and Becker, J. J. (1967) *J. Appl. Phys.*, **38**, 1001.
19. Debye, P. (1926) *Ann. Physik*, **81**, 1154.
20. Giauque, W. F. (1927) *Am. Chem. Soc. J.*, **49**, 1864.
21. Fidler, J., Bernard, J. and Skalicky, P. (1987) in *High Performance Permanent Magnet Materials* (ed. S. G. Sankar, J. F. Herbst and N. C. Koon) Materials Research Society, New York, p. 181.

FURTHER READING

- Bozorth, R. M. (1951) *Ferromagnetism*, Van Nostrand, New York.
- Heck, C. (1974) *Magnetic Materials and their Applications*, Crane Russak and Co. New York.
- Hummel, R. (1985) *Electronic Properties of Materials*, Springer–Verlag, Berlin, Ch. 17.
- Jorgensen, F. (1988) *The Complete Handbook of Magnetic Recording*, 3rd edn, TAB publishers, Pennsylvania.
- McCaig, M. (1977) *Permanent Magnets in Theory and Practice*, Wiley, New York.
- Snelling, E. C. (1988) *Soft Ferrites, Properties and Applications*, 2nd edn, Butterworths, London.

EXAMPLES AND EXERCISES

Example 4.1 Properties of ferromagnets. Explain the difference between a ferromagnet and a paramagnet on the basis of macroscopic measurements. What is the saturation magnetization and how does it differ as a material is heated through its Curie point?

What criteria are used to distinguish between hard and soft magnetic materials?

In deciding on a material for use in (a) an electromagnet (b) a transformer what magnetic properties would you take into consideration?

Example 4.2 Use of initial magnetization curve to find flux in core. Explain the meaning of hysteresis loss, coercivity and remanence. How do the magnitudes of these quantities determine the suitability of a ferromagnet for applications? Explain what is meant by the initial magnetization curve.

The initial magnetization curve for a specimen of steel is given in Fig. 4.7 below, a toroid of this steel has a mean circumference of 40 cm and a cross-sectional area of 4 cm^2 . It is wound with a coil of 400 turns. What will be the total flux in the material for currents of 0.1, 0.2, 0.3, 0.4 and 0.5 amps?

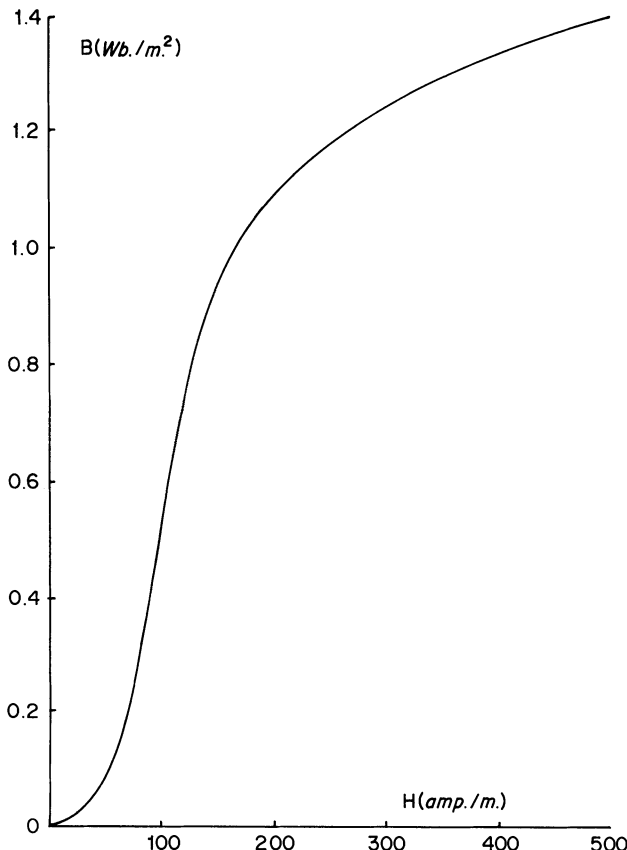


Fig. 4.7 Initial magnetization curve for a low-carbon steel.

Example 4.3 Calculation of atomic magnetic moment. The saturation magnetization of iron is $1.7 \times 10^6 \text{ A/m}$. If the density of iron is 7970 kg/m^3 and Avogadro's number is 6.025×10^{26} per kilogram atom calculate the magnetic moment per iron atom in amp metre² and in Bohr magnetons. (1 Bohr magneton $\mu_B = 9.27 \times 10^{-24}$ joule/tesla or 1.16×10^{-29} joule/amp metre⁻¹. Relative atomic mass of iron = 56.)

5

Magnetic Properties

We will now look at the causes of hysteresis in ferromagnets and how the variation of magnetization with magnetic field can be quantified in restricted cases such as at low field and in the approach to saturation. High-resolution measurements of the variation of \mathbf{M} with \mathbf{H} indicate that there are discontinuities. These are known as the Barkhausen effect. We will also consider the change in length of a ferromagnet as it is magnetized, that is the magnetostriction, and discuss anisotropy in relation to magnetostriction.

Which are the most important macroscopic magnetic properties of ferromagnets?

We have shown in the previous chapter that most of the important macroscopic magnetic properties of ferromagnets can be represented on a \mathbf{B}, \mathbf{H} plot or hysteresis loop. From this the magnetization can be calculated at every point on the hysteresis curve using the totally general formula $\mathbf{B} = \mu_0(\mathbf{H} + \mathbf{M})$. As the magnetization curve is traversed there are discontinuous, irreversible changes in magnetization known as the Barkhausen effect after their discoverer. In recent years the Barkhausen effect has become an important tool for investigating the microstructural properties of ferromagnetic materials.

One important bulk property of interest which is not contained in the hysteresis plot is the magnetostriction. This is the change in length of a material either as a result of a magnetic order (spontaneous magnetostriction) or under the action of a magnetic field (field-induced magnetostriction). This will also be discussed in the chapter.

5.1 HYSTERESIS AND RELATED PROPERTIES

What information can be obtained from the hysteresis curve?

From the hysteresis curve such as the one shown in Fig. 5.1 we can define a number of magnetic properties of the material which can be used to characterize the hysteresis loop. A question immediately arises: how many degrees of freedom are there in a hysteresis loop? Or to put the question another way: how many parameters are needed to characterize a hysteresis loop? Clearly there is no general answer to this but for the commonly encountered sigmoid-shaped hysteresis loop

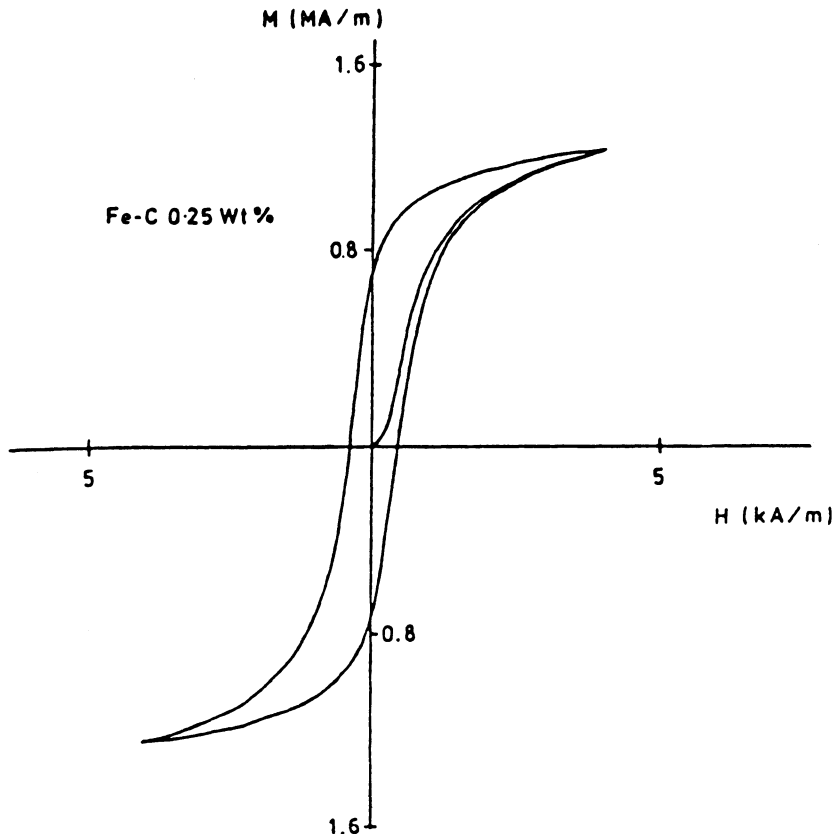


Fig. 5.1 Typical sigmoid-shaped hysteresis curve of a specimen of iron containing 0.25% by wt carbon.

such as the one in Fig. 5.1 we can start to enumerate the important properties and thereby make an estimate.

5.1.1 Parametric characterization of hysteresis

Which are the parameters that can be used to define hysteresis?

First of all the saturation magnetization M_0 will give us an upper limit to the magnetization that can be achieved. At temperatures well below the Curie point the technical saturation M_s can be used instead. The width of the loop across the H axis which is twice the coercivity H_c is also an independent parameter since this can be altered by heat treatment and hence is not dependent on M_s . The height of the curve along the B axis, that is the remanence B_R , is also an independent parameter since it is not wholly dependent on M_s and H_c . The orientation of the whole hysteresis curve, which can be expressed as μ'_{\max} the slope of the curve at the coercive point, can change independently of the other parameters.

Table 5.1 Magnetic properties of various high-permeability ferromagnetic materials. Relative permeability at a magnetic induction of 2 tesla μ_{2T} , maximum relative permeability μ_{\max} , saturation magnetic induction B_s , d.c. hysteresis loss W_H and coercivity H_c

Material	μ_{2T}	μ_{\max}	B_s (tesla)	W_H (J/m ³)	H_c (A/m)
Purified iron	5000	180 000	2.15	30	4
Iron	200	5000	2.15	500	80
Carbonyl iron	55	132	2.15	—	—
Cold rolled steel	180	2000	2.1	—	144
Iron–4% silicon	500	7000	1.97	350	40
45 Permalloy	2500	25 000	1.6	120	24
Hipernik	4500	70 000	1.6	22	4
Monimax	2000	35 000	1.5	—	8
Sinimax	3000	35 000	1.1	—	—
78 Permalloy	8000	100 000	1.07	20	4
Mumetal	20 000	100 000	0.65	—	4
Supermalloy	100 000	800 000	0.8	—	0.16
Permendur	800	5000	2.45	1200	160
2V Permendur	800	4500	2.4	600	160
Hiperco	650	10 000	2.42	—	80
Ferroxcube	1000	1500	2.5	—	8

The hysteresis loss W_H may also be an independent parameter as may the initial permeability μ'_{in} . Finally the curvature of the sides of the hysteresis loop, which although not immediately obvious as an independent parameter, is clearly not dependent on such factors as coercivity or maximum differential permeability. This parameter emerges more clearly from a consideration of anhysteretic magnetization given below, which requires at least two independent parameters in addition to M_s in order to characterize it.

From the above simplistic considerations we may expect to be able to characterize the bulk magnetic properties of a material in terms of perhaps five or six independent parameters. In fact we often find that when the magnetic properties of ferromagnetic materials are displayed in tabular form the properties are represented in terms of coercivity, remanence, hysteresis loss, initial permeability, maximum permeability and saturation magnetization or saturation magnetic induction, as in Table 5.1.

5.1.2 Causes of hysteresis

What are the underlying mechanisms behind hysteresis?

It is well known that if a specimen of iron or steel is subjected to cold working the hysteresis loss and the coercivity increase (Fig. 5.2). It is also well known that the addition of other non-magnetic elements to iron such as carbon in making steel,

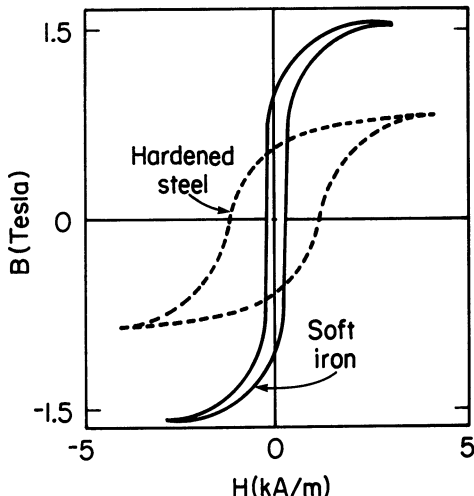


Fig. 5.2 Dependence of the hysteresis loop of iron or steel on hardness caused by the addition of carbon or other non-magnetic material or by cold working.

increases the hysteresis loss and coercivity. These empirical facts were known long before theories of hysteresis were suggested.

From these results it would appear that ‘imperfections’, whether in the form of dislocations or impurity elements in the metal, cause an increase in the energy lost during the magnetization process, in the form of a kind of internal friction. It is these ‘imperfections’ which give rise to hysteresis.

Another mechanism which gives rise to hysteresis is caused by magneto-crystalline anisotropy. Ferromagnetic materials with higher anisotropy have greater hysteresis. This is well known by those working with permanent magnets. In an anisotropic solid certain crystallographic axes are favoured by the magnetic moments which will prefer to lie along these directions as this leads to a lower energy. The magnetic moments can be dislodged from the direction they are occupying by application of a magnetic field but when this occurs they jump to crystallographically equivalent axes which are closer to the field direction, and hence of lower energy. This results in discontinuous and irreversible rotation of the magnetic moments which leads to a kind of switching action.

In order to discuss this second process properly we need some additional background knowledge of domain processes which have yet to be discussed (Chapter 8). Therefore we will defer the discussion until after the necessary background material has been presented.

5.1.3 Anhysteretic, or hysteresis-free, magnetization

What happens in the case of a material without defects such as dislocations or impurity elements?

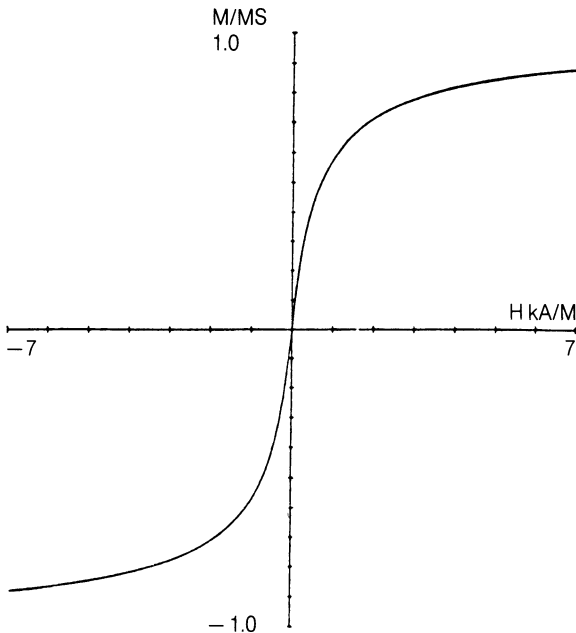


Fig. 5.3 Anhysteretic magnetization curve. This is antisymmetric with respect to the magnetic field. The differential susceptibility is greatest at the origin and decreases monotonically with increasing field. The curve has no hysteresis and is completely reversible.

If we accept the hypothesis that it is the imperfections, whatever their nature, which cause hysteresis, then we must also ask ourselves what the magnetization curve would look like if the material were devoid of all imperfections. The answer is that, ignoring anisotropic effects for the moment, it would be hysteresis free. That is the magnetic induction would be a single-valued function of the magnetic field H . The magnetization curve would therefore be reversible.

We can briefly speculate on the form of such a curve before presenting a simple model for it. Suppose we consider a plot of magnetization against field for such an ideal case. Since the magnetization of a ferromagnet saturates it is clear that as H increases so M tends towards M_s . Furthermore, we would expect that at first the magnetization would change fairly rapidly with H but as H increased the rate of change would decrease, since this is in the nature of physical systems which saturate. So we would expect M to be a monotonically increasing function of H while dM/dH was monotonically decreasing. This would give the S-shaped curve of Fig. 5.3.

5.1.4 The Frohlich–Kennelly relation

Can we find a simple equation for the anhysteretic?

94 Magnetic properties

A quantitative relationship between magnetization \mathbf{M} and magnetic field \mathbf{H} is clearly highly desirable since any such equation provides a means of telling how the magnetization or magnetic induction of a material will change with field. An empirical relationship between \mathbf{M} and \mathbf{H} along the anhysteretic magnetization curve was suggested by Frohlich [1] and later in a different, but equivalent, form by Kennelly [2].

The Frohlich equation for the anhysteretic magnetization is

$$\mathbf{M} = \frac{\alpha \mathbf{H}}{1 + \beta \mathbf{H}},$$

where $\alpha/\beta = M_s$ since as $H \rightarrow \infty$ the magnetization must tend to M_s .

Independently Kennelly arrived at an expression for the high-field susceptibility as the magnetization approached saturation. If Kennelly's expression is converted to SI units it becomes

$$\frac{1}{\mu - \mu_0} = a + bH,$$

which can easily be shown to be equivalent to the Frohlich equation in which $\mu_0 a = 1/\alpha$ and $\mu_0 b = \beta/\alpha = 1/M_s$.

This equation can also be rewritten in the form of a series

$$\mathbf{M} = M_s [1 - aM_s/H + (aM_s/H)^2 \dots].$$

This is the form of equation used by Weiss [3] for finding M_s from magnetization curves by extrapolation, using only the terms up to $1/H$. It is also of interest in section 5.1.7 when we compare it with the law of approach to saturation given much later by Becker and Doring [4].

5.1.5 Measurement of anhysteretic magnetization

If the anhysteretic is so important how do we measure it?

Elimination of all defects within a material is not usually practicable, however there is a way of reaching the anhysteretic magnetization by other means. This is by cycling the magnetization by applying an alternating field of gradually decreasing amplitude superimposed on the d.c. field of interest. As the a.c. field is cycled the hysteresis is gradually removed and the magnetization converges on the anhysteretic value for the prevailing d.c. field strength. This procedure can be thought of as 'shaking' the magnetization so that it overcomes the internal frictional forces, and anisotropic or switching hysteresis effects, and reaches its true equilibrium value. The same effect can also be brought about by stress cycling although this is generally more difficult to achieve.

In magnetic recording (Chapter 14) the use of field cycling is well known as a method of reaching the anhysteretic magnetization [5]. The anhysteretic susceptibility at the origin is typically an order of magnitude greater than the

normal d.c. susceptibility at the origin. The anhysteretic magnetization also varies linearly with field at low values which is one of the prime considerations for magnetic recording.

5.1.6 Low-field behaviour: the Rayleigh law

Is there a simple equation for the initial magnetization curve?

We now go on to consider the initial magnetization curve, that is the variation of magnetization with field obtained when a d.c. field is first applied to a demagnetized ferromagnet. It was noticed by Rayleigh [6] that in the low-field region of the initial magnetization curve the permeability could be represented by an equation of the form

$$\mu(\mathbf{H}) = \mu(0) + v\mathbf{H},$$

which leads to the following parabolic dependence of \mathbf{B} on \mathbf{H} along the initial magnetization curve

$$\mathbf{B}(\mathbf{H}) = \mu(0)\mathbf{H} + v\mathbf{H}^2.$$

According to Rayleigh the term $\mu(0)\mathbf{H}$ represented the reversible change in magnetic induction while the term $v\mathbf{H}^2$ represented the irreversible change in magnetic induction. Furthermore, Rayleigh indicated that low-amplitude hysteresis loops could be represented by parabolic curves which have a reversible differential permeability at the loop tips which is equal to $\mu(0)$ as shown in Fig. 5.4.

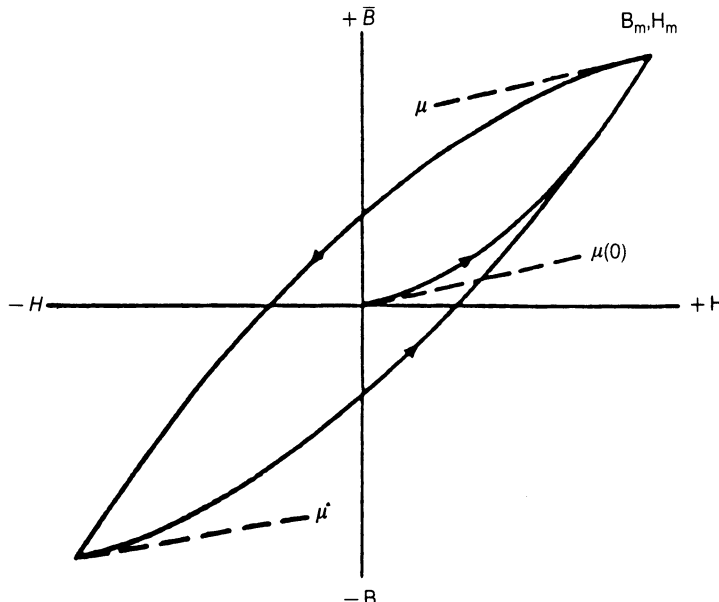


Fig. 5.4 Hysteresis loops of low-field amplitude in the Rayleigh region.

96 Magnetic properties

It follows from this assumption and the Rayleigh law that in the low-field region the small-amplitude hysteresis loops can be described by an equation of the form

$$\mathbf{B} = [\mu(0) + v\mathbf{H}_m]\mathbf{H} \pm (v/2)(\mathbf{H}_m^2 - \mathbf{H}^2),$$

where \mathbf{H}_m is the maximum field at the loop tip. Low-amplitude hysteresis loops for which this parabolic relation applies are known as Rayleigh loops.

This leads to two further results of interest: expressions for the hysteresis loss W_H and the remanence B_R . In SI units these are

$$\begin{aligned} W_H &= \int \mathbf{H} \cdot d\mathbf{B} \\ &= (4/3)v\mathbf{H}_m^3 \end{aligned}$$

and

$$B_R = (v/2)\mathbf{H}_m^2.$$

It must be remembered of course that these relations only hold true in the low-field region. As \mathbf{H}_m is increased the parabolic relation breaks down. In order to model the hysteresis behaviour over a wider range of \mathbf{H} it is necessary to gain further insight into the microscopic mechanisms occurring within the material.

5.1.7 High-field behaviour: the law of approach to saturation

Is there an equation for the magnetization at high fields?

In the high-field region the magnetization approaches saturation. The first attempt to give an equation describing the behaviour in this region was Lamont's law [7, p. 484],

$$\chi = \frac{dM}{dH} = \text{constant} \times (M_s - M),$$

which states simply that at high fields the susceptibility is proportional to the displacement from saturation. This was later shown to be equivalent to the Frohlich–Kennelly relation. This is of interest in relation to the development of the hysteresis model in section 8.2

Later work indicated that the high-field behaviour can be modelled by the law of approach to saturation as given by Becker and Doring [4] and Bozorth [7, p. 484]. This is expressed in the form of a series,

$$\mathbf{M} = M_s \left(1 - \frac{a}{\mathbf{H}} - \frac{b}{\mathbf{H}^2} - \dots \right) + k\mathbf{H}$$

where the final term $k\mathbf{H}$ represents the forced magnetization, that is the field induced increase in spontaneous magnetization, which is a very small contribution except at high fields. Typically \mathbf{H} has to be of the order of 10^5 or 10^6 Oe before this last term becomes significant.

It is interesting to note that this law which was only derived at high

magnetizations is also very similar to the series form of the Frohlich–Kennelly relation. The reason for this is that at high fields the initial magnetization curve, the upper and lower branches of the hysteresis loop and the anhysteretic magnetization approach each other asymptotically.

5.2 THE BARKHAUSEN EFFECT AND RELATED PHENOMENA

5.2.1 The Barkhausen effect

Does the magnetization change smoothly with magnetic field?

The Barkhausen effect is the phenomenon of discontinuous changes in the flux density B within a ferromagnet as the magnetic field H is changed continuously. This was first observed in 1919 [8] when a secondary coil was wound on a piece of iron and connected to an amplifier and loudspeaker. As the H field was increased smoothly a series of clicks were heard over the loudspeaker which were due to small voltage pulses induced in the secondary coil. These voltages were caused through the law of electromagnetic induction by small changes in flux density through the coil arising from discontinuous changes in magnetization M and hence in the induction B .

If the initial magnetization curve, which looks to be a smooth variation of B with H under normal circumstances, is greatly magnified, then the discontinuous changes in B which constitute the Barkhausen effect can be observed directly as in Fig. 5.5. At first these discontinuities in induction were attributed to sudden discontinuous rotation of the direction of magnetization within a domain, a mechanism known as domain rotation, but it is now known that discontinuous domain boundary motion is the most significant factor contributing to Barkhausen emissions [9]. Nevertheless both of these mechanisms do occur and contribute to the Barkhausen effect.

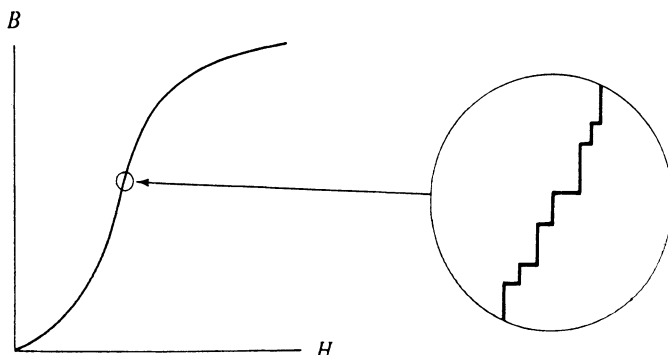


Fig. 5.5 Barkhausen discontinuities along the initial magnetization curve observed by amplifying the magnetization.

98 Magnetic properties

The Barkhausen emissions are greatly affected by changes in the microstructure of the material and also by stress. Therefore Barkhausen measurements have found an important role in materials evaluation as discussed by Matzkanin, Beissner and Teller [10].

5.2.2 Magnetoacoustic emission

What other effects occur as a result of sudden discontinuous domain-wall motion?

Magnetoacoustic emission, also known sometimes as the acoustic Barkhausen effect, is closely related to the magnetic Barkhausen effect described above. Magnetoacoustic emission consists of bursts of low-level acoustic energy generated by sudden discontinuous changes in magnetization involving localized strains or magnetostriction (section 5.3). These can be detected by a broad-band ultrasonic transducer. They are caused by microscopic magnetostrictive pulses as the domain walls move, and in non-magnetostrictive materials such as Fe–20%Ni are almost non-existent. Therefore the effect depends on both sudden discontinuous domain processes and magnetostriction.

Magnetoacoustic emission was first observed by Lord [11]. Subsequently investigations were carried out by Ono and Shibata [12] and others [13]. Because the effect depends on magnetostriction it cannot be generated by 180° domain-wall motion or rotation, as these involve no change in magnetostriction. These 180° domain boundaries exist between neighbouring domains in which the magnetization vectors point in exactly opposite directions. The relative number density of 180° and non-180° domain walls is affected by the application of uniaxial stress. Therefore the method has been suggested as a means of detecting stress in ferromagnetic materials and this has been shown to be viable by Buttle, Scruby, Briggs and Jakubovics [14].

5.3 MAGNETOSTRICTION

Do the dimensions of a specimen change when it is magnetized?

The magnetization of a ferromagnetic material is in nearly all cases accompanied by changes in dimensions. The resulting strain is called the magnetostriction λ . From a phenomenological viewpoint there are really two main types of magnetostriction to consider: spontaneous magnetostriction arising from the ordering of magnetic moments into domains at the Curie temperature; and field-induced magnetostriction. These are manifestations of the same effect but can be usefully treated as distinct.

In both cases the magnetostriction is simply defined as λ , the fractional change in length.

$$\lambda = \frac{dl}{l}$$

The existence of magnetostriction was first discovered by Joule [15,16]. Spontaneous magnetostriction within domains arises from the creation of domains as the temperature of the ferromagnet passes through the Curie (or ordering) temperature. Field-induced magnetostriction arises when domains that have spontaneous magnetostriction are reoriented under the action of a magnetic field. Magnetostriction can be measured by using resistive strain gauges or by optical techniques.

We will first consider the magnetostriction of a hypothetical isotropic solid, since this leads to the simplest mathematical results.

5.3.1 Spontaneous magnetostriction in isotropic materials

Does the length of a specimen change when it becomes ferromagnetic?

When a ferromagnetic material is cooled through its Curie point the previously disordered magnetic moments, which had completely random alignment above the Curie point, become ordered over volumes containing large numbers (typically

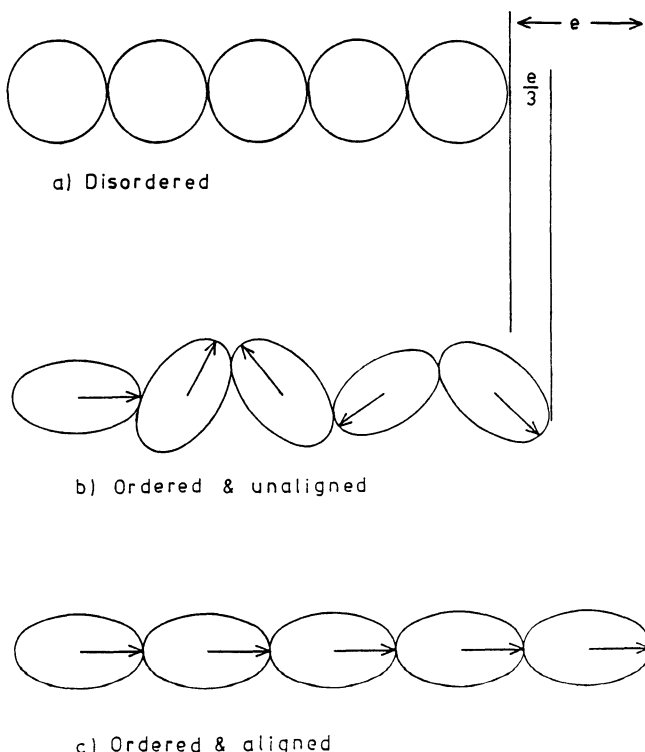


Fig. 5.6 Schematic diagram illustrating the magnetostriction in: (a) the disordered (paramagnetic) regime; (b) the ferromagnetic regime demagnetized; and (c) the ferromagnetic regime, magnetized to saturation.

10^{12} – 10^{15}) of atoms. These volumes in which all moments lie parallel are called domains and can be observed under a microscope. The direction of spontaneous magnetization \mathbf{M}_s varies from domain to domain throughout the material to ensure that the bulk magnetization is zero.

The transition to ferromagnetism is said to cause the onset of ‘long-range order’ of the atomic moments. By this we mean of course long-range compared with atomic dimensions, since the range is still microscopic, and three or four orders of magnitude smaller than the range of magnetic order imposed when the material is magnetically saturated.

Let us therefore consider spherical volumes of unstrained solid within the solid above the Curie temperature and hence in the disordered phase as shown in Fig. 5.6(a). When the material becomes ferromagnetic at the Curie point, spontaneous magnetization appears within the domains and with it an associated spontaneous strain e or magnetostriction λ_0 , along a particular direction, as shown in Fig. 5.6(b).

For the present isotropic case the amplitudes of these spontaneous magnetostrictions are independent of crystallographic direction. Within each ‘isotropic’ domain the strain varies with angle θ from the direction of spontaneous magnetization according to the relation

$$e(\theta) = e \cos^2 \theta.$$

The average deformation throughout the solid due to the onset of spontaneous magnetostriction can then be obtained by integration assuming that the domains are oriented at random so that any particular direction is equally likely.

$$\begin{aligned} \lambda_0 &= \int_{-\pi/2}^{\pi/2} e \cos^2 \theta \sin \theta d\theta \\ &= e/3. \end{aligned}$$

This then is the spontaneous magnetostriction caused by ordering of the magnetic moments at the onset of ferromagnetism. We should note that since we have assumed an isotropic material the domains are arranged with equal probability in any direction and therefore the strain is equivalent in all directions. Therefore in this case although the sample undergoes changes in dimensions its shape remains the same.

5.3.2 Saturation magnetostriction λ_s

What is the maximum change in length when a ferromagnet is magnetized?

Next we will consider saturation magnetostriction which is the fractional change in length between a demagnetized ferromagnetic specimen and the same specimen in a magnetic field sufficiently strong to saturate the magnetization along the field direction. In this case there will be a change of shape since the applied field generates a preferred direction.

Using the very simple model above we cause the transition from the ordered but demagnetized state to the ordered saturated state by application of a magnetic field. In the saturated state of course the magnetic moments in the domains are all aligned parallel to the field and hence the strains are parallel as shown in Fig. 5.6(c).

$$\begin{aligned}\lambda_s &= e - \lambda_0 \\ &= \frac{2}{3}e.\end{aligned}$$

This gives us a method of measuring the spontaneous strain e within a material due to magnetic ordering along a particular direction, by measuring λ_s .

5.3.3 Technical saturation and forced magnetostriction

Can the saturation increase even after the magnetization has reached technical saturation?

As discussed in section 2.1.4 technical saturation of magnetization occurs when all magnetic domains within a material have been aligned in the same direction to form a single-domain specimen. However if the magnetic field is increased further there is still a very slow rise in M and this process is called forced magnetization.

Similar behaviour is observed in the magnetostriction. Technical saturation magnetostriction is reached when the specimen has been converted to a single domain. However a very slow increase in magnetostriction, called forced magnetostriction, is observed as the field is increased further. Forced magnetostriction is a very small effect, being appreciable only at fields of the order of 800 kA/m (10 000 Oe).

The phenomenon is caused by an increase in the ordering of individual atomic magnetic moments within the single domain which is treated in detail in Chapter 9. This is the same mechanism which leads to an increase in the spontaneous magnetization within a domain. The statistical ordering of magnetic moments within a domain is highly temperature dependent [17] and consequently so is the magnitude of the forced magnetostriction.

5.3.4 Magnetostriction at an angle θ to the magnetic field

How does the saturation magnetostriction vary as a function of angle?

Since we are still considering a completely isotropic medium, we can write down an equation for the saturation magnetostriction $\lambda_s(\theta)$ at any angle θ to the field direction.

$$\lambda_s(\theta) = \frac{3}{2}\lambda_s(\cos^2\theta - \frac{1}{3}),$$

where λ_s is the saturation magnetostriction along the direction of magnetization.

This leads to an explanation of some of the magnetostriction measurements which you will often find in the literature in which the magnetostriction with the

field parallel to a given direction $\lambda_{s\parallel}$, and the magnetostriction with the field perpendicular to the given direction $\lambda_{s\perp}$, are measured and the difference taken. The difference between them gives the spontaneous strain within a single domain.

$$\lambda_{s\parallel} - \lambda_{s\perp} = \lambda_s + \lambda_s/2 = \frac{3}{2}\lambda_s = e$$

5.3.5 Anisotropic materials

Are the magnetic properties identical in all directions in a crystal?

Although nickel comes fairly close to having isotropic properties such as magnetostriction, the reality is that all solids are anisotropic to some degree, and therefore the magnetostriction needs to be defined in relation to the crystal axis along which the magnetization lies. An extensive review of magnetostriction in anisotropic materials has been given by Lee [18].

The magnetostrictions or spontaneous strains are defined along each of the principal axes of the crystal. For cubic materials there are two independent magnetostriction constants λ_{100} and λ_{111} as shown in Table 5.2.

The saturation magnetostriction in cubic materials is then given by a generalized version of the equation for isotropic materials above,

$$\begin{aligned}\lambda_s = & \frac{3}{2}\lambda_{100}(\alpha_1^2\beta_1^2 + \alpha_2^2\beta_2^2 + \alpha_3^2\beta_3^2 - \frac{1}{3}) \\ & + 3\lambda_{111}(\alpha_1\alpha_2\beta_1\beta_2 + \alpha_2\alpha_3\beta_2\beta_3 + \alpha_3\alpha_1\beta_3\beta_1),\end{aligned}$$

where λ_{100} is the saturation magnetostriction measured along the $\langle 100 \rangle$ directions and λ_{111} is the saturation magnetostriction along the $\langle 111 \rangle$ directions. The spontaneous strains along these axes when the material cools through its Curie point are clearly $e_{111} = (3/2)\lambda_{111}$ and $e_{100} = (3/2)\lambda_{100}$.

In this equation $\beta_1, \beta_2, \beta_3$ are the direction cosines, relative to the field direction, in which the saturation magnetostriction is measured, while $\alpha_1, \alpha_2, \alpha_3$ are the direction cosines, relative to the field direction, of the axis along which the magnetic moments are saturated. These equations of course only apply to the magnetostriction within a domain. The anisotropic magnetostriction equations for cubic and other crystal classes have been given by Lee [19].

Usually we will wish to know the saturation magnetostriction in the same

Table 5.2 Magnetostriction coefficients of cubic materials

Material	$\lambda_{100}(10^{-6})$	$\lambda_{111}(10^{-6})$
Iron	21	-21
Nickel	-46	-24
Terfenol	90	1600

direction as the field in which case the above expression reduces to

$$\lambda_s = \lambda_{100} + 3(\lambda_{111} - \lambda_{100})(\alpha_1^2 \alpha_2^2 + \alpha_2^2 \alpha_3^2 + \alpha_3^2 \alpha_1^2).$$

Once again as in the case of isotropic materials the two constants λ_{100} and λ_{111} can be determined by saturating the magnetostriction along the axis of interest and then at right angles. The difference in strain remains $(3/2)\lambda_{100}$ and $(3/2)\lambda_{111}$ depending on the axis chosen.

The behaviour of the magnetostriction of an assembly of domains, a polycrystal for example, can only be calculated by averaging the effects. This is not possible in general and therefore it is assumed that the material consists of a large number of domains and hence that the strain is uniform in all directions. In a randomly oriented polycrystalline cubic material (i.e. one in which there is no preferred grain orientation) this formula simplifies further to become,

$$\lambda_s = \frac{2}{5}\lambda_{100} + \frac{3}{5}\lambda_{111}.$$

5.3.6 Field-induced magnetostriction

How does the length of a ferromagnet change with magnetic field?

The field-induced magnetostriction is the variation of λ with \mathbf{H} or \mathbf{B} and is often the most interesting feature of the magnetostrictive properties to the materials scientist. However the variations $\lambda(\mathbf{H})$ or $\lambda(\mathbf{B})$ are very structure sensitive so that it is not possible to give any general formula for the relation of magnetostriction to field. This may at first seem strange when we have already been able to give equations for the saturation magnetostriction.

The magnetostrictions of polycrystalline iron, cobalt and nickel are shown in Fig. 5.7 which indicates some of the problems immediately, since for example the bulk magnetostriction of iron actually changes sign from positive to negative as \mathbf{H} or \mathbf{B} is increased. Lee [19] has reported on the magnetostriction curves of polycrystalline ferromagnets.

There is one case at least where a fairly simple solution occurs. If the magnetic field is applied in a direction perpendicular to the easy axis in a single crystal with uniaxial anisotropy, or perpendicular to the axis in which the moments have been completely aligned in a polycrystalline material such as nickel under extreme tension or terfenol under compression.

In this case magnetization takes place entirely by rotation of magnetization. So we may make the substitution

$$\mathbf{M} = \mathbf{M}_s \cos \theta,$$

which gives the magnetization along the field axis in terms of the angle θ which the saturation magnetization within the domains makes with this axis. The magnetostriction along the field axis is given by

$$\lambda = \frac{3}{2}\lambda_s \cos^2 \theta$$

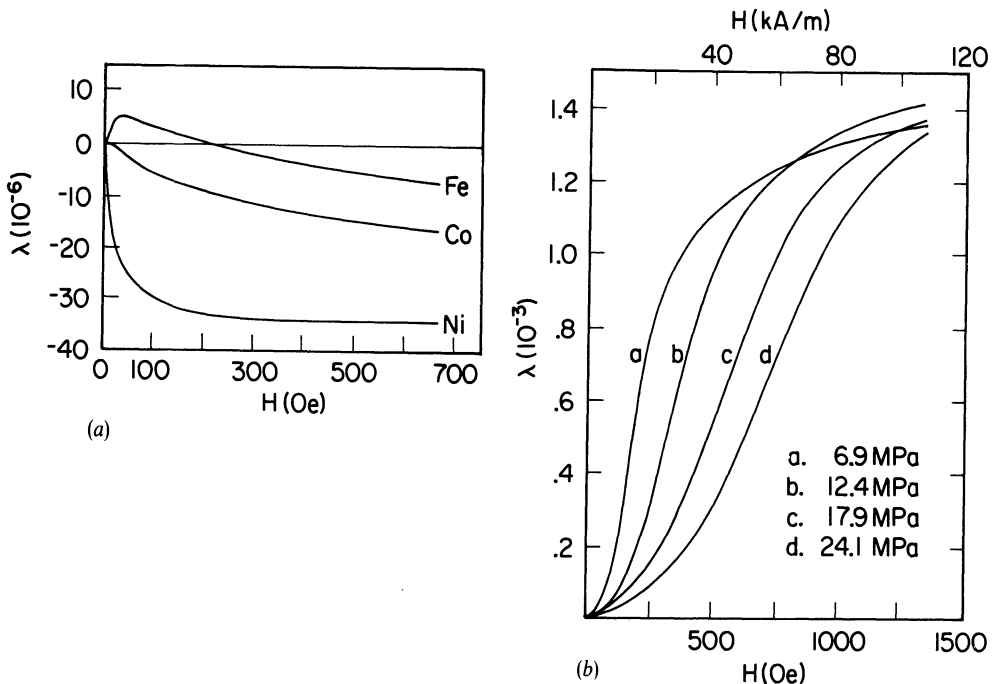


Fig. 5.7 Dependence of the bulk magnetostriction on applied magnetic field in: (a) iron, nickel and cobalt; and (b) a highly magnetostrictive rare earth–iron alloy $Tb_{0.27}Dy_{0.73}Fe_{1.95}$

and substituting for $\cos^2 \theta$ leaves

$$\lambda = (3/2)\lambda_s(M/M_s)^2$$

which gives the variation of the observed magnetostriction with magnetization M .

5.3.7 Transverse magnetostriction

When the length of a ferromagnet changes what happens to the cross section?

Between the demagnetized state and saturation magnetization the volume of a ferromagnet remains fairly constant (although there is a very small volume magnetostriction in most materials). Therefore there is a transverse magnetostriction of one half the longitudinal magnetostriction and opposite in sign.

$$\lambda_t = -\lambda/2.$$

REFERENCES

1. Frohlich, O. (1881) *Electrotech Z.*, **2**, 134.
2. Kennelly, A. E. (1891) *Trans. Am. IEE.*, **8**, 485.

3. Weiss, P. (1910) *J. Phys.*, **9**, 373.
4. Becker, R. and Doring, W. (1938) *Ferromagnetismus*, Springer, Berlin.
5. Mee, C. D. (1964) *The Physics of Magnetic Recording*, North Holland, Amsterdam.
6. Rayleigh, Lord (1887) *Phil. Mag.*, **23**, 225.
7. Bozorth, R. M. (1951) *Ferromagnetism*, Van Nostrand, New York.
8. Barkhausen, H. (1919) *Phys. Z.*, **29**, 401.
9. Schroeder, K. and McClure, J. C. (1976) The Barkhausen effect, *CRC Critical Reviews of Solid State Science*, **6**, 45.
10. Matzkanin, G. A., Beissner, R. E. and Teller, C. M. (1979) The Barkhausen effect and its application to NDE, SWRI Report No. NTIAC-79-2, Southwest Research Institute, San Antonio, Texas.
11. Lord, A. E. (1975) Acoustic emission, in *Physical Acoustics*, Vol. XI (ed. W. P. Mason and R. N. Thurston), Academic Press, New York.
12. Ono, K. and Shibata, M. (1980) *Materials Evaluation*, **38**, 55.
13. Kusanagi, H., Kimura, H. and Sasaki, H. (1979) *J. Appl. Phys.*, **50**, 1989.
14. Buttle, D. J., Scruby, C. B., Briggs, G. A. D. and Jakubovics, J. P. (1987) *Proc. Roy. Soc. Lond.*, **A414**, 469.
15. Joule, J. P. (1842) *Ann. Electr. Magn. Chem.*, **8**, 219.
16. Joule, J. P. (1847) *Phil. Mag.*, **30**, 76.
17. Kittel, C. (1987) *Introduction of Solid State Physics*, 6th edn, Wiley, p. 248, New York.
18. Lee, E. W. (1955) Magnetostriction and magnetomechanical effects, *Reports on Prog. in Phys.*, **18**, 184.
19. Lee, E. W. (1958) Magnetostriction curves of polycrystalline ferromagnets, *Proc. Phys. Soc.*, **72**, 249.

FURTHER READING

- Cullity, B. D. (1971) *Fundamentals of Magnetostriction*, *Int. J. Magnetism*, **1**, 323.
 Cullity, B. D. (1972) *Introduction to Magnetic Materials*, Addison-Wesley, Reading, Mass.
 Heck, C. (1974) *Magnetic Materials and their Applications*, Crane Russak & Co., New York, Ch. 4.

EXAMPLES AND EXERCISES

Example 5.1 Determination of Rayleigh coefficients at low fields. Using the results for the initial magnetization of iron given in Table 5.3, plot the initial magnetization curve. Estimate the extent of the Rayleigh region. Calculate the Rayleigh coefficients and use them to determine the remanence that would be observed if the field were reduced to zero after reaching a maximum value of (a) 10 A/m (b) 20 A/m. Find the hysteresis loss when the field is given one complete cycle at an amplitude of 20 A/m.

Example 5.2 Magnetostriction of terfenol without stress. In polycrystalline terfenol which is not subjected to stress and does not have a preferred orientation, the domains are aligned randomly. If $\lambda_{111} = 1600 \times 10^{-6}$ and $\lambda_{100} = 90 \times 10^{-6}$ calculate the saturation magnetostriction along the field direction on the basis of initial random alignment of domains.

For the same specimen of terfenol calculate the 'saturation magnetostriction' $\lambda_{\parallel} - \lambda_{\perp}$ obtained by applying a saturating field at right angles to a given direction

Table 5.3 Magnetic properties of annealed iron

H (A/m)	B (T)
0	0
5	0.0019
10	0.0042
15	0.0069
20	0.010
40	0.028
50	0.043
60	0.095
80	0.45
100	0.67
150	1.01
200	1.18
500	1.44
1000	1.58
10 000	1.72

and setting the strain at an arbitrary value of zero, then rotating the field into the direction of interest. How does this value of magnetostriction compare with the saturation magnetostriction obtained by the first method?

Example 5.3 Magnetostriction of terfenol under compressive load. By applying a uniaxial compressive stress to terfenol the moments can also be made to line up perpendicular to the stress axis. Using the saturation magnetostriction calculated above for the non-oriented terfenol determine how the magnetostriction of stressed terfenol varies with magnetization (assume the stress is sufficient to align all domains at right angles to the stress axis) and hence find the magnetostriction at $M = M_s/2$ and at $M = M_s$. How does this compare with $\lambda_{\parallel} - \lambda_{\perp}$ which was calculated in exercise 5.2?

Discuss how the magnetostriction along the field axis would be changed if instead of having a non-oriented sample we had one with the (111) directions aligned preferentially along the field axis.

6

Magnetic Domains

We now consider the organization of the magnetic moments within ferromagnets. Two questions arise: are the magnetic moments permanent or field induced, and are they randomly aligned or ordered? It is shown that the moments are permanent and are aligned parallel within volumes containing large numbers of atoms, but these ‘magnetic domains’ are still on the microscopic scale in most cases.

6.1 DEVELOPMENT OF DOMAIN THEORY

What microscopic theories are needed to account for the observed macroscopic properties of ferromagnets?

On the macroscopic scale the bulk magnetization \mathbf{M} is clearly field induced. On the microscopic scale we need to find how the magnetization varies within a ferromagnet. In the demagnetized state for example is the magnetization everywhere zero or are there large local values of magnetic moment which sum to zero on the macroscopic scale? If there are large local magnetic moments we need to find how these are arranged and what happens to them when subjected to a field.

6.1.1 Atomic magnetic moments

Do the atoms of a ferromagnet have permanent magnetic moments or are the moments induced by the magnetic field?

Since atoms are the units from which solids are composed it is reasonable to suppose that when a ferromagnetic solid is magnetized there is a net magnetic moment per atom. For example in Chapter 4 we have calculated the net magnetic moment per atom in saturated iron. There are two possible origins for the atomic magnetic moments in ferromagnets. The material could already have small atomic magnetic moments within the solid which are randomly aligned (or at least give a zero vector sum over the whole solid) in the demagnetized state but which became ordered (or aligned) under the action of a magnetic field. This was first suggested by Weber [1]. Alternatively the atomic magnetic moments may not exist at all in the demagnetized state but could be induced on the application of a magnetic field as suggested by Poisson [2].

The existence of saturation magnetization and remanence support the former idea, and in fact it has been established beyond doubt that in ferromagnets permanent magnetic moments exist on the atomic scale and that they do not rely on the presence of a field for their existence. The origin of the atomic moments was first suggested by Ampère [3] who with extraordinary insight, suggested that they were due to ‘electrical currents continually circulating within the atom’. This was some seventy-five years before J. J. Thomson discovered the electron and at a time when it was not known whether charge separation existed within an atom or even whether atoms existed.

We should note that both paramagnets and ferromagnets have permanent atomic magnetic moments. Next it is necessary to distinguish between them on a microscopic scale knowing that on the macroscopic scale the permeabilities of ferromagnets are much higher.

6.1.2 Magnetic order in ferromagnets

Are the ferromagnets already in an ordered state before a magnetic field is applied or is the order induced by the field?

Ewing [4] followed the earlier ideas of Weber in explaining the difference between a magnetized and demagnetized ferromagnet as due to the atomic moments (or ‘molecular magnets’ as they called them in those days) being randomly oriented in demagnetized iron but aligned in the magnetized material. Ewing was particularly interested in explaining hysteresis on the basis of interactions between the atomic dipole moments of the type envisaged by Weber. As we shall see this was inevitably to fail because he did not realize that the demagnetized iron was actually already in an ordered state with large numbers of atomic magnetic moments aligned locally in parallel.

6.1.3 Permeability of ferromagnets

Can the properties of ferromagnets be explained best by assuming that a magnetic field rearranges existing ordered-volume magnetic moments or by assuming that the field aligns disordered (randomly oriented) atomic magnetic moments?

One of the problems in the field of magnetism that needed to be addressed was the very large permeabilities and susceptibilities of ferromagnets. In their original state the bulk magnetization of ferromagnets is zero, but on application of a magnetic field they become ‘magnetically polarized’ that is they acquire a magnetization. However the magnetizations of ferromagnets are mostly orders of magnitude greater than the field strengths which produce them.

There are two possible explanations: either the atomic magnetic moments are randomly oriented on the interatomic scale and the field gradually aligns them as in the case of paramagnets. Alternatively, the moments could be aligned on the

interatomic scale but at some larger scale the magnetizations of whole aligned regions, known as domains, could be randomly aligned from one domain to the next.

The properties of ferromagnets can be explained if long-range magnetic order exists within the solid but the volumes, or domains, containing the magnetic moments are randomly aligned in the demagnetized state. Magnetization is then simply the process of rearranging these volumes so that their magnetizations are aligned parallel. The paramagnets, which also have permanent atomic magnetic moments, can then be distinguished from the ferromagnets because the paramagnets do not exhibit long-range order such as is found in ferromagnetic domains. In fact in paramagnets the atomic magnetic moments are randomly aligned in the absence of a field due to the thermal, or Boltzmann, energy.

6.1.4 Weiss domain theory

If the atomic magnetic moments are ordered then how do we explain the demagnetized state?

Some years after Ewing's work one of the most important advances in the understanding of ferromagnetism was made by Weiss in two papers in 1906 and 1907 [5, 6]. In these papers Weiss built on the earlier work of Ampère, Weber and Ewing and suggested the existence of magnetic domains in ferromagnets, in which the atomic magnetic moments were aligned parallel over much larger volumes of the solid than had previously been suspected. In these domains large numbers of atomic moments, typically 10^{12} to 10^{15} , are aligned parallel so that the magnetization within the domain is almost saturated. However the direction of alignment varies from domain to domain in a more or less random manner, although certain crystallographic axes are preferred by the magnetic moments, which in the absence of a magnetic field will align along one of these equivalent 'magnetic easy axes'.

The immediate consequences of this were (a) atomic magnetic moments were in permanent existence (Weber's hypothesis), (b) the atomic moments were ordered (aligned) even in the demagnetized state, (c) it was the domains only which were randomly aligned in the demagnetized state, and (d) the magnetization process consisted of reorienting the domains so that either more domains were aligned with the field, or the volumes of domains aligned with the field were greater than the volume of domains aligned against the field.

6.1.5 Weiss mean field theory

What is the underlying cause of the alignment of atomic magnetic moments?

If the atomic moments are aligned within the domains of ferromagnets it is necessary to explain this ordering and if possible to explain why when a

ferromagnet is heated up it eventually undergoes a transition to a paramagnet at the Curie temperature.

In order to explain these observations Weiss further developed the statistical thermodynamic ideas of Boltzmann and Langevin as they applied to magnetic materials. Some years previously Langevin [7] had produced a theory of paramagnetism based on classical Boltzmann statistics. Weiss used the Langevin model of paramagnetism and added an extra term, the so called Weiss mean field, which was in effect an interatomic interaction which caused neighbouring atomic magnetic moments to align parallel because the energy was lower if they did so.

In the original Weiss theory the mean (or ‘molecular’) field was proportional to the bulk magnetization \mathbf{M} so that

$$\mathbf{H}_e = \alpha \mathbf{M},$$

where α is the mean field constant. This can be proved to be equivalent to assuming that each atomic moment interacts equally with every other atomic moment within the solid. This was found to be a viable assumption in the paramagnetic phase because due to the homogeneous distribution of magnetic moment directions the local value of magnetization, obtained by considering a microscopic volume of the material surrounding a given atomic magnetic moment, is equal to the bulk magnetization.

However in the ferromagnetic phase the magnetization is locally inhomogeneous on a scale larger than the domain size due to the variation in the direction of magnetization from domain to domain. Therefore subsequent authors preferred to apply the idea of a Weiss mean field only within a domain, arguing that the interaction between the atomic moments decayed with distance and that therefore such an interaction was unlikely to extend beyond the domain. It is generally considered that the Weiss field is a good approximation to the real situation within a given domain because within the domain the magnetization is homogeneous and has a known value \mathbf{M}_s . So the interaction field which is responsible for the ordering of moments within domains can be expressed as

$$\mathbf{H}_e = \alpha \mathbf{M}_s,$$

where \mathbf{M}_s is the spontaneous magnetization within the domain which has been discussed in section 2.1.4; it is equal to the saturation magnetization at 0 K but decreases as the temperature is increased, becoming zero at the Curie point.

Subsequent models, such as the Ising model [8] applied to ferromagnets, have been based on interaction fields only between nearest neighbours. This gives rise to ordering of moments within a domain as shown in Fig. 6.1. When $\alpha > 0$ the ordering is parallel, leading to ferromagnetism. When $\alpha < 0$ the ordering is antiparallel leading to simple antiferromagnetism. At this state we should note that a number of different types of magnetic order are possible depending on the nature of the interaction parameter α . Some of these configurations are shown in Fig. 6.2.

In Chapter 9 we will discuss the Langevin and Weiss theories in detail, showing

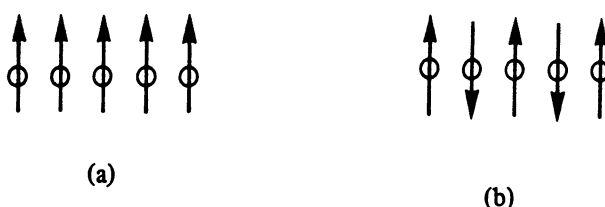


Fig. 6.1 Ordered arrangement of a linear chain of atomic magnetic moments when $\alpha > 0$ leading to ferromagnetism as shown in (a), and $\alpha < 0$ leading to simple antiferromagnetism, as shown in (b).

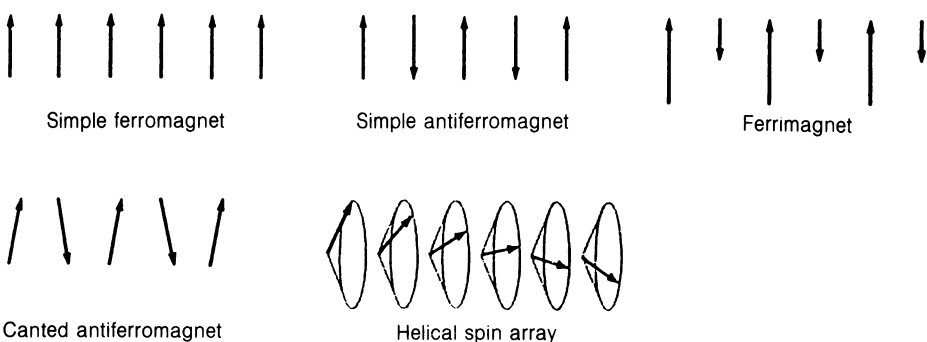


Fig. 6.2 Examples of different types of magnetic order using a linear array of localized moments. These include ferromagnetism, simple antiferromagnetism, ferrimagnetism and helical antiferromagnetism.

derivation of the equations and how the Curie temperature is determined by the mean field parameter. We will also leave the explanation of the Weiss mean field until later, although we should note in passing that it cannot be explained in classical terms and depends entirely on quantum mechanical considerations. In quantum mechanics it is known as the exchange interaction and we shall refer to it as such occasionally.

Example 6.1 The equivalent field strength of the Weiss mean field. Suppose the field experienced by any magnetic moment \mathbf{m}_i within a domain due to its interaction with any other moment \mathbf{m}_j is $\mathbf{H}_e = \alpha_{ij}\mathbf{m}_j$. (a) Find the field experienced by this moment as a result of its interactions with all other moments. (b) The energy of the moment as a result of this interaction. (c) If each moment interacts equally with all other moments within the domain show that this is equivalent

112 Magnetic domains

to a mean field. (d) Calculate the field strength if the mean field parameter in iron is $\alpha = 400$ in SI units ($= 400 \times 4\pi$ in CGS units).

If the interaction with one moment is

$$\mathbf{H}_e = \alpha_{ij} \mathbf{m}_j$$

then the interaction with all moments is simply the sum over the moments within the domain,

$$\mathbf{H}_e = \sum \alpha_{ij} \mathbf{m}_j$$

and the energy of the moment will be

$$\begin{aligned} E &= -\mu_0 \mathbf{m}_i \cdot \mathbf{H}_e \\ &= -\mu_0 \mathbf{m}_i \cdot \sum \alpha_{ij} \mathbf{m}_j. \end{aligned}$$

If the interactions with all moments are equal then all the α_{ij} are equal. Let these be α

$$\mathbf{H}_e = \alpha \sum \mathbf{m}_j$$

the vector sum over all the moments within a domain gives the spontaneous magnetization \mathbf{M}_s

$$\mathbf{H}_e = \alpha \mathbf{M}_s$$

which is equivalent to a mean field.

It is known that $\mathbf{M}_0 = 1.7 \times 10^6 \text{ A/m}$, and at room temperature the spontaneous magnetization \mathbf{M}_s in iron may be taken as almost equal to the saturation magnetization \mathbf{M}_0 . If $\alpha = 400$ in iron it follows that the mean field is

$$\begin{aligned} \mathbf{H}_e &= \alpha \mathbf{M}_s \\ &= (400)(1.7 \times 10^6) \text{ A/m} \\ &= 6.8 \times 10^8 \text{ A/m} \end{aligned}$$

which is equivalent to a magnetic induction of 855 tesla.

Notice in particular the size of this field. Remember that a standard laboratory electromagnet generates an induction of typically 2 tesla. The expected field based on simple classical dipole interactions between the moments in a solid is of the order of $8 \times 10^4 \text{ A/m}$ or equivalently 0.1 tesla. The exchange field is therefore several orders of magnitude greater than expected classically.

6.1.6 Energy states of different arrangements of moments

If bar magnets in a linear chain prefer to align antiparallel why do atomic magnetic moments align parallel?

Consider the two configurations of magnetic moments in Fig. 6.3. It can easily be shown that for $\alpha > 0$ that the configuration with all moments aligned parallel is a lower energy state than the configuration with one moment antiparallel.

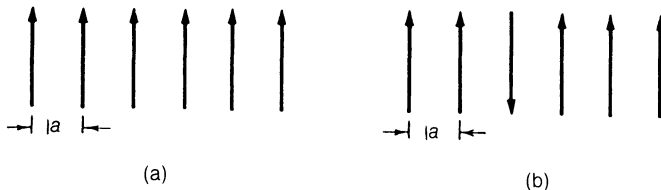


Fig. 6.3 Two possible configurations of a linear array of magnetic moments. When $\alpha > 0$ the parallel alignment is the ground state.

If we only consider the exchange energy of the six-moment system shown in Fig. 6.3 the energy of any moment \mathbf{m}_i is simply

$$E_i = -\mu_0 \mathbf{m}_i \cdot \sum \alpha_{ij} \mathbf{m}_j$$

with the mean field approximation

$$E_i = -\mu_0 \alpha \mathbf{m}_i \cdot \sum \mathbf{m}_j.$$

The total energy is therefore

$$E = -\mu_0 \alpha \sum \mathbf{m}_i \cdot \sum \mathbf{m}_j.$$

When all moments are parallel

$$\begin{aligned} E &= -\mu_0 \alpha (6\mathbf{m})(5\mathbf{m}) \\ &= -30 \mathbf{m}^2 \mu_0 \alpha. \end{aligned}$$

With one moment antiparallel

$$\begin{aligned} E &= -\mu_0 \alpha (5\mathbf{m}3\mathbf{m} - \mathbf{m}5\mathbf{m}) \\ &= -10 \mathbf{m}^2 \mu_0 \alpha. \end{aligned}$$

Therefore as a result of the positive exchange interaction the energy is lower when all moments are aligned parallel within the domain and hence the aligned state is preferred.

6.1.7 Early observational evidence of domains

If these magnetic domains exist how can we see them?

There were two important experimental observations in the years after Weiss' work which served to confirm the essential correctness of his theories. There have subsequently been innumerable observations of ferromagnetic domains, both direct and indirect. The first confirmation was the indirect detection of domains by the Barkhausen effect [9], in which the reorientation of domains caused discrete changes in magnetic induction within a ferromagnet which could be detected by suitable amplification of the signals from a search coil wound around the specimen. The Barkhausen effect leads to discontinuities in other bulk properties if they are

measured accurately enough. Recent discontinuities in magnetoresistance have been reported, for example [10], and of course acoustic emissions can be generated as discussed in section 5.2.2.

The second confirmation was by direct observations of domain patterns on the surfaces of ferromagnetic materials made by Bitter in [11]. He used a very fine magnetic powder suspended in a carrier liquid which was spread on the surface of the material. Patterns were observed in the particle accumulations when viewed under a microscope. The particles accumulate at positions where the magnetic field gradient is greatest. This occurs where domain walls intersect the surface. It seems likely that the idea of doing this had come from the magnetic particle inspection techniques of Hoke and DeForest [12] which had been developed a few years before.

More recently colloidal solutions of ferromagnetic particles in a carrier liquid ('ferrofluids') have been used. The particles are usually Fe_3O_4 and the commercially available ferrofluids usually have to be diluted for the best observation of domains. In order to produce optimum surface conditions for domain observations the surface of the material should be electropolished to remove strains which would otherwise reduce the size of domains. Some Bitter patterns produced by magnetic colloids such as ferrofluid on the surface of iron from the work of Williams, Bozorth and Shockley [13] are shown in Fig. 6.4.

Although the Bitter method is a mature technique, and consequently not many new developments are reported now, one new variation of this method has evolved

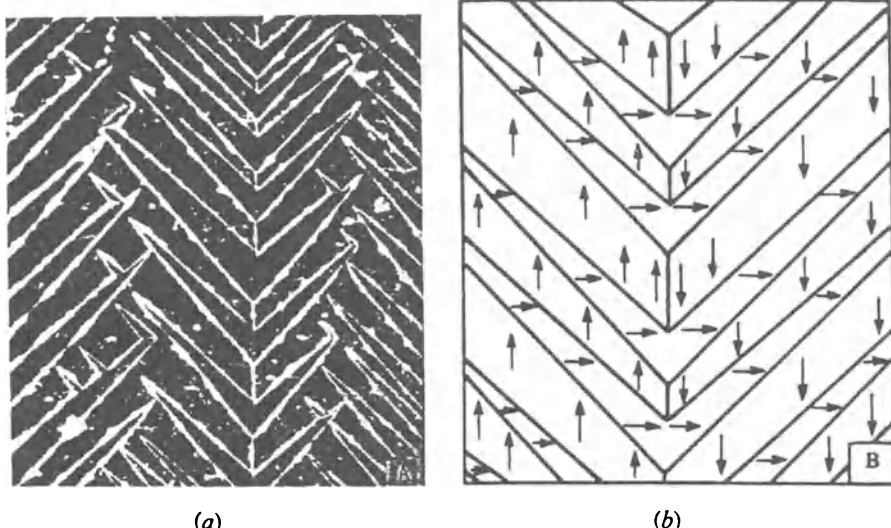


Fig. 6.4 (a) Magnetic domains in the surface of iron observed using the Bitter method (magnification $\times 120$), after Williams *et al.* [13], (b) interpretation of domain pattern in (a) showing the direction of the spontaneous magnetizations within the domains.

recently [14]. In this the conventional Bitter colloid pattern was observed in polarized light in order to study stray field-induced birefringence on the surfaces of magnetic materials. Results on garnets were reported.

6.1.8 Techniques for domain observation

What other methods are available for looking at domains?

Several other techniques are regularly used for the observation of domains. Two of these are related optical methods the Faraday and Kerr effects, in which the axis of polarization of a linearly polarized light beam is rotated by the action of a magnetic field.

The rotation of the direction of polarization of a polarized light beam reflected from the surface of a magnetic material is known as the Kerr effect [15]. The angle of rotation of the axis of polarization is dependent upon the magnitude and direction of the magnetization \mathbf{M} at the surface of the material. This is determined by the domain configuration in the surface and hence an image of the domain structure at the surface can be formed. One of the difficulties with the Kerr effect is that the angle of rotation is usually very small so that there is little contrast between the different domains.

There are three types of Kerr effect which can be observed depending on the relative orientation of the magnetization with respect to the plane of incidence of the light beam and the plane of the reflecting surface. These are known as the polar, longitudinal and transverse Kerr effects [16] and are shown in Fig. 6.5. In the polar Kerr effect, Fig. 6.5(a), the domain magnetization \mathbf{M} has a component perpendicular to the surface of the specimen. In this case the angle of rotation is largest and may be up to 20 minutes of arc. However the demagnetizing energy strongly favours the alignment of magnetization in the plane of the surface, so unless there is sufficient anisotropy to maintain a component of \mathbf{M} perpendicular to the surface this method can not be used. In the longitudinal Kerr effect, Fig. 6.5(b), the domain magnetization \mathbf{M} lies in the plane of incidence and also in the plane of the surface. In this case the rotation of the direction of polarization is much smaller, typically being up to 4 minutes of arc. The maximum rotation in the longitudinal Kerr effect is obtained at an angle of incidence of 60°. In the transverse Kerr effect, Fig. 6.5(c), \mathbf{M} lies in the surface plane but is perpendicular to the plane of incidence. This leads to an effective rotation of the direction of polarization, as described originally by Ingersoll [17]. This is comparable in magnitude to the rotation observed in the longitudinal Kerr effect.

Hubert and coworkers [18] have developed a new technique based on the Kerr effect which uses digital image processing based on a combination of longitudinal and transverse Kerr effect measurements. This enables quantitative determination of the magnetization and its direction in the domain patterns of soft magnetic materials.

The Faraday effect [19], which is less useful for domain observations, is similar

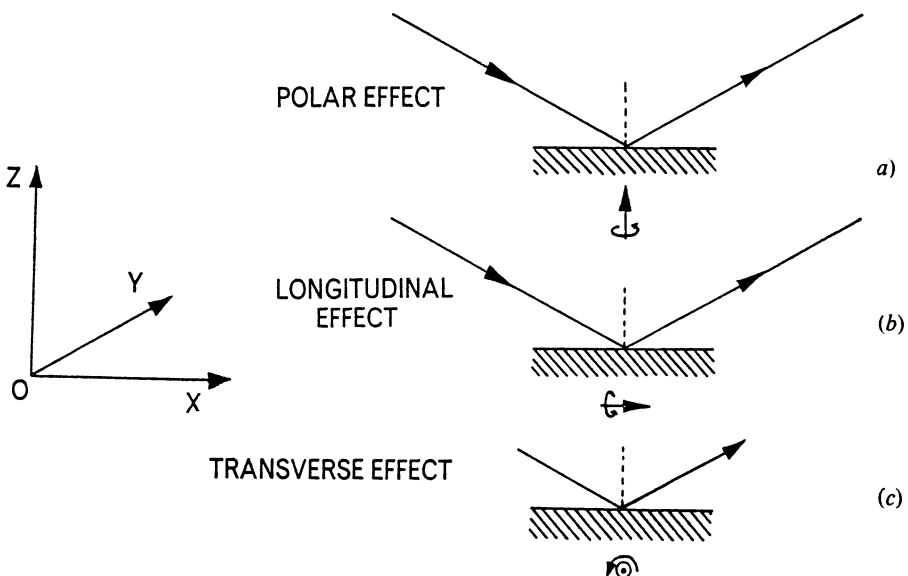


Fig. 6.5 Arrangement for polar, longitudinal and transverse Kerr effect observation of surface domain structures showing the relative orientation of the magnetization \mathbf{M} with respect to the incident linearly polarized light beam. The plane of incidence is the X - Z plane and the surface is in the X - Y plane.

except that the rotation of the axis of polarization is caused during transmission of a polarized light beam through a ferromagnetic solid. This can therefore only be applied to a thin transparent sample of a ferromagnetic material and is hence restricted to thin slices of ferromagnetic oxide or to metal films. In both cases the resulting beam is analysed using a second polarizing filter which then reveals the location of various domains as either light or dark regions in the polarized image.

A combination of magneto-optic Faraday and Kerr effects with the Bitter pattern technique has been reported by Hartmann [20]. This method provides a high contrast image of the surface domain pattern and can be used for both transparent and opaque magnetic materials. It is known as the interference contrast colloid technique.

The most recent development in the general area of magneto optic methods for domain observations is the laser magneto-optic microscope (LAMOM) of Argyle and Herman [21]. This is a highly sophisticated application of the Kerr effect which has been used for domain studies in read and write heads for magnetic recording devices [22].

Another method of domain observation is transmission electron microscopy, TEM [23], also known as Lorentz microscopy, in which the specimens are usually in the form of thin films. The transmitted electrons are deflected by the local magnetic field gradients in the material and this can be used to produce an image of the domain structure [24, 25]. The angular deflection of the electrons in

ferromagnetic materials such as iron is typically 0.01° . In order to obtain images normal bright-field imaging conditions cannot be used. Instead the image must be either under- or over-focused, since as the focus is changed the images of domains with different magnetizations move in different directions. The domain walls then either appear as dark or bright lines. The TEM pictures obtained under these conditions reveal only the domain walls.

The force on an electron as it passes through the material is

$$\mathbf{F} = -\mu_0 e \mathbf{v} \times \mathbf{M},$$

where \mathbf{M} is the local magnetization and \mathbf{v} is the velocity. For 100 keV electrons the maximum thickness of the ferromagnetic material that can usefully be observed is about 200 nm. This method is capable of a spatial resolution of 5 nm however one problem is that the electron beam uses a strong magnetic field to focus it and therefore a ferromagnetic specimen cannot be placed in the usual location in the microscope without some magnetic shielding, otherwise the domain structure will be disturbed. An alternative is to move the specimen from the normal position inside the objective lens.

Scanning electron microscopy (SEM) can also be used for domain imaging [26]. This has the added advantage over TEM that it can be used to image domains in thick specimens. Two methods are used in SEM, one which depends on the deflection of incident electrons after they enter the material, so that the number of backscattered electrons at a given angle is dependent on the direction of magnetization within a domain [27]. The second method depends on the deflection of secondary electrons by stray magnetic fields near the specimen surface [28].

X-ray topography is another technique of domain imaging [29]. It is well known that the diffraction of X-rays by a solid is dependent on the lattice spacing. In ferromagnets because of spontaneous magnetostriction the lattice parameter is dependent upon the direction of magnetization within the domain. This means that domains with magnetic moments aligned at angles other than 180° can be distinguished on the basis of Bragg diffraction of X-rays. This method can be used on thick specimens but the diffraction of X-rays is affected by dislocations and grain boundaries and therefore the method is best suited to fairly pure single-crystal materials with few dislocations or other defects.

Another method which has been reported in recent years is neutron diffraction topography [30]. The neutron carries a magnetic moment but no charge and therefore can be affected by a magnetic field or the magnetization within a domain. In this method a beam of polarized neutrons passes through a specimen and the angle of rotation of polarization is detected. The results are then used to reconstruct an image of the domain pattern in the material.

A very recent technique for imaging the domains is the atomic force method. At this time there is little information available although there have been brief reports in conference proceedings [31, 32].

6.2 ENERGY CONSIDERATIONS AND DOMAIN PATTERNS

6.2.1 Existence of domains as a result of energy minimization

Why do domains exist at all? Surely the moments should simply be aligned throughout the solid?

Since Weiss has shown that there exists an interaction field between the atomic moments within a ferromagnet which causes alignment of the magnetic moments, we are left once again with the question why a ferromagnet is not spontaneously magnetized, or if you wish, why the domains themselves are not aligned throughout the whole volume of the solid.

Clearly Weiss, in postulating the existence of domains, had sought to provide an empirical explanation of why the mean field did not lead to spontaneous magnetization of the material. It was left to Landau and Lifschitz in 1935 [33] to show that the existence of domains is a consequence of energy minimization. A single domain specimen has associated with it a large magnetostatic energy, but the breakup of the magnetization into localized regions (domains), providing for flux closure at the ends of the specimen, reduces the magnetostatic energy. Providing that the decrease in magnetostatic energy is greater than the energy needed to form magnetic domain walls then multi-domain specimens will arise.

6.2.2 Magnetostatic energy of single-domain specimens

What is the self energy of a single-domain particle?

The energy per unit volume of a dipole of magnetization \mathbf{M} in a magnetic field \mathbf{H} is given by

$$E = -\mu_0 \int \mathbf{H} \cdot d\mathbf{M},$$

as given earlier in section 1.2.4. When it is subjected only to its own demagnetizing field \mathbf{H}_d , which is of course generated by \mathbf{M} anyway, we can put $\mathbf{H}_d = -N_d \mathbf{M}$ in the integral where N_d is the demagnetizing factor so that the energy becomes

$$\begin{aligned} E &= -\mu_0 N_d \int \mathbf{M} \cdot d\mathbf{M} \\ E &= \frac{\mu_0}{2} N_d M^2. \end{aligned}$$

The calculation of the energy of a multi-domain specimen is more complex and we shall consider it later, but we can note immediately that if \mathbf{M} can be reduced by the emergence of domains the magnetostatic self energy will be reduced. The size of domains is determined by another factor which we have not considered yet: the domain wall energy.

6.2.3 Domain patterns and configurations

How do the domains arise from a single-domain specimen as the magnetic field is reduced?

Many direct observations of domain patterns have been made by Bitter pattern techniques or by other methods such as the magneto-optic Kerr and Faraday effects. Figure 6.6 shows diagrammatically the emergence of domains as a sample which is originally in the saturated condition is demagnetized. The lower diagram shows a closure domain at the end of a single crystal of iron. Closure domains usually emerge fairly early in the demagnetizing process since they provide return paths for the magnetic flux within the solid. They are nucleated by defects including the boundary of the material. They are also usually the last domains to be swept out at higher fields.

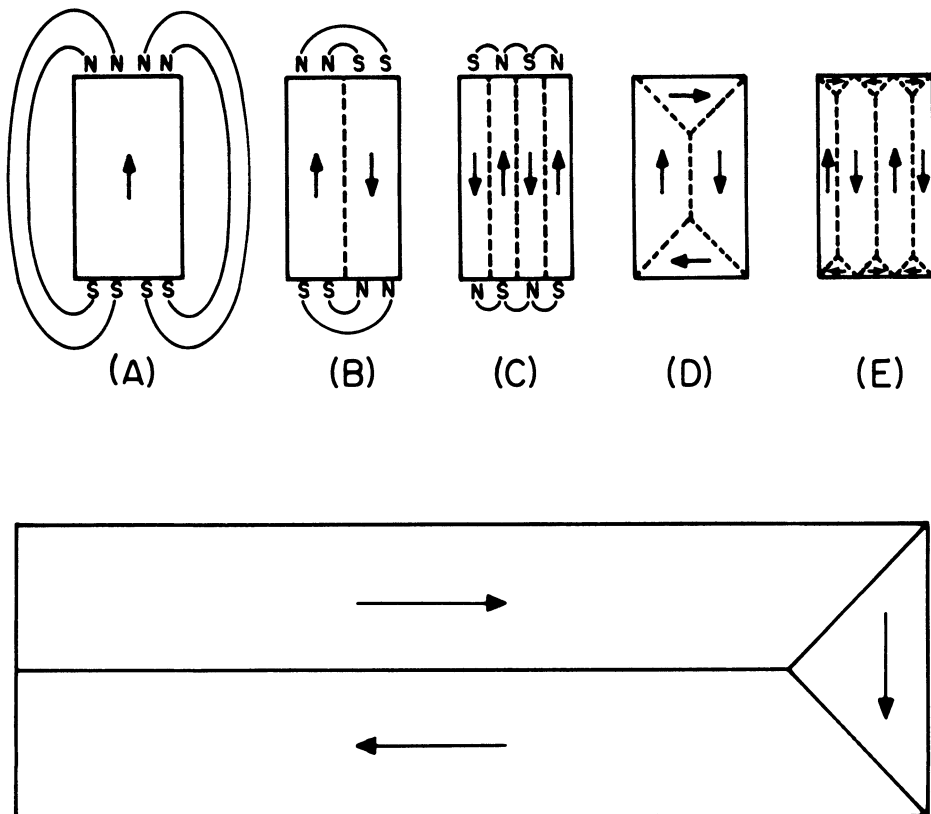


Fig. 6.6 Changing domain patterns as a sample of single-crystal iron is demagnetized (after Coleman, Scott and Isin).

6.2.4 Magnetization process in terms of domain theory

What changes occur within domains as a magnetic field is applied and gradually increased?

Since according to the domain theory the atomic magnetic moments are ordered even in the demagnetized state in a ferromagnet, the difference between the demagnetized state and the magnetized state must be due to the configuration of the domains.

When a magnetic field is applied to a demagnetized ferromagnetic material the changes in magnetic induction B when traced on the B, H plane generate the initial magnetization curve. At low fields the first domain process occurs which is a growth of domains which are aligned favourably with respect to the field according to the minimization of the field energy $E = -\mu_0 M_s \cdot H$ and a consequent reduction

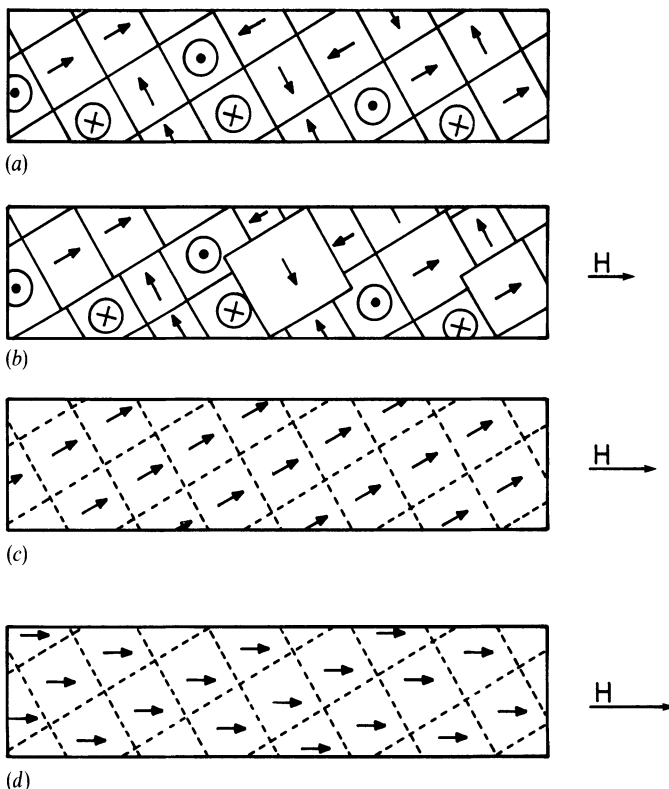


Fig. 6.7 Domain processes occurring as a material is magnetized to saturation; from the demagnetized state (a) to partial magnetization (b) by domain wall movement; from partial magnetization to the knee of the magnetization curve (c) by irreversible rotation of domain magnetization, from the knee of the magnetization curve to technical saturation (d) by reversible rotation.

in size of domains which are aligned in directions opposing the field, as shown in Fig. 6.7.

At moderate field strengths a second mechanism becomes significant; this is domain rotation, in which the atomic magnetic moments within an unfavourably aligned domain overcome the anisotropy energy and suddenly rotate from their original direction of magnetization into one of the crystallographic 'easy' axes which is nearest to the field direction.

The final domain process which occurs at high fields is coherent rotation. In this process the magnetic moments, which are all aligned along the preferred magnetic crystallographic easy axes lying close to the field direction, are gradually rotated into the field direction as the magnitude of the field is increased. This results in a single-domain sample.

6.2.5 Technical saturation magnetization

Why is the magnetization within the domains not equal in magnitude to the saturation magnetization?

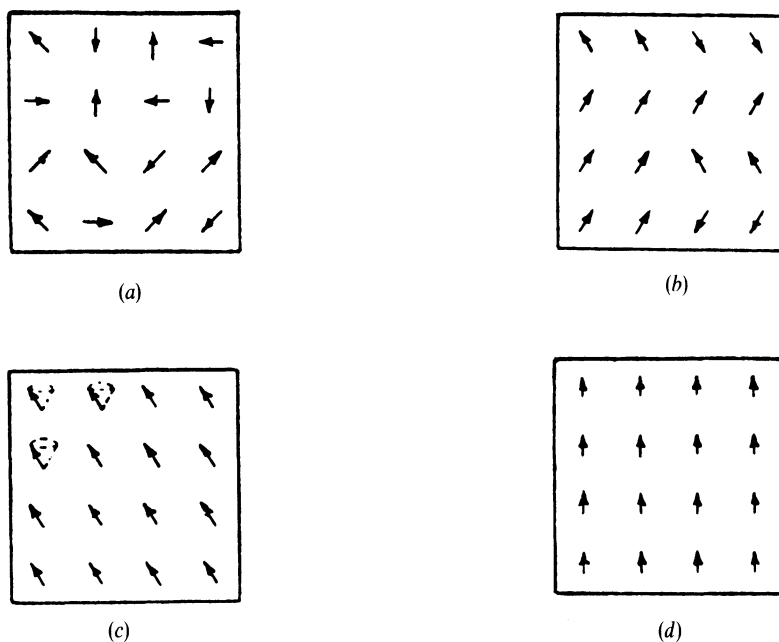


Fig. 6.8 Alignment of individual magnetic moments within a domain at various temperatures: (a) above the Curie point showing random alignment; (b) below the Curie point; (c) at low temperatures in which the magnetic moments precess about the field direction in low-level excited states; and (d) perfect alignment at 0 K where there is no thermal energy for precession.

122 Magnetic domains

When all domains have been aligned with their spontaneous magnetization vectors parallel to the field the material consists of a single magnetic domain and is said to have reached technical saturation magnetization. If the magnetic field is increased further it is noticed however that the magnetization does continue to increase very slowly. This is due to an increase in the spontaneous magnetization M_s within the domain as the atomic magnetic moments within the single domain which are not perfectly aligned with the field because the thermal activation, are brought into complete alignment.

The spontaneous magnetization is temperature dependent as we have noted earlier. At 0 K it is equal to the saturation magnetization but decays to zero at the Curie point. At temperatures above 0 K the individual magnetic moments have thermal energy which causes them to precess about the field direction as shown in Fig. 6.8. The precession becomes greater as the temperature increases. It is the precession which causes the spontaneous magnetization to be smaller than the saturation magnetization. Ultimately when all of the magnetic moments within the domain are completely aligned parallel due to a very high magnetic field the magnetization reaches M_0 .

6.2.6 Domain rotation and anisotropy

How does anisotropy affect the ability of domains to change the direction of their magnetization?

Although the domain growth process is not much affected by anisotropy, both the incoherent (irreversible) rotation and coherent (reversible) rotation are determined principally by the magnetocrystalline anisotropy. The rotation of the domains can be considered as a competition between the anisotropy energy $E_a(\theta, \phi)$ and the field energy E_H giving a total energy E_{tot} of

$$E_{\text{tot}} = E_a(\theta, \phi) + E_H$$

where

$$E_H = -\mu_0 \mathbf{M}_s \cdot \mathbf{H}.$$

\mathbf{M}_s is the magnetization within a domain, which is often replaced by the saturation magnetization M_0 of the material for the purpose of calculation.

6.2.7 Hexagonal anisotropy

What is the simplest representation of hexagonal (i.e. uniaxial) anisotropy?

In this case the anisotropy can be represented by the one-constant approximation

$$E_a = K_{u1} \sin^2 \phi,$$

where ϕ is the angle of the magnetization with respect to the unique axis, which for $K > 0$ is the easy axis, while for $K < 0$ it is the hard axis. In the case of single-crystal cobalt which is hexagonal $K_{u1} = 4.1 \times 10^5 \text{ J/m}^3$.

Example 6.2 Anisotropy 'field'. Calculate the anisotropy field for a cobalt crystal whose magnetization is close to the hexagonal axis. Use $M_s = M_0 = 1.42 \times 10^6 \text{ A/m}$ and $K_{u1} = 4.1 \times 10^5 \text{ J/m}^3$. Assume that for small angles $E_a = K_{u1}\phi^2$ and that $E_H = \text{constant} + (1/2)\mu_0 H\phi^2$.

The anisotropy energy for a uniaxial material such as cobalt is given by

$$E_a = K_{u1} \sin^2 \phi$$

and for small angles ϕ we can put $\sin^2 \phi \approx \phi^2$,

$$E_a = K_{u1} \phi^2.$$

If a magnetic field is applied along the unique axis then the field energy is given by,

$$E_H = -\mu_0 M_s H \cos \phi$$

and for small angles ϕ , $\cos \phi = 1 - \phi^2/2$

$$E_H = -\mu_0 M_s H (1 - \phi^2/2).$$

Removing the constant term, which has no bearing on the equilibrium condition

$$E_H = \frac{\mu_0 M_s H \phi^2}{2}.$$

Equating these energies will give the magnetic field along the unique axis which is equivalent to the anisotropy

$$K_{u1} = \frac{\mu_0 M_s H}{2}$$

and hence

$$H = \frac{2K_{u1}}{\mu_0 M_s}.$$

Substituting in the values for cobalt

$$H = \frac{(8.2 \times 10^5)}{(4\pi \times 10^{-7})(1.42 \times 10^6)}$$

$$H = 4.6 \times 10^5 \text{ A/m.}$$

6.2.8 Cubic anisotropy

What is the simplest representation of cubic anisotropy?

In the case of cubic anisotropy a one-constant anisotropy equation can also be used as a first approximation

$$E_a = K_1 (\cos^2 \theta_1 \cos^2 \theta_2 + \cos^2 \theta_2 \cos^2 \theta_3 + \cos^2 \theta_3 \cos^2 \theta_1),$$

where θ_1 , θ_2 , θ_3 are angles which the magnetization makes relative to the three crystal axes.

Table 6.1 Anisotropy constants for various ferromagnetic materials

<i>Material</i>		K_1	K_{u1} (10^5 J/m^3)	K_2	K_{u2}
Iron	Cubic	0.480	—	0.050	—
Nickel	Cubic	-0.045	—	0.023	—
Cobalt	Hexagonal	—	4.1	—	1.0
SmCo_5	Hexagonal	—	1100	—	—

So, for example, if we consider the anisotropy in, say, the (001) plane only, we will have $\theta_3 = \pi/2$, and consequently $\cos\theta_3 = 0$

$$E_{(001)} = K_1(\cos^2\theta_1 \cos^2\theta_2).$$

Once we have established that we are only considering moments in this plane, $\theta_1 = 90^\circ - \theta_2$

$$E_{(001)} = (K_1/4)\sin^2 2\theta,$$

where now $\theta = 0$ is the direction of the magnetic easy axis within the plane (001) when $K_1 > 0$, that is the $\langle 100 \rangle$ directions, as in the case of iron for which $K_1 = 4.8 \times 10^4 \text{ J/m}^3$. When $K_1 < 0$ the magnetic easy axes are $\langle 111 \rangle$ as in nickel for which $K_1 = -4.5 \times 10^3 \text{ J/m}^3$.

REFERENCES

1. Weber, W. (1852) *Pogg. Ann.*, **LXXXVII**, 167.
2. Poisson, S. D. (1893) in *Magnetic Induction in Iron and Other Metals* (ed. J. A. Ewing), Electrician Publishing Company, London, p. 282.
3. Ampère, A. M. (1827) *Theorie Mathematique des Phenomenes Electro-dynamiques Uniquelement Deduite de l'Experience*, Reprinted by Blanchard, Paris (1958).
4. Ewing, J. A. (1893) *Magnetic Induction in Iron and Other Metals*, The Electrician Publishing Company, London.
5. Weiss, P. (1906) *Compt. Rend.*, **143**, 1136.
6. Weiss, P. (1907) *J. Phys.*, **6**, 661.
7. Langevin, P. (1905) *Ann. Chem. et Phys.*, **5**, 70.
8. Ising, E. (1925) *Z. Phys.*, **31**, 253.
9. Barkhausen, H. (1919) *Physik Z.*, **20**, 401.
10. Tsang, C. and Decker, S. K. (1981) *J. Appl. Phys.*, **52**, 2465.
11. Bitter, F. (1931) *Phys. Rev.*, **38**, 1903.
12. Betz, C. E. (1967) *Principles of Magnetic Particle Testing*, Magnaflux Corporation, Chicago, p. 48.
13. Williams, H. J., Bozorth, R. M. and Shockley, W. (1949) *Phys. Rev.*, **75**, 155.
14. Jones, G. A. and Puchalska, I. (1979) *Phys. Stat. Sol.*, **A51**, 549.
15. Kerr, J. (1876) *Rep. Brit. Assoc.*, **5**.
16. Carey, R. and Isaac, E. D. (1966) *Magnetic Domains and Techniques for their Observation*, Academic Press, Ch. 5. London.
17. Ingersoll, L. P. (1912) *Phys. Rev.*, **35**, 315.

18. Rave, W. Schafer, R. and Hubert, A. (1987) *J. Mag. Mag. Mater.*, **65**, 7.
19. Faraday, M. (1846) *Phil. Trans. Roy. Soc.*, **136**, 1.
20. Hartmann, U. (1987) *Appl. Phys. Letts.*, **51**, 374.
21. Argyle, B. and Herman, D. (1986) *IEEE Trans. Mag.*, **MAG-22**, 772.
22. Herman, D. and Argyle, B. (1987) *J. Appl. Phys.*, **61**, 4200.
23. Hale, M. E., Fuller, H. W. and Rubinstein, H. (1959) *J. Appl. Phys.*, **30**, 789, and (1960) *J. Appl. Phys.*, **31**, 238.
24. Hwang, C., Laughlin, D. E., Mitchell, P. V., Layadi, A., Mountfield, K., Snyder, J. E. and Artman, J. O. (1986) *J. Mag. Mag. Mater.*, **54-7**, 1676.
25. Lodder, J. C. (1983) *Thin Solid Films*, **101**, 61.
26. Mayer, L. (1957) *J. Appl. Phys.*, **28**, 975.
27. Koike, K., Matsuyama, H., Todokoro, H. and Hayakawa, K. (1985) *Jap. J. Appl. Phys.*, **24**, 1078.
28. Unguris, J., Hembree, G., Celiotta, R. J. and Pierce, D. T. (1986) *J. Mag. Mag. Mater.*, **54-7**, 1629.
29. Polcarova, M. and Lang, A. R. (1962) *Appl. Phys. Letts.*, **1**, 13.
30. Baruchel, J., Palmer, S. B. and Schlenker, M. (1981) *J. de Phys.*, **42**, 1279.
31. Saenz, J. J. and Garcia, N. (1987) *J. Appl. Phys.*, **62**, 4293.
32. Wickramsinghe, H. K. and Martin, Y. (1988) *J. Appl. Phys.*, **63**, 2948.
33. Landau, L. D. and Lifschitz, E. M. (1935) *Physik Z. Sowjetunion*, **8**, 153.

FURTHER READING

- Argyle, B. and Herman, D. (1986) *IEEE Trans. Mag.*, **MAG-22**, 772.
 Carey, R. and Isaac, E. D. (1966) *Magnetic Domains and Techniques for their Observation*, Academic Press, London.
 Craik, D. J. and Tebble, R. S. (1965) *Ferromagnetism and Ferromagnetic Domains*, North Holland, Amsterdam.
 Crangle, J. (1977) *The Magnetic Properties of Solids*, Arnold, London, Ch. 6.
 Cullity, B. D. (1972) *Introduction to Magnetic Materials*, Addison-Wesley, Reading, Mass., Ch. 7.
 Kittel, C. and Galt, J. K. (1956) Ferromagnetic domains, *Solid State Physics*, **3**, 437.

EXAMPLES AND EXERCISES

Example 6.3 Effects of anisotropy on rotation of magnetization. Derive an expression for the magnetization of a specimen with cubic anisotropy when a field is applied along the (110) direction and the easy axes are the (100) directions. You may assume that the material is a perfect single crystal so that the domain wall motion all occurs at negligibly small fields, leaving the magnetizations within domains aligned along either of the (100) directions closest to the field direction. Also you may use the one-constant approximation for the anisotropy.

Example 6.4 Critical fields as determined by anisotropy. A magnetic field is applied in the base plane of cobalt. The easy direction is the unique axis. Using a one-constant model for the anisotropy with $K_{u1} = 4.1 \times 10^5 \text{ J/m}^3$ and $M_s = 1.42 \times 10^6 \text{ A/m}$ calculate the field needed to rotate the magnetic moments (a) into the base plane (i.e. perpendicular to the unique axis) and (b) 45° from the hexagonal axis.

126 Magnetic domains

Example 6.5 Stress-induced anisotropy. If the saturation magnetostriction of a randomly oriented rod of polycrystalline terfenol is $\lambda_s = 1067 \times 10^{-6}$, and assuming the anisotropy constant is $K_1 = -2 \times 10^4 \text{ J/m}^3$, *determine the stress needed completely to align the moments in the easy plane perpendicular to the stress.

You may use the one-constant approximation to the cubic anisotropy and since the material has no preferred orientation in the bulk sense, you may use the expression $E_\sigma = -(3/2)\lambda_s\sigma \cos^2 \theta$ for the stress-induced anisotropy, where σ is the stress and θ is the angle from the stress axis.

*The anisotropy constant of this alloy varies significantly with temperature and alloy composition. Therefore this value, although in the correct range, should not be assumed to be generally valid for terfenol.

Domain Walls

In this chapter we shall investigate the local magnetic properties in the vicinity of domain boundaries. These regions are called domain walls and have properties which are very different from the rest of the domain. Most of the magnetic changes under the action of weak and moderate magnetic fields occur at the domain walls and hence an understanding of domain-wall behaviour is essential to describing the magnetizing process.

7.1 PROPERTIES OF DOMAIN BOUNDARIES

How do the magnetic moments behave in the domain boundaries?

Once we have accepted the idea of domains within ferromagnets there arises the question of how the moments change direction in the vicinity of the domain

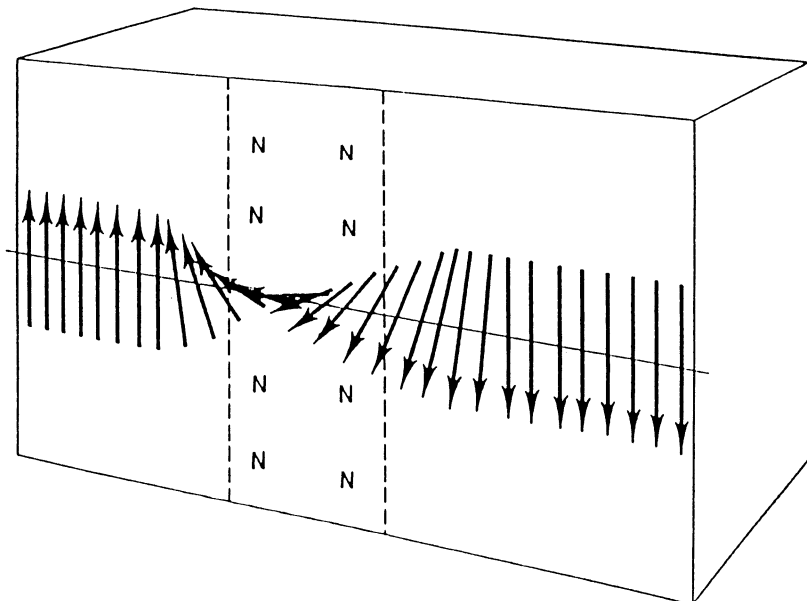


Fig. 7.1 Alignment of individual magnetic moments within a 180° domain wall, after Kittel (1949).

boundary. There are two possibilities, either the domain boundary is infinitesimal in width with nearest-neighbour moments belonging either to one domain or the other. Alternatively there could be a transition region in which the magnetic moments realign between the domains and therefore belong to neither domain, as for example in Fig. 7.1.

7.1.1 Bloch walls

How thick are the domain walls?

The existence of these transition layers between domains, in which the magnetic moments undergo a reorientation, was first suggested by Bloch [1]. The transition layers are commonly referred to as domain walls or Bloch walls, although we should note immediately that not all domain walls are necessarily Bloch walls. The total angular displacement across a domain wall is often 180° or 90° , particularly in cubic materials because of the anisotropy and, as we shall see, the change in direction of the moments takes place gradually over many atomic planes.

7.1.2 Domain wall energy

Is there any additional energy associated with the domain wall?

We may define the domain wall energy most conveniently as the difference in energy of the magnetic moments when they are part of the wall and when they are within the main body of the domain. This is usually expressed as the energy per unit area of the wall.

It is found by considering the changes in energy of the moments in the domain wall caused by Weiss-type interaction coupling between the atomic magnetic moments (or exchange interaction energy as it is now known because of its quantum mechanical origin) and the anisotropy. The anisotropy tends to make the domain walls thinner because anisotropy energy is lowest with all moments aligned along crystallographically equivalent axes. The exchange energy tends to make the walls thicker since the exchange energy in a ferromagnet is minimized when neighbouring moments are aligned parallel.

Exchange energy

If we consider only the interactions between the magnetic moments these give rise to the interaction or exchange energy

$$E_{\text{ex}} = -\mu_0 \mathbf{m} \cdot \mathbf{H}_e,$$

where \mathbf{H}_e is the interaction field. In the Weiss mean field model we have said that \mathbf{H}_e is proportional to the magnetization within the domain, that is \mathbf{M}_s , which at

temperatures well below the Curie temperature is almost equal to M_0 , consequently

$$H_e = \alpha M_s$$

where α is the mean field parameter. If we consider this in terms of an interaction with the individual magnetic moments \mathbf{m} , then, since $M_s = N\mathbf{m}$, where N is the number of atoms per unit volume

$$H_e = \alpha N\mathbf{m}.$$

In order to consider the domain walls we now wish to go on and look at situations where only the nearest neighbour interactions are significant. We need to do this because the directions of the magnetic moments within a domain wall vary with position and hence the mean field approximation is not valid. We consider nearest neighbour interactions in order to provide a tractable solution for the domain wall energy.

The energy per moment due to this interaction is then

$$E_{ex} = -\mu_0 \alpha N \mathbf{m}_i \cdot \mathbf{m}_j$$

where \mathbf{m}_i and \mathbf{m}_j are neighbouring moments.

Once we allow the moments to have different orientations in the domain wall the mean field interaction as defined above becomes meaningless. We therefore will replace it with an analogous interaction \mathcal{J} for use between nearest neighbours only. This will be defined such that the interaction energy per moment becomes

$$E_{ex} = -\mu_0 z \mathcal{J} \mathbf{m}_i \cdot \mathbf{m}_j,$$

where z is the number of nearest neighbours and the magnetic moments \mathbf{m}_i and \mathbf{m}_j are in units of $A\ m^2$. (The approach used here in defining the exchange interaction in terms of magnetic moment will be useful in introducing the quantum mechanical exchange in terms of electron spins in section 7.1.4).

In this case the interaction energy per moment becomes dependent on the turn angle between neighbouring moments. If ϕ is the angle between the neighbouring moments \mathbf{m}_i and \mathbf{m}_j the interaction energy per moment becomes

$$E_{ex} = -\mu_0 z \mathcal{J} \mathbf{m}^2 \cos\phi.$$

If we consider a linear chain, each moment has two nearest neighbours. Making the substitution $\cos\phi = 1 - \phi^2/2$ for small ϕ , the energy per moment becomes

$$E_{ex} = \mu_0 \mathcal{J} \mathbf{m}^2 (\phi^2 - 2).$$

The extra interaction energy due to the rotation of the angle of moments within the wall is therefore the sum of the individual interaction energies over the number of moments in the wall,

$$E_{ex} = \mu_0 \mathcal{J} \mathbf{m}^2 \phi^2 n,$$

where n is the number of moments in the wall.

130 Domain walls

For a 180° domain wall of thickness n lattice parameters, each of size a , $\phi = \pi/n$, and the energy per unit area is then

$$E_{\text{ex}} = \frac{\mu_0 J m^2 \pi^2}{na^2}.$$

From this result [2] it is clear that the interaction energy is minimized when ϕ is very small, corresponding to a very wide domain wall. Therefore the exchange interaction energy favours wide domain walls.

Anisotropy energy

The anisotropy of a cubic crystal expressed using the one constant approximation, gives the energy of the p th moment in the wall as

$$E_a = (K_1/4) \sin^2 2p\phi$$

and summing this over the width of the domain wall gives [3] the energy per unit area as

$$E_a = K_1 na,$$

where a is the lattice spacing and n is the number of layers of atoms in the domain wall. If l_d is the thickness of the wall $l_d = na$.

$$E_a = K_1 l_d.$$

Therefore the anisotropy energy is minimized for a very thin wall.

Energy per unit area of the wall

If the anisotropy and exchange energies are summed this gives

$$E_{\text{tot}} = \frac{\mu_0 J m^2 \pi^2}{l_d a} + K_1 l_d$$

which is the domain wall energy per unit area.

If the anisotropy is the dominant term then energy is minimized at small l_d , whereas if the exchange is dominant then energy is minimized at large l_d . The domain wall thickness is determined by competing influence of these two factors.

7.1.3 Width of domain walls

How wide are the domain walls and what determines the width?

The width of the domain walls in a ferromagnet is determined by minimizing energy of the wall with respect to its width. Therefore differentiating the energy with respect to l_d to find the equilibrium, remembering that $\phi = \pi/n$ and $l_d = na$

$$\frac{dE_{\text{tot}}}{dl_d} = \frac{-\mu_0 J m^2 \pi^2}{l_d^2 a} + K_1 = 0.$$

This leads to

$$l_d = \sqrt{\frac{\mu_0 J m^2 \pi^2}{K_1 a}}$$

This is the width of the domain wall which increases with the exchange energy but decreases with anisotropy. The anisotropy favours alignment of moments only along the crystallographic easy axes, such as the (100) axes in iron or the (111) axes in nickel.

Example 7.1 Domain wall thickness in iron. Determine the domain wall width of a 180° domain wall in iron. For iron $K_1 = 4.8 \times 10^4 \text{ J/m}^3$, $a = 2.5 \text{ \AA}$, $m = 2.14 \text{ Bohr magnetons} (= 1.98 \times 10^{-23} \text{ A m}^2)$ and $J = 1.9 \times 10^{-21} \text{ Joules}$ ($J = 386 \times 10^{28}$).

If l_d is the domain wall thickness then, from the above,

$$l_d^2 = (\mu_0 J m^2 \pi^2 / K_1 a).$$

Substituting in the various values

$$l_d^2 = \frac{(4\pi \times 10^{-7})(386 \times 10^{28})(1.98 \times 10^{-23})^2 \pi^2}{(4.8 \times 10^4)(2.5 \times 10^{-10})}$$

$$l_d^2 = 15.59 \times 10^{-16} \text{ m}^2$$

Hence,

$$\begin{aligned} l_d &= 3.95 \times 10^{-8} \text{ m} = 395 \text{ \AA} \\ &= 160 \text{ lattice parameters (or atomic layers).} \end{aligned}$$

This is an approximate value for the domain wall widths in iron. Actually the width depends on the type of domain wall. Typical values of domain wall thicknesses in iron, nickel and cobalt along different crystallographic directions have been given by Lilley [4].

7.1.4 Interaction energy in terms of electron spin and quantum mechanical exchange energy

Can the interaction energy be expressed in terms of the exchange interaction between two electrons on neighbouring atomic sites?

There is an alternative expression for the wall energy and width that you will encounter more frequently. This is in terms of the quantum mechanical exchange constant J [5], which is really an alternative representation of our nearest-neighbour interaction \mathcal{J} , and which also determines the Weiss mean-field coupling α where such an approximation is appropriate. The wall energy is then expressed in

terms of the exchange constant and the spin on the electrons in the atom S . The spin on one electron s is always $1/2$, which corresponds to a magnetic moment of one Bohr magneton or $9.27 \times 10^{-24} \text{ A m}^2$. In iron each atom has a net spin of $S = 1$, which gives 2 Bohr magnetons per atom [6].

In practice the magnetic moments on the atoms are not always integral multiples of a Bohr magneton because there is a contribution to the magnetic moment from the electron orbital motion and indeed the magnetic electrons in solids such as iron, cobalt and nickel may not be localized at the atomic sites which can also lead to non-integral values of magnetic moment as discussed in Chapter 10. In iron the moment corresponds closely to a spin of $S = 1$. However in nickel this is quite seriously in error since if we take $S = 1/2$ this indicates a moment per atom of $0.93 \mu_B$, whereas the true value is $0.6 \mu_B$. Therefore the use of the quantum mechanical exchange interaction J , apart from making first principles calculations for very simple systems, is limited. Practical estimates of the value of J can be made using the Curie temperature, the low-temperature saturation magnetization or the specific heat [7,8].

The relation between the classical nearest-neighbour interaction, \mathcal{J} , and the quantum mechanical exchange energy, J , is

$$\mu_0 \mathcal{J} \mathbf{m}^2 = JS^2,$$

and consequently,

$$\mathcal{J} = \frac{J}{43.5 \times 10^{-53}}$$

and where appropriate, using the mean-field model

$$\mu_0 N \alpha \mathbf{m}^2 = zJS^2,$$

where z is the number of nearest-neighbour atoms, S is the total electron spins per atom and J is the exchange constant (also known as the exchange integral).

For iron, assuming $S = 1$, the exchange constant $J = 11.9 \times 10^{-3} \text{ eV}$, or $1.9 \times 10^{-21} \text{ J}$ between each pair of nearest-neighbour atoms, this gives rise to an exchange energy per atom of $J_{\text{atom}} = 8J$ since iron has $z = 8$ nearest neighbours with which it interacts in the b.c.c. crystal structure.

$$\begin{aligned} J_{\text{atom}} &= 95.2 \times 10^{-3} \text{ eV} \\ &= 15.2 \times 10^{-21} \text{ J/atom} \end{aligned}$$

and a volume energy of NJ_{atom} , where N is the number of atoms per unit volume. ($N = 8.58 \times 10^{28}$ atoms per m^3 in iron.)

$$J_v = 1.30 \times 10^9 \text{ J m}^{-3}.$$

The mean-field parameter α can be related to the exchange coupling since within the body of a domain we can use the mean-field approximation

$$\mu_0 N \alpha \mathbf{m}^2 = zJS^2$$

and in the case of iron we have $S = 1$.

$$\begin{aligned}\alpha &= \frac{(8)(1.9 \times 10^{-21})}{\mu_0 N(1.98 \times 10^{-23})^2} \\ &= \frac{15.2 \times 10^{-21}}{3.92 \times 10^{-46} \mu_0 N} \\ &= \frac{3.88 \times 10^{25}}{(8.58 \times 10^{28})(4\pi \times 10^{-7})} \\ &= \frac{3.88 \times 10^{25}}{108 \times 10^{21}} \\ &= 360.\end{aligned}$$

The interaction parameter \mathcal{J} is given by

$$\begin{aligned}\mu_0 \mathcal{J} \mathbf{m}^2 &= JS^2 \\ \mathcal{J} &= \frac{1.9 \times 10^{-21}}{(4\pi \times 10^{-7})(3.92 \times 10^{-46})} \\ \mathcal{J} &= 3.86 \times 10^{30} \text{ (dimensionless)},\end{aligned}$$

a rather cumbersome number to deal with. In most cases when these types of interactions are considered the quantum mechanical exchange energy is used. The drawback, as already mentioned, is that the magnetic moments per atom, whether localized on the atomic sites or itinerant, are seldom integral numbers of electron spins.

Example 7.2 Domain wall energy. Estimate the domain wall energy of a 180° domain wall in iron. For iron $K_1 = 4.8 \times 10^4 \text{ J/m}^3$, $a = 2.5 \text{ \AA}$, $\mathbf{m} = 2.14 \text{ Bohr magnetons}$, $J = 1.9 \times 10^{-21} \text{ J}$ ($\mathcal{J} = 3.86 \times 10^{30}$).

Using the equation,

$$E_{\text{tot}} = \frac{\mu_0 \mathcal{J} \mathbf{m}^2 \pi^2}{la} + K l_1,$$

where the wall thickness is $4 \times 10^{-8} \text{ m}$

$$\begin{aligned}E_{\text{tot}} &= \frac{(4\pi \times 10^{-7})(386 \times 10^{28})(1.98 \times 10^{-23})^2 \pi^2}{(4 \times 10^{-8})(2.5 \times 10^{-10})} + (4.8 \times 10^4)(4 \times 10^{-8}) \\ &= 1.87 \times 10^{-3} + 1.92 \times 10^{-3} \\ &= 3.8 \times 10^{-3} \text{ J m}^{-2}.\end{aligned}$$

Table 7.1 Magnetic properties of iron, cobalt and nickel

	<i>Fe</i>	<i>Co</i>	<i>Ni</i>
Magnetic moment per atom [6] at 0 K (in Bohr magnetons)	2.22	1.72	0.62
Saturation magnetization (in 10^6 A m^{-1}) at 0 K	1.74	1.43	0.52
at 300 K	1.71	1.40	0.48
Exchange energy J [3, 7] (in J)	2.5×10^{-21}		3.2×10^{-21}
(in meV)	0.015		0.020
Curie temperature [6] (in °C)	770	1131	358
(in K)	1043	1404	631
Anisotropy energy K_1 [8, 9, 10, 11] (in J m^{-3}) 300 K	4.8×10^4	45×10^4	-0.5×10^4
0 K	5.7×10^4	68×10^4	-5.7×10^4
Lattice spacing [12] (in nm) a	0.29	0.25	0.35
c		0.41	
Domain wall thickness [3, 4] (in nm)	40	15	100
(in lattice parameters)	138	36	285
Domain wall energy [6, 11] (in J/m^2)	3×10^{-3}	8×10^{-3}	1×10^{-3}

Note: Domain wall thicknesses and energies are approximate values only, since they will depend on the crystallographic direction of the moments in the domains on either side of the wall. For further details consult the paper by Lilley [4].

7.1.5 180° and non-180° domain walls

What different types of domain wall exist and how may we classify them?

Generally domain walls can be classified into 180° and non-180° walls. The 180° domain walls occur in virtually all materials and are distinct from all other non-180° walls in that they are not affected by stress [13]. In 180° walls the directions of magnetization in the neighbouring domains are antiparallel and consequently the moments in the two domains always lie in equivalent crystallographic directions.

In cubic materials with $K > 0$ the non-180° walls are all 90°, so that the direction of the moments in neighbouring domains are at right angles. Therefore in iron the easy axes are all the $\langle 100 \rangle$ directions, and domain walls between the [100] and [$\bar{1}00$] directions are 180° walls, while those between [100] and [010] are 90°

walls. In nickel for which $K < 0$ the easy axes are all the $\langle 111 \rangle$ directions. Consequently the non- 180° domain walls will be either 71° or 109° .

Often all non- 180° domain walls are incorrectly referred to collectively as '90° walls' to distinguish the stress-sensitive from the non-stress sensitive walls.

7.1.6 Effects of stress on 180° and non- 180° domain walls

Why are 90° domain walls stress sensitive but 180° domain walls are not?

Suppose for example a uniaxial stress is applied along the [100] direction in iron. If this is a tensile stress it will make that particular [100] direction lower in energy than the [010] and the [001] directions which were degenerate in energy in the unstressed state. However the energy of the $[\bar{1}00]$ direction will be reduced by the same amount. Consequently, a 180° wall separating domains aligned along these two directions will not be affected by stress.

Consider now a 90° wall between domains along the [100] and [010] directions in iron which are energetically equal. Application of tensile stress along the [100] direction causes the [100] domain to be energetically favoured, so the 90° wall will move under the action of such a stress to increase the volume of the [100] domain at the expense of the [010] domain. It can be seen therefore that the 90° domain walls are stress-sensitive.

7.1.8 Closure domains

Where do these different types of domain wall occur?

Closure domains occur more often in cubic materials than in hexagonal materials because the cubic anisotropy ensures that the directions at right angles to the

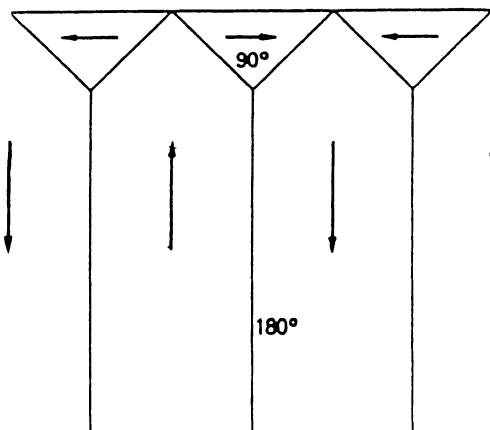


Fig. 7.2 Closure domains at the surface in a material with cubic crystal structure, in this case grain-oriented silicon–iron.

magnetisation in a given domain are also magnetically easy axes. Therefore it is energetically favourable to have 90° as well as 180° domain walls. In a material such as cobalt in which the unique axis is the easy direction it is difficult to form 90° walls since the magnetic moments in one of the domains must then lie in the hexagonal basal plane which is energetically unfavourable.

One example of where 90° domain walls occur is in the closure domains of grain-oriented silicon iron, Fig. 7.2. Of course there are many other instances of 90° walls, and they certainly are not dependent on high anisotropy, in fact high anisotropy impedes the formation of closure domains as in the case of hexagonal materials such as cobalt. The domain boundaries between the neighbouring longitudinal domains are 180° walls, while those between the closure domains at the end of the material and the main longitudinal domains are 90° walls.

7.1.8 Neel walls

Are there other types of domain wall apart from Bloch walls?

If a specimen is in the form of a thin film the ferromagnetic domains can extend across the whole width of the specimen. In this case the Bloch wall, which would have its magnetization normal to the plane of the material, as shown in Fig. 7.3, causes a large demagnetization energy, whereas the Neel wall [14], in which the moments rotate within the plane of the specimen, results in a lower energy.

Neel walls do not occur in bulk specimens because they generate a rather high demagnetization energy within the volume of the domain wall. It is only in thin films that this energy becomes lower than the demagnetization energy of the Bloch wall.

7.1.9 Antiferromagnetic domain walls

What about domain walls in other ordered magnetic materials?

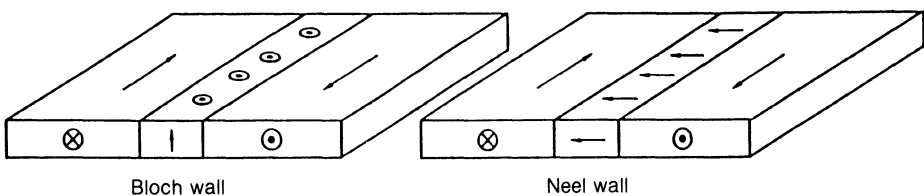


Fig. 7.3 A conventional Bloch wall and Neel wall in a thin film of ferromagnetic material. The Bloch wall requires that some of the magnetic moments be oriented normal to the plane of the film. This leads to a demagnetization energy associated with the Bloch wall. The Neel wall has all moments oriented in the plane. The Neel wall is energetically favoured once the film thickness decreases below a certain critical value.

Magnetic domain walls occur in all forms of ordered magnetic materials and so there are correspondingly many different forms of domain walls. Domain walls in simple antiferromagnets and ferrimagnets are similar to domain walls in ferromagnets. However the helical antiferromagnet such as occurs in dysprosium and terbium presents a very interesting case. Domains in these materials were first suggested by Palmer [15] in which it was suggested that the domains consisted of helices of different chirality. These were subsequently observed experimentally [16]. The domain walls are transition regions between helical domains and are regions in which the neighbouring moments are aligned nearly parallel, or at least the turn angle between successive moments ϕ is very small compared to within the domain.

Generally the two senses of helix are energetically equal so that either may occur. Application of a field perpendicular to the unique axis of the helix can cause favourably oriented domain walls to grow. Therefore the helical to ferromagnetic transition, which can be induced by application of a field perpendicular to the unique axis, is caused by growth of domain walls in this type of magnet.

7.2 DOMAIN WALL MOTION

What changes occur at the domain walls when the magnetic field increases?

In discussing the magnetizing process we have mentioned the rotation of magnetic moments within a domain as a result of the competing effects of anisotropy and field energy. We have also touched very briefly on the idea of the growth of favourably oriented domains without really explaining what is meant by this.

In fact on application of a field it is the moments within domain walls which can most easily be rotated. This is because the resulting directions of the moments within the walls are a fine balance between the exchange and anisotropy energies. So a change in the field energy $E = -\mu_0 \mathbf{m} \cdot \mathbf{H}$ can alter this balance causing the moments to rotate. Within the main body of the domain the moments are locked into a particular direction by the exchange interaction so that an applied field can not immediately alter the balance of the energy in favour of another direction.

7.2.1 Effect of magnetic field on the energy balance in domain walls

Why do magnetic changes under the action of weak and moderate fields occur at domain boundaries?

Consider for example Fig. 7.1. If a weak field is applied in the 'up' direction the moments within the 'down' domain will not change direction because they are at the bottom of a deep energy well caused by their mutual interactions through the exchange field. However in the domain wall the energy introduced by the magnetic field can just tip the balance slightly in favour of the 'up' direction.

The net result is that the moments within the wall rotate slightly into the field

direction as the field is increased. To an observer it therefore appears as though the domain wall moves towards the right. This process is called domain-wall motion, although in truth there is no translational motion at all. The movement is more like that of a wave, and in fact Kittel [17] and others have considered the movement of Bloch walls to be an example of the motion of a soliton, that is a solitary wave.

In discussing domain-wall motion it is conventional to treat the domain wall as an entity in itself and to discuss its motion through the material in terms similar to those used for interfaces such as elastic membranes.

7.2.2 Domain walls as elastic membranes

Is there a simple model that we can use to envisage the behaviour of domain walls?

Since domain walls have an energy associated with them which is proportional to the area the walls behave in such a way as to minimize their area. We may therefore consider them to be analogous to the surfaces of liquids where the domain-wall energy is equivalent to the surface tension of the liquid. This analogy works well in trying to understand the behaviour of domain walls, particularly the reversible bowing of domain walls [18, 19] under the action of a magnetic field, and their tendency to become attached to non-magnetic particles, impurities or second-phase materials within the solid [20] and to regions of inhomogeneous microstrain [21, 22].

7.2.3 Forces on domain walls

What is the force exerted on a domain wall by a magnetic field?

If a magnetic field is applied to a ferromagnetic material this results first in the movement of domain walls, in such a way that domains aligned favourably with the field direction grow at the expense of those aligned unfavourably. The energy per unit volume of such a domain when subjected to a field \mathbf{H} is

$$E_H = -\mu_0 \mathbf{M}_s \cdot \mathbf{H}.$$

Consequently the energy change caused by displacement of a 180° domain wall through a distance x is

$$E = -2\mu_0 A \mathbf{M}_s \cdot \mathbf{H}x,$$

where A is the area of the wall. Therefore the force per unit area on such a wall is

$$\begin{aligned} F &= -(1/A) \left(\frac{dE}{dx} \right) \\ &= 2\mu_0 \mathbf{M}_s \cdot \mathbf{H}. \end{aligned}$$

7.2.4 Planar displacement of rigid, high-energy domain walls: the potential approximation

How do walls with high surface energy compared to pinning energy behave?

Walls with high surface energy tend to remain planar. Planar domain-wall motion has been considered by Kersten [23, 24]. The movement of planar domain walls under the action of a magnetic field in a specimen of high-purity iron are shown in Fig. 7.4. The energy supplied by a magnetic field \mathbf{H} to a ferromagnet is given by

$$\Delta E = -\mu_0 \int \mathbf{H} \cdot d\mathbf{M},$$

and consequently if a 180° domain wall with unit cross sectional area is moved through a distance dx , the change in magnetization is

$$d\mathbf{M} = 2\mathbf{M}_s dx.$$

Therefore the change in field energy is given by,

$$\begin{aligned}\Delta E_H &= -2\mu_0 \mathbf{M}_s \cdot \mathbf{H} \int dx \\ &= -2\mu_0 \mathbf{M}_s \cdot \mathbf{H} x,\end{aligned}$$

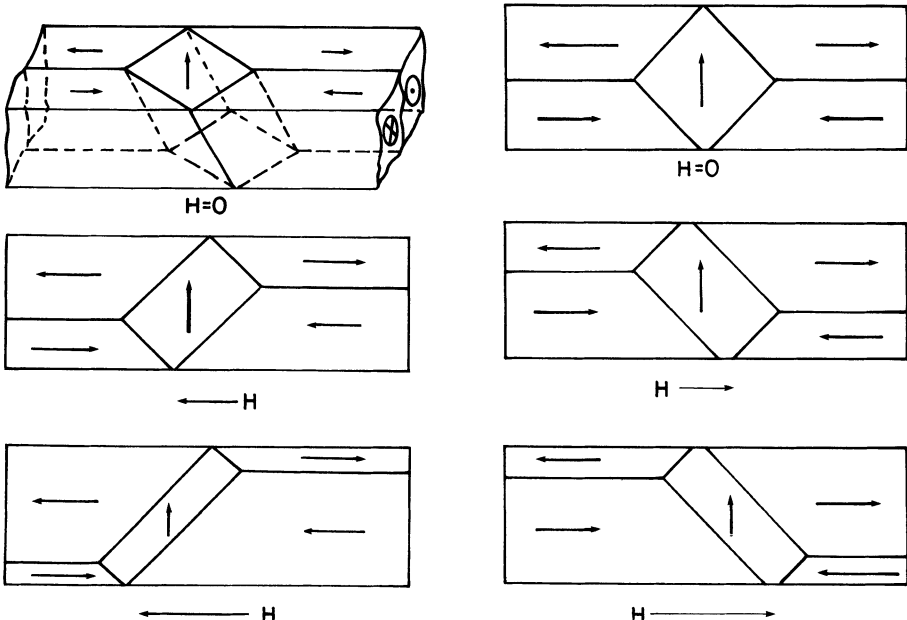


Fig. 7.4 Translational motion of planar domain walls in high-purity iron.

where x is the displacement of the wall. We assume in this analysis that the \mathbf{H} field is parallel to the direction of magnetization in one of the domains and antiparallel to the other domain.

If the domain wall is subject to a potential energy E_p within the material then the total energy is, [25, 26]

$$E_{\text{tot}} = E_p - 2\mu_0 \mathbf{M}_s \cdot \mathbf{H}x.$$

The potential E_p will vary throughout the solid since the defects within the solid provide minima in E_p , while regions of inhomogeneous microstress, associated with dislocations, can provide either energy minima or maxima depending on the sign of the stress and the magnetostriction coefficient. In general the form of this potential will be irregular as shown in Fig. 7.5, where the energy is plotted against wall displacement.

The displacement x of the 180° wall can then be calculated from the condition

$$\begin{aligned}\frac{dE_{\text{tot}}}{dx} &= 0 \\ &= \frac{dE_p}{dx} - 2\mu_0 \mathbf{M}_s \cdot \mathbf{H}.\end{aligned}$$

Specific solutions may be attempted if the form of E_p is known or can be approximated. As an example consider the simplest form of potential

$$E_p = \frac{1}{2}ax^2.$$

In this case the solution for x is

$$x = \frac{2\mu_0 \mathbf{M}_s \cdot \mathbf{H}}{a}.$$

This refers to a small displacement, and hence to a completely reversible process since if the field is removed then x returns to zero. As might be expected the wall displacement increases as the potential well becomes flatter and decreases as it becomes steeper.



Fig. 7.5 Potential energy seen by domain wall as a function of position. This variation of energy with displacement is used in models based on the rigid wall approximation.

7.2.5 Magnetization and initial susceptibility in the rigid wall approximation

What value of initial reversible susceptibility is expected on the basis of the rigid wall model?

This enables us to calculate the initial reversible change in magnetization. Suppose $x = 0$ corresponds to the demagnetized state $\mathbf{M} = 0$, then the magnetization is given by

$$\mathbf{M} = 2\mathbf{M}_s A \cos \theta x,$$

where A is the cross-sectional area of the wall, and θ is the angle between the magnetization vector in the domain and the direction of displacement. Substituting for x

$$\mathbf{M} = \frac{4\mu_0 A H \mathbf{M}_s^2 \cos^2 \theta}{a}$$

and consequently the initial reversible susceptibility is

$$\begin{aligned} \chi_{in} &= \frac{d\mathbf{M}}{dH} \\ &= \frac{4\mu_0 A \mathbf{M}_s^2 \cos^2 \theta}{a}. \end{aligned}$$

In a cubic material such as iron the average of $\cos^2 \theta$ over the three easy axes is $1/3$, so for a multidomain specimen,

$$\chi_{in} = \frac{4\mu_0 A \mathbf{M}_s^2}{3a}.$$

The initial reversible susceptibility calculated on the basis of the rigid wall approximation therefore depends on the saturation magnetization and on the potential seen by the wall as expressed in this simple case by the parameter a . As the potential well becomes steeper so the initial susceptibility decreases.

7.2.6 Bending of flexible, low-energy domain walls: the wall bowing approximation

How do walls with low surface energy compared to pinning energy behave?

Walls with low surface energy show a tendency to bend. In practice domain walls exhibit both reversible bending and reversible translation under the action of a magnetic field. Wall bending is shown in Fig. 7.6. Of course the amount of bending that the walls undergo depends on many factors, including the field strength, but most particularly on the domain-wall energy [27–31]. Walls with high energy do not bend easily while those with a low energy are more flexible.

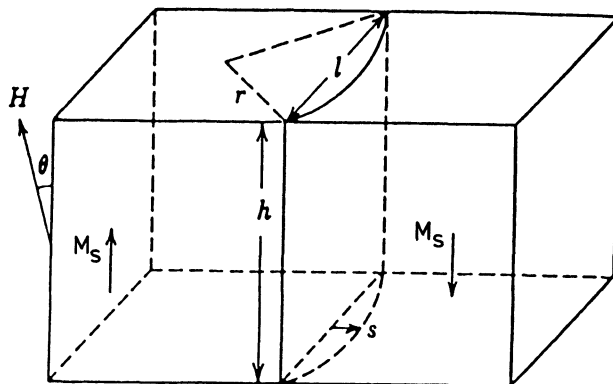


Fig. 7.6 Bending of a domain wall under the action of a field. The domain wall is pinned at the boundaries and expands in the manner of an elastic membrane as described by Kersten and Neel [27,29].

To give some indication the wall energies, based on a one-constant anisotropy model calculation, of 180° domain walls in iron are about 2.9 ergs/cm², in nickel 0.7 ergs/cm² and in cobalt 7.6 ergs/cm². Clearly the domain walls in cobalt are more rigid than the domain walls in nickel. However if a specimen is very pure and free of defects the domain walls can still move in a planar manner.

Now let us suppose that a 180° domain wall extends throughout a single grain of a relatively pure specimen. Therefore the grain boundary is the principal impediment to domain-wall motion. The domain wall will be attached to the grain boundary in much the same way that it becomes attached to any other defect in the material. If a field is applied along the direction of one of the domains that domain will grow by domain-wall motion. However as the domain wall is attached to the grain boundary it will first move by bending.

The force per unit area on the domain wall is, as before,

$$F = 2\mu_0 M_s \cdot H.$$

The difference in wall energy caused by bending will be,

$$E = \gamma [A(H) - A(0)]$$

where γ is the wall energy, $A(0)$ is the area at zero magnetic field, that is before deformation, and $A(H)$ is the area under a field H .

Assuming for simplicity a cylindrical deformation, this leads to an expression for the force per unit area on the wall in terms of its radius of curvature

$$F = \frac{\gamma}{r},$$

as in the expression for excess pressure across an elastic membrane such as a liquid interface where γ is the surface tension.

7.2.7 Magnetization and initial susceptibility in the flexible approximation

What initial reversible susceptibility is expected on the basis of the wall-bending model?

Once again it is possible to calculate the initial reversible susceptibility. The change in magnetization as a result of bending of the domain wall is

$$\mathbf{M} = 2\mathbf{M}_s dV,$$

where $dV = (2/3)lhx$, x being the displacement of the wall at its centre, and h and l the spatial extent of the undeformed wall.

$$\mathbf{M} = \frac{4}{3}\mathbf{M}_s lhx.$$

Since for small x , $x \doteq l^2/8r$

$$\mathbf{M} = \frac{1}{6} \frac{\mathbf{M}_s l^3 h}{r}$$

and at equilibrium the force due to the field must equal the force due to the surface tension of the wall. Equating the pressures,

$$\frac{\gamma}{r} = 2\mu_0 \mathbf{M}_s \mathbf{H}.$$

This allows a substitution to be made for r , since now $r = \gamma/(2\mu_0 \mathbf{M}_s \mathbf{H})$

$$\mathbf{M} = \frac{\mu_0 \mathbf{M}_s^2 \mathbf{H} l^3 h}{3\gamma}.$$

The initial susceptibility is thus

$$\chi_{in} = \frac{\mu_0 \mathbf{M}_s^2 l^3 h}{3\gamma}.$$

This is the reversible susceptibility, which depends on the saturation magnetization and on the domain wall surface energy γ . As the domain wall surface energy increases so the wall becomes more rigid and the initial susceptibility decreases.

We see therefore that two types of wall motion can occur: wall displacement and wall bending. The strength of the domain wall pinning and the surface energy of the wall determine which of these occurs in a particular case.

REFERENCES

1. Bloch, F. (1932) *Z. Physik*, **74**, 295.
2. Kittel, C. and Galt, J. K. (1956) Ferromagnetic domain theory, *Solid State Physics*, **3**, 437.
3. Chen, C. W. (1977) *Magnetism and Metallurgy of Soft Magnetic Materials*, North Holland, p. 84.

4. Lilley, B. A. (1950) *Phil. Mag.*, **41**, 792.
5. Kittel, C. (1949) *Revs. Mod. Phys.*, **21**, 541.
6. Cullity, B. D. (1972) *Introduction to Magnetic Materials*, Addison-Wesley, Reading, Mass., p. 617.
7. Hoffmann, J. A., Paskin, A., Tauer, K. J. and Weiss, R. J. (1956) *J. Phys. Chem. Sol.*, **1**, 45.
8. Graham, C. D. (1958) *Phys. Rev.*, **112**, 1117.
9. Sato, H. and Chandrasekar, B. S. (1957) *J. Phys. Chem. Sol.*, **1**, 228.
10. Pauthenet, R., Barnier, Y. and Rimet, G. (1962) Proceedings of the International Conference on Magnetism and Crystallography, Kyoto, 1961, *J. Phys. Soc. Japan*, **17** (Sup. B-1), 309.
11. Chikazumi, S. (1964) *Physics of Magnetism*, Wiley, New York, p. 130.
12. Kittel, C. (1986) *Introduction to Solid State Physics*, 6th edn, Wiley, New York, p. 23.
13. Chikazumi, S. (1964) *Physics of Magnetism*, Wiley, New York, p. 192.
14. Neel, L. (1955) *Comptes Rendu*, **241**, 533.
15. Palmer, S. B. (1975) *J. Phys. F.*, **5**, 2370.
16. Palmer, S. B., Baruchel, J., Drillat, A., Patterson, C. and Fort, D. (1986) *J. Mag. Mag. Mater.*, **53–7**, 1626.
17. Kittel, C. (1986) *Introduction to Solid State Physics*, 6th Edn, Wiley, New York.
18. Kersten, M. (1956) *Z. Angewandte Phys.*, **8**, 496.
19. Neel, L. (1944) *Cahiers de Phys.*, **25**, 21.
20. Kersten, M. (1943) *Grundlagen einer Theorie der Ferromagnetischen Hysterese und der Koerativkraft*, Hirzel, Leipzig.
21. Becker, R. (1932) *Phys. Zeits.*, **33**, 905.
22. Kondorsky, E. (1937) *Phys. Z. Sovietunion*, **11**, 597.
23. Kersten, M. (1938) *Phys. Zeits.*, **39**, 860.
24. Kersten, M. (1938) in *Problem der Technischen Magnetisierungskurve* (ed. R. Becker), Springer, Berlin, p. 42.
25. Hoselitz, K. (1952) *Ferromagnetic Properties of Metals and Alloys*, Oxford, Ch. 2, p. 79.
26. Chikazumi, S. (1964) *Physics of Magnetism*, Wiley, p. 267.
27. Neel, L. (1946) *Annales Univ. Grenoble*, **22**, 299.
28. Neel, L. (1944) *Cahiers de Phys.*, **25**, 21.
29. Kersten, M. (1956) *Z. Angewandte Phys.*, **7**, 313.
30. Kersten, M. (1956) *Z. Angewandte Phys.*, **8**, 382.
31. Kersten, M. (1956) *Z. Angewandte Phys.*, **8**, 496.

FURTHER READING

- Chikazumi, S. (1964) *Physics of Magnetism*, John Wiley, New York, Ch. 9.
 Crangle, J. (1977) *The Magnetic Properties of Solids*, Arnold, London, Ch. 6.
 Cullity, B. D. (1972) *Introduction to Magnetic Materials*, Addison-Wesley, Reading, Mass., Ch. 9.
 Kittel, C. (1949) Physical theory of ferromagnetic domains, *Revs. Mod. Phys.*, **21**, 541.
 Kittel, C. and Galt, J. K. (1956) Ferromagnetic domain theory, *Solid State Physics*, **3**, 437.

EXAMPLES AND EXERCISES

Example 7.3 Critical dimensions for single-domain particles in nickel. Calculate the magnetostatic energy of a small spherical particle of nickel of radius r and magnetized to saturation $M_s = 5.1 \times 10^5$ A/m. (You can assume the magnetostatic

energy of a sphere with magnetization \mathbf{M} and volume V is $E_{\text{ms}} = \mu_0 \mathbf{M}^2 V / 6$ and that this energy is halved when the particle is divided into two domains.) The energy required to form a Bloch wall is $\gamma = 0.7 \times 10^{-3} \text{ J m}^{-2}$ in nickel. Hence find the critical radius for single-domain particles which will be such that the reduction in magnetostatic energy obtained by division into two domains is less than the energy needed to form a wall.

Example 7.4 Calculation of wall energy and thickness from anisotropy energy, saturation magnetization and exchange energy. Find the domain-wall energy γ , wall thickness l and critical dimension r_c for single-domain particles for a material with anisotropy energy $K = 33 \times 10^4 \text{ J m}^{-3}$, saturation magnetization $\mathbf{M}_s = 0.38 \times 10^6 \text{ A/m}$, lattice spacing $3 \times 10^{-10} \text{ m}$ and exchange energy $J = 3 \times 10^{-21} \text{ J}$. You may assume this material has a spin of $S = 1/2$, or magnetic moment per atom of one Bohr magneton.

Example 7.5 Estimation of domain spacing in cobalt. Estimate the domain spacing d in a specimen of single-crystal cobalt in the form of a plate of infinite per unit area is $1.7 \times 10^{-7} \mathbf{M}_s^2 d$. The domain-wall energy for cobalt is $7.6 \times 10^{-3} \text{ J m}^{-2}$ and $\mathbf{M}_s = 1.42 \times 10^6 \text{ A/m}$.

Calculate the domain spacing when $l = 0.01 \text{ m}$.

8

Domain Processes

In this chapter we will look at the behaviour of domains under the action of a changing magnetic field. We are interested principally in the changes which occur in the domain structure and the mechanisms by which these are brought about. We will look at reversible and irreversible changes in magnetization and describe them in terms of the two main mechanisms: domain-wall motion and rotation. Finally we will use some of these ideas to formulate a model of hysteresis.

8.1 REVERSIBLE AND IRREVERSIBLE DOMAIN PROCESSES

Are the changes in magnetization reversible or irreversible or both?

The changes in magnetization arising from the application of a magnetic field to a ferromagnet can be either reversible or irreversible depending on the domain processes involved. A reversible change in magnetization is one in which after application and removal of a magnetic field, the magnetization returns to its original value. In ferromagnetic materials this only occurs for small field increments.

More often both reversible and irreversible changes occur together, so that on removal of the field the magnetization does not return to its initial value. If the magnetic field is cycled under these conditions hysteresis is observed in \mathbf{M} . The next task is to interpret such changes in magnetization in terms of domain mechanisms so that both reversible and irreversible changes can be explained.

8.1.1 Domain rotation and wall motion

What mechanisms are available for interpreting and describing the changes in magnetization with field?

The domain mechanisms which we have discussed so far are rotation and wall motion. Both of these processes can be manifested as either reversible or irreversible mechanisms, and the transition from reversible to irreversible is in both cases dependent on the amplitude of the magnetic field.

Wall motion incorporates two distinct effects: bowing of domain walls and

translation. Domain-wall bowing is a reversible process at low field amplitudes. The domain wall expands like an elastic membrane under the action of the magnetic field. When the field is removed the wall returns to its original position. Wall bowing becomes irreversible once the domain wall is sufficiently deformed that the expansion continues without further increase of field. The bending of the domain wall which begins as reversible can also become irreversible if during this process the wall encounters further pinning sites which prevent it relaxing once the field is removed.

The translation of domain walls is usually irreversible unless the material is sufficiently pure that the domain wall can exist in a region of the material that is free from defects. The displacement of planar walls can be modelled using a potential energy which fluctuates as a function of distance, as in Fig. 8.1. There are two possible origins for the short-range fluctuations in potential experienced by the domain walls. These are short-range variations in strain associated with dislocations within the material and the presence of particles of a second phase within the matrix material, for example the presence of carbides in steel. There is no general way of treating these energy fluctuations since they are random in nature, however we can consider a simple case of a sinusoidal variation of potential energy, as in Example 8.1, which will have many of the essential features of the real solid.

Rotation of magnetic moments within a domain has been discussed in Chapter 6. At low field amplitudes the direction of alignment of the magnetic moments which corresponds to minimum energy is displaced slightly from the crystallographic easy axes towards the field direction. This results in a reversible rotation of the magnetic moments within a domain.

At intermediate to high field amplitudes there is an irreversible mechanism within the domain when the moments rotate from their original easy axis to the easy axis closest to the field direction. This occurs when the field energy overcomes the anisotropy energy. In this case once the magnetic moments within the domain

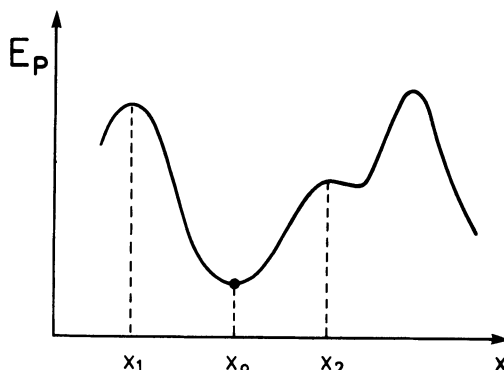


Fig. 8.1 Magnetic energy potential as a function of distance seen by a magnetic domain wall.

have rotated into a different easy axis the moments remain within the potential well surrounding this easy axis if the field is reduced.

At high fields the energy minimum of the easy axis closest to the field is perturbed by the field energy until the minimum lies in the field direction. This results in a reversible rotation of the moments into the field direction and hence a reversible change in magnetization at high fields. Finally at very high fields there is a reversible change in which the magnetic moments within the specimen, which is already a single domain, are aligned more closely with the field direction. This occurs because the individual magnetic moments precess about the field direction due to thermal energy. This precession does not give any net moment in other directions but does reduce the component of magnetization along the field direction. As the field strength increases the angle of precession is reduced. Similarly if the temperature is lowered the angle of precession is reduced due to a reduction in thermal energy.

8.1.2 The strain theory: pinning of domain walls by strains

What causes domain wall motion to be irreversible?

Even before Bloch's theoretical prediction of the existence of a finite transition region between domains, which he called domain walls, it was realized that the principal domain process occurring at low fields was caused by domain boundary motion. Early experiments on domain boundary motion were reported by Sixtus and Tonks [1]. In view of the hysteresis loss, most of which occurs at low fields, it was necessary to explain the loss mechanism in terms of wall motion.

One of the earliest suggestions was by Becker [2] that the domain walls were impeded in their movements by regions of inhomogeneous strain which interacted via the magnetostriction with the magnetic moments to provide local energy barriers which the domain walls needed to overcome. An excellent survey of this early work has been given by Hoselitz [3]. The first calculations were by Becker and Kersten [4] and by Kondorsky [5]. Becker and Kersten determined the initial susceptibility and the coercivity as a function of internal stress. The results of Kersten's investigations are shown in Fig. 8.2.

The strain theory of coercivity was treated in detail by Becker and Doring [6] and by Kersten [7]. During the time in which the effects of stress on magnetization were being investigated, the existence of dislocations within crystals was first suggested by Orowan, Polanyi and Taylor [8, 9, 10]. Dislocations have an associated local stress field which gives rise to highly inhomogeneous microstrains within a solid [11].

Through the magnetoelastic coupling the dislocations pin domain walls, and therefore the higher the dislocation density within a ferromagnet the greater the impedance to domain wall motion. This explains why cold-worked specimens have higher coercivity and lower initial susceptibility than the same material in a well-annealed state, a fact that can be exploited for non-destructive evaluation of the

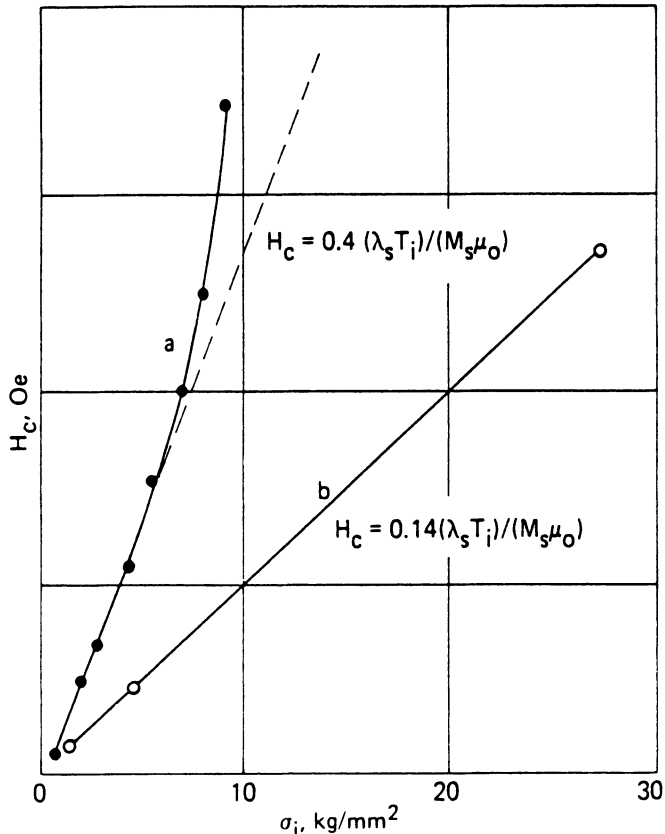


Fig. 8.2 Variation of coercivity of nickel with internal stress calculated by Kersten: (a) recrystallized nickel, and (b) hard-drawn nickel. This result confirmed the strain theory of coercivity.

mechanical state of a ferromagnetic material such as iron or steel using magnetic measurements.

Example 8.1 Initial susceptibility as a result of planar wall displacement in a sinusoidal potential. Suppose the stress σ within a material can be represented as a function of distance by

$$\sigma = \sigma_0 \left(1 - \cos\left(\frac{2\pi x}{l}\right) \right)$$

as shown in Fig. 8.3, where l is the periodicity of the stresses and σ_0 the maximum amplitude.

The stress energy per unit volume E_σ is

$$E_\sigma = \left(\frac{3}{2}\right) \lambda_s \sigma.$$

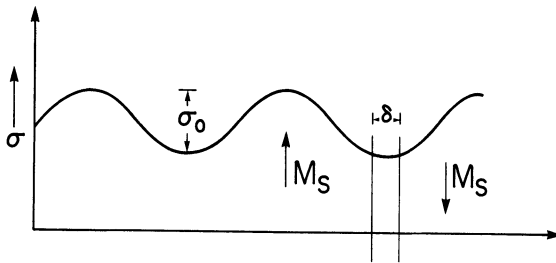


Fig. 8.3 Idealized variation of internal microstress with displacement, approximated by a sinusoidal function.

where λ_s is the magnetostriction coefficient. Substituting for σ in this equation and differentiating, for a domain wall of unit area

$$\frac{dE_\sigma}{dx} = \left(\frac{3\pi}{l}\right) \lambda_s \sigma_0 \sin\left(\frac{2\pi x}{l}\right).$$

The energy per unit volume of a domain under the action of a field \mathbf{H} is

$$E_H = -\mu_0 \mathbf{M}_s \cdot \mathbf{H}.$$

Therefore the change in field energy caused by moving a 180° domain wall of unit area through a distance x will be

$$E_H = -2\mu_0 \mathbf{M}_s \cdot \mathbf{H}x$$

$$\frac{dE_H}{dx} = -2\mu_0 \mathbf{M}_s \cdot \mathbf{H}.$$

The total energy will be the sum of the field energy and the stress energy

$$E_{\text{tot}} = E_H + E_\sigma$$

and differentiating with respect to x to find equilibrium

$$\frac{dE_{\text{tot}}}{dx} = \left(\frac{3\pi}{l}\right) \lambda_s \sigma_0 \sin\left(\frac{2\pi x}{l}\right) - 2\mu_0 \mathbf{M}_s \mathbf{H} \cos \theta = 0$$

At equilibrium

$$2\mu_0 \mathbf{M}_s \mathbf{H} \cos \theta = \left(\frac{3\pi}{l}\right) \lambda_s \sigma_0 \sin\left(\frac{2\pi x}{l}\right),$$

which can be solved for the displacement x . For small x we can make the approximation $\sin 2\pi x/l \approx 2\pi x/l$

$$2\mu_0 \mathbf{M}_s \mathbf{H} \cos \theta = \frac{6\lambda_s \sigma_0 \pi^2 x}{l^2}$$

$$x = \frac{l^2 \mu_0 \mathbf{M}_s \mathbf{H} \cos \theta}{3\pi^2 \lambda_s \sigma_0}$$

The initial susceptibility can be obtained by noting that for a 180° domain wall the change in magnetization is

$$\begin{aligned} \mathbf{M} &= 2AM_s x \cos \theta \\ \frac{d\mathbf{M}}{dH} &= \left(\frac{d\mathbf{M}}{dx} \right) \left(\frac{dx}{dH} \right) \\ &= \frac{2Al^2 \mu_0 M_s^2 \cos^2 \theta}{3\pi^2 \lambda_s \sigma_0} \\ &= \text{constant} \times \frac{M_s^2 l^2}{\lambda_s \sigma_0}. \end{aligned}$$

Therefore the initial susceptibility decreases with $\lambda_s \sigma_0$ and increases with the separation of stress maxima l .

8.1.3 The inclusion theory: pinning of domain walls by impurities

What other factors cause irreversibility in domain wall motion?

Isolated regions of second-phase materials with magnetic properties different from those of the matrix material are known as magnetic inclusions. These reduce the

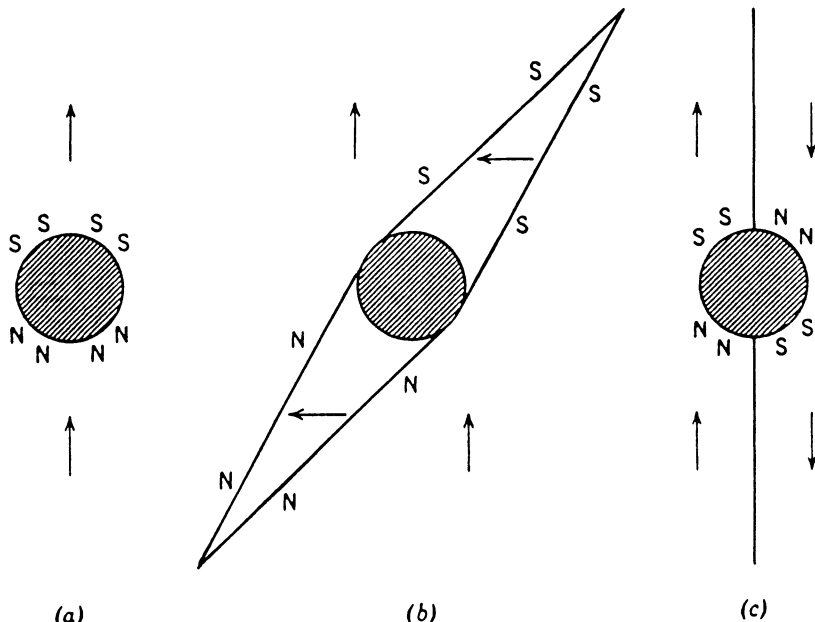


Fig. 8.4 (a) Free-pole distribution on a naked inclusion, (b) spike domain attached to an inclusion and (c) reduction of magnetostatic energy associated with an inclusion when intersected by a domain wall.

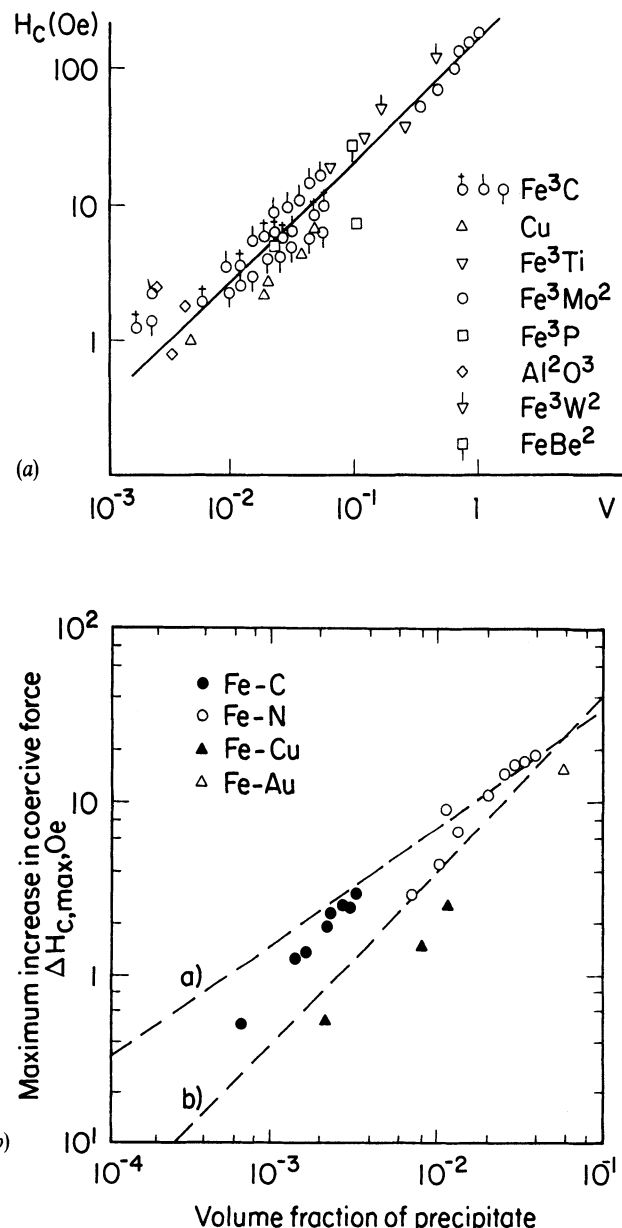


Fig. 8.5 (a) Coercivity of various steels as a function of the total volume fraction of inclusions. Experimental results of Kersten and calculations by Neel (1946). (b) Increase in coercivity of iron caused by precipitates of interstitial or substitutional solutes. Theoretical calculations are represented by the two dashed lines: (a) due to Kersten and (b) due to Neel.

energy of domain walls when the domain walls intersect them and consequently the domain walls are attracted to the inclusions which effectively impede wall motion.

The inclusion theory of domain-wall pinning was suggested by Kersten [12, 13]. He assumed that the magnetic domain walls move in a planar manner through the solid and that the energy of the walls is reduced when they intersect inclusions. The inclusions themselves may take many forms such as insoluble second-phase material which appears if the solubility limit has been exceeded, they may be oxides or carbides, or they may be pores, voids, cracks or other mechanical inhomogeneities. Well-known examples of magnetic inclusions are cementite (Fe_3C) particles in iron and steels.

Neel [14] criticised the assumption of planar wall motion and further indicated that Kersten's interpretation ignored the fact that the magnetic free poles associated with a defect such as a void or crack would be a greater source of energy. So that a naked inclusion totally enclosed within the body of a domain would have free poles attached, as shown in Fig. 8.4(a), with an attendant magnetostatic energy of $2\pi\mu_0 M_s^2 r^3/9$ but when the wall bisects the defect there occurs a change in distribution of the free poles on the defect as shown in Fig. 8.4(c) which results in a reduction of the magnetostatic energy to $\pi\mu_0 M_s^2 r^3/9$. Neel's model became known as the disperse field theory (or the variable field theory).

The energy reduction of the domain wall using the simple elastic membrane model is the reduction in area of the wall times the wall energy per unit area. This can be calculated as $\pi r^2 \gamma$, where γ is the domain-wall energy. For a 1 μm diameter non-magnetic inclusion in iron with $\gamma = 1.5 \text{ erg/cm}^2$ the energy reduction due to free poles is about 140 times the energy reduction due to wall area. Figure 8.5 shows the results of a comparison of calculated and observed coercivities in steels by Neel [15].

An attempt to describe the effect of carbide inclusions on the coercivity of iron was made by Dijkstra and Wert [16]. In their model the domain wall was considered to be an elastic surface, so that the difference in energy between the wall when it intersected the defect and when it was free was determined simply from the difference in area of the wall. In reality an inclusion would not be entirely free from spike domains when within the body of a domain as shown in Fig. 8.4(b). These spike domains themselves lower the magnetostatic energy of the inclusion. Nevertheless the energy of the inclusion and spike domains is still reduced when intersected by a domain wall and the energy reduction is still considerably higher than the energy obtained from reducing the wall area.

8.1.4 Critical field when a domain wall is strongly pinned

What is the field strength needed to break a domain wall away from a pinning site in the situation where the wall bends?

Kersten [17] modified the assumptions of his previous model and calculated the initial susceptibility of a solid with flexible domain walls. Consider for example the

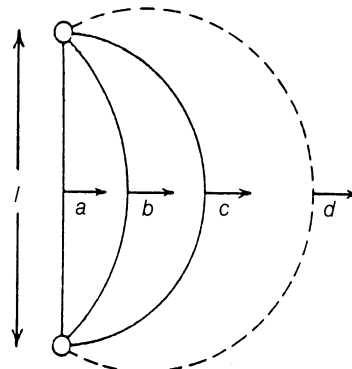


Fig. 8.6 Reversible and irreversible expansion of a domain wall according to Kersten.

case where the pinning strength of the defect sites is relatively high and the wall energy is relatively low. In this case the domain wall will bend under the action of a field. The process will be reversible until the radius of curvature reaches a critical value, after which the wall expands discontinuously and irreversibly.

Consider the situation depicted in Fig. 8.6. The radius of curvature r of the domain wall as it bends under the influence of an applied field \mathbf{H} is such that the excess pressure on the wall γ/r exactly balances the force per unit area due to the field. For a 180° wall

$$\frac{\gamma}{r} = 2\mu_0 \mathbf{M}_s \mathbf{H} \cos \theta,$$

where θ is the angle between the direction of the \mathbf{H} field and the magnetization within one of the domains. The critical condition arises when the radius of curvature of the wall reaches $l/2$ where l is the distance between the pinning sites.

$$\mathbf{H}_{c180} = \frac{\gamma}{\mu_0 \mathbf{M}_s l \cos \theta}$$

and similarly for a 90° wall

$$\mathbf{H}_{c90} = \frac{\gamma\sqrt{2}}{\mu_0 \mathbf{M}_s l \cos \theta}.$$

Kersten used these equations to determine the coercivity of nickel–iron alloys. This tells us that for strong pinning the critical field, and hence the coercivity, are dependent on the number density of pinning sites, expressed through the coefficient l , and the domain-wall energy γ .

8.1.5 Critical field when a domain wall is weakly pinned

What is the field strength needed to break a domain wall away from its pinning site before it bends?

156 Domain processes

In this case the walls move in a planar manner because they break away from the pinning sites before they have a chance to bend. The walls experience a certain potential as a result of the distribution of defects and dislocations. The force exerted on unit area of a 180° domain wall by a field \mathbf{H} is given by

$$F = 2\mu_0 M_s H \cos \theta,$$

where θ is the angle between the magnetization and the magnetic field.

If the potential energy is given by

$$E_p = E_p(x)$$

and the maximum slope of this is $[dE_p(x)/dx]_{\max}$, then at the critical field we must have the maximum force per unit area exerted on the wall,

$$F_{\max} = \left[\frac{dE_p(x)}{dx} \right]_{\max}.$$

So the critical field, beyond which the domain wall breaks away from its pinning site is given by

$$H_{\text{crit}} = \frac{F_{\max}}{2\mu_0 M_s \cos \theta}$$

$$H_{\text{crit}} = \frac{1}{2\mu_0 M_s \cos \theta} \left[\frac{dE_p(x)}{dx} \right]_{\max}$$

In the case of a sinusoidal variation of the potential energy of

$$E_p(x) = E_{\max} \sin\left(\frac{2\pi x}{l}\right)$$

and therefore

$$\left[\frac{dE_p(x)}{dx} \right]_{\max} = \frac{2\pi E_{\max}}{l}$$

this leads to

$$\begin{aligned} H_{\text{crit}} &= \frac{E_{\max}(2\pi/l)}{2\mu_0 M_s \cos \theta} \\ &= \frac{E_{\max}\pi}{l\mu_0 M_s \cos \theta}. \end{aligned}$$

In this case therefore the critical field and hence the coercivity are dependent on the maximum pinning energy E_{\max} and the number density of pinning sites, expressed via the separation l .

8.2 DETERMINATION OF MAGNETIZATION CURVES FROM PINNING MODELS

Can realistic models of the magnetization process be devised from the concept of domain-wall pinning?

One of the most difficult problems in the field of magnetism is to describe the magnetization curves of a ferromagnet in terms of materials properties. The complexity of domain-wall interactions with randomly distributed structural features is further compounded by the possibility of magnetization changes by domain rotation. Therefore attempts at deriving the underlying theory have dealt only with the simplest situations.

8.2.1 Effects of microstructural features on magnetization

How do dislocations and other defects affect coercivity and initial susceptibility?

The investigations of Becker, Kersten and Neel have served to clarify the processes taking place on the domain level when a domain wall interacts with defects. To be useful such a theory must be related to the observed bulk properties. As we have shown calculations were made by Kersten of the initial susceptibility based on a single Bloch wall model. The next development in understanding the magnetization process was a generalization of the earlier models to include the interaction of domain walls with defects such as dislocations. Dislocations have an associated stress field which impedes the motion of magnetic domain walls. The suggestion that dislocations affect the coercive force was first made by Vicena [18]. Subsequently there were a number of papers published by Kronmuller and coworkers on this subject.

Seeger *et al.* [19] considered the influence of lattice defects on the magnetization curve. They noted that the internal stresses in the earlier work of Becker were of an unspecified origin and were characterized by an average stress amplitude. Their theoretical calculations, based on a rigid wall approximation, indicated that the product of coercivity and initial susceptibility should be a constant.

$$\chi_{\text{in}} H_c = \text{constant}.$$

In addition it was shown that in the rigid wall approximation the coercivity was dependent on the square root of dislocation density ρ which in an f.c.c. material is proportional to applied stress.

$$\frac{H_c}{\sqrt{\rho}} = \text{constant}.$$

Kronmuller [20] derived a statistical theory of Rayleigh's law in the low-field magnetization region based on a rigid wall approximation model of domain-wall motion. The Rayleigh law (section 5.1.6.) gives the relation between magnetization M and magnetic field H as

$$M = \chi_{\text{in}} H + v H^2,$$

where v is the Rayleigh constant and χ_{in} is the initial susceptibility. The coefficients were shown to be determined by the domain wall potential, and it was found that they were related to the dislocation density ρ by the following

$$\chi_{\text{in}} \sqrt{\rho} = \text{constant}$$

$$v\rho = \text{constant}.$$

Hilzinger and Kronmuller [21] also investigated theoretically the coercive field of hard ferromagnetic materials. In particular they found that the interaction of domain walls in hard magnetic materials with defects lead to the experimentally observed temperature dependence of coercivity of SmCo₅. They have shown that high coercivities can be obtained by (a) pinning of domain walls by defects and (b) elimination of domain walls by using single-domain particles. For multidomain materials the first mechanism is the most important and it is known that in many materials the most significant mechanism for pinning is the interaction between dislocations and domain walls. However in SmCo₅ they considered that point defects are the most important pinning sites because the domain walls in this material are so thin, being typically 30 Å in width.

Further investigation of Bloch wall pinning in rare-earth cobalt alloys [22] suggested that antiphase boundaries are the dominant mechanism determining coercive force in these materials. (Antiphase boundaries occur when the A and B sublattices within an ordered superlattice become out of phase, with the type of atoms which were on sublattice A switching to sublattice B and vice versa. The nearest-neighbour coordination of the superlattice is therefore disrupted locally.)

Hilzinger and Kronmuller [23] developed and generalized these theories further for rigid (planar) domain-wall motion, considering the pinning of Bloch walls by randomly distributed defects. As they have indicated, the theories of domain-wall pinning basically still fall into two categories: potential theories with rigid domain walls and wall bowing theories with flexible walls. The problem of domain wall defect interactions has been treated previously for dislocations, point defects, and antiphase boundaries. They have shown that the coercivity depends upon defect density, the interaction (or pinning force) and the area and flexibility of domain walls. These concepts have also been considered by Jiles and Atherton [24].

In the case of potential theories Hilzinger and Kronmuller have shown further that the coercive force H_c , depends on the square root of the total domain wall area A_B as well as the defect density ρ

$$H_c \sim \frac{\sqrt{\rho}}{\sqrt{A_B}}.$$

In the case of domain-wall bowing models the coercive field was found to be dependent on $\rho^{2/3}$,

$$H_c \sim \rho^{2/3}$$

according to Labusch [25]. The question of how much domain wall bowing takes place is still slightly controversial. In Kronmuller's statistical theory of Rayleigh's law the domain walls were assumed to remain planar, but the papers of Kersten [17] and Dietze [26] assumed that bowing took place. It seems that the amount of domain-wall bowing that occurs depends on the strength of the pinning sites and the domain wall surface energy. Chikazumi [27, p. 193] has considered that the domain walls remain planar along the axis of magnetization within the domain, such as the [100] direction in iron, in order to avoid the appearance of free poles at the curved portion of the walls, but the walls are free to bend in other directions.

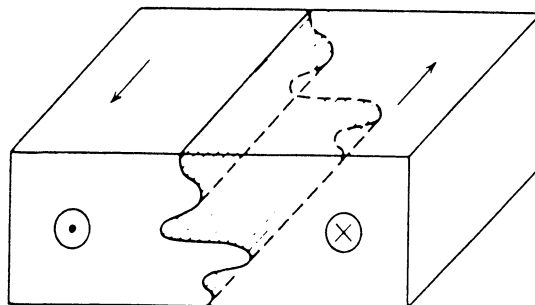


Fig. 8.7 Domain wall in iron showing its planar and bowing aspects in different crystallographic planes.

For example magnetizations along the [100] and [$\bar{1}00$] direction on either side of a domain wall lead to a planar wall when viewed from either the (001) or (010) planes. But when viewed from the (100) plane the wall can bend, as in Fig. 8.7.

Finally after considering only planar walls in their earlier papers Hilzinger and Kronmuller [28] considered the pinning of curved domain walls by randomly distributed defects. The two theories, the potential theory for planar walls and the bowing theory for flexible walls, were shown to be merely limiting cases of a more general theory. In this more general theory the coercive force was found to depend on $\rho^{1/2}$ for weak defect domain wall interactions and on $\rho^{2/3}$ for strong defect domain wall interactions. So the two models provided limiting ranges of a single curve. The result was important because it brought together the two principal wall mechanisms under a unified theory of domain-wall motion.

8.2.2 Domain-wall defect interactions in metals

What do experimental observations of domain-wall defect interactions show?

The problem of describing the magnetization process in terms of Bloch wall motion has also been discussed in a series of papers by Portesel, Astie and coworkers. In these papers a number of observations of domain-wall motion were made and the results were interpreted in terms of theoretical models. Portesel and Vergne in a theoretical paper [29] calculated the magnetization curve of a polycrystal using a single isolated Bloch wall model. They investigated conditions under which a single irreversible event remained independent and when it lead to an avalanche effect with numerous subsequent irreversible wall jumps or Barkhausen discontinuities.

Astie, Degauque, Portesel and Vergne [30] studied the influence of dislocation structures on the magnetic and magnetomechanical properties of high-purity iron. The dislocation structures were formed by strain hardening of polycrystalline iron. They criticized earlier work on domain-wall defect interactions because earlier studies failed to make precise observations of lattice defects. Their

investigation involved the dependence of the initial susceptibility χ_{in} , the Rayleigh coefficient v and the coercivity H_c on the strain hardening $\Delta\sigma = \sigma - \sigma_0$, where σ_0 is the yield strength and σ is the maximum stress applied. The authors concluded that there were three distinct regions on the strain hardening curve between $\Delta\sigma = 0$ and $\Delta\sigma = 100$ MPa and these were identified both from transmission electron microscopy (TEM) and from the magnetic parameters.

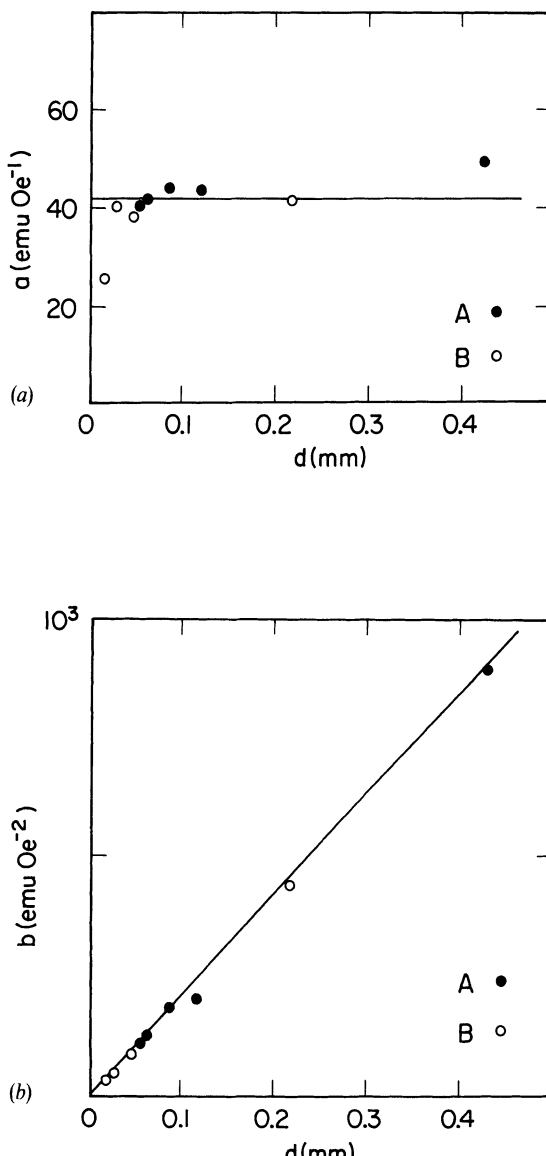


Fig. 8.8 Dependence of Rayleigh coefficient v on the grain diameter d in high-purity iron after Degauque, Astie, Portesel and Vergne [32].

Interestingly in the low stress region ($< 30 \text{ MPa}$) the coercivity and initial permeability were almost independent of stress. However at higher stresses, which resulted in larger dislocation densities in the form of tangles of dislocations separated by relatively large distances with lower dislocation densities, H_c increased rapidly, while χ_{in} was less affected. Further studies of the interaction of magnetic domain walls with defects in high-purity iron were reported by Degauque and Astie [31]. The evolution of domain structures under an applied field was studied using high-voltage electron microscopy (HVEM). Once again it was remarked that there have been many theoretical studies on the subject of domain-wall defect interactions, but very few direct observations of these interactions.

The effect of grain size on the magnetic properties of high-purity iron was reported by Degauque, Astie, Portesel and Vergne [32]. The coercivity H_c , the initial susceptibility χ_{in} and the Rayleigh coefficient v were studied together with the remanent induction B_R . The study concluded that the initial susceptibility was independent of grain size but the Rayleigh coefficient was proportional to grain diameter d

$$v/d = \text{constant},$$

as shown in Fig. 8.8. They also found that coercivity was linearly dependent on $1/d$ as shown in Fig. 8.9.

$$H_c d = \text{constant}.$$

The potential model for domain-wall motion was used by Astie, Degauque, Portesel and Vergne [33] to interpret results obtained on polycrystalline iron. From the work of Hilzinger and Kronmuller reported above it was known that the theory predicted

$$H_c \chi_{in} = \text{constant}$$

and

$$v H_c^2 = \text{constant}.$$

However it was found from experimental measurements on polycrystalline iron in which the density of defects was altered, that these values did change in contradiction of the predictions of the potential model of Hilzinger and Kronmuller. The authors found that the initial susceptibility χ_{in} was independent of grain size in iron. This is because χ_{in} is determined by the short-range reversible motion of domain walls in low fields. Under these conditions the dislocations are the predominant factor contributing to χ_{in} . The Rayleigh coefficient v was however found to be dependent on grain size d and increased with grain size, whereas the coercivity decreased with grain size.

In summary the predictions of invariance for $H_c \chi_{in}$ and $v H_c^2$ follow from the model only if the assumption is valid that the potential curve $V(x)$ is only altered by effectively scaling both V and x maintaining a similar shape of potential. However Astie *et al.* indicate that such an assumption is unlikely to be valid in many cases,

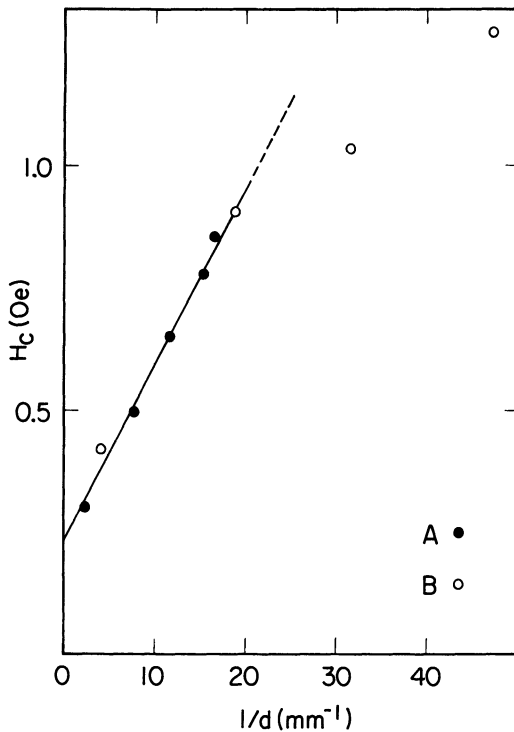


Fig. 8.9 Dependence of the coercivity H_c on the grain diameter d in high-purity iron after Degauque, Astie, Portesel and Vergne [32].

and as observed in their results and those of Jiles *et al.* [34] these products do not remain constant.

8.2.3 Magnetization processes in materials with few defects

Which factors influence the magnetization curve in materials with few defects?

The investigation of domain-wall motion in materials such as ferrites, garnets and spinels, which are relatively free of defects compared with iron, steel and nickel, has been conducted by Globus *et al.* in a series of papers. The effects of grain boundaries on the bulk magnetization curves of these materials proved to be the most significant microstructural factor, and in fact the domain-wall motion in these materials can be modelled with relatively few parameters, due to the simplicity of the situation.

In the Globus model which was suggested in the earliest paper of this series [35], it was assumed that domain walls are pinned at the grain boundaries. The model assumes that the magnetic domain walls are fixed by the pinning sites on the grain boundaries and that the walls deform by bending like an elastic membrane under the action of a magnetic field as was first described by Kersten. Therefore in experimental studies Globus and Duplex [36] prepared specimens which had only one variable parameter: the grain size. They investigated ferrites such as nickel

ferrite $\text{NiO}\cdot\text{Fe}_2\text{O}_3$, spinels such as nickel-zinc ferrite $\text{Ni}_x\text{Zn}_{1-x}\text{O}\cdot\text{Fe}_2\text{O}_3$ and yttrium-iron-garnet $5\text{Fe}_2\text{O}_3\cdot3\text{Y}_2\text{O}_3$. Precautions were taken to avoid other features such as non-magnetic inclusion, pores and dislocations within the grains, since the authors acknowledged that these strongly influence the domain-wall motion and hence the bulk magnetization curve.

From the model it was possible to calculate the wall curvature which corresponded to the initial susceptibility. It was found that χ_{in} depended linearly on the grain diameter d as shown in Fig. 8.10. They also concluded that the initial susceptibility of these materials is due almost entirely to wall motion. From the results it was therefore possible to separate the influence of wall motion (proportional to d) and rotation (independent of d) on the initial susceptibility. These contributions can be found in Fig. 8.10 (b) from the slope of the line, which is due to wall pinning, and the intercept at $d = 0$, which is due to rotation of the magnetic moments. The rotational contribution to χ_{in} is, according to Globus and Duplex [37], dependent on anisotropy but independent of structure, whereas the wall motion contribution

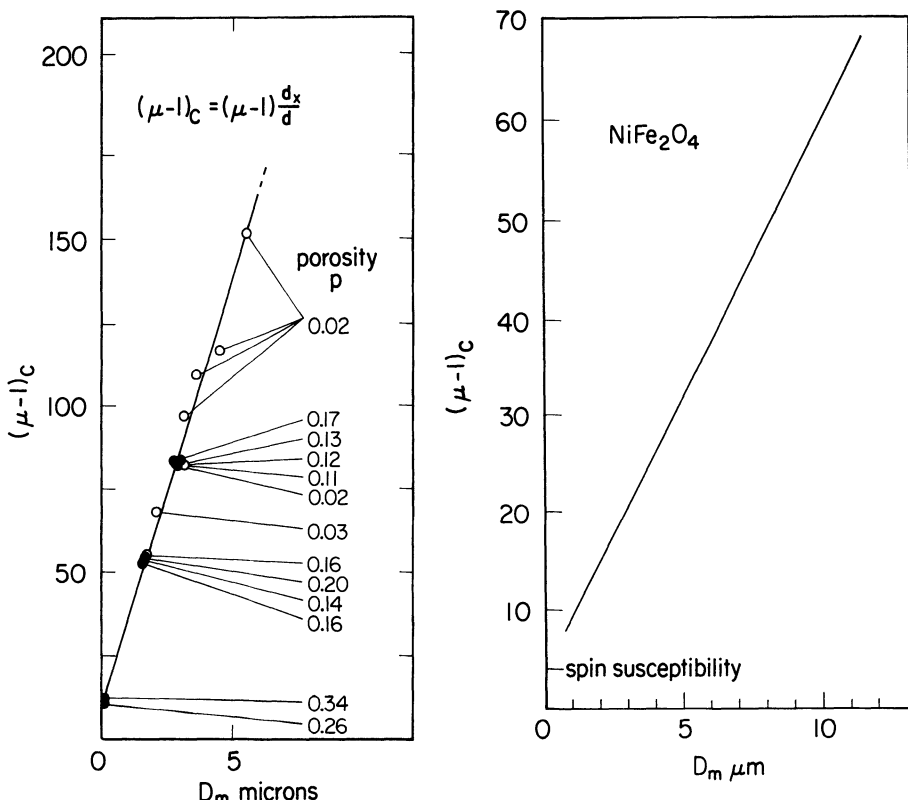


Fig. 8.10 Dependence of the initial susceptibility χ_{in} on grain diameter d in yttrium-iron-garnet and nickel ferrite, after Globus and Duplex [36 and 39]. © (1966) IEEE.

is highly structure-sensitive. Subsequently, Globus and Duplex [38] applied the same model to spinels and garnets.

Globus, Duplex and Guyot [39] have considered the magnetization process in yttrium–iron–ganet in terms of domain-wall processes. In their work the reversible component of magnetization was considered to be due to wall bulging, while the irreversible component of magnetization was due to domain-wall displacement, since the fields used were well below those required for domain rotation. In this paper an explicit formula for the susceptibility in terms of domain-wall bending was given.

The extended Globus–Guyot model [40] included both wall bulging and displacement. From this they provided a model for coercivity and remanence. In the extended model the authors determined a critical field strength beyond which wall translation, and hence irreversible processes, begin.

Further work by Guyot and Globus [41, 42] attempted to relate hysteresis loss to the creation and annihilation of domain-wall surface area and the energy lost by continual pinning and unpinning of magnetic domain walls. They concluded that the losses in these materials cannot be explained solely on the basis of pinning losses. The first loss term is of course a solid friction term due to the pinning and unpinning of domain walls. The second contribution comes from the variations in the magnetic domain surface area. Both of these lead to hysteresis loss.

From this work the authors concluded that the magnetization curves of these materials all had the same general form which was dependent upon grain size d , saturation magnetization M_s and the magnetic anisotropy field H_{eff} . In general the critical field for wall motion was much smaller than the anisotropy field ($H_{\text{cr}}/H_{\text{eff}} = 0.003$) so that domain rotation mechanisms could not play a significant role.

Finally Globus [43] has summarized earlier work giving a universal curve for the initial magnetization and hysteresis loss of spinels, ferrites and garnets. This universal curve depends upon M_s , the anisotropy K and the grain size d . The model seems to work well for these materials because they have very few intragranular defects and therefore the factors influencing the magnetization curve are relatively few and can be expressed in an analytic form of the magnetization curve. In metals such as iron and nickel the presence of other defects such as non-magnetic inclusions and dislocations play a significant role, and consequently the whole mechanism is more complicated.

8.2.4 The Barkhausen effect and domain-wall motion

How can other magnetic phenomena be interpreted in terms of wall motion?

The related phenomena of the Barkhausen effect and magnetoacoustic emission are both due to discontinuous irreversible changes in magnetization. These irreversible changes can occur as a result of irreversible domain-wall motion, either

as the unpinning of planar or non-planar domain walls from their pinning sites, or as the discontinuous expansion of a domain wall once its curvature has exceeded the critical value.

Barkhausen emissions can also result from the discontinuous rotation of moments within a domain from one of the easy axes into the easy axis aligned closest to the field direction. However in practice the contribution from this type of process is less significant.

The Barkhausen effect can be caused by the motion of either 180° or non-180° walls. However magnetoacoustic emission is only caused by the discontinuous motion of non-180° walls, or the irreversible rotation of domains through angles other than 180°. The reason for this is that to generate acoustic pulses there must be generation of stresses. No stresses are generated as a result of 180° wall motion or rotation because the strain along a particular axis is independent of the direction of magnetic moments if they lie along the axis.

8.2.5 Magnetostriiction and domain-wall motion

Are there differences in the contribution to magnetostriiction from different types of domain wall?

There is no change in the bulk magnetostriiction as a result of 180° wall motion or rotation. So in the case of terfenol and other highly magnetostrictive materials it is important to arrange for as much non-180° activity as possible to optimize the performance of the material, that is to maximize the bulk magnetostriiction. This is achieved by inducing stress anisotropy via an applied compressive stress to align the domains at right angles to the field direction.

8.3 THEORY OF FERROMAGNETIC HYSTERESIS

How can the bulk magnetic properties of ferromagnets be described with a minimum number of parameters?

It would obviously be very useful to be able to describe hysteresis mathematically in order to model magnetic properties of ferromagnetic materials. Therefore we will now consider how the ideas developed so far can be brought together to provide a theoretical model of hysteresis in ferromagnets. A few models are in use at present; these include the Preisach model [44] which is widely used in the magnetic recording industry for describing the magnetization characteristics of recording tapes, and the Stoner–Wohlfarth model [45] of rotational hysteresis, which really only applies to single-domain particles, but has been used for modelling properties of hard magnetic materials. We will consider a recent model of hysteresis [24] based on domain-wall motion which, as we have mentioned previously, is the principal cause of hysteresis in multidomain specimens.

8.3.1 Energy loss through wall pinning

Can we describe the energy loss in pinning of a domain wall?

Consider a 180° domain wall of area A between two domains aligned parallel and antiparallel to a magnetic field \mathbf{H} . If the wall moves through a distance dx under the action of a field the change in energy due to this movement is

$$dE = -2\mu_0 M_s \cdot H A dx.$$

Suppose the pinning energy of a given pinning site is $\mu_0 \varepsilon_\pi$ for a 180° domain wall, and that the pinning energy is proportional to the change in energy per unit volume caused by moving the wall.

$$\varepsilon_{\text{pin}} = \frac{1}{2} \varepsilon_\pi (1 - \cos \phi),$$

where ϕ is the angle between the moments in the neighbouring domains. This gives us an expression for the pinning energy of a given site as a function of angle ϕ . Clearly when $\phi = 0$ the pinning energy must go to zero since the wall no longer exists. In the case of a 180° wall $\varepsilon_{\text{pin}} = \varepsilon_\pi$. If there are n pinning sites per unit volume the energy lost by moving a domain wall is

$$dE_{\text{loss}} = \mu_0 n \varepsilon_\pi A dx,$$

where A is the cross-sectional area of the wall. The change in magnetization will be

$$dM = 2M_s A dx.$$

Therefore

$$dE_{\text{loss}} = \frac{\mu_0 n \varepsilon_\pi dM}{2M_s}.$$

Replacing $(n \varepsilon_\pi / 2M_s)$ by the constant k gives

$$dE_{\text{loss}} = \mu_0 k dM.$$

8.3.2 Irreversible magnetization changes

If we know the energy loss can we write down an energy equation for the magnetization process?

Suppose the change in energy of a ferromagnet is manifested either as a change in magnetization or as hysteresis loss. Then we can write the energy equation as follows

$$\left(\begin{array}{c} \text{Energy supplied to} \\ \text{material} \end{array} \right) = \left(\begin{array}{c} \text{Change in} \\ \text{magnetostatic} \\ \text{energy} \end{array} \right) + \left(\begin{array}{c} \text{Hysteresis} \\ \text{loss.} \end{array} \right)$$

In the case where there is no hysteresis loss, then the change in magnetostatic energy must equal the total energy supplied. When there is no hysteresis the

magnetization follows the anhysteretic curve $\mathbf{M}_{\text{an}}(\mathbf{H})$

$$\mu_0 \int \mathbf{M}_{\text{an}}(\mathbf{H}) d\mathbf{H} = \mu_0 \int \mathbf{M}(\mathbf{H}) d\mathbf{H} + \mu_0 \int \left(\frac{n\epsilon_\pi}{2M_s} \right) \left(\frac{d\mathbf{M}}{d\mathbf{H}} \right) d\mathbf{H}$$

and consequently

$$\begin{aligned} \mathbf{M}_{\text{an}}(\mathbf{H}) &= \mathbf{M}(\mathbf{H}) + k \left(\frac{d\mathbf{M}}{d\mathbf{H}} \right) \\ \frac{d\mathbf{M}}{d\mathbf{H}} &= \frac{\mathbf{M}_{\text{an}}(\mathbf{H}) - \mathbf{M}(\mathbf{H})}{k}. \end{aligned}$$

This simple result states that the rate of change of magnetization \mathbf{M} with field \mathbf{H} is proportional to the displacement of the magnetization from the anhysteretic magnetization. That is the bulk magnetization \mathbf{M} experiences a harmonic potential about $\mathbf{M}_{\text{an}}(\mathbf{H})$.

In fact the situation is a little more complex than this in reality due to the coupling between the magnetic domains which is of the form envisaged by Weiss, so that the effective field becomes $\mathbf{H}_e = \mathbf{H} + \alpha\mathbf{M}$ resulting in the following equation, which we should note represents only the irreversible component of magnetization

$$\frac{d\mathbf{M}_{\text{irr}}}{d\mathbf{H}} = \frac{\mathbf{M}_{\text{an}}(\mathbf{H}) - \mathbf{M}_{\text{irr}}(\mathbf{H})}{k - \alpha[\mathbf{M}_{\text{an}}(\mathbf{H}) - \mathbf{M}_{\text{irr}}(\mathbf{H})]}.$$

8.3.3 Reversible magnetization changes

Can we incorporate reversible changes in magnetization into the differential equation of hysteresis?

There is of course also a reversible component of magnetization due to reversible domain wall bowing, reversible translation and reversible rotation. In the model this has the form

$$\mathbf{M}_{\text{rev}} = c(\mathbf{M}_{\text{an}} - \mathbf{M}_{\text{irr}})$$

and since we must have either reversible or irreversible changes in magnetization, the total magnetization \mathbf{M}_{tot} is given by

$$\mathbf{M}_{\text{tot}} = \mathbf{M}_{\text{rev}} + \mathbf{M}_{\text{irr}}.$$

In fact the above equation is not really very helpful since magnetization changes which begin as reversible can become locked in and end up as irreversible. A much more useful expression however is the expression for the change in magnetization with field. In this case we are more justified in distinguishing between a reversible component of susceptibility and an irreversible component of susceptibility

$$\frac{d\mathbf{M}_{\text{tot}}}{d\mathbf{H}} = \frac{d\mathbf{M}_{\text{irr}}}{d\mathbf{H}} + \frac{d\mathbf{M}_{\text{rev}}}{d\mathbf{H}}.$$

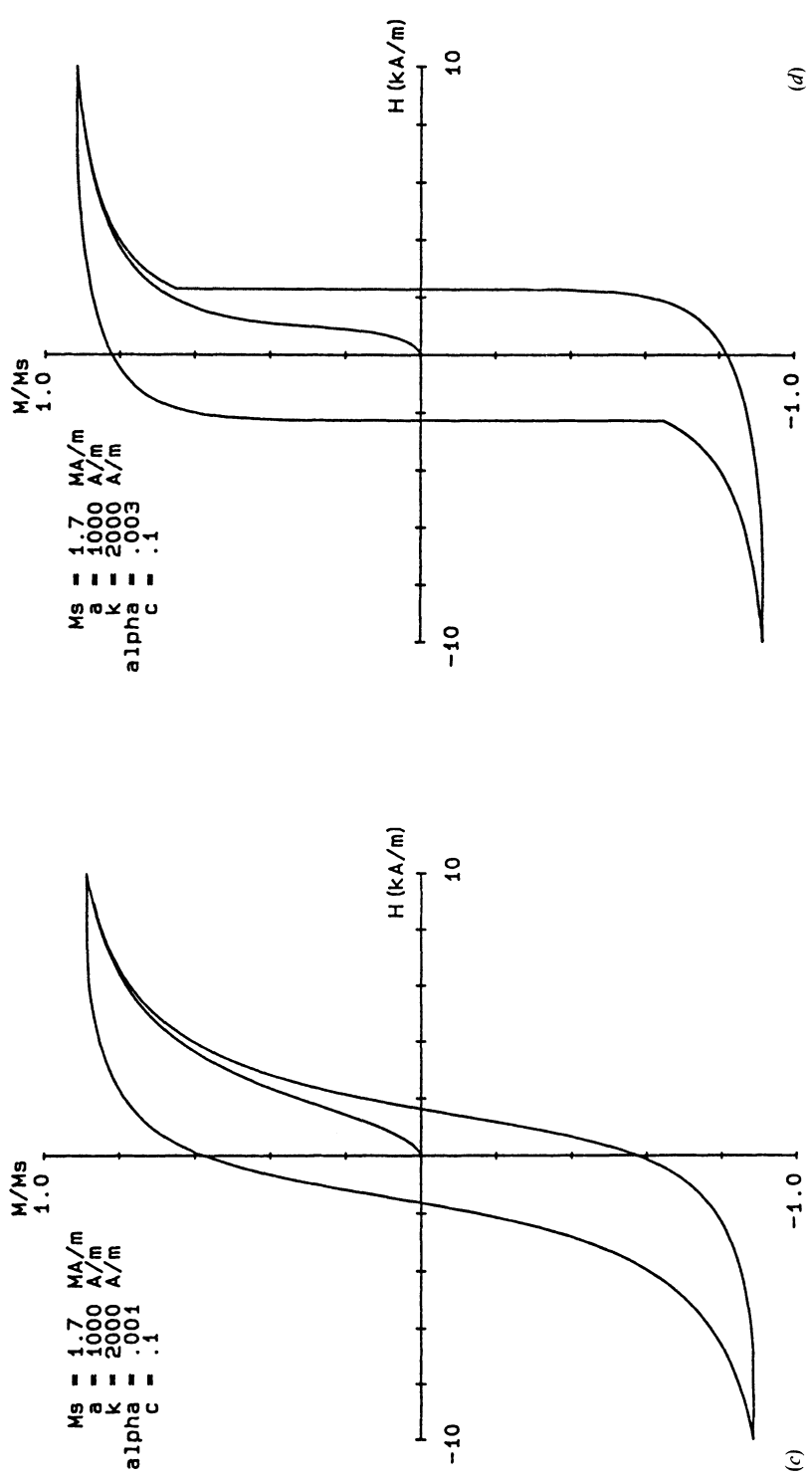
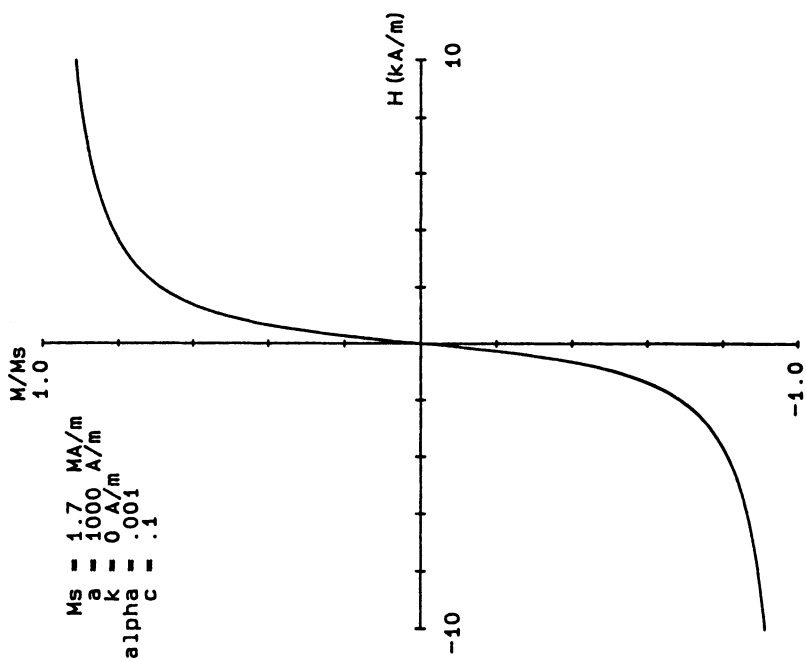
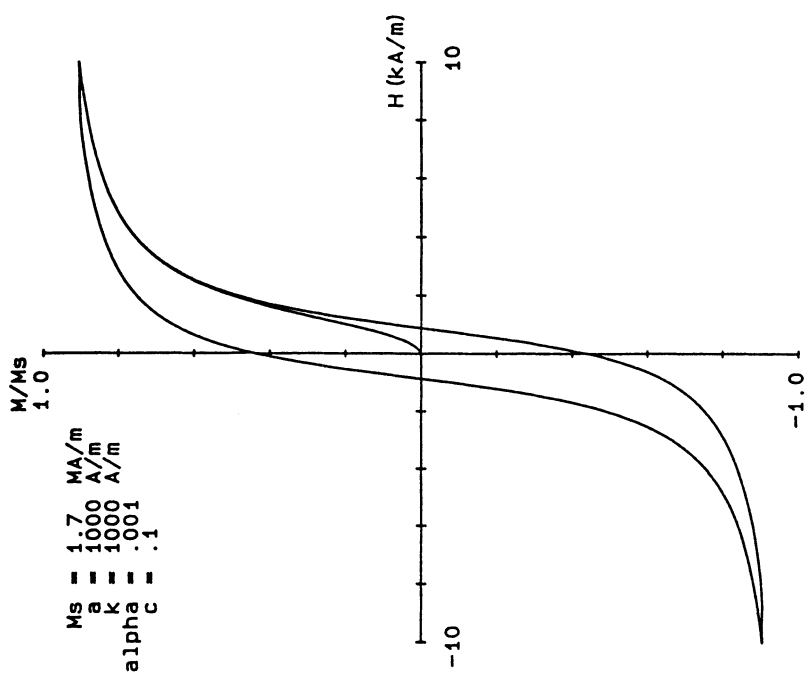


Fig. 8.11 Theoretical hysteresis loops calculated using the equations derived in the theory of hysteresis by Jiles and Atherton.



Removing the subscript and assuming that whenever we talk about a change in magnetization without further qualification, we mean the total magnetization

$$\frac{d\mathbf{M}}{dH} = \frac{(\mathbf{M}_{an} - \mathbf{M}_{irr})}{k - \alpha(\mathbf{M}_{an} - \mathbf{M}_{irr})} + c \left(\frac{d\mathbf{M}_{an}}{dH} - \frac{d\mathbf{M}_{irr}}{dH} \right).$$

It is clear from this model that if $k \rightarrow 0$ then $\mathbf{M} \rightarrow \mathbf{M}_{an}(H)$ which conforms with earlier comments that if there are no pinning sites then the magnetization will follow the anhysteretic magnetization curve. Solutions of this differential equation for various values of the parameters are shown in Fig. 8.11.

8.3.4 Relationship between hysteresis coefficient and measured magnetic properties

How can these theoretical parameters be calculated from the conventional magnetization curve?

It is clearly important from the viewpoint of applications to be able to calculate the values of these various parameters governing hysteresis from a measured magnetization curve [46]. From the equations it is easily shown that the initial susceptibility of the normal magnetization curve is given by

$$\chi_{in} = c\chi_{an},$$

where χ_{an} is the differential susceptibility of the anhysteretic curve at the origin. This concept agrees well with Rayleigh's idea that χ_{in} represents the reversible component of magnetization at the origin of the initial magnetization curve.

In the case where k is constant and the reversible component is negligible, that is $c = 0$, we have the following very simple solution for k in terms of the coercivity H_c and the slope χ'_{H_c} of the hysteresis loop at H_c

$$k = M_{an}(H_c) \left(\alpha + \frac{1}{\chi'_{H_c}} \right).$$

when $c \neq 0$ this becomes

$$k = M_{an}(H_c) \left\{ \frac{\alpha}{(1-c)} + \left[\frac{1}{(1-c)\chi'_{H_c} - c \frac{dM_{an}(H_c)}{dH}} \right] \right\}.$$

In the case of soft magnetic materials which have a low coercivity we can make some approximations which lead to an interesting relation between k and H_c . For low coercivity materials the slope of the hysteresis loop at the coercive point is approximately equal to the slope of the anhysteretic curve at the origin. Setting these equal,

$$\begin{aligned} \chi'_{an} &= \chi'_{H_c} \\ \frac{M_s}{3a - \alpha M_s} &= \frac{M_{an}(H_c)}{k - \alpha M_{an}(H_c)} \end{aligned}$$

which leads to the following equation for k ,

$$k = \frac{3a}{M_s} M_{\text{an}}(H_c).$$

Secondly, the slope of the anhysteretic curve at the origin is quite linear and therefore, for small H_c we can write

$$M_{\text{an}}(H_c) = \chi'_{\text{an}} H_c = \left(\frac{M_s}{3a - \alpha M_s} \right) H_c$$

and substituting this result into the expression for k gives

$$k = \frac{H_c}{1 - \left(\frac{\alpha M_s}{3a} \right)}.$$

This brings us to the important result that the coercivity of a soft ferromagnetic material is determined principally by the pinning of domain-wall motion. In fact $k \approx H_c$ for soft magnetic materials.

8.3.5 Effects of microstructure and deformation on hysteresis

How does the hysteresis depend on the details of the material microstructure?

Changes in microstructure, in the form of additional magnetic inclusions such as second-phase particles with different magnetic properties from those of the matrix material, cause changes in the hysteresis properties by introducing more pinning sites that impede domain-wall motion and thereby lead to increased coercivity and hysteresis loss [47, 48, 49]. The same is also true of dislocations when their number density is increased by plastic deformation, either in tension or compression [50]. So for example the addition of carbon in the form of iron carbide particles increases coercivity and hysteresis loss. Cold working of the material has a similar effect.

The effect of these pinning sites is expressed via the coefficient k in the theory of ferromagnetic hysteresis. Clearly as their numbers increase k will increase proportionally and this results in an increase in the coercivity H_c as given in the equations above.

In the low field limit the coercivity is $H_c = k$ and consequently the coercivity is proportional to the product of number density and average pinning energy per site.

8.3.6 Effects of stress on bulk magnetization

How does applied stress alter the hysteresis properties?

Following classical thermodynamics of reversible systems the Gibbs energy is

$$G = U - TS + \frac{3}{2}\sigma\lambda,$$

where λ is the bulk magnetostriction, σ is the stress, U is the internal energy, T is the

thermodynamic temperature and S is the entropy. The Helmholtz energy is

$$A = G + \mu_0 \mathbf{H} \cdot \mathbf{M},$$

where \mathbf{H} is the field and \mathbf{M} is the magnetization. The internal energy U due to magnetization is

$$U = \frac{1}{2} \alpha \mu_0 \mathbf{M}^2.$$

The total effective field is given by [51]

$$\mathbf{H}_{\text{eff}} = \left(\frac{1}{\mu_0} \right) \left(\frac{dA}{d\mathbf{M}} \right)_T$$

assuming the material is under a constant stress σ we can write the effective field as

$$\mathbf{H}_{\text{eff}} = \mathbf{H} + \alpha \mathbf{M} + \frac{3}{2} \sigma \left(\frac{d\lambda}{d\mathbf{M}} \right)_T,$$

where \mathbf{H} is the magnetic field, $\alpha \mathbf{M}$ is the mean field coupling to the magnetization and \mathbf{H}_σ is an equivalent stress field [51].

$$\mathbf{H}_\sigma = \frac{3}{2} \sigma \left(\frac{d\lambda}{d\mathbf{M}} \right)_T.$$

This can be used to determine the reversible magnetization under the action of stress. So for example the anhysteretic magnetization curve, which is a reversible magnetization curve, can be determined by adding the stress equivalent field \mathbf{H}_σ to the sum of the true field \mathbf{H} and the internal field due to coupling between the magnetic moments $\alpha \mathbf{M}$. Using the Frohlich–Kennelly relation with $\alpha = 0$ (the Frohlich–Kennelly equation does not contain any coupling to the magnetization) this would become under the action of a stress σ

$$\mathbf{M}_{\text{an}}(\mathbf{H}) = \frac{\alpha \left[\mathbf{H} + \frac{3}{2} \left(\frac{d\lambda}{d\mathbf{M}} \right)_T \right]}{\left\{ 1 + \beta \left[\mathbf{H} + \frac{3}{2} \sigma \left(\frac{d\lambda}{d\mathbf{M}} \right)_T \right] \right\}}$$

This result tells us how the anhysteretic magnetization curve is altered under the action of a constant stress σ for a material with magnetostriction λ . We should note that this analysis applies only to a reversible process. In the case of irreversible processes the thermodynamic relationships become more complicated.

REFERENCES

1. Sixtus, K. J. and Tonks, L. (1931) *Phys. Rev.*, **37**, 930.
2. Becker, R. (1932) *Phys. Zeits.*, **33**, 905.
3. Hoselitz, K. (1952) *Ferromagnetic Properties of Metals and Alloys*, Oxford University Press, Oxford.
4. Becker, R. and Kersten, M. (1930) *Z. Phys.*, **64**, 660.

5. Kondorsky, E. (1937) *Physik. Z. Sowjetunion*, **11**, 597.
6. Becker, R. and Doring, W. (1938) *Ferromagnetismus*, Springer-Verlag, Berlin.
7. Kersten, M. (1938) in *Problems of the Technical Magnetisation Curve* (ed. R. Becker), Springer, Berlin.
8. Orowan, E. (1934) *Z. Phys.*, **89**, 605.
9. Taylor, G. I. (1934) *Proc. Roy. Soc. Lond.*, **145A**, 362.
10. Polanyi, M. (1934) *Z. Phys.*, **89**, 660.
11. Hull, D. and Bacon, D. J. (1964) *Introduction to Dislocations*, 3rd edn, Pergamon Oxford.
12. Kersten, M. (1943) *Underlying Theory of Ferromagnetic Hysteresis and Coercivity*, Hirzel, Leipzig.
13. Kersten, M. (1943) *Phys. Z.*, **44**, 63.
14. Neel, L. (1944) *Cahiers de Phys.*, **25**, 21.
15. Neel, L. (1946) Basis of a new general theory of the coercive field, *Ann. Univ. Grenoble*, **22**, 299.
16. Dijkstra, L. J. and Wert, C. (1950) *Phys. Rev.*, **79**, 979.
17. Kersten, M. (1956) *Z. Angew. Phys.*, **7**, 313; **8**, 382; **8**, 496.
18. Vicena, F. (1955) *Czech. J. Phys.*, **5**, 480.
19. Seeger, A., Kronmuller, H., Rieger, H. and Trauble, H. (1964) *J. Appl. Phys.*, **35**, 740.
20. Kronmuller, H. (1970) *Z. Angew. Phys.*, **30**, 9.
21. Kronmuller, H. and Hilzinger, H. R. (1973) *Int. J. Magnetism*, **5**, 27.
22. Hilzinger, H. R. and Kronmuller, H. (1975) *Phys. Letts.*, **51A**, 59.
23. Hilzinger, H. R. and Kronmuller, H. (1976) *J. Mag. Mag. Mater.*, **2**, 11.
24. Jiles, D. C. and Atherton, D. L. (1986) *J. Mag. Mag. Mater.*, **61**, 48.
25. Labusch, R. (1969) *Cryst. Latt. Def.*, **1**, 1.
26. Dietze, H. D. (1957) *Z. Phys.* **149**, 276.
27. Chikazumi, S. (1964) *Physics of Magnetism*, Wiley, New York.
28. Hilzinger, H. R. and Kronmuller, H. (1977) *Physica*, **86-8B**, 1365.
29. Porteseil, J. L. and Vergne, R. (1979) *J. de Phys.* (1981) **40**, 871.
30. Astie, B., Degauque, J., Porteseil, J. L. and Vergne, R. (1981) *IEEE Trans. Mag.*, **17**, 2929.
31. Degauque, J. and Astie, B. (1982) *Phys. Stat. Sol.*, **A74**, 201.
32. Degauque, J., Astie, B., Porteseil, J. L. and Vergne, R. (1982) *J. Mag. Mag. Mater.*, **26**, 261.
33. Astie, B., Degauque, J., Porteseil, J. L. and Vergne, R. (1982) *J. Mag. Mag. Mater.*, **28**, 149.
34. Jiles, D. C., Chang, T. T., Hougen, D. R. and Ranjan, R. (1988) *J. Appl. Phys.*, **64**, 3620.
35. Globus, A. (1962) *Comptes Rendus Acad. Seances*, **255**, 1709.
36. Globus, A. and Duplex, P. (1966) *IEEE Trans. Mag.*, **2**, 441.
37. Globus, A. and Duplex, P. (1969) *Phys. Stat. Sol.*, **31**, 765.
38. Globus, A. and Duplex, P. (1970) *Phys. Stat. Sol.*, **A3**, 53.
39. Globus, A. Duplex, P. and Guyot, M. (1971) *IEEE Trans. Mag.*, **7**, 617.
40. Globus, A. and Guyot, M. (1972) *Phys. Stat. Sol.*, **B52**, 427.
41. Guyot, M. and Globus, A. (1973) *Phys. Stat. Sol.*, **B59**, 447.
42. Guyot, M. and Globus, A. (1977) *J. de Phys.*, **38**, C1-157.
43. Globus, A. (1977) *Physica*, **86-8B**, 943.
44. Preisach, F. (1935) *Z. Phys.*, **94**, 277.
45. Stoner, E. C. and Wohlfarth, E. P. (1948) *Phil. Trans. Roy. Soc.*, **A240**, 599.
46. Jiles, D. C. and Thoelke, J. B. (1989) Proceedings of the 1989 Intermag Conference, *IEEE Trans. Mag.*, **25**, 3928, 1989.
47. Leslie, W. C. and Stevens, D. W. (1964) *Trans. ASM*, **57**, 261.
48. English, A. T. (1967) *Acta. Metall.*, **15**, 1573.
49. Jiles, D. C. (1988) *J. Phys. D. (Appl. Phys.)*, **21**, 1186.

50. Jiles, D. C. (1988) *J. Phys. D. (Appl. Phys.)*, **21**, 1196.
 51. Sablik, M. J., Kwun, H., Burkhardt, G. L. and Jiles, D. C. (1988) *J. Appl. Phys.*, **63**, 3930.

FURTHER READING

- Becker, R. and Doring, W. (1939) *Ferromagnetismus*, Springer-Verlag, Berlin.
 Chikazumi, S. (1964) *Physics of Magnetism*, Wiley, Ch. 11, 13, 14.
 Crangle, J. (1977) *The Magnetic Properties of Solids*, Arnold, Ch. 6.
 Cullity, B. D. (1972) *Introduction to Magnetic Materials*, Addison-Wesley, Reading, Mass, Ch. 9.
 Hoselitz, K. (1952) *Ferromagnetic Properties of Metals and Alloys*, Oxford, Ch. 2.
 Stoner, E. C. (1948) *Phil. Trans. Roy. Soc.*, **A240**, 599.

EXAMPLES AND EXERCISES

Example 8.2 Magnetostatic energy associated with a void. Show that the magnetostatic energy of a spherical void enclosed entirely within a domain as shown in Fig. 8.4 is $2\mu_0 M_s^2 \pi r^3 / 9$ where M_s is the saturation magnetization of the material and r is the radius of the void.

Assuming that the reduction in energy when a 180° domain wall intersects such a void is $\mu_0 M_s^2 \pi r^3 / 9$, calculate the energy reduction when a domain wall in iron intersects spherical voids of $r = 5 \times 10^{-8}$ m and $r = 10^{-6}$ m. Compare this to the

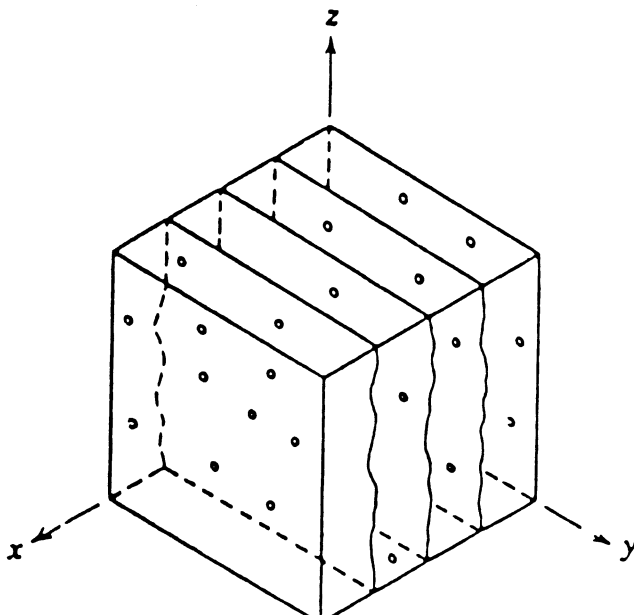


Fig. 8.12 Domain walls within a ferromagnetic material stabilized by inclusions distributed within the material. In this case the inclusions are voids.

difference in wall energy caused by the intersection with the void, assuming the domain-wall energy in iron is $2 \times 10^{-3} \text{ J/m}^2$ and $M_s = 1.7 \times 10^6 \text{ A/m}$.

Example 8.3 Reduction of domain-wall energy by voids. If the reduction in energy when a domain wall intersects a void is given by $\mu_0 M_s^2 \pi r^3 / 9$, estimate the reduction in energy per unit volume in a material which has N voids per unit volume each of radius r . (Assume all domain walls form parallel planes of separation d within a cube of unit volume as shown in Fig. 8.12.)

If the wall energy is to be completely compensated for by the decrease in energy associated with the voids estimate the number density of voids of radius r which can generate domain walls in a crystal.

Calculate this number for iron with $M_s = 1.7 \times 10^6 \text{ A/m}$, $r = 0.01 \text{ mm}$ and a wall energy of $2 \times 10^{-3} \text{ J/m}^3$.

Example 8.4 Effect of stress on anhysteretic susceptibility. Derive an expression for the susceptibility of a 180° domain wall moving in a linear stress field $\sigma = ax^2$, where a is a constant. Assume there is no change in wall energy as it moves in the stress field.

Determine the anhysteretic susceptibility at the origin $\chi'_{\text{an}}(\sigma)$ of a magnetic material under a compressive stress of -20 MPa , if the zero stress value of $\chi'_{\text{an}}(0)$ is 1000, and the low-field magnetostriction increases with magnetization M according to $\lambda = b(\sigma)M^2$, where $b(\sigma) = 1.8 \times 10^{-12} (\text{A/m})^{-2}$ when $\sigma = -20 \text{ MPa}$. The saturation magnetization of this material $M_s = 0.9 \times 10^6 \text{ A/m}$.

9

Magnetic Order and Critical Phenomena

In this chapter we discuss theories of magnetic behaviour of materials, particularly the alignment of magnetic moments within the material. These theories can provide quite useful phenomenological models of the magnetic properties including order-disorder transitions such as occur at the Curie temperature. These models assume each atom in a paramagnet or ferromagnet has a fixed magnetic moment but make no assumptions about the electronic structure of the atoms or origin of the atomic magnetic moment.

9.1 THEORIES OF PARAMAGNETISM AND DIAMAGNETISM

What atomic scale theories do we have to account for the properties of diamagnets and paramagnets?

Diamagnets are solids with no permanent net magnetic moment per atom. Diamagnetic susceptibility arises from the realignment of electron orbitals under the action of a magnetic field. Therefore all materials exhibit a diamagnetic susceptibility, although not all are classified as diamagnets. Some materials have a net magnetic moment per atom, due to an unpaired electron spin in each atom which leads to paramagnetism or even to ordered magnetic states such as ferromagnetism. In either case the paramagnetic or ferromagnetic susceptibility is much greater than the diamagnetic susceptibility and therefore is the dominant effect.

Paramagnetism occurs at higher temperatures in all materials which have a net magnetic moment. The atomic magnetic moments are randomly oriented but can be aligned by a magnetic field.

9.1.1 Diamagnetism

What causes the negative susceptibility observed in some materials?

The magnetic moments associated with atoms in magnetic materials have three origins. These are the electron spins, the electron orbital motion and the change in orbital motion of the electrons caused by an applied magnetic field. Only the

change in orbital motion gives rise to a diamagnetic susceptibility. Diamagnetism leads to a very weak magnetization which opposes the applied field. The diamagnetic susceptibility is therefore negative and has an order of magnitude of 10^{-5} or 10^{-6} . It is also found to be independent of temperature. Most elements in the periodic table are diamagnetic, we mention as examples copper, gold, silver and bismuth.

9.1.2 Langevin theory of diamagnetism

How can we explain the negative susceptibility of diamagnets in terms of the motion of electrons?

The susceptibility of diamagnets was first explained by Langevin [1]. In this work he applied some of the earlier ideas of Ampère, Weber and Lenz on the effect of a magnetic field on a current-carrying conductor, to the motion of an electron within an atom. An electron in orbit about an atomic nucleus can be compared with current passing through a loop of conductor and it will therefore have an orbital magnetic moment \mathbf{m}_0 since as we already know from Chapter 1 electric charge in closed loop motion generates a magnetic moment.

In the case of a current loop the magnetic moment is

$$\mathbf{m}_0 = iA,$$

where i is the current and A is the area of the loop. For an electron in orbital motion

$$\mathbf{m}_0 = \frac{eA}{\tau},$$

where e is the charge on the electron and τ is the orbital period. If we have circular orbital of area $A = \pi r^2$ and $\tau = 2\pi r/v$, where v is the instantaneous tangential velocity of the electron and r is the radius of the orbital

$$\mathbf{m}_0 = \frac{evr}{2}.$$

This is the magnetic moment obtained as a result of the orbital motion of an electron. In the absence of a magnetic field the orbital moments of paired electrons within an atom will cancel. An applied magnetic field \mathbf{H} will accelerate or decelerate the orbital motion of the electron and thereby contribute to a change in the orbital magnetic moment. Once a magnetic field has been applied the perturbation of the electron velocity can be determined. The change in magnetic flux through the current loop described by the electron about the nucleus gives rise to an emf V_e in the current loop. This leads to an electric field E given by

$$\begin{aligned} E &= \frac{V_e}{L} \\ &= -\left(\frac{1}{L}\right) \frac{d\phi}{dt}, \end{aligned}$$

where L is the orbit length ($= 2\pi r$) and V_e is the induced voltage.

$$E = \left(\frac{-1}{L} \right) \frac{d(BA)}{dt}$$

$$= \left(\frac{-A}{L} \right) \frac{d\mathbf{B}}{dt}.$$

The acceleration of the electron is

$$a = \frac{dv}{dt}$$

$$= \frac{eE}{m_e},$$

where $F = eE$ is the force on the electron due to the field E and m_e is the mass of the electron.

$$\begin{aligned} \frac{dv}{dt} &= \frac{eE}{m_e} \\ &= - \left(\frac{eA}{m_e L} \right) \frac{d\mathbf{B}}{dt} \\ &= - \left(\frac{er}{2m_e} \right) \frac{d\mathbf{B}}{dt} \\ &= - \left(\frac{\mu_0 er}{2m_e} \right) \frac{d\mathbf{H}}{dt}. \end{aligned}$$

Now integrating from zero field strength to an arbitrary field strength \mathbf{H} gives

$$\begin{aligned} \int_{v_1}^{v_2} dv &= - \left(\frac{\mu_0 er}{2m_e} \right) \int_0^H d\mathbf{H} \\ v_2 - v_1 &= - \left(\frac{\mu_0 er}{2m_e} \right) H. \end{aligned}$$

The change in magnetic moments arising from this is

$$\Delta \mathbf{m}_0 = \left(\frac{er}{2} \right) (v_2 - v_1)$$

$$\Delta \mathbf{m}_0 = - \frac{\mu_0 e^2 r^2 \mathbf{H}}{4m_e}.$$

This result only applies in the case where the magnetic field is perpendicular to the plane of motion of the electron. In the case where the field \mathbf{H} is in the plane of motion the net change is zero. In the general case therefore we have the projection

R of the orbit radius r on a plane normal to the field

$$R = r \sin \theta,$$

where $\theta = 0$ corresponds to a field in the plane of orbit and $\theta = \pi/2$ corresponds to a field perpendicular to the plane.

$$\Delta \mathbf{m}_0 = -\left(\frac{\mu_0 e^2}{4m_e}\right) \int \left(\frac{R^2}{A}\right) \sin^2 \theta \, dA,$$

where now A is the area of a hemisphere and $dA = 2\pi R^2 \sin \theta \, d\theta$, as shown in Fig. 9.1. The average value of R^2 is

$$\langle R^2 \rangle = \left(\frac{2}{3}\right)r^2$$

and consequently

$$\Delta \mathbf{m}_0 = -\frac{\mu_0 e^2 r^2 H}{6m_e},$$

where now the radius r can have any orientation. If we consider Z outer electrons in

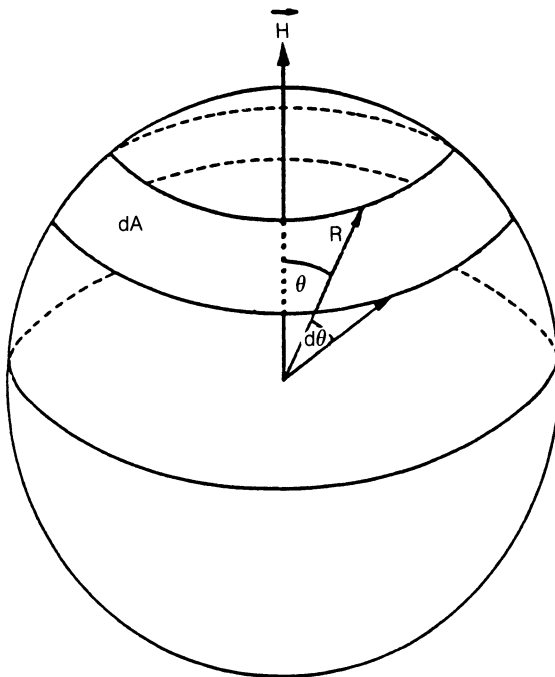


Fig. 9.1 Unit sphere defining the parameters R , θ and A used to describe the orbital motion of an electron about the nucleus.

the atom then the change in magnetic moment per atom is

$$\Delta \mathbf{m}_0 = -\frac{\mu_0 Ze^2 r^2 \mathbf{H}}{6m_e}$$

and of course if we wish to convert this to a bulk magnetization

$$\Delta \mathbf{M} = -\left(\frac{N_0 \rho}{W_a}\right) \left(\frac{\mu_0 Ze^2 r^2 \mathbf{H}}{6m_e}\right)$$

where N_0 = Avogadro's number, ρ is the density and W_a the relative atomic mass.

$$\begin{aligned} \chi &= \frac{\mathbf{M}}{\mathbf{H}} \\ &= -\left(\frac{N_0 \rho}{W_a}\right) \frac{(\mu_0 Ze^2 r^2)}{6m_e}. \end{aligned}$$

This deduction tells us that in the case of a diamagnet, which has no net atomic magnetic moment in the absence of a field, the action of a magnetic field causes changes in the velocity of electrons in the atom in such a way that the induced moment opposes the field producing it. It is also clear that the above expression for diamagnetic susceptibility is independent of temperature, which is in accordance with experimental observations.

The result that is often quoted as confirmation of the Langevin model of diamagnetism is the susceptibility of carbon, for which

$$N_0 = 6.02 \times 10^{-29}$$

$$\rho = 2220 \text{ kg/m}^3$$

$$e = 1.6 \times 10^{-19} \text{ C}$$

$$Z = 6$$

$$\langle R^2 \rangle = (0.7 \times 10^{-10})^2 \text{ m}^2.$$

The expected value of susceptibility on the basis of the Langevin model is

$$\chi = -18.85 \times 10^{-6},$$

the true value is

$$\chi = -13.82 \times 10^{-6}.$$

9.1.3 Paramagnetism

How can we explain the paramagnetic susceptibility of solids which have a permanent magnetic moment per atom?

Both the electron spin and the orbital angular momentum give contributions to the magnetization which lead to positive susceptibility. The susceptibilities of

182 Magnetic order and critical phenomena

paramagnets are typically of the order of $\chi \approx 10^{-3}$ to 10^{-5} , and at low fields M is proportional to H , although deviations from proportionality occur at very high fields where the magnetization begins to saturate. Examples of paramagnets are aluminum, platinum and manganese above its Neel temperature of 100 K.

There are a number of possible explanations of paramagnetic behaviour in solids. These range from the localized moments model of Langevin [1], in which the non interacting electronic magnetic moments on the atomic sites are randomly oriented as a result of their thermal energy, to the Van Vleck model [2] of localized moment paramagnetism, which leads to a temperature-independent susceptibility under certain circumstances. Finally, there is the Pauli paramagnetism model [3], which depends on the weak spin paramagnetism of the conduction-band electrons in metals. In this model the conduction electrons are considered essentially to be free and so non-localized. The Pauli model also leads to a temperature-independent paramagnetic susceptibility.

9.1.4 Curie's law

How does the susceptibility of a paramagnet depend on temperature?

The susceptibilities of a number of paramagnetic solids were measured over a wide temperature range by Curie [4]. In this he found that the susceptibility varied inversely with temperature, as shown in Fig. 9.2.

$$\chi = \frac{C}{T},$$

where C is a constant known as the Curie constant.

The materials which obey this law are materials in which the magnetic moments are localized at the atomic or ionic sites. These can be considered to be 'dilute' magnetic materials, in which the magnetic atoms are surrounded by a number of non-magnetic atoms. Hydrated salts of transition metals such as $\text{CuSO}_4 \cdot 5\text{H}_2\text{O}$ and $\text{CrK}(\text{SO}_4) \cdot 12\text{H}_2\text{O}$ obey the Curie law.

9.1.5 Langevin theory of paramagnetism

If the electronic magnetic moments are localized on the atom how does the susceptibility depend on magnetic field and temperature?

In materials with unpaired electrons, and consequently in which the orbital magnetic moments are not balanced, there is a net permanent magnetic moment per atom. If this net atomic magnetic moment is \mathbf{m} , which will be the vector sum of the spin \mathbf{m}_s and orbital \mathbf{m}_o components, then the energy of the moment in a magnetic field \mathbf{H} will be

$$E = -\mu_0 \mathbf{m} \cdot \mathbf{H}.$$

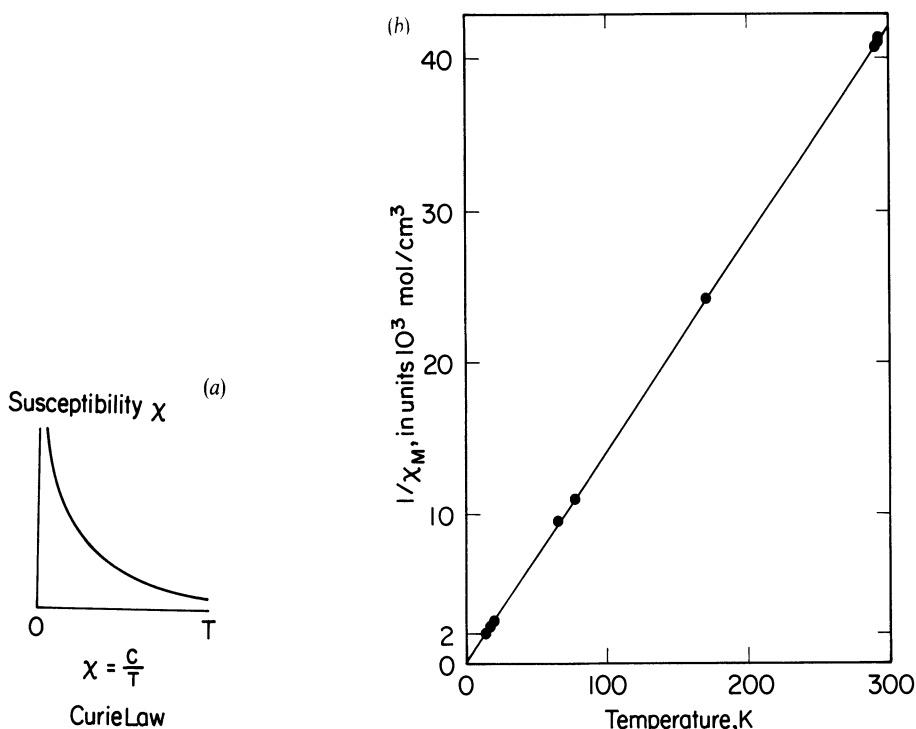


Fig. 9.2 Temperature dependence of paramagnetic susceptibility. Left-hand diagram shows a schematic of the variation of χ with T . The right-hand diagram shows the variation of $1/\chi$ with temperature for the paramagnetic salt $\text{Gd}(\text{C}_2\text{H}_5\cdot\text{SO}_4)_3 \cdot 9\text{H}_2\text{O}$. The circles are experimental points; the straight line is the Curie law prediction.

Thermal energy tends to randomize the alignment of the moments. Langevin [1] supposed that the moments are non-interacting in which case we can use classical Boltzmann statistics to express the probability of any given electron occupying an energy state E . If $k_B T$ is the thermal energy

$$p(E) = \exp(-E/k_B T).$$

We evaluate the probability function for the case of an isotropic material. The number of moments lying between angles θ and $\theta + d\theta$ is dn which will be proportional to the surface area dA

$$dA = 2\pi r^2 \sin \theta \, d\theta$$

$$dn = C 2\pi r^2 \sin \theta \, d\theta,$$

where C is a normalizing constant which gives the total number of moments per unit area. Now incorporating the probability of occupation of any given state

$$dn = C 2\pi \sin \theta \, d\theta \exp\left(\frac{\mu_0 \mathbf{m} \cdot \mathbf{H} \cos \theta}{k_B T}\right).$$

Integrating this expression over a hemisphere gives the resultant total number of moments per unit volume N

$$N = 2\pi C \int_0^\pi \sin \theta \exp\left(\frac{\mu_0 \mathbf{mH}}{k_B T}\right) d\theta$$

$$C = \frac{N}{2\pi \int_0^\pi \sin \theta \exp\left(\frac{\mu_0 \mathbf{mH}}{k_B T}\right) d\theta}.$$

The magnetization is then given by the expression

$$\begin{aligned} \mathbf{M} &= \int_0^N \mathbf{m} \cos \theta dn \\ \mathbf{M} &= \frac{N \mathbf{m} \int_0^\pi \cos \theta \sin \theta \exp\left(\frac{\mu_0 \mathbf{mH} \cos \theta}{k_B T}\right) d\theta}{\int_0^\pi \sin \theta \exp\left(\frac{\mu_0 \mathbf{mH} \cos \theta}{k_B T}\right) d\theta} \end{aligned}$$

If we put $x = \cos \theta$, $dx = -\sin \theta d\theta$ and integrate this gives

$$\begin{aligned} \mathbf{M} &= N \mathbf{m} \left[\coth\left(\frac{\mu_0 \mathbf{mH}}{k_B T}\right) - \frac{k_B T}{\mu_0 \mathbf{mH}} \right] \\ \mathbf{M} &= N \mathbf{m} \mathcal{L}\left(\frac{\mu_0 \mathbf{mH}}{k_B T}\right). \end{aligned}$$

This is the Langevin equation for the magnetization of a paramagnet. $\mathcal{L}(x)$ is called the Langevin function and always lies in the range $-1 < \mathcal{L}(x) < 1$. The Langevin function can be expressed as an infinite power series in $\mu_0 \mathbf{mH}/k_B T$. In most cases $\mu_0 \mathbf{mH}/k_B T \ll 1$, so that the expression for \mathbf{M} becomes equal to the first term in the series

$$\mathbf{M} = \frac{N \mu_0 \mathbf{m}^2 \mathbf{H}}{3 k_B T}$$

which leads immediately to the Curie law, since

$$\begin{aligned} \chi &= \frac{\mathbf{M}}{\mathbf{H}} \\ &= \frac{N \mu_0 \mathbf{m}^2}{3 k_B T} \\ &= \frac{C}{T} \end{aligned}$$

which is Curie's law. This demonstrates that the Langevin model leads to a paramagnetic susceptibility which varies inversely with the temperature.

9.1.6 Curie–Weiss law

Is there a more general law for the dependence of paramagnetic susceptibility on temperature?

It was found that the susceptibilities of a number of paramagnetic metals obey a modified or generalized law known as the Curie–Weiss law [5]. In metals such as nickel and the lanthanides it was found to vary as shown in Fig. 9.3, which can be represented at least in the paramagnetic region by an equation of the form

$$\chi = \frac{C}{(T - T_c)},$$

where C is again the Curie constant and T_c is another constant with dimensions of temperature.

T_c can be either positive, negative or zero. $T_c = 0$ corresponds of course to the earlier Curie law. For materials that undergo a paramagnetic to ferromagnetic transition $T_c > 0$ corresponds to the Curie temperature. For materials that undergo a paramagnetic to antiferromagnetic transition the term T_c is less than zero, although in practice the transition temperature between the paramagnetic and antiferromagnetic phases occurs at a positive temperature T_N known as the Neel temperature.

It should be remembered that the susceptibility only follows the Curie–Weiss law in the paramagnetic region. Once the material becomes ordered the

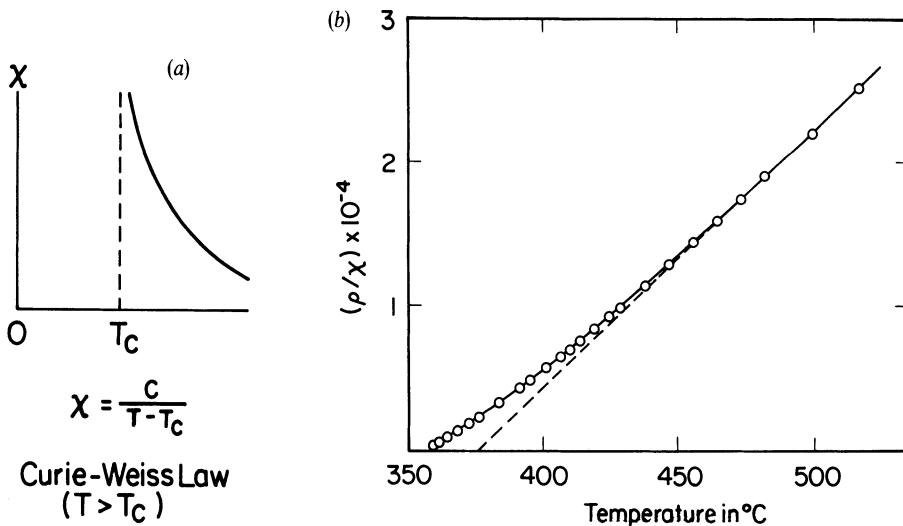


Fig. 9.3 Variation of χ with temperature for paramagnetic materials which undergo a transition to ferromagnetism at the Curie temperature T_c . Left-hand diagram shows a schematic of the variation of χ with T . The right-hand diagram shows the variation of $1/\chi$ with temperature for nickel.

susceptibility behaves in a very complicated way and no longer has a unique value for a given field strength.

9.1.7 Weiss theory of paramagnetism

What does the Curie–Weiss law tell us about the interactions between the individual electronic magnetic moments?

Weiss [6] showed that the variation of paramagnetic susceptibility with temperature of materials which obeyed the Curie–Weiss law could be explained if the individual atomic magnetic moments interacted with each other via an interaction field \mathbf{H}_e which Weiss called the ‘molecular field’ but more accurately should be called the atomic field.

Since in paramagnets the magnetization is locally homogeneous the magnetic moment per unit volume will be everywhere equal to the bulk magnetization \mathbf{M} (unlike in ferromagnets where the local magnetic moment per unit volume, the ‘spontaneous magnetization’, is unrelated to the bulk magnetization because of the existence of domains). Therefore interactions between any individual magnetic moment and other moments within a localized volume can be expressed as an interaction between the given moment and the bulk magnetization \mathbf{M} .

This is represented as an interaction field \mathbf{H}_e which can be written as

$$\mathbf{H}_e = \alpha \mathbf{M},$$

where so far we have made no assumptions about the nature of α . The total magnetic field experienced by a magnetic moment then becomes

$$\mathbf{H}_{\text{tot}} = \mathbf{H} + \mathbf{H}_e$$

and hence

$$\mathbf{H}_{\text{tot}} = \mathbf{H} + \alpha \mathbf{M}.$$

Consider the paramagnetic susceptibility of a material in which such a field operates. This is a perturbation of the Langevin model, so a Curie-type law should still be obeyed providing that the orientation of the magnetic moments is in thermal equilibrium and obeys Boltzmann statistics.

$$\frac{\mathbf{M}}{\mathbf{H}_{\text{tot}}} = \frac{C}{T}$$

The susceptibility is still given by

$$\chi = \frac{\mathbf{M}}{\mathbf{H}}$$

and substituting $\mathbf{H} = \mathbf{H}_{\text{tot}} - \alpha \mathbf{M}$ leads to

$$\chi = \frac{C}{T - \alpha C}$$

$$\chi = \frac{C}{T - T_c}.$$

This is the Curie–Weiss law. The derivation shows that a paramagnetic solid with localized but interacting atomic moments will have a susceptibility that obeys the Curie–Weiss law. The critical temperature T_c is known as the Curie temperature and marks the boundary between the paramagnetic and ferromagnetic states of the material.

9.1.8 Consequences of the Weiss theory

What is the magnetization equation for a material with a Weiss interaction field?

Having established the concept of an interatomic coupling it is possible to provide an equation for the paramagnetic magnetization as a function of the applied magnetic field using a perturbation of the Langevin function. In this case the energy of a magnetic moment within a magnetic field needs to be modified slightly to

$$E = -\mu_0 \mathbf{m}(\mathbf{H} + \alpha \mathbf{M})$$

and consequently the magnetization as a function of field becomes

$$\mathbf{M} = \mathbf{M}_s \left\{ \coth \left[\frac{\mu_0 \mathbf{m}(\mathbf{H} + \alpha \mathbf{M})}{k_B T} \right] - \frac{k_B T}{\mu_0 \mathbf{m}(\mathbf{H} + \alpha \mathbf{M})} \right\}.$$

This means that the paramagnetic susceptibility is greater in the case of the interacting moment system. It is also apparent however that at the critical temperature T_c there arises a discontinuity in the function on the right-hand side of the equation. So that below T_c the behaviour is very different.

9.1.9 Critique of the Langevin–Weiss theory

In what way does the classical Langevin–Weiss theory of paramagnetism fail?

The Langevin model requires that the magnetic moments be localized on the atomic sites. The model does not apply to a material in which the moments are not localized and such materials should not follow the Curie or Curie–Weiss law. Although a number of paramagnetic materials obey the Curie law most metals do not. In these cases the susceptibility is independent of temperature.

The Langevin theory does not work for most metals because the magnetic electrons are usually the outer electrons of the atom which are not localized at the atomic core. The unpaired electrons must exist in unfilled shells and for many elements this means that the magnetic electrons are the outer electrons which are only loosely bound. These are unlikely to remain localized at the atomic sites.

Despite this the Curie–Weiss law still works very well for some metals such as nickel for which it is unlikely that the magnetic electrons are tied to the ionic sites. One possible explanation is that the electrons do migrate but that they spend a large amount of their time close to the ionic sites which results in behaviour that is similar to that predicted by a localized model. Also in the rare earth metals and their alloys and compounds, the 4f electrons which determine the magnetic properties, are closely bound to the atomic core. Hence these materials do exhibit the Curie–Weiss type behaviour.

9.2 THEORIES OF ORDERED MAGNETISM

What types of ordered magnetic structures exist and how do they differ?

There are a number of different types of magnetic order in solids including ferromagnetism, antiferromagnetism, ferrimagnetism and helimagnetism. Some materials, such as the heavy rare earths, exhibit more than one ordered magnetic state. These ordered states undergo transitions at critical temperatures so that every solid that exhibits one of these types of magnetic order will become paramagnetic at higher temperatures. For example in a ferromagnet the Curie point is the transition temperature above which the material becomes paramagnetic and below which an ordered ferromagnetic state exists. The Neel point is the temperature below which an ordered antiferromagnetic state exists. Some solids such as terbium, dysprosium and holmium have both Curie and Neel temperatures.

9.2.1 Ferromagnetism

What causes the transition from paramagnetism to ferromagnetism?

In ferromagnetic solids at temperatures well below the Curie temperature the magnetic moments within domains are aligned parallel. This can be explained phenomenologically by the Weiss interaction field which was originally suggested in order to explain the dependence of paramagnetic susceptibility on temperature in certain materials.

Examples of ferromagnetic elements are the three familiar transition metal ferromagnets iron, $T_c = 770^\circ\text{C}$, nickel, $T_c = 358^\circ\text{C}$, and cobalt, $T_c = 1131^\circ\text{C}$. Several of the rare earth metals also exhibit ferromagnetism including gadolinium, $T_c = 293\text{ K}$, dysprosium $T_c = 85\text{ K}$, terbium $T_c = 219\text{ K}$, holmium $T_c = 19\text{ K}$, erbium $T_c = 19.5\text{ K}$ and thulium $T_c = 32\text{ K}$.

The alignment of magnetic moments in various ordered ferromagnetic solids is shown in Fig. 9.4. As the temperature of a ferromagnet is increased the thermal energy increases while the interaction energy is unaffected. At a critical temperature the randomizing effect of thermal energy overcomes the aligning effect of the

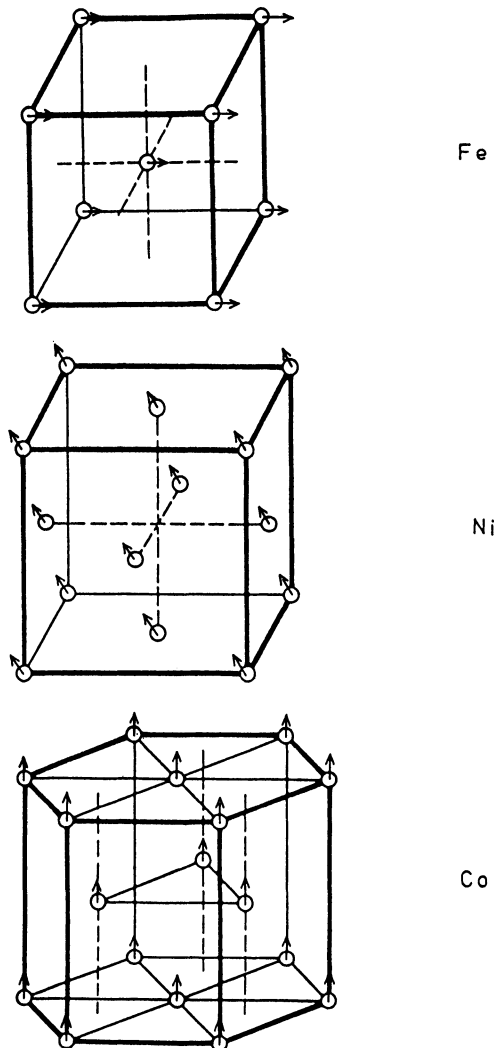


Fig. 9.4 Crystallographic alignment of the magnetic moments in various ferromagnetic solids.

interaction energy and above this temperature the magnetic state becomes disordered.

9.2.2 Weiss theory of ferromagnetism

How can the Weiss interaction be used to explain magnetic order in ferromagnets?

If the unpaired electronic magnetic moments which are responsible for the magnetic properties are localized on the atomic sites then we can consider an

interaction between the unpaired moments of the form discussed above in section 9.1.7. This interaction, which Weiss introduced to explain the paramagnetic susceptibilities of certain materials, leads to the existence of a critical temperature below which the thermal energy of the electronic moments is insufficient to cause random paramagnetic alignment. This means that the effective field \mathbf{H}_e can be used to explain the alignment of magnetic moments within domains for temperatures below T_c .

There are a number of possible variations on the theme of the interatomic interaction or exchange field. We will look at two of these: the mean-field approximation, which was used successfully in the paramagnetic region, and a nearest-neighbour-only coupling which is more appropriate in the ferromagnetic regime. We will begin by considering the interaction between just two magnetic moments.

Suppose that any atomic magnetic moment \mathbf{m}_i experiences an effective field \mathbf{H}_{eij} due to another moment \mathbf{m}_j . If we assume that this field is also in the direction of \mathbf{m}_j we can write

$$\mathbf{H}_{eij} = \mathcal{J}_{ij} \mathbf{m}_j.$$

The total exchange interaction field at the moment \mathbf{m}_i will then simply be the vector sum of all the interactions with other moments

$$H_{ei} = \sum_{\text{all } j} \mathcal{J}_{ij} \mathbf{m}_j.$$

9.2.3 Mean-field approximation

Is there a simple explanation of the Weiss interaction?

So far we have made no assumption about the form of \mathcal{J}_{ij} . We can show that if the interactions between all moments are identical and hence independent of displacement between the moments, then all of the \mathcal{J}_{ij} are equal. Let these be α as we have used before for the mean-field interaction in section 6.1.5. Hence

$$\mathbf{H}_e = \alpha \sum_{\text{all } j} \mathbf{m}_j$$

so that within a domain

$$\begin{aligned} \mathbf{H}_e &= \alpha(\mathbf{M}_s - \mathbf{m}_i) \\ &\approx \alpha \mathbf{M}_s. \end{aligned}$$

The interaction energy of the moment under these conditions is

$$\begin{aligned} E_e &= -\mu_0 \mathbf{m}_i \cdot \mathbf{H}_e \\ &= -\mu_0 \alpha \mathbf{m}_i \cdot \mathbf{M}_s. \end{aligned}$$

This was the original formulation of the Weiss theory. In essence the mean-field

approximation is not very realistic because each moment does not interact equally with all others in the domain. However for moments within the body of a domain it works out quite well in practice simply because each moment will experience the same exchange field as its neighbours, and this will be in the direction of the spontaneous magnetization M_s in the domain. Therefore if the mean-field parameter is treated completely empirically it can give a reasonable model of the behaviour of the moments.

If we consider the case of a zero external field, then the only field operating within a domain will be the Weiss field

$$H_{\text{tot}} = H_e.$$

When considering the magnetic moments within the body of a domain if we apply the mean-field model the interaction field will be proportional to the spontaneous magnetization M_s within a domain. Following an analogous argument to that given by Langevin for paramagnetism then if there are no constraints on the possible direction of \mathbf{m} we arrive at

$$\frac{M_s}{M_0} = \coth\left(\frac{\mu_0 m \alpha M_s}{k_B T}\right) - \frac{k_B T}{\mu_0 m \alpha M_s}.$$

The solution of this equation leads to perfect alignment of magnetic moments

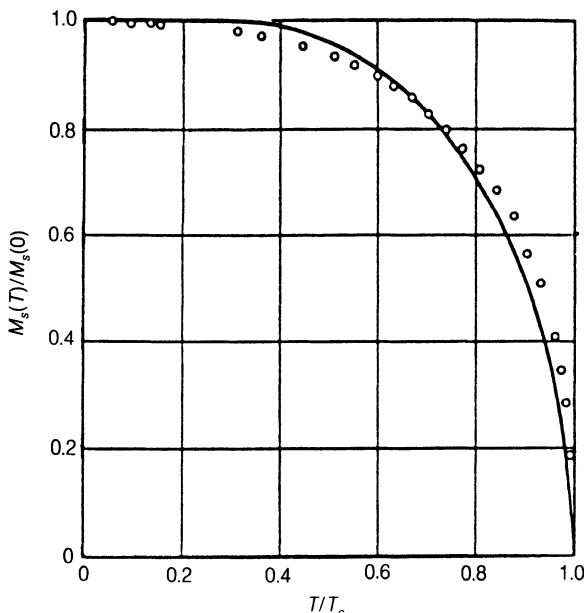


Fig. 9.5 Variation of the spontaneous magnetization M_s of nickel within a domain as a function of temperature according to the Weiss mean-field model, after Weiss and Forrer (1929).

within a domain as the temperature approaches absolute zero. As T increases the spontaneous magnetization within a domain decreases as shown in Fig. 9.5. At a finite temperature which corresponds to the Curie point the spontaneous magnetization tends rapidly to zero representing the transition from ferromagnetism to paramagnetism. The above expression can be generalized to include the effects of a magnetic field \mathbf{H} , so that the energy of a moment within a domain becomes

$$E = -\mu_0 \mathbf{m} \cdot (\mathbf{H} + \alpha \mathbf{M}_s)$$

which leads immediately to the following magnetization within a domain

$$\frac{\mathbf{M}_s}{\mathbf{M}_0} = \coth \left[\frac{\mu_0 \mathbf{m}(\mathbf{H} + \alpha \mathbf{M}_s)}{k_B T} \right] - \frac{k_B T}{[\mu_0 \mathbf{m}(\mathbf{H} + \alpha \mathbf{M}_s)]}.$$

This equation is not encountered very often however because $\alpha \mathbf{M}_s \gg \mathbf{H}$ in ferromagnets (e.g. in iron $\mathbf{M}_s = 1.7 \times 10^6 \text{ A/m}$, and so $\alpha \mathbf{M}_s$ can be up to $6.8 \times 10^8 \text{ A/m}$, while \mathbf{H} will rarely exceed $2 \times 10^6 \text{ A/m}$). Consequently within the body of a domain the action of the \mathbf{H} field is not very significant when compared with the interaction field.

However it is well known that moderate magnetic fields ($\mathbf{H} \approx 8 \times 10^3 \text{ A/m}$) can cause significant changes in the bulk magnetization \mathbf{M} in ferromagnets. Therefore these changes occur principally at the domain boundaries where the exchange interaction is competing with the anisotropy energy to give an energy balance. Under these conditions the additional field energy can just tip the balance and result in changes in the direction of magnetic moments within the domain wall. This mechanism manifests itself as domain-wall motion, as described in Chapter 8.

The magnetic moments in the domain wall, being on the periphery of the domain do not couple to the spontaneous magnetization of the domains although the Weiss-type coupling is still strong between nearest neighbours. The net interaction field per moment is different in this case because the domains on either side are aligned in different directions. Therefore the energy is very finely balanced in the domain wall and slight perturbations due to an applied magnetic field can cause changes in the direction of alignment of the moments which would not be possible within the body of the domain.

9.2.4 Nearest-neighbour interactions

Can the Weiss model be interpreted on the basis of localized interactions only?

Another variation of the Weiss model which provides mathematically tractable solutions is the nearest-neighbour approximation [7] in which the electronic moments interact only with those of its z nearest neighbours. So for a simple cubic lattice $z = 6$, for body-centred cubic $z = 8$, for face-centred cubic $z = 12$ and for a hexagonal lattice $z = 12$. The nearest-neighbour approach is particularly useful for

considering magnetic moments in the domain walls since in this case the moments do not couple to the magnetization within the body of the domain simply because they lie between domains with different magnetic directions and the direction of magnetization changes within the wall.

In this approximation we can write the exchange interaction field as

$$\mathbf{H}_e = \sum_{\text{nearest neighbours}} \mathcal{J}_{ij} \mathbf{m}_j$$

We assume that each nearest-neighbour interaction is identical and equal to \mathcal{J} , where once again $\mathcal{J} = 0$ corresponds to the non-interacting limit described by Langevin theory. When \mathcal{J} is non-zero it is usually convenient to consider that each moment interacts equally with each of its nearest neighbours. (In order to arrive at the same order of magnitude of the exchange field as the mean-field approximation we need to have $N\alpha \approx z\mathcal{J}$.)

$$\begin{aligned} \mathbf{H}_e &= \sum_{\text{nearest neighbours}} \mathcal{J} \mathbf{m}_j \\ &= \mathcal{J} \sum_{\text{nearest neighbours}} \mathbf{m}_j. \end{aligned}$$

On the basis of this nearest-neighbour interaction we find that $\mathcal{J} > 0$ corresponds to ferromagnetic alignment while $\mathcal{J} < 0$ corresponds to antiferromagnetic alignment. This can easily be seen by considering the configuration of moments which leads to a minimum in the interaction energy.

$$E_e = -\mu_0 \mathbf{m} \mathcal{J} \sum_{\text{nearest neighbours}} \mathbf{m}_j$$

and summing over the z nearest neighbours

$$E_e = -\mu_0 z \mathcal{J} \mathbf{m}^2.$$

Having established the existence of the Weiss interaction it is possible to provide a description of ferromagnets which is similar to the Langevin model of paramagnetism. Such a model is strictly only correct for ferromagnets in which the moments are localized on the atomic cores. Thus it applies to the lanthanide series because the 4f electrons which determine the magnetic properties, are tightly bound to the nuclei. The model also works reasonably well for nickel, which obeys the Curie-Weiss law.

9.2.5 Curie temperature on the basis of the mean-field model

How does the Weiss interaction explain the existence of a critical temperature?

In the original papers by Weiss [5, 6] it was shown that the existence of an internal or atomic field proportional to the magnetization \mathbf{M} led to a modified form of

Curie's law known as the Curie–Weiss law

$$\chi = \frac{C}{T - T_c}.$$

From the Curie–Weiss law the Curie constant is given by

$$C = \frac{N\mu_0 m^2}{3k_B}$$

and the Curie temperature $T_c = \alpha C$ is therefore given by

$$T_c = \frac{\mu_0 N \alpha m^2}{3k_B}.$$

We see from this that it is possible to determine the mean-field coupling or Weiss constant α from the Curie temperature providing the magnetic moment per atom is known.

Similarly for a nearest-neighbour coupling the interaction parameter \mathcal{J} can be found from the Curie temperature using the equation

$$T_c = \frac{\mu_0 z \mathcal{J} m^2}{3k_B}.$$

9.2.6 Antiferromagnetism

Is it also possible to explain antiferromagnetic order by a Weiss interaction?

Simple antiferromagnetism [8] in which nearest-neighbour moments are aligned antiparallel can also be interpreted on the basis of the Weiss model. There are two ways of considering this. One is to divide the material into two sublattices A and B, with the moments on one sublattice interacting with the moments on the other sublattice with a negative coupling coefficient, but interacting with the moments on their own sublattice with a positive coupling coefficient. This ensures that the magnetic moments on the two sublattices point in different directions. Another way to envisage the problem is on the basis of nearest-neighbour interactions. With a negative interaction between nearest neighbours this leads to simple antiferromagnetism.

The Curie–Weiss law also applies to antiferromagnets above their ordering temperatures. However the sign of the constant term T_c in the denominator is positive so that the law becomes

$$\chi = \frac{C}{T + T_c}.$$

It therefore appears superficially as though the critical temperature in this case is below 0 K. In fact the plot of $1/\chi$ against temperature for these antiferromagnets does appear to be a straight line intercepting the temperature axis at $-T_c$, but at a temperature above 0 K known as the Neel temperature the materials undergo an

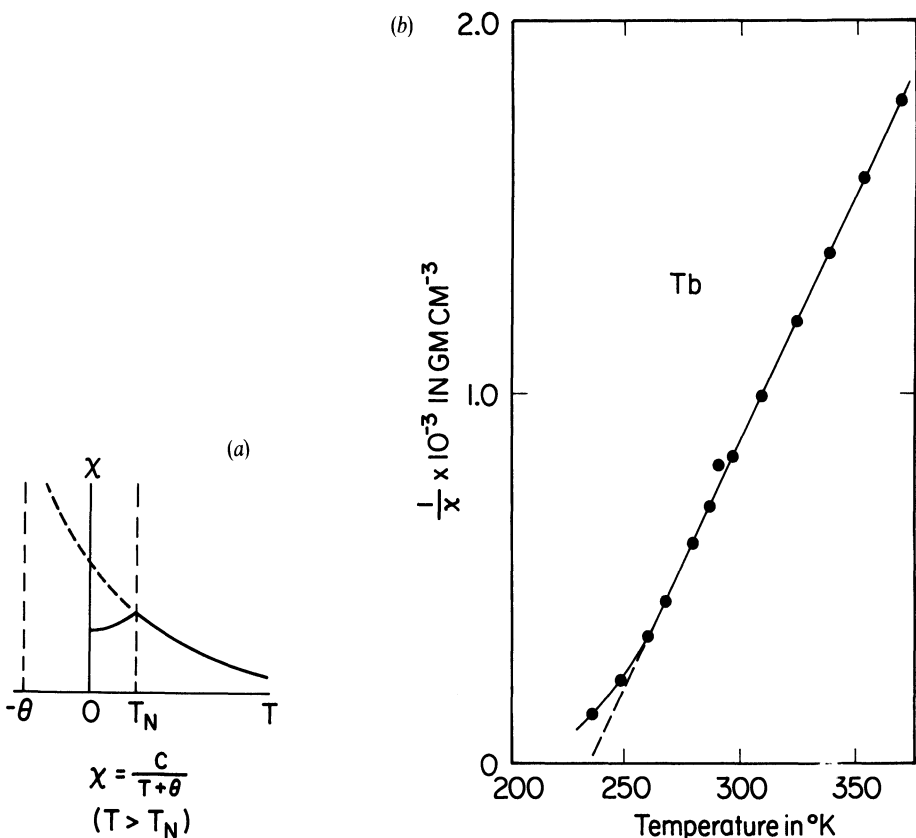


Fig. 9.6 The left-hand diagram is the schematic variation of χ with temperature in the paramagnetic regime of materials which undergo a transformation to antiferromagnetism. The right-hand diagram is $1/\chi$ versus T data for terbium.

order-disorder transition after which they cease to obey the Curie-Weiss law, as shown in Fig. 9.6.

Examples of antiferromagnetic materials are chromium, below its Neel temperature of 37 °C, and manganese below its Neel temperature of 100 K.

9.2.7 Ferrimagnetism

How can the properties of ferrites be explained?

Ferrimagnetism is a particular case of antiferromagnetism in which the magnetic moments on the A and B sublattices while still pointing in opposite directions have different magnitudes. Ferrimagnetic order was first suggested by Neel in 1948 [9] to explain the behaviour of ferrites. The ferrimagnets behave on a macroscopic scale very much like ferromagnets so that it was not realized for many years that there was a distinction. They have a spontaneous magnetization below the Curie

temperature and are organized into domains. They also exhibit hysteresis and saturation in their magnetization curves.

The most familiar ferrimagnet is Fe_3O_4 , although other magnetic ferrites with the general formula $MO \cdot \text{Fe}_2\text{O}_3$ where M is a transition metal such as manganese, nickel, cobalt, zinc or magnesium are widely used. These ferrites are cubic and have the ‘spinel’ crystal structure referred to in Chapter 8.

Another class of ferrites is made up of the hexagonal ferrites such as barium ferrite $\text{BaO} \cdot 6(\text{Fe}_2\text{O}_3)$ and strontium ferrite $\text{SrO} \cdot 6(\text{Fe}_2\text{O}_3)$. These are magnetically hard and have been extensively used as permanent-magnet materials. They have a high anisotropy with the moments lying along the c axis. Their critical temperatures are typically in the range $T_c = 500\text{--}800^\circ\text{C}$.

A third group of ferrimagnets are the garnets which have the chemical formula $5\text{Fe}_2\text{O}_3 \cdot 3R_2\text{O}_3$ where R is a rare earth ion. The best known of these is yttrium–iron garnet, $5\text{Fe}_2\text{O}_3 \cdot 3\text{Y}_2\text{O}_3$. These materials have a complicated cubic crystal structure. Their order–disorder transition temperatures are around 550°C .

Another ferrimagnetic material is gamma iron oxide $\gamma\text{-Fe}_2\text{O}_3$ which is widely used as a magnetic recording medium. This is obtained by oxidizing magnetite Fe_3O_4 . Above 400°C this transforms to rhombohedral alpha iron oxide, or haematite, which is a canted antiferromagnet.

9.2.8 Helimagnetism

Are there other types of ordered magnetic materials?

So far we have discussed the situations where the nearest-neighbour interaction is positive (ferromagnetic) and negative (antiferromagnetic). There is a more general case in which we consider nearest- and next-nearest-neighbour interactions.

As an example we will look at the case of dysprosium as treated by Enz [10] and later by Nicklow [11]. In the base plane the moments are all aligned ferromagnetically, however successive base planes have their moments inclined at an angle θ to the moments in the next base plane. This gives a helical magnetic structure.

If \mathcal{J}_{i1} is the interaction between nearest-neighbour planes and \mathcal{J}_{i2} the interaction between next-nearest-neighbour planes, the total exchange energy E_{ex} becomes

$$E_{\text{ex}} = - \sum_i \sum_j \mathcal{J}_{ij} \cos(\theta_{i+j} - \theta_i) \mathbf{m}^2.$$

If the turn angle between moments in successive base planes is θ

$$j\theta_t = \theta_{i+j} - \theta_i$$

and if $\mathcal{J}_{i1} = \mathcal{J}_1$, and $\mathcal{J}_{i2} = \mathcal{J}_2$ for all i , then

$$E_{\text{ex}} = - N \sum_j \mathcal{J}_j \cos(j\theta_t) \mathbf{m}^2.$$

If we assume that the interaction from further than two planes away is negligible by comparison

$$E_{\text{ex}} = -Nm^2(\mathcal{J}_0 + 2\mathcal{J}_1 \cos \theta_t + 2\mathcal{J}_2 \cos 2\theta_t).$$

At equilibrium

$$\begin{aligned} \frac{dE_{\text{ex}}}{dH_t} &= 0 \\ &= Nm^2(2\mathcal{J}_1 \sin \theta_t + 4\mathcal{J}_2 \sin 2\theta_t) \\ \cos \theta_t &= -\frac{\mathcal{J}_1}{4\mathcal{J}_2}. \end{aligned}$$

This gives the value of the turn angle θ_t between successive base planes which leads to the minimum exchange energy. For ferromagnetic alignment we need $\cos \theta_t = 1$, or $\mathcal{J}_1 = -4\mathcal{J}_2$, while for simple antiparallel antiferromagnetic alignment we need $\cos \theta_t = -1$, $\mathcal{J}_1 = 4\mathcal{J}_2$.

Examples of this form of helimagnetic order occur in terbium, dysprosium and holmium.

9.3 MAGNETIC STRUCTURE

How is the magnetic structure within a domain determined?

The magnetic structure of materials is usually deduced from neutron diffraction and magnetization/susceptibility measurements. The use of neutron diffraction for investigating the structure of magnetic materials has been discussed by Bacon [12] and more recently by Lovesey [13]. The first material to be studied in this way was MnO in 1949 and this was followed by other antiferromagnetic oxides. The determination of the magnetic structure of the 3d series metals iron, nickel and cobalt by neutron diffraction was first made by Koehler and coworkers at Oak Ridge National Laboratory beginning in 1951. The magnetic structures of the 4f series metals, the lanthanides, was also studied by the same group using neutron diffraction in an extensive research program in the 1950s and 1960s. The results of this were summarized by Koehler [14] in a review of the magnetic properties of the rare earths.

9.3.1 Neutron diffraction

How do neutrons interact with magnetic materials?

Although the various different types of magnetic order described in sections 9.1 and 9.2 can be inferred from measurements of magnetic anisotropy and susceptibility, their existence has only been directly verified by neutron diffraction. In the older and perhaps more familiar technique of X-ray diffraction a beam of X-

rays is diffracted by the distribution of electric charge at the periodic lattice sites in the solid. This is known as Bragg reflection. Neutrons however are diffracted both by the distribution of the nuclei on the lattice sites and by the magnetic moments associated with the electron distribution on each atom. This leads to both Bragg peaks and magnetic peaks in the resulting neutron diffraction spectrum.

Neutrons have a net magnetic moment of 5.4×10^{-4} Bohr magnetons ($= 5.0 \times 10^{-27} \text{ A m}^2$) but have no electric charge. This presence of magnetic moment in the absence of charge is itself an anomaly, but we shall not discuss the problem here. Nevertheless this combination of properties means that neutrons can pass relatively easily through a solid since they are not influenced by the localized electric charge distribution. The neutrons do interact with the nuclei to a greater or lesser extent depending on the type of nuclei present as shown in Table 9.1. This gives rise to a nuclear scattering component in the total neutron diffraction spectrum. For the wavelengths used in neutron diffraction the nuclei act as point scatterers and the nuclear scattering spectrum is therefore isotropic.

The neutrons necessary for neutron diffraction studies of this type must have wavelengths comparable with the atomic dimensions, which are typically 0.1 nm. Neutrons with de Broglie wavelengths of this order of magnitude are produced in a nuclear reactor as thermal neutrons at a temperature of about 300 K and hence an energy of $4 \times 10^{-21} \text{ J}$ (25 meV) and a corresponding wavelength of 0.18 nm.

The neutron diffraction spectra of magnetic materials contain at least three different contributions which can be used to examine different properties of the materials. There is elastic neutron scattering which has two components; the first of these is the nuclear (or Bragg type) diffraction peaks which are determined by the periodicity of the lattice, and the neutron scattering cross-section of the nucleus; the second is the magnetic scattering which is determined by the magnetic order in the solid and the magnetic scattering cross-section. Finally there is inelastic

Table 9.1 Comparison of nuclear and magnetic scattering amplitudes of various atoms (after Bacon [12])

Atom or ion	Nuclear scattering amplitude (10^{-12} cm)	Effective spin quantum number S	Magnetic scattering amplitude	
			$P (10^{-12} \text{ cm})$	$\theta = 0$ $(\sin \theta / \lambda = 0.25 \text{ \AA}^{-1})$
Cr^{2+}	0.35	2	1.08	0.45
Mn^{2+}	-0.37	5/2	1.35	0.57
Fe	0.96	1.11	0.60	0.35
Fe^{2+}	0.96	2	1.08	0.45
Fe^{3+}	0.96	5/2	1.35	0.57
Co	0.28	0.87	0.47	0.27
Co^{2+}	0.28	2.2	1.21	0.51
Ni	1.03	0.3	0.16	0.10
Ni^{2+}	1.03	1.0	0.54	0.23

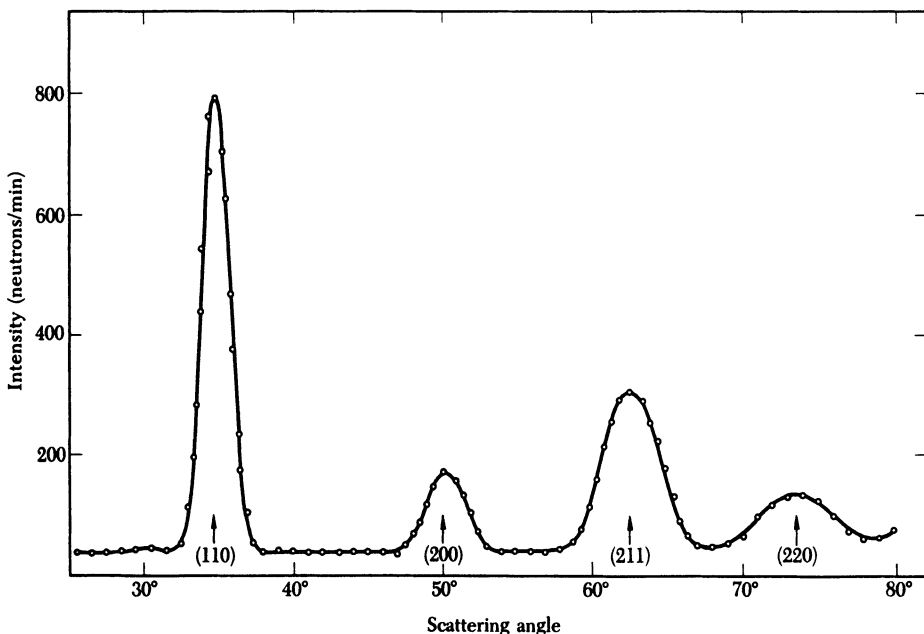


Fig. 9.7 Neutron diffraction spectrum of iron showing the intensity of diffracted peaks as a function of scattering angle. The peaks have been indexed with the corresponding crystallographic directions (after Shull *et al.* [51]).

neutron scattering which results in the creation or annihilation of a magnon (spin wave excitation) and from such measurements it is possible to study the spin wave spectrum of the solid.

The experimental arrangement for neutron diffraction investigations is similar to that used in X-ray diffraction. A collimated, monochromatic (i.e. single-energy) and in some cases polarized beam of neutrons is directed on to the specimen. A neutron detector can be moved around the specimen to any angle in order to measure the angular dependence of the intensity of the diffracted beam. Nuclear scattering patterns have the same criteria as for X-rays and so the Bragg angle θ can be defined as $\sin \theta = \lambda/2|G|$ where λ is the de Broglie wavelength of the neutrons, and $|G|$ is the magnitude of the reciprocal lattice vector. The magnetic reflections are superimposed on the Bragg reflection spectrum. Generally both are referenced to the crystallographic unit cell, as indicated in Fig. 9.7 which is taken from the work of Shull *et al.* [15].

9.3.2 Elastic neutron scattering

What can elastic neutron scattering tell us about the magnetic structure of a material?

The idea of using neutrons for investigating directly the magnetic structure of materials was suggested first by Bloch [16] and later in more detail by Halpern and

Johnson [17]. Elastic neutron scattering gives two types of diffraction peaks. One group is due to nuclear scattering and these are isotropic, that is they do not depend on the scattering angle, and they also persist above the magnetic ordering temperature as shown in Fig. 9.8. The second group, the magnetic scattering spectrum, is caused by the presence of localized magnetic moments in the solid. This spectrum is anisotropic and also depends on temperature, the intensity of the peaks decreasing with increasing temperature until at the magnetic ordering

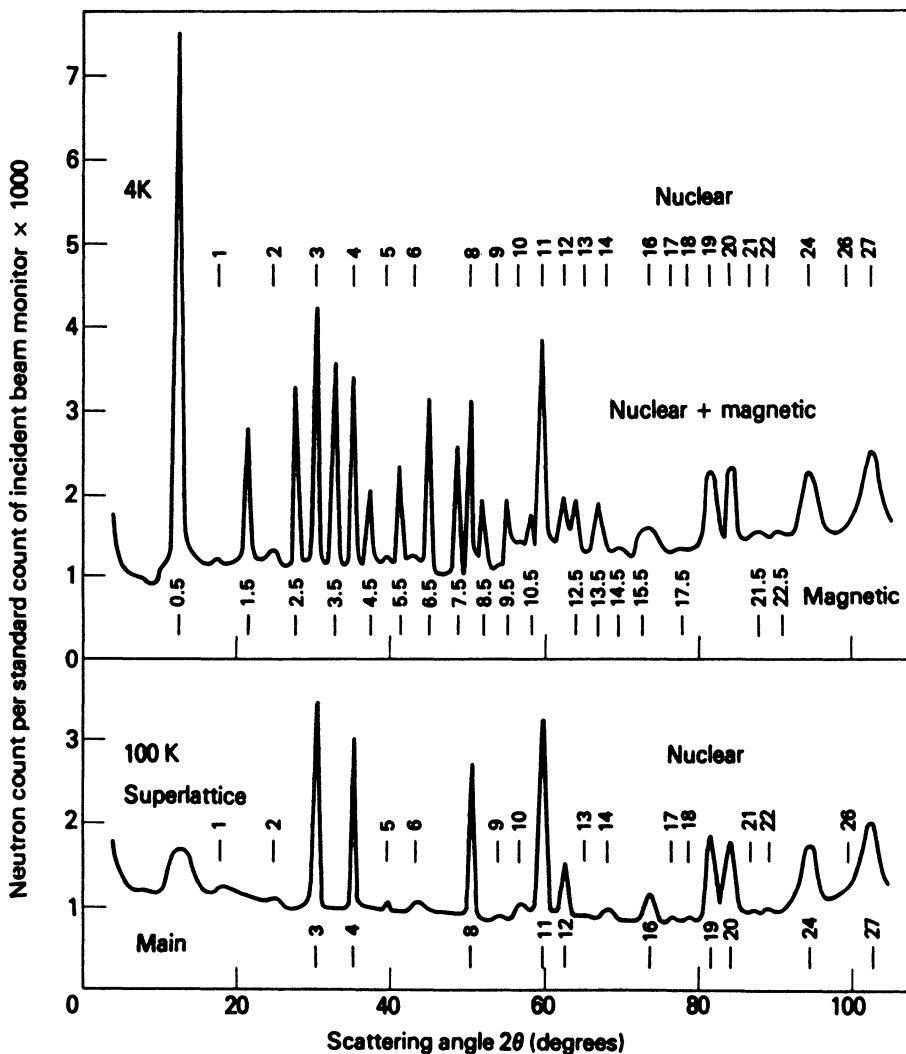


Fig. 9.8 Neutron diffraction spectra for TbIn_3 above and below the magnetic ordering temperature (after Crangle [18]).

temperature the spectrum disappears to become a diffuse background due to paramagnetic scattering.

The cross-sections for neutron-electron and neutron-nuclear scattering are usually comparable in magnitude, with either being larger depending on the particular case. This means that the spectral peaks due to Bragg diffraction and magnetic scattering are usually comparable in magnitude. The two contributions can however be distinguished for example by the application of a magnetic field (since the nuclear component remains isotropic) or by raising the temperature above the magnetic ordering temperature (whereupon the magnetic component becomes diffuse due to paramagnetic scattering). Once the magnetic scattering contribution to the spectrum has been isolated the distribution, direction and ordering of the magnetic moments within the solid can be determined.

Paramagnetic scattering

In the case of a paramagnet the magnetic scattering is diffuse and appears as a contribution throughout the background which decreases in intensity with increasing angle of scatter θ . Paramagnetic scattering is found by subtracting all other contributions from the spectrum, providing that the magnetic contribution is sufficiently large compared with the other contributions to render this calculation accurate enough.

Ferromagnetic scattering

The Bragg and magnetic scattering spectra have peaks in the same locations when neutrons are diffracted by a ferromagnet. Therefore the two components of the spectrum will be completely superposed as shown in Fig. 9.9(a). The magnetic contribution however decreases with temperature and therefore the two contributions can be distinguished by making measurements above and below the Curie point.

Simple antiferromagnetic scattering

In the case of simple antiferromagnetism the magnetic moments on neighbouring atoms point in opposite directions. This leads to a doubling of the crystallographic repeat distance for magnetic moments and hence to a halving of the repeat distance in the reciprocal lattice. Therefore additional magnetic peaks appear midway between the nuclear scattering peaks in the spectrum as shown in Fig. 9.9(b). The magnetic peaks occur at $\sin \theta$ values which are half those of the expected nuclear diffraction peaks. The scattering of neutrons by antiferromagnets is discussed in detail by Bacon [12 (p. 208)].

Helical antiferromagnetic scattering

In helimagnetic materials the diffraction peaks consist of the central nuclear peaks each accompanied by a pair of satellite peaks due to the magnetic scattering as

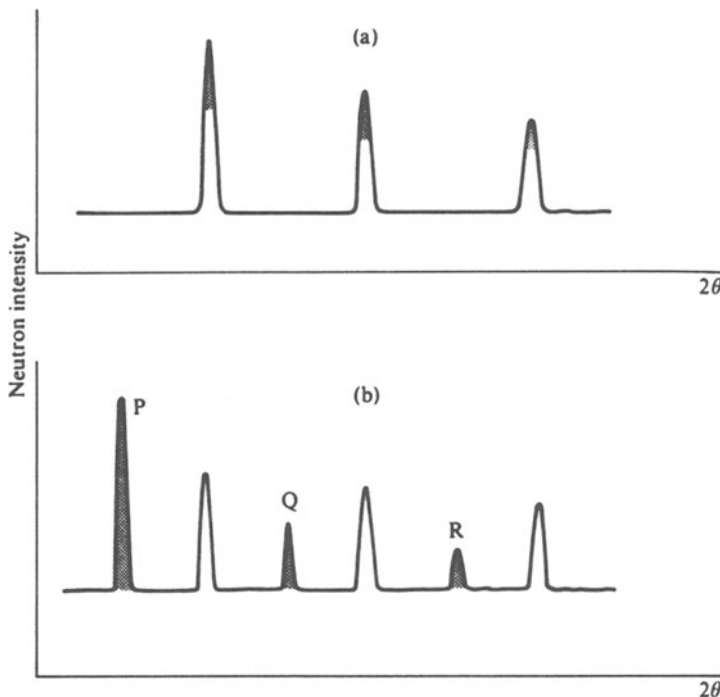


Fig. 9.9 Neutron diffraction spectra: (a) for a ferromagnetic solid showing superposition of nuclear and magnetic peaks; and (b) for a simple antiferromagnetic solid in which the nuclear and magnetic peaks occur at different locations (after Bacon [12]).

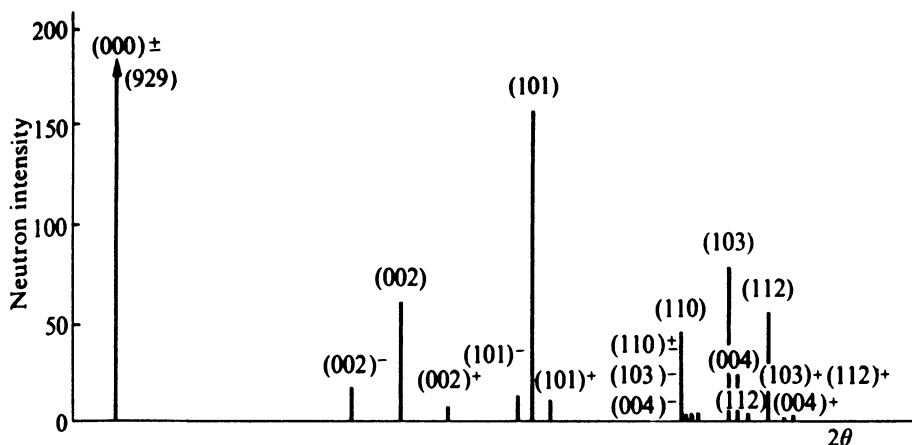


Fig. 9.10 Neutron diffraction spectrum for a helical antiferromagnetic structure (after Bacon [12]).

shown in Fig. 9.10. The displacement of the satellite peaks from the nuclear peaks can be used to determine both the direction of the helical axis and the magnitude of the turn angle between successive helical planes.

The technique of neutron diffraction finds its greatest use in the investigation of antiferromagnetic (including helical antiferromagnetic) and ferrimagnetic structures. The case of ferromagnetic materials is fairly trivial by comparison since all moments lie parallel within a domain, and therefore little further information can be obtained, since the crystallographic easy axes can be determined from anisotropic susceptibility measurements. However information about the spin wave spectrum can be obtained from inelastic neutron scattering data on ferromagnets as they approach the Curie point.

9.3.3 Inelastic neutron scattering

How can we study higher energy states (magnetic excitations) in the magnetic structure?

The thermal fluctuations of the individual atomic magnetic moments in a magnetically ordered solid become particularly prevalent as the magnetic ordering temperature is approached. These spin waves can be studied by inelastic neutron scattering. It was observed for example by Squires [19] that the magnetic scattering cross-section for iron has a peak at the Curie point as shown in Fig. 9.11 which is caused by inelastic scattering of neutrons by spin clusters. This scattering becomes greater as the temperature is increased towards the Curie temperature as the spin fluctuations become greater. A further example for nickel [20] is given in Fig. 9.12.

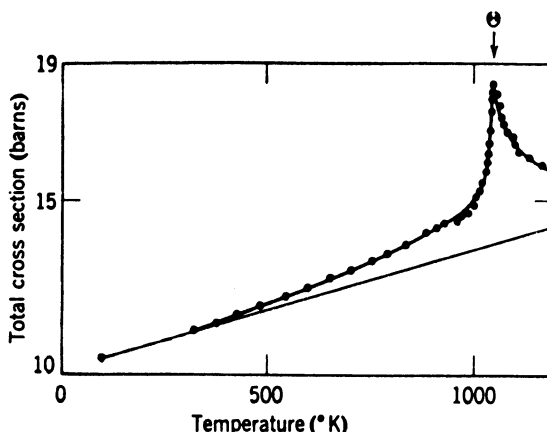


Fig. 9.11 Total scattering cross-section for inelastic scattering of neutrons by iron as a function of temperature (after Cribier *et al.* [19]).

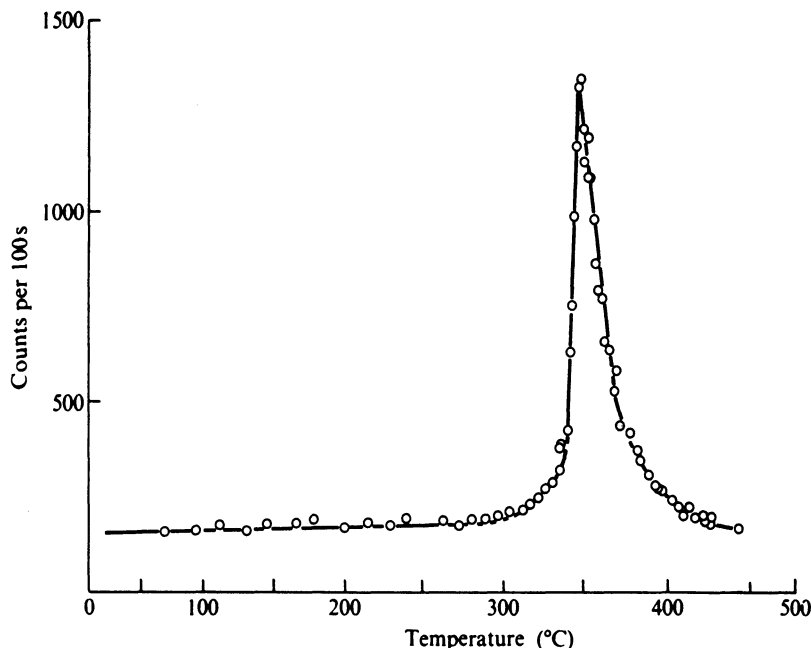


Fig. 9.12 Total scattering cross-section for inelastic scattering of neutrons by nickel as a function of temperature (after Cribier *et al.* [20]).

A more detailed discussion of neutron diffraction by magnetic solids is beyond the intended scope of this book. However those interested in this area of magnetism are referred to the excellent, recent, two-volume work by Lovesey [13] which provides a comprehensive summary of the subject.

9.3.4 Magnetic order in various solids

What examples do we have of these many different types of magnetic order?

The ordering of the magnetic moments within domains in various rare earth metals is shown in Fig. 9.13. For the cubic metals such as iron and nickel the magnetic moments align preferentially along the $\langle 100 \rangle$ and $\langle 111 \rangle$ axes respectively [21, 22]. The magnetization curves along the various crystal axes in iron are shown in Fig. 9.14, and in nickel in Fig. 9.15. From these it is clear that the initial and low-field susceptibility of iron is highest along the $\langle 100 \rangle$ axes and in nickel is highest along the $\langle 111 \rangle$ axes. Conversely it is more difficult to magnetize iron along the $\langle 111 \rangle$ axes and nickel along the $\langle 100 \rangle$ axes. Cobalt has a hexagonal crystal lattice. In this case the moments are aligned along the unique axis [0001] which is the easy direction [23], while the [10\bar{1}0] axis in the base plane is the hard axis. The magnetization curves along these directions are shown in Fig. 9.16.

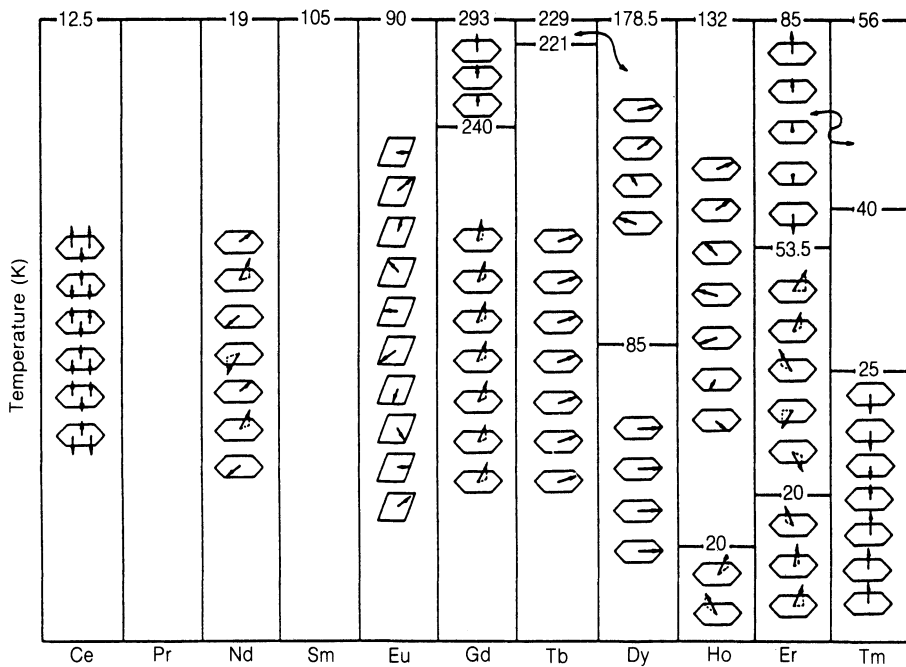


Fig. 9.13 Magnetic ordering of magnetic moments within the domains of various rare earth metals under zero applied magnetic field.

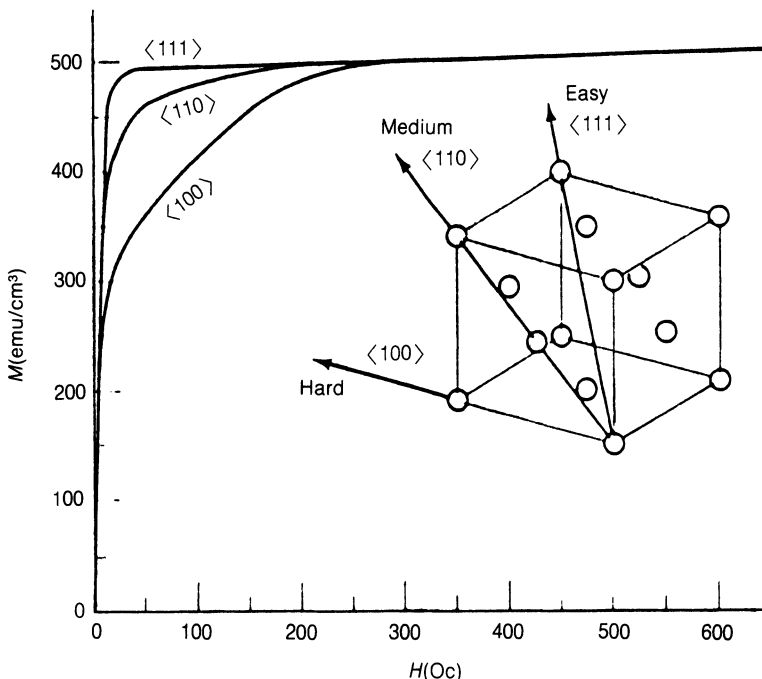


Fig. 9.14 Magnetization curves for iron along the three axes $\langle 100 \rangle$, $\langle 110 \rangle$ and $\langle 111 \rangle$.

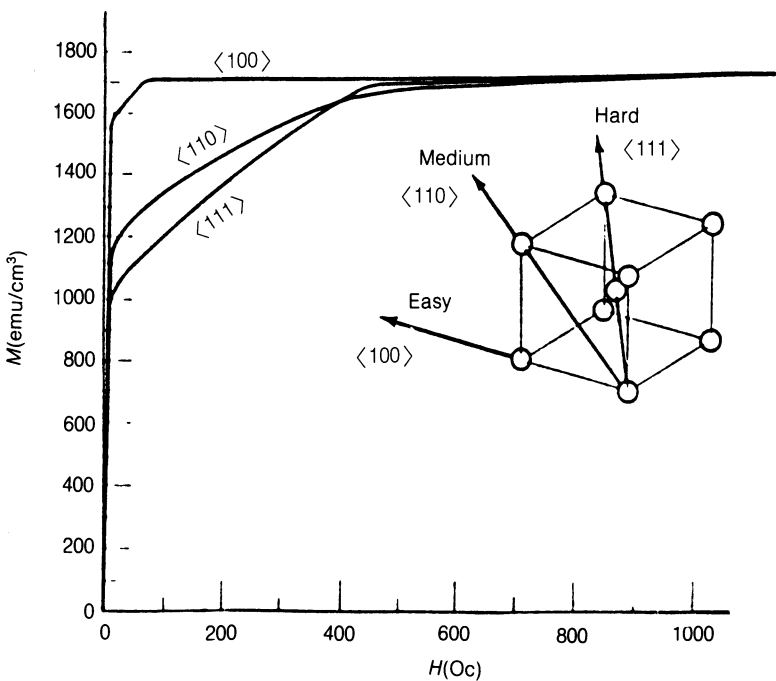


Fig. 9.15 Magnetization curves for nickel along the three axes $\langle 100 \rangle$, $\langle 110 \rangle$ and $\langle 111 \rangle$.

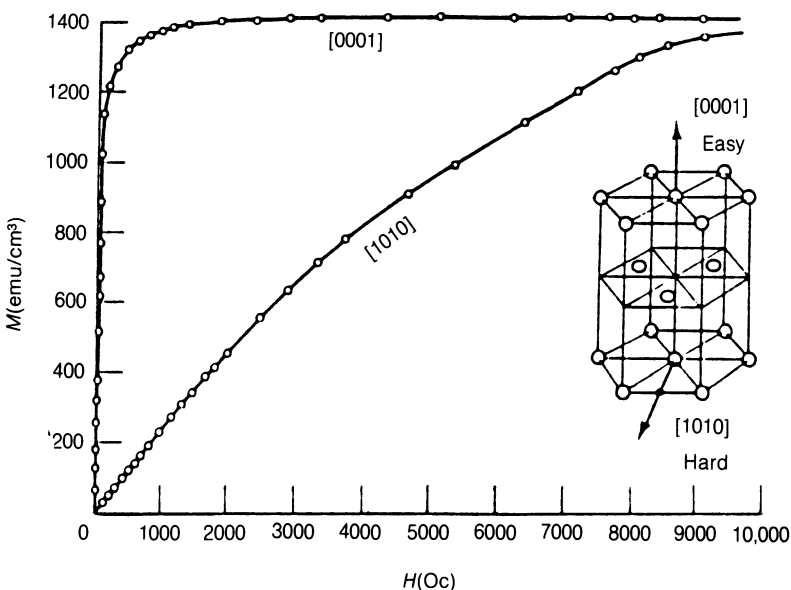


Fig. 9.16 Magnetization curves for cobalt along the unique axis $\langle 0001 \rangle$ and the base plane $\langle 10\bar{1}0 \rangle$.

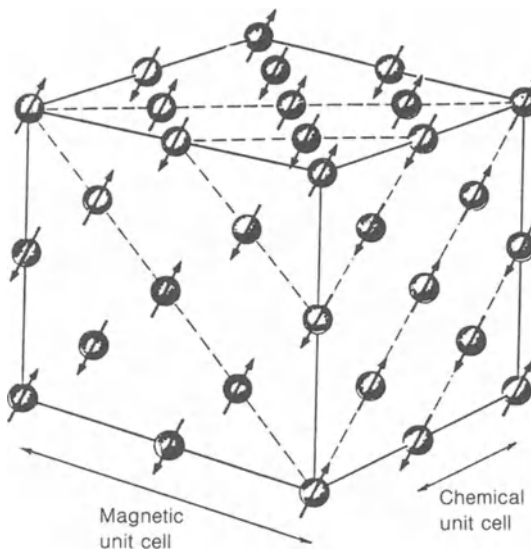


Fig. 9.17 Simple antiferromagnetism in manganese.

Simple antiparallel antiferromagnetism occurs in chromium and manganese and these ordered structures are shown in Fig. 9.17 [24, 25]. Antiferromagnetism is actually far more commonly occurring than ferromagnetism, but so far no use has been found for this type of magnetic order in solids.

In the rare earth metals the magnetic ordering can be much more complex. In gadolinium [26–29], which exhibits the simplest magnetic structure among the rare earths, the magnetic moments are aligned along the *c* axis when the temperature lies between the Curie point of 293 K and the spin-reorientation temperature of 240 K. Below 240 K the moments deviate from the (001) axis and the angular deviation increases continuously as the temperature is reduced. In this temperature range we speak of gadolinium as a ‘canted’ ferromagnet.

Terbium [30] and dysprosium [31, 32, 33], the next two elements in the periodic table, behave very differently from gadolinium. At the Neel temperature, $T_n = 230$ K for terbium and $T_n = 180$ K for dysprosium, which is the ordering temperature for antiferromagnets, they both form base-plane helical antiferromagnets. In terbium the easy axis is the [10̄10] direction (the *b* axis) while in dysprosium it is the [1000] direction (or *a* axis). At a lower temperature of 219 K in terbium or 85 K in dysprosium (which are the Curie temperatures) they form base-plane ferromagnets. In terbium the domains have their axes along the *b* axes while in dysprosium the moments align along the *a* axes.

Holmium has an ordering temperature of 132 K, below which it forms a base-plane antiferromagnet [34] that is similar to dysprosium, with an easy axis along the [1000] direction. This helical structure is retained down to 20 K, the Curie

point, below which there appears a ferromagnetic c axis component, while the base plane continues to exhibit helical antiferromagnetic order.

Erbium has a Neel point of 85 K, below which the magnetization is sinusoidally modulated along the c axis [34, 35, 36]. At 53 K a further transition occurs when the base plane orders helically, and the c axis structure begins to change to a square-wave modulation of four moments up followed by four moments down. This square-wave modulation is never completed, however. At the Curie point of 20 K the c axis components become ferromagnetic, while the base plane continues its helical order. This leads to a ‘conical’ ferromagnetic structure of the type observed also in holmium.

Ferrimagnetism is exhibited by a number of transition metal oxides known as ferrites. These fall into three classes: the cubic ferrites, also known as spinels, such as $\text{NiO}\cdot\text{Fe}_2\text{O}_3$, which are soft magnetic materials with the exception of cobalt ferrite which is hard; the hexagonal ferrites such as $\text{BaO}\cdot 6(\text{Fe}_2\text{O}_3)$ which are hard magnetic materials used to make ceramic magnets; and the garnets such as yttrium–iron garnet $5\text{Fe}_2\text{O}_3\cdot 3\text{Y}_2\text{O}_3$.

9.3.5 Excited states and spin waves

How does temperature affect the alignment of magnetic moments within a domain?

We have noted above in section 6.2.5 that the spontaneous magnetization within a domain M_s is only equal to the saturation magnetization $M_0 = Nm$ at absolute zero of temperature (0 K). The reason for this is that the thermal energy at temperatures above 0 K causes some misalignment of the directions of magnetic moments within the domains. We shall now explain how this misalignment occurs.

Consider the ground state of a six-moment linear ferromagnet as shown in Fig. 9.18(a). The ground state is clearly when all six moments are aligned parallel. On the basis of nearest-neighbour-only interaction this has a ground energy of E_0 given by

$$E_0 = -10\mu_0 J m^2.$$

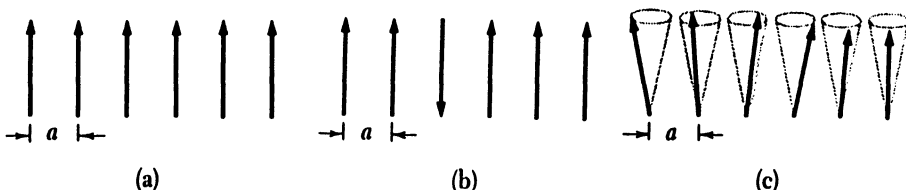


Fig. 9.18 A six-moment linear ferromagnetic chain: (a) ground state, (b) a state with one moment antiparallel, and (c) a state with each successive moment at an angle θ to its neighbours.

There are several possible candidates for the lowest-level excited state. One possible candidate is the configuration with one moment pointing antiparallel to the rest as shown in Fig. 9.18(b). This will have an energy of

$$\begin{aligned} E_1 &= -2\mu_0 \mathcal{J} \mathbf{m}^2 \\ &= E_0 + 8\mu_0 \mathcal{J} \mathbf{m}^2 \end{aligned}$$

and in fact for a linear chain with any number of moments greater than 2 the energy of the system with one moment antiparallel is always $8\mu_0 \mathcal{J} \mathbf{m}^2$ above the ground state.

Another candidate excited state is one in which each moment is aligned at an angle θ to the direction of the previous moment as shown in Fig. 9.18(c). In this case the energy of the system is

$$\begin{aligned} E(\theta) &= -10\mu_0 \mathcal{J} \mathbf{m}^2 \cos \theta \\ &= E_0 + 10\mu_0 \mathcal{J} \mathbf{m}^2(1 - \cos \theta). \end{aligned}$$

This allows for much lower-energy excited states which in the classical approximation form a continuum of allowed energy states above the ground state, each with gradually increasing values of θ .

The spontaneous magnetization within a domain therefore decreases as the temperature increases above 0 K. It can be shown from an analysis of the spin-wave structure [37] that

$$\begin{aligned} M_s &= M_0(1 - aT^{3/2}) \\ &= M_0 \left[1 - c \left(\frac{k_B T}{\mu_0 \mathcal{J} \mathbf{m}^2} \right)^{3/2} \right], \end{aligned}$$

where $\mu_0 \mathcal{J} \mathbf{m}^2$ is the nearest-neighbour exchange constant in joules and c is a constant. $c = 0.118$ for a simple cubic lattice, $c = 0.059$ for a body-centred cubic lattice, and $c = 0.029$ for a face-centred cubic lattice.

9.3.6 Critical behaviour at the ordering temperature

What happens to other bulk properties of a ferromagnet at the Curie temperature?

The bulk properties of magnetic materials show anomalous behaviour in the vicinity of the transition temperatures such as the Curie and Neel points. The anomalous behaviour is due to coupling between the particular bulk property and the magnetic structure. The effects are known as critical phenomena. We have already remarked that the bulk susceptibility has anomalous behaviour close to T_c , for example. Other properties such as the specific heat, elastic moduli, magnetostriction, magnetoresistance and thermal expansion all reveal critical behaviour at the magnetic transition temperatures.

9.3.7 Susceptibility anomalies

How does the susceptibility behave at the ordering temperature?

We have shown that the susceptibility of ferromagnets, ferrimagnets and antiferromagnets behaves in an anomalous way as the temperature is reduced in the paramagnetic regime towards the critical temperature T_c . In many cases these materials obey the Curie–Weiss law and this leads to a dependence of susceptibility on temperature of the form $\chi = C/(T - T_c)$ in the paramagnetic regime. The susceptibility therefore starts to become very large as T_c is approached from above.

Work on the magnetization curves and susceptibility of a number of rare earth metals which obey the Curie–Weiss law was performed by Legvold, Spedding and coworkers in a series of papers [38–42].

9.3.8 Specific heat anomalies

How does the specific heat behave at the ordering temperature?

The specific heats of materials which undergo order–disorder transitions show lambda-type anomalies at the critical temperature. Some examples are shown in Fig. 9.19 from the work of Hofmann *et al.* [43]. Measurements of the heat capacities of several heavy rare earth elements were made by Spedding *et al.* [44–48].

The specific heat of a magnetic material has a magnetic component C_m given by

$$C_m = \left(\frac{1}{\mu_0 \rho} \right) \left(\frac{dE_{ex}}{dT} \right)$$

where E_{ex} is the total exchange self energy of the material per unit volume.

$$E_{ex} = -\mu_0 \mathcal{J} M_s^2$$

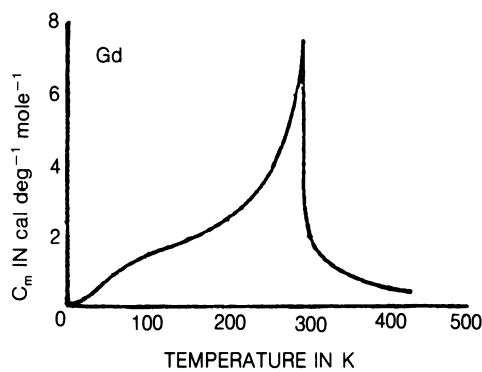
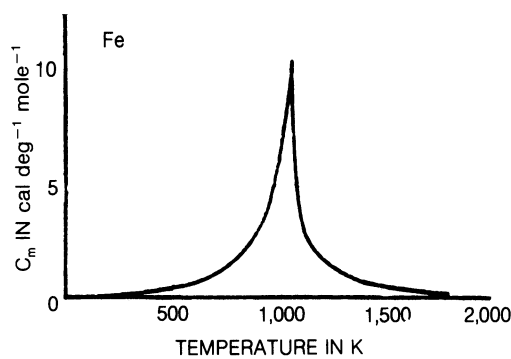
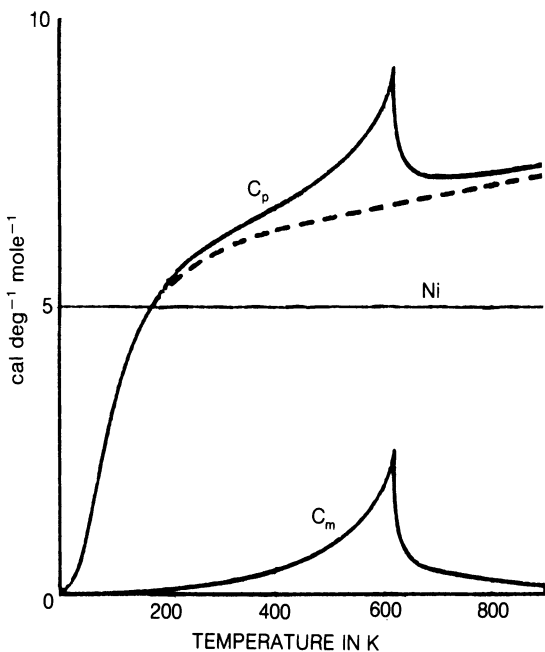
$$C_m = -2 \left(\frac{\mathcal{J} M_s}{\rho} \right) \frac{dM_s}{dT}.$$

The dependence of M_s on temperature is known from the equation, given in section 9.2.3,

$$\frac{dM_s}{dT} = M_0 \frac{d}{dT} \left[\coth \left(\frac{\mu_0 m \alpha M_s}{k_B T} \right) - \frac{k_B T}{\mu_0 m \alpha M_s} \right].$$

The variation of C_m with temperature is plotted for nickel in Fig. 9.20. The behaviour gives a remarkably good fit to the experimental data for such a simple model. The experimental results show some broadening of the lambda anomaly in the paramagnetic region.

Fig. 9.19 Examples of specific heat anomalies in nickel, iron and gadolinium close to their ordering temperatures (after Hofmann *et al.* (1956)).



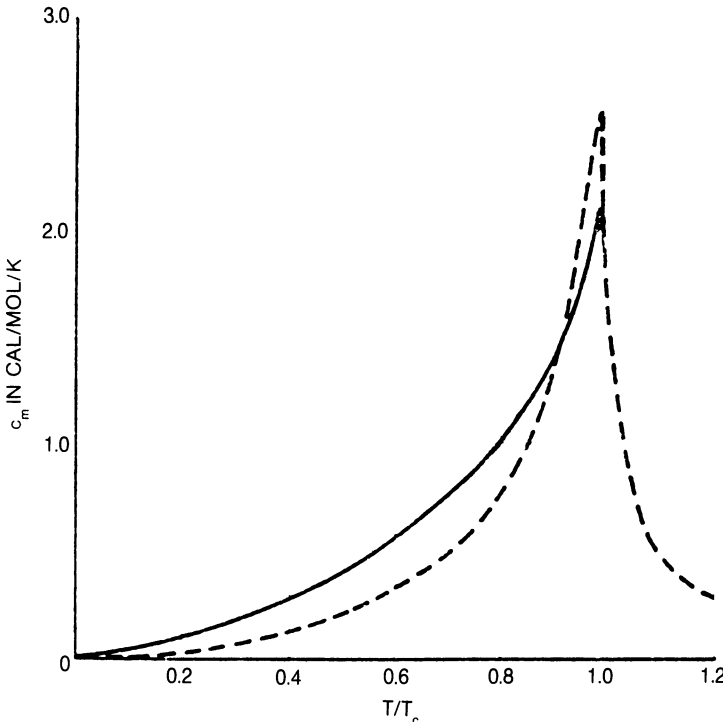


Fig. 9.20 Specific heat anomaly for nickel at its Curie point compared with the theoretical prediction.

9.3.9 Elastic constant anomalies

How do the elastic properties behave at the ordering temperature?

The elastic constants of materials show critical behaviour close to magnetic phase transitions such as the Curie point as shown in Fig. 9.21. Magnetoelastic anomalies are known to occur in rare earth metals as a result of the very strong magnetoelastic coupling. These have been thoroughly investigated by Palmer and coworkers in a series of papers [49–55] and Moran and Luthy [56, 57]. Some of the theoretical aspects have been addressed by Tachiki and Maekawa [58].

The dependence of elastic modulus on magnetization, the so called ΔE effect in iron is well known and has been reported by Bozorth [59].

9.3.10 Thermal expansion anomalies

How does the thermal expansion behave at the ordering temperature?

The thermal expansion and magnetostriction also undergo unusual behaviour at phase transitions such as at the Curie and Neel points as shown in Fig. 9.22. This is

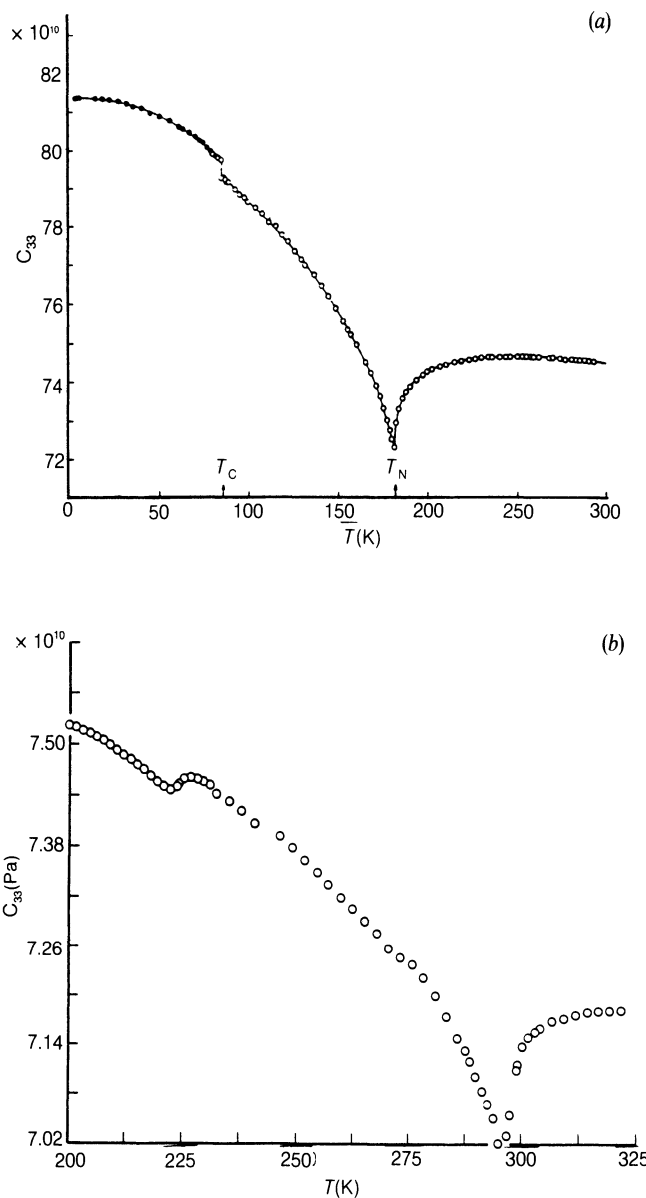


Fig. 9.21 Critical behaviour of the elastic constants of dysprosium (above) and gadolinium (below).

because there is the sudden appearance of spontaneous magnetostriction at the order-disorder transition temperature. Anomalous thermal expansion and magnetostriction have been investigated by Bozorth and Wakayama [60] and by Greenough and coworkers in a number of papers [61–63].

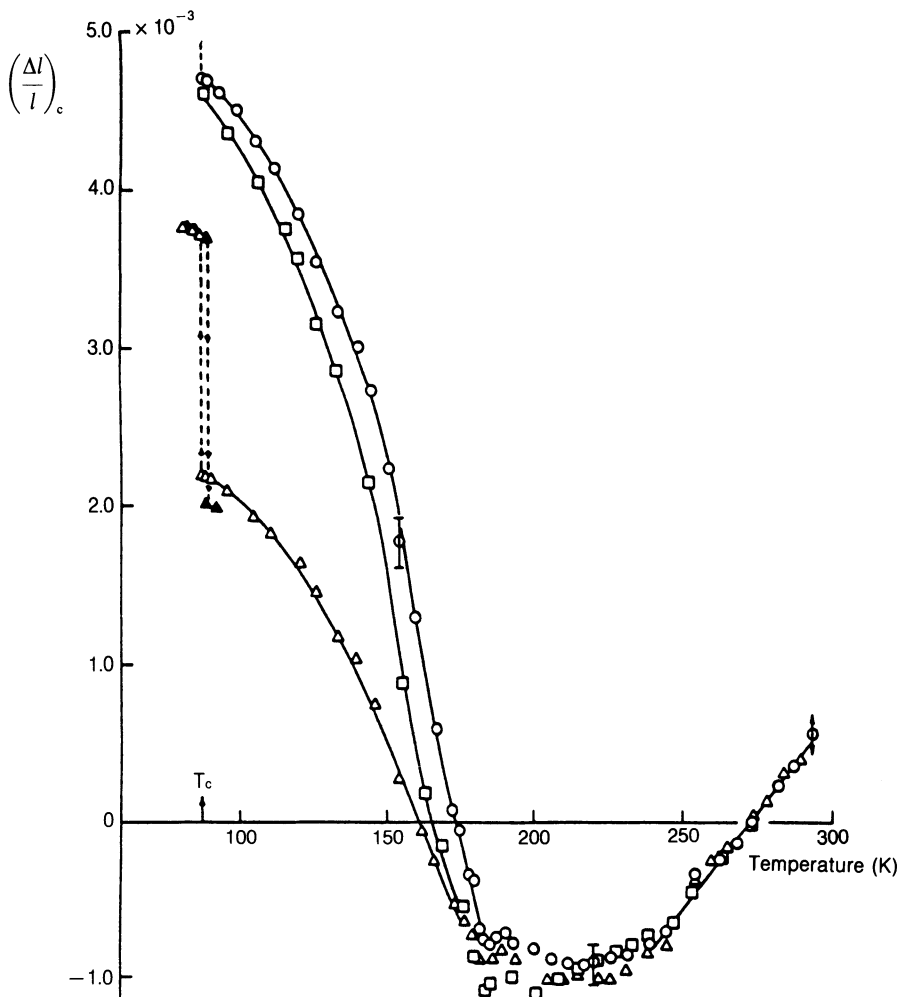


Fig. 9.22 Anomalous behaviour of the *c*-axis thermal expansion of dysprosium at its Neel temperature of 180 K and Curie temperature of 85 K.

9.3.11 The Ising model

Is there a thermodynamic model which can be used to describe the behaviour of magnetic materials as a function of temperature and field?

The idea of a Weiss-type coupling between electronic moments can be incorporated into a simple classical model which describes the effects of temperature and magnetic field on the magnetization. The Ising model [64] provides a useful mathematical description of critical phenomena and is particularly relevant to magnetic materials. It has the unique distinction of being

the only model of a second-order phase transition which has so far yielded a mathematical solution.

In the Ising model as applied to magnetic materials [65, 66] the solid is divided into ‘cells’ each of which contains one magnetic moment or spin. Each cell is allowed a limited number of possible states and in the simplest models only two states are allowed which correspond to ‘spin up’ and ‘spin down’. At first sight this restriction may appear to be unrealistic, because classically the spins can point in any direction. But in quantum mechanics the spins are restricted to certain directions and in particular the directions of the spins can be referenced parallel and antiparallel to an applied magnetic field \mathbf{H} to which they are restricted in quantum mechanics. Therefore this actually results in a quite reasonable approximation of reality.

One drawback however is that in the simple Ising model described here the restriction on orientation of the spins does not allow spin waves. The lowest excited energy state that can be produced is therefore when one spin is antiparallel to the rest and consequently there exists an energy gap of $8\mu_0\mathcal{J}\mathbf{m}^2$ between the ground state and the first excited state.

The Ising model has then two imposed restrictions and these are (a) that the spins have two states and (b) that there are interactions between the spins which correlate their orientations, but the interactions are restricted to nearest-neighbour, or nearest-neighbour and second-nearest-neighbour, or else all moments interact equally (which is equivalent to the mean-field approximation).

As before the magnetic interaction has the form

$$E_{\text{ex}} = -\mu_0 \sum \mathcal{J} \mathbf{m}_i \cdot \mathbf{m}_j.$$

We can define an order parameter for the Ising model η given by

$$\eta = \frac{(p_+ - p_-)}{(p_+ + p_-)}$$

such that when $\eta = 0$ the system is paramagnetic and when $\eta \neq 0$ the system is ferromagnetic. A phase transition therefore occurs when η reaches zero.

A mathematical treatment of the probable configuration of magnetic moments on the atomic sites in the two-dimensional Ising lattice has shown that an order-disorder transition occurs at a Curie temperature of

$$\begin{aligned} T_c &= \frac{0.88 E_{\text{ex}}}{k_B} \\ &= \frac{0.88 J s^2}{k_B} \\ &= \frac{0.88 \mu_0 \mathcal{J} \mathbf{m}^2}{k_B}, \end{aligned}$$

where E_{ex} is the nearest-neighbour coupling energy between the spins. Similarly, as shown above for the mean-field model the specific heat has a lambda anomaly.

REFERENCES

1. Langevin, P. (1905) *Annales de Chem. et. Phys.*, **5**, 70.
2. Van Vleck, J. H. (1932) *The Theory of Electric and Magnetic Susceptibilities*, Oxford.
3. Pauli, W. (1926) *Z. Phys.*, **41**, 81.
4. Curie, P. (1895) *Ann. Chem. Phys.*, **5**, 289.
5. Weiss, P. (1906) *Compt. Rend.*, **143**, 1136.
6. Weiss, P. (1907) *J. de Phys.*, **6**, 661.
7. Weiss, P. (1948) *Phys. Rev.*, **74**, 1493.
8. Neel, L. (1932) *Annales de Phys.*, **18**, 5.
9. Neel, L. (1948) *Annales de Phys.*, **3**, 137.
10. Enz, U. (1960) *Physica*, **26**, 698.
11. Nicklow, R. M., Wakabayashi, N., Wilkinson, M. K. and Read, R. E. (1971) *Phys. Rev. Letts.*, **26**, 140.
12. Becon, G. E. (1975) *Neutron Diffraction*, 3rd edn. Clarendon Press, Oxford.
13. Lovesey, S. W. (1984) *Theory of Neutron Scattering from Condensed Matter*, Vol. 2: *Polarization Effects and Magnetic Scattering*, Clarendon Press, Oxford.
14. Koehler, W. C. (1965) *J. Appl. Phys.*, **36**, 1078.
15. Shull, C. G., Wollan, E. O. and Koehler, W. C. (1951) *Phys. Rev.*, **84**, 912.
16. Bloch, F. (1936) *Phys. Rev.*, **50**, 259.
17. Halpern, O. and Johnson, M. H. (1939) *Phys. Rev.*, **55**, 898.
18. Crangle, J. (1977) *The Magnetic Properties of Solids*, Edward Arnold, London.
19. Squires, G. L. (1954) *Proc. Phys. Soc. Lond.* **A67**, 248.
20. Cribier, D., Jacrot B. and Parette, G. (1962) *J. Phys. Soc. Jap.* **17** (Suppl. BIII Proceedings of the International Conference on Magnetism and Crystallography, Kyoto), **67**.
21. Honda, K. and Kaya, (1926) *S. Sci. Reps. Tohoku Univ.* **15**, 721.
22. Kaya, S. (1928) *Sci. Reps. Tohoku Univ.* **17**, 639.
23. Kaya, S. (1928) *Sci. Reps. Tohoku Univ.* **17**, 1157.
24. Corliss, L. M., Hastings, J. M. and Weiss, R. J. (1959) *Phys. Rev. Letts.*, **3**, 211.
25. Shull, C. G. and Wilkinson, M. K. (1953) *Revs. Mod. Phys.* **25**, 100.
26. Cable, J. W. and Wollan, E. O. (1968) *Phys. Rev.*, **165**, 733.
27. Graham, C. D. (1963) *J. Appl. Phys.*, **34**, 1341.
28. Corner, W. D., Roe, W. C. and Taylor, K. N. R. (1962) *Proc. Phys. Soc.*, **80**, 927.
29. Corner, W. D. and Tanner, B. K. (1976) *J. Phys. C.*, **9**, 627.
30. Koehler, W. C., Child, H. R., Wollan, E. O. and Cable, J. W. (1963) *J. Appl. Phys.*, **34**, 1335.
31. Bly, P. H., Corner, W. D. and Taylor, K. N. R. (1969) *J. Appl. Phys.*, **40**, 4787.
32. Landry, P. C. (1967) *Phys. Rev.*, **156**, 578.
33. Wilkinson, M. K., Koehler, W. C., Wollan, E. O. and Cable, J. W. (1961) *J. Appl. Phys.*, **32**, 48S.
34. Koehler, W. C., Cable, J. W., Wollan, E. O. and Wilkinson, M. K. (1962) *J. Phys. Soc. Jap.*, **17**, (Suppl. BIII Proceedings of the International Conference on Magnetism and Crystallography, Kyoto), 32.
35. Rhyne, J. J., Foner, S., McNiff, E. J. and Doclo, R. (1968) *J. Appl. Phys.*, **39**, 892.
36. Cable, J. W., Wollan, E. O., Koehler, W. C. and Wilkinson, M. K. (1961) *J. Appl. Phys.*, **32**, 49S.
37. Bloch, F. (1930) *Z. Phys.* **61**, 206.
38. Nigh, H. E., Legvold, S. and Spedding, F. H. (1963) *Phys. Rev.*, **132**, 1092.
39. Hegland, D. E., Legvold, S. and Spedding, F. H. (1963) *Phys. Rev.*, **131**, 158.
40. Behrendt, D. R., Legvold, S. and Spedding, F. H. (1958) *109*, 1544.
41. Strandburg, D. L., Legvold, S. and Spedding, F. H. (1962) *Phys. Rev.*, **127**.
42. Green, R. W., Legvold, S. and Spedding, F. H. (1961) *Phys. Rev.*, **122**, 827.

43. Hofmann, J. A., Paskin, A., Tauer, K. J. and Weiss, R. J. (1956) *J. Phys. Chem. Sol.*, **1**, 45.
44. Jennings, L. D., Stanton, R. M. and Spedding, F. H. (1957) *J. Chem. Phys.*, **27**, 909.
45. Skochedopole, R. E., Griffel, M. and Spedding, F. H. (1955) *J. Chem. Phys.*, **23**, 2258.
46. Griffel, M., Skochedopole, R. E. and Spedding, F. H. (1954) *Phys. Rev.*, **93**, 657.
47. Griffel, M., Skochedopole, R. E. and Spedding, F. H. (1956) *J. Chem. Phys.*, **25**, 75.
48. Gerstein, B. C., Griffel, M., Jennings, L. D., Miller, R. E., Skochedopole, R. E. and Spedding, F. H. (1957) *J. Chem. Phys.*, **27**, 394.
49. Palmer, S. B. and Lee, E. W. (1972) *Proc. Roy. Soc.*, **A327**, 519.
50. Palmer, S. B., Lee, E. W. and Islam, M. N. (1974) *Proc. Roy. Soc.*, **A338**, 341.
51. Isci, C. and Palmer, S. B. (1977) *J. Phys. Chem. Sol.*, **38**, 1253.
52. Isci, C. and Palmer, S. B. (1978) *J. Phys. F.*, **8**, 247.
53. Jiles, D. C., Blackie, G. N. and Palmer, S. B. (1981) *J. Mag. Mag Mater.*, **24**, 75.
54. Jiles, D. C. and Palmer, S. B. (1980) *J. Phys. F.*, **10**, 2857.
55. Jiles, D. C. and Palmer, S. B. (1981) *J. Phys. F.*, **11**, 45.
56. Luthi, B., Moran, T. J. and Pollina, R. J. (1970) *J. Phys. Chem. Soc.*, **31**, 1741.
57. Moran, T. J. and Luthi, B. (1970) *J. Phys. Chem. Sol.*, **31**, 1735.
58. Tachiki, M. and Maekawa, S. (1974) *Prog. Theor. Phys. Jap.*, **51**, 1.
59. Bozorth, R. M. (1951) *Ferromagnetism*, Van Nostrand, New York.
60. Bozorth, R. M. and Wakiyama, T. (1963) *J. Phys. Soc. Jap.*, **18**, 97.
61. Greenough, R. D. and Isci, C. and Palmer, S. B. (1977) *Physica*, **86–88B**, 61.
62. Greenough, R. D. and Isci, C. (1978) *J. Mag. Mag. Mater.*, **8**, 43.
63. Greenough, R. D. (1979) *J. Phys. C.*, **12**, 1113.
64. Ising, E. (1925) *Z. Phys.* **31**, 253.
65. Stanley, H. E. (1971) *Introduction to Phase Transition and Critical Phenomena*, Clarendon Press, Oxford.
66. Green, H. S. and Hurst, C. A. (1964) *Order–Disorder Phenomena*, Wiley Interscience, London.

FURTHER READING

- Bacon, G. E. (1975) *Neutron Diffraction*, 3rd edn, Clarendon Press, Oxford.
- Chikazumi, S. (1964) *Physics of Magnetism*, Wiley, New York, Ch. 4 and 5.
- Coqblin, B. (1977) *The Electronic Structure of Rare Earth Solids*, Wiley, New York.
- Cullity, B. D. (1977) *Introduction to Magnetic Materials*, Addison-Wesley, Reading, Mass., Ch. 3, 4 and 5.
- Elliott, R. J. (1972) *Magnetic Properties of Rare Earth Metals*, Plenum London.
- Lovesey, S. W. (1984) *Theory of Neutron Scattering from Condensed Matter*, Clarendon Press, Oxford.
- Mackintosh, A. R. (1977) *The Magnetism of Rare Earth Metals*, Physics Today, June, 23.

EXAMPLES AND EXERCISES

Example 9.1 Paramagnetic susceptibility of oxygen. Calculate the susceptibility at 0 °C of a paramagnetic gas of molecular mass 32 with a magnetic moment of 3 Bohr magnetons per molecule ($S = 3/2$).

Example 9.2 Magnetic mean interaction field for iron. Derive the relationship between the Weiss ‘molecular’ field of a ferromagnet and the Curie temperature. Calculate the value of this field for iron which has a Curie temperature of 770 °C and an effective magnetic moment per atom of 2.2 Bohr magnetons.

218 Magnetic order and critical phenomena

Example 9.3 Critical behaviour of spontaneous magnetization. In the mean-field approximation for a system with two possible microstates (e.g. magnetic moments either parallel or antiparallel to a unique axis) the spontaneous magnetization within a domain is given by $M_s = M_0 \tanh [\mu_0 m \alpha M_s / k_B T]$. Show that at just below the Curie point the spontaneous magnetization varies with $\sqrt{(T_c - T)}$.

10

Electronic Magnetic Moments

In this chapter we discuss the prime cause of the magnetic moment within an individual atom. We will look at the properties of electrons which are of central importance to magnetism and in particular the origin of the electron's magnetic moment which is a result of its angular momentum. We also look at how the magnetic properties of the electrons lead to differences in the available energy states in the presence of a magnetic field. Finally we show how the magnetic moments of the electrons are combined to give the magnetic moment of the atom.

10.1 THE CLASSICAL MODEL OF ELECTRONIC MAGNETIC MOMENTS

Why do electrons have a magnetic moment?

In the classical model the angular momentum of the electrons can be used to determine the magnetic moments of the electrons by invoking the concept of electrical charge in motion. It is known from Chapter 1 for example that a current loop behaves as a magnetic dipole and has an associated magnetic moment. There are two contributions to the electronic magnetic moment: an orbital magnetic moment due to orbital angular momentum, and a spin magnetic moment due to electron spin.

10.1.1 Electron orbital magnetic moment

How does the angular momentum of an electron lead to a net magnetic moment?

We can envisage an electron moving in an orbit about an atomic nucleus, as shown in Fig. 10.1, with orbital area A and period τ . This would then be equivalent to a current i given by

$$i = \frac{e}{\tau}$$

From the earlier definitions, in sections 2.1.1 and 9.1.2, this gives an orbital

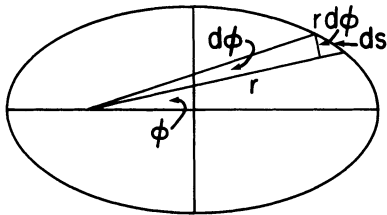


Fig. 10.1 Classical model of an electron in an elliptical orbit around a nucleus.

magnetic moment \mathbf{m}_0

$$\begin{aligned}\mathbf{m}_0 &= i\mathbf{A} \\ &= -\frac{e\mathbf{A}}{\tau}.\end{aligned}$$

The angular momentum of such an orbital \mathbf{p}_0 will be

$$\mathbf{p}_0 = m_e r^2 \frac{d\phi}{dt},$$

where m_e is the mass of an electron and r is the radius

$$\mathbf{A} = \left(\frac{1}{2}\right) \mathbf{p}_0 \frac{\tau}{m_e}.$$

We can therefore write down the orbital magnetic moment \mathbf{m}_0 of the electron in terms of the orbital angular momentum \mathbf{p}_0 as

$$\mathbf{m}_0 = -\left(\frac{e}{2m_e}\right) \mathbf{p}_0$$

remembering that the magnetic moment vector points in the opposite direction to the angular momentum vector because the electron has negative charge.

10.1.2 Electron spin magnetic moment

How does the electron spin contribute to the magnetic moment?

The electronic spin angular momentum \mathbf{p}_s also generates a spin magnetic moment \mathbf{m}_s . In this case the relation is

$$\mathbf{m}_s = -\frac{e\mathbf{p}_s}{m_e}.$$

Notice that for a given angular momentum the spin gives twice the magnetic moment of the orbit.

10.1.3 Total electronic magnetic moment

How can we combine the spin and orbital angular momentum contributions to get the total electron magnetic moment?

If we consider the total magnetic moment per electron as the vector sum of the orbital and spin magnetic moments

$$\begin{aligned}\mathbf{m}_{\text{tot}} &= \mathbf{m}_s + \mathbf{m}_0 \\ &= -\left(\frac{e}{2m_e}\right)2\mathbf{p}_s - \left(\frac{e}{2m_e}\right)\mathbf{p}_0.\end{aligned}$$

These terms on the right-hand side can then be combined to give

$$\mathbf{m}_{\text{tot}} = -g\left(\frac{e}{2m_e}\right)\mathbf{p}_{\text{tot}},$$

where now \mathbf{p}_{tot} is the total angular momentum of the electron. The term ‘ g ’ is called the Lande splitting factor, which has a value of $g = 2$ for spin-only components and $g = 1$ for orbital-only components of magnetic moment. The value of the splitting factor must therefore lie between 1 and 2 depending on the relative sizes of the contributions from the spin and orbit to the total angular momentum.

10.2 THE QUANTUM MECHANICAL MODEL OF ELECTRONIC MAGNETIC MOMENTS

How are the above definitions modified as a result of quantum mechanics?

We have shown above how the angular momentum of electrons leads to a net magnetic moment. However in the discussion we have so far allowed all values of \mathbf{p}_0 and \mathbf{p}_s . In fact this is not realistic, the possible values of angular momentum are restricted by quantum mechanics, and consequently the magnetic moments are also quantized. We begin by defining the quantum numbers needed to fully describe electrons within atoms, then look at the restrictions on magnetic moment, and finally look at experimental evidence confirming the quantization of magnetic moments, specifically the Zeeman effect and the Stern–Gerlach experiment.

We need to use four quantum numbers in order to define uniquely each electron in an atom. These are the principal quantum number n , defined by Bohr, the angular momentum quantum number l defined by Sommerfeld, the orbital magnetic quantum number m_l and the spin magnetic quantum number m_s .

10.2.1 Principal quantum number n

What energies can electrons have within the atom?

This n is the quantum number introduced by Bohr in his theory of the atom [1]. It determines the shell of the electron, and hence its energy. In Bohr’s original

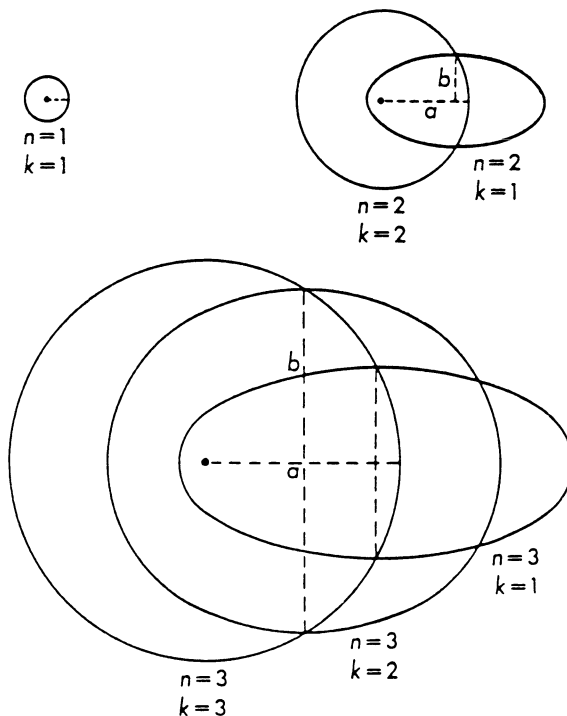


Fig. 10.2 Electron orbitals with the same energy but with different angular momentum described in the Bohr–Sommerfeld theory.

formulation it also defined the orbital angular momentum but in later models several different orbitals with different angular momenta, but degenerate energy, were found to exist for a given n , as shown in Fig. 10.2.

The energy E_n of an electron with principal quantum number n is then,

$$E_n = -\frac{Z^2 m_e e^4}{8n^2 h^2 \epsilon_0^2},$$

where

$$n = 1, 2, 3, \dots,$$

and Z is the atomic number, m_e the mass of the electron, e the electronic charge and ϵ_0 the permittivity of free space. The maximum number of electrons permitted in the n th shell is $2n^2$.

10.2.2 Orbital angular momentum quantum number l

What values of orbital angular momentum are possible for electrons within the atom?

This l is synonymous with the quantum number k introduced in the Sommerfeld theory of the atom [2] except that $l = k - 1$. It was needed to define the orbital

angular momentum p_0 of the electron once it was realized that one energy level could have more than one allowed value of angular momentum. It is a measure of the orbital angular momentum of the electron when multiplied by $(h/2\pi)$. It also gives a measure of the eccentricity of the electron orbit.

$$p_0 = l \left(\frac{h}{2\pi} \right).$$

It can have value of $l = 0, 1, 2, 3 \dots (n - 1)$ where n is the principal quantum number.

10.2.3 Spin quantum number s

What values of spin angular momentum can electrons have within the atom?

Electrons have spin angular momentum which can be represented by the spin quantum number s . The value of s is always $1/2$ for an electron. The angular momentum due to spin $sh/2\pi$ is therefore always a multiple of $h/4\pi$

$$p_s = s \left(\frac{h}{2\pi} \right).$$

The total angular momentum quantum number j of an electron is not an independent quantum number since it is determined by l and s . However it is a useful quantity to define, particularly since it gives a measure of the total magnetic moment of an electron. It is the vector sum of the spin and orbital angular momenta and is necessarily quantized

$$\begin{aligned} p_j &= j \left(\frac{h}{2\pi} \right) \\ &= (l + s) \left(\frac{h}{2\pi} \right) \end{aligned}$$

10.2.4 Magnetic quantum numbers m_l and m_s

What orientations can the spin and orbit angular momentum vectors of an electron take when subjected to a magnetic field?

The angular momentum vector precesses about the direction of an applied field as shown in Fig. 10.3. This was predicted by Larmor's theorem [3] which states that the effect of a magnetic field on an electron moving in an orbit is to impose on the electron a precession motion about the direction of the magnetic field with an angular velocity given classically by $\omega = \mu_0(e/2m_e)\mathbf{H}$. The component of the angular momentum along the field axis is $m_0 \cos \theta$, where θ is the angle of precession. The component perpendicular to this direction is time averaged to zero.

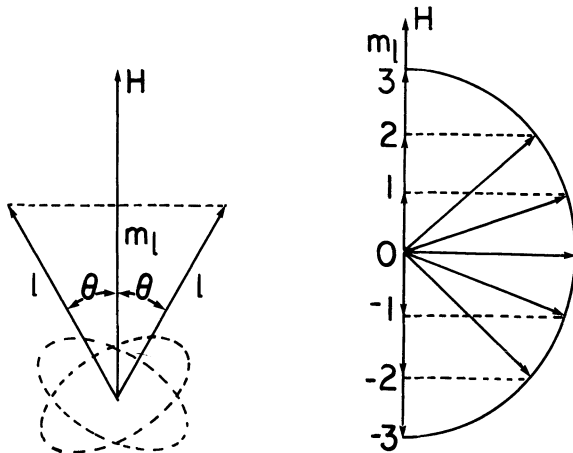


Fig. 10.3 (a) Precession of the orbital angular momentum vector \mathbf{l} about the magnetic field axis. (b) Quantization of the allowed projection of angular momentum \mathbf{l} along the field direction.

The component of angular momentum along the axis of a magnetic field is restricted to discrete values by quantum mechanics. The magnetic quantum number m_l which represents these discrete values arises from the solution of Schrödinger's equation for a single electron atom. It gives the component l_z of the orbital angular momentum \mathbf{l} along the z -axis of a coordinate system

$$l_z = m_l \left(\frac{\hbar}{2\pi} \right),$$

where the z -axis is defined as the axis perpendicular to the plane in which the electron orbit lies.

The values of m_l are restricted to $m_l = -l, \dots, -2, -1, 0, 1, 2, \dots, +l$. The

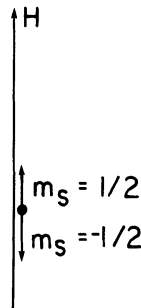


Fig. 10.4 Quantization of the allowed projection of the spin s along the magnetic field direction.

physical significance of this number is that when a magnetic field is applied to an atom the electron's orbital angular momentum l can only have certain values of the component parallel to the magnetic field direction, and these are given by the magnetic quantum number m_l .

Electron spins are constrained to lie either parallel or antiparallel to a magnetic field. The orientation of the electron can be represented by the spin magnetic quantum number m_s which is always constrained to have the values $m_s = +\frac{1}{2}$ or $-\frac{1}{2}$ as shown in Fig. 10.4.

10.2.5 Quantized angular momentum and magnetic moments

What restrictions does quantum theory impose on the allowed values of the electronic magnetic moment?

If we express the orbital angular momentum in units of $h/2\pi$ then the equation of section 10.1.1 becomes

$$\begin{aligned}\mathbf{m}_0 &= -\left(\frac{eh}{4\pi m_e}\right)\left(\frac{2\pi p_0}{h}\right) \\ &= -\left(\frac{eh}{4\pi m_e}\right)l,\end{aligned}$$

where l is the orbital angular momentum quantum number, since by the quantum theory we expect the angular momentum of an electron to be an integral multiple of $h/2\pi$ (remembering that from Bohr's atomic theory $p_0 = nh/2\pi$ and from Sommerfeld's theory $p_0 = kh/2\pi$).

This means that on this basis we expect the orbital contribution to the magnetic moment to be an integral multiple of $eh/4\pi m_e$. This quantity is known as the Bohr magneton, designated μ_B , which has a value of $9.27 \times 10^{-24} \text{ A m}^2$ (A m^2 is equivalent to J/T).

$$\mathbf{m}_0 = -\mu_B l,$$

where l must be an integer.

The spin on an electron is $\frac{1}{2}$, and so if we suppose p_s is an integer multiple of $(h/2\pi)$ then $p_s = sh/2\pi$, where s is the spin quantum number. The magnetic moment \mathbf{m}_s due to the spin is then

$$\mathbf{m}_s = -\frac{eh}{2\pi m_e}\left(\frac{2\pi p_s}{h}\right).$$

Replacing $2\pi p_s/h$ by the spin quantum number s

$$\mathbf{m}_s = -2\left(\frac{eh}{4\pi m_e}\right)s.$$

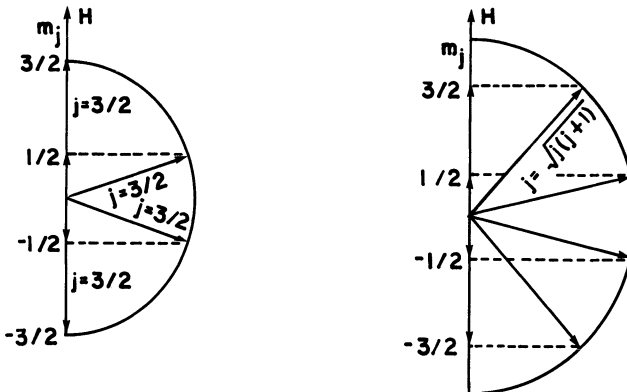


Fig. 10.5 Projection of the total angular momentum j along the magnetic field direction.

Again replacing $(eh/4\pi m_e)$ by μ_B the Bohr magneton

$$\mathbf{m}_s = -2\mu_B \mathbf{s},$$

where now because of the quantization of angular momentum $2s = 4\pi p_s/h$. Since s must be $+\frac{1}{2}$ or $-\frac{1}{2}$ this means that the spin magnetic moment of an electron is one Bohr magneton.

The total magnetic moment of an electron can be expressed in terms of multiples of the total angular momentum $(h/2\pi)j$ of the electron.

$$\begin{aligned} \mathbf{m}_{\text{tot}} &= -g\left(\frac{e\mathbf{h}}{4\pi m_e}\right)\left(\frac{2\pi\mathbf{p}_{\text{tot}}}{h}\right) \\ &= -g\mu_B\left(\frac{2\pi\mathbf{p}_{\text{tot}}}{h}\right) \end{aligned}$$

$$\mathbf{m}_{\text{tot}} = -g\mu_B \mathbf{j},$$

where j is the total angular momentum quantum number, and for a particular electron

$$\begin{aligned} \mathbf{m}_{\text{tot}} &= \mathbf{m}_0 + \mathbf{m}_s \\ &= -(g\mu_B l + 2\mu_B s). \end{aligned}$$

The projection m_j of the total angular momentum along the direction of a magnetic field is also quantized as shown in Fig. 10.5.

10.2.6 The Vector model of the atom

Do we have a simple model that can be used to interpret the electronic properties of an atom?

We know that an electron has a total angular momentum j which arises from its spin angular momentum s and its orbital angular momentum l . In the vector model

of the atom the total angular momentum of an electron is simply the vector sum of its spin and orbital angular momenta.

$$j = l + s$$

as indicated in Fig. 10.6(a). Of course the vector sum must always be half integral. For any given value of l the total angular momentum j can only have two possible values, $l \pm s$, depending on whether s is parallel or antiparallel to l . An exception is the case $l = 0$ when j must be $\frac{1}{2}$.

For an atom with a single electron in an outer unfilled shell, and with all other shells filled, these values become the angular momenta of the atom. For a multielectron atom, that is one with more than one electron in an unfilled shell, we use the terms J , L and S to designate the total, orbital and spin angular momenta of the atom respectively where L is the vector sum of all the orbital components m_l , S is the vector sum of all spin components m_s and J is the vector sum of total angular momenta of the electrons which can be calculated in at least two ways. For an atom with completely filled shells $J = 0$, $L = 0$ and $S = 0$.

We shall see shortly the assumption that the angular momentum is an integral multiple of the orbital quantum number l and the spin quantum number s is not quite valid. More precise values according to wave mechanics are $p_0^2 = (h/2\pi)^2 l(l+1)$ and $p_s^2 = (h/2\pi)^2 s(s+1)$. The respective magnetic moments become $\mathbf{m}_0 = \mu_B \sqrt{l(l+1)}$ and $\mathbf{m}_s = \mu_B \sqrt{s(s+1)}$. Similarly the total angular

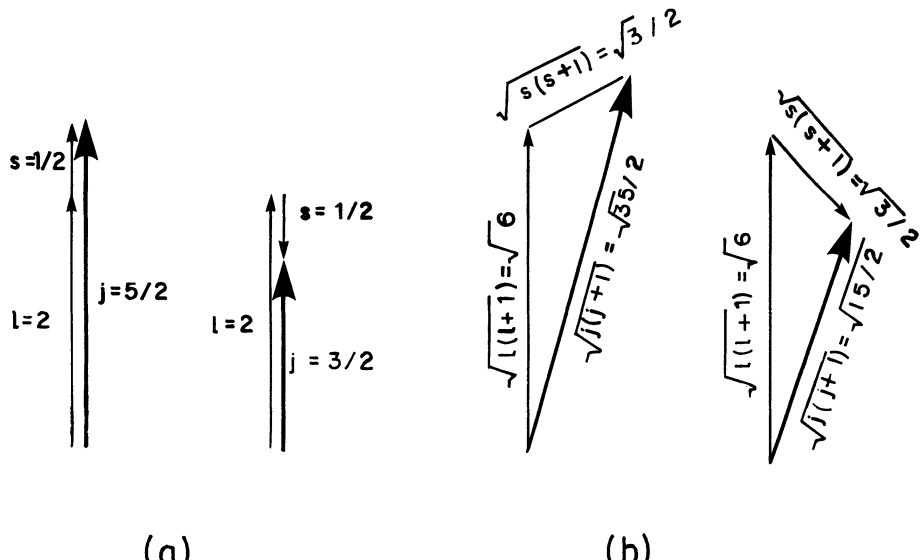


Fig. 10.6 (a) Vector addition of the components of angular momentum l and s to form the total angular momentum j according to the semi-classical vector model of the atom. (b) Vector addition of the components of angular momentum l and s to form the total angular momentum j .

momentum needs a correction from wave mechanics because $\mathbf{p}_{\text{tot}} \neq (h/2\pi)\mathbf{j}$, but is in fact given by $\mathbf{p}_{\text{tot}} = (h/2\pi)\sqrt{[j(j+1)]}$. This has been shown for example by Sherwin [4].

10.2.7 Wave mechanical corrections to angular momentum of electrons

Why is the angular momentum of an electron not simply the quantum number multiplied by $(h/2\pi)$, as expected on the ‘old quantum theory’?

We may now consider very briefly the quantum theory of angular momentum. This will be needed to provide the expectation value of the angular momentum $\hat{\mathbf{p}}_0 = h/2\pi\sqrt{l(l+1)}$ for the following discussion of the quantum theories of ferro-

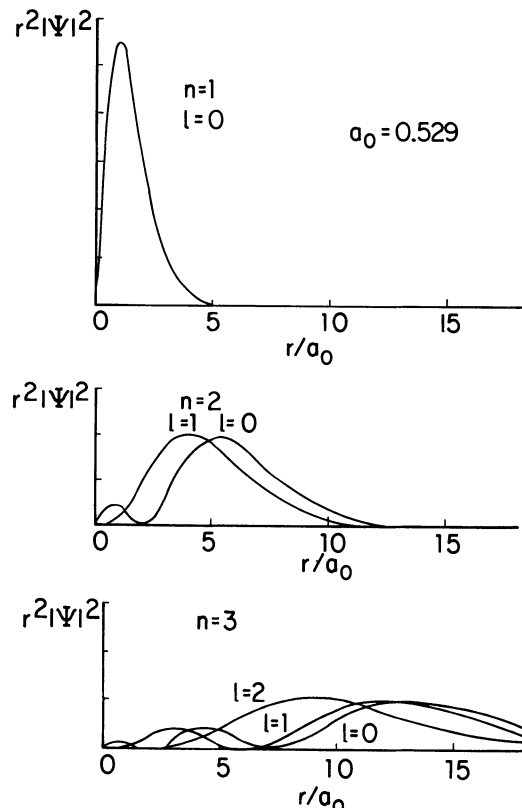


Fig. 10.7 Probability functions $\psi^*\psi$ for an electron as a function of radial distance from the nucleus in a simple atom such as hydrogen.

magnetism and paramagnetism. The treatment given here is abbreviated and only intended to be a guide to the derivation.

Consider a very simple case of a single electron orbiting an ionic core. We are interested only in the angular momentum of this one electron. We could approximate the situation with the wave function of the single electron in a hydrogen atom. In this case the wave function can be represented by the expression

$$\Psi(r, \theta, \phi) = R(r)\Theta(\theta)\Phi(\phi)$$

always assuming that the dependences on r , θ and ϕ are independent of each other and hence can be separated. The solutions of the Schroedinger equation in this case are shown in Figs. 10.7 and 10.8. These show the possible electron states.

If $\langle p_0^2 \rangle$ is the operator for the orbital angular momentum squared, and $\overline{p_0^2}$ is the expectation value of the same quantity, then $\langle p_0^2 \rangle \Psi(r, \theta, \phi) = p_0^2 \Psi(r, \theta, \phi)$. Replacing $\langle p_0^2 \rangle$ by $(h/2\pi)^2 \langle l^2 \rangle$ and $\overline{p_0^2}$ by $(h/2\pi)^2 l^2$ gives

$$-\left[\frac{1}{\sin^2 \theta} \frac{d^2}{d\phi^2} + \frac{1}{\sin \theta} \frac{d}{d\theta} \left(\sin \theta \frac{d}{d\theta} \right) \right] \Psi(r, \theta, \phi) = \overline{l^2} \Psi(r, \theta, \phi)$$

where the first term on the left-hand side is the expression for $\langle l^2 \rangle$. If we suppose

$$\begin{aligned} \Phi(\phi) &= \exp(im\phi) \\ \frac{d^2\Phi(\phi)}{d\phi^2} &= -m^2 \exp(im\phi) \end{aligned}$$

where m is an integer, the operator for $\langle l^2 \rangle$ is modified, and separating the terms in the wave function, the previous equation becomes

$$\left[\frac{-m^2}{\sin^2 \theta} \frac{d^2}{d\phi^2} + \frac{1}{\sin \theta} \frac{d}{d\theta} \left(\sin \theta \frac{d}{d\theta} \right) \right] \Theta(\theta) = \overline{l^2} \Theta(\theta)$$

It can be shown by a rather lengthy proof that this equation only has well behaved solutions when $\overline{l^2} = l(l+1)$ for $l = 0, 1, 2, 3, \dots$. The expected values of the angular momentum are therefore

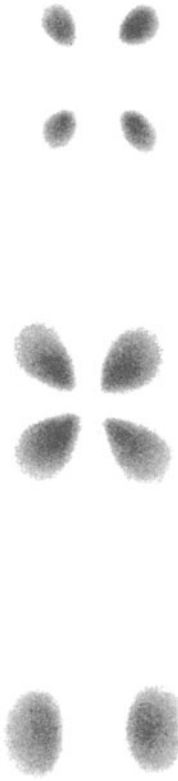
$$\overline{p_0} = \left(\frac{h}{2\pi} \right) \overline{l} = \left(\frac{h}{2\pi} \right) \sqrt{l(l+1)}$$

The result of this is that an electron with orbital angular momentum quantum number l will have an angular momentum of $(h/2\pi) \sqrt{l(l+1)}$ and not $(h/2\pi)l$ as might have been expected on the basis of the old quantum theory.

The same argument holds for the spin angular momentum $(h/2\pi) \sqrt{[(s(s+1)]}$ and the total angular momentum $(h/2\pi) \sqrt{[j(j+1)]}$. The vector addition of these quantities is then shown in Fig. 10.6(b).



$m_l = 0$ $m_l = \pm 1$ $m_l = \pm 2$ $m_l = \pm 3$



$m_l = 0$ $m_l = \pm 1$ $m_l = \pm 2$

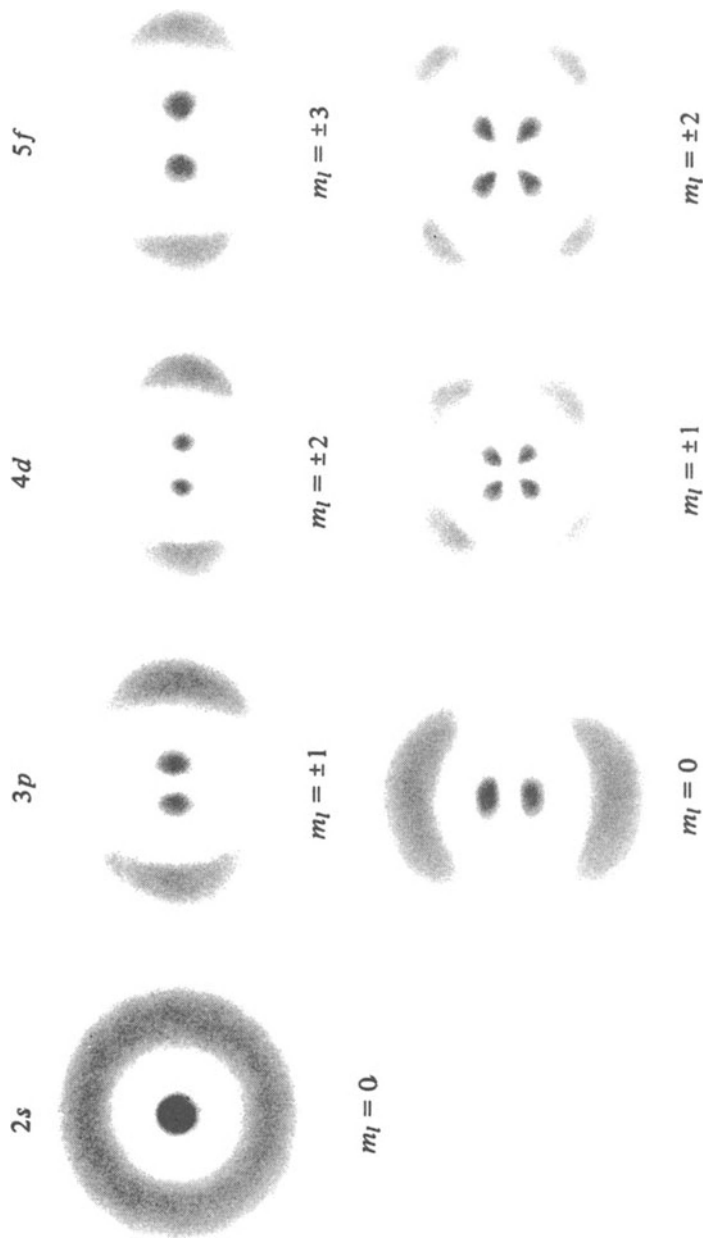


Fig. 10.8 Probability density functions in real space for various electronic levels in hydrogen.

10.2.8 The normal Zeeman effect

What effect does a magnetic field have on the energy levels of electrons within atoms?

The energy levels of electrons within the atom are altered by the presence of a magnetic field. This is shown in the optical spectra for example, where the emissions from the atoms in the form of light quanta are the result of electrons moving to lower energy levels. These spectra are altered by the presence of a magnetic field as shown in the Zeeman effect [5, 6].

The normal Zeeman effect is exhibited by atoms in which the net spin angular momentum is zero. A spectral line of frequency v_0 in zero field is split into two lines displaced symmetrically about the original zero-field line at frequencies of $v_0 + \Delta v$ and $v_0 - \Delta v$. The displacement in frequency Δv is proportional to the magnetic field strength. When viewed perpendicular to the field direction all three lines are observed, but when viewed along the direction of the field only the two displaced spectral lines are observed.

The normal Zeeman effect occurs in calcium (the singlet at $\lambda = 422.7\text{ nm}$), magnesium and cadmium (the singlet at $\lambda = 643.8\text{ nm}$), for example. The displacement in energy is $0.93 \times 10^{-23}\text{ J}$ or $0.58 \times 10^{-4}\text{ eV}$ in magnetic inductions of 1 T , corresponding in the optical region to a shift in wavelength of typically 0.01 nm .

Under the action of a magnetic field the allowed changes in the electron energy levels $\Delta E_H = E_0 \pm E_H$ are quantized and are given by

$$\Delta E_H = -\mu_0 \Delta m H,$$

where Δm is the difference in the component of magnetic moment along the field direction. This can take only the values given by $m_l (eh/4\pi m_e)$ where $m_l = -l, -l+1, -l+2, 0, l-1, l$

$$\Delta E_H = m_l \left(\frac{eh}{4\pi m_e} \right) \mu_0 H.$$

Therefore a P state, which has $l = 1$ splits into three levels, $m_l = -1, 0, +1$, while a D state which has $l = 2$ splits into five levels, $m_l = -2, -1, 0, 1, 2$.

There is also a selection rule which governs allowable transitions between states with different values of m_l [7]. This rule, which is found empirically states that an electron undergoing a transition from different energy levels can not change its magnetic quantum number by more than 1. This rule ensures that there are no more than three available transition energies in the normal Zeeman effect.

$$\Delta m_l = 0 \text{ or } \pm 1.$$

The shift in energy of the spectral lines is

$$hv - hv_0 = \left(\frac{eh}{4\pi m_e} \right) \mu_0 H.$$

By measuring the change in frequency the ratio of charge to mass of an electron can be found from

$$\nu - \nu_0 = \left(\frac{e}{4\pi m_e} \right) \mu_0 H.$$

Experimental measurements of the change in frequency yield the value

$$e/m_e = 1.7587 \times 10^{11} \text{ C/kg.}$$

Notice that the expression for the change in spectral frequency does not depend on Planck's constant. In fact an explanation of the normal Zeeman effect of spectral frequency can be given by classical physics [8].

An example of the splitting of the electron energy levels of the D states ($l = 2$) and the P states ($l = 1$) in cadmium is shown in Fig. 10.9. In the absence of a net spin the P levels have three states corresponding to $m_l = 1, 0, -1$ which are degenerate in zero field. The D levels have five states. Once a magnetic field is applied the degeneracy is lifted, and on application of the selection rule this results in three allowed transition energies. The shift in spectral lines is also shown in Fig. 10.9.

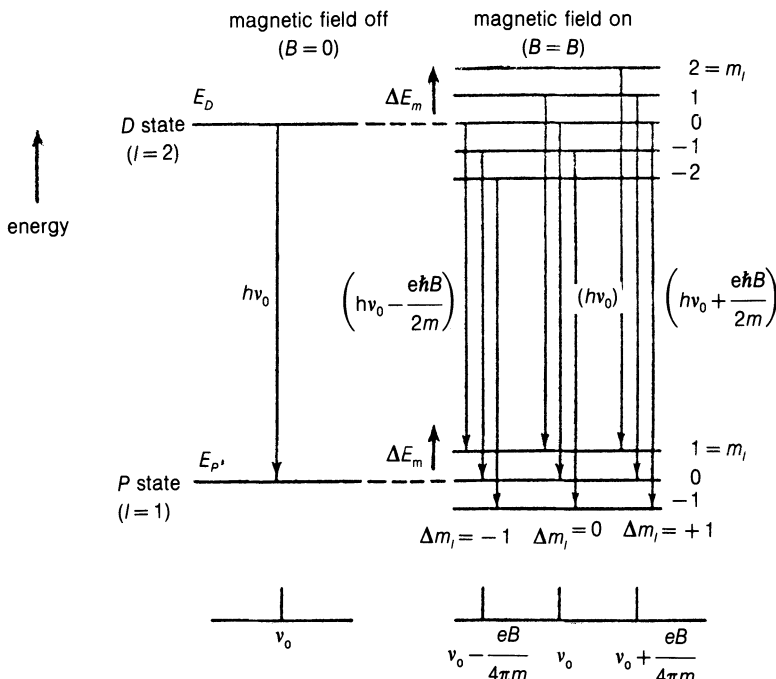


Fig. 10.9 Splitting of the electronic D and P states in the normal Zeeman effect.

234 Electronic magnetic moments

We should note that the quantization of the various states with $m_l = -l, \dots, 0, \dots, +l$ remains even when the field is removed (that is, it is not the field which induces the quantization), but in zero field the various states are degenerate (i.e. have the same energy) and therefore they all contribute to the same spectral line. All electronic transitions for which $\Delta l = \pm 1$ lead to the same Zeeman effect, that is the splitting of one spectral line into three.

10.2.9 The anomalous Zeeman effect

Why do most atoms not exhibit the simple ‘normal’ Zeeman effect?

The spectra of most atoms do not show the simple normal Zeeman effect. In these cases the spectral lines split into more than three levels described above. The resulting behaviour is called the anomalous Zeeman effect, even though it occurs more often than the ‘normal’ Zeeman effect.

These spectra cannot be accounted for on the basis of quantization of the orbital angular momentum alone under the action of a magnetic field, and therefore it is necessary to look for further explanations. In order to account for the anomalous Zeeman effect Goudsmit and Uhlenbeck [9] suggested that the electrons have a spin angular momentum which leads to a magnetic moment associated with the spin.

The spectra of most atoms exhibit fine structure even in the absence of a magnetic field and hence the name anomalous Zeeman effect since it does not need a magnetic field to cause splitting of the energy states. When such zero-field fine structure is present it is indicative that the element will exhibit the anomalous Zeeman effect under the action of a field also. The energy splitting between states with spin up and spin down in the presence of a magnetic field \mathbf{H} is

$$\Delta E_s = 2s \left(\frac{e\hbar}{4\pi m_e} \right) \mu_0 \mathbf{H}$$

using $\mu_B = e\hbar/4\pi m_e$

$$\Delta E_s = 2s \mu_B \mu_0 \mathbf{H}$$

and $\mathbf{m}_s = 2s \mu_B$

$$\Delta E_s = \mu_0 \mathbf{m}_s \cdot \mathbf{H}.$$

Therefore since any energy state can be occupied by electrons in degenerate spin-up spin-down states it will be split into two, that is it has the degeneracy lifted, by a magnetic field.

A well-known example of the anomalous Zeeman effect occurs in the sodium

spectrum. The zero-field transitions can be resolved into a doublet with wavelengths 589.0 nm and 589.6 nm. Each of these lines itself exhibits fine structure and can be resolved further into two or three lines. The doublet is due to the $3P - 3S$ transition as shown in Fig. 10.10. Application of a magnetic field splits the P states into four new levels (compare with P level splitting into two new levels in Fig. 10.9) and the S state into two new levels compared with none in the normal Zeeman effect.

The diagram of Fig. 10.10 is kept relatively simple because the P state ($l = 1$) is split by the normal Zeeman into only two levels which are each further split into two by the spin. If we had looked at a D state ($l = 2$) for example there would have been a total of ten levels in an applied field, five as a result of the normal Zeeman splitting ($m_l = 2, 1, 0, -1, -2$) each of which are further split into two by the spin splitting ($m_s = +\frac{1}{2}$ or $-\frac{1}{2}$).

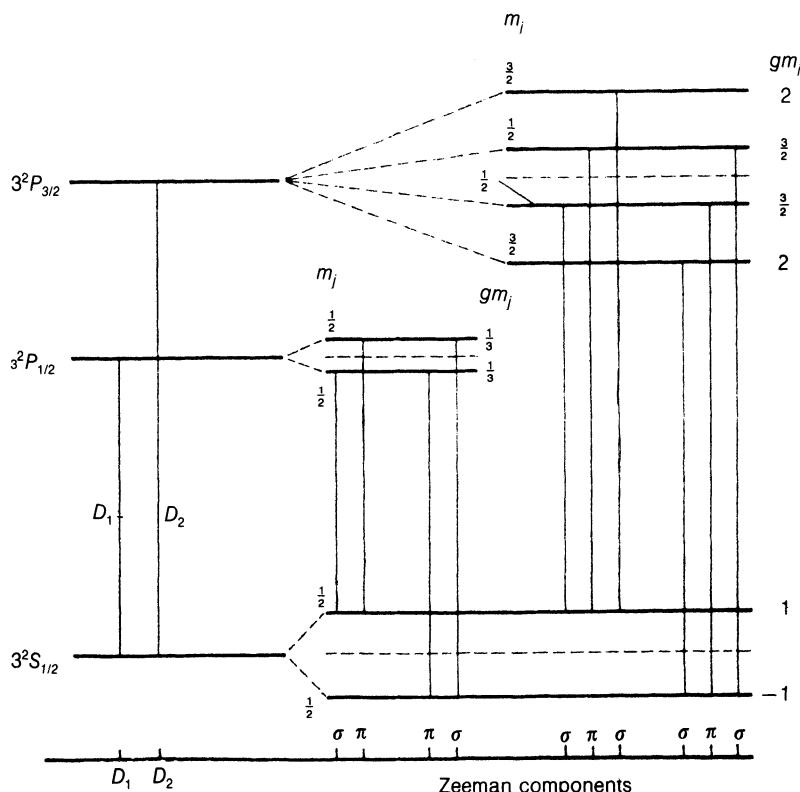


Fig. 10.10 Splitting of the electronic D and P states in the anomalous Zeeman effect.

10.2.10 The Stern–Gerlach experiment

How do we know that the electronic angular momentum is quantized?

In zero field of course all of the values of m_l represent degenerate energy levels, although the quantization is still present. In the presence of a field the component of angular momentum along the field direction is determined by Larmor precession of the angular momentum as shown in Fig. 10.3. The total orbital angular momentum remains the same for each of these electrons but by precessing at an angle to the field direction the component perpendicular to the field direction averages to zero. The quantization of the component of the angular momentum, or magnetic moment, along the direction of a magnetic field represented by the magnetic quantum numbers was first confirmed by the experiment of Stern and Gerlach [10].

Stern and Gerlach tested the space quantization of the angular momentum using atoms of silver in which $J = S = \frac{1}{2}$. The only contribution to the magnetic moment comes from the spin of a single electron which according to theory should be quantized with value $+\frac{1}{2}$ or $-\frac{1}{2}$ along the field direction. The arrangement of the experiment is shown in Fig. 10.11. Silver atoms leaving an oven at high speeds, were collimated by slits and passed through an inhomogeneous magnetic field generated by the pole pieces shown. They were stopped by a photographic plate where their final positions were recorded. It was found that the locations of the atoms arriving on the photographic plate were not continuous but instead were in two lines corresponding to silver in the two allowed spin states of $m_s = +\frac{1}{2}$ and $-\frac{1}{2}$.

10.3 MAGNETIC PROPERTIES OF FREE ATOMS

What determines the magnetic moment of an atom?

The magnetic properties of an atom are determined principally by the magnetic moments of its electrons. We have shown in the previous chapter that the magnetic

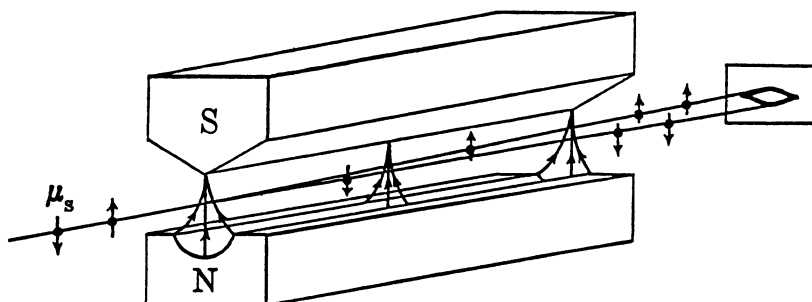


Fig. 10.11 Experimental arrangement in the Stern–Gerlach experiment.

moments of these electrons can be calculated from the sum of orbital and spin angular momentum. The net magnetic moment of a filled electron shell is zero so that only the unfilled shell needs to be considered. This simplifies the problem of calculation greatly.

The angular momentum of the atom can be found by summing vectorially the spin and orbital angular momenta of its electrons. This can be done in two ways, either the values of j for each electron can be found and the vector sum of these calculated to give J . Alternatively the orbital angular momentum L of all the electrons can be found by vector sum and the spin angular momentum S of all the electrons can be found. L and S can then be added vectorially to provide the J for the atom. These two methods do not give identical answers.

10.3.1 Magnetic moment of a closed shell of electrons

Does a closed shell of electrons have any net magnetic moment?

The total J , orbital L and spin S angular momenta of a closed shell of electrons are always zero. This result enables us to simplify calculations of the net magnetic moment of an atom by considering only the contributions due to the partially filled shells.

Example 10.1. To demonstrate that a closed shell of electrons has zero angular momentum consider the Zn^{2+} ion which has ten electrons in its 3d shell. For the 3d series $l = 2$, the electron configuration is

m_1	2	1	0	-1	-2	2	1	0	-1	-2
m_s	$\frac{1}{2}$	$\frac{1}{2}$	$\frac{1}{2}$	$\frac{1}{2}$	$\frac{1}{2}$	$-\frac{1}{2}$	$-\frac{1}{2}$	$-\frac{1}{2}$	$-\frac{1}{2}$	$-\frac{1}{2}$
s	↑	↑	↑	↑	↑	↓	↓	↓	↓	↓

Consequently $L = \sum m_1 = 0$ and $S = \sum m_s = 0$.

10.3.2 Atomic magnetic moment

How can we calculate the magnetic moment of an atom from a knowledge of its electron structure?

We can find the magnetic moment of an atom from its total angular momentum. The vector model of the atom is a simple semi-classical model which allows us to calculate the total angular momentum J from the orbital and spin angular momenta of the electrons belonging to an atom. The model is semi-classical because although the sum $J = L + S$ is made in the classical vector manner the actual values of L and S are calculated from quantum mechanics.

238 Electronic magnetic moments

Corrections are made to the model as a result of quantum mechanics in order to find the magnitude of the vectors $|\mathbf{L}|$, $|\mathbf{S}|$ and $|\mathbf{J}|$ in terms of the quantum numbers L , S and J . Fortunately the correction is very simple and is the same as the correction needed for individual electrons as discussed in the previous chapter.

We should mention that there is a very small contribution to the total angular momentum of the atom from the nucleus due to nuclear spin. This contribution is about 10^{-3} of the spin of an electron. The nuclear magnetic moment is measured in units of nuclear magnetons, denoted μ_N . The value of μ_N is $5.05 \times 10^{-27} \text{ A m}^2$, compared with $9.27 \times 10^{-24} \text{ A m}^2$ for the Bohr magneton.

10.3.3 Atomic orbital angular momentum L

How does the atomic orbital angular momentum depend on the electronic angular momenta?

The atomic orbital angular momentum, denoted by the quantum number L , is the vector sum of the orbital angular momenta of the electrons within the atom.

$$\mathbf{L} = \sum \mathbf{l}_i.$$

An example of the vector summation for an atom with two electrons in its unfilled shell with quantum numbers $l = 1$ and $l = 2$ is shown in Fig. 10.12.

The magnitude of the orbital angular momentum vector $|\mathbf{L}|$ in terms of the orbital angular momentum quantum number L is

$$|\mathbf{L}| = \sqrt{[L(L + 1)]}$$

which is identical in form to the relation between $|\mathbf{l}|$ and the orbital angular momentum quantum number l of a single electron.

10.3.4 Atomic spin angular momentum S

How does the atomic spin depend on the electron spins?

The spin angular momentum \mathbf{S} for an atom can be found in a similar way using the vector model. It is the vector sum of the spin angular momenta of the electrons.

$$\mathbf{S} = \sum \mathbf{s}_i.$$

The summation process is indicated in Fig. 10.13(a) for an atom with three electrons in its unfilled shell and in Fig. 10.13(b) for an atom with four electrons in its unfilled shell.

The magnitude of the spin angular momentum vector $|\mathbf{S}|$ in terms of the spin

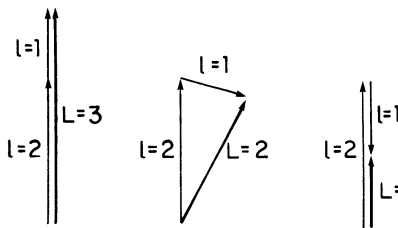


Fig. 10.12 Vector addition of the orbital angular momentum in a two-electron system.

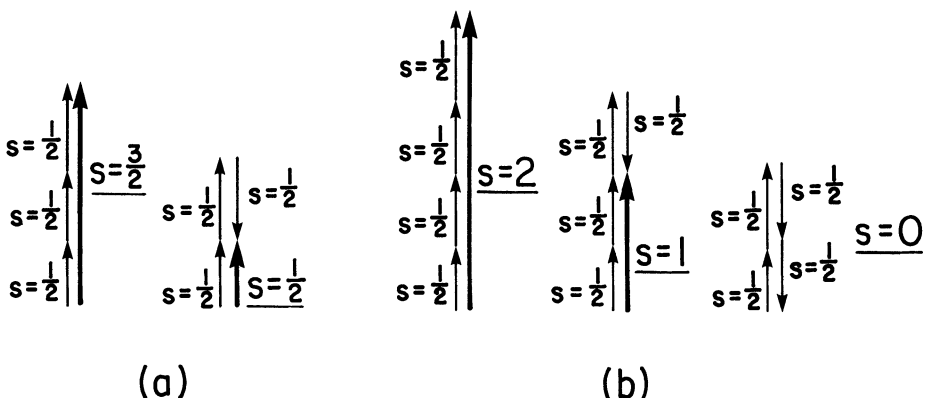


Fig. 10.13 Vector addition of electron spins for: (a) a three-electron system; and (b) a four-electron system.

quantum number S is according to quantum mechanics,

$$|S| = \sqrt{[S(S + 1)]}$$

which is again identical to the relation for a single electron.

10.3.5 Hund's rules: occupancy of available electron states

How do electrons decide which values of s and l to take?

There is a set of empirical rules which determine the occupancy of the available electronic states within an atom. These rules identify how the possible electronic states are filled and can be used therefore to calculate L , S and J for an atom from the electron configuration in its unfilled shell.

The Hund rules [11] can be applied to electrons in a particular shell to determine the ground state of the atom. The three rules apply to the atomic spin S , the atomic

240 Electronic magnetic moments

orbital angular momentum L and the atomic angular momentum J respectively. Electrons occupy available states as follows:

- such that the maximum total atomic spin $S = \sum m_s$ is obtained without violating the Pauli exclusion principle;
- such that the maximum value of total atomic orbital angular momentum $L = \sum m_l$ is obtained, while remaining consistent with the given value of S ; and
- the total atomic angular momentum J is equal to $|L - S|$ when the shell is less than half full, and is equal to $|L + S|$ when the shell is more than half full. When the shell is exactly half full $L = 0$ so that $J = S$.

This means that the electrons will occupy states with all spins parallel within a shell as far as is possible. They will also start by occupying the state with the largest orbital angular momentum followed by the state with the next largest orbital angular momentum, and so on.

The next two examples show how Hund's rules are applied in specific cases to calculate L , S and J .

Example 10.2. The Sm^{3+} ion which has 5 electrons in its 4f shell ($n = 4, l = 3$), must have the electrons arranged with the following configuration.

m_l	3	2	1	0	-1	-2	-3
m_s	$\frac{1}{2}$						
occupancy	s	\uparrow	\uparrow	\uparrow	\uparrow	\uparrow	

This gives $S = \sum m_s = \frac{5}{2}$ and $L = \sum m_l = 5$. The shell is less than half full so that $J = L - S = \frac{5}{2}$.

10.3.6 Total atomic angular momentum J

How is the total atomic angular momentum related to the spin and orbit components?

The coupling between the orbital angular momentum of the atom L and the spin angular momentum S gives the total atomic angular momentum J . This summation can be obtained in two ways, by independently summing the orbital and spin moments of the unpaired electrons

$$\mathbf{J} = \sum \mathbf{l}_i + \sum \mathbf{s}_i.$$

This form of coupling is known as Russell-Saunders coupling [12]. In this case the l vectors of individual electrons are coupled together ($l-l$) and the vectors are coupled together ($s-s$). These couplings are stronger than the coupling between the resultant L and S vectors.

Another method of obtaining \mathbf{J} is by summing the total angular momenta of the electrons, which are obtained for each electron individually by summing l and s

first

$$J = \sum j_i = \sum (l_i + s_i).$$

This is the so called $j-j$ coupling. This type of coupling occurs if there is a strong spin orbit coupling ($l-s$) for each electron. Then the coupling between l and s for a particular electron is stronger than the coupling between l and l for separate individual electrons.

In these calculations the vectors which are strongly coupled together must always be added first. In practice the most common form of coupling is the first kind. Russell-Saunders (or $l-s$) coupling is the most appropriate form of coupling to consider for magnetism.

10.3.7 Russell-Saunders coupling

How do the spin and orbital angular momenta combine to form the total angular momentum of an atom?

Russell-Saunders coupling, in which the spin-spin and orbit-orbit couplings are strongest applies in most cases. It occurs in all of the light elements and situations in which the multiplet splitting is small compared with the energy difference of levels having the same electron structure but different values of L .

In this coupling it is assumed that when several electrons are present in an unfilled shell the orbital angular momenta are so strongly coupled with each other that states with a different total L have a different energy. Similarly it is assumed that states with a different total S have a significant difference in energy. The resultant vectors L and S are then less strongly coupled with one another.

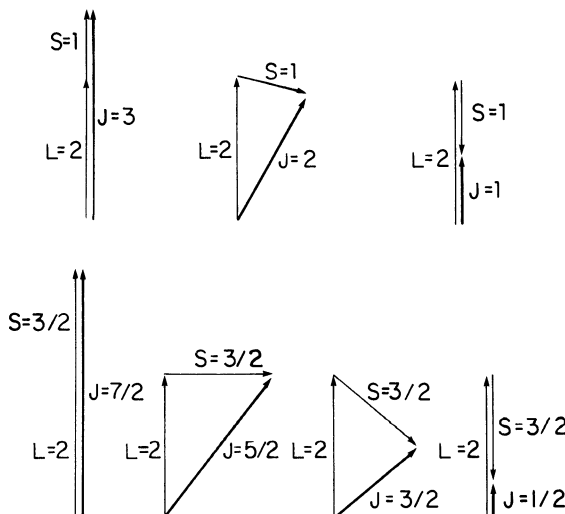


Fig. 10.14 Vector addition of atomic orbital angular momentum L and atomic spin angular momentum S to give the total atomic angular momentum J .

In Russell–Saunders coupling the orbital momentum vectors combine to form a total orbital angular momentum L while the spin momentum vectors combine independently to form a total spin momentum vector S . This means that the calculated S is not affected by the value of L .

This leads to a total angular momentum J of the atom which is simply the vector sum of the two non-interacting momenta L and S .

$$\mathbf{J} = \mathbf{L} + \mathbf{S}$$

as shown in Fig. 10.14. There are certain restrictions on this however. J must be an integer if S is an integer, and J must be a half integer if S is half integral. Russell–Saunders coupling applies to iron and the rare earth atoms.

10.3.8 The j - j coupling

Are there other ways of coupling to form the total angular momentum of an atom?

The alternative form of coupling, spin–orbit coupling, in which the orbital and spin angular momenta are dependent on each other is called j - j coupling. This form of coupling is more applicable to very heavy atoms. It assumes there is a strong spin–orbit ($l-s$) coupling for each electron and that this coupling is stronger than the $l-l$ or $s-s$ coupling between electrons. Since the strongly coupled vectors are summed first these give a resultant j for each electron. The j vectors are then summed to obtain J for the whole atom.

10.3.9 Quenching of the orbital angular momentum

Why do the magnetic moments of the 3d series elements imply that $\mathbf{L} = 0$ in all cases?

In the 3d series of elements it has been found experimentally that $\mathbf{J} = \mathbf{S}$ as shown in Table 10.1. This implies that $\mathbf{L} = 0$ throughout the 3d series, which is a surprising result if we only consider the properties of electrons in isolated atoms. In these cases we speak of the orbital angular momentum being ‘quenched’. The phenomenon has been discussed by Morrish [13] and Kittel [14]. Here we shall merely note that under certain circumstances the plane of the orbit can move about and this can average to zero over the whole atom. This results in a net zero value of L . Notice from Table 10.2 that this does not occur in the 4f series which is the other principal group of magnetic materials.

Example 10.3. The Fe^{2+} ion has 6 electrons in its 3d shell. Since $l = 2$ for this series the electron configuration is

m_1	2	1	0	-1	-2	2	1	0	-1	-2
m_s	$\frac{1}{2}$	$-\frac{1}{2}$	$-\frac{1}{2}$	$-\frac{1}{2}$						
occupancy	s	↑	↑	↑	↑	↑	↓			

Table 10.1 Magnetic moments of isolated ions of the 3d transition metal series

Ion	Configuration	Calculated moment		Measured moment
		$9\sqrt{[J(J+1)]}$	$2\sqrt{[S(S+1)]}$	
Ti ³⁺ , V ⁴⁺	3d ¹	1.55	1.73	1.8
V ³⁺	3d ²	1.63	2.83	2.8
Cr ³⁺ , V ³⁺	3d ³	0.77	3.87	3.8
Mn ³⁺ , Cr ³⁺	3d ⁴	0	4.90	4.9
Fe ³⁺ , Mn ²⁺	3d ⁵	5.92	5.92	5.9
Fe ²⁺	3d ⁶	6.70	4.90	5.4
Co ²⁺	3d ⁷	6.63	3.87	4.8
Ni ²⁺	3d ⁸	5.59	2.83	3.2
Cu ²⁺	3d ⁹	3.55	1.73	1.9

Table 10.2 Magnetic moments of isolated ions of the 4f transition metal series

Ion	Configuration	Calculated moment		Measured moment
		$g\sqrt{[J(J+1)]}$		
Ce ³⁺	4f ¹ 5s ² p ⁶	2.54		2.4
Pr ³⁺	4f ² 5s ² p ⁶	3.58		3.5
Nd ³⁺	4f ³ 5s ² p ⁶	3.62		3.5
Pm ³⁺	4f ⁴ 5s ² p ⁶	2.68		—
Sm ³⁺	4f ⁵ 5s ² p ⁶	0.84		1.5
Eu ³⁺	4f ⁶ 5s ² p ⁶	0		3.4
Gd ³⁺	4f ⁷ 5s ² p ⁶	7.94		8.0
Tb ³⁺	4f ⁸ 5s ² p ⁶	9.72		9.5
Dy ³⁺	4f ⁹ 5s ² p ⁶	10.63		10.6
Ho ³⁺	4f ¹⁰ 5s ² p ⁶	10.60		10.4
Er ³⁺	4f ¹¹ 5s ² p ⁶	9.59		9.5
Tm ³⁺	4f ¹² 5s ² p ⁶	7.57		7.3
Yb ³⁺	4f ¹³ 5s ² p ⁶	4.54		4.5

This leads to $S = 2$ and $L = 2$. Since the orbital angular momentum is quenched in these elements $J = S$ and therefore the total magnetic moment is

$$\mathbf{m} = 2\mu_B \sqrt{[S(S+1)]}$$

which corresponds to 4.90 Bohr magnetons for the isolated Fe²⁺ atom. This agrees reasonably well with the observed value of 5.36 Bohr magnetons. The expected value without quenching of the orbital angular momentum is 6.7 Bohr magnetons which is clearly in serious error.

We should note that these calculations apply only to the isolated paramagnetic (i.e. non-interacting) atoms or ions. When a large number of atoms are brought together in a solid the electron energy levels are drastically altered and the

244 Electronic magnetic moments

magnetic moment per atom is in most cases significantly different from the values calculated above.

10.3.10 Electronic behaviour in strong magnetic fields

Is the coupling between the spin and orbital angular momenta different in a strong magnetic field?

As the magnetic field is increased and the field splitting becomes greater than the multiplet splitting the anomalous Zeeman effect changes over to a normal Zeeman effect. The reason for this is that the precessional velocity of J about the field axis becomes greater than the precession of the S and L vectors about J . Therefore this is described better as independent precessions of S and L about the field direction, that is the L - S coupling breaks down. We speak of L and S being decoupled by the magnetic field. This transition is known as the Paschen–Back effect [15] and only occurs in high magnetic fields.

REFERENCES

1. Bohr, N. (1913) *Phil. Mag.*, **26**, 1.
2. Sommerfeld, A. (1916) *Annln. Physik.* **51**(1), 125.
3. Larmor, J. (1897) *Phil. Mag.*, **44**, 503.
4. Sherwin, C. W. (1959) *Introduction to Quantum Mechanics*, Holt, Rinehart and Winston, New York.
5. Zeeman, P. (1897) *Phil. Mag.*, **43**, 226.
6. Hertzberg, G. (1937) *Atomic Spectra and Atomic Structure*, Prentice-Hall, New York.
7. Weidner, R. and Sells, R. L. (1968) *Elementary Modern Physics*, 2nd edn, Allyn and Bacon, Boston.
8. Lorentz, H. A. (1897) *Kon. Ak. van Wetenscheppen*, **6**, 193; (1898) *Ecl. Electr.*, **14**, 311.
9. Goudsmit, S. and Uhlenbeck, G. E. (1926) *Nature*, **117**, 264.
10. Gerlach, W. and Stern, O. (1924) *Ann. Physik.*, **74**, 673.
11. Hund, F. (1927) *Linienspektren und Periodische System der Elemente*, Springer, Berlin. (*Trans. Line Spectra and Periodicity of the Elements*)
12. Russell, H. N. and Saunders, F. A. (1925) *Astrophys. J.*, **61**, 38.
13. Morrish, A. H. (1965) *The Physical Principles of Magnetism*, Wiley, New York.
14. Kittel, C. (1986) *Introduction to Solid State Physics*, 6th edn, Wiley, New York.
15. Paschen, F. and Back, E. (1913) *Ann. Physik.*, **40**, 960.

FURTHER READING

- Chikazumi, S. (1964) *Physics of Magnetism*, Wiley, New York, Ch. 3.
Cullity, B. D. (1972) *Introduction to Magnetic Materials*, Addison-Wesley, Reading, Mass, Ch. 3.
Hertzberg, G. (1937) *Atomic Spectra and Atomic Structure*, Prentice Hall, New York.
Semat, H. (1972) *Introduction to Atomic and Nuclear Physics*, Holt, Rinehart and Winston, New York, Ch. 8 and 9.
Sherwin, C. W. (1959). *Introduction to Quantum Mechanics*, Holt, Rinehart and Winston, New York.

Weidner, R. and Sells, R. L. (1968) *Elementary Modern Physics*, 2nd edn, Allyn and Bacon, Boston.

EXAMPLE AND EXERCISES

Example 10.4 Orbital and spin angular momentum of an electron (a) Explain the significance of the four quantum numbers n, l, s and m_l . Describe how to calculate the orbital, spin and total angular momentum of an electron from its quantum numbers using the ‘classical’ vector model of the atom. Why do the values of l_s and j differ from the classically expected results when calculated using quantum mechanics?

(b) Using vector diagrams determine the different values for the total orbital angular momentum of a two-electron system. (i.e. atom) for which $l_1 = 3$ and $l_2 = 2$. What are the possible values for L , for S and for J of the atom?

(c) Find the values of L , S and J for the Co^{2+} ion.

Example 10.5 The Zeeman effect. Calculate the normal Zeeman effect separation in energy levels in cadmium when subjected to magnetic field strengths of 1.6×10^6 , 0.4×10^6 and $0.064 \times 10^6 \text{ A/m}$ (equivalent to a free space magnetic induction of 2.0, 0.5 and 0.1 tesla). The wavelength of the main $6^1\text{D}_2 - 5^1\text{P}_1$ transition is $\lambda = 643.8 \text{ nm}$, which is a spectral line at the red end of the visible spectrum. Calculate the shift in wavelength.

Example 10.5 The Zeeman Effect. Calculate the normal Zeeman effect separation in energy levels in cadmium when subjected to magnetic field strengths of (equivalent to a free space magnetic induction of 0.1, 0.5 and 2.0 tesla). The wavelength of the main $6^1\text{D}_2 - 5^1\text{P}_1$ transition is $\lambda = 643.8 \text{ nm}$, which is a spectral line at the red of the visible spectrum. Calculate the shift in wavelength.

Draw an energy level diagram showing the 6^1D_2 and 5^1P_1 states before and after application of a magnetic field and explain why the original singlet is split only into a triplet and not into a larger number of spectral lines.

Example 10.6 Determination of atomic angular momentum. Using vector diagrams determine the possible values of J for an atom with

- (a) $L = 2, S = 3$
- (b) $L = 3, S = 2$
- (c) $L = 3, S = 5/2$
- (d) $L = 2, S = 5/2$

What are the values of L , S and J for the ground state of the paramagnetic carbon atom?

11

Quantum Theory of Magnetism

In the previous chapter we discussed the origin of the atomic magnetic moment. In this chapter we look at how these magnetic moments interact to give cooperative magnetic phenomena such as ferromagnetism and paramagnetism in solids. We then consider theories of magnetism based on two mutually exclusive models: the localized moment model and the band or itinerant electron model. The localized model works well for the rare earth metals, while the itinerant electron model describes the magnetic properties of the 3d transition metals and their alloys quite well.

11.1 ELECTRON–ELECTRON INTERACTIONS

The exchange interaction is obviously crucial to an understanding of ordered magnetic states, but where does it come from?

We have seen that the behaviour of the susceptibility of many ferromagnets above their Curie temperature follows a Curie–Weiss law and that this implies the existence of an internal field which has been called the Weiss molecular field, or more accurately the atomic field. The field originates from quantum mechanical interactions. A discussion of these together with a derivation of the exchange interaction from considering overlap of the electron wave functions has been given in detail by Martin [1].

11.1.1 Wavefunctions of a two-electron system

How do we form the wavefunction for a system consisting of two electrons?

The wave function of two electrons can be represented as $\Psi(r_1, r_2)$ where r_1 is the coordinate of the first electron and r_2 is the coordinate of the second electron. Then we may consider possible representations of this wave function using linear combinations of the separate wave functions of the individual electrons $\psi(r_1)$ and $\psi(r_2)$.

There are four possibilities

$$\Psi(r_1, r_2) = \psi_a(r_1)\psi_b(r_2)$$

$$\Psi(r_1, r_2) = \psi_a(r_2)\psi_b(r_1)$$

$$\Psi(r_1, r_2) = \psi_a(r_1)\psi_b(r_2) + \psi_a(r_2)\psi_b(r_1)$$

$$\Psi(r_1, r_2) = \psi_a(r_1)\psi_b(r_2) - \psi_a(r_2)\psi_b(r_1),$$

where $\psi_a(r_1)$ represents the wave function of electron 1 on atom a, and $\psi_b(r_2)$ represents the wave function of electron 2 on atom b and so on. We need a solution such that the ‘observed’ properties $\Psi^*\Psi$ are unaltered by interchanging electrons, while the electrons remain distinct, that is $\Psi(r_1, r_2)$ must be antisymmetric. This is an important point; if the wave function is symmetric and $\Psi^*\Psi$ is identical then the wavefunctions of the two electrons are identical and hence they have the same four quantum numbers, which is not allowed.

In both cases 1 and 2 above the interchange of electrons, r_1 for r_2 alters the value of $\Psi^*\Psi$ and hence alters the electron distribution at all points. Therefore these cannot be solutions of the wave function. Another possibility is

$$\Psi(r_1, r_2) = \psi_a(r_1)\psi_b(r_2) + \psi_a(r_2)\psi_b(r_1).$$

In this case the function remains symmetric after interchanging the electrons and $\Psi^*\Psi$ is also unaltered. However according to the Pauli exclusion principle the probability of finding both electrons in an identical state (that is with the same set of quantum numbers) is zero.

If the wavefunctions of the separate electrons are otherwise identical the Pauli principle can only be satisfied among this group of candidate wave functions by

$$\Psi(r_1, r_2) = \psi_a(r_1)\psi_b(r_2) - \psi_a(r_2)\psi_b(r_1).$$

See for example Fig. 11.1.

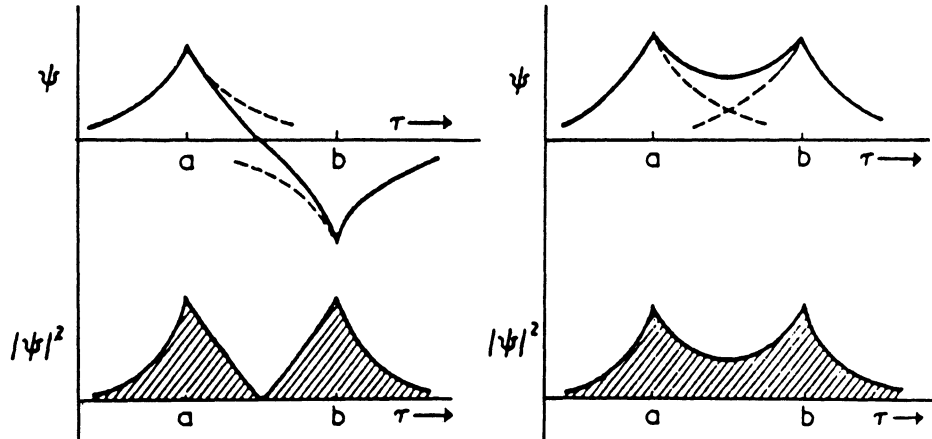


Fig. 11.1 Wave function for a two-electron system using a linear combination of atomic orbitals as in the Heitler–London approximation [2], ψ is antisymmetric, while $\psi^*\psi$ is symmetric.

11.1.2 Heitler-London approximation

What is the total energy of two interacting electrons according to quantum theory? Do we find a result that is just a modification of classical theory or something radically different?

The Heitler-London approximation [2] is merely a method of obtaining the orbital wave function of two electrons by assuming that it can be approximated by a linear combination of the atomic orbital wave functions of two electrons localized on the two atomic sites.

Consider the orbital functions and in particular the energy for such a system of two atoms with one electron each. Heitler and London calculated the energy of this system by evaluating the integral

$$E = \int \int \Psi(r_1, r_2) \langle H \rangle \Psi^*(r_1, r_2) d\tau_1 d\tau_2$$

and the Hamiltonian $\langle H \rangle$ must contain the separate Hamiltonians $\langle H_1 \rangle$ and $\langle H_2 \rangle$ for each electron and an interaction Hamiltonian $\langle H_{12} \rangle$

$$\langle H \rangle = \langle H_1 \rangle + \langle H_2 \rangle + \langle H_{12} \rangle.$$

Of course $\langle H_1 \rangle$ contains only the coordinate r_1 and $\langle H_2 \rangle$ contains only the coordinate r_2 .

$$\langle H_1 \rangle \Psi_a(r_1) = E_a \Psi_a(r_1)$$

$$\langle H_2 \rangle \Psi_b(r_2) = E_b \Psi_b(r_2).$$

The solution of the total energy equation leads to

$$\begin{aligned} E = E_a \int \int \Psi^*(r_1) \Psi(r_1) d\tau_1 + E_b \int \int \Psi^*(r_2) \Psi(r_2) d\tau_2 \\ + \frac{1}{(1 \pm \alpha^2)} \int \int \psi_a^*(r_1) \psi_b^*(r_2) \langle H_{12} \rangle \psi_a(r_1) \psi_b(r_2) d\tau_1 d\tau_2 \\ + \frac{1}{(1 \pm \alpha^2)} \int \int \psi_a^*(r_1) \psi_b^*(r_2) \langle H_{12} \rangle \psi_b(r_1) \psi_a(r_2) d\tau_1 d\tau_2. \end{aligned}$$

The last energy term is obtained by exchanging the electrons 1 and 2 between the atoms a and b and so is called the ‘exchange energy’.

11.1.3 Exchange interaction

What is the cause of the extra energy term?

We can write this expression for the energy obtained from evaluating these integrals in the form,

$$E = E_a + E_b + \left[\frac{1}{(1 \pm \alpha^2)} \right] (Q \pm J),$$

250 Quantum theory of magnetism

where $[1/(1 \pm \alpha^2)]$ is a normalizing constant. In this equation we have on the right-hand side the energy of the electrons when they belong to their separate atoms E_a and E_b , plus some additional energy which results from their interactions. Q is the coulomb electrostatic energy. J is an energy which arises from exchange of the electrons, as can be seen from the form of the wave function. We have already encountered this exchange constant in Chapter 6. Here it is italicized to distinguish it from J the atomic angular momentum. It is immediately clear that the existence of the term J depends on the necessity of an antisymmetric wave function above, since if $\Psi(r_1, r_2)$ were symmetric then J would automatically become zero.

11.1.4 Wave function including electron spin

What is the form of the two-electron wavefunction if we include electron spin?

We have shown from the very simple quantum mechanical treatment above that there exists an exchange energy which has no classical analog. It is now necessary to show that the ordering of the electron spins arises from this. Suppose we write the spin wave functions as $\varphi_1(s)$ and $\varphi_2(s)$. Then the spin state for two electrons can be represented, using the same approximation as before, as a linear combination of the individual spin wave functions.

$$\begin{aligned}\varphi(s_1, s_2) &= \varphi_a(s_1)\varphi_b(s_2) - \varphi_a(s_2)\varphi_b(s_1) \\ \varphi(s_1, s_2) &= \varphi_a(s_1)\varphi_b(s_2) + \varphi_a(s_2)\varphi_b(s_1) \\ \varphi(s_1, s_2) &= \varphi_a(s_1)\varphi_b(s_2) \\ \varphi(s_1, s_2) &= \varphi_a(s_2)\varphi_b(s_1).\end{aligned}$$

The total wave function of the two electrons system with spins can then be represented as

$$\Psi_{\text{Tot}} = \Psi(r_1, r_2)\varphi(s_1, s_2)$$

which as we already know must be antisymmetric with respect to interchange of the electrons. So if $\Psi(r_1, r_2)$ is antisymmetric then $\varphi(s_1, s_2)$ must be symmetric, and vice versa, in order to maintain the antisymmetric nature of the total electronic wave function Ψ_{Tot} .

Symmetric and antisymmetric φ 's correspond to parallel and antiparallel spins. Therefore the exchange energy as derived above can be considered as really the interaction between the spins, since it is the spins which maintain the total wave function Ψ_{Tot} antisymmetric. In other words the spin can be used to distinguish between two electrons which are otherwise identical because the spins can be used to satisfy the Pauli principle when the other three quantum numbers of the two electrons are identical. For parallel spins the exchange energy is then simply $[1/(1 \pm \alpha^2)](-J)$. This means that a positive J corresponds to parallel spin alignment, and hence to ferromagnetic ordering. A negative J leads to antiparallel alignment.

11.1.5 Exchange energy in terms of electron spin

Can we separate the exchange energy and make it dependent only on spin?

From the above discussion the exchange energy dictates a lower energy and hence ferromagnetic order when $J > 0$, and antiferromagnetic alignment when $J < 0$. The model has only discussed two localized electrons on neighbouring atoms and so has some obvious limitations when we wish to apply it to a solid. The exchange Hamiltonian can however now be written simply in terms of the spins on two electrons

$$\langle H \rangle = -2J_{ij}\mathbf{s}_i \cdot \mathbf{s}_j$$

which leads to the Heisenberg model of ferromagnetism [3] which was also proposed by Dirac [4].

11.1.6 The Heisenberg model of ferromagnetism

How might the direct exchange energy between two neighbouring electrons account for long-range magnetic order in ferromagnets and antiferromagnets?

The Heisenberg model of ferromagnetism, like the classical Weiss model [5], is another local moment theory which considers the quantum mechanical exchange interaction between two neighbouring electrons with overlapping wave functions. The idea of direct exchange between electrons on neighbouring atoms first occurred in the Heitler-London treatment of electron orbitals. Heisenberg was the first to include the electron spins in the wave function and then apply the same Heitler-London approximation to obtain the total wave function of a two-electron system. The energy integral was evaluated but now including spin and this showed that the relative orientations of the spins of two interacting electrons can be changed only at the expense of changing the spatial distribution of the charge.

If two electron wave functions overlap then the Pauli exclusion principle [6] applies to the region of overlap. Since no two electrons can have the same set of quantum numbers, when the orbital wave function is symmetrical the spins must be antisymmetric and vice versa. This leads immediately to a correlation between the spins on the two electrons, which is all that is needed to cause a magnetically ordered state. The correlation can be expressed in the form of a magnetic field (although strictly it is not of magnetic origin but is rather electrostatic) or as an energy. The interaction energy is proportional to the dot product of the spins.

$$E_{\text{Heis}} = -2J\mathbf{s}_1 \cdot \mathbf{s}_2.$$

Here $J > 0$ gives ferromagnetism and $J < 0$ gives antiferromagnetism.

When considering a solid it is then necessary to sum the exchange over all the electrons which can contribute to this energy so that

$$\langle H \rangle = -2\sum_i \sum_j J_{ij}\mathbf{s}_i \cdot \mathbf{s}_j.$$

252 Quantum theory of magnetism

In many cases we are only interested in nearest-neighbour interactions and this simplifies the Heisenberg Hamiltonian considerably.

$$\langle H \rangle = -2J \sum_{\text{nearest neighbours}} \mathbf{s}_i \cdot \mathbf{s}_j,$$

where it is assumed that the exchange integral J is identical for all nearest-neighbour pairs. The exchange integral J has no classical analogue, so it is difficult to understand it from a classical viewpoint. However a brief consideration of the Pauli principle tells us that two electrons with like spins cannot approach one another closely. This leads to an effective energy which influences the alignment of the moments.

Empirical values of the exchange interaction J for various ferromagnetic metals have been calculated from specific heat measurements and from spin wave considerations. Some of these have been reported by Hofmann *et al.* [7] which indicate that for iron and nickel $J \approx 0.01$ to 0.02 eV and for gadolinium $J \approx 0.0002$ eV.

Wohlfarth [8] had encountered problems with first principles calculation of J , obtaining the wrong sign when using spherical wave functions. Later Stuart and Marshall [9] made detailed calculations of the direct Heisenberg exchange in iron. They obtained a value of 6.8×10^{-3} eV for two neighbouring localized electron interactions, and on this calculation a similar result would be obtained for both cobalt and nickel. This is about a third of the value obtained from experimental measurements. Watson and Freeman [10, 11] refined the calculations of Stuart and Marshall to include additional terms neglected in the earlier work and with improved orbital wave functions. They confirmed that the magnitude of J is in serious error, being much smaller than is required to explain magnetic order in these 3d metals, but furthermore they found that J should be negative.

Finally in the rare earth metals the magnetic 4f electrons which determine the magnetic properties are highly localized so that there is no significant overlap and hence no direct exchange mechanism of the Heisenberg type can occur, although these metals show a range of different magnetic order. Therefore an additional exchange mechanism involving indirect exchange needs to be invoked.

It seems therefore that although the Heisenberg model is a useful concept the interactions between electrons in real solids is not the simple direct Heisenberg exchange.

11.1.7 Exchange interactions between electrons in filled shells

In order to determine the type of magnetic order is it then necessary to find the exchange energy between every electron in one atom and every electron in a neighbouring atom?

It is easy to show on the basis of the Heisenberg model that the exchange energy between electrons in a filled shell of one atom and electrons in a filled shell of a

neighbouring atom is zero.

$$\begin{aligned} E_{\text{ex}} &= -2J \sum \sum \mathbf{s}_i \cdot \mathbf{s}_j \\ &= -2J \sum \mathbf{s}_i \sum \mathbf{s}_j \end{aligned}$$

and in a filled shell $\sum \mathbf{s}_i = 0$. The exchange energy is consequently zero. This is a useful result in that we only need to take into account interactions from electrons in partially filled shells which simplifies the analysis considerably.

11.1.8 The Bethe–Slater curve

Can we make any simple and verifiable predictions of magnetic order in materials based on the quantum theory of exchange interactions?

The magnetic behaviour of the 3d elements chromium, manganese, iron, cobalt and nickel was of interest to the early investigators of the quantum theory of magnetism. Slater [12, 13] published values of the interatomic distances r_{ab} and the radii of the incompletely filled d subshell r_d of some transition elements. It was found that the values of r_{ab}/r_d seemed to correlate with the sign of the exchange interaction. For large values of r_{ab}/r_d the exchange was positive while for small values it was negative.

Bethe [14] made some calculations of the exchange integral in order to obtain J as a function of interatomic spacing and radius of d orbitals. He found the exchange integral for the electrons on two one electron atoms is given by

$$J = \int \int \psi_a^*(r_1) \psi_b^*(r_2) \left[\frac{1}{r_{ab}} - \frac{1}{r_{a2}} - \frac{1}{r_{b1}} + \frac{1}{r_{21}} \right] \psi_b(r_1) \psi_a(r_2) d\tau,$$

where r_{ab} is the distance between the atomic cores, r_{21} is the distance between the two electrons, r_{a2} and r_{b1} are the distances between the electrons and the respective nuclei. Evaluation of this integral was made using the results of Slater and it was found that the exchange integral J becomes positive for small r_{12} and small r_{ab} . It also become positive for large r_{a2} and r_{b1} . The exchange integral can therefore be plotted against the ratio r_{ab}/r_d where r_d is the radius of the 3d orbital. This gives the Bethe–Slater curve as shown in Fig. 11.2 which correctly separates the ferromagnetic 3d elements such as iron, cobalt and nickel from the antiferromagnetic 3d elements chromium and manganese.

This means that if two atoms of the same kind are brought closer together without altering the radius of their 3d shells then r_{ab}/r_d will decrease. When r_{ab}/r_d is large then J is small and positive. As the ratio is decreased J at first increases and then after reaching a maximum decreases and finally becomes negative, indicating antiferromagnetic order at small values of r_{ab} . The exact nature of the exchange interaction is therefore dependent on the interatomic and interelectronic spacing.

Subsequently Slatter [15], Wohlfarth and Stuart and Marshall [9] expressed dissatisfaction with the Bethe–Slater model after difficulties with the sign and

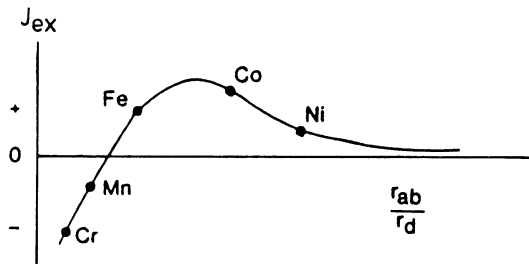


Fig. 11.2 The Bethe–Slater curve representing the variation of the exchange integral J with interatomic spacing r_{ab} and radius of unfilled d shell r_d . The positions of various magnetic elements on this curve are indicated. The rare earth elements lie to the right of nickel on the curve.

magnitude of J . Finally Herring [16] showed that the Heitler–London method of calculating the spin coupling is ultimately unreliable.

Therefore although the whole approach of Heitler–London, Heisenberg and Bethe still provides a useful conceptual framework for discussing the magnetic interactions of electrons, the method seems to be ultimately inadequate and we await a better description which can give more accurate values of J from first principles.

11.2 THE LOCALIZED ELECTRON THEORY

Can the magnetic properties of a solid be described in terms of the properties of electrons localized at the atomic sites?

We now go on to look at the magnetic properties in solids rather than isolated atoms. The most natural extension of the above discussion of atomic magnetism is to consider that the magnetic moments of atoms in a solid are due to electrons localized at the ionic sites. This means that we can deal with the magnetic properties of solids as merely a perturbation of the magnetic properties of the individual atoms. We shall see how far this proves to be correct in the two main groups of magnetic elements the 3d and 4f series.

11.2.1 Atomic magnetic moment due to localized electrons

How is the atomic magnetic moment determined from the angular momentum of the atom?

We can apply the above ideas to calculate the magnetic moment of an atom if we assume that the electrons in the unfilled shell which contribute to the magnetic moment are all localized at the ionic site. The magnetic moment of an atom is determined on this basis from the total angular momentum of the isolated atom

$(\hbar/2\pi)\mathbf{J}$ which is obtained as a vector sum of the orbital and spin angular momenta of electrons in unfilled shells.

$$\mathbf{m} = -g\mu_B \mathbf{J},$$

where μ_B is the Bohr magneton and g is the Lande splitting factor which is equal to

$$g = 1 + \frac{J(J+1) + S(S+1) - L(L+1)}{2J(J+1)}.$$

The magnetic moment can equally well be expressed as

$$\mathbf{m} = \gamma \left(\frac{\hbar}{2\pi} \right) \mathbf{J}$$

as discussed in Chapter 3 where γ is the gyromagnetic ratio and \hbar is Planck's constant.

We should note however that the values of J will not always be the same in the solid as in the free atoms discussed above. In the 3d series metals there are significant differences, even allowing for the quenching of the orbital angular momentum, but in the 4f or lanthanide series there is good agreement between the magnetic moments in the solid and the isolated atoms.

11.2.2 Quantum theory of paramagnetism

How do all these ideas combine to provide an explanation of paramagnetism, and how different is this theory from the classical models?

Single-electron atoms

By single-electron atoms we mean atoms with only one unpaired electron contributing to the magnetic properties. A good example is nickel. If we consider the energy of a single magnetic moment \mathbf{m} under the action of a magnetic field \mathbf{H} , the energy is given by

$$E = -\mu_0 \mathbf{m} \cdot \mathbf{H}.$$

We have now an expression for the magnetic moment of an isolated, and hence paramagnetic atom

$$\mathbf{m} = g\mu_B \mathbf{J}$$

$$E = -\mu_0 g\mu_B \mathbf{J} \cdot \mathbf{H}.$$

If we consider only the spins on the electrons and ignore the orbital contribution then $g = 2$ and $J = S = s = \frac{1}{2}$ for a single-electron spin. As the spin can only have the values $m_s = \pm \frac{1}{2}$ this means that, in the case of a single-electron atom, the electronic magnetic moment, as a result of quantization, can align only either parallel ($m_s = \frac{1}{2}$) or antiparallel ($m_s = -\frac{1}{2}$) to the field direction.

An atom with one unpaired electron therefore has two possible energy states in the magnetic field. The estimation of the magnetization using Boltzmann statistics

leads to

$$\begin{aligned}\mathbf{M} &= N\mathbf{m} \tanh(\mu_0\mathbf{mH}/k_B T) \\ &= NgJ\mu_B \tanh(\mu_0gJ\mu_B H/k_B T),\end{aligned}$$

where \mathbf{M} is the bulk magnetization or magnetic moment per unit volume, N is the number of atoms per unit volume and \mathbf{m} is the magnetic moment per atom. Solutions of this equation as a function of H/T are shown as a special case of the Brillouin function with $J = \frac{1}{2}$ in Fig. 11.3.

For values of $\mu_0\mathbf{mH}/k_B T \ll 1$ this leads to the approximation

$$\begin{aligned}\mathbf{M} &= N\mathbf{m}^2\mu_0\mathbf{H}/k_B T \\ \chi &= \frac{N\mathbf{m}^2\mu_0}{k_B T}\end{aligned}$$

which of course is the Curie law.

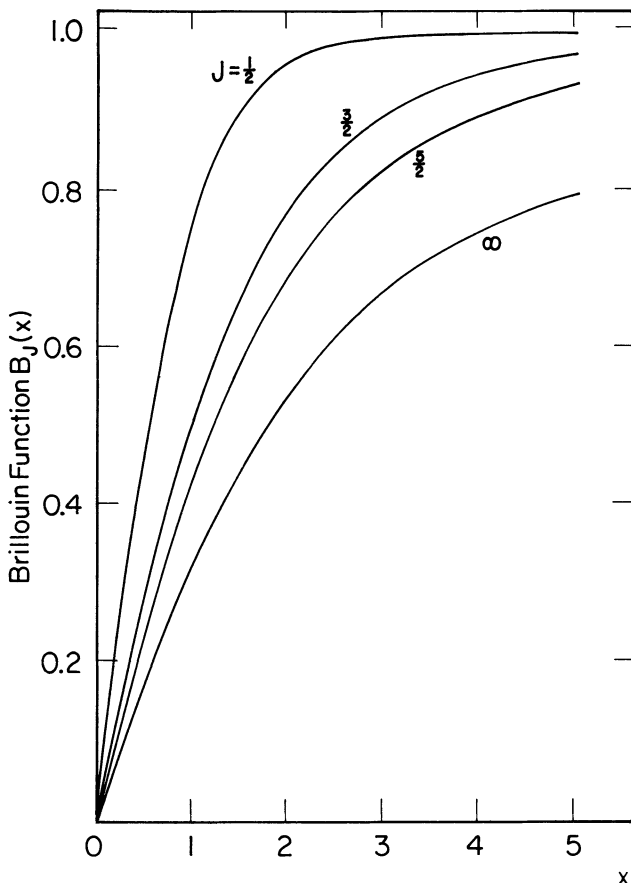


Fig. 11.3 The value of the Brillouin function $B_J(x)$ for various values of J ($\frac{1}{2}, \frac{3}{2}, \frac{5}{2}$, and infinity) and as a function of x . In the quantum theory of paramagnetism, for example $x = \mu_0gJ\mu_B H/k_B T$.

Multielectron atoms

By multielectron atoms we mean simply atoms with more than one electron contributing to the magnetic properties. Nickel is by this definition a single-electron atom, while iron is a multielectron atom.

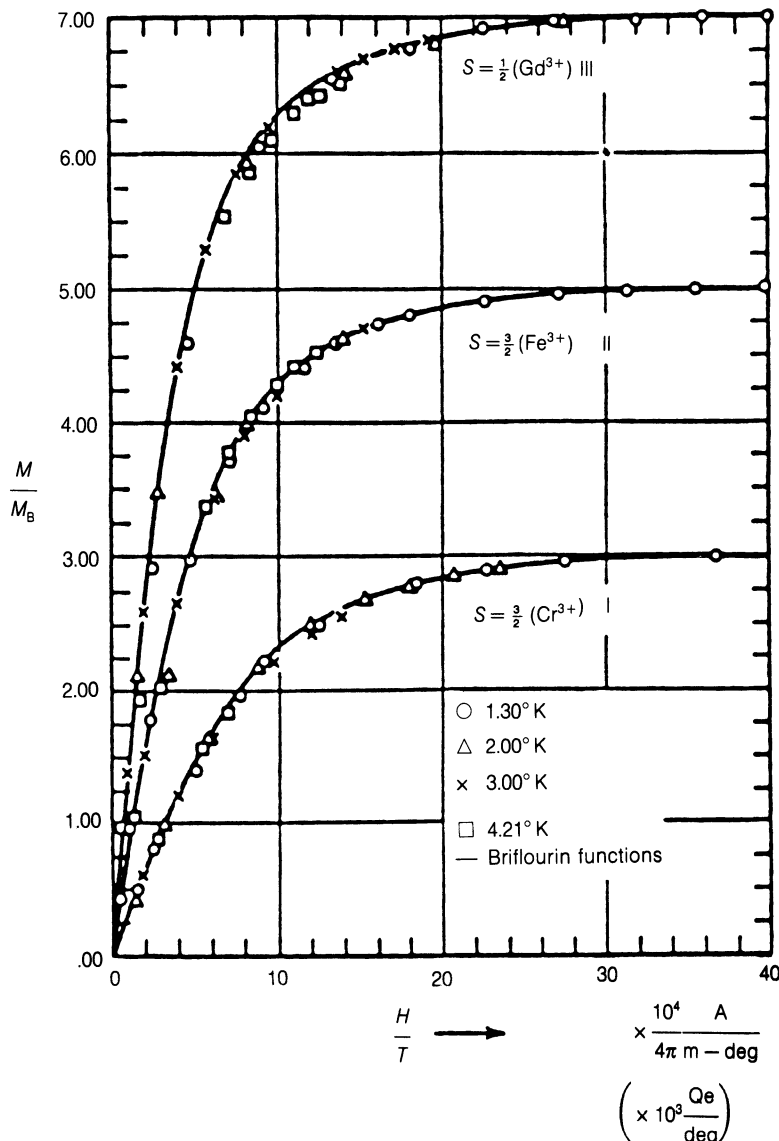


Fig. 11.4 Comparison of theory and experiment for the magnetization curves of three paramagnetic salts containing Gd^{3+} , Fe^{3+} and Cr^{3+} ions, respectively, after Henry [19]. These salts are potassium chromium alum, ferric ammonium alum and gadolinium sulphate octahydrate.

In these more complex situations there are $2J + 1$ energy levels and so the expression for the magnetization is

$$\mathbf{M} = N g J \mu_B B_J \left(\frac{g J \mu_B \mu_0 \mathbf{H}}{k_B T} \right),$$

where $B_J(x)$ is the Brillouin function [17] which is defined as

$$B_J(x) = \left(\frac{(2J+1)}{2J} \right) \coth \left(\frac{(2J+1)x}{2J} \right) - \left(\frac{1}{2J} \right) \coth \left(\frac{x}{2J} \right).$$

The above equations for the single-electron atoms are then seen to be merely special or restricted cases of this general function.

The equation for the magnetization of the multiple-electron atom is the quantum analogue of the Langevin function [18] given in Chapter 9. In the limiting case when $J \rightarrow \infty$, that is when there are no quantum mechanical restrictions on the allowed directions and values of magnetic moment in the atom we arrive at the classical Langevin expression for magnetization.

Solutions for the paramagnetic magnetization equation are shown for different values of S in Fig. 11.4 together with experimental values for three paramagnetic salts as determined by Henry [19].

Curie's law

The Curie law of paramagnetic susceptibilities can be derived from the quantum theory of paramagnetism. For $\mu_0 \mathbf{m} \mathbf{H} / k_B T \ll 1$ the Brillouin function becomes

$$B_J(\mu_0 \mathbf{m} \mathbf{H} / k_B T) = \mu_0 \mathbf{m} \mathbf{H} / 3k_B T$$

$$\mathbf{M} = \frac{N \mu_0 \mathbf{m}^2 \mathbf{H}}{3k_B T}$$

$$\begin{aligned} \chi &= \frac{\mathbf{M}}{\mathbf{H}} = \frac{N \mu_0 \mathbf{m}^2}{3k_B T} \\ &= \frac{N \mu_0 g^2 \mu_B^2 J(J+1)}{3k_B T} \\ \chi &= \frac{C}{T}, \end{aligned}$$

which is the Curie law, with

$$C = \frac{N \mu_0 g^2 \mu_B^2 J(J+1)}{3k_B}.$$

We see from this discussion that the quantum theory of paramagnetism provides qualitatively similar results to the classical theories, however the classical Langevin function needs to be replaced by its quantum mechanical analogue, the Brillouin function which leads to different numerical results.

11.2.3 Quantum theory of ferromagnetism

How can we extend the above theories to a quantum theory of ferromagnetism and how different is this from the classical models?

The quantum theory of ferromagnetism is derived from the quantum theory of paramagnetism in much the same way as the classical Weiss theory of ferromagnetism was derived from the Langevin theory of paramagnetism. A perturbation in the form of an interaction, or exchange coupling, is introduced into the quantum theory of paramagnetism so that the electrons on neighbouring atoms interact with one another. The energy of an electron in a magnetic field therefore becomes, as before

$$E = -\mu_0 \mathbf{m}(\mathbf{H} + \alpha \mathbf{M}),$$

where $\alpha \mathbf{M}$ represents the interaction of the electron moment with those other electrons closeby.

Magnetization

In the case of an atom with one electron this leads via statistical thermodynamics to

$$\mathbf{M} = NgJ\mu_B \tanh \left[\frac{\mu_0 g J \mu_B (\mathbf{H} + \alpha \mathbf{M})}{k_B T} \right]$$

and, for multielectron atoms, to

$$\mathbf{M} = NgJ\mu_B B_J \left[\frac{gJ\mu_B \mu_0 (\mathbf{H} + \alpha \mathbf{M})}{k_B T} \right]$$

where $B_J(x)$ is the Brillouin function.

The Curie–Weiss law

At higher temperatures this system will be paramagnetic, so that \mathbf{M} will be uniform throughout the material, and hence

$$\begin{aligned} \mathbf{M} &= \frac{N\mu_0 g^2 \mu_B^2 J(J+1)(\mathbf{H} + \alpha \mathbf{M})}{3k_B T} \\ \chi &= \frac{\mathbf{M}}{\mathbf{H}} = \frac{N\mu_0 g^2 \mu_B^2 J(J+1)/3k_B T}{1 - \alpha N\mu_0 g^2 \mu_B^2 J(J+1)/3k_B T} \\ \chi &= \frac{N\mu_0 g^2 \mu_B^2 J(J+1)}{3k_B T - \alpha N\mu_0 g^2 \mu_B^2 J(J+1)}, \end{aligned}$$

which is the Curie–Weiss law in which

$$C = N\mu_0 g^2 \mu_B^2 J(J+1)$$

$$T_c = \alpha N\mu_0 g^2 \mu_B^2 J(J+1)/3k_B T.$$

We see therefore that the quantum theory of ferromagnetism also leads to qualitatively similar results to the classical theory.

In the ferromagnetic regime the magnetization M will not be uniform throughout the solid. Since any individual magnetic moment is likely to be more affected by other moments nearby than by distant magnetic moments, the moments will couple to the spontaneous magnetization within the domain M_s rather than the bulk magnetization M when in the ferromagnetic state. Therefore a nearest-neighbour model, with possible extension to next and higher order neighbours, is more appropriate in the ferromagnetic regime.

11.2.4 Temperature dependence of the spontaneous magnetization within a domain

How does the magnetization within a domain vary with temperature according to the quantum theory of ferromagnetism?

The spontaneous magnetization within a domain M_s is determined by solving the ferromagnetic Brillouin function in the absence of a field

$$M_s = N g J \mu_B B_J \left(\frac{\mu_0 g J \mu_B \alpha M_s}{k_B T} \right).$$

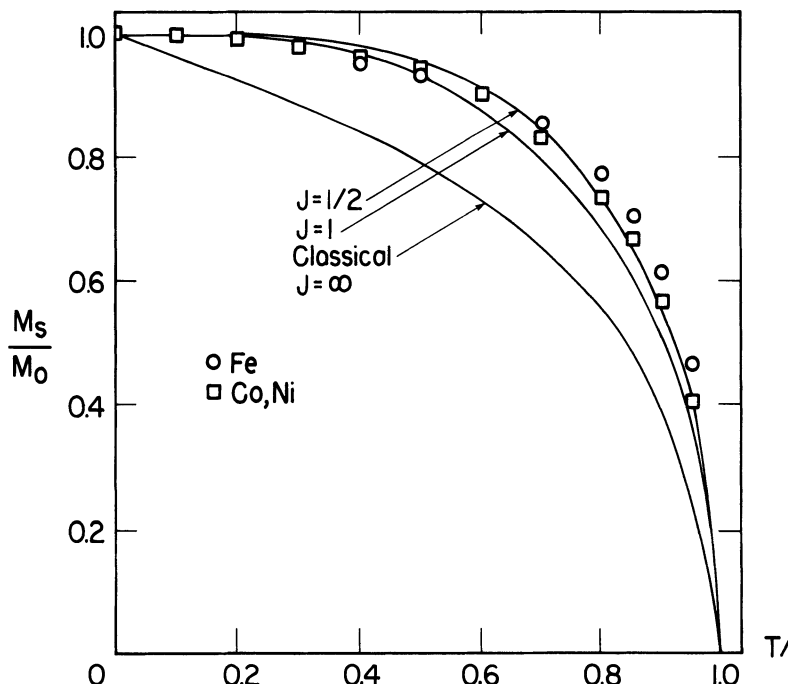


Fig. 11.5 Temperature dependence of the spontaneous magnetization within a domain for iron, cobalt and nickel, compared with calculations based on the ferromagnetic Brillouin function.

In the case of nickel we can use the $S = \frac{1}{2}$ solution so that

$$\mathbf{M}_s = NgJ\mu_B \tanh\left(\frac{\mu_0 g J \mu_B \alpha M_s}{k_B T}\right).$$

Solutions of this are shown in Fig. 11.5. It is seen from this that the spontaneous magnetization is only weakly dependent on temperature until it reaches $0.75T_c$. Above that it decreases rapidly towards zero at the Curie temperature.

11.2.5 Critique of the local moment model

How well does this model work and how realistic is it?

The local moment model works well in that it does provide relatively simple mathematical functions for the dependence of magnetization on magnetic field and temperature. It is quite realistic for the lanthanides with their closely bound 4f electrons which determine the magnetic properties of the solid. In most other cases the magnetic properties of paramagnets and the other main group of ferromagnets the 3d series, the ‘magnetic’ electrons are outer electrons which are relatively free to move through the solid. Therefore the localized model, despite its successes, is not a realistic model for these cases.

11.3 THE ITINERANT ELECTRON THEORY

What happens if the ‘magnetic’ electrons are not localized at the atomic sites?

If the magnetic electrons are in unfilled shells then in a number of metals these magnetic electrons are unlikely to be localized as described above. The unfilled shells are in most cases among the furthest removed from the nucleus and it is these electrons which are most easily removed. This means that alternative models must be sought for these metals in order to provide a realistic theory.

11.3.1 The magnetism of electrons in energy bands

What are the magnetic properties of electrons in energy bands?

So far we have only considered the magnetic properties of solids in terms of localized magnetic moments which behave as if they were attached to the atomic cores in the material. Thus we have talked about atomic magnetic moments. However we have come to realize that these magnetic moments are really due to the angular momentum of unpaired electrons in unfilled shells. With the exception of the lanthanides the unpaired ‘magnetic’ electrons are usually outer electrons and so are unlikely to be closely bound to the atoms.

Metals such as the alkali metal series lithium, sodium, potassium, rubidium and caesium all show temperature independent paramagnetism for example which can not be explained by the local moment model. In this case the paramagnetism is due to the outer electrons which behave as a free electron gas.

This is true of the 3d transition elements iron, nickel and cobalt. We therefore need to find a theoretical description of magnetism due to itinerant electrons in these cases.

11.3.2 Pauli paramagnetism of ‘free’ electrons

Can paramagnetism be described simply on the basis of changes in population of nearly free electrons in bands?

The Langevin theory of paramagnetism and its quantum mechanical analogue work for dilute paramagnets such as the hydrated salts of transition metal ions. However it is well known that the paramagnetic susceptibility of most metals is independent of temperature and hence does not follow the classical Langevin theory. In addition the paramagnetism of most metals is considerably weaker than would be expected on the basis of the localized model.

The reason that the paramagnetic susceptibility is so much lower is that the electrons are in general not free to rotate into the field direction as required by the Langevin model. This is because, as a result of the Pauli exclusion principle [6], the electron states needed for reorientation are already occupied by other electrons. Only those electrons within an energy $k_B T$ of the Fermi level are able to change

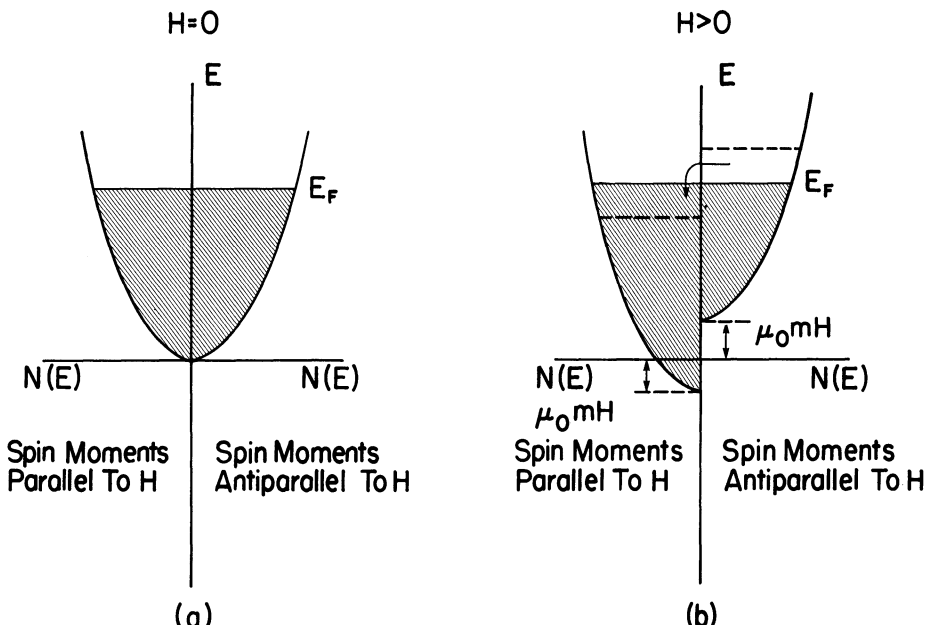


Fig. 11.6 Pauli paramagnetism for nearly free electrons in a magnetic field H . In (a) the field is zero so that both up and down spin sub-bands have identical energy. In (b) the field causes an energy difference between sub-bands with spins aligned parallel and antiparallel to the field.

orientation. We therefore need to consider an alternative model of paramagnetism due to the band electrons as conceived by Pauli [20].

Consider therefore the parabolic distribution of nearly free electrons as shown in Fig. 11.6. Only the fraction T/T_f of the total number of electrons can contribute to the magnetization where T is the thermodynamic temperature and T_f is the Fermi temperature, defined such that $E_f = k_B T_f$. Therefore

$$\begin{aligned} \mathbf{M} &= \left(\frac{N\mu_0 \mathbf{m}^2 \mathbf{H}}{3k_B T} \right) \left(\frac{T}{T_f} \right) \\ &= \frac{N\mu_0 \mathbf{m}^2 \mathbf{H}}{3k_B T_f}. \end{aligned}$$

The number density of electrons parallel to the field is

$$\begin{aligned} N_+ &= \frac{1}{2} \int f(\varepsilon) D(\varepsilon + \mu \mathbf{H}) d\varepsilon \\ &\approx \frac{1}{2} \int f(\varepsilon) D(\varepsilon) d\varepsilon + \frac{1}{2} \mu_0 \mathbf{m} \mathbf{H} D(\varepsilon_f) \end{aligned}$$

and the number density of those antiparallel to the field

$$\begin{aligned} N_- &= \frac{1}{2} \int f(\varepsilon) D(\varepsilon - \mu_0 \mathbf{H}) d\varepsilon \\ &\approx \frac{1}{2} \int f(\varepsilon) D(\varepsilon) d\varepsilon - \frac{1}{2} \mu_0 \mathbf{m} \mathbf{H} D(\varepsilon_f). \end{aligned}$$

The magnetization is then given by

$$\begin{aligned} \mathbf{M} &= \mathbf{m}(N_+ - N_-) \\ &= \mathbf{m}^2 \mu_0 \mathbf{H} D(\varepsilon_f) \\ &= \frac{3N\mathbf{m}^2 \mu_0 \mathbf{H}}{2k_B T_f}. \end{aligned}$$

This equation gives the Pauli spin magnetization of the paramagnetic conduction band electrons. The susceptibility is then

$$\chi = \frac{3N\mathbf{m}^2 \mu_0}{2k_B T_f}$$

which is temperature independent since T_f is a constant.

11.3.3 Band theory of ferromagnetism

How do electrons in bands behave when there is an exchange interaction which causes alignment of the spins?

The band theory of ferromagnetism is a simple extension of the band theory of paramagnetism by the introduction of an exchange coupling between the

electrons. The simplest case is to consider the electrons to be entirely free, that is a parabolic energy distribution. This simplifying assumption does not alter the main conclusions of the theory. The band theory of ferromagnetism was first proposed by Stoner [21] and then independently by Slater [22].

Since magnetic moments can only arise from unpaired electrons it is immediately clear that a completely filled energy band cannot contribute a magnetic moment since in such an energy band all electron spins will be paired giving $L = 0$ and $S = 0$. In a partially filled energy band it is possible to have an imbalance of spins leading to a net magnetic moment per atom. This arises because the exchange energy removes the degeneracy of the spin up and spin down half bands as shown in Fig. 11.7. The larger the exchange energy the greater the difference in energy between these two half bands. Electrons fill up the band by occupying the lowest energy levels first. If the half bands are split as in Fig. 11.7(a) the electrons can begin to occupy the spin down half band before the spin up half band is full. This usually leads to a non integral number of magnetic moments per atom. A larger exchange splitting can lead to a separation between the half bands as in Fig. 11.7(b). In this case the spin up band must be filled before electrons can enter the spin down band. This leads to an integral number of magnetic moments per atom.

For example consider the situation in Fig. 11.8, where 10 electron states exist

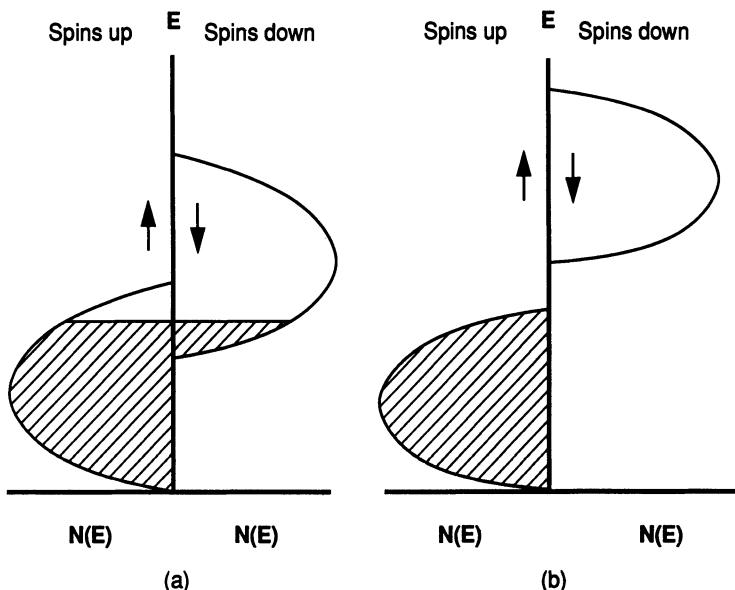


Fig. 11.7 (a) Schematic band structure density of states, showing exchange splitting of the spin up and spin down half bands, with remaining overlap between the two half bands leading to a magnetic moment with a non integral number of Bohr magnetons per atom. (b) Schematic band structure density of states with a larger exchange splitting leading to complete energy separation of the half bands and to a magnetic moment with an integral number of Bohr magnetons per atom.

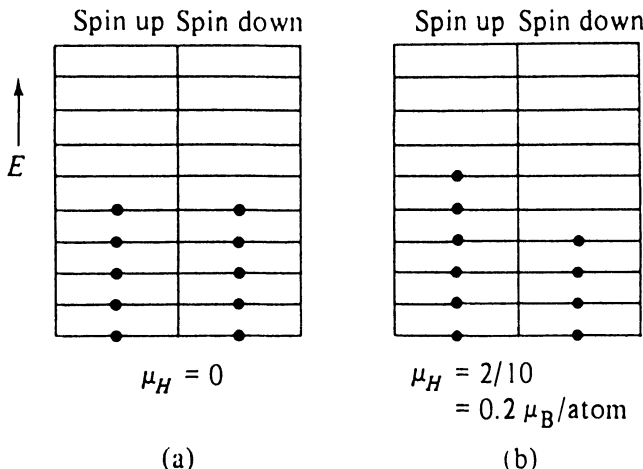


Fig. 11.8 Diagram representing the occupation of allowed energy states in an electron band: (a) balanced numbers of spin up and spin down electrons; (b) unbalanced numbers of spin up and spin down electrons due to the exchange interaction, leading to a net magnetic moment per atom.

in close proximity in an electronic band. A spin imbalance of 2 can be created by flipping one of the moments into the opposite direction. This then gives rise to a magnetic moment of $0.2 \mu_B$ per atom. We now see the possibility of atomic magnetic moments that are non-integral multiples of the Bohr magneton.

11.3.4 Magnetic properties of 3d band electrons

Can the band theory provide a satisfactory description of the magnetic properties of the 3d metals?

In the transition metals iron, nickel and cobalt which are the three ferromagnetic elements with electronic structure for which the band theory should apply, the magnetic properties are due to the 3d band electrons. Of course there is also a 4s electron band but this contains two paired electrons and so does not affect magnetic properties.

The 3d band can hold up to 10 electrons (5 up and 5 down) and it is here that we must concentrate attention in order to explain the observed properties. The exchange interaction is responsible for creating the imbalance in spin up and spin down states. In the absence of the exchange energy the spin imbalance would be an excited state but this does not require too much energy in the 3d band because of the high density of states and therefore a positive exchange interaction can be sufficient to cause the alignment resulting in a spin imbalance and a net magnetic moment per atom.

If we suppose that in these metals the exchange interaction causes 5 of the 3d electrons to align 'up' and the remainder 'down', we arrive at an equation which approximates observed magnetic moments in these elements very well. Let n be the

number of 3d + 4s electrons per atom, x be the number of 4s electrons per atom, and $n - x$ the number of 3d electrons per atom

$$\begin{aligned}\mathbf{m} &= [5 - (n - x - 5)] \mu_B \\ &= [10 - (n - x)] \mu_B.\end{aligned}$$

We can approximate observed magnetic properties by the assumption that $x = 0.6$.

$$\mathbf{m} = (10.6 - n) \mu_B$$

which for nickel with $n = 10$, cobalt with $n = 9$ and iron $n = 8$ gives the following

$$\begin{array}{ll}\text{Ni:} & \mathbf{m} = 0.6 \mu_B \\ \text{Co:} & \mathbf{m} = 1.6 \mu_B \\ \text{Fe:} & \mathbf{m} = 2.6 \mu_B.\end{array}$$

These results are quite close to the known values.

In this way the band theory can account for the non-integral atomic magnetic moments in these metals, a result that is more difficult to justify on the localized moments model.

11.3.5 The Slater–Pauling curve

How well does the itinerant electron model describe the magnetic properties of 3d alloys?

The above argument can be used to explain the moment per atom of several of the 3d transition metals from manganese to copper. The Slater–Pauling curve [23, 24] gives the magnetic moments of these 3d metals and their alloys from the premises of the itinerant electron theory. This is shown in Fig. 11.9. Most alloys fall on to a locus consisting of two straight lines beginning at chromium with 0 Bohr magnetons rising to 2.5 Bohr magnetons between iron and cobalt and dropping to 0 Bohr magnetons again between nickel and copper. The metals in this range chromium, manganese, iron, cobalt, nickel and copper have total numbers of electrons ranging from 24 to 29, while the number of 3d electrons ranges from 5 in chromium to 10 in copper.

The interpretation of the results in Fig. 11.9 is in terms of the rigid band model. It is considered that the alloy metals share a common 3d band to which both elements contribute electrons. The maximum magnetic moment occurs at a point between iron and cobalt. It appears from this model that, as expected, the 3d and 4s electrons are responsible for the magnetic properties of these metals and alloys, and that they are relatively free. Therefore it is a reasonable assumption that they are shared between the ions in a common 3d band.

Pauling [24] has suggested that the 3d band is broken into two parts: the upper part capable of holding 4.8 electrons (2.4 up and 2.4 down) and the lower part capable of holding 5.2 electrons (2.6 up and 2.6 down). This means that as electrons are removed beginning with zinc for example the magnetic moment is increased by

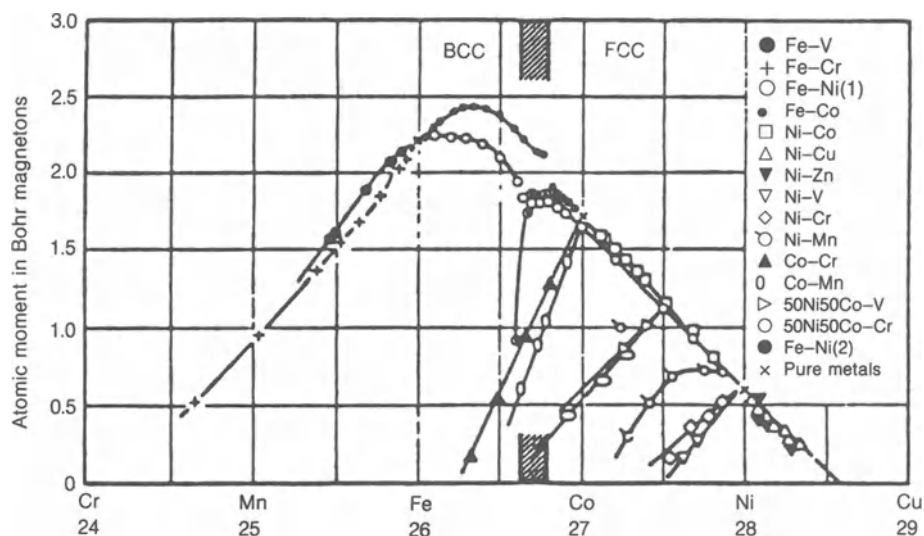


Fig. 11.9 The Slater–Pauling curve which gives the net magnetic moment per atom as a function of the number of 3d electrons per atom. The various 3d elements are shown at the relevant points on the x-axis, but the curve is more general, being primarily of interest in explaining the magnetic moments of various intra-3d alloys.

depletion of spin down electrons in the upper part of the band until a magnetic moment of 2.4 Bohr magnetons is reached between iron and cobalt. Then the moment begins to decrease again towards chromium because the removal of further electrons results in a reduction in spin up electrons from the upper part of the 3d band.

11.3.6 Critique of the itinerant electron model

What are the strengths and weaknesses of the itinerant electron model?

The itinerant electron model has had successes and these include the ability to explain non-integral values of atomic magnetic moments and to predict some aspects of the magnetic behaviour of the 3d series metals and alloys. Furthermore the localized moment model, which is the main alternative, is certainly open to the objection that it is unrealistic in so far as the magnetic electrons of most atoms, with the exception of the lanthanides, are relatively free being in the outer shells.

The drawback of the itinerant electron theory is that it is extremely difficult to make fundamental calculations based on it. Unlike the local moment theory which lends itself readily to simple models such as the Weiss [25] and Heisenberg [26] models of ferromagnetism, the itinerant electron theory does not provide any simple model from which first principles calculations can be made. Therefore although the current opinion is that the itinerant theory is intrinsically closer to reality in most cases, interpretations of magnetic properties are still more often made on the basis of the localized moment model.

REFERENCES

1. Martin, D. H. (1967) *Magnetism in Solids*, Illife, London, Ch. 5.
2. Heitler, W. and London, F. (1927) *Z. Phys.*, **44**, 455.
3. Heisenberg, W. (1928) *Z. Phys.*, **49**, 619.
4. Dirac, P. A. M. (1929) *Proc. Roy. Soc.*, **A123**, 714.
5. Weiss, P. (1907) *J. de Phys.*, **6**, 661.
6. Pauli, W. (1925) *Z. Phys.*, **31**, 765.
7. Hofmann, J., Paskin, A., Tauer, K. J. and Weiss, R. J. (1956) *J. Phys. Chem. Sol.*, **1**, 45.
8. Wohlfarth, E. P. (1949) *Nature*, **163**, 57.
9. Stuart, R. and Marshall, W. (1960) *Phys. Rev.*, **120**, 353.
10. Watson, R. E. and Freeman, A. J. (1961) *Phys. Rev.*, **123**, 2027.
11. Watson, R. E. and Freeman, A. J. (1962) *J. Phys. Soc. Jap.*, **17**, **B-1**, 40.
12. Slater, J. C. (1930) *Phys. Rev.*, **35**, 509.
13. Slater, J. C. (1930) *Phys. Rev.*, **36**, 57.
14. Bethe, H. (1933) *Handb. d. Phys.*, **24**, 595.
15. Slater, J. C. (1936) *Phys. Rev.*, **49**, 537; **49**, 931.
16. Herring, C. (1962) *Rev. Mod. Phys.*, **34**, 631.
17. Brillouin, L. (1927) *J. de Phys. Radium*, **8**, 74.
18. Langevin, P. (1905) *Ann. de Chem. et Phys.*, **5**, 70.
19. Henry, W. E. (1952) *Phys. Rev.*, **88**, 559.
20. Pauli, W. (1926) *Z. Phys.*, **41**, 81.
21. Stoner, E. C. (1933) *Phil. Mag.*, **15**, 1080.
22. Slater, J. C. (1936) *Phys. Rev.*, **49**, 537.
23. Slater, J. C. (1937) *J. Appl. Phys.*, **8**, 385.
24. Pauling, L. (1938) *Phys. Rev.*, **54**, 899.
25. Weiss, P. (1907) *J. de Phys.*, **6**, 661.
26. Heisenberg, W. (1928) *Z. Phys.*, **49**, 619.

FURTHER READING

- Chikazumi, S. (1964) *Physics of Magnetism*, Ch. 3, Wiley, New York.
 Cullity, B. D. (1972) *Introduction to Magnetic Materials*, Ch. 3, Addison-Wesley, Reading, Mass.
 Morrish, A. H. (1965) *The Physical Principles of Magnetism*, Wiley, New York.

EXAMPLES AND EXERCISES

Example 11.1 The exchange interaction. Explain the origin of the exchange interaction J . Does this have a classical analogue? If not how can it be interpreted classically? Since the exchange interaction is only invoked to prevent two electrons occupying the same energy levels with the same set of quantum numbers it would seem that the exchange interaction should lead only to antiferromagnetism by ensuring that the ‘exchanged’ electrons have antiparallel spins. Explain why the exchange interaction does not lead only to antiferromagnetism.

Example 11.2 Magnetic moment of dysprosium ions. Dy^{3+} has nine electrons in its 4f shell. What are the values of L , S and J ? Calculate the susceptibility of a salt containing 1 g mole of Dy^{3+} at 4 K.

Example 11.3 Paramagnetism of $S = 1$ system. Find the magnetization as a function of magnetic field and temperature of a system with $S = 1$, moment \mathbf{m} and concentration N atoms per unit volume. Show that the limit $\mu_0 \mathbf{m} \mathbf{H} \ll k_B T$ leads to $\mathbf{M} \approx (2\mu_0 N \mathbf{m}^2 \mathbf{H}) / (3k_B T)$.

12

Soft Magnetic Materials

Applications of soft ferromagnetic materials are almost exclusively associated with electrical circuits in which the magnetic material is used to amplify the flux generated by the electric currents. In this chapter we will consider both a.c. and d.c. applications of soft magnetic materials. These each require somewhat different material properties, although in general high permeability and low coercivity are needed in all cases.

12.1 PROPERTIES AND USES OF SOFT MAGNETIC MATERIALS

Soft ferromagnetic materials find extensive applications as a result of their ability to enhance the flux produced by an electrical current. Consequently the uses of soft materials are closely connected with electrical applications such as electrical power generation and transmission, receipt of radio signals, microwaves, inductors, relays and electromagnets. The available range of magnetic properties of materials is continually being increased and here we shall give some indication of the present status.

12.1.1 Permeability

Permeability is the most important parameter for soft magnetic materials since it indicates how much magnetic induction is generated by the material in a given magnetic field. In general the higher the permeability the better for these materials. Initial permeabilities range from $\mu_r = 100\,000$ [1] in materials such as permalloy down to as low as $\mu_r = 1.1$ in some of the cobalt–platinum permanent magnets. It is well known that initial permeability and coercivity have in broad terms a reciprocal relationship, so that materials with high coercivity necessarily have a low initial permeability and vice versa.

12.1.2 Coercivity

Coercivity is the parameter which is used to distinguish hard and soft magnetic materials. Traditionally a material with a coercivity of less than 1000 A/m is

considered magnetically ‘soft’. A material with a coercivity of greater than 10 000 A/m is considered magnetically ‘hard’. Low coercivities are achieved in nickel alloys such as permalloy in which the coercivity can be as low as 0.4 A/m [2]. In some of the recent permanent magnet materials intrinsic coercivities in the range 1.2×10^6 A/m are commonly observed.

12.1.3 Saturation magnetization

The highest saturation magnetization available is 2.43 T which is achieved in an iron–cobalt alloy containing 35% cobalt. The possible values of saturation magnetization then range downward continuously to effectively zero.

12.1.4 Hysteresis loss

The hysteresis loss is the area enclosed by the d.c. hysteresis loop on the B , H plane as discussed in section 5.1. It represents the energy expended during one cycle of the hysteresis loop. The hysteresis loss increases as the maximum magnetic field reached during the cycle increases. Clearly for a.c. applications in which energy dissipation should be minimized the hysteresis loss should be as low as possible. This loss is closely related to the coercivity so that processing of materials to reduce coercivity also reduces the hysteresis loss. However in a.c. applications the hysteresis loss is not the only dissipative or loss mechanism.

12.1.5 Conductivity and a.c. electrical losses

One of the most important parameters of a magnetic material for a.c. applications is its electrical loss. The electrical losses are shown for various materials in Table 12.1 at 50 Hz and an amplitude of excitation of 1 T [3].

The electrical losses depend on the frequency of excitation v , the amplitude of magnetic induction B_{\max} , the hysteresis loss W_H , the sheet thickness t (due to the

Table 12.1 Total electrical losses of various soft magnetic materials with sheet thicknesses t between 0.2 mm and 0.5 mm at a frequency of 50 Hz and an induction amplitude of 1 T [3, p. 46]

Material	Total losses W_{tot} (W/kg)
Commercial iron	5–10
Si–Fe hot rolled	1–3
Si–Fe cold rolled, grain oriented	0.3–0.6
50% Ni–Fe	0.2
65% Ni–Fe	0.06

penetration depth of the a.c. magnetic field) and the eddy current dissipation W_{ec} . In addition there is usually a discrepancy between the measured loss and the loss expected from the sum of hysteresis and eddy current losses and this is usually referred to as the anomalous loss W_a . The total electrical power loss W_{tot} can be expressed as the sum of these components

$$W_{\text{tot}} = W_H + W_{\text{ec}} + W_a,$$

where the hysteresis loss and eddy current loss are frequency dependent. The hysteresis loss increases linearly with frequency while the eddy current loss increases with the frequency squared.

The eddy current loss, at frequencies which are low enough for the inductive effects of the eddy currents to be neglected, is given by the general equation

$$W_{\text{ec}} = \frac{\pi^2 B_{\max}^2 d^2 v^2}{\rho \beta}$$

where d is the cross sectional dimension, ρ is the bulk resistivity in $\Omega \cdot \text{m}$ and β is a coefficient which has different values for different geometries. For example $\beta = 6$ for laminations, in which d represents the thickness t . For cylinders $\beta = 16$ and d represents the diameter. For spheres $\beta = 20$ and d represents the diameter. Stephenson [4] has shown that for low alloy, non oriented electrical steel sheets the above equation, which reduces to

$$W_{\text{ec}} = \frac{1.644 B_{\max}^2 t^2 v^2}{\rho D}$$

where D is the density in kilograms/m³, gives the eddy current loss in watts per kilogram. The anomalous loss at 60 Hz and an induction amplitude of 1.5 to 1.7 T was found to be dependent on t^2/ρ , so that

$$W_a = W_{\text{ao}} + \frac{kt^2}{\rho},$$

where W_{ao} and k are empirical constants. From the empirical Steinmetz law [5] the d.c. hysteresis loss is known to depend on induction amplitude B_{\max} and frequency v according to the relation

$$W_H = \eta B_{\max}^n v$$

where η is a material constant and n is an exponent which lies in the range 1.6–2.0.

The total losses can be reduced if the conductivity of the material is reduced. This is exploited in transformer material such as silicon iron in which the silicon is added principally to reduce the conductivity, although it has an adverse effect on the permeability but does reduce the coercivity. The losses in Ni–Fe alloys are lower than for silicon–iron, and this is also used in a.c. applications such as inductance coils and transformers, but silicon–iron has a higher saturation magnetization.

12.1.6 Electromagnets and relays

The most important d.c. uses which soft magnetic materials find are in electromagnets and relays. An electromagnet is any device in which a magnetic field H is generated by an electric current and the resulting flux density B is increased by the use of a high-permeability core. The simplest example is a solenoid carrying a d.c. current wound around a ferromagnetic core. In electromagnets soft iron is still the most widely used material because it is relatively cheap and can produce high magnetic flux densities. It is often alloyed with a small amount of carbon (< 0.02 wt%) without seriously impairing its magnetic properties for this application. Also the alloy Fe–35%Co is used in electromagnet pole tips to increase the saturation magnetization.

A relay is a special form of d.c. electromagnet with a moving armature which operates a switch. This can be used for example to open and close electrical circuits and is therefore important as a control device.

12.1.7 Transformers, motors and generators

A transformer is a device which can transfer electrical energy from one electrical circuit to another although the two circuits are not connected electrically. This is achieved by a magnetic flux which links the two circuits through an inductance coil in each circuit. The two coils are connected by a high-permeability magnetic core. The main consideration for the purpose of this chapter is the choice of a suitable material for the magnetic core of the transformer. Transformers have also been described in section 4.2.3. The material used for transformer cores is almost exclusively grain-oriented silicon–iron, although small cores still use non-oriented silicon–iron. High-frequency transformers use cobalt–iron although this represents only a small volume of the total transformer market.

Generators are devices for converting mechanical energy into electrical energy. Motors are devices for converting electrical energy into mechanical energy. Both are constructed from high-induction, high-permeability magnetic materials. The most common material used for these applications is non-oriented silicon–iron but many smaller motors use silicon-free low-carbon steels.

12.2 MATERIALS FOR A.C. APPLICATIONS

We will first look at uses in power generation and transmission since these are easily the most important areas in which soft ferromagnetic materials are employed. The desirable properties here are, as in most soft magnetic materials applications, high permeability and saturation magnetization with low coercivity and power loss. In addition suitable mechanical properties are a consideration since silicon–iron becomes very brittle at high silicon content. Generally it is not possible to have all of these properties in a single material so it is necessary to decide which is the most crucial property in any given situation. For high power applications silicon–iron is widely used. Non-oriented silicon–iron is the material

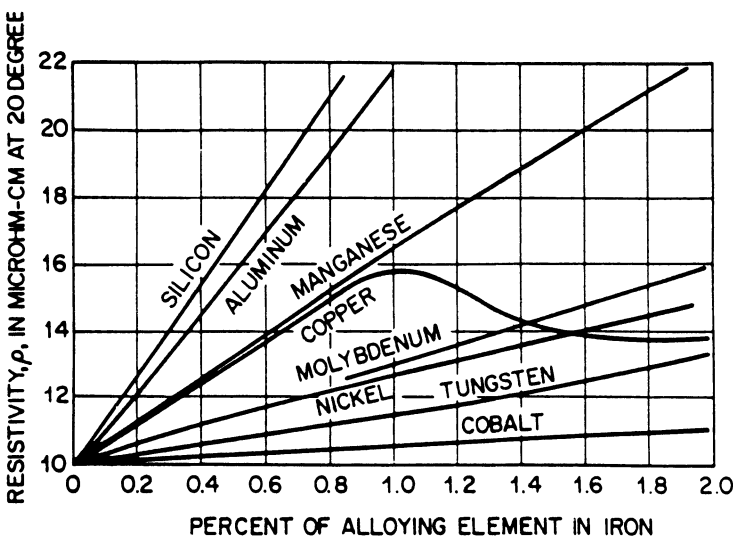


Fig. 12.1 Variation of the electrical resistivity of iron with the addition of different alloying elements.

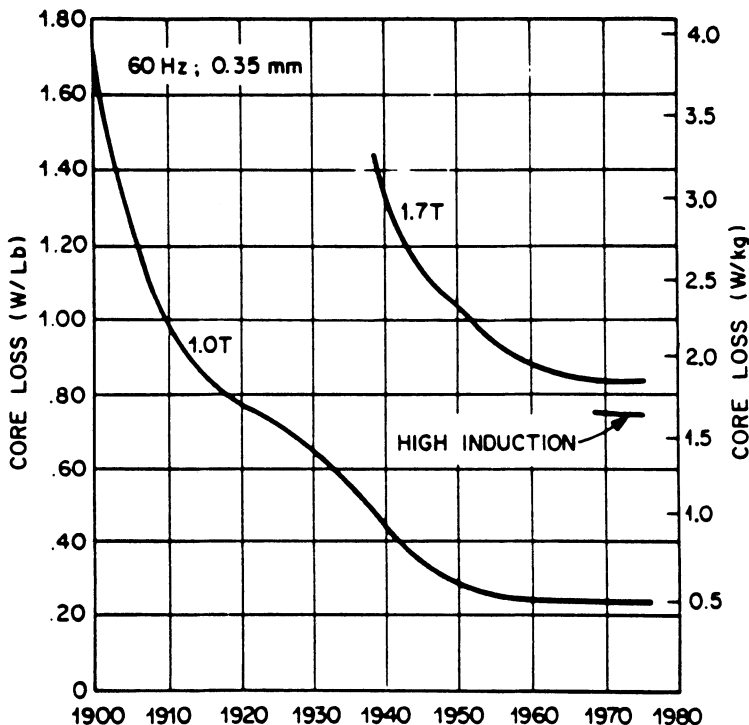


Fig. 12.2 Reduction of core loss of 0.35 mm thick silicon-iron at 60 Hz from the year 1900 until 1975.

of choice in motors and generators while grain-oriented silicon–iron is used for transformers.

12.2.1 Iron–silicon alloys

In electrical power generation and transmission the greatest demand is for transformer cores. In this area silicon–iron is used to the exclusion of all others. This is also known as ‘electrical steel’ or silicon steel both of which are misnomers since these materials are not really steels.

In the power industry the electrical voltage is almost always low-frequency a.c. at 50 or 60 Hz. This leads to an alternating flux in the cores of the electromagnetic

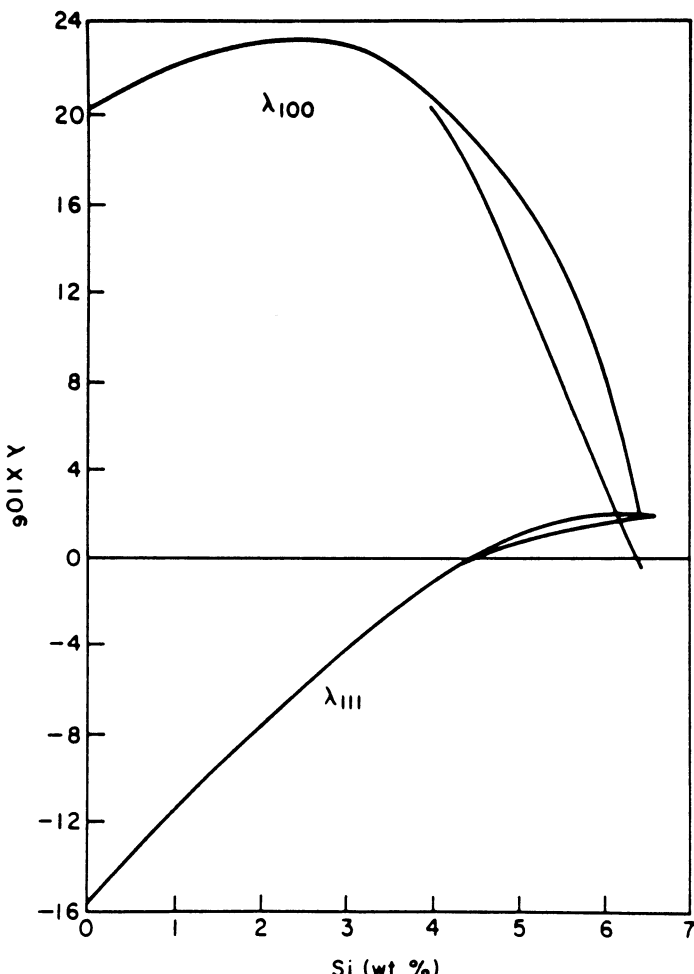


Fig. 12.3 Dependence of the magnetostriction coefficients λ_{100} and λ_{111} of silicon–iron on silicon content. The lower curves in the range 4–7% Si are for slowly cooled samples.

devices and consequently to the generation of 'eddy currents' if the material is an electrical conductor. Eddy currents reduce the efficiency of transformers because some of the energy is lost through eddy current dissipation.

There are several ways in which the properties of pure iron can be improved in order to make it more suitable for transformer cores at low frequencies and these have been discussed in a review paper by Littman [6]. First the resistivity can be increased so that the eddy current losses become less. This is achieved by the alloying of silicon with iron. The variation of resistivity of silicon-iron with silicon content is shown in Fig. 12.1. Iron containing 3% silicon has four times the resistivity of pure iron [7]. Over the years there have been substantial improvements in the core losses of silicon iron. These improvements for 0.35 mm thick sheets are shown in Fig. 12.2.

Silicon of course is a very cheap material which is an important consideration

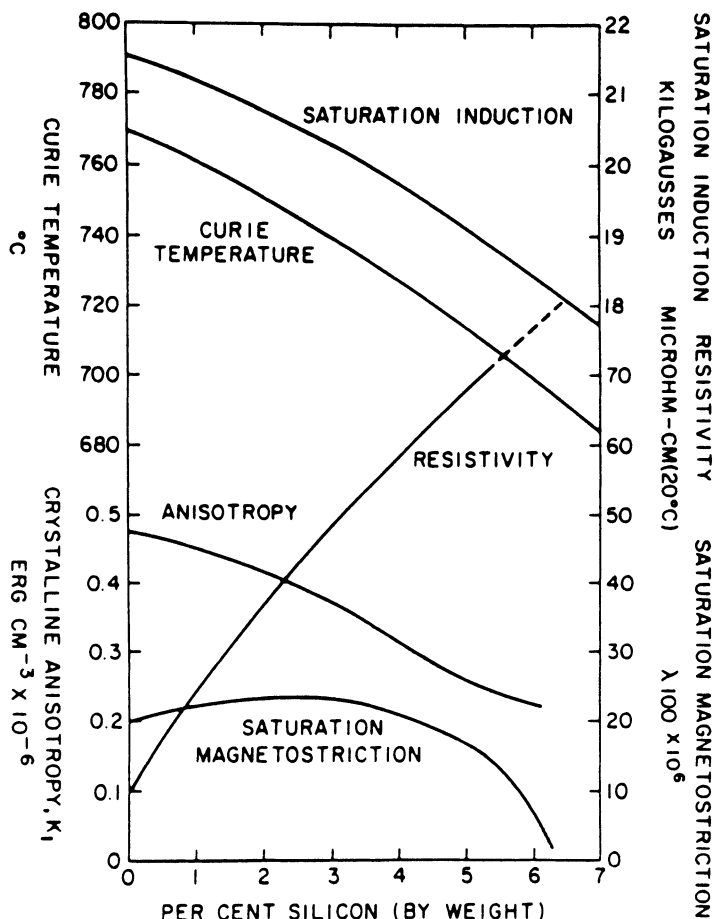


Fig. 12.4 Various magnetic and electrical properties of silicon-iron as a function of silicon content. © 1971 IEEE.

when so much transformer iron is needed. It has two main beneficial effects on the properties of the alloy. The conductivity is reduced as silicon is added and the magnetostriction is reduced as shown in Fig. 12.3. For a.c. applications this reduction of magnetostriction is an additional advantage since the cyclic stresses resulting from magnetostrictive strains at 50 or 60 Hz produce acoustic noise. Therefore any reduction of magnetostriction is desirable, particularly if it arises as a result of modifying the material to suit other unrelated requirements. A third benefit caused by the addition of silicon is that it reduces the anisotropy (Fig. 12.4) of the alloy leading to an increase in permeability in the non-oriented silicon-iron.

It is also beneficial to laminate the cores in such a way that the laminations run parallel to the magnetic field direction. This does not interfere with the magnetic flux path but does reduce the eddy current losses, by only allowing the eddy currents to exist in a narrow layer of material. The dependence of core losses at 60 Hz on sheet thickness is shown in Fig. 12.5. Furthermore the coating of laminations with an insulating material also improves the eddy current losses by preventing current passing from one layer to the next. The thickness of the laminations is comparable with the skin depth at 50 or 60 Hz, which is typically 0.3–0.7 mm [8], for optimum performance.

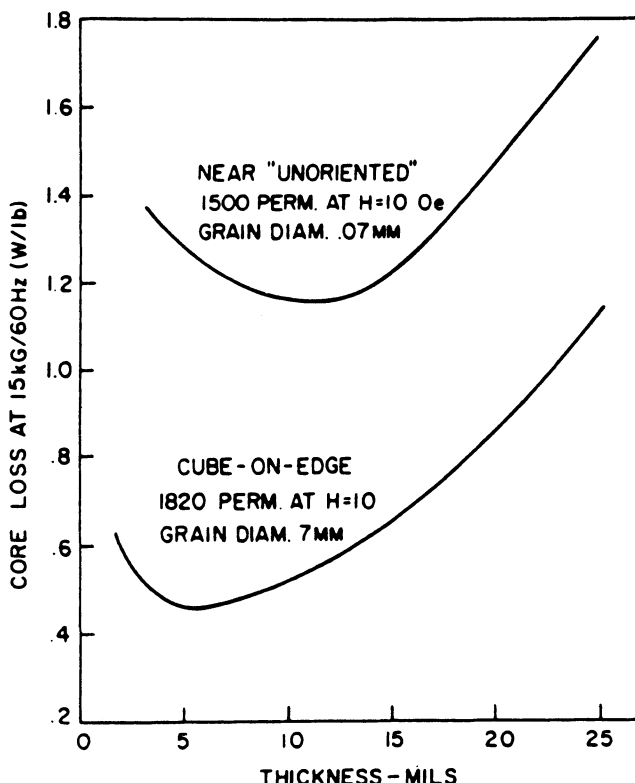


Fig. 12.5 Dependence of core loss on sheet thickness in 3.15% silicon-iron.

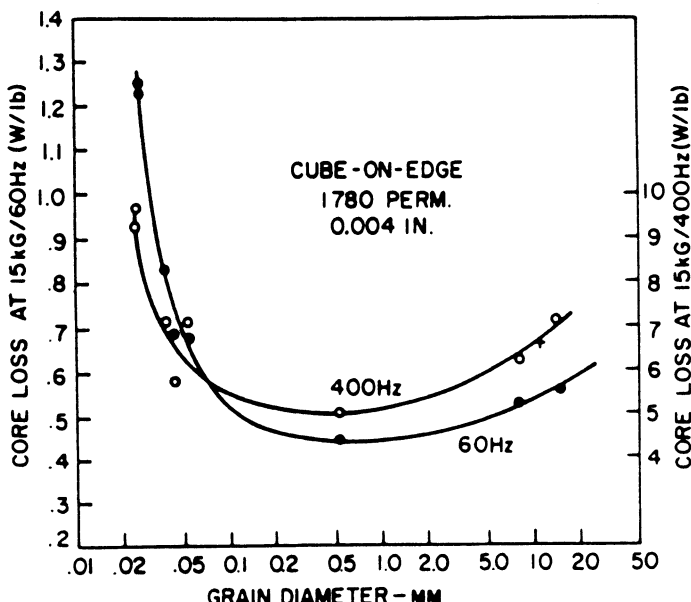


Fig. 12.6 Dependence of core loss on grain size in 3.15% silicon-iron sheets.

Since in these applications the magnetic flux only passes in one direction along the laminations it is advantageous to ensure that the permeability is highest along this direction. Therefore techniques have been devised for producing grain-oriented silicon-iron by hot and cold rolling and annealing which result in the [001] direction lying along the length of the laminations. The <001> directions are the magnetically easy axes. The addition of silicon to iron increases the grain size so that the grain diameters in 3% silicon-iron can be as large as 10 mm. The core losses of 3.15% silicon-iron vary with grain size as shown in Fig. 12.6 in which a minimum in core loss occurs at a grain diameter of between 0.5 and 1.0 mm.

There are nevertheless some disadvantages involved with the addition of silicon to iron. At higher silicon contents the alloy becomes very brittle and this makes a practical limitation on the level of silicon that can be added without the material becoming too brittle to use. This limit is about 4% and most silicon-iron transformer material has a composition of 3–4% Si, although material with a silicon content of 6% with adequate mechanical properties for transformer applications has recently been developed. Another disadvantage resulting from the addition of silicon to iron is the reduction of saturation induction.

12.2.2 Iron-aluminum alloys

The properties of aluminum-iron are very similar to those of silicon-iron and since aluminum is rather more expensive than silicon these alloys are unlikely to replace silicon-iron in applications where they compete. Furthermore the

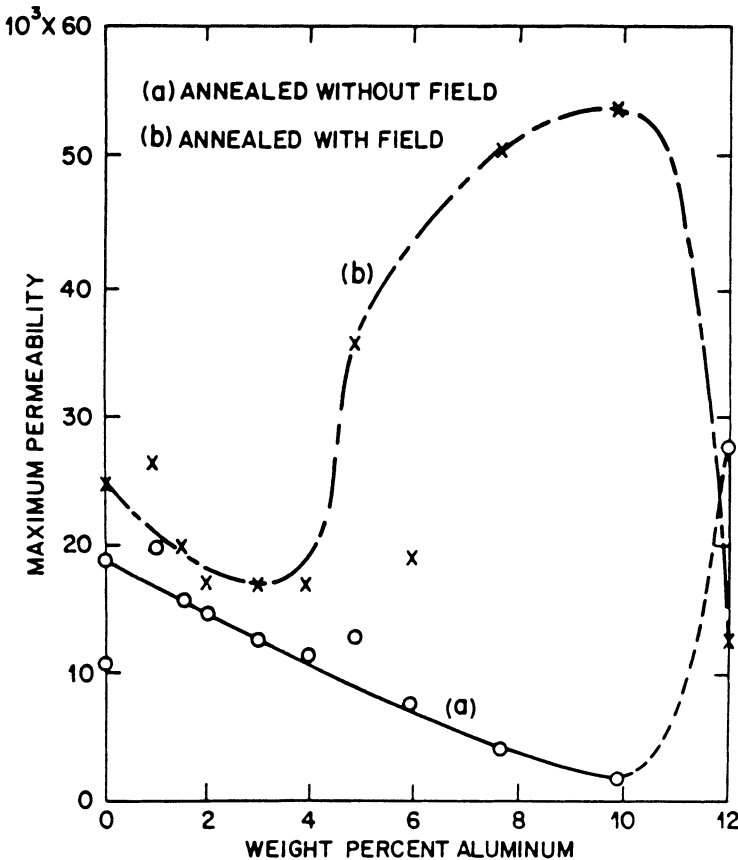


Fig. 12.7 Maximum permeability of iron–aluminium alloys as a function of aluminium content after two different types of anneal. The field anneal was in a magnetic field of 136 A/m. Specimens were 0.35 mm thick laminations.

presence of Al_2O_3 particles in iron–aluminum alloys causes rapid wear of punching dies which is disadvantageous. To date therefore the binary aluminum–iron alloys have made little commercial impact.

The magnetic properties of some aluminum–iron alloys are shown in Figs. 12.7 and 12.8. Alloys of up to 17% Al are ferromagnetic but at higher aluminum contents the alloys become paramagnetic. Often aluminum is used as an addition in silicon–iron because it promotes grain growth, which can lead to lower losses. Furthermore the addition of aluminum produces higher resistivity with less danger from brittleness. Therefore ternary alloys of iron, silicon and aluminum are used in electrical steels for special applications.

12.2.3 Nickel–iron alloys (Permalloy)

These alloys are the most versatile of all soft magnetic materials for electromagnetic applications. Only the alloys with above 30% nickel are widely

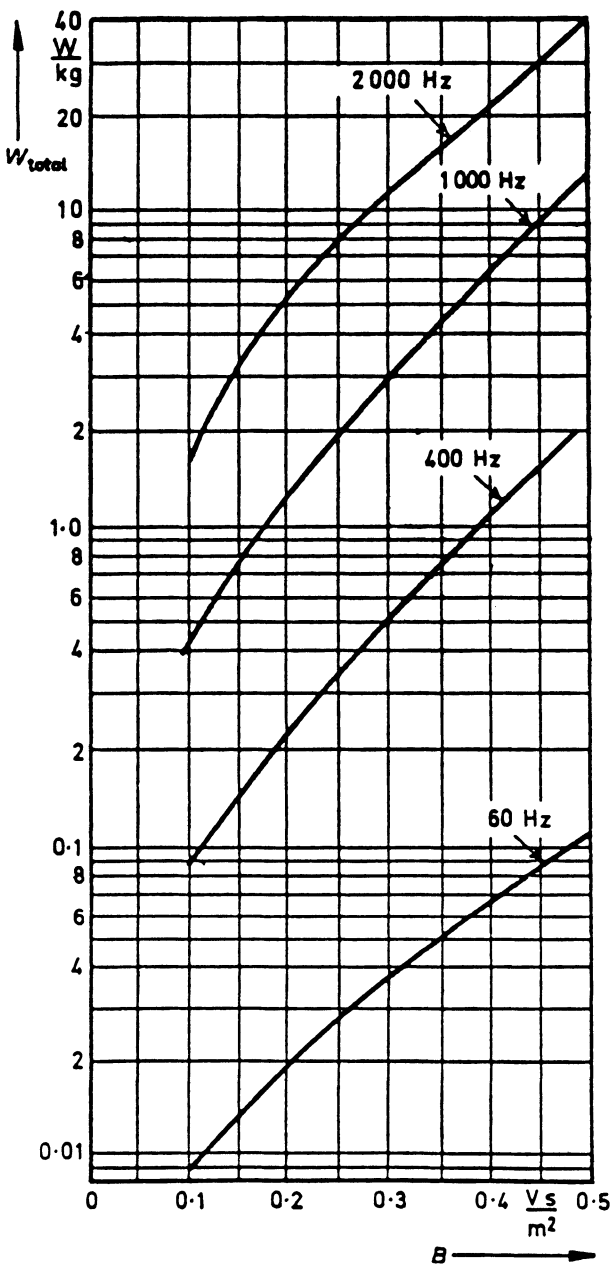


Fig. 12.8 Total core loss as a function of peak magnetic induction for laminated 0.35 mm sheets of iron-16% aluminium.

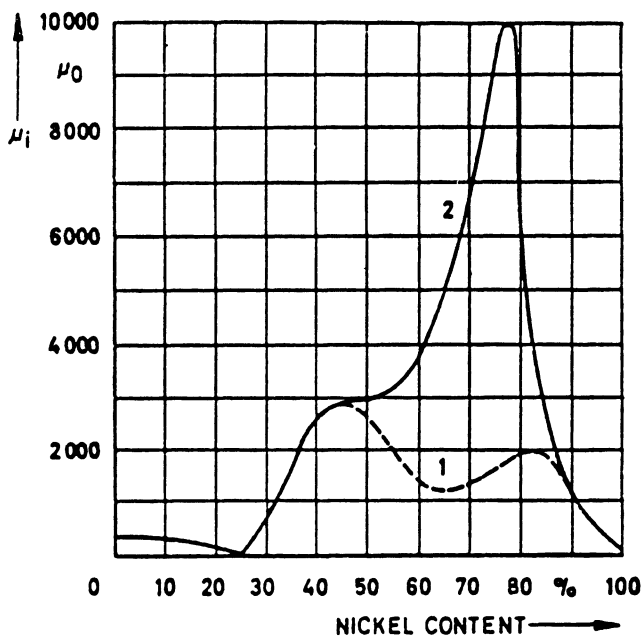


Fig. 12.9 Initial permeability of iron–nickel alloys: 1, slow cooled; and 2, normal permalloy treatment.

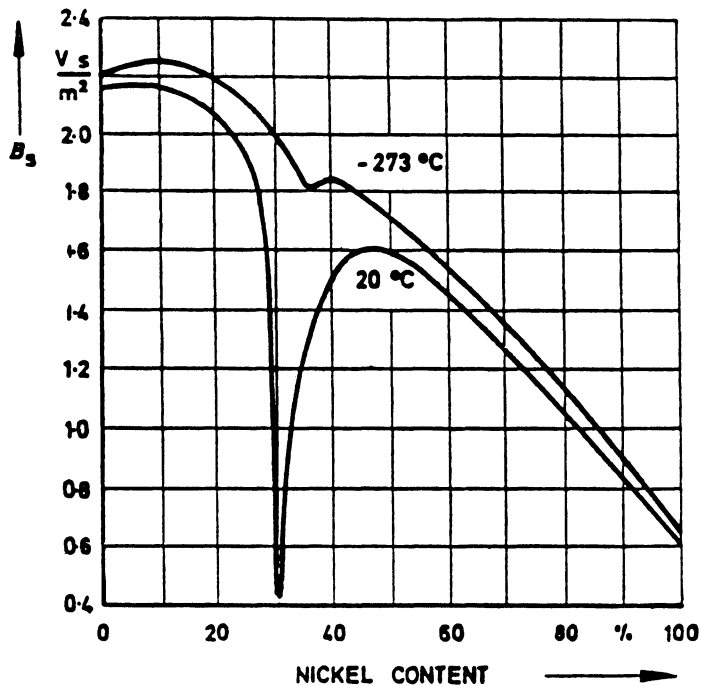


Fig. 12.10 Saturation magnetic induction in iron–nickel alloys.

used because at lower nickel contents there is a lattice transformation which occurs as a function of temperature. This transformation exhibits temperature hysteresis and hence there is no well-defined Curie temperature. As a result of this complication the alloys in this range are not widely used.

Three groups of these alloys are commonly encountered [9]. These have nickel contents close to 80%, 50% or in the range 30–40%. The permeability is highest for the alloys close to 80% Ni, as shown in Fig. 12.9. The saturation magnetization is highest in the vicinity of 50% Ni (Fig. 12.10). The electrical resistivity is highest in the 30% Ni range (Fig. 12.11). These are the three magnetic properties which are of most interest in soft magnetic material applications and so the alloys used are often close to one of these compositions depending on the specific application.

The main uses of these alloys are in inductance coils and transformers, particularly power supply transformers. They are used at audio frequencies as transformer cores and also for much higher frequency applications. They can be made with low, or even zero, magnetostriction (Fig. 12.12). Some of the high permeability alloys, Mumetal and Supermalloy, have relative permeabilities of up

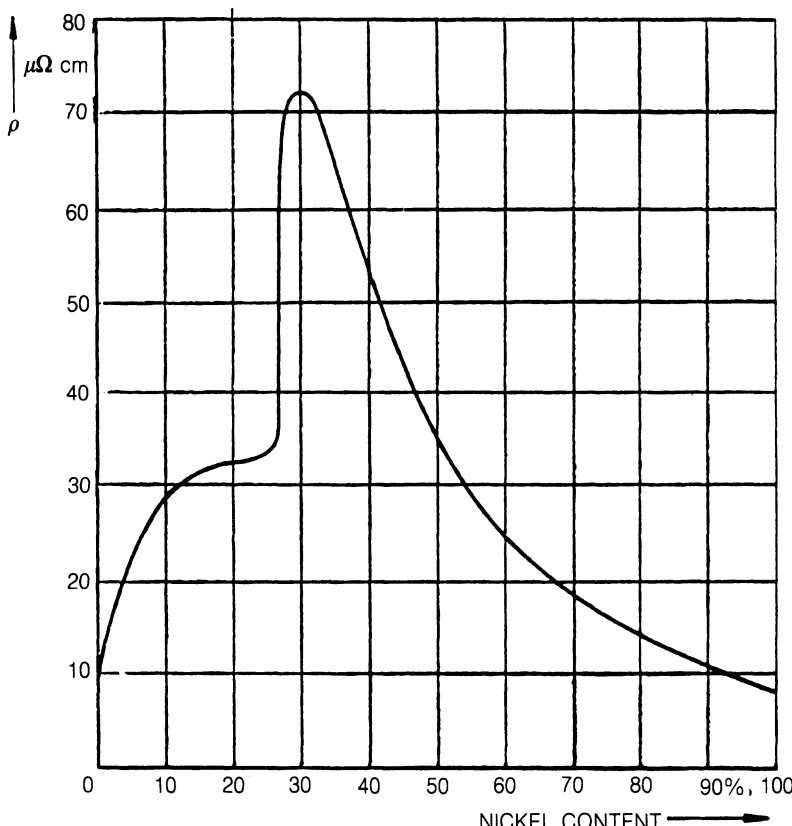


Fig. 12.11 Electrical resistance in iron–nickel alloys.

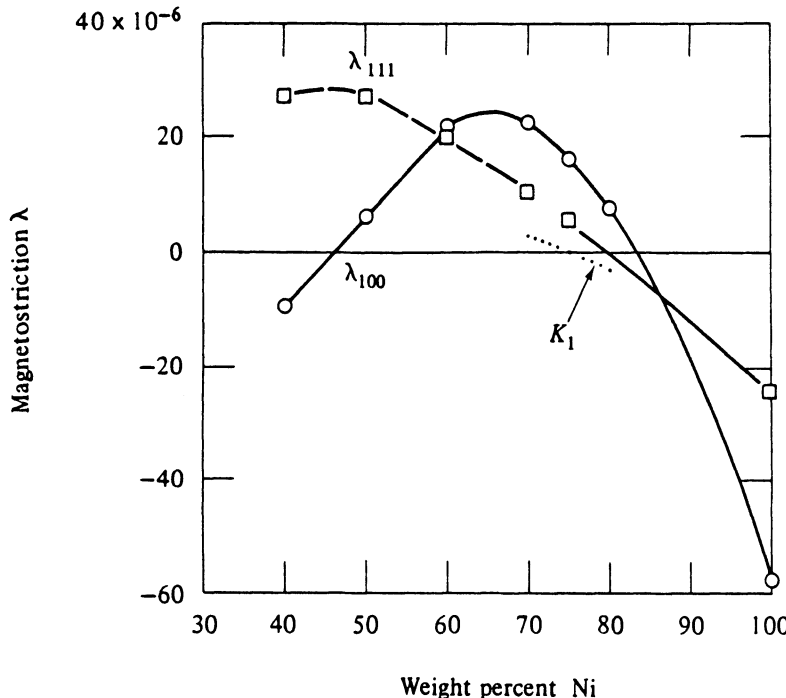


Fig. 12.12 Dependence of magnetostriction coefficients λ_{100} and λ_{111} with nickel content in iron–nickel alloys.

to 3×10^5 and coercivities down to 0.4 A/m. They also have low anisotropy and this contributes to their high permeability in the polycrystalline form.

Permalloy and Mumetal, both Ni–Fe alloys with close to 80% Ni, are used in magnetic screening because of very high permeability. Some of these alloys can reach an induction of 0.6 T in a field as low as 1.6 A/m, corresponding to a relative permeability of $\mu_r = 3 \times 10^5$. In these applications the low saturation of the material is not a disadvantage since the magnetic screen can always carry more magnetic flux if it is made thicker.

Alloy additions to the basic iron–nickel alloy and processing allow the magnetic properties of these alloys to be varied within wide limits. Cold working by rolling gives rise to high permeability perpendicular to the field as in Isoperm, a 50%–50% Fe–Ni alloys. Invar is a 64% Fe 36% Ni alloy with zero thermal expansion.

High-quality transformers are often made of this material. Relative permeabilities of up to 100 000 are attainable with coercivities in the range 0.16–800 A/m (0.002 to 10 Oe) and these can be adjusted with precision by suitable processing of the material. The core losses of two commercial Ni–Fe alloys are shown in Fig. 12.13.

This alloy system is also used in some magnetic memory devices and amplifiers. For high-frequency applications of up to 100 kHz the alloy can be used in the form of powdered cores in which each particle is by virtue of its nature electrically insulated from others and therefore the bulk conductivity of the material is low.

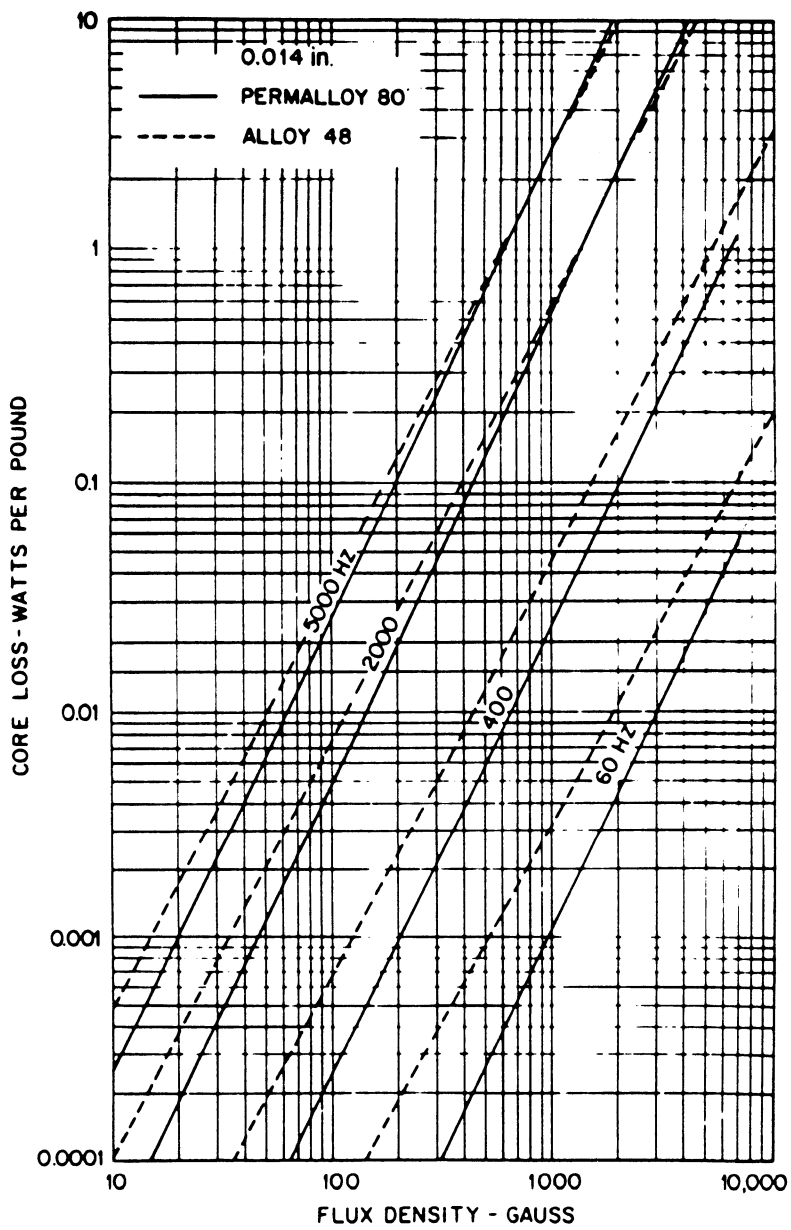


Fig. 12.13 Core losses against peak magnetic induction and frequency for 0.35 mm thick laminations of two commercial nickel-iron alloys; Permalloy 80 and Alloy 48.

12.2.4 Amorphous metals (metallic glasses)

These materials have only been developed in the last 20 years. They are produced by rapid cooling (quenching) of magnetic alloys consisting of iron, nickel and/or cobalt together with one or more of the following elements: phosphorus, silicon, boron and sometimes carbon [10]. Even in the as cast condition these alloys have very soft magnetic properties but the rapidly quenched material has even better properties for soft magnetic material applications. The molten metal is sprayed in a continuous jet under high pressure on to a rapidly moving cold surface such as the surface of a rotating metal wheel. The material is produced in the form of a thin ribbon.

As a result of the rapid cooling the materials do not form a crystalline state but instead produce a solid with only short-range order with otherwise random microstructural properties. These materials can be considered as a random packing of spheres. They are also known as 'metallic glasses' because of this random structure. The materials produced in this way have large internal strains, which as we know lead to high coercivity and low permeability. This can be altered by annealing the material at intermediate temperatures in order to relieve the strains without leading to recrystallization.

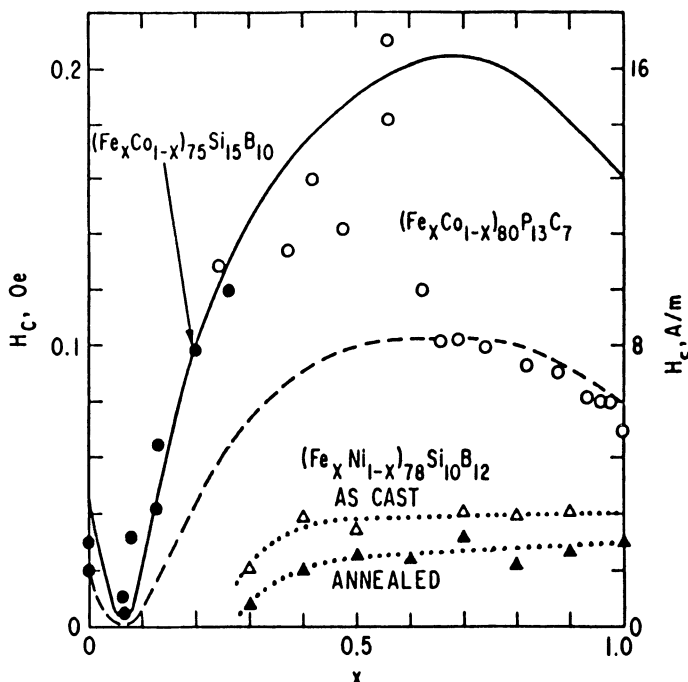


Fig. 12.14 Variation of coercivity of a number of amorphous alloys with chemical composition.

About ten years ago amorphous alloys were considered to have great promise and a large effort was expended to further develop them. The main interest arose from the low coercivities, as shown in Fig. 12.14., which were an order of magnitude smaller than silicon–iron while the permeability was about an order of magnitude greater. The hysteresis loops of the Fe₈₀B₂₀ material (Metglas 2605CO) at different frequencies are shown in Fig. 12.15. Core losses are also very low as indicated in Figs. 12.16 and 12.17. Such properties were perceived to be a distinct advantage, however certain disadvantages turned out to be even more significant.

One of the disadvantages is the low saturation magnetization of the alloys, as shown in Fig. 12.18, which limits their use in heavy current engineering when compared for example with silicon–iron. Secondly at higher flux densities their core losses begin to increase rapidly. Therefore their general applicability has fallen far short of expectations.

There is a better market for these alloys in rather low-current applications and specialized small-device applications in which transformers are needed with only moderate flux densities where the amorphous alloys can compete successfully with the nickel–iron alloys such as Permalloy. These alloys are now being produced in large quantities and are finding specific uses in pulsed power transformers and in magnetic sensors and magnetostrictive transducers. Also because of their unique metallurgical properties they continue to provide scientific interest for researchers in magnetism.

Amorphous alloys with widely differing magnetic hysteresis properties can be produced by annealing in the presence of a magnetic field. They can be used in low-

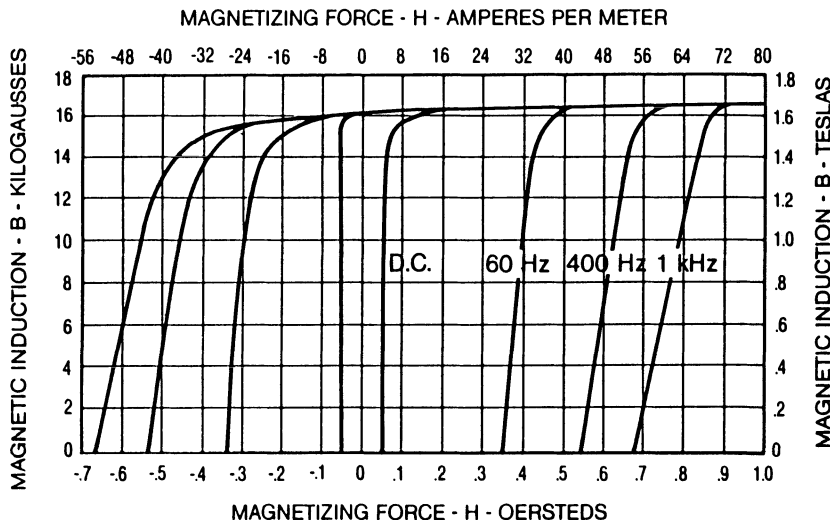


Fig. 12.15 Upper two quadrants of the hysteresis loops of Metglas 2605CO at different frequencies.

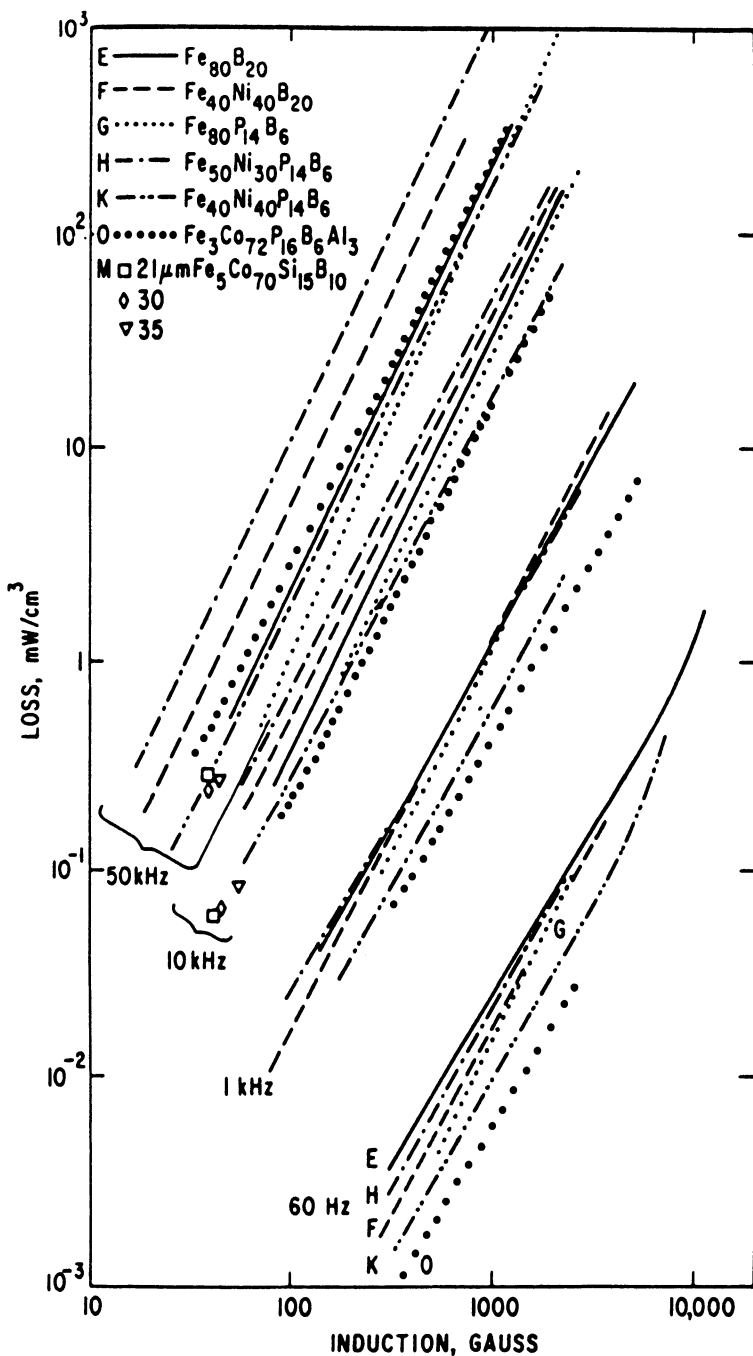


Fig. 12.16 Dependence of core loss on magnetic induction and frequency for various amorphous alloys. All sample thicknesses were in the range 25–50 μm .

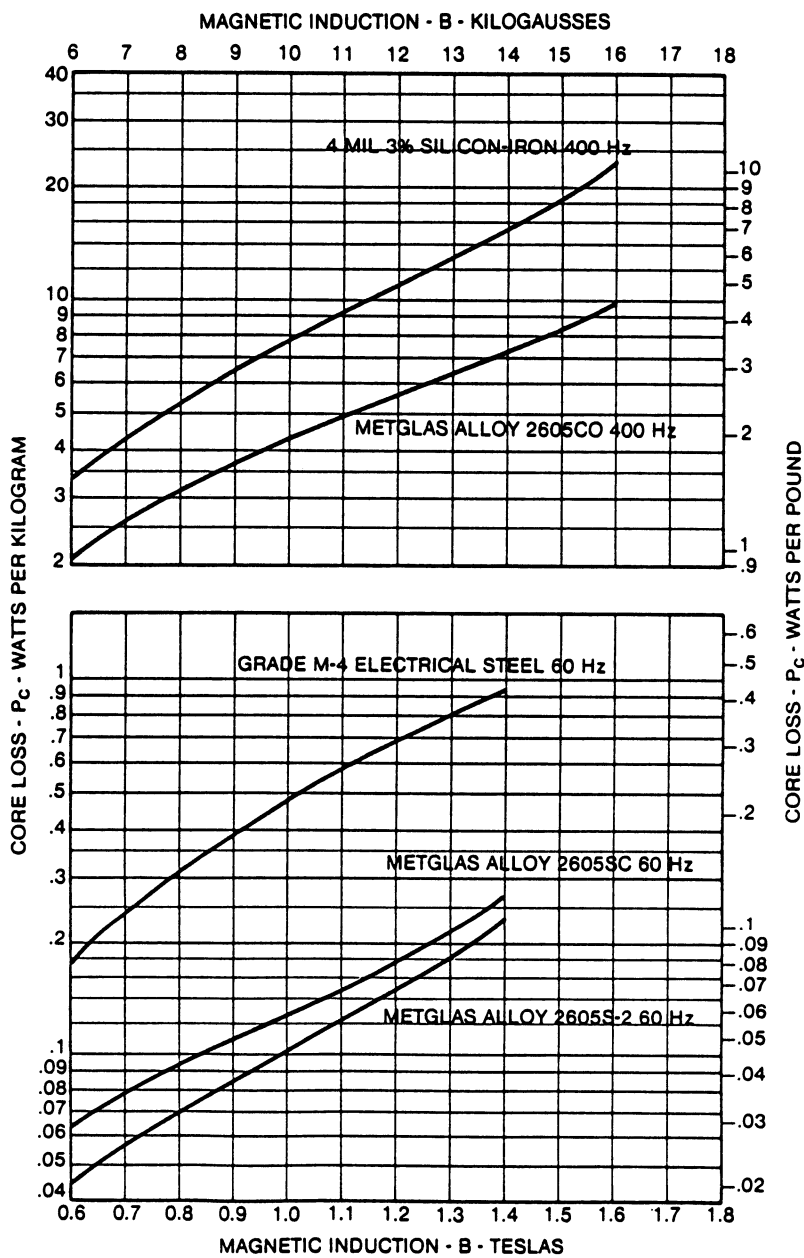


Fig. 12.17 Comparison of core losses for different soft magnetic materials as a function of peak magnetic induction.

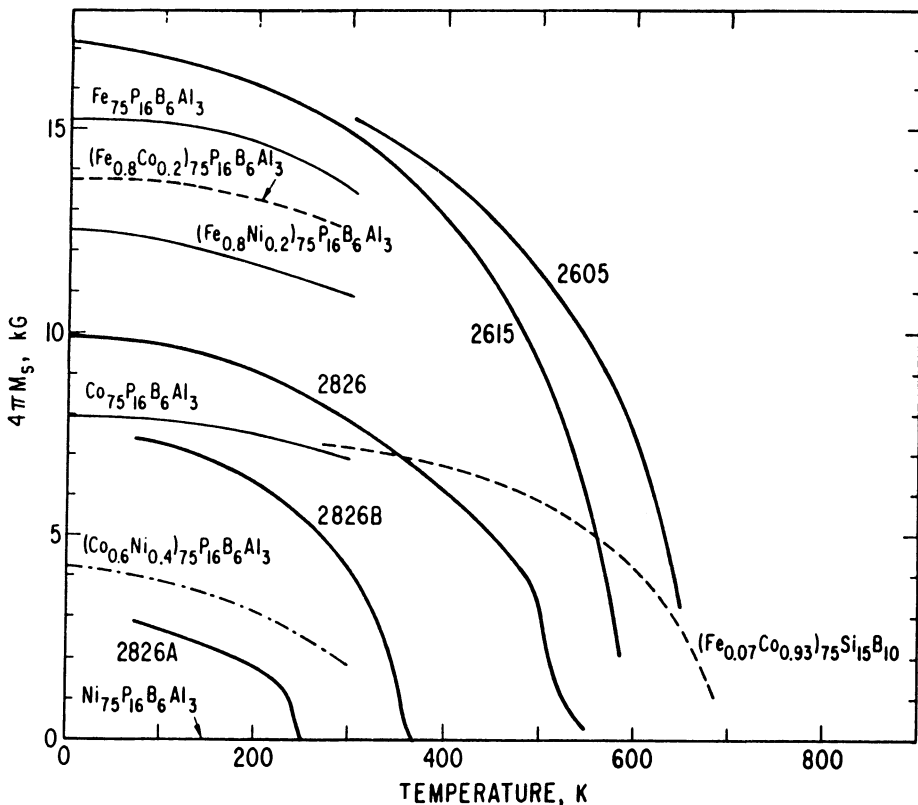


Fig. 12.18 Temperature dependence of the saturation magnetic induction for different amorphous alloys. Allied Chemical Metglas alloys are as follows: 2605 is $\text{Fe}_{80}\text{B}_{20}$; 2615 is $\text{Fe}_{80}\text{P}_{16}\text{C}_3\text{B}$; 2826 is $\text{Fe}_{40}\text{Ni}_{40}\text{P}_{14}\text{B}_6$; 2826A is $\text{Fe}_{32}\text{Ni}_{36}\text{Cr}_{14}\text{P}_{12}\text{B}_6$; and 2826B is $\text{Fe}_{29}\text{Ni}_{49}\text{P}_{14}\text{B}_6\text{Si}_2$.

power transformers which are needed in communications equipment for example. The magnetic properties of a range of amorphous alloys is shown in Table 12.2.

12.2.5 High-frequency applications: soft ferrites

For high-frequency applications the conductivity of metals limits their use and so we must turn to magnetic insulators. These materials must of course exhibit the usual properties associated with soft ferromagnets: high permeability, low coercivity and high saturation magnetization. In these applications soft ferrites are widely used. Ferrites are ceramic magnetic solids which first appeared commercially in 1945. They are ferrimagnetic but on the bulk scale behave in much the same way as ferromagnets. The cubic or soft ferrites all have the general chemical formula $MO \cdot \text{Fe}_2\text{O}_3$, where M is a transition metal such as nickel, iron, manganese, magnesium or zinc. The most familiar of these is Fe_3O_4 . The ferrite

Table 12.2 Magnetic properties of amorphous alloys under d.c. conditions

Alloy	Shape	As cast			Annealed		
		H_c (A/m)	M_r/M_s	μ_{\max} (10^3)	H_c (A/m)	M_r/M_s	μ_{\max} (10^3)
Metglas #2605 $\text{Fe}_{80}\text{B}_{20}$	Toroid	6.4	0.51	100	3.2	0.77	300
Metglas #2826 $\text{Fe}_{40}\text{Ni}_{40}\text{P}_{14}\text{B}_6$	Toroid	4.8	0.45	58	1.6	0.71	275
Metglas #2826 $\text{Fe}_{29}\text{Ni}_{44}\text{P}_{14}\text{B}_6\text{Si}_2$	Toroid	4.6	0.54	46	0.88	0.70	310
$\text{Fe}_{4.7}\text{Co}_{70.3}\text{Si}_{15}\text{B}_{10}$ $(\text{Fe}_{8.2}\text{Ni}_{1.2})_{78}\text{Si}_8\text{B}_{14}$	Strip	1.04	0.36	190	0.48	0.63	700
Metglas #2615 $\text{Fe}_{80}\text{P}_{16}\text{C}_3\text{B}$	Toroid	4.96	0.4	96	4.0	0.42	130

$\text{CoO}\cdot\text{Fe}_2\text{O}_3$ although of the same general type is nevertheless a hard ferrite rather than a soft ferrite. The magnetic garnets were discovered by Bertaut and Forret [11]. Yttrium–iron garnet is the best-known example of these.

Soft ferrites can be further classified into the ‘non-microwave ferrites’ [12] for frequencies from audio up to 500 MHz and ‘microwave ferrites’ for frequencies from 100 MHz to 500 GHz [13]. Microwave ferrites, such as yttrium–iron garnet, are used as waveguides for electromagnetic radiation and in devices such as phase shifters.

Soft ferrites are also used in frequency selective circuits in electronic equipment, for example in telephone signal transmitters and receivers. Manganese–zinc ferrite, which is sold under the commercial name of Ferroxcube, is widely used for applications at frequencies of up to 10 MHz, while beyond that frequency nickel–zinc ferrites are preferred because they have lower conductivity. Another area where ferrites find wide application is in antennae for radio receivers. Almost all radio receivers using amplitude modulation of signals are now provided with ferrite rod antennae. Other applications include waveguides and wave shaping for example in pulse-compression systems.

The permeability of these materials does not change much with frequency up to a critical frequency but then decays rapidly with increasing frequency. The critical frequency of these materials varies between 10 MHz and 100 MHz. The saturation magnetization of ferrites is typically 0.5 T, which is low compared with iron and cobalt alloys.

For very high-frequency applications, beyond 100 MHz, there are other materials such as the hexagonal ferrites which have special properties which make them suitable for use at these frequencies. These materials are uniaxial with magnetic moments confined to the hexagonal base plane.

12.3 MATERIALS FOR D.C. APPLICATIONS

In d.c. applications the need for a low conductivity does not arise and so there are fewer constraints on the type of material suitable for particular applications. These applications generally require low coercivity and high permeability. High permeability is best achieved through high saturation magnetization and this means that alloys of iron and cobalt are widely used. A review of soft magnetic materials for d.c. applications has been given by Chin and Wernick [14].

12.3.1 Iron and low-carbon steels (soft iron)

These were the original materials for transformers, motors and generators but have been superseded by silicon–iron both in its oriented form for transformers and in its non-oriented form for motors and generators.

Soft iron is used as a core material for d.c. electromagnets such as laboratory electromagnets for which it remains the best material. The prime concern is merely to obtain either high fields and/or very uniform magnetic fields. Iron with low levels of impurities such as carbon (0.05%) and nitrogen has a coercivity of about 80 A/m (1 Oe) and a maximum relative permeability of the order of 10 000. By annealing in hydrogen the impurities can be removed and this results in a reduction in coercivity to 4 A/m (0.05 Oe) and an increase in maximum relative permeability to about 100 000 as shown in Table 12.3. The highest relative permeability obtained

Table 12.3 Magnetic properties of various high-purity forms of iron

	<i>Saturation induction</i> B_s (T)	<i>Coercivity</i> H_c (A/m)	<i>Relative permeability at</i> 80 A/m	800 A/m	<i>Maximum relative permeability</i> μ_{\max}
Cast magnetic ingot iron	2.15	68	3500	1500	—
Magnetic ingot iron (2 mm sheet)	2.15	89	1800	1575	—
Electromagnet iron (2 mm sheet)	2.15	81.6	2750	1575	—
Ingots iron (vacuum melted)	—	24.8	—	—	21 000
Electrolytic iron (annealed)	—	18.4	—	—	41 500
Electrolytic iron (vacuum melted and annealed)	—	7.2	—	—	61 000
Puron (H_2 treated)	2.16	4.0	—	—	100 000

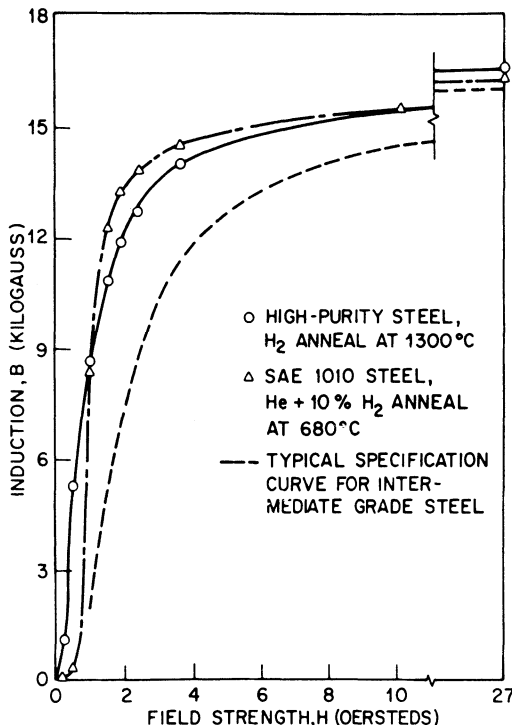


Fig. 12.19 Initial magnetization curves for two high-purity steels, after annealing in a reducing atmosphere of hydrogen and a typical intermediate-grade steel, after Swisher (1969) [15] and Swisher and Fuchs (1970) [16].

for pure iron is 1.5×10^6 , however the problem with this from a commercial viewpoint is that it is too expensive for many applications.

In most applications ultra-high-purity iron is unnecessary. A typical commercial soft iron for electromagnet applications will therefore contain about 0.02% C, 0.035% Mn, 0.025% S, 0.015% P and 0.002% Si in the form of impurities. The magnetization curves of high-purity iron and a commercial soft iron after annealing in hydrogen to remove impurities are shown in Fig. 12.19.

For electromagnets the principle question that arises is what field is necessary to produce an induction of 1.0 T or 1.5 T. For the commercial soft iron given above the values are typically 200 A/m and 700 A/m, respectively.

Any form of mechanical deformation will result in a deterioration of the magnetic properties of soft iron for electromagnet applications. The internal stresses produced by such cold working can be removed by annealing at temperature between 725 °C and 900 °C providing the material does not suffer oxidation during the anneal which would also result in impaired magnetic properties. The usual procedure now is to anneal in a hydrogen atmosphere which has the additional advantage of removing some of the impurities. The variation of coercivity with impurity nitrogen and carbon content is shown in Figs. 12.20 and 12.21.

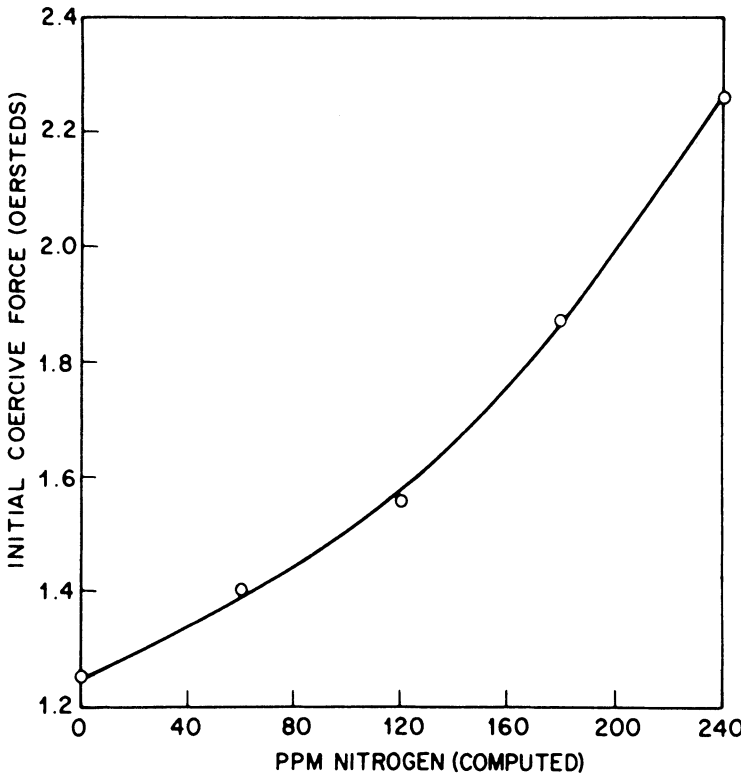


Fig. 12.20 Dependence of coercivity on nitrogen content in high-purity iron, after Swisher (1969) and Swisher and Fuchs (1970).

12.3.2 Iron–nickel alloys (Permalloy)

Iron and nickel form a number of commercially important alloys, most of which are in the ‘Permalloy’ range with nickel contents above 35%. For d.c. applications the iron–nickel alloys are very versatile since by suitable alloying they can be produced with a wide range of properties. Among these it is possible to produce for example an alloy with zero magnetostriction (19%Fe–81%Ni).

The low coercivity of these alloys can be seen from Table 12.4 and this has made them ideal for relays with a short release time. Both 30% Fe–50% Ni and Mumetal are used for the cores. However the low saturation magnetization of these alloys has meant that they are not widely used in relays in general.

The nickel–iron alloys in general have very high permeabilities, as shown in Tables 12.4 and 12.5. The maximum permeability of the polycrystalline alloy is expected to occur when the anisotropy and magnetostriction are small. The value of the anisotropy constant K_1 is zero at a nickel content of 78%. The addition of 5% copper to Permalloy produces the alloy known as Mumetal, although these days commercial Mumetal also contains 2% Cr. Its magnetic properties are no better

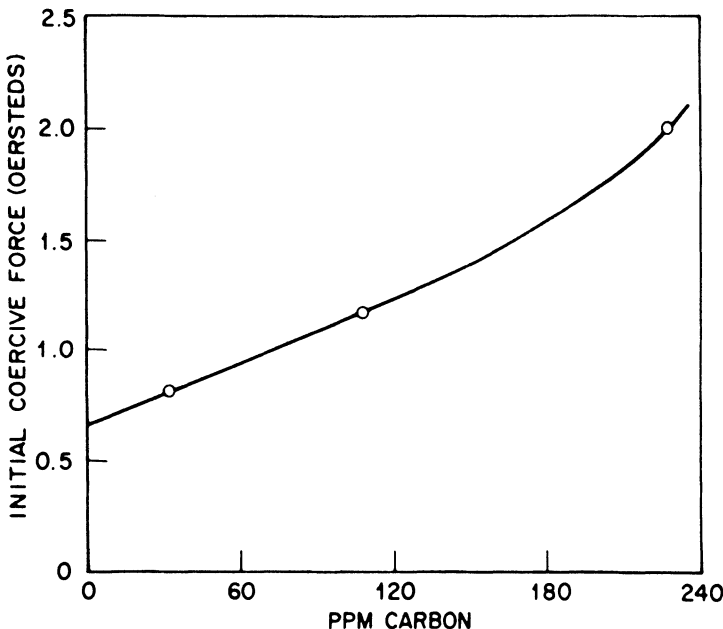


Fig 12.21 Dependence of coercivity on carbon content in high-purity iron, after Swisher (1969) and Swisher and Fuchs (1970).

Table 12.4 Selected magnetic properties of materials used for relays

	<i>Relative permeability</i> μ_{\max}	<i>Saturation induction</i> B_s (T)	<i>Coercivity</i> H_c (A/m)	<i>Remanence</i> B_r (T)
<i>Unalloyed iron</i>				
Auto machining iron	4300–8000	2.05	60–140	0.8
Open smelted iron	2200–7500	2.15	24–120	0.9
Vacuum smelted iron	—	2.15	16–40	—
Carbonyl iron	30 000	2.15	8–24	0.8
Carbonyl iron (critically stretched)	40 000	2.15	6–10	0.8
<i>Silicon steels</i>				
Fe-1% Si	4000–15 000	2.1	30–120	0.9–1.45
Fe-2.5% Si	4000–12 000	2.0	12–120	0.8–1.2
Fe-4% Si	5000–20 000	2.0	5–90	0.8–1.2
<i>Nickel Steels</i>				
Fe-36% Ni	6000–14 000	1.3	8–24	0.8
Fe-50% Ni	15 000–60 000	1.55	5–14	0.8–1.2
Fe-78% Ni	5000–300 000	0.7	1–8	0.5–0.75

Table 12.5 Selected magnetic properties of different soft magnetic materials

	<i>Composition</i>	<i>Relative permeability</i> μ_i	μ_{\max}	<i>Coercivity</i> H_c (A/m)	<i>Saturation induction</i> B_s (T)
Iron	100% Fe	150	5000	80	2.15
Silicon–iron (Non-oriented)	96% Fe 4% Si	500	7000	40	1.97
Silicon–iron (Grain-oriented)	97% Fe 3% Si	1500	40 000	8	2.0
78 Permalloy	78% Ni 22% Fe	8000	100 000	4	1.08
Hipernik	50% Ni 50% Fe	4000	70 000	4	1.60
Supermalloy	79% Ni 16% Fe, 5% Mo	100 000	1 000 000	0.16	0.79
Mumetal	77% Ni, 16% Fe 5% Cu, 2% Cr	20 000	100 000	4	0.65
Permendur	50% Fe 50% Co	800	5000	160	2.45
Hiperco	64% Fe 35% Co, 0.5% Cr	650	10 000	80	2.42
Supermendur	49% Fe 49% Co, 2% V	—	60 000	16	2.40

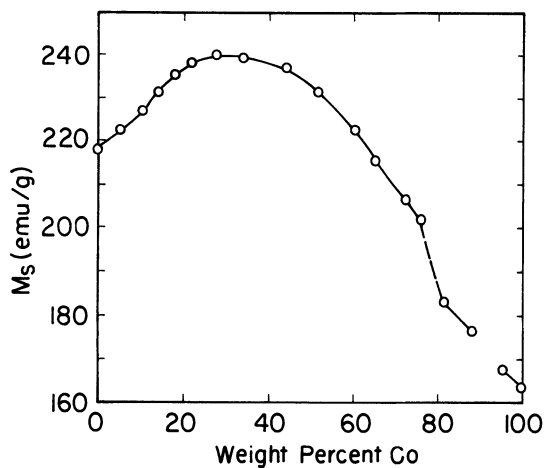


Fig. 12.22 Variation of saturation magnetization with composition in iron–cobalt alloys, after Weiss and Forrer (1929).

than permalloy but this metal is rather more ductile than permalloy and is therefore used in the form of thin sheets in magnetic shielding in order to prevent stray magnetic fields from affecting sensitive components.

Addition of cobalt to iron-nickel gives the so-called 'perminvar' ternary alloys which have constant permeability and zero hysteresis losses at low fields of up to 200 A/m.

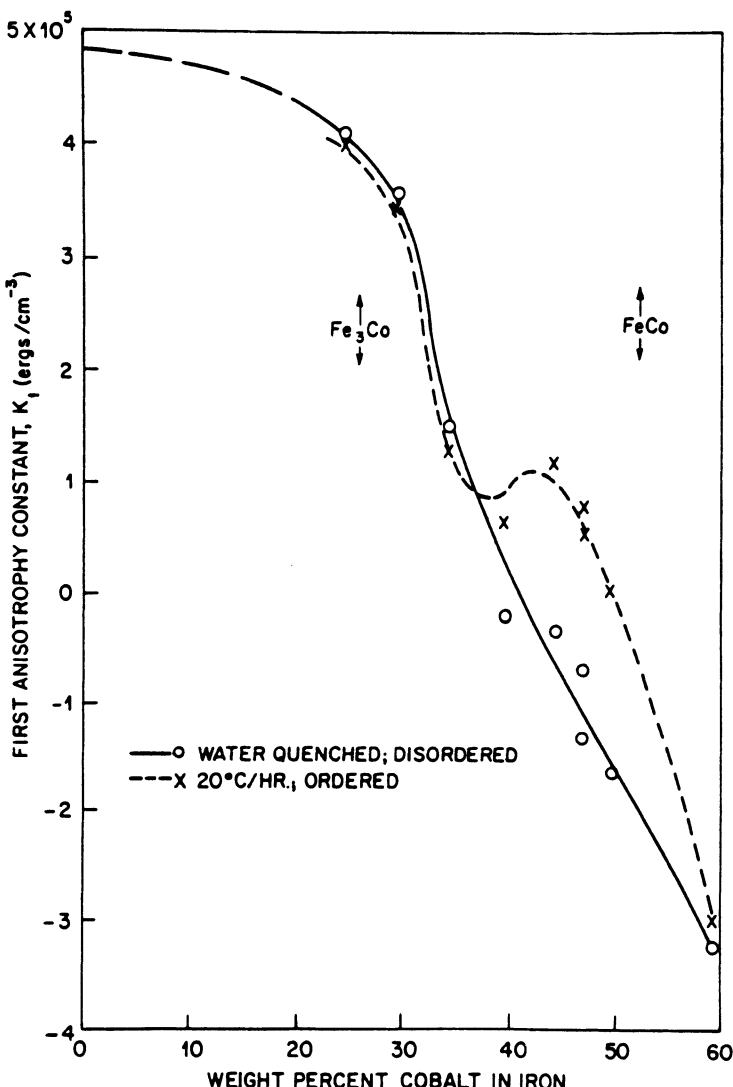


Fig. 12.23 Variation of the first anisotropy constant with composition in iron-cobalt alloys, after Hall (1960).

12.3.3 Iron-cobalt alloys (Permendur)

Cobalt is the only element which when alloyed with iron causes an increase in saturation magnetization (Fig. 12.22) and Curie temperature and so the cobalt-iron alloys are of some interest. These alloys have low anisotropy (Fig. 12.23) and high permeability (Fig. 12.24). They have found some applications in both a.c. and d.c. devices but the high cost of cobalt has been a limiting factor. Nickel and niobium are also now used as alloying constituents in iron-cobalt alloys.

The highest saturation magnetization occurs in 65% iron-35% cobalt alloys in which it reaches 1.95 MA/m. These binary alloys are brittle, but improved mechanical properties can be obtained by alloying with vanadium. Permendur which has a composition of 49% Fe, 49% Co, 2% V known as vanadium permendur has a saturation magnetization which is close to the maximum 1.95 MA/m and also has a permeability which remains constant with H over a wide range of fields.

The rather expensive cost of cobalt has also prevented the use of these alloys in

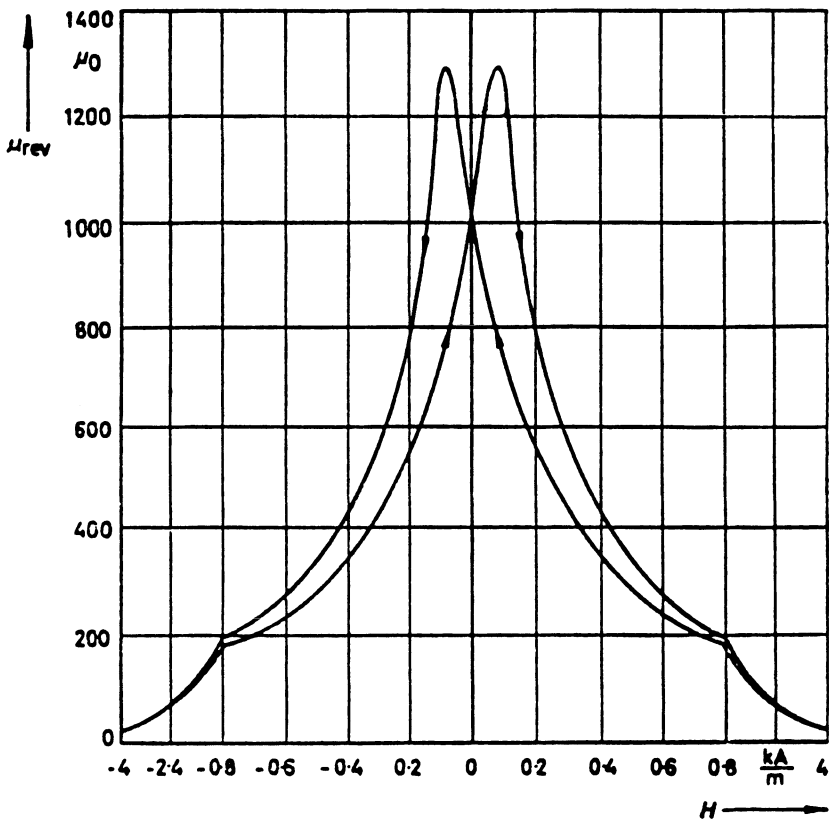


Fig. 12.24 Reversible permeability of permendur as a function of field strength measured with a small superimposed cyclic field of amplitude 0.34 A/m at a frequency of 200 Hz.

relay armatures where they would otherwise be the ideal material in view of their high saturation magnetization which would give rise to a large attractive force with which to operate the moving parts of the relay.

The ternary alloys are used in magnetic amplifiers and in some switching and memory-storage cores. They are used in diaphragms of high-quality telephone receivers, where the high value of reversible permeability at high flux density is important, and as the pole pieces of servomotors in the aircraft industry where high flux density is crucial. These alloys were also used previously to a lesser extent as magnetostrictive transducers, however there are now far superior magnetostrictive transducer materials available.

REFERENCES

1. Elmen, G. W. (1935; 1936) Magnetic alloys of iron, nickel and cobalt, *Elect. Engng*, **54**, 1292; **54**, 887.
2. Jakubovics, J. (1987) *Magnetism and Magnetic Materials*, Institute of Metals, London, p. 97.
3. Boll, R. (1978) *Vacuumschmelze Handbook of Soft Magnetic Materials*, Heyden, London.
4. Stephenson, E. T. (1985) *J. Appl. Phys.*, **57**, 4226.
5. Steinmetz, C. (1891) *Electrician*, **26**, 261.
6. Littmann, M. F. (1971) *IEEE Trans. Mag.*, **7**, 48.
7. Chen, C. W. (1977) *Magnetism and Metallurgy of Soft Magnetic Materials*, North Holland Publishing Company, Amsterdam p. 276.
8. Cullity, B. D. (1972) *Introduction to Magnetic Materials*, Addison-Wesley, Reading, Mass., p. 494.
9. Heck, C. (1974) *Magnetic Materials and their Applications*, Crane and Russak, New York, p. 392.
10. Luborsky, F. E. (1980) Amorphous ferromagnets, in *Ferromagnetic Materials*, Vol. 1 (ed. E. P. Wohlfarth), North Holland, Amsterdam.
11. Bertraut, F. and Forret, F. (1956) *Comptes Rend. Hebd. Seance. Acad. Sci.*, **242**, 382.
12. Slick, P. I. (1980) Ferrites for non-microwave applications, in *Ferromagnetic Materials*, (ed. E. P. Wohlfarth) North Holland, Amsterdam.
13. Nicolas, J. (1980) Microwave ferrites, in *Ferromagnetic Materials*, Vol. 2 (ed. E. P. Wohlfarth) North Holland, Amsterdam.
14. Chin, G. Y. and Wernick, J. H. (1980) Soft magnetic materials, in *Ferromagnetic materials*, (ed. E. P. Wohlfarth) North Holland, Amsterdam.
15. Swisher, J. H., English, A. T. and Stoffers, R. C. (1969) *Trans. A. S. M.*, **62**, 257.
16. Swisher, J. H. and Fuchs, E. O. (1970) *J. Iron. Steel. Inst.* August, 777.

FURTHER READING

- Boll, R. (ed.) (1978) *Vacuumschmelze Handbook of Soft Magnetic Materials*, Heyden, London.
- Chin, G. Y. and Wernick, J. H. (1980) Soft magnetic materials, in *Ferromagnetic materials*, Vol. 2 (ed. E. P. Wohlfarth), North Holland, Ch. 2.
- Cullity, B. D. (1972) *Introduction to Magnetic Materials*, Addison-Wesley, Reading, Mass., Ch. 13.
- Heck, C. (1972) *Magnetic Materials and their Applications*, Crane Russak & Co. New York Ch. 10-13.

298 Soft magnetic materials

- Hummel, R. E. (1985) *Electronic Properties of Materials*, Springer-Verlag, Ch. 17 Berlin.
- Luborsky, F. E. (1980) Amorphous ferromagnets, in *Ferromagnetic Materials*, Vol. 1 (ed. E. P. Wohlfarth), North Holland, Ch. 6.
- Siemens Akgt (1987) *Siemens Ferrites: Soft Magnetic Materials Data Book*, Munich.
- Snelling, E. C. (1988) *Soft Ferrites, Properties and Applications*, 2nd edn, Butterworths, London.
- Valvo Inc. (1987) Ferroxcube Datenbuch, Huthig Verlag GmbH, Heidelberg.

13

Hard Magnetic Materials

In this chapter we consider the properties of ferromagnets that make them useful as permanent magnets. A number of different materials are now available and improvements in properties such as coercivity and maximum energy product continue to be made, as in the recent discovery of neodymium–iron–boron permanent magnets. There is a wide range of applications of permanent magnets from heavy current engineering such as in electrical motors and generators to very small-scale uses for example control devices for electron beams and moving-coil meters, and intermediate power range applications such as microphones and loudspeakers.

13.1 PROPERTIES AND APPLICATIONS

A permanent magnet is a passive device used for generating a magnetic field. That is to say it does not need an electric current flowing in a coil or solenoid to maintain the field. The energy needed to maintain the magnetic field has been stored previously when the permanent magnet was ‘charged’ (i.e. magnetized initially to a high field strength and then to remanence when the applied field was removed). Permanent magnets are used for field generation in a variety of situations in which it is difficult to provide electrical power, as in portable equipment, or where geometrical constraints such as space restrictions dictate their use rather than electromagnets.

When ferromagnetic materials are used as permanent magnets they must operate in conditions where at best they are subject to their own demagnetizing field and at worst can be subjected to various demagnetizing effects of other magnetic materials or magnetic fields in their vicinity. It is therefore essential that they are not easily demagnetized.

In addition a permanent magnet is only of use if it has a relatively high magnetization when removed from the applied magnetic field. Therefore a high remanence is also desirable and this inevitably means a high saturation magnetization. However most of the other properties that were considered desirable in soft magnetic materials, such as high permeability and low conductivity, are irrelevant in hard magnetic materials.

13.1.1 Coercivity

Since the permanent magnets operate without an applied field their ability to resist demagnetization is an important quality and consequently a high coercivity is desirable. Over the years there has been continual progress in the discovery of new permanent magnet materials with higher coercivities [1]. The coercivity is used to distinguish between hard and soft magnetic materials. The hard magnetic materials are classified rather arbitrarily to have coercivities above 10 kA/m (125 Oe). Recent permanent magnet materials have coercivities two orders of magnitude greater than this. For example the intrinsic coercivity is typically 1.1 MA/m (14 000 Oe) in neodymium–iron–boron, 0.69 MA/m (8700 Oe) in samarium–cobalt and 56 kA/m (700 Oe) in Alnico [2].

Unlike soft magnetic materials, in which B is approximately equal to $\mu_0 M$, in permanent magnets the magnetization is not simply an approximate linear function of the flux density because the values of magnetic field H used in the permanent magnets are generally much larger than in soft magnetic materials. The result is that the coercivity can be defined as either the field at which the magnetization is zero, the intrinsic coercivity $_m H_c$, or the field at which the magnetic flux density in the material is zero $_B H_c$. These quantities have quite different values in hard magnetic materials, and the greater the difference the better the material is as a permanent magnet. It should be noted that $_m H_c$ is always greater than $_B H_c$.

13.1.2 Remanence

No matter what the coercivity of the permanent magnet is it will be of little use if the remanent magnetization is low. Therefore a high remanence combined with a high coercivity is essential. The remanence M_R is the maximum residual magnetization which can be obtained only in a closed-loop configuration in which there is no demagnetizing field. Since all permanent magnets must be operated in an ‘open circuit’ configuration to be of any use, the residual magnetization at which the permanent magnet operates in open circuit will always be below the remanence value M_R . The remanence in neodymium–iron–boron is for example typically $M_R = 1.05 \text{ MA/m}$ (1050 emu/cc), $B_R = 1.3 \text{ T}$ (13 kG).

13.1.3 Saturation magnetization

The remanence is of course dependent on the saturation magnetization, and for this reason the saturation magnetization of a permanent magnet should be large. While this condition is necessary it is not sufficient since the squareness ratio M_R/M_s must also be as close to 1 as can be achieved in order to ensure a large remanence. The saturation magnetization in neodymium–iron–boron is 1.27 MA/m [3], in samarium–cobalt it is 0.768 MA/m [4, p. 80] and in Alnico alloys typically 0.87–0.95 MA/m [5, p. 574].

13.1.4 Energy product

One parameter that is often of interest to permanent magnet manufacturers and users is the maximum energy product, which is the maximum value of BH obtained in the second quadrant, as shown in Fig. 13.1. This is clearly closely related to the total hysteresis loss or area enclosed by the hysteresis loop. The maximum energy product is the maximum amount of useful work that can be performed by the magnet.

The improvement in the maximum energy product of various permanent magnet materials over the years are shown in Fig. 13.2 [6]. We can estimate the ultimate limits of the maximum energy product that may be achieved in the future. For a material with a remanence M_R and a very square hysteresis loop the coercivity H_c can never exceed M_R . Therefore the maximum energy product is $\mu_0 M_R^2 / 4$. Clearly remanence can never be greater than the saturation magnetization, and the largest saturation known is $1.95 \times 10^6 \text{ A/m}$ in some cobalt–iron alloys. Therefore it has been suggested [7] that the maximum energy product cannot exceed $1.19 \times 10^6 \text{ J/m}^3$ (150 MG Oe).

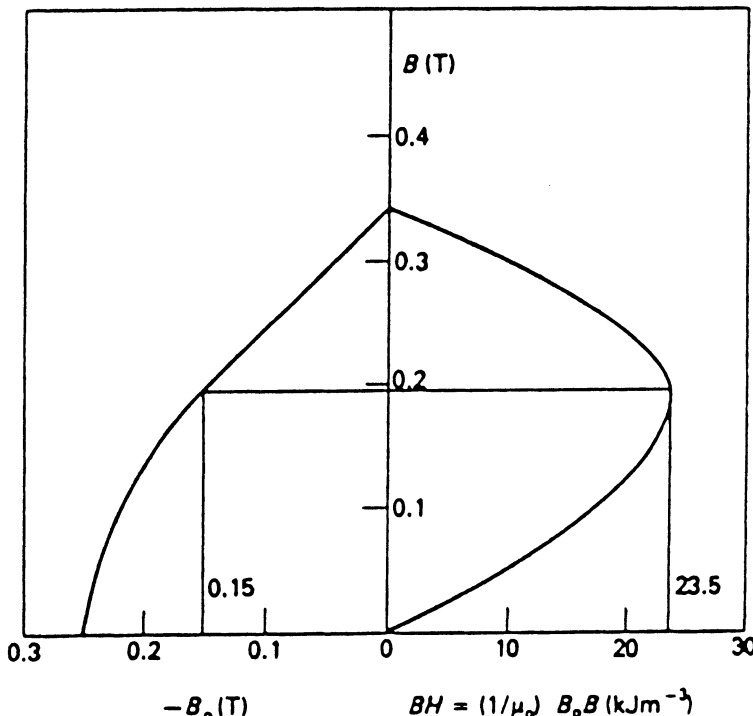


Fig. 13.1 Second quadrant ‘demagnetization curve’ of the ceramic magnet barium ferrite (left half of the diagram) and energy product as a function of induction (right half of the diagram).

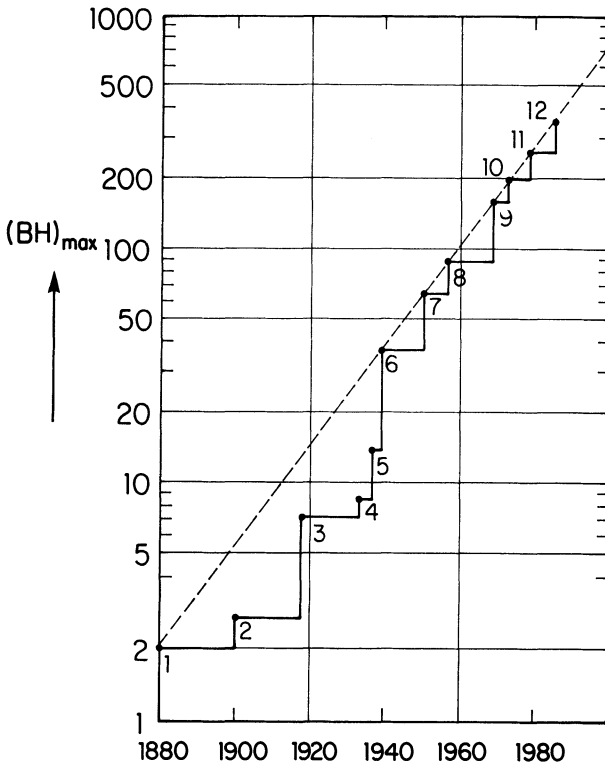


Fig. 13.2 Improvements in maximum energy product $(BH)_{\max}$ in kJ/m³ over the years 1880 to 1980: 1, carbon steel; 2, tungsten steel; 3, cobalt steel; 4, Fe–Ni–Al alloy; 5, Ticonal II; 6, Ticonal G; 7, Ticonal GG; 8, Ticonal XX; 9, SmCo₅; 10, (SmPr)Co₅; 11, Sm₂(Co_{0.85}F_{0.11}Mn_{0.04})₁₇; and 12, Nd₂Fe₁₄B.

A high energy product results from high coercivity and remanence, however it is certainly not adequate merely to choose the material with the highest energy product for any given application since the optimum operating conditions, which are affected by geometrical considerations, may dictate that other properties are more important. In order to understand this it is necessary to consider the complete demagnetization curve of the permanent magnet.

In most cases in industry the maximum energy product is measured in non-standard units of megaGauss–Oersted (MG Oe). The conversion factors between MG Oe, J/m³ and ergs/cc are as follows

$$1 \text{ MG Oe} = (10^6/4\pi) \text{ ergs/cc} = 7.96 \text{ kJ/m}^3.$$

13.1.5 Demagnetization curve

The maximum energy product by itself gives insufficient information about the properties of a permanent magnet. A more useful way of displaying the magnetic

properties of a permanent magnet is to plot the portion of the hysteresis loop in the second quadrant, that is from the remanence to the coercivity. This is known as the demagnetization curve and is the information which is always used in order to decide on the suitability of a permanent magnet for particular applications. Such a curve contains information about the maximum energy product, but also contains additional information for the designer if the permanent magnet cannot be operated at its optimum condition.

This demagnetization curve indicates that magnetization under various demagnetizing fields. The strength of the demagnetizing field of a permanent magnet in open-circuit configuration depends on the shape of the permanent magnet. It is therefore immediately apparent that the choice of material is dependent as much on its shape as on the intrinsic material properties.

The operating conditions for a permanent magnet are determined by the demagnetizing field as shown in Fig. 13.3. If the geometry is known, that is either the length of the air gap or the total length of magnet that can be used, the designer must select a material with the largest possible value of BH on the load line. The load line is the locus of possible operating points as dictated by the demagnetizing factor for the particular geometry of specimen. This is discussed in the following section.

13.1.6 Permanent magnet circuit design

The operating point of a permanent magnet is the point of intersection of the load line with the demagnetization curve. The slope of the load line is determined by the demagnetizing factor and hence by the shape of the magnet. Consider for example a permanent magnet with length to diameter ratio $1:d$ which has a demagnetizing factor N_d . Under these circumstances it is fairly easy to show [5, p. 560] that the demagnetizing field H_d is related to the induction B by

$$H_d = - \left(\frac{N_d}{\mu_0(1 - N_d)} \right) B.$$

Hence a load line of slope $-\mu_0(1 - N_d)/N_d$ passing through the origin on the B, H plane gives the locus of possible operating conditions for a magnet with the given geometry, as shown in Fig. 13.3. The slope of this load line $B/\mu_0 H_d = -(1 - N_d)/N_d$ is called the permeance coefficient. It is often one of the parameters supplied to the designer because it contains information on the shape of the permanent magnet required and therefore is important in determining the suitability of a material for a particular application.

The field in the gap of a permanent magnet is given by, [5, p. 561].

$$H_g = \sqrt{\left(\frac{H_m B_m V_m}{\mu_0 V_g} \right)},$$

where H_m is the field inside the magnet, B_m is the flux density inside the magnet, V_m

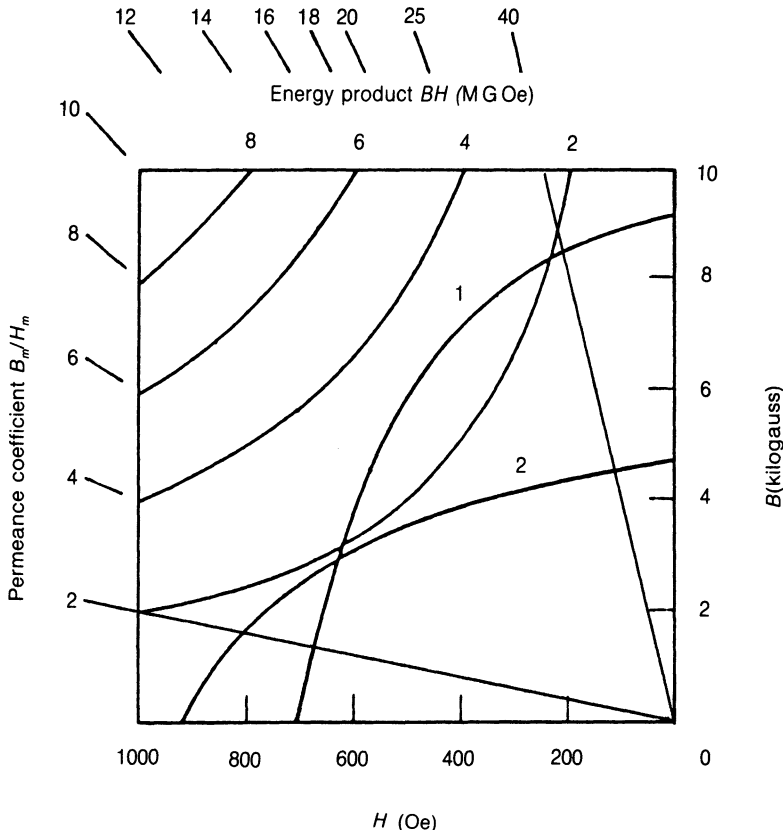


Fig. 13.3 Demagnetization curves, load lines and energy product values in the second quadrant of the magnetization curve. Two load lines are shown, one for a short specimen with $l:d = 1:1$, giving a permeance coefficient of 2 ($N_d = 0.23$) and the other for a longer specimen with $l:d = 7:1$, giving a permeance coefficient of 40 ($N_d = 0.244$).

is the volume of the magnet and V_g is the volume of the gap. The important result here is that the maximum field is obtained by operating the permanent magnet at maximum energy product (BH_{\max}).

Combining these two results it is clear that the most appropriate material for a given application is the one with the largest value of BH along the load line dictated by geometrical constraints of the given application. Conversely given a particular material for an application it should be shaped such that its load line passes through $(BH)_{\max}$ in order to optimize its performance.

For example if a short permanent magnet is required the demagnetizing field may be large so that the operating conditions are far from the $(BH)_{\max}$ point. Under these circumstances the material with the largest coercivity may be the best. If a long permanent magnet is used then the demagnetizing field may be quite low so that the magnet operates closer to the remanence. Under this condition the

material with the largest remanence may be the best. These two conditions are depicted by the load lines in Fig. 13.3.

13.1.7 Stoner–Wohlfarth model of rotational hysteresis

The Stoner–Wohlfarth model [8] describes the magnetization curves of an aggregation of single-domain particles with uniaxial anisotropy either as a result of particle shape or from the magnetocrystalline anisotropy. If the anisotropy energy, whether due to crystalline anisotropy or shape, can be represented as a single constant expression, then

$$E_{\text{an}} = -K \sin^2 \theta.$$

When the magnetization is oriented at an angle θ to the easy direction, as shown in Fig. 13.4 this will give rise to a torque of

$$\begin{aligned} \tau_{\text{an}} &= \frac{-dE_{\text{an}}}{d\theta} \\ &= 2K \sin \theta \cos \theta. \end{aligned}$$

The torque produced by a field H will be dependent on the angle ϕ between the magnetization and the field direction as shown in Fig. 13.4

$$\begin{aligned} \tau_H &= \mu_0 H \times M_s \\ &= \mu_0 H M_s \sin \phi \end{aligned}$$

and when the torque produced by the field H equals the torque due to the anisotropy we will have equilibrium.

$$\begin{aligned} \tau_H &= \tau_{\text{an}} \\ \mu_0 H M_s \sin \phi &= 2K \sin \theta \cos \theta. \end{aligned}$$

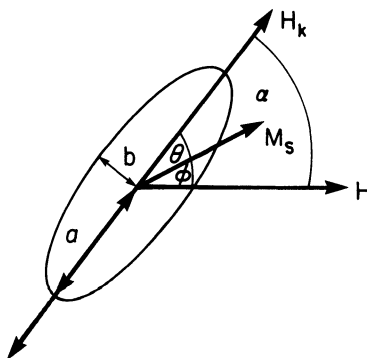


Fig. 13.4 Shape anisotropy of an ellipsoidal single-domain particle assumed to have neither crystal or stress anisotropy. The particle has higher demagnetizing factor N_d along the short axis than along the long axis. This leads to shape anisotropy.

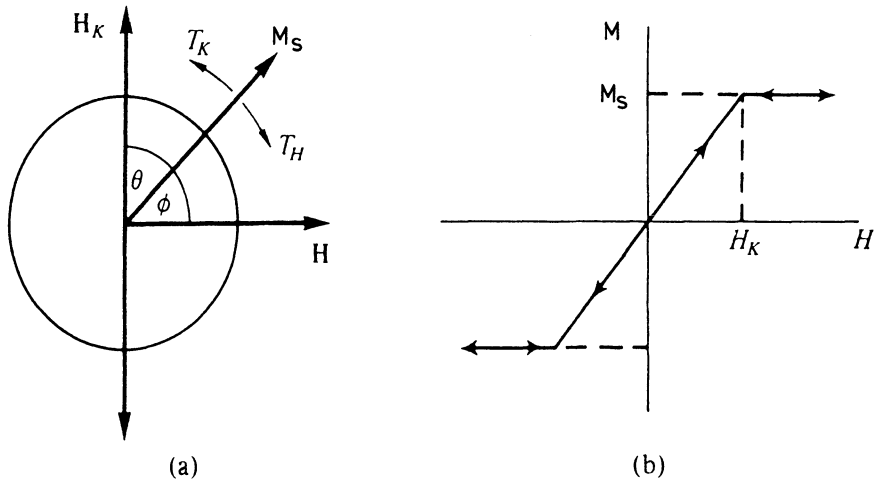


Fig. 13.5 (a) A spherical single-domain particle with anisotropy field H_K and with the magnetic field H perpendicular to the easy axis. (b) Magnetization curve obtained for the situation depicted in (a).

The field strength H_s needed to saturate the magnetization in a polycrystalline specimen is therefore the field needed to overcome the anisotropy and rotate the magnetic moments from the easy axes at 90° to the field direction into the field direction. This field strength is easily shown from the above equations to be

$$H_s = \frac{2K}{\mu_0 M_s}.$$

If H is perpendicular to the anisotropy field this gives completely reversible changes in magnetization as shown in Fig. 13.5. If H is antiparallel to the anisotropy field there arises irreversible switching of magnetization as soon as H exceeds $2K/\mu_0 M_s$, as shown in Fig. 13.6. If H is at some arbitrary angle θ to the anisotropy field then the behaviour is partly reversible and partly irreversible as shown in Fig. 13.7. In these cases whenever θ is greater than 45° it is found that τ_H increases with θ while τ_{an} decreases. A discontinuity occurs in the magnetization at a critical field H_c where

$$H_c = \frac{K}{\mu_0 M_s}.$$

When various different possible combinations of domain direction are investigated this forms a domain distribution and we obtain the kind of curves shown in Fig. 13.8. Stoner and Wohlfarth considered a random assembly of such single-domain particles, each with uniaxial anisotropy. From their calculations the composite hysteresis loop of Fig. 13.9 was obtained.

The Stoner–Wohlfarth model has been used by permanent magnet producers to

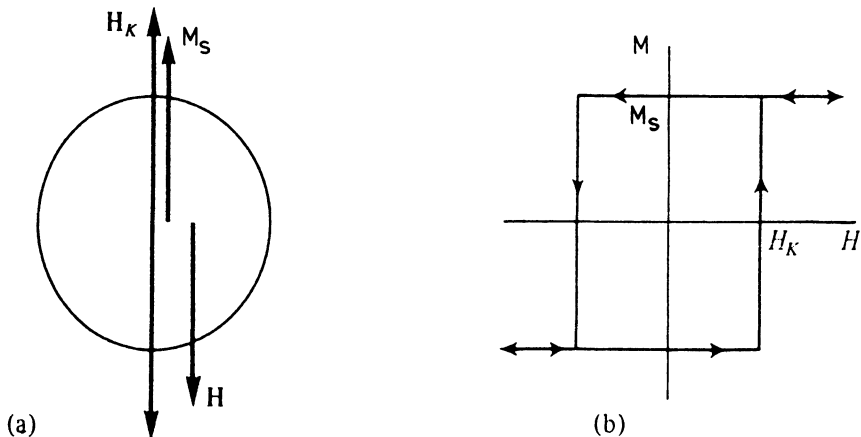


Fig. 13.6 (a) A spherical single-domain particle with anisotropy field H_K and with the magnetic field H parallel to the easy axis. (b) Magnetization curve obtained for the situation depicted in (a).

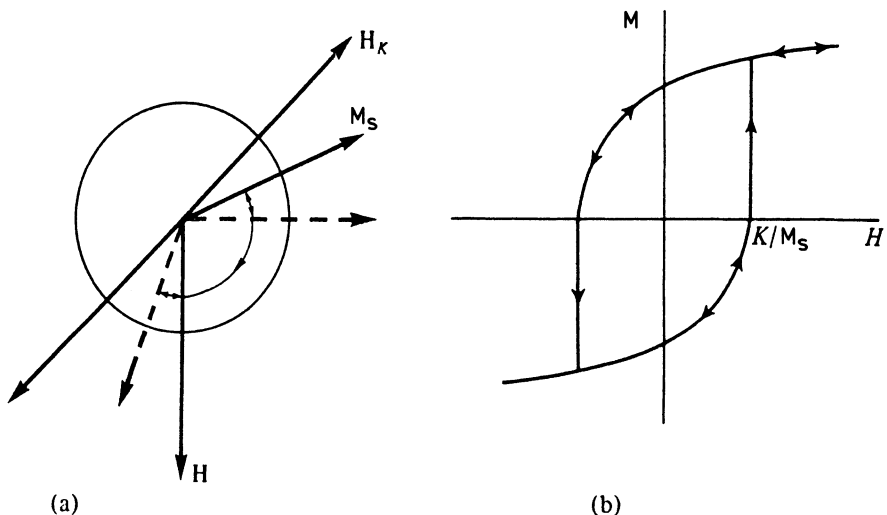


Fig. 13.7 (a) A spherical single-domain particle with anisotropy field H_K and with the magnetic field H at an arbitrary angle to the easy axis. (b) Magnetization curve obtained for the situation depicted in (a).

indicate ways in which improved properties can be obtained essentially by increasing the anisotropy. Despite the wide use of this theory there are questions about its general validity for most real permanent magnet materials. One of the most serious weaknesses of the theory is that it makes no provision for interactions between the single-domain particles. In addition real permanent magnet materials

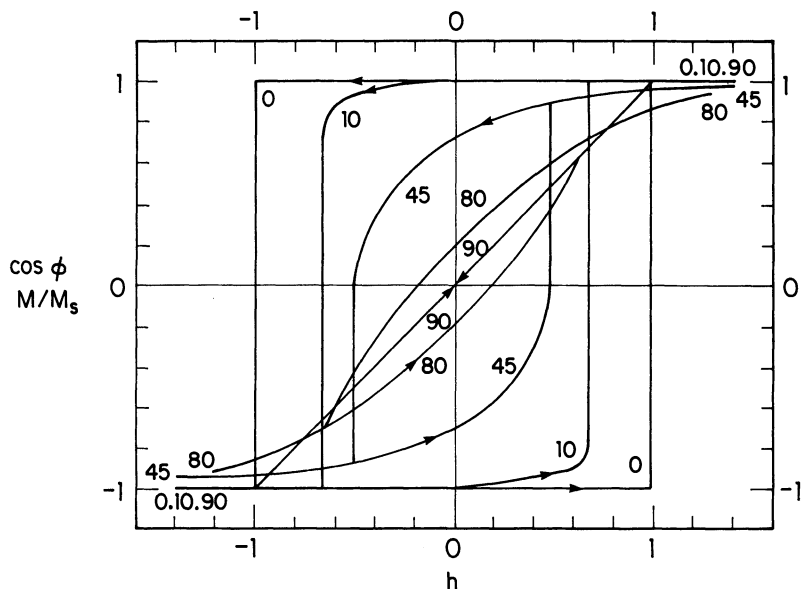


Fig. 13.8 Magnetization curves obtained on the Stoner–Wohlfarth model for various angles between the direction of the magnetic field and the easy axis.

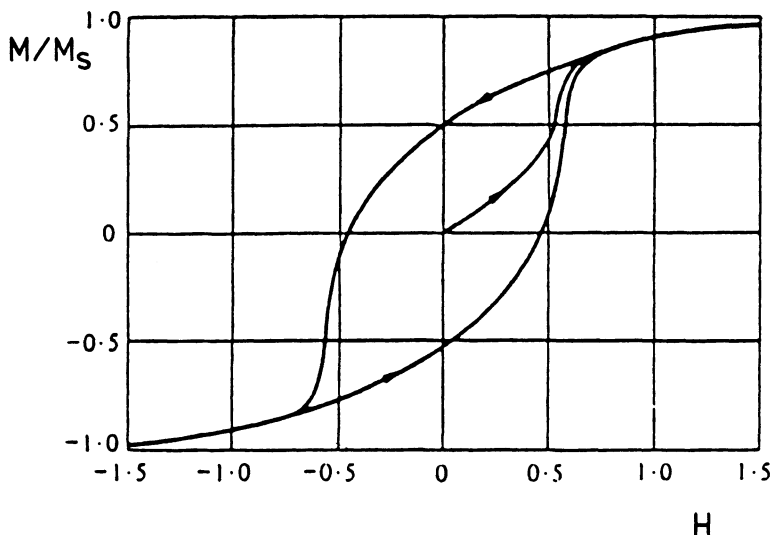


Fig. 13.9 Composite hysteresis loop obtained from summing the elementary magnetization curves for a particular distribution of easy axes (i.e. magnetic texture) with respect to the field direction. In this case the distribution of easy axes is random.

are in no sense arrays of isolated single-domain particles, although particulate media used in magnetic recording give a rather more valid approximation to the model as discussed in the next chapter.

Recently therefore there has been a shift in emphasis towards explaining properties of these materials in terms of domain-wall motion which is a more valid physical model. The problem is that domain-wall motion is much more difficult to describe theoretically than is domain rotation. At present there is considerable debate over the details of the magnetization mechanism in hard magnetic materials such as neodymium–iron–boron, particularly over the cause of the high coercivity of these materials. Chikazumi [9] has indicated that domain-wall mechanisms are probably the dominant factor in permanent magnet materials such as samarium–cobalt and neodymium–iron–boron. Some authors have argued that the high coercivity is due to difficulty in nucleating domains after the material has been magnetized to near saturation [10]. Others suggest that the high coercivity is due principally to domain-wall pinning [11]. Current evidence seems to favour the strong pinning mechanism [12].

It is certainly true that higher anisotropy will lead to improved properties for permanent magnet materials [13], however this result is not unique to the Stoner–Wohlfarth model it is far more general and applies just as well to domain-wall motion models. Therefore the essential feature of the Stoner–Wohlfarth model that has proved so useful is rather more general than the model itself.

The idea of producing a very fine microstructure for permanent magnets is also well established. This has little to do with the anisotropy (shape or otherwise), but a lot to do with the creation of a large number of impediments to domain-wall motion, both through the particle or grain sizes and through the presence of localized residual strains which pin domain walls and lead to higher coercivity.

13.1.8 Applications

Permanent magnets generate stable magnetic fields without continuous expenditure of electrical energy. This is an advantage in certain circumstances. There are many different applications of permanent magnets [14, 15] and as we have seen considerations of geometry lead to many different materials requirements. Therefore there remains a wide range of permanent magnet materials available commercially. The main applications of permanent magnets are in electric motors, generators, loudspeakers, moving-coil meters, magnetic separators, control devices for electron beams such as in TV sets, frictionless bearings and magnetic levitation systems, and various forms of holding magnets such as door catches.

Electric motors, in which electrical energy is converted into mechanical energy, and electric generators in which mechanical energy is converted into electrical energy are the most important single application of permanent magnets. The recent neodymium–iron–boron permanent magnet material was developed by General Motors for use in the starter motors of their cars and trucks. The size of

310 Hard magnetic materials

motors can be reduced greatly by the use of stronger permanent magnet materials and this is often an important consideration which outweighs the additional cost of the high-performance magnets. Neodymium–iron–boron permanent magnets are also now being used in magnetic resonance imaging systems [16]. This application requires a very high field homogeneity, typically 5 parts per million over a volume 0.6 m in diameter [17]. Previously such fields had to be produced using superconducting magnet technology as discussed in section 15.2.5.

13.1.9 Stability of permanent magnets

It is important to know under what conditions a permanent magnet will perform to its design specifications. Two problems may arise (a) temporary effects due to operating at temperatures beyond those for which the material was designed, and (b) permanent deterioration of the magnetic properties caused by exposure to very high fields (demagnetization) or by alteration of microstructure caused by exposure to elevated temperatures (ageing).

The temporary or reversible changes in the magnetic properties with temperature are caused by the reduction of spontaneous magnetization within the domains as the temperature is raised. This becomes more significant the closer the temperature is to the Curie point. The permanent changes which occur as a result of exposure to elevated temperatures are caused by acceleration of the ageing

Table 13.1 Important magnetic properties of selected permanent magnet materials

Material	Composition		Remanence (T)	Coercivity (kA/m)	$(BH)_{\max}$ (kJ/m ³)
Steel	99% Fe,	1% C	0.9	4	1.59
36Co Steel	36% Co, 5.75% Cr,	3.75% W 0.8% C	0.96	18.25	7.42
Alnico 2	12% Al, 3% Cu,	26% Ni 63% Fe	0.7	52	13.5
Alnico 5	8% Al, 24% Co,	15% Ni 3% Cu, 50% Fe	1.2	57.6	40
Alnico DG	8% Al, 24% Co,	15% Ni 3% Cu, 50% Fe	1.31	56	52
Ba Ferrite	BaO·6Fe ₂ O ₃		0.395	192	28
PtCo	77% Pt,	23% Co	0.645	344	76
Remalloy	12% Co, 71% Fe	17% Mo	1.0	18.4	9
Vicalloy	13% V, 35% Fe	52% Co	1.0	36	24
Samarium–cobalt	SmCO ₅		0.9	696	160
Neodymium–iron–boron	Nd ₂ Fe ₁₄ B		1.3	1120	320

process. Many permanent magnet materials exist in a metastable metallurgical state so that a phase transformation does occur but at room temperature this proceeds very slowly. At higher temperature the transformation proceeds more rapidly. Other factors such as mechanical treatments, corrosion and radiation effects can alter the properties of permanent magnets. These have been discussed in detail by McCaig [18].

13.2 PERMANENT MAGNET MATERIALS

In this section we look at the various different materials which have been used as permanent magnets. Materials that were considered ‘hard’ magnetic materials in the past are in many instances not recognized as hard materials today because of the great improvement of magnetic properties such as coercivity and maximum energy product which have taken place in the last fifty years. The magnetic properties of various permanent magnet materials are shown in Table 13.1. A summary of the properties of various permanent magnet materials has been given by Becker *et al.* [19] which covers developments up to 1968. A later review paper by Buschow [20] considered recent permanent magnet materials, concentrating principally on the rare earth–iron and rare earth–cobalt magnet materials.

13.2.1 Magnetite or ‘lodestone’

This material Fe_3O_4 which is a naturally occurring oxide of iron was the first ‘permanent magnet’ material to be recognized. Today it is not even considered to be a hard magnetic material.

13.2.2 Permanent magnet steels

The addition of carbon to iron has long been known to increase coercivity and hysteresis loss, and this has been discussed in earlier chapters. The first commercially produced permanent magnets were high-carbon steels containing about 1% carbon. These were also mechanically hard while the low-carbon steels and iron were mechanically soft. Hence the classification ‘hard’ and ‘soft’, which, for those involved in magnetism, later came to be a measure of coercivity rather than of mechanical properties.

Later permanent magnet steels were made with the addition of tungsten and chromium which improved the coercivity compared with the carbon steels. Later still came the cobalt steels. In these materials the improved magnetic properties arose from the presence of second-phase particles which impeded the motion of domain walls, thereby leading to higher coercivity and maximum energy product.

These permanent magnet steels have coercivities of up to 20 kA/m and maximum product of up to 7 kJ/m³. The magnetic properties of some chromium and cobalt steels are shown in Fig. 13.10 [12].

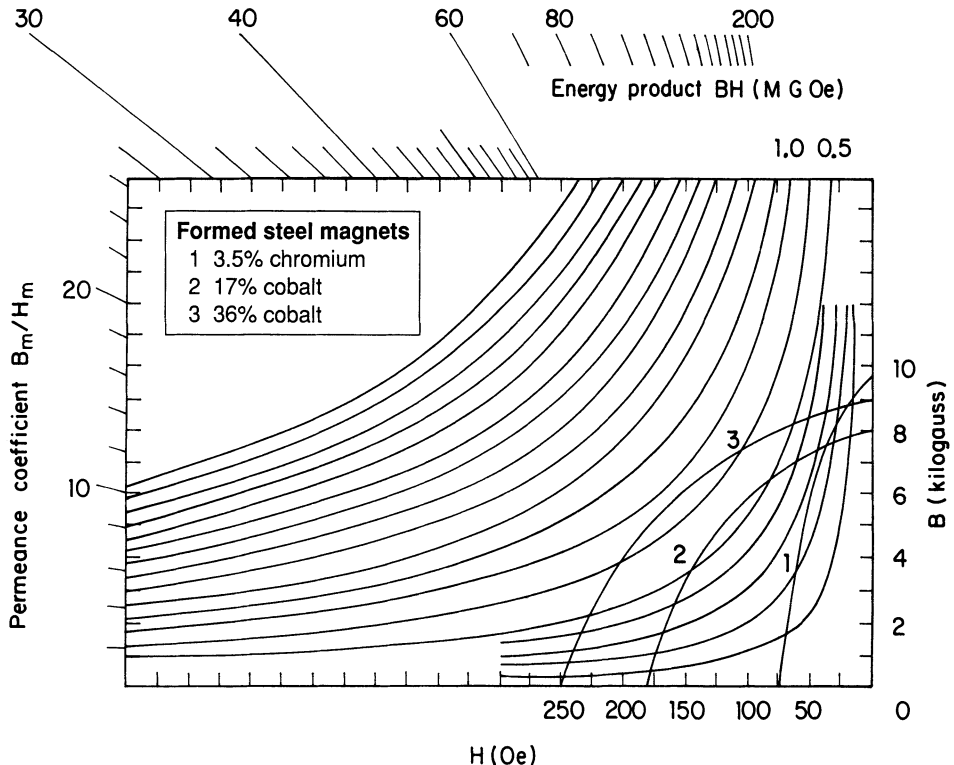


Fig. 13.10 Demagnetization curves of three permanent magnet steels.

13.2.3 Alnico alloys

The Alnico alloys were developed in the 1930s. The discovery of their important magnetic properties was quite fortuitous during the development of a new type of steel for other purposes. The Alnico alloys consist mainly of iron, cobalt, nickel and aluminum with small amounts of other metals such as copper [22]. These constituents form a finely intermixed two-phase alloy consisting of a strongly magnetic α_1 phase (Fe–Co) and a very weakly magnetic α_2 phase (Ni–Al) which provides pinning sites to restrain the motion of the magnetic domain walls.

The magnetic properties of the alloy are improved by suitable heat treatment involving quenching followed by tempering at 700 °C. They are also improved by annealing in a magnetic field. This raises the coercivity and maximum energy product. The magnetic properties of these alloys were superior to other materials available at that time as a result of the formation of long rod-shaped grains of iron–cobalt which give rise to shape anisotropy. The particles are also embedded in a nickel–aluminum matrix which impeded domain-wall motion. One disadvantage of these alloys is that they are very hard and brittle and therefore can only be shaped by casting or by pressing and sintering of metal powder.

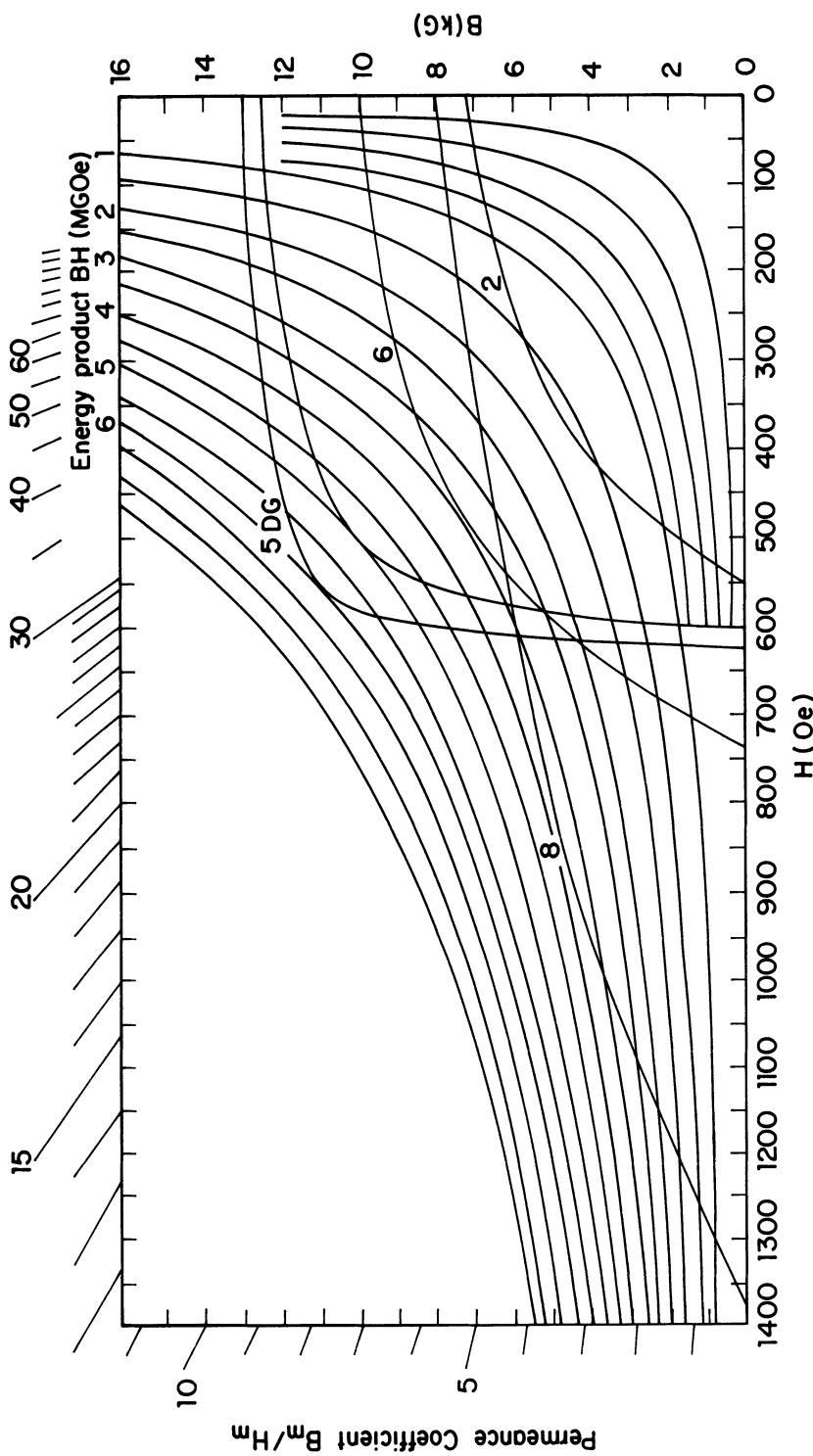


Fig. 13.11 Demagnetization curves of various forms of Alnico, After Parker and Studders (1962) [21].

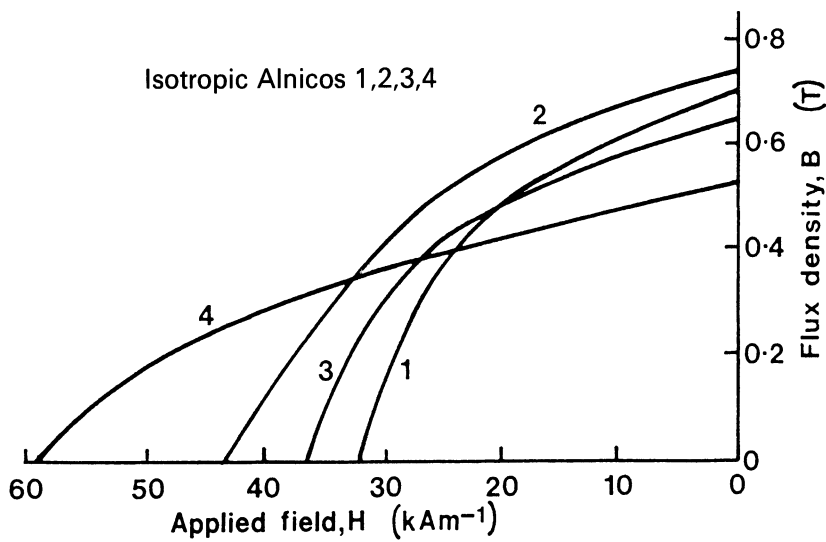


Fig. 13.12 Demagnetization curves of the isotropic forms of Alnico; Alnicos 1, 2, 3 and 4.

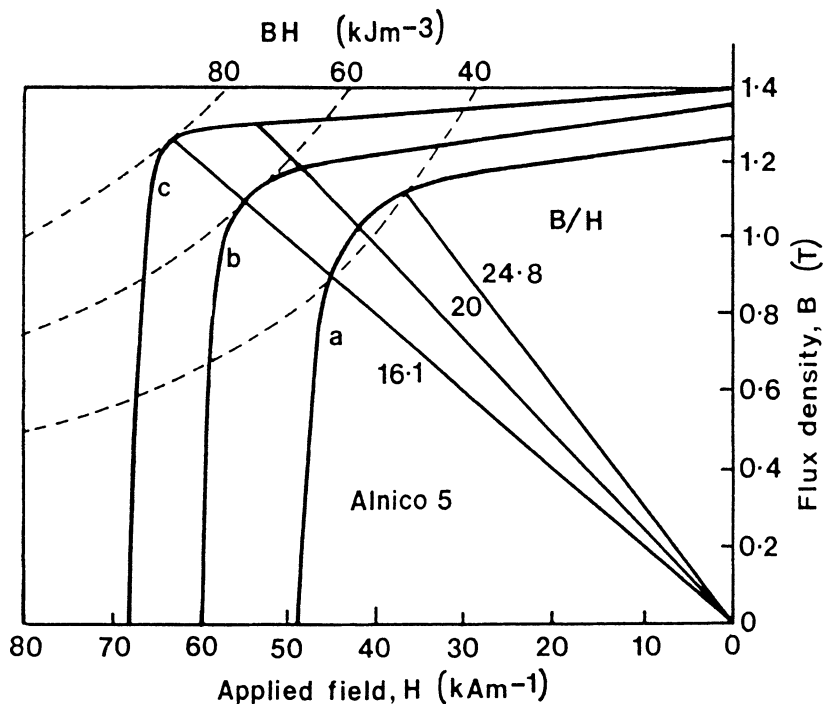


Fig. 13.13 Demagnetization curves of oriented forms of Alnico 5: (a) equiaxed, (b) grain-oriented and (c) single-crystal.

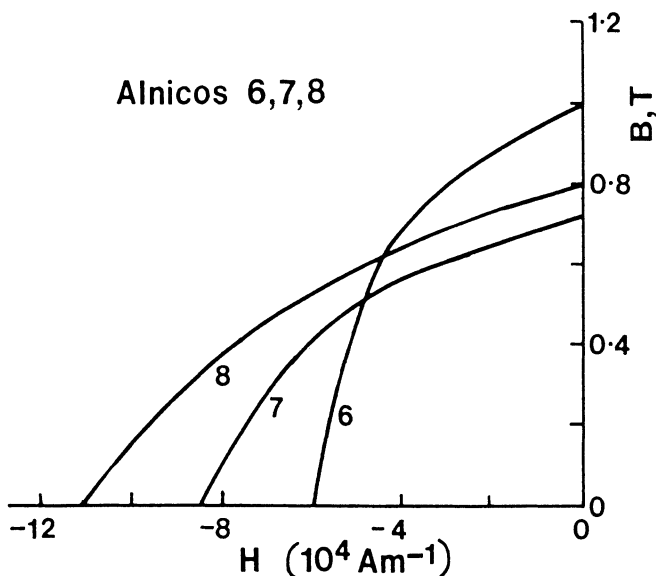


Fig. 13.14 Demagnetization curves of the anisotropic forms of Alnico: Alnicos 6, 7 and 8.

Alnico alloys have remanences in the range 50–130 kA/m with maximum energy products of 50–75 kJ/m³. These alloys represent a mature technology and no significant improvements in their magnetic properties have occurred in the last twenty years. Typical magnetic properties of some Alnico alloys are shown in Figs. 13.11 to 13.14.

13.2.4 Hard ferrites

These materials, also known as ceramic magnets, were developed in the 1950s as a result of the Stoner–Wohlfarth theory which indicated that the coercivity of a system of single-domain particles was proportional to the anisotropy. The theory thus provided a direction for the permanent magnet industry by indicating the types of materials which should prove to be good permanent magnets.

This led the permanent magnet manufacturers to try to develop highly anisotropic materials in the form of aggregations of single-domain particles. The cause of the anisotropy could be either crystalline or small-particle shape effects. However it has been found that the coercivities of real materials have always been much smaller than the theoretical predictions of Stoner and Wohlfarth since mechanisms other than coherent domain rotation are almost always available and these can take place at lower coercivities.

The hard hexagonal ferrites in widespread use are usually either barium or strontium ferrite ($\text{BaO}\cdot 6\text{Fe}_2\text{O}_3$ or $\text{SrO}\cdot 6\text{Fe}_2\text{O}_3$). These materials are relatively cheap to produce and commercially remain the most important of the permanent

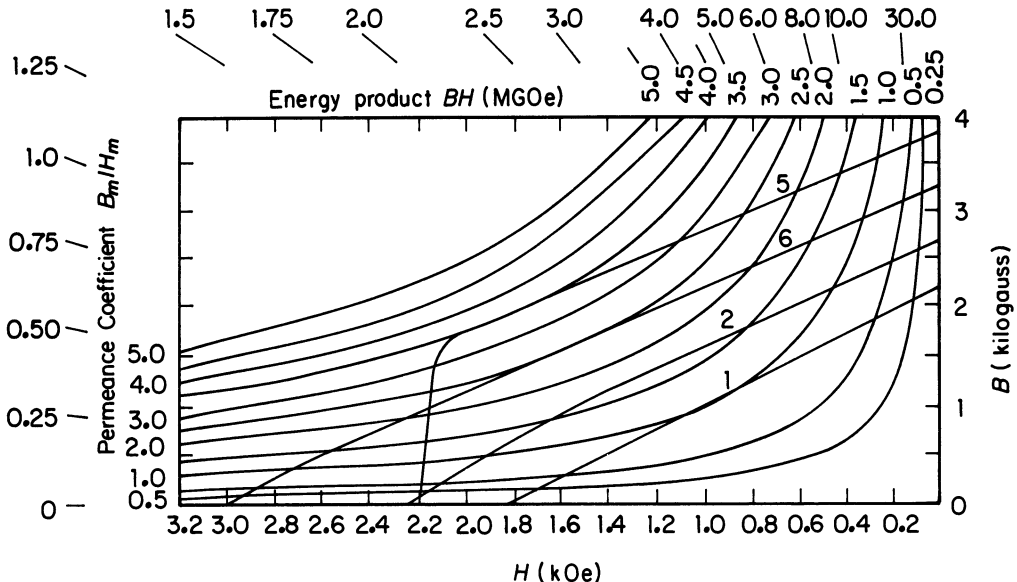


Fig. 13.15 Demagnetization curves for: 1, isotropic barium ferrite; and 2, 5, and 6, anisotropic barium ferrite permanent magnets.

magnet materials. The ferrites are often used to produce the so called ‘plastic magnets’ by embedding the ferrite in a flexible plastic matrix.

The coercivities are larger than the Alnicos for example, being typically 150–250 kA/m, but their maximum energy product is low, being typically 20 kJ/m³. The magnetic properties of some barium ferrite magnets are shown in Fig. 13.15. Reviews of the properties of the hard ferrites have been given by Stablein [23] and by Kojima [24].

13.2.5 Platinum–cobalt

This permanent magnet material was developed in the late 1950s. Although its magnetic properties were an improvement over other materials that were available at the time, its cost made it impractical for any except the smallest magnets. Other cheaper magnets with superior properties are now available so this permanent magnet material is no longer in use. It has coercivities of typically, 400 kA/m and a maximum energy product of, typically, 80 kJ/m³.

13.2.6 Samarium–cobalt

Samarium–cobalt permanent magnet material was developed in the late 1960s as a result of a concerted research effort to identify new permanent magnet materials based on alloys of the rare earths with the 3d transition series ferromagnets, iron,

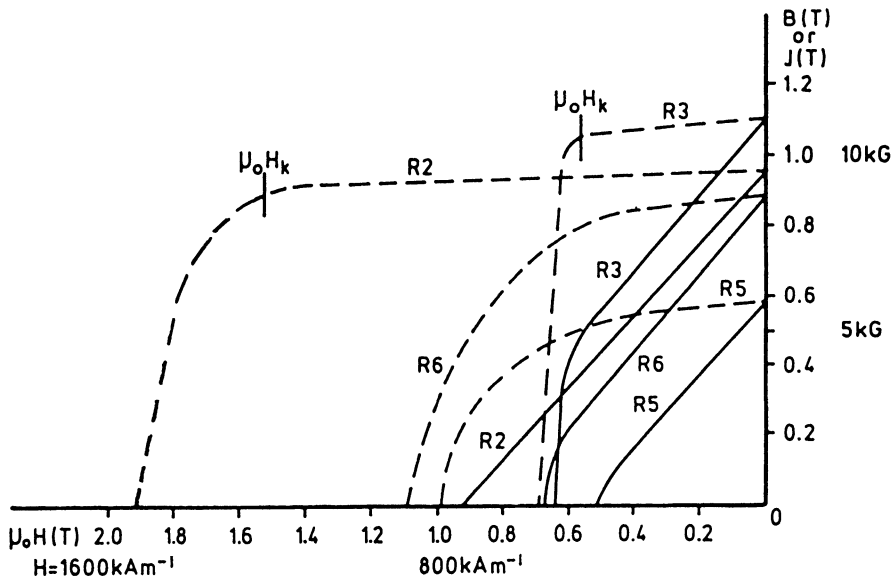


Fig. 13.16 Second quadrant demagnetization curves for four specimens of samarium cobalt permanent magnet material. The broken lines are curves of M against H , the full lines are curves of B against H . R2 = sintered SmCo_5 , R3 = sintered $\text{Sm}_2\text{Co}_{17}$, R5 = bonded SmCo_5 , R6 = bonded $\text{Sm}_2\text{Co}_{17}$. (From M. McCaig and A. G. Clegg [31].)

cobalt and nickel [25]. It was found that the cobalt–rare earth alloys had higher anisotropies than the nickel– or iron–rare earth alloys. Furthermore the alloys with the light rare earths generally had higher saturation magnetizations. The first alloy to be developed was SmCo_5 which has a saturation magnetization of 780 kA/m , a coercivity typically of $B_{\text{c}} = 760 \text{ kA/m}$ ($m_{\text{c}} = 3 \text{ MA/m}$) with a maximum energy product of 150 – 200 kJ/m^3 . This was followed by $\text{Sm}_2\text{Co}_{17}$, which has $B_{\text{c}} = 800 \text{ kA/m}$ and maximum energy product of 260 kJ/m^3 . The demagnetizing curves of four typical samples of samarium–cobalt permanent magnet material are shown in Fig. 13.16. The samarium–cobalt alloys have been discussed in detail by Nesbitt and Wernick [26].

13.2.7 Neodymium–iron–boron

This material was discovered in the early 1980s largely because of the intervention of economic circumstances. At that time due to problems with the supply of cobalt there was a need for a new permanent magnet material to replace samarium–cobalt even though the properties of the samarium–cobalt were adequate for the applications for which the new material was to be used. There had been some attempts to develop neodymium–iron materials which were known to have large coercivities, but the properties of these alloys were not sufficiently reproducible. From this research the addition of a small amount of boron was found to improve the properties dramatically.

The main neodymium–iron–boron alloy developed contained the $\text{Nd}_2\text{Fe}_{14}\text{B}$ phase [27, 28], which has greater coercivity and energy product than samarium–cobalt. It is the presence of this very hard magnetic phase which leads to improved magnetic properties. Demagnetization curves of three specimens of the material are shown in Fig. 13.17. The magnetic properties of the neodymium–iron–boron material are very sensitive to the metallurgical processing. Two principal methods of production have been devised. The material is produced either by powdering and sintering, as in samarium–cobalt, or by rapidly quenching from the melt.

In the powder sintering method developed by Sagawa *et al.* [27] the constituents are induction melted in an alumina crucible under an inert atmosphere, of argon for example, to prevent oxidation. The alloy is then milled into a powder with particles of diameter 3 μm . The particles are aligned in a 800 kA/m field, compacted under 200 MPa pressure and then sintered in an argon atmosphere at temperatures in the range 1050–1150 °C. This process is followed by a post-sintering anneal.

The rapid quenching process, known as ‘magnequench’ was developed by Croat *et al.* [28]. Constituents are arc melted together and then ‘melt spun’ in an argon atmosphere by ejecting the molten alloy through a hole in the quartz crucible on to a rapidly rotating substrate where the metal cools rapidly to form ribbons. This

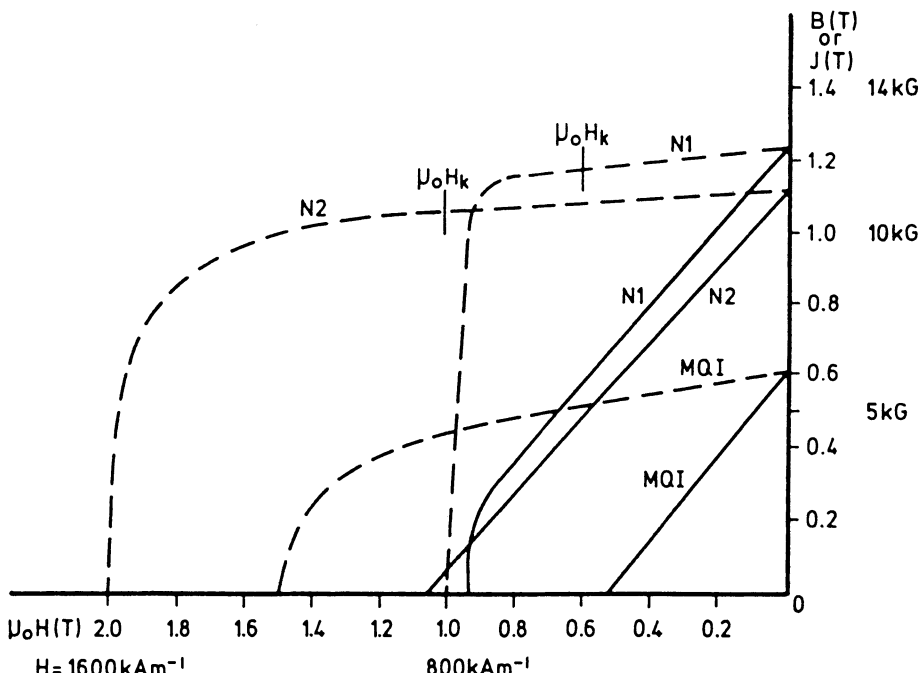


Fig. 13.17 Second quadrant demagnetization curves for three specimens of neodymium–iron–boron permanent magnet material. The broken lines are curves of M against H , the full lines are curves of B against H . N1 = sintered NdFeB, N2 = high coercivity NdFeB, MQ1 = bonded ‘magnequench’ NdFeB’. (From M. McCaig and A. G. Clegg [31].)

Table 13.2 Magnetic properties of domains and domain walls in permanent magnet materials samarium–cobalt and neodymium–iron–boron

	<i>Domain wall surface energy</i> (mJ/m ²)	<i>Domain wall width</i> (nm)	<i>Single-domain particle diameter</i> (μm)
Nd ₂ Fe ₁₄ B	30	5.2	0.26
SmCo ₅	85	5.1	1.6
Sm ₂ Co ₁₇	43	10.0	0.66

gives a fine-grained microstructure of the equilibrium Nd₂Fe₁₄B phase. Particle sizes are in the range 20–80 nm. The ribbons then undergo one of two further processes: either they are bonded with epoxy to form a ‘bonded magnet’ with intermediate maximum energy product typically of 72 kJ/m³; or the ribbon fragments are vacuum hot pressed and vacuum die upset to form aligned magnets with high maximum energy products, typically of 320 kJ/m³.

The principle advantage of these alloys compared with samarium–cobalt is that the alloy constituents, iron and neodymium, are cheaper than samarium and cobalt. One disadvantage of the alloy is its rather low Curie point of around 300–500 °C. This means that the magnetic properties are rather more sensitive to temperature than are those of samarium–cobalt ($T_c = 720$ °C) and are not suitable for some higher temperature applications. Typical coercivities of these permanent magnet alloys are in the range 1100 kA/m with maximum energy product of 300–350 kJ/m³.

Sagawa *et al.* [29] have reviewed the development of neodymium–iron–boron permanent magnet materials over the period 1984–7. A recent summary of research and development covering this another rare earth permanent magnet materials has been given by Strnat [30]. Finally the most comprehensive treatment of all aspects of permanent magnets and their applications can be found in the revision of McCaig’s text by Clegg [31].

The domain wall surface energies, domain wall widths and single-domain particles diameters of the three most widely used rare earth transition metal alloy permanent magnets are given in Table 13.2 which is taken from the review by Sagawa *et al.* [29]. These may be compared with the values for iron, nickel and cobalt in Table 7.1 whence it is seen that the permanent magnets have much higher surface energies and correspondingly thinner domain walls than the soft magnetic materials.

REFERENCES

1. Moskowitz, L. R. (1976) *Permanent Magnet Design and Application Handbook*, Cahners Books International, Boston.

2. Hummel, R. (1985) *Electronic Properties of Materials*, Springer-Verlag, New York, p. 255.
3. Hilscher, G., Grossinger, R., Heisz, S., Sassik, H. and Wiesinger, G. (1986) *J. Mag. Mag. Mater.*, **54-7**, 577.
4. Nesbitt, E. A. and Wernick, J. H. (1973) *Rare Earth Permanent Magnets*, Academic Press, New York.
5. Cullity, B. D. (1972) *Introduction to Magnetic Materials*, Addison-Wesley, Reading, Mass.
6. Zijlstra, H. (1982) Permanent magnets; theory, in *Ferromagnetic Materials*, Vol. 3 (ed. E. P. Wohlfarth) Amsterdam.
7. Graham, C. D. (1987) *Conference on Properties and Applications of Magnetic Materials*, Illinois Institute of Technology, Chicago.
8. Stoner, E. C. and Wohlfarth, E. P. (1948) *Phil. Trans. Roy. Soc.*, **A240**, 599.
9. Chikazumi, S. (1986) *J. Mag. Mag. Mater.*, **54-7**, 1551.
10. Durst, K. D. and Kronmuller, H. (1987) *J. Mag. Mag. Mater.*, **68**, 63.
11. Pinkerton, F. E. and Van Wingerden, D. J. (1986) *J. Appl. Phys.*, **60**, 3685.
12. Hadjipanayis, G. C. (1988) *J. Appl. Phys.*, **63**, 3310.
13. Becker, J. J. (1968) *IEEE Trans. Mag.*, **4**, 239.
14. Bradley, F. N. (1971) *Materials for Magnetic Functions*, Hayden, New York.
15. McCaig, M. (1968) *IEEE. Trans. Mag.*, **4**, 221.
16. Molfino, P., Repetto, M., Bixio, A., Del Mut, G. and Marabotto, R. (1988) *IEEE Trans. Mag.*, **24**, 994.
17. Bobrov, E. S. and Punchard, W. F. B. (1988) *IEEE Trans. Mag.*, **24**, 553.
18. McCaig, M. (1977) *Permanent Magnets in Theory and Practice*, Wiley, New York.
19. Becker, J. J., Luborsky, F. E. and Martin, D. L. (1968) *IEEE Trans. Mag.*, **4**, 84.
20. Buschow, K. H. J. (1986) *Materials Science Reports*, **1**, 1.
21. Parker, R. J. and Studders, R. J. (1962) *Permanent Magnets and their Applications*, Wiley, New York.
22. McCurrie, R. A. (1982) The structure and properties of Alnico permanent magnet alloys, in *Ferromagnetic Materials*, Vol. 3 (ed. E. P. Wohlfarth) Amsterdam.
23. Stablein, H. (1982) Hard ferrites, in *Ferromagnetic Materials*, Vol. 3 (ed. E. P. Wohlfarth) Amsterdam.
24. Kojima, H. (1982) Fundamental properties of hexagonal ferrites with magnetoplumbite structure, in *Ferromagnetic Materials*, Vol. 3 (ed. E. P. Wohlfarth) Amsterdam.
25. Strnat, K., Hoffer, G., Olson, J., Ostertag, W. and Becker, J. J. (1967) *J. Appl. Phys.*, **38**, 1001.
26. Nesbitt, E. A. and Wernick, J. H. (1973) *Rare Earth Permanent Magnets*, Academic Press, New York.
27. Sagawa, M., Fujimura, S., Togawa, N., Yamamoto, H. and Matsuura, Y. (1984) *J. Appl. Phys.*, **55**, 2083.
28. Croat, J. J., Herbst, J. F., Lee, R. W. and Pinkerton, F. E. (1984) *J. Appl. Phys.*, **55**, 2078.
29. Sagawa, M., Hirosawa, S., Yamamoto, H., Fujimura, S. and Matsuura, Y. (1987) *Jap. J. Appl. Phys.*, **26**, 785.
30. Strnat, K. J. (1987) *IEEE Trans. Mag.*, **23**, 2094.
31. McCaig, M. and Clegg, A. G. (1987) *Permanent Magnets in Theory and Practice*, 2nd edn, Pentech Press, London.

FURTHER READING

- Bradley, F. N. (1971) *Material for Magnetic Functions*, Hayden, New York.
- Cullity, B. D. (1972) *Introduction to Magnetic Materials*, Addison-Wesley, Reading, Mass, Ch. 14.

- Hadfield, D. (1962) *Permanent Magnets and Magnetism*, Iliffe Books, London.
- Hummel, R. (1985) *The Electronic Properties of Solids*, Springer-Verlag, Berlin.
- Jakubovics, J. (1987) *Magnetism and Magnetic Materials*, Institute of Metals, London.
- Kojima, H. (1987) Fundamental properties of hexagonal ferrites with magnetoplumbite structure, in *Ferromagnetic Materials*, Vol. 3 (ed. E. P. Wohlfarth) Amsterdam.
- McCaig, M. and Clegg, A. G. (1987) *Permanent Magnets in Theory and Practice*, 2nd edn, Pentech Press, London.
- Nesbitt, E. A. and Wernick, J. H. (1973) *Rare Earth Permanent Magnets*, Academic Press, New York.
- Stablein, H. (1982) Hard ferrites, in *Ferromagnetic Materials*, Vol. 3 (ed. E. P. Wohlfarth) Amsterdam.

14

Magnetic Recording

In this chapter we look at the various magnetic methods available for information storage. The most important of these are magnetic tape recording, which is widely used for both audio and video, and magnetic disk recording which is vital for the permanent storage of computer information. We also look at the magnetic recording process.

14.1 MAGNETIC RECORDING MEDIA

The hysteresis of magnetization versus magnetic field in ferromagnets and ferrimagnets can be used to good effect in magnetic recording. Without hysteresis the magnetic state of the material in zero field would be independent of the field that it had last experienced. However in hysteretic systems the remanent magnetization is a kind of memory of the last field maximum, both in magnitude and direction, experienced by the magnetic material. Therefore data, either in digital form for computers and related devices, or analog signals as in sound recording, can be stored in the form of magnetic ‘imprint’ on magnetic media.

Of course to make this of any practical use it must be possible to store large amounts of data in as small a space as possible. So we notice that in the recording industry there is a continual desire to increase the recording density of storage media.

The information must also be able to be retrieved with a minimum of distortion, that is it must not be easily erased or changed by the presence of extraneous magnetic fields since the information should be capable of being stored permanently. Nor should it be altered by the reading process since it is usually necessary to reread the data many times without loss of information. Furthermore it should be written and read with minimal power requirements.

The magnetic recording media must have high saturation magnetization to give as large a signal as possible during the reading process. The coercivity must be sufficient to prevent erasure, but small enough to allow the material to be reused for recording. Coercivities in the range of 20–100 kA/m are common for magnetic recording tapes and disks.

14.1.1 History and background of magnetic recording

Analog magnetic recording of the human voice was first demonstrated by Poulsen [1], a Danish engineer, as long ago as 1898. In his device, called the 'telephone', acoustic signals were recorded on a ferromagnetic wire using an electromagnet connected to a microphone. However the reproduction was very weak due to the absence of an amplifier.

By 1920 with the development of amplifiers the signals from the magnetic medium could be recreated more strongly and the sound reproduction was easily audible. However there was also a low signal to noise ratio, due to the nonlinear nature of the recording process, which still meant that the quality of the sound was not good.

The a.c. biasing method of recording was devised in 1921 [2] and resulted in much better signal to noise ratios because the recorded magnetization could be made linearly dependent on the signal level. However it was not exploited properly for another twenty years [3].

Magnetic tape was invented in 1927 in both the USA, using a paper tape coated with dried ferrimagnetic liquid, and in Germany using a tape containing iron powder. Oxide tapes were developed in 1947 by 3M Corporation and audio recorders became available in 1948. Video recording began in 1956. Digital recording for storage of computer information was developed by IBM and the first magnetic disk drive became available in 1955.

Since the 1950s there has been a growth in digital magnetic recording for the storage of computer data which, together with the consumer demand for audio analog magnetic recording, particularly recording of music, form commercially the most important areas of the magnetic recording industry. The industry is currently worth about \$80 billion a year.

14.1.2 Magnetic tapes

Magnetic tapes are the most widely used recording medium for audio and video signals, and also to a lesser extent for computer data. Magnetic recording tapes usually consist of a coating of fine particles of ferrimagnetic material (usually gamma ferric oxide) on a flexible, non-magnetic, plastic substrate or base of thickness about $25\text{ }\mu\text{m}$. The particles are typically of dimensions $0.25\text{--}0.75\text{ }\mu\text{m}$ in length by $0.05\text{--}0.15\text{ }\mu\text{m}$ in width [4, p. 34, 5, p. 105] and are single domains which can relatively easily be magnetized parallel to their long axes. Their saturation magnetization is 370 kA/m (370 emu/cc) and the Curie temperature is in the vicinity of $600\text{ }^{\circ}\text{C}$.

Magnetic tapes are magnetically anisotropic. Gamma ferric oxide tapes usually have larger particle sizes than do chromium dioxide tapes in which the particle size is typically $0.4 \times 0.05\text{ }\mu\text{m}$. [5, p. 105]. At present the particles are aligned in the plane of the tape. In order to align the single-domain particles the tapes are placed in a magnetic field oriented in the plane of the tape. The field is applied before the

solvent which carries the magnetic particles evaporates and leaves the dry binder which carries the magnetic particles. The tape is then heated to completely dry the coating and is rolled or squeezed to densify the coating. Efforts have been made to develop cobalt–chromium tapes for so-called perpendicular recording media in which the long axes of the particles are aligned at right angles to the tape surface. This should in principle allow higher recording densities to be achieved although several difficulties have been encountered in the development of perpendicular recording including flying height of the head [6] and noise during the reading process [7].

14.1.3 Magnetic disks

The principles of recording on magnetic disks are almost identical to those of recording on magnetic tapes and these will be discussed shortly. Magnetic recording disks come in two categories: floppy disks and hard disks. The materials used as a magnetic recording medium on disk are also broadly similar to those used on tapes. Floppy disks are made in the same way as tapes, and are usually either $5\frac{1}{4}$ " or $3\frac{1}{2}$ " diameter. The floppies are widely used in microcomputers. Hard disks were previously more often associated with large computers, however there is an increasing demand for hard disks in the microcomputer industry now because of their great storage capabilities.

One of the advantages of disks over tapes is that access time is much shorter on disks. This is mainly because the reading heads can be moved quickly to the right sector of the disk, whereas in tape recording it is necessary to rewind the tape to find the data. In disk recording the access time can also be improved by rotating the disk at a higher angular velocity. This by itself can bring problems of additional wear on floppy disks but not on hard disks. The reason for this is that on floppy disks the read/write head is in contact with the disk during the reading and writing process, but in hard disks, such as the Winchester disk systems, there is no direct contact during reading or writing.

In magnetic tape recording the contact between tape and the read and write heads is a crucial factor in determining performance but in that case actual contact is acceptable because of the relatively low number of replay head/magnetic tape passes expected. The heads are even contoured to improve contact with tape. In magnetic floppy disks the head also rides in contact with the disk. On hard disks the read/write head is not in contact with the disk. In order to optimize the performance of hard disks while ensuring that there is no direct contact head and disk an air bearing is used. In this way the head can be maintained close to, but not actually in direct contact with the disk. This is the so-called 'flying head'. The air flow is caused by the relative velocity between the disk and head and this maintains a small gap. When this arrangement fails, as it does occasionally, we encounter the so called 'disk head crash' which usually results in some damage in the form of lost data.

In Winchester disk drives [8] the load applied to the heads is so small that the

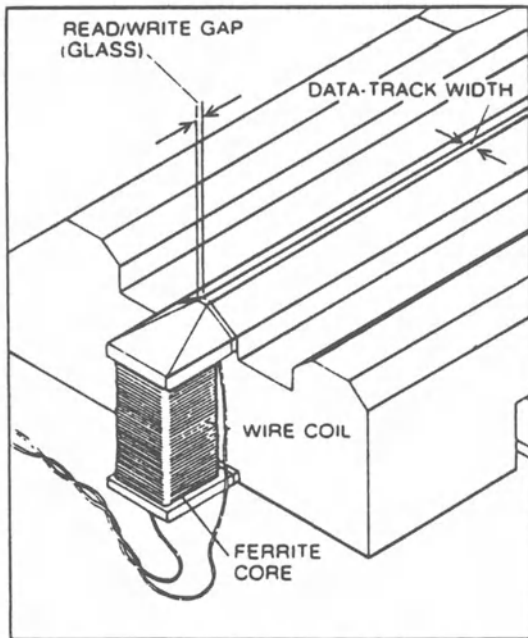
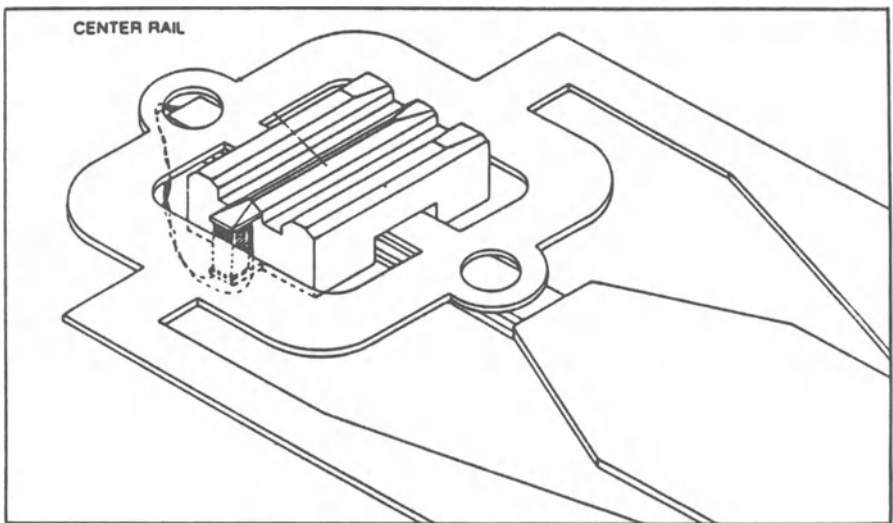


Fig. 14.1 Winchester read/write head showing the air bearing which enables the heads to start and stop in contact with the disk. © 1985 IEEE.

heads can start and stop in contact with the disk. The Winchester head air bearing is shown in Fig. 14.1. In other earlier systems the heads were gradually lowered on to the disk once it was spinning.

14.1.4 Materials for magnetic recording media

Gamma ferric oxide

The most widely used magnetic recording material is gamma ferric oxide ($\gamma\text{-Fe}_2\text{O}_3$) which has been used in magnetic tapes since 1937. Gamma ferric oxide is not a commonly occurring form of Fe_2O_3 but is produced by oxidation of specially prepared Fe_3O_4 . The coercivity of these tapes is in the range 20–30 kA/m (250–375 Oe) [4, p. 34, 5, p. 104]. The particle size is typically a few tenths of a micrometre with a length-to-diameter ratio of anything from 10:1 to 3:1. The shape anisotropy of the particles of course also determines their magnetization characteristics such as coercivity.

Saturation magnetization of the gamma ferric oxide is 370 kA/m (370 emu/cc) while the Curie temperature is about 600 °C which is sufficiently high to avoid undue temperature dependence of the properties of the medium while operating under normal conditions in the vicinity of room temperature.

Chromium dioxide

Chromium dioxide was also popular as a high-performance material for audio recording, before the cobalt-doped surface modification process was invented, in order to produce a magnetic recording material with higher coercivity than gamma ferric oxide [4, p. 39, 5, p. 110]. Chromium dioxide has a coercivity of 40–80 kA/m and can usefully be employed with a rather smaller particle size of 0.4 by 0.05 μm and hence higher recording densities are possible. Its saturation magnetization is slightly higher than gamma ferric oxide at 500 kA/m (500 emu/cc), but it has a rather low Curie temperature of 128 °C which makes its performance more temperature sensitive, a factor which is a distinct disadvantage. It is also more expensive than iron oxide which reduces its commercial attraction. It has been replaced by the cobalt-doped gamma ferric oxide as a high-performance recording material.

Cobalt surface-modified gamma ferric oxide

Cobalt surface-modified gamma ferric oxide was discovered in Japan and is now used as a magnetic recording medium because it has a higher coercivity than gamma ferric oxide [4, p. 38, 5, p. 108]. The cobalt accumulates preferentially in the surface of the tape to a depth of about 30 Å. The addition of cobalt increases the anisotropy of the material leading to higher coercivity. The disadvantage is that it lowers the Curie point leading to greater temperature sensitivity.

The cobalt is added to the ferric oxide at the last stage of processing before it is coated on to the substrate. Most video tape now contains cobalt surface-modified ferric oxide which has a coercivity of 48 kA/m (600 Oe).

Hexagonal ferrites

Hexagonal ferrites have much higher coercivities than any of the above and are used for more specialized applications such as credit cards where there is less likelihood of a need for rerecording, but where it is imperative that there is little chance of demagnetization by unanticipated exposure to low and moderate external magnetic fields.

Ferromagnetic powders

Iron powder is also used as a recording medium [5, p. 111]. This has higher saturation magnetization than the oxide particulate media described above and so can be used in thinner coatings. The coercivity of these fine particles is typically 120 kA/m. The production of the iron particle tapes is a modification of the production process for iron oxide tapes in which the oxide is finally reduced to metallic iron under a hydrogen atmosphere at 300 °C. However these tapes also need a surface coating of tin to prevent sintering whereby the particles coalesce and are no longer single domains. Typical magnetic properties are saturation magnetization 1700 kA/m (1700 emu/cc), and coercivity 120 kA/m (1450 Oe).

Thin metallic films

Metallic films are also coming under consideration for recording tapes because of their high saturation magnetization and remanence. They can be used in the form of very thin coatings since the leakage magnetic fields, which are used in the reading process, are proportional to the remanent magnetization on the tape. The higher saturation magnetization therefore ensures that these leakage fields are rather larger than for similar thin films of other materials. The pick up voltage in the read head is proportional to the magnetic field from the tape. Thinner recording media allow higher recording densities since the rate of change of field with distance dH/dx along the tape can be made larger.

Their disadvantage is that they do not wear very well and so their lifetimes are relatively short. Particulate media in a plastic binder have lubricants built in. Thin metallic films need surface coatings of lubricant and corrosion inhibitor. Metal evaporated films of nickel–cobalt alloy have been tried with varying degrees of success as have sputtered films of gamma ferric oxide.

Thin metallic films have now become the principal medium for rigid disk recording media. Aluminum disks are coated with a paramagnetic layer of nickel–phosphorus, then covered with a magnetic recording medium such as cobalt–nickel–phosphorus, cobalt–nickel–chromium or cobalt–chromium–tantalum.

This is then coated with a non-magnetic protective layer of carbon to provide lubrication and improve wear. These films have typical coercivities of 60–100 kA/m (750–1250 Oe) and saturation magnetization of (1000 emu/cc) 1000 kA/m.

Perpendicular recording media

Perpendicular recording media have been pioneered by Iwasaki in Japan [9]. These media offer higher recording density but so far seem to suffer from other problems which have prevented them becoming viable, such as the need for a very small head-to-medium distance and noise problems in the reading process. The material which has been used for this is a sputtered cobalt–chromium film containing greater than 18% Cr, which forms columns about 100–200 nm in diameter normal to the surface of the substrate. In addition, due to the nature of the growth of these films, the magnetic moments remain perpendicular to the plane of the film, unlike the previous materials in which the magnetic moments lie in the plane of the material. When the moments are perpendicular to the plane it is believed that the transitions between neighbouring ‘bits’ become much sharper leading to an increased recording density. Another material that has been tried is oriented barium ferrite.

In principle perpendicular recording has been shown to be possible, however it has yet to become more than merely of scientific interest. In practice there are problems with mechanical failure of the medium on floppy disks and also the small head-to-medium separation needed is less than present technology is capable of handling [10].

14.1.5 Bubble domain devices

Bubble domains are cylinder-shaped domains with their magnetization vector perpendicular to the plane of a thin ferromagnetic film. Until quite recently the potential uses of bubble domain devices for providing compact data storage for computers were thought to be sufficient to make them competitive with semiconductor memory devices. Their access time is relatively slow compared with other magnetic storage techniques, and much slower than semiconductor memory. However their storage capacity is very large compared with the semiconductor devices. A number of companies were actively engaged in research and development of bubble memory devices in the 1970s. Among these were Bell Telephones, Texas Instruments, Motorola and particularly Intel, but few are now active in this area.

Bubble domains are produced in thin ferrimagnetic films with high uniaxial anisotropy such that the easy axis is perpendicular to the plane of the film. This means that only two types of domain can be produced: those with magnetization ‘up’ and those with magnetization ‘down’, as shown in Fig. 14.2. There are many criteria for the development of workable bubble memory devices. Among these are

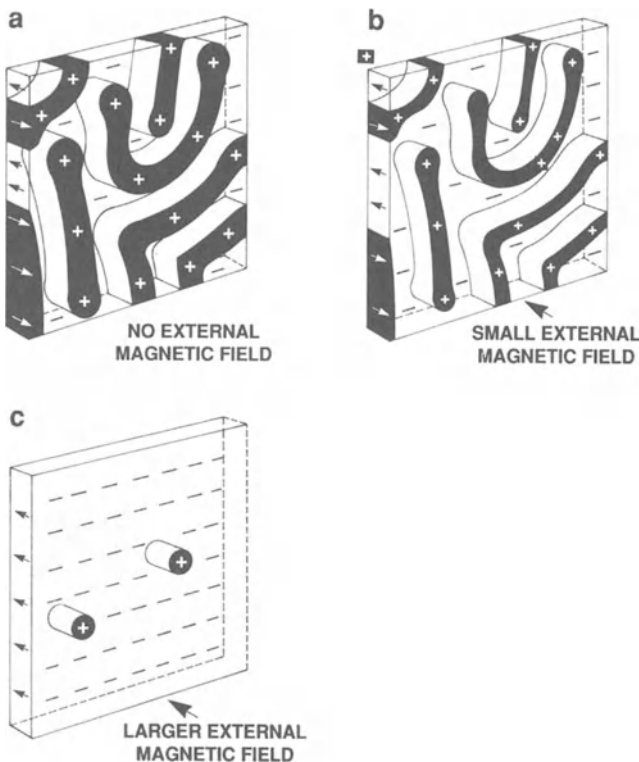


Fig. 14.2 Magnetic bubble domain patterns in a thin layer of magnetic garnet. The relative numbers of 'magnetization up' domains (white) and 'magnetization down' domains (black) are dependent on the strength of the magnetic field. The domains are observed by the magneto-optic Faraday effect. © 1985 IEEE.

the need for a magnetocrystalline anisotropy much greater than the magnetostatic energy to give stable magnetic bubbles which prefer to align along the magnetic easy axis rather than in the plane of the film, which would be preferred by the demagnetizing field. Another criterion concerns the film thickness which must not be much greater than the bubble diameter.

The materials used in bubble domain devices are rare earth iron oxides $R\cdot FeO_3$ (garnets) and their derivatives such as substituted yttrium–iron garnet $(EuY)_3(GaFe)_5O_{12}$. These superseded the orthoferrites which had high bubble mobility but large bubble size, and hexagonal ferrites, which had small bubble size but low mobility.

Once the bubble domains are created by nearly saturating the magnetization normal to the film they are very stable and can be moved around within the film without being destroyed. They even repel each other which is a useful property since it inhibits coalescence of bubbles. There are limits to the field strengths under

which the bubbles are stable however, and if this is exceeded (collapse field) the material merely becomes saturated when all bubbles disappear, or if the lower limit is exceeded (stripe-out field) the bubbles grow to form stripes and again are no longer useful. The bubbles are moved along a 'track', which is usually made by evaporating Ni–Fe on to a non-conducting, non-magnetic substrate. The bubbles are moved by using current pulses to generate local magnetic fields or by a rotating magnetic field.

The problem with bubble memories seems to be that they are just too slow successfully to compete with either magnetic tape or disk or semiconductor memory. The high-capacity tape, disk and semiconductor memories that have become available over the last few years have been able to provide sufficient storage capacity for nearly all applications at much faster speeds and the bubble memory chips are rather bulky by comparison because they need magnetic field coils. The bubble domain chips are also more expensive than magnetic tapes and disks and therefore they are not commercially competitive for mass storage of data.

14.1.6 Magneto-optic recording devices

Another area of interest in magnetic recording is that of magneto-optic devices. These make use of the Faraday and Kerr effects in which the direction of polarization of light is rotated in the presence of a magnetic field (see sections 3.2.4 and 6.1.8). In this way two oppositely magnetized regions on a magnetic medium can be distinguished. The advantage of magneto-optical disks is that the storage density can be more than 1000 times greater than for floppy disks [11, 12], while access time for magneto-optic disks are 40–100 ms which are about ten times faster than for floppy disks but are not yet competitive with access times for Winchester disks which are typically 20–60 ms [12]. The total storage capacity of a 5.25" magneto-optic disk is currently 600 MBytes. This compares with the top capacity 5.25" Winchester disks which can store 300 MBytes, and the typical 5.25" floppy which can store about 350 kBytes.

The recording of information depends on thermomagnetic magnetization in which an intense light source such as a focused laser beam is used to heat a small region of a thin film of ferrimagnetic material above its 'compensation' or Curie point and then it is allowed to cool again. If the material is exposed to a reverse magnetic field throughout the process (i.e. is operating in the second quadrant of its magnetic hysteresis loop) then we know from earlier discussion of the anhysteretic magnetization that its optimum magnetic energy state corresponds to magnetization in the opposite direction.

As it cools through the Curie point the magnetization taken by the region exposed to the laser beam will be the anhysteretic magnetization under the prevailing field, which will be in the third quadrant. This means that the regions which have been exposed to the laser beam will be magnetized in the opposite direction, as shown in Fig. 14.3.

The subsequent reading of magnetic information on the medium depends on the

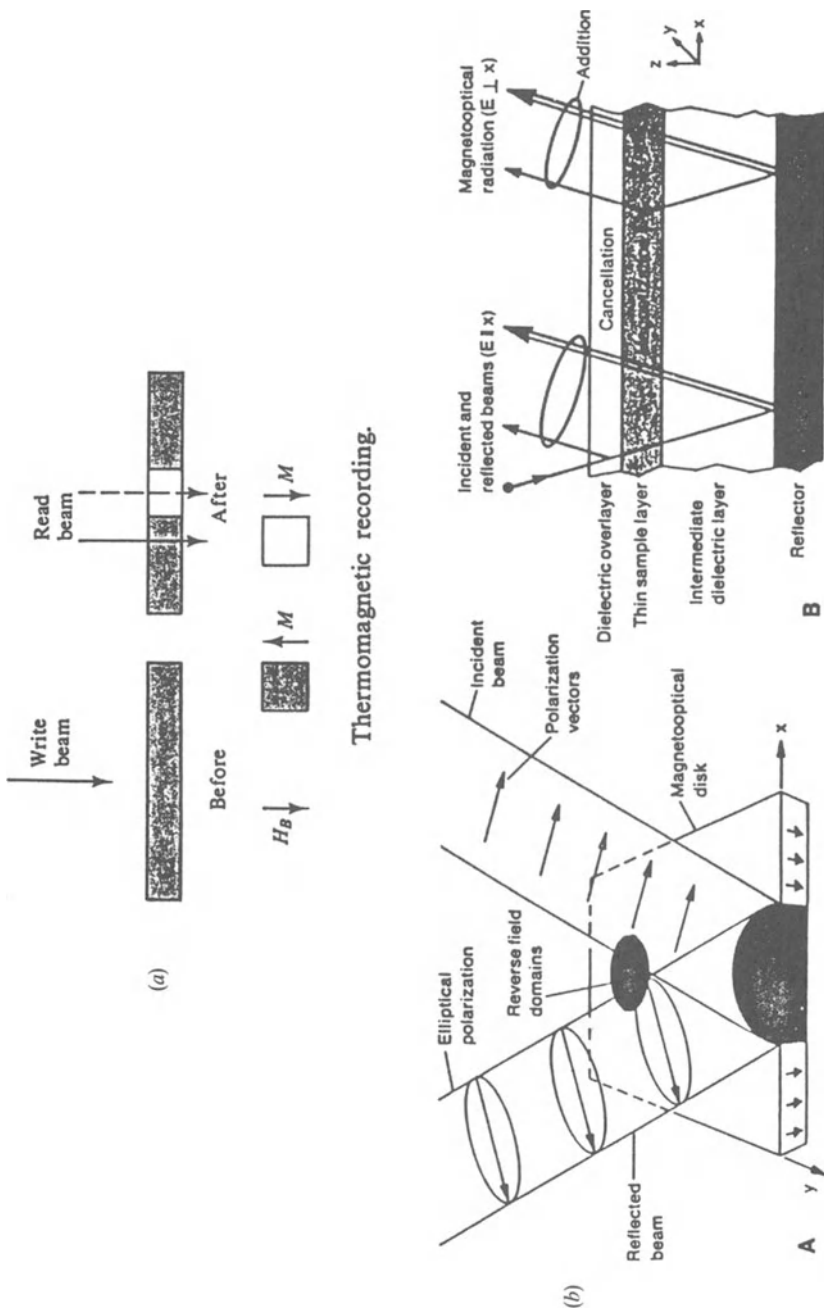


Fig. 14.3 The magneto-optic recording and reading process. In the recording process a laser beam heats a small region of the material so that its magnetization can more easily be changed by a magnetic field. In the reading process the direction of polarization of a light beam is altered by the magnetization of these regions (the Kerr effect) and this is used to determine the direction of magnetization in the region of interest. © 1985 IEEE.

magneto-optic Kerr effect. A polarized laser beam of weaker intensity than that used for writing is reflected from the surface of the magnetic recording medium, as in Fig. 14.4 and is then passed through a polarized analyser before being detected. The presence or absence of the reverse domains can then represent either '0' or '1'. The film can later be wiped clean by saturating the magnetization in the original direction.

It should be noted that for purposes of detection this technique works best in perpendicularly magnetized media. Signal to noise ratios are comparable with conventional magnetic disk recording. Magneto-optic disks made by Philips have a 500 Å thick magnetic coating on a transparent 3 mm thick plastic substrate. Their method uses a 3 mW laser with a spot size of 2×5 micrometres reading the disk by the Faraday effect. Whereas the recording densities of these magneto-optic disks are about two or three times greater than that of high-performance conventional magnetic hard disk drives, the access time is generally about twice as long.

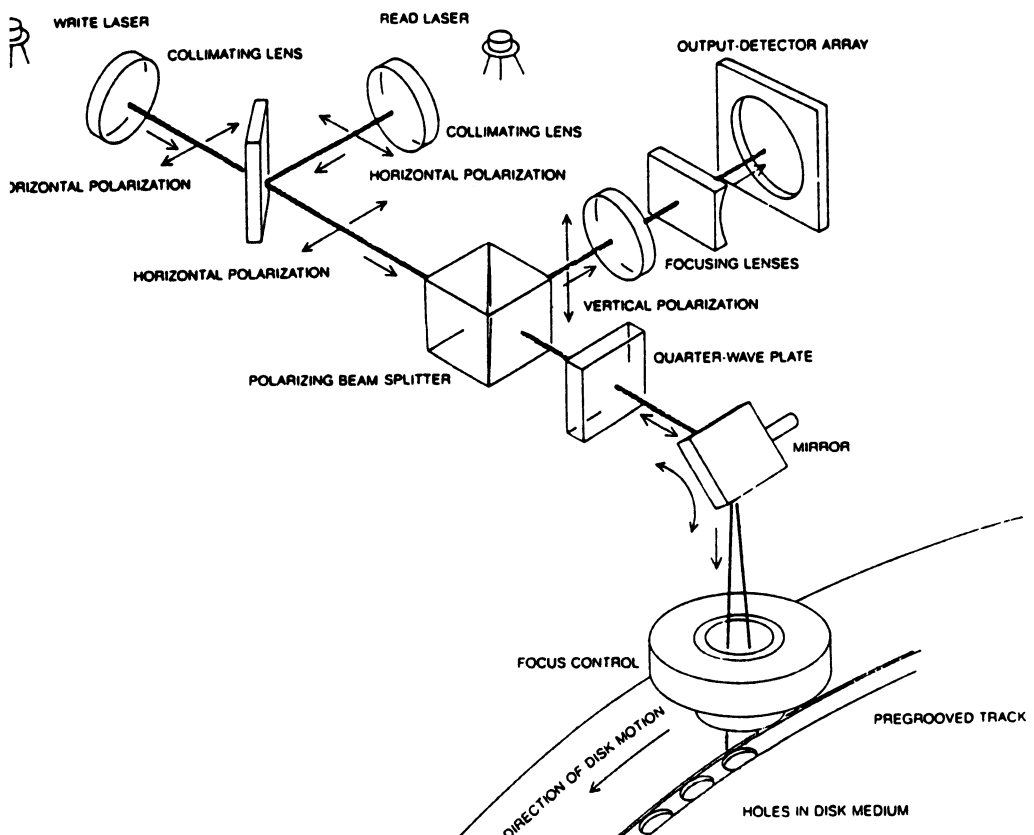


Fig. 14.4 A simplified diagram showing the conventional optical recording method using a laser to burn holes in the optical disk. This is a non-erasable process unlike magneto-optic recording. © 1985 IEEE.

14.2 THE RECORDING PROCESS AND APPLICATIONS OF MAGNETIC RECORDING

The recording process involves the mechanism by which a magnetic imprint is left on the magnetic medium and the mechanism by which this imprint is read from the medium and the original information, whether an audio signal or some digital data, is recreated. A recent detailed review which discusses the fundamentals of the magnetic recording process has been given by Bertram [13].

The writing process is the means of transferring electrical impulses in a coil wound on an electromagnet (the writing head) into magnetic patterns on the storage medium. The reading process is the inverse of this mechanism. The reading process is quite well understood since it requires no knowledge of the magnetization characteristics of the medium. Only the remanent magnetization of the medium determines the response. However the writing process, which involves the effect of an applied field on the magnetization of a magnetic medium, is by comparison still rather poorly understood. This is because it is difficult accurately to model the dependence of magnetization of the medium on the magnetic field even when the field is completely uniform, and in these cases the field is not even uniform.

14.2.1 Recording heads

Recording heads are small electromagnets in the form of a ferromagnetic core with a very small pole gap of typical width $0.3\ \mu\text{m}$, as shown in Fig. 14.5. The recording head material must have high saturation magnetization in order to leave a large imprint (high magnetization) on the tape but it must also have low remanence to ensure that there is no writing when the current in the coil is zero. Further it is also clear that a low coercivity is desirable. Recording heads are constructed of magnetically soft material. Many of the soft magnetic materials described in Chapter 12 are suitable for the cores of recording heads; these include soft ferrites, Al–Fe, Al–Fe–Si, Permalloy, and amorphous cobalt–zirconium.

The magnetic tape or disk passes the head where the fringing field causes a realignment of the magnetization within the single-domain articles. The magnetization in the tape is then a record of the strength of the field in the gap of the recording head at the time that the tape passed it. In reading mode the passage of the tape causes a variation in flux density in the reading head which is then converted into a voltage in the coil wound on the reading head. The signal is then amplified and, in the case of audio recording, used to activate a loudspeaker.

The magnetic field in the gap of the write head, which is the main region of interest to the magnetic recording engineer in the writing process, can be determined by the finite-element techniques described briefly in Chapter 1. This fringing field is shown in Fig. 14.6. With present technology which uses parallel recording media the tape responds to the component of the fringing field which is parallel to the tape surface. However for perpendicular recording the fringing field

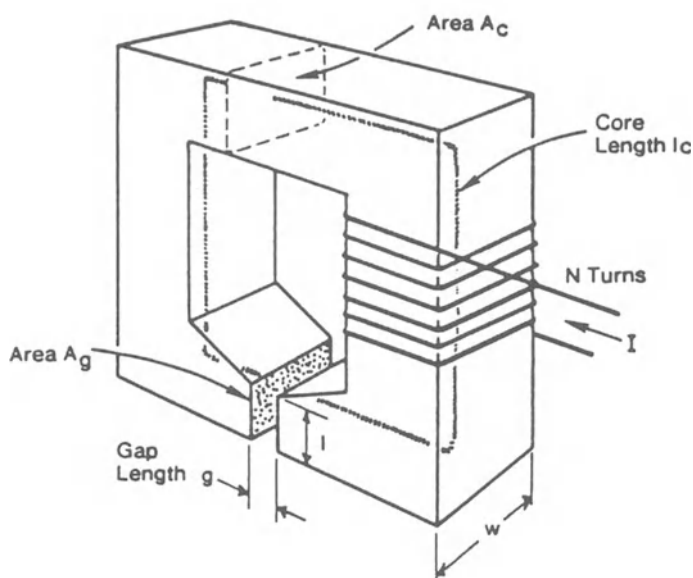
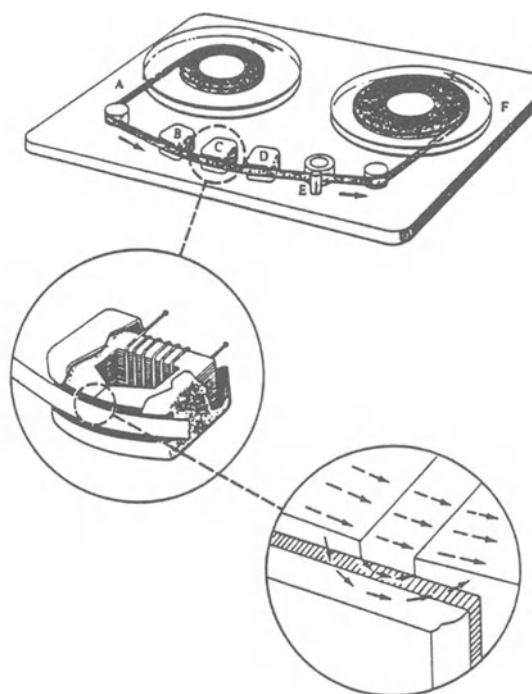


Fig. 14.5 Magnetic recording heads used in tape recording.

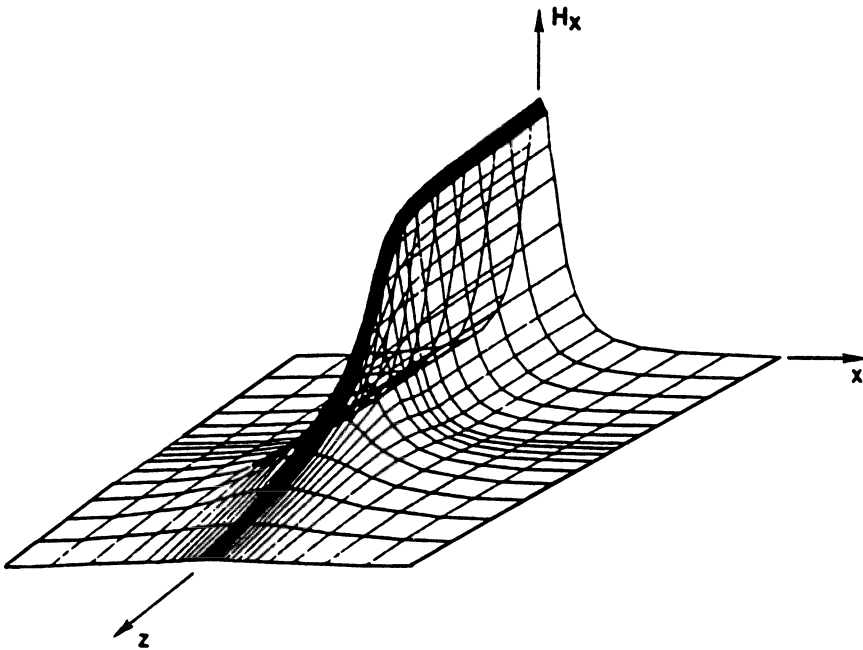


Fig. 14.6 The magnetic fringing field in the gap of a recording head.

needs to be normal to the plane of the tape or disk and this leads to differences in the design of the read and write heads.

14.2.2 Writing head efficiency

Head efficiency is the ratio of magnetomotive force obtained across the head gap to the magnetomotive force supplied by the energizing coil. This is determined from consideration of the magnetic circuit formed by the magnetic core and air gap of the head.

In the air gap

$$B_g = \mu_0 H_g$$

In the core

$$B_c = \mu_r \mu_0 H_c$$

where μ_r is the relative permeability of the core and here H_c is the field in the core.

The magnetomotive force of the driving coil is also the magnetomotive force across the whole magnetic circuit. If l_g is the length of the gap and l_c is the length of the ferromagnetic core

$$Ni = H_c l_c + H_g l_g$$

The efficiency of the core, being simply the ratio of magnetomotive force across the gap $H_g l_g$ to the magnetomotive force supplied from the coil Ni is then

$$\eta = \frac{H_g l_g}{(H_c l_c + H_g l_g)}$$

$$\eta = \frac{H_g l_g}{Ni}$$

The efficiency can also be expressed in terms of the reluctances of the magnetic paths R_c in the core and R_g in the gap.

$$\begin{aligned} \eta &= \frac{R_g}{(R_c + R_g)} \\ &= \frac{\left(\frac{l_g}{A_g}\right)}{\left(\frac{l_g}{A_g} + \frac{l_c}{\mu_r A_c}\right)} \end{aligned}$$

where A_c is the cross-sectional area of the core and A_g is the cross-sectional area of the gap. This means that a large gap field, and hence a large fringing field, requires a large permeability μ_r in the core and a large ratio A_c/A_g .

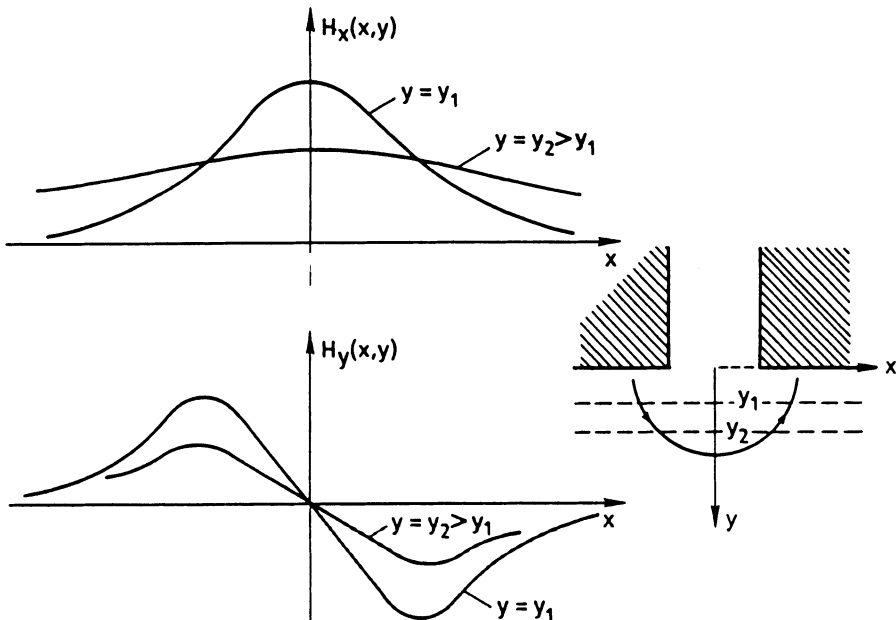


Fig. 14.7 Vertical and horizontal components of the magnetic field in the vicinity of a Karlqvist head.

The head gap together with the saturation magnetization of the head material determines the field in the gap, as indicated from the discussion of air gaps in magnetic circuits in Chapter 2. This determines the fringing field in the vicinity of the gap and consequently the maximum coercivity of the recording medium that can be used with the head.

Karlqvist heads [14] are an idealization often used for calculating the field in the vicinity of the gap. In Karlqvist heads the pole gap is small compared with the pole tip lengths, such as in the head depicted in Fig. 14.7. These provide a relatively simple geometrical situation for determining the magnetic field in the gap. The heads on a Winchester disk drive are a good example of Karlqvist heads.

14.2.3 The writing process

We now consider the process of magnetizing the recording media. Specifically we wish to know how the medium responds to an applied field in the head gap. In general this is a rather difficult problem which is not very well understood although some empirically based models can be used to good effect. One problem that arises as the medium passes close to the head is that the magnetic fields at different depths in the magnetic medium are different, as shown in Fig. 14.8. Secondly, as the medium passes the gap the field it experiences changes with time.

To give an example of the writing process we will suppose that a given region of the recording medium passing the head begins at the positive remanence point on its hysteresis curve, as shown in Fig. 14.9. Then as it passes the gap with a negative field the material passes down the second quadrant of the hysteresis loop to its coercive point $-H_c$ for example. As it passes the head the magnetic field it experiences from the head gap decreases to zero and the material magnetization passes along a recoil minor hysteresis loop to $H = 0$, ending with a small positive remanence.

This means that even where the magnetization had been reduced to zero at the coercive point the magnetization will actually finally increase again to give a positive remanent magnetization. Therefore to result in a completely demagnetized state $\mathbf{M} = 0$ the field experienced by the medium must be greater than $-H_c$, a point referred to as the remanent coercivity H_{cr} . A very square hysteresis loop in which the recoil minor loops are very flat ($dM/dH \approx 0$) is therefore desirable.

During the writing process the time-varying current in the writing head coil changes thereby altering the field in the gap. This causes localized changes in the magnetization in the recording medium which passes the write head at a constant speed. It has proved very difficult to determine the magnetization of the tape in two dimensions and therefore theoretical models have only limited usefulness in the predictions of tape magnetization.

Models for the magnetization of the recording medium usually make use of some very simplistic approximations to the magnetization characteristics of the medium such as assuming \mathbf{M} is a single-valued function of field. One such model is the Williams–Comstock [15] model. This is a one-dimensional model which

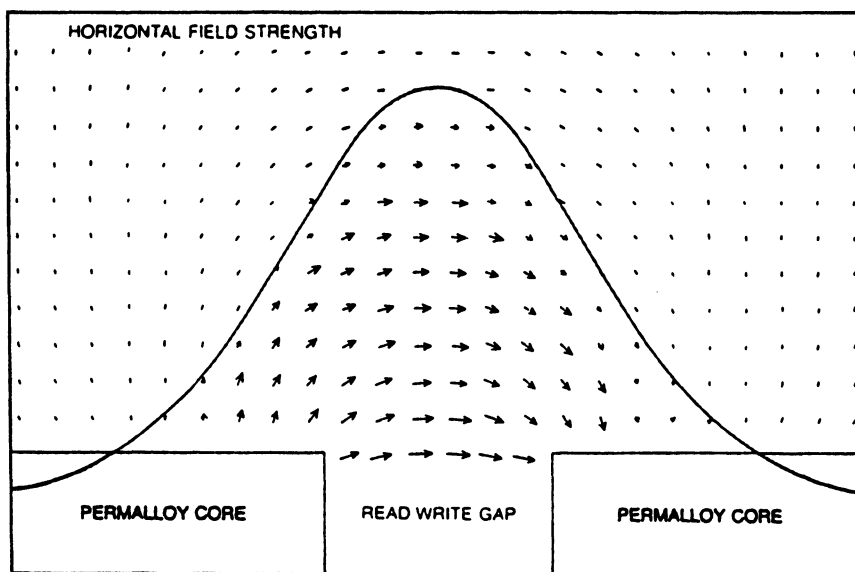
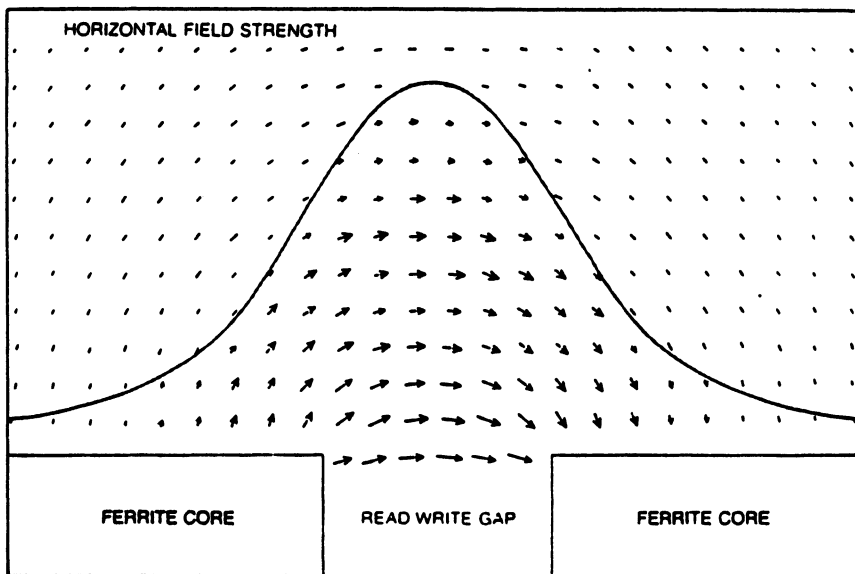


Fig. 14.8 Variation of the magnetic field strength in both direction and magnitude close to
(a) a Winchester head and (b) a thin film head. © 1985 IEEE.

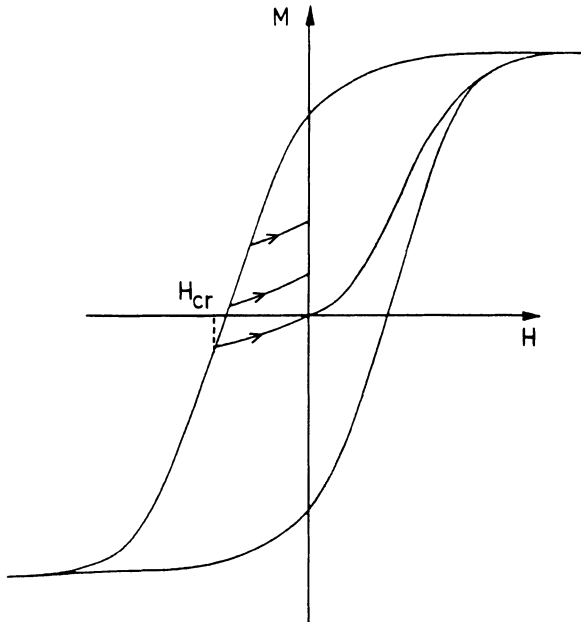


Fig. 14.9 Recoil minor loops during the writing process for different regions of a magnetic recording medium as it passes a recording head.

employs the arctangent function. The magnetization $M(x)$ in the tape can be expressed as a function of distance in response to a step function change in field in the gap by the equation

$$M(x) = \left(\frac{2M_R}{\pi} \right) \text{Arctan} \left(\frac{x}{a} \right),$$

where x is the distance along the tape or disk, a is an adjustable parameter which is determined by the rate of change of magnetization with distance and M_R is the remanent magnetization.

14.2.4 Recording density

The recording density in a medium depends on the magnetic properties of the medium and the characteristics of the writing head. The recording density is determined by the product of bits per inch (BPI) and the number of tracks per inch (TPI). The maximum attainable BPI can be measured by the parameter a , known as the transition length, which is the minimum distance along the tape that is needed to reverse completely the magnetization from saturation remanence in one direction to saturation remanence in the other direction.

The transition length in which a signal can be made to change is dependent on dM/dx in the recording medium. This can be expressed as the product $(dM/dH)(dH/dx)$, where (dM/dH) is a property of the medium, specifically the

slope of the hysteresis curve, while (dH/dx) is a property of the writing head. If we make the approximation that the slope of the hysteresis loop is constant then for a fixed field gradient in the head gap we have the following expression for the transition length a

$$a = \frac{\left(\frac{2M_R}{\pi}\right)}{\left(\frac{dM}{dx}\right)}$$

$$= \frac{\left(\frac{2M_R}{\pi}\right)}{\left(\frac{dM}{dH}\right)\left(\frac{dH}{dx}\right)}.$$

This can be verified from the Williams–Comstock equation above. The transition length a is therefore made smaller for large field gradient dH/dx and large dM/dH on the major hysteresis loop, that is for a square hysteresis loop. Of course there are other factors which have not been taken into account in this simple analysis, such as the demagnetizing field in the tape and the spatial variation in the transition region. However these do not alter the basic conclusion about the desirability of high field gradient in the gap and square hysteresis loop materials. Notice that while large dM/dH on the major hysteresis loop is desirable this should coincide with small dM/dH on the recoil minor loops.

14.2.5 a.c. bias recording

When signals are recorded in analog form, such as in audio recording, it is advantageous to have the recorded signal proportional to the amplitude of the input signal. The recorded signal is the remanent magnetization on a region of the magnetic tape, while the input signal voltage is converted to an applied field in the recording head gap. Because the initial part of the magnetization curve is nonlinear the remanent magnetization on the tape would be a nonlinear function of the applied field if the d.c. initial magnetization curve of the tape were used. However by a.c. biasing, which produces the anhysteretic magnetization curve, the variation of remanence with applied field is linear at low fields, and this produces a more desirable recording characteristic which also improves the signal to noise ratio.

14.2.6 The reading process

The reading process in magnetic recording is very well understood. The tape or disk passes below the read head and causes a fluctuation in the flux density in the magnetic core of the read head. The fringing fields from the tapes can be dealt with using simple models.

For example, consider the situation shown in Fig. 14.10. As the tape passes near

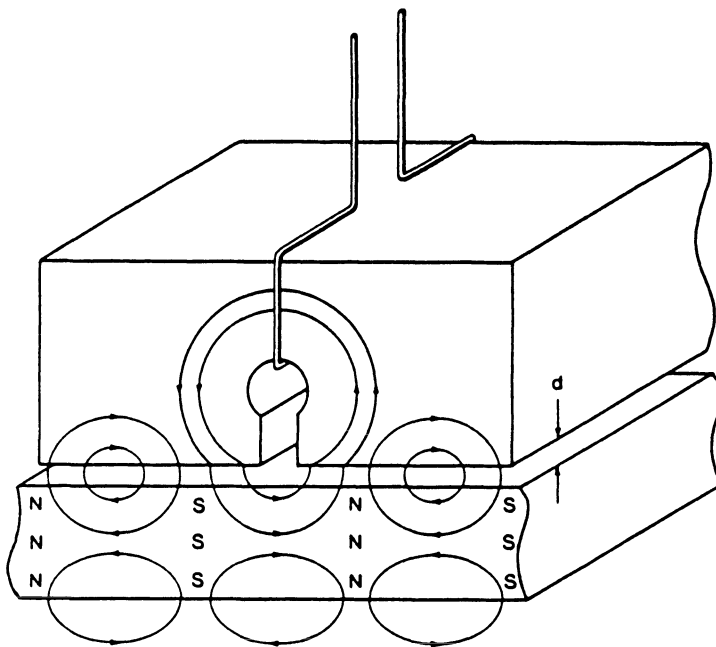


Fig. 14.10 Schematic diagram of magnetic flux capture by the high-permeability read head during the reading process.

to the reading head the stray field associated with the magnetic imprint on the medium enters the reading head. At the gap this field passes through the coil giving a voltage which, as we have shown earlier, is proportional to $-dB/dt$, the rate of change of magnetic induction linking the coil. Therefore the voltage in the reading head will be dependent on the stray magnetic induction emanating from the tape which is collected by the head and passed through the coil.

The reading head efficiency is defined as the ratio of the tape flux entering the reading head that actually passes through the sensing coil.

14.2.7 Various types of recording devices

The most common form of magnetic recorders are audio recorders. These have traditionally been analog recording devices which use a.c. bias recording, that is they make use of the linearity of the anhysteretic remanent magnetization curve to avoid distortion of the reproduced signal. By this method it is possible to make the magnetization imprinted on the recording medium proportional to the amplitude of the signal. In audio recording, particularly music, any distortion of the signal is undesirable. Therefore the reading and recording processes take place relatively slowly. The typical tape velocity in professional audio recording is 40 cm/s [13], while on audio cassettes it is less than 5 cm/s [13, 16].

Video recorders use frequency modulation in which the signal $S(t)$ imprinted on the tape is related to the original input signal $f(t)$ by

$$S(t) = \cos\left(\omega t + 2\pi\beta \int f(t) dt\right),$$

where ω is the carrier frequency and β is the modulation index. The video signals range from 30 Hz to 7 MHz so that tape velocities are relatively fast and may be up to 500 cm/s [13].

Digital recorders are in most cases peripheral devices for computers, whether disks or tapes. Lately, however, digital recording of music has also become available. In digital recording it is only necessary to distinguish between '0' and '1' so these devices can function with much lower signal to noise ratios than are acceptable in analog recording. Furthermore since in digital recording the actual level of the signal is not really crucial, providing that a '0' and '1' can be distinguished, the reading and writing process is very fast. However, even though the signal to noise ratio can be relatively small in digital recording the tolerable error rate is also very low.

14.2.8 The Preisach model

In the magnetic recording industry the magnetic properties of the medium are usually represented using a model for magnetization as a function of field that was devised in the 1930s by Preisach in Germany [17]. This model really does not give much physical insight into the magnetic properties of materials, being a essence merely a complicated curve-fitting procedure, but it can be used to give reasonable mathematical representations of hysteresis curves once the curves are already known. It has been found useful for modelling the magnetic properties of the recording media and is quite widely used in the recording industry [18].

The essential idea of the Preisach model is that the observed bulk magnetic hysteresis loop of a material is due to a summation of more elementary hysteresis loops of domains with differing switching fields (coercivities). These domains can only have two states within the confines of the model, with magnetization parallel or antiparallel to a given direction. The model relies on a density function called the Preisach function which is defined on a plane described by the positive and negative fields H_+ and H_- . This function is used to determine how many domains switch their orientation from + to -, or vice versa, as the field is swept between limiting values of magnetic field H .

The model works fairly well for weak interactions between domains such as occur in these media, which are simply aggregates of single-domain particles, and because the magnetic moments within the elongated single-domain particles can only have magnetic moments along one axis leading to a magnetization either parallel or antiparallel to the long axis of the particles.

14.2.9 Stoner–Wohlfarth theory

The Stoner–Wohlfarth theory [19] which was discussed in the previous chapter has far more relevance to particulate recording media than to hard ferromagnetic alloys. In the particulate media the isolated single-domain particles are deliberately created on the tapes or disks and these are clearly well-suited for the application of Stoner–Wohlfarth. The model has therefore found appropriate applications in determining the magnetization characteristics of fine-particle recording media [20].

REFERENCES

1. Poulsen, V. (c. 1899) Danish patent No. 2653; (1905) US patent No. 789,336.
2. Carlson, W. L. and Carpenter, G. W. (1921) referenced in White, R. M. (1984) *Introduction to Magnetic Recording*, IEEE, p. 1.
3. Holmes, L. C. and Clark, D. L. (1945) *Electronics*, **18**, 126.
4. Mallinson, J. C. (1987) *The Foundations of Magnetic Recording*, Academic Press, San Diego.
5. Camras, M. *Magnetic Recording Handbook*, Van Nostrand, New York.
6. Jeanniot, D. and Bull, S. A. (1988) *IEEE Trans. Mag.*, **24**, 2476.
7. deBie, R. W., Luitjens, S. B., Zieren, V., Schrauwen, C. P. G. and Bernards, J. P. C. (1987) *IEEE Trans. Mag.*, **23**, 2091.
8. Harker, J. M. (1981) A quarter century of disk file innovation, *IBM J. Res. Develop.*, **25**, 677.
9. Ouchi, K and Iwasaki, S. (1987) *IEEE Trans. Mag.*, **23**, 180.
10. Bonnebat, C. (1987) *IEEE Trans. Mag.*, **23**, 9.
11. White, R. M. (1983) *IEEE Spectrum*, **20**(8), 32.
12. Freese, R. P. (1988) *IEEE Spectrum*, **25**(2), 41.
13. Bertram, H. N. (1986) *Proceedings IEEE*, **74**, 1512.
14. Karlqvist, O. (1954) *Trans. Roy. Inst. Techn. (Stockholm)*, 86.
15. Williams, M. L. and Comstock, R. L. (1971) *AIP Conf. Proc. No. 5*, 758.
16. Crangle, J. (1977) *The Magnetic Properties of Solids*, Edward Arnold, London.
17. Preisach, F. (1935) *Zeit. Phys.*, **94**, 277.
18. Della Torre, E. and Kadar, G. (1988) *J. Appl. Phys.*, **63**, 3004.
19. Stoner, E. C. and Wohlfarth, E. P. (1948) *Phil. Trans. Roy. Soc. Lond.*, **A240**, 599.
20. Chantrell, R. W., O'Grady, K., Bradbury, A., Charles, S. W. and Hopkins, N. (1987) *IEEE Trans. Mag.*, **23**, 204.

FURTHER READING

- Bate, G. (1980) Recording materials, in *Ferromagnetic Materials*, Vol. 2 (ed. E. P. Wohlfarth), North Holland Amsterdam.
- Camras, M. (1988) *Magnetic Recording Handbook*, Van Nostrand, New York.
- Hoagland, A. S. (1983) *Digital Magnetic Recording*, Robert Krieger, Orlando, Florida.
- Jorgensen, F. (1980) *Handbook of Magnetic Recording*, TAB Books, Blue Ridge Summit, Pennsylvania.
- Mallinson, J. C. (1987) *The Foundations of Magnetic Recording*, Academic Press, San Diego.
- Mee, C. D. (1964) *The Physics of Magnetic Recording*, North Holland, Amsterdam.
- White, R. M. (1980) Disc storage technology, *Scientific American*, August.
- White, R. M. (1983) Magnetic disks: Storage densities on the rise, *IEEE Spectrum*, August.
- White, R. M. (1984) *Introduction to Magnetic Recording*, IEEE Press, New York.

15

Superconductivity

Superconductivity is not really part of magnetism but the two subjects do have considerable common ground, for example in the unusual magnetic properties arising from the Meissner effect and in the generation of high magnetic fields using superconducting coils. It is a subject in its own right and consequently we can only present a summary here which, while omitting much of the detail, gives a guide to the main results and ideas with suggestions for further reading.

15.1 BASIC PROPERTIES OF SUPERCONDUCTORS

Electrical resistivity in solids is such a familiar property that it came as rather a surprise when zero d.c. resistivity was discovered in mercury at low temperature by Kamerlingh Onnes in 1911 [1]. This phenomenon was named superconductivity. Since the original discovery a number of elements and many alloys have been found to exhibit this state. The elements known to exhibit superconductivity together with their transition temperatures are shown in Fig. 15.1.

It is of course well known that the resistivity of metals increases with temperature due to the scattering of electrons by various means, including the ionic sites which vibrate with greater amplitude as the temperature increases (phonon scattering). As the temperature decreases towards absolute zero the resistivity decreases continuously due to the reduction in phonon scattering, but does not reach zero because of impurity and defect scattering which leaves a residual resistance even when resistivity is extrapolated to absolute zero of temperature.

This continuous reduction of resistivity with decreasing temperature does not lead to superconductivity. In superconductivity, as the temperature decreases there occurs a rapid or in some cases nearly discontinuous reduction in resistivity. It is this which marks the onset of the superconducting state and it appears to be the result of a totally different conduction mechanism rather than merely a limiting case of the normal conduction mechanism.

One model that was proposed for understanding the properties of superconductors was the two-carrier model of Gorter and Casimir [2] and this is still a useful concept. The model assumes there are two types of charge carrier:

¹ H																² He	
³ Li	⁴ Be									⁵ B	⁶ C	⁷ N	⁸ O	⁹ F	¹⁰ Ne		
¹¹ Na	¹² Mg									¹³ Al 1.20	¹⁴ Si	¹⁵ P	¹⁶ S	¹⁷ Cl	¹⁸ A		
¹⁹ K	²⁰ Ca	²¹ Cs	²² Tl 0.39	²³ V 5.3	²⁴ Cr	²⁵ Mn	²⁶ Fe	²⁷ Co	²⁸ Ni	²⁹ Cu	³⁰ Zn 0.88	³¹ Ga 1.09	³² Ge	³³ As	³⁴ Se	³⁵ Br	³⁶ Kr
³⁷ Rb	³⁸ Sr	³⁹ Y	⁴⁰ Zr 0.6	⁴¹ Nb 9.3	⁴² Mo 0.95	⁴³ Tc 8	⁴⁴ Ru 0.49	⁴⁵ Rh	⁴⁶ Pd	⁴⁷ Ag	⁴⁸ Cd 0.56	⁴⁹ In 3.4	⁵⁰ Sn 3.7	⁵¹ Sb	⁵² Te	⁵³ I	⁵⁴ Xe
⁵⁵ Cs	⁵⁶ Ba	⁵⁷ La $\alpha 4.9$ $\beta 6$	⁷² Hf 0.1	⁷³ Ta 4.5	⁷⁴ W 0.01	⁷⁵ Re 1.7	⁷⁶ Os 0.66	⁷⁷ Ir 0.14	⁷⁸ Pt	⁷⁹ Au	⁸⁰ Hg $\alpha 4.15$ $\beta 3.95$	⁸¹ Tl 2.4	⁸² Pb 7.2	⁸³ Bi	⁸⁴ Po	⁸⁵ At	⁸⁶ Rn
⁸⁷ Fr	⁸⁸ Ra	⁸⁹ Ac	⁹⁰ Th 1.37	⁹¹ Pa 1.4	⁹² U $\alpha 0.68$ $\beta 1.80$												

Fig. 15.1 Periodic table showing elements which exhibit superconductivity.

1. ‘superconducting’ carriers condensed into an ordered state with zero entropy which are not scattered by collisions with the lattice; and
2. ‘normal’ carriers which are scattered by collisions with the lattice.

It must be remembered that although the d.c. resistivity in these materials is zero in the superconducting state, the a.c. losses remain finite due to eddy currents, but at low frequencies these losses are very small (see also section 15.1.4).

15.1.1 Critical temperature

The most characteristic feature of the superconductor is the complete disappearance of d.c. electrical resistivity at a critical temperature T_c . In zero field this is a second-order transition. The results of Fig. 15.2 are the original data of Kamerlingh Onnes for the resistance of mercury which can be seen to exhibit a sudden change at close to 4.2 K. In nearly perfect single crystals the transition is very sharp, occurring over a range of less than a millikelvin in some cases.

The resistance of superconductors is so low that persistent electrical currents have been found to circulate in a superconducting loop for several years without diminution. This absence of detectable decay of current has indicated an upper limit to the resistivity of $10^{-25} \Omega \text{m}$ which may be compared with the lowest resistivity of pure copper at low temperatures of $10^{-12} \Omega \text{m}$. It is also found that

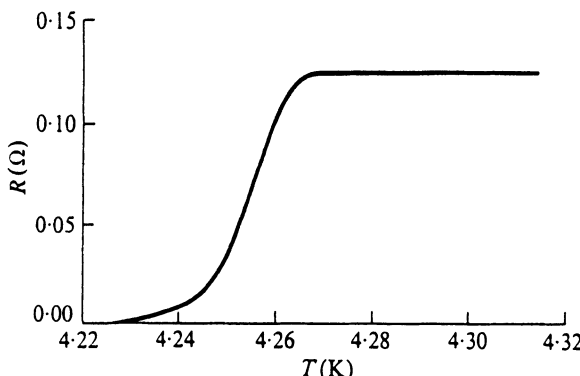


Fig. 15.2 Original data of Kamerlingh Onnes showing the superconduction transition in mercury.

there is no correlation between the normal electrical resistivity of the superconductors above their critical temperature and their performance below the critical temperature. In fact superconductors have relatively high resistivity at room temperature, for example lead which has $\rho \approx 20 \times 10^{-8} \Omega \text{ m}$.

Until quite recently the highest known critical temperature was 23.2 K observed in Nb_3Ge , but in 1986 there began a series of developments in the ceramic

Table 15.1 Table showing the sudden progress in high T_c superconductors in 1986–8

Date	Development	Researchers	Institution
Apr. '86	La–Ba–Cu–O superconducts at 30 K	Bednorz and Muller	IBM, Zurich
Dec. '86	Confirmation of IBM result La–Ba–Cu–O under pressure superconducts at 40 K	Tanaka and Kitazawa Chu	Tokyo University Houston University
	La–Sr–Cu–O superconducts at 36 K	Cava	AT&T Bell Labs
Jan. '87	La–Ba–Cu–O superconducts at 70 K	Zhao	Chinese Academy of Sciences
Feb. '87	Y–Ba–Cu–O superconducts at 95 K	Chu and Wu	Houston University
May. '87	Critical current densities in excess of 10^5 A/cm^2 in Y–Ba–Cu–O	Chaudhari	IBM Yorktown Heights
Nov. '87	Critical current density of 7000 A/cm^2 in bulk Y–Ba–Cu–O	Jin	AT&T Bell Labs
Jan. '88	Bi–Sr–Ca–Cu–O superconducts at 106 K	Maeda	NRIM Tsukuba, Japan
Feb. '88	Th–Ba–Ca–Cu–O superconducts at 106 K	Herman and Sheng	University of Arkansas
Mar. '88	Th–Ba–Ca–Cu–O superconducts at 125 K	Parkin	IBM Almaden

superconductors [3, 4] based on cuprate materials with a perovskite structure, such as lanthanum–barium–copper oxide. This lead to the highest known critical temperature being raised to 125 K for $\text{Th}_2\text{Ba}_2\text{Ca}_2\text{Cu}_3\text{O}_{10}$ by early 1988, Table 15.1.

15.1.2 Critical field

A few years after the discovery of superconductivity it was found that the superconducting state can be destroyed by application of a magnetic field above a certain strength. The value of the critical field depends on the temperature and on the material. In type I superconductors (see section 15.1.3) it can be accurately represented by the simple equation

$$H_c = H_0[1 - (T/T_c)^2]$$

Table 15.2 Critical temperature and critical field strengths for the superconducting elements

Element		T_c (K)	H_0 (kA/m)
Aluminum		1.2	7.9
Cadmium		0.5	2.4
Gallium		1.1	4.1
Indium		3.4	22
Iridium		0.1	1.6
Lanthanum	α	4.8	
	β	4.9	
Lead		7.2	64
Mercury	α	4.2	33
	β	4.0	27
Molybdenum		0.9	
Niobium		9.3	Type II
Osmium		0.7	5
Rhenium		1.7	16
Ruthenium		0.5	5.3
Tantalum		4.5	66
Technetium		8.2	
Thallium		2.4	14
Thorium		1.4	13
Tin		3.7	24
Titanium		0.4	
Tungsten		0.01	
Uranium	α	0.6	
	β	1.8	
Vanadium		5.3	Type II
Zinc		0.9	4.2
Zirconium		0.8	3.7

which means that the critical field becomes zero at the critical temperature T_c . Values H_0 for the elements are shown in Table 15.2. It must also be remembered that the critical field strength can be caused by the current carried by a superconductor as well as by an externally applied field.

15.1.3 Type I and type II superconductors

There are two main classifications of superconductors based on the nature of their transition to the normal state when a magnetic field is applied. The type I superconductors follow the Meissner–Ochsenfeld [5] behaviour up to their critical field H_c . Type II superconductors undergo a transition region from the type I superconducting state at a critical field H_{c1} to the ‘mixed’ state, also known as the ‘vortex’ state, in which the applied field does partially penetrate the material. At a higher field H_{c2} the material undergoes a further transition from the ‘mixed’ state to the normal state.

Type I superconductors exclude the magnetic field until the superconductivity is spontaneously destroyed at the critical field H_c as shown in Fig. 15.3(a). These superconductors have generally rather low critical fields and are not found very useful for applications.

Type II superconductors exclude the field entirely up to the field H_{c1} . Beyond this field the flux partly penetrates the material (the vortex state) but some superconducting volume remains until the critical field H_{c2} is reached, when the flux penetrates completely and the superconducting state is destroyed (Fig. 15.3(b)). These are the superconductors used for applications such as superconducting solenoids.

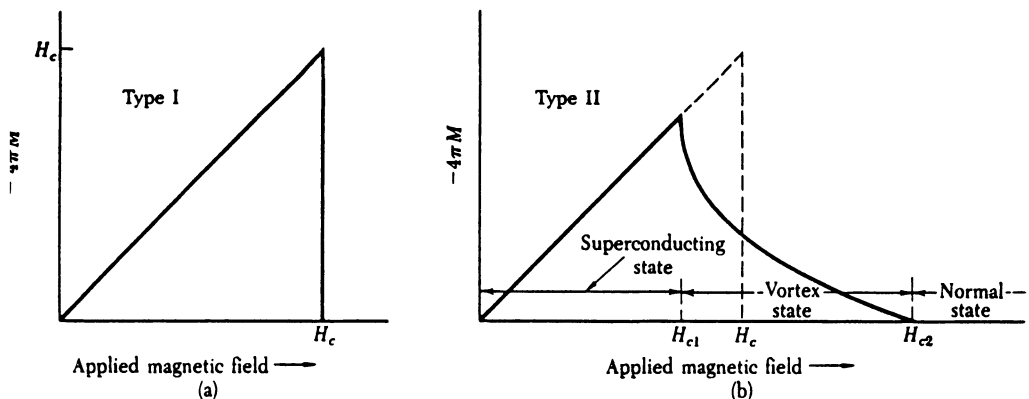


Fig. 15.3 Magnetization function of applied field in superconductors. (a) A type I superconductor which exhibits perfect diamagnetism via the Meissner effect, up to its critical field strength H_c . At field strengths above H_c the material is a normal conductor. (b) A type II superconductor which exhibits perfect diamagnetism up to the field strengths H_{c1} whereupon the field begins to penetrate the material. The material is in the ‘vortex’ state between H_{c1} and H_{c2} . At field strengths above H_{c2} the material is a normal conductor.

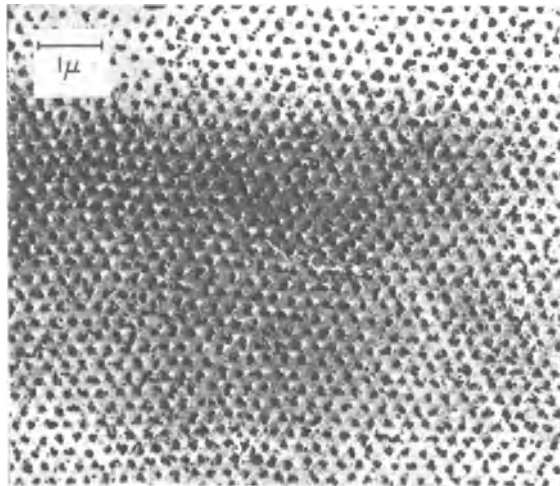


Fig. 15.4 Mixed state in a type II superconductor. The dark regions are normal material within a matrix of superconducting material (the light regions).

In the intermediate ‘mixed’ state, of type II superconductors the material consists of tubes or bundles of normal (i.e. non-superconducting) metal, known as vortices, carrying magnetic flux lying inside a matrix of superconducting material in which there is no flux penetration. Figure 15.4. shows a photograph of the end of a type II superconductor in its vortex state. The dark regions represent the normal metal where the magnetic flux emerges from the surface. The radius of the vortices is equal to the penetration depth. Each vortex carries one quantum of magnetic flux $B = h/2e = 2.067 \times 10^{-15}$ Wb.

Pure metals tend to be type I superconductors while alloys tend to be type II. Type I can be changed to type II by the addition of a small amount of an alloying element. For many years it was thought that the type II superconductors were an imperfect form of type I caused by the presence of impurities in the metal, but it is now understood that the type II superconductors are a different class of materials with fundamentally different properties. The theory of type II superconductors has been developed by Abrikosov [6] Ginzburg and Landau [7] and Gorkov [8].

15.1.4 Flux pinning in type II superconductors

In type II superconductors the vortices in the normal material through which the magnetic flux penetrates are pinned by microstructural defects and grain boundaries. So long as the vortices remain pinned the material exhibits superconductivity. However as the magnetic field is increased the vortices pile up and eventually overcome the pinning forces. They then swirl through the material and provide resistance to the passage of electrons causing loss of the

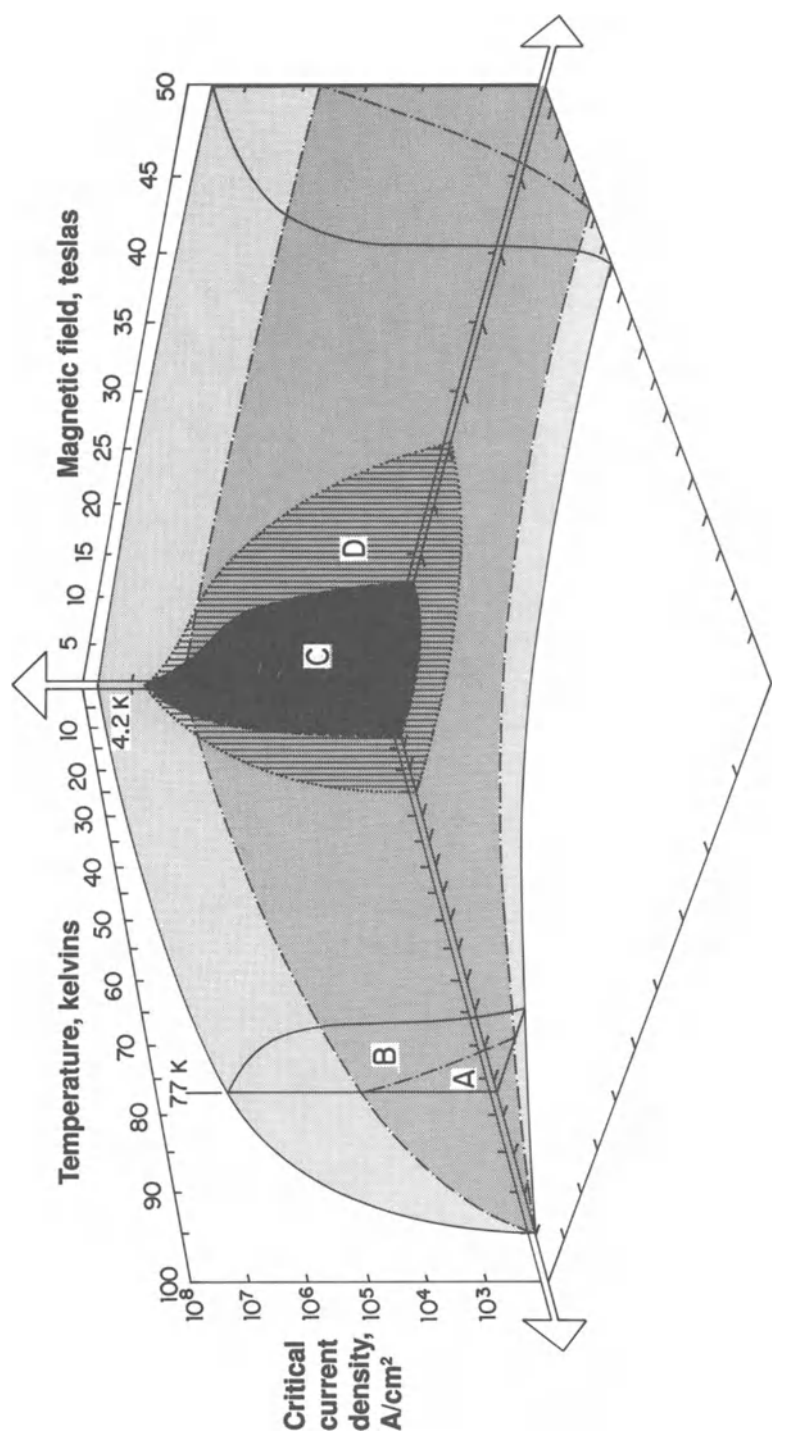


Fig. 15.5 Limiting region of the superconducting state in temperature, current density and magnetic field parameter space.

A: Y-Ba-Cu-O (bulk material)

B: Y-Ba-Cu-O (thin films)

C: Niobium-titanium

D: Niobium-tin

superconducting state. A moving vortex causes a time-varying magnetic field which by Faraday's law generates a voltage and consequently power loss.

15.1.5 Critical current density

When an electrical current is passing in a conductor it generates a magnetic field as described in Chapter 1. When the surface magnetic field generated by this current in a superconductor exceeds the critical field H_c the type I superconductor undergoes a transition to the normal state. This is known as the Silsbee effect [9]. The current density at which the material goes normal is called the critical current density, which for superconducting wire is dependent on the radius of the superconducting specimen. In a type II superconductor when the surface field exceeds H_{c1} the material undergoes a transition to its mixed state. In this state the magnetic field penetrates the material and it is no longer useful to consider the concept of a surface field.

The three parameters temperature, magnetic field and current density form a parameter space within which the material is superconducting, as shown in Fig. 15.5. The critical current density depends on both temperature and applied magnetic field. It is clear from Fig. 15.5 that the further the temperature is below T_c the higher the critical current density and magnetic field a superconductor can sustain before going 'normal'.

15.1.6 The Meissner effect: diamagnetism in superconductors

The type I superconductors are perfect diamagnets if subjected to a magnetic field that is lower than the critical field H_c . This means that once the material makes the transition to its superconducting state the magnetic flux inside becomes zero, an observation first made by Meissner and Ochsenfeld in 1933 [5] and depicted in Fig. 15.6. Type II superconductors are also perfect diamagnets below their lower

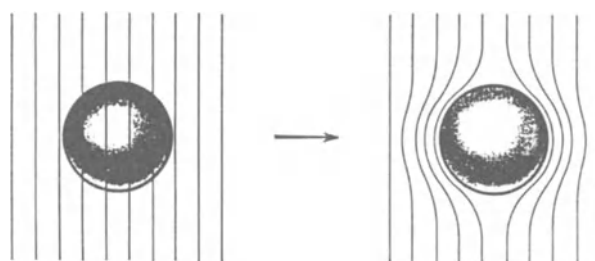


Fig. 15.6 The Meissner effect – flux exclusion in a superconductor cooled in a constant magnetic field. The solid sphere on the left is in the normal state in which the magnetic flux can still penetrate. As it is cooled it passes into the superconducting state, whereupon the magnetic flux is immediately expelled.

critical field H_{c1} .

$$\mathbf{B} = \mu_0(\mathbf{H} + \mathbf{M})$$

so that

$$\mathbf{M} = -\mathbf{H}$$

and hence

$$\begin{aligned}\chi &= -1 \\ \mu &= 0.\end{aligned}$$

It should be noted here however that there is no magnetization in the superconductor in the sense that there is magnetization in a ferromagnet. The flux density inside is zero due to the existence of surface currents which set up a totally opposing magnetic field, as in Lenz's law, because the resistivity is zero. This prevents the flux in the specimen from being non-zero no matter what the magnitude of the external field is, providing it is below the critical field strength, since the surface current will always exactly balance the external field.

We should note that this result is not a consequence of the zero resistivity of the superconductor which would lead only to the conclusion that the flux in the superconductor remains constant once it has passed into the superconducting state.

An important result here is that the Meissner effect suggests that the state of a superconductor can be described using equilibrium thermodynamics (i.e. is not path dependent). Clearly if the flux in the material was trapped this would result in a path-dependent state because the flux then depends on what the prevailing field was on entering the superconducting state. Note that the magnetic field does not penetrate the bulk of the material, but it does actually penetrate a certain depth of the surface of the superconductor, a distance known as the penetration depth λ .

In type II superconductors the situation is slightly different. The magnetic field is excluded, with a susceptibility of -1 , up to the field strength H_{c1} ; beyond this field strength the flux does partially penetrate the bulk of the material and the material is therefore no longer perfectly diamagnetic.

15.1.7 Flux trapping

Another consequence of the Meissner effect occurs if flux passes through a toroid of superconductor when we observe the phenomenon of flux trapping. If a magnetic field passes through a solenoid or toroid of material in its normal state and this material is then cooled into a superconducting state the magnetic field is pushed out of the superconductor (the Meissner effect) but not out of the hole in the toroid. Instead the flux passing through the solenoid or toroid becomes trapped and remains at the value it had at the moment of transition to the superconducting state.

We know that

$$\nabla \times \mathbf{E} = -d\mathbf{B}/dt$$

354 Superconductivity

and further that

$$\rho \mathbf{J} = \mathbf{E},$$

where \mathbf{E} is the electric field, ρ is the resistivity and \mathbf{J} the current density. Since \mathbf{J} is finite and ρ is zero this gives zero electric field \mathbf{E} inside a superconductor, so that \mathbf{B} must remain constant.

15.1.8 The London equations: surface currents

Classical electromagnetism can be used to describe some of the bulk properties of superconductors in terms of surface currents flowing in the superconductor. The zero value of the flux density inside a superconductor is a consequence of the induced surface currents generated by an applied field which, in accordance with Lenz's law, oppose the field producing them. Such surface currents of course flow in a surface layer of finite thickness which means that the applied field does penetrate the solid to a certain depth, and this depth is called the penetration depth, denoted λ . The field strength decays exponentially with depth x according to the equation

$$\mathbf{H} = \mathbf{H}_0 e^{-x/\lambda}.$$

The Meissner effect and the field penetration depth cannot be determined from the Maxwell equations alone. Two additional equations are needed which were proposed by London and London [10]. These are

$$\nabla \times \mathbf{J}_s = -\frac{\mathbf{B}}{\Lambda}$$

and

$$\frac{d\mathbf{J}_s}{dt} = \frac{\mathbf{E}}{\Lambda},$$

where $\Lambda = m/(n_s e^2)$, m is the electronic mass, e the electronic charge, n_s the number density of paired electrons, \mathbf{E} is the electric field and \mathbf{J}_s is the superconducting current density.

The penetration depth λ can then be shown to be

$$\lambda = \sqrt{\left(\frac{\Lambda}{\mu_0}\right)} = \sqrt{\left(\frac{m}{\mu_0 n_s e^2}\right)}.$$

As the number of superconducting electrons decreases on approaching T_c so the penetration depth increases.

15.1.9 Coherence length

We have mentioned above that the superconducting state is one of long-range order. The understanding of superconductivity is dependent on the 'coherence length', that is the long-range correlation of the behaviour of electrons. We may

Table 15.3 The coherence length and penetration depth at absolute zero of temperature for various metals

Metal	Pippard coherence length ξ_0 (10^{-6} cm)	London penetration depth λ_L (10^{-16} cm)	λ_L/ξ_0
Sn	23	3.4	0.16
Al	160	1.6	0.01
Pb	8.3	3.7	0.45
Cd	76	11	0.14
Nb	3.8	3.9	1.02

think of this as in some ways analogous to the ordering of two electron spins in ferromagnetism. The coherence length ξ is the distance over which these electron states can be correlated. In fact the paired, or correlated, electrons can be thousands of lattice spacings apart (i.e. $\xi \approx 10^{-6}$ metre).

In the London equations which have been given above it was assumed that the number density of superconducting electrons was identical to the number density of total electrons. This is only true at the absolute zero of temperature, $T = 0$. At higher temperatures $n_s < n$ and so the penetration depth λ given by the above equation becomes larger as the temperature rises. However experimental results on the temperature dependence of λ indicated that the penetration depth was greater than could be explained even on this basis. These larger than expected skin depths which were observed in superconductors were termed ‘anomalous’. An explanation was given by Pippard [11] who showed that when the coherence length was greater than the skin depth predicted by the classical London equations the observed skin depth would be greater than expected by the London theory. This coherence length is known as the Pippard coherence length. It can therefore be considered to be the minimum spatial extent of a transition layer between a normal and a superconducting region in the material. In type I superconductors λ is small compared with ξ while in type II superconductors the opposite is true. The values of these parameters for various metals are shown in Table 15.3.

15.1.10 Ginzburg–Landau theory

The Ginzburg–Landau theory [7] is a quantum mechanical alternative to the classical London theory which we shall only mention in passing. It does have the benefit of including some known facts about the electronic behaviour of these materials, but ultimately also includes *ad hoc* assumptions whose only justification is that they correctly describe the behaviour in zero field.

In this theory the concept of long-range order of electron pairs is central in determining the equilibrium state of a superconductor in an external magnetic

field. An order parameter ψ is introduced such that $|\psi|$ equals the density of superconducting electrons pairs. At any temperature T this is dependent on the location inside the material, that is to say it is not constant. This can then be used to predict the properties of surface layers and the boundary between the normal and superconducting regions of the solid. The equilibrium state is found by minimizing the Gibbs free energy G which is a function of both \mathbf{B} and ψ . The Gibbs function minimum contains the coherence length over which ψ slowly varies.

The theory was able to determine the effect of field on penetration depth, and to predict the behaviour of type II superconductors with their two critical fields H_{c1} and H_{c2} .

15.1.11 The Bardeen–Cooper–Schrieffer (BCS) theory

The two outstanding properties of a superconductor are perfect conductivity and perfect diamagnetism. The Bardeen–Cooper–Schrieffer theory [12] is able to explain these and in addition accounts for the variation of all the thermodynamic variables including the dependence of critical field on temperature below T_c .

The isotope effect [13] was discovered in 1950, in which it was found that the critical temperature T_c of mercury depended on the isotopic mass such that T_c was proportional to M^{-a} where $a = \frac{1}{2}$. In other elements the exponent is not always $\frac{1}{2}$ but T_c does remain dependent on the isotopic mass. Clearly the lattice structure, chemical and electronic properties are independent of the isotopic mass. Therefore some other effects such as the vibration or deformation of the lattice must play a role in determining the superconducting properties. The only explanation remaining is that it is the lattice–electron interactions.

The BCS theory was able to show the existence of an attractive force between two electrons due to the polarization of the lattice during deformation. The interaction which binds the electrons is therefore indirect, being communicated through the lattice. An attractive force between electrons instead of the usual Coulomb repulsive force results which gives rise to loosely bound electron pairs with wave vectors \mathbf{k} and $-\mathbf{k}$ and with antiparallel spins. Therefore each pair has a total wavevector of 0 and total spin of 0 while having a mass of $2m^*$ and charge $2e$.

The zero wavevector of these electrons in the form of Cooper pairs corresponds to very long wavelengths which are not scattered by the lattice and this explains why they experience no electrical resistance, whereas the normal conducting electrons with $\mathbf{k} \approx \mathbf{k}_f$, where \mathbf{k}_f is the wave vector at the Fermi surface, are easily scattered by the lattice. The penetration depth and coherence length emerged as a natural consequence of the theory. The London equations and the Meissner effect also emerged naturally from the theory.

In the original BCS theory in which other interactions are ignored the exponent in the isotopic dependence of the critical temperature was found to be $\frac{1}{2}$. However if the Coulomb interaction is also included this gives rise to other values of the exponent.

15.1.12 Energy gap

In a superconductor there is an energy gap of $E \approx 3.5 k_B T_c$ caused by the fact that the superconducting Cooper pairs have a lower energy than two unpaired electrons. This gap only exists below T_c , separating the superconducting electrons below the gap from the normal electrons above the gap. The conductivity of the superconducting electrons effectively ‘short circuits’ the conductivity of the normal electrons above the gap. The origin of this gap is however entirely different from that in insulators and semiconductors. In semiconductors the gap arises from Bragg scattering of the electrons by the lattice. In superconductors the energy gap is determined by electron–electron interactions, not by electron–lattice interactions. The energy gap decreases continuously to zero as the critical temperature is approached.

15.1.13 Thermal conductivity

In normal metals there is a close relation between the electrical and thermal conductivities since both are due almost entirely to electronic conduction. This is expressed as the Wiedemann–Franz ratio and can be explained on the basis of a free electron model of metals. In superconductors the situation is different because the Cooper pairs which cause the electrical superconductivity, cannot interact with thermal phonons (lattice vibrations) because of their very long wavelength and hence can not transfer heat. Only the unpaired electrons interact with the lattice and as the temperature is reduced these become fewer in number. Therefore the thermal conductivity in the superconductors is below that in the normal state. There are some exceptions to this statement however, notably lead, in which phonons are responsible for a substantial fraction of the thermal conductivity and so thermal conductivity rises at the critical temperature because there are fewer normal electrons available to scatter the thermal phonons.

The number of unpaired electrons decreases so markedly with temperature T in these materials that phonon conduction becomes the dominant mechanism for heat transport, and the conductivity therefore follows at T^3 dependence. This means of course that the thermal conductivity is much less than the normal state in which it is proportional to T .

15.1.14 Flux quantization

When flux passes through a toroid of superconductor this flux will be quantized in units of $h/2e$, where h is Planck’s constant and e is the electronic charge. This happens because the electron pairs cannot be scattered and so the flow of a superconducting current leads to long-range phase coherence. This means that no matter what the frequency with which the electron pairs circulate the toroid they must remain in phase and hence the phase around the inner circumference must be

$2\pi n$, where n is an integer. The resulting flux density is

$$\Phi = n(h/2e) = n\Phi_0.$$

This can be used in superconducting devices such as SQUIDS to detect fields with resolution down to a flux quantum. The value of the flux quantum is

$$\Phi = 2.067 \times 10^{-15} \text{ Wb.}$$

Dirac [14] has shown that the flux quantum is related to the flux generated by a magnetic monopole, the ultimate unit of magnetic ‘charge’, which has a predicted pole strength of 3.29×10^{-9} Am and emits a total flux of 4.136×10^{-15} Wb.

15.2 APPLICATIONS OF SUPERCONDUCTORS

In order to make superconductors more useful it is obviously desirable to increase the critical temperature and the critical current density. This has been a constant goal of researchers in the field but for many years the critical temperatures advanced very slowly so that even by 1986 the highest known critical temperature was 23.2 K in niobium–germanium.

15.2.1 Development of improved superconducting materials

Properties

In October 1986 Bednorz and Muller [3] reported that lanthanum–barium–copper oxide became superconducting at 30 K and this opened a new era in superconductivity. Within months critical temperatures of the new class of ceramic superconductors had been found as high as 95 K in yttrium–barium–copper oxide (YBCO) [4]. This meant that the critical temperature was above the liquid nitrogen point of 77 K and so it was no longer necessary to cool with expensive liquid helium at 4.2 K in order to observe superconductivity. This was a significant advance, which meant that many uses which were impractical with earlier superconductors came within the realm of feasibility although there are still many problems to be overcome, particularly in the fabrication of these materials. Unfortunately this advance also led inevitably to unjustifiable and exaggerated speculations about applications to power transmission, cheaper domestic electricity and heavy current engineering which at present remain beyond the technological horizon.

One unfortunate property of these materials is their brittleness which does make the production of wires a problem. However the materials are quite flexible before being given their final heat treatment at 900 °C and so can be formed into wire before the material processing ends. However once heat treated they can no longer be formed into other shapes. Another problem is that the critical current density in these ceramics (1500 A/cm^2 at 4.2 K) is quite inferior to that in materials such as

niobium–tin (10 MA/cm^2 at 4.2 K). At 77 K this critical current density has dropped to 400 A/cm^2 . Even the recent bismuth and thallium superconductors discovered in 1988 [15,16] which have been higher critical temperatures have comparable critical current densities in the bulk.

The critical magnetic fields in these ceramics are however very high, higher than has been possible to measure at this time, and estimates have been made that they are as high as 300 T . Since the critical current density is usually linked to the critical field this property of the ceramic superconductors has been puzzling.

Conductivity mechanism

One of the crucial questions regarding the conductivity mechanisms in these superconductors appears to have been solved. The unit cell of YBCO is shown in Fig. 15.7. For a long time it was not known whether the superconductivity proceeded via a two-dimensional mechanism (in planes of copper and oxygen) or a one-dimensional mechanism (in chains). This remained unanswered until two newer materials with critical temperatures above 100 K were found, bismuth-

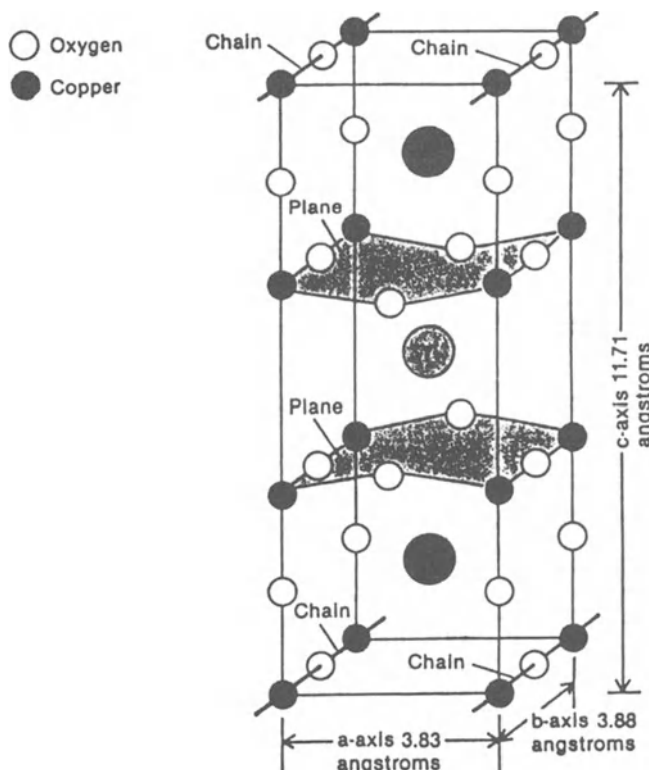


Fig. 15.7 The unit cell in the crystal lattice of the yttrium–barium–copper oxide.
© 1988 IEEE.

strontium–calcium–copper oxide and the most recent superconductor thallium–barium–calcium–copper oxide which has $T_c = 125$ K, these have planes of copper and oxygen but not chains.

Theories of the conduction mechanism in these superconductors lie outside the BCS theory that has been so successful in earlier materials. Most theories concentrate on the copper–oxygen bonds. The amount of oxygen present seems to affect the ability of these materials to superconduct by changing the valence state of the copper. These materials are not subject to the isotope effect which seems to rule out lattice vibrations (phonons) which are central to the earlier theories.

The yttrium–barium–copper oxide is highly anisotropic being able to conduct 100 times more current along two directions in the crystal lattice than along the third. This gives partial explanation of why the sputtered single-crystal thin films have superior properties to the bulk of the material. The other reason is that it appears that fewer grain boundaries help to raise the critical current density. This is a result that is contrary to observations in other superconductors in which flux pinning by grain boundaries and other microstructural defects keeps the vortices in place ensuring that the superconducting electrons meet no resistance. Recent results announced by Tanaka and Itozaki of Sumitomo [17] have reported a critical current density of 3.5 MA/cm^2 in epitaxially grown thin-film YBCO deposited on a magnesium oxide substrate.

Applications

Electronic applications for the new superconductors look relatively promising. The material can be laid down in thin films for Josephson junction devices and chip interconnections. Thicker films will need to be used for connecting devices on printed circuit boards. The sputtered films have shown critical current densities at 77 K as high as 4 MA/cm^2 which is 2 to 3 orders of magnitude greater than that obtained in the bulk material. It must be remembered however that the resistance of copper itself is very low at 77 K and not much advantage may be gained here by replacing copper with superconducting material.

Applications using bulk material are proving much more difficult. In fact there has been much less progress towards useful materials here. The highest critical current density obtained to date is 17 kA/cm^2 in zero magnetic field by Jin *et al.* at AT & T [18], although in view of the effort being expended on improving the critical current density it is likely that this will soon be raised.

15.2.2 Superconducting solenoids and magnets

Superconductors have found important applications in the generation of high magnetic fields using superconducting solenoids. In superconducting wires very high currents can be obtained with no Joule heating and furthermore once started such currents will persist almost indefinitely without any power input. The problem was of course to find a material with a sufficiently high critical field, since otherwise the actual generation of the field would destroy the superconductivity.

This was not achieved until the 1960s when niobium–zirconium, niobium–titanium and niobium–tin were discovered to have superconducting states with very high critical fields. Niobium–tin (NbSn_3) was found to remain superconducting even at fields of $17 \times 10^6 \text{ A/m}$ and this paved the way for the development of superconducting magnets. Niobium–tin can carry currents of up to 10^5 A/cm^2 and this material remains the most widely used material for construction of superconducting magnets.

Fields of up to $12 \times 10^6 \text{ A/m}$ (150 kOe , $B = 150 \text{ kG}$, 15T) are obtained in commercially available superconducting magnets. This should be compared with the $2 \times 10^6 \text{ A/m}$ (25 kOe , $B = 2.5\text{T}$) fields available from a typical laboratory electromagnet. Applications of these superconducting magnets were found in high-energy physics such as in bubble chambers and in fusion research, in magnetic detectors (SQUIDS) and in medical applications such as magnetic resonance imaging (MRI).

15.2.3 Josephson junction devices

If two pieces of superconductor are separated by a weak link such as a constriction or a very thin insulating layer superconducting electrons can tunnel through the link. This effect was first discovered by Josephson [19]. The critical current density can be affected by the presence of a small field so the state of the junction can easily be controlled by varying the current in a nearby wire to generate a critical magnetic field.

The junction therefore has two states which can be used as a switch to direct current across the barrier when its resistance is zero but along a different path when the resistance of the barrier is finite, that is when it is driven ‘normal’. The switching speed is of the order of picoseconds. These junctions have found widespread use in SQUIDS.

15.2.4 SQUIDS

Superconducting quantum interference devices are high-resolution magnetometers which rely on the Josephson effect. The first type of SQUID was the two-junction d.c. SQUID (1964), later the one-junction SQUID, the r.f. SQUID, appeared (1970).

In the d.c. SQUID two Josephson junctions connected in parallel as shown in Fig. 15.8 demonstrate quantum interference. As the magnetic flux Φ threading the superconducting loop changes the critical current of the two junctions oscillates with a period equal to that which corresponds to the flux quantum. When the flux through the loop changes the voltage–current characteristic oscillates smoothly as shown in Fig. 15.9. The SQUID is therefore a highly sensitive flux-to-voltage converter.

In general for practical field strength or induction measurements one usually needs a dynamic range somewhat greater than fractions of a flux quantum. Therefore the SQUID is often used as a null detector in a feedback circuit in which

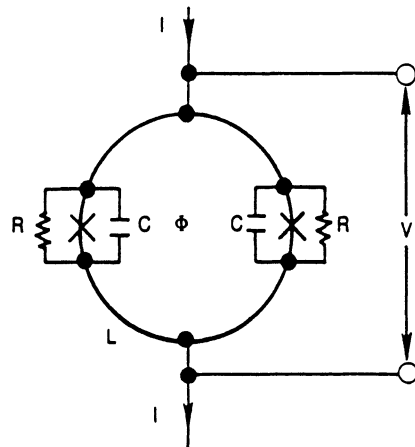


Fig. 15.8 Schematic diagram of the connection of two Josephson junctions in parallel to form a SQUID.

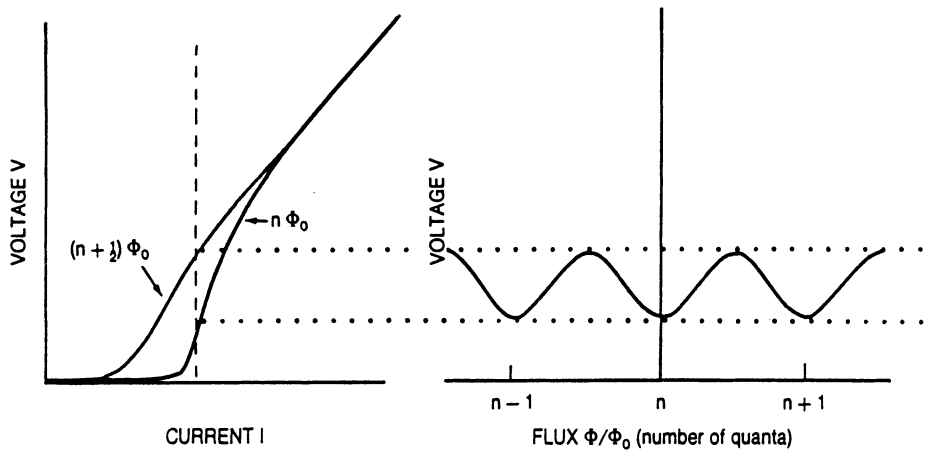


Fig. 15.9 Current-voltage characteristics of a SQUID. The voltage is an oscillating function of the flux threading the circuit. The current-voltage characteristics are for a SQUID with fluxes $n\phi_0$ and $(n + \frac{1}{2})\phi_0$. The variation of voltage across the SQUID with flux linking the circuit is shown on the right. Notice that the voltage is a sinusoidal function of the flux linking the circuit (see section 3.3.3).

any change in voltage across the SQUID is amplified and converted to a current through a coil coupled to the SQUID to produce an equal and opposite flux. This allows large magnetic fields to be measured to an accuracy of much less than a flux quantum.

15.2.5 Magnetic resonance imaging

One of the most interesting developments in the medical field in recent years has been magnetic resonance imaging (MRI) [20]. This needs large, 1 m diameter, magnets capable of generation high-intensity uniform 2 T fields. This has been one of the most important markets for superconducting magnets.

The MRI image is a representation of the spatial distribution of nuclear magnetic resonance signals which can identify the location of elements at different points within a test specimen, for example a human body. Field strengths of 0.15–2.0 T are used and the fields must be very uniform, typically 0.1 p.p.m. over a 10 cm diameter sphere. The first MRI systems became operational in 1979.

It should be noted that as a result of recent developments superconducting magnets are no longer essential to the operation of magnetic resonance imaging systems. Permanent magnet based MRI systems have now been developed using the new neodymium–iron–boron magnets, as discussed in sections 13.1.8 and 13.2.7. Nevertheless the superconducting magnet based systems are far more prevalent.

REFERENCES

1. Kamerlingh Onnes, H. (1911) *Akad. van Wertenschappen (Amsterdam)*, **14**, 113.
2. Gorter, C. J. and Casimir, H. B. G. (1934) *Physica*, **1**, 305.
3. Bednorz, J. G. and Muller, A. (1986) *Z. Phys.*, **B64**, 189.
4. Wu, M. K., Ashburn, J. R., Torng, C. J., Hor, P. H., Meng, R. L., Gao, L., Huang, Z. J., Wang, Y. Q. and Chu, C. W. (1987) *Phys. Rev. Letts.*, **58**, 908.
5. Meissner, W. and Ochsenfeld, R. (1933) *Naturwiss.*, **21**, 787.
6. Abrikosov, A. A. (1957) *Sov. Phys. JETP*, **5**, 1174.
7. Ginzburg, V. L. and Landau, L. D. (1950) *Sov. Phys. JETP*, **20**, 1064.
8. Gorkov, L. P. (1959) *Sov. Phys. JETP*, **9**, 1364.
9. Silsbee, F. B. (1916) *J. Wash. Acad. Sci.*, **6**, 597.
10. London, F. and London, H. (1935) *Proc. Roy. Soc. Lond.*, **A149**, 71.
11. Pippard, A. B. (1953) *Proc. Roy. Soc.*, **A216**, 547.
12. Bardeen, J., Copper, L. N. and Schrieffer, J. R. (1957) *Phys. Rev.*, **108**, 1175.
13. Maxwell, E. (1950) *Phys. Rev.*, **78**, 477.
14. Dirac, P. A. M. (1931) *Proc. Roy. Soc. Lond.*, **A133**, 60.
15. Sheng, Z. Z. and Herman, A. M. (1988) *Nature*, **332**, 138.
16. Maeda, M., Tanaka, Y., Fukutomi, M. and Asano, T. (1988) *Jap. J. Appl. Phys.*, **27**, L209.
17. Tanaka, S. and Itozaki, H. (1988) *Jap. J. Appl. Phys. Letts.*, **27**, L622.
18. Jin, S., Tieffel, T. H., Sherwood, R. C., Davis, M. E., Van Dover, R. B., Kammlott, G. W., Fastnacht, R. A. and Keith, H. D. (1988) *Appl. Phys. Letts.*, **52**, 2074.
19. Josephson, B. D. (1962) *Phys. Letts.*, **1**, 251.
20. Schwall, R. E. (1987) *IEEE Trans. Mag.*, **23**, 1287.

FURTHER READING

- Anil Khurana (1987) Superconductivity seen above the boiling point of liquid nitrogen, *Physics Today*, April, 17.
- Bleaney, B. I. and Bleaney, B. (1976) *Electricity and Magnetism*, 3rd edn, Oxford University Press, Oxford Ch. 13.

- de Bruyn Ouboter, R. (1987) *IEEE Trans. Mag.*, **23**, 355.
Kittel, C. (1986) *Introduction to Solid State Physics*, 6th edn, Wiley Ch. 12.
Pippard, A. B. (1987) *IEEE Trans. Mag.*, **23**, 371.
Rose-Innes, A. C. and Rhoderick, E. H. (1978) *Introduction to Superconductivity*, 2nd edn, Pergamon, Oxford.
Rosenberg, H. M. (1978) *The Solid State*, 2nd edn, Oxford University Press, Oxford Ch. 14.
Tilley, D. R. and Tilley, J. (1974) *Superfluidity and Superconductivity*, Van Nostrand Reinhold, London.
Tinkham, M. (1975) *Introduction to Superconductivity*, McGraw-Hill, New York.
Superconductivity, Special issue, *Physics Today*, March (1986).
Superconductivity: Special report, *IEEE Spectrum*, May (1988).

16

Magnetic Methods for Materials Evaluation

In this chapter we look at applications of magnetism to engineering problems and in particular to the non destructive evaluation (NDE) of materials properties. Magnetic methods can be used to solve two main classes of problem: detection of defects and evaluation of intrinsic properties such as residual stress. The subject of magnetic NDE has received little attention in the past due to the complexity of the magnetic response of materials. It is now one of the fastest developing fields in NDE.

16.1 METHODS FOR EVALUATION OF INTRINSIC PROPERTIES

More iron and steel is produced each year than any other metal. In 1986 world production of crude steel was 622×10^6 tons and of pig iron and ferro alloys 484×10^6 tons. So economically steel must be considered one of the most important industrial commodities. It is of course under widespread use as a constructional material on large-scale projects such as pipelines, railroads and bridges while also being used for the fabrication of high-strength components. Consequently there is a growing need for nondestructive inspection of steel structures both for the detection of corrosion, cracks and other defects and for the evaluation of stresses, elastic and plastic deformation and the likelihood of failure due to creep or fatigue.

A number of nondestructive testing techniques have appeared over the years, but today the subject of NDE has assumed a vital role, as more industries become aware of the potential benefits of plant life extension, the cost effectiveness of only retiring defective components (retirement for cause) and the possibilities of avoiding potentially catastrophic failures by monitoring the condition of structures both for defects and the presence of high levels of stress.

While various NDE techniques may be used on steels the magnetic methods are unique because they utilize the inherent ferromagnetic properties of the steel. They can be used for nondestructive evaluation of a wide range of material properties from cracks to residual strain. In general the changes in magnetic properties that are observed are easily measurable and unlike ultrasonic methods do not need high-resolution electronics for their use. Nevertheless the magnetic methods have not yet fully been exploited when compared for example with ultrasound.

Probably this is because other techniques can be applied to a wide variety of materials and previously there was more incentive for their development. Now however, as the limitations of other techniques become apparent, as for example in the important area of detection and prediction of failure such as fatigue or thermomechanical degradation (creep damage), attention has focused on the capabilities of magnetic methods applied to steels.

16.1.1 The magnetic Barkhausen effect (MBE)

The Barkhausen effect [1] was discovered in 1919, but it was many years before its potential as an NDE tool was realized. It is now one of the most popular magnetic NDE methods for investigating intrinsic properties of magnetic materials such as grain size, heat treatment, strain and other mechanical properties such as hardness.

The Barkhausen effect consists of discontinuous changes in flux density, known as Barkhausen jumps, as shown in Fig. 16.1. These are caused by sudden irreversible motion of magnetic domain walls when they break away from pinning sites as a result of changes in magnetic field H . The Barkhausen spectrum, which is the number of events against pulse height, as shown in Fig. 16.2, is dependent on the number density and nature of pinning sites within the material. These may be grain boundaries, dislocations or precipitates of a second phase with different magnetic properties from the matrix material, such as iron carbide in steels. Most Barkhausen activity occurs close to the coercive field H_c . Double peaks in the count rate can occur, as shown in Fig. 16.3. Also the location and size of the peaks can shift as a result of changes in the defect distribution, Fig. 16.3, where results are for two specimens of the same material with different defect distributions.

The first attempt to use the magnetic Barkhausen effect to determine stress was reported by Leep in 1967, but the method really only began to gain acceptance after the work of Pasley who showed distinct variations in Barkhausen signal amplitude

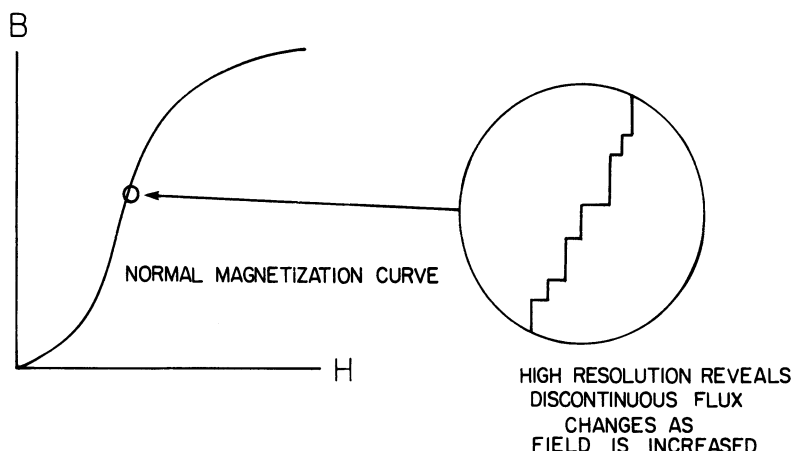


Fig. 16.1 Discontinuous changes in flux density B as the magnetic field H is changed.

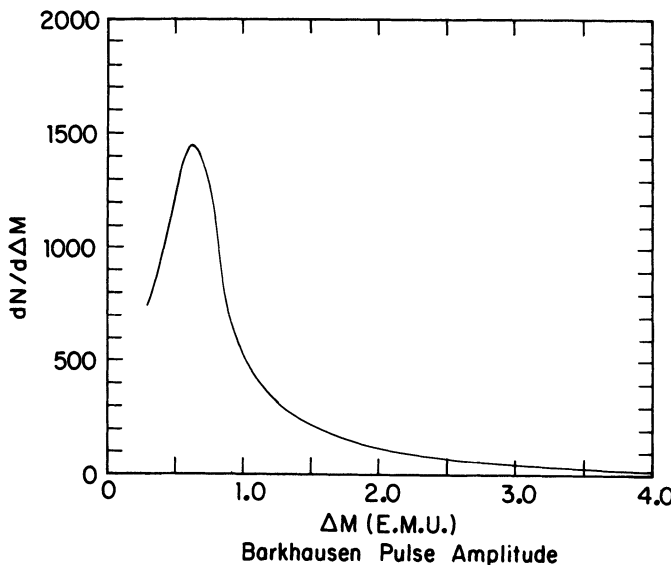


Fig. 16.2 Magnetic Barkhausen spectrum (pulse height distribution) after Tebble *et al.* [2].

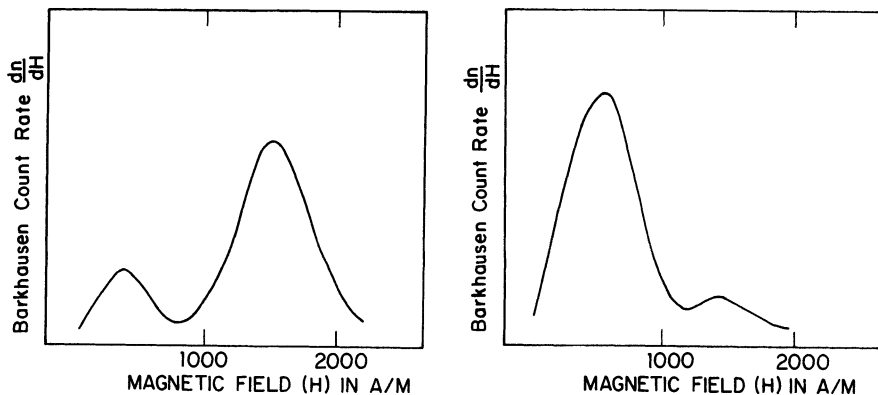


Fig. 16.3 Barkhausen count rate as function of magnetic field H for specimens with two different defect distributions.

with applied and residual stress. As stress increased in tension the peak Barkhausen amplitude in steel was found to increase while in compression it was found to decrease. Subsequently there were a number of investigations in Finland by Tiitto and co-workers [3,4]. Tiitto investigated the effects of elastic and plastic strain on the MBE in silicon–iron and the microstructural dependence of MBE in steels. He was also able to show that MBE could be used to determine grain size in steels. Sundstrom and Torronen reported that MBE can be used for the determination of microstructure, mechanical and electrical properties while Karjalainen and Moilanen investigated the effects of plastic deformation and

fatigue on MBE. Otala and Saynajakangas devised an MBE instrument for grain size determination.

The effect of tensile and cyclic loading on the RMS value of MBE signals in mild steel was the subject of an investigation by Karjalainen *et al.* [5]. They found that residual strains in unloaded specimens could be identified from MBE. But changes occurring under cyclic loading (fatigue cycling) were very complex so that the Barkhausen signals could not simply be related to the applied load. However subsequent investigations by Ruuskanen and Kettunen were able to demonstrate that the median Barkhausen pulse amplitude could be used to assess whether the applied stress amplitude was above or below the fatigue limit.

Lomaev has reviewed the literature relating to nondestructive evaluation applications of MBE [6]. In these papers he identified five mechanisms by which MBE is caused: (a) discontinuous, irreversible domain-wall motion; (b) discontinuous rotation within a domain; (c) appearance and disappearance of Neel peaks; (d) inversion of magnetization in single-domain particles; and (e) displacement of Bloch or Neel lines in two 180° walls with oppositely directed magnetizations. The first of these mechanisms has been studied most intensively and is often, incorrectly, quoted as the sole mechanism for generation of MBE. It is interesting to note that in the early years of MBE the effect was attributed to the second mechanism, irreversible domain rotation.

A number of other papers have appeared on MBE in the Soviet literature, usually in *Defektoskopia* (Soviet Journal of NDT). Klyuev *et al.* have reported that on the basis of their results there does not seem to be any single unambiguous correlation between their MBE measurements and the parameters of magnetic hysteresis. This is an interesting and very significant result since it shows that the magnetic Barkhausen effect provides independent nondestructive information on the state of a material from that gained by bulk magnetic properties such as hysteresis.

Filinov *et al.* have shown that MBE can be used to probe surface plastic deformation of steel components by using different magnetization frequencies. Such a technique can be used for evaluation of a variety of different types of surface condition such as case hardening or surface decarburization. A combination of MBE at different frequencies and hysteresis measurements has been used by Mayos *et al.* [7] for the determination of surface decarburization in steels. By this method different depths of the material were inspected to investigate changes in magnetic properties. Segalini *et al.* have used MBE for evaluation of heat treatment and microstructure of constructional steels.

In Germany Theiner and co-workers have used MBE in conjunction with incremental permeability and ultrasonic measurements for the evaluation of stress [8, 9]. As they have noted, all ferromagnetic NDE methods are sensitive to both mechanical stress and the microstructure of the material. In order to determine stress it is therefore necessary to use two or three independent measurement parameters. They found that Barkhausen effect, incremental permeability X-ray and hardness measurements were successful in estimating residual stress. As might

have been anticipated, they found changes in the density of dislocations affected the MBE signals. They also found that MBE could be used to distinguish between microstructures which cannot be distinguished on the basis of optical microscopy.

In the United States a large amount of work on MBE has been conducted at Southwest Research Institute by Matzkanin, Beissner and co-workers. Much of this work has been summarized in 'The Barkhausen effect and its applications to NDE' [10] by Matzkanin, Beissner and Teller which remains the most comprehensive work on the subject to date. Other reviews are also available, the most notable being by McClure and Schroeder [11].

16.1.2 Magneto-acoustic emission (MAE)

Magneto-acoustic emission is an effect which is very closely related to the magnetic Barkhausen effect. It is caused by microscopic changes in strain due to magnetostriction when discontinuous irreversible domain-wall motion of non- 180° domain walls occurs. It therefore arises in ferromagnetic materials when subjected to a time-dependent field (Fig. 16.4). The acoustic emissions may be detected by a piezoelectric transducer bonded on to the test part. The amplitude of MAE depends on the spontaneous magnetostriction, being zero if $\lambda_0 = 0$ and

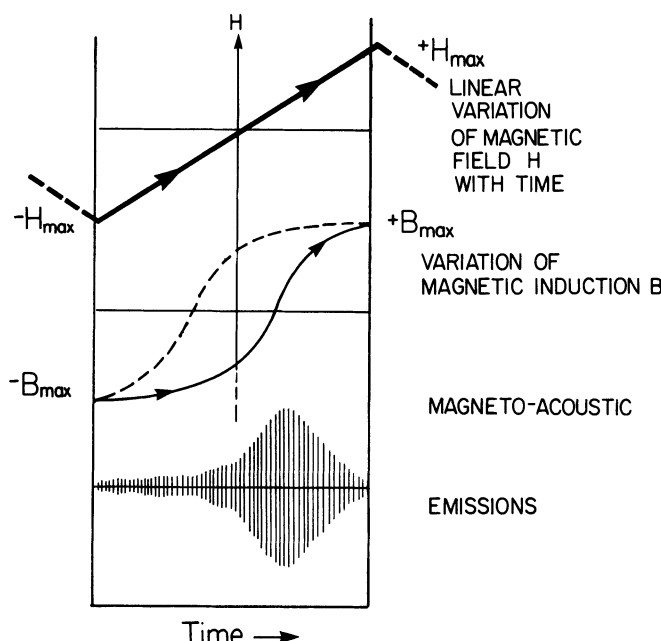


Fig. 16.4 Schematic diagram showing magnetic field H with time, variation in flux density over the same period and the emergence of magneto-acoustic emission pulses as flux density changes.

increasing with λ_0 . The amplitude of emissions is also a function of the frequency and amplitude of the driving field.

It is clearly apparent that MAE must change with applied stress, since stress alters the magnetocrystalline anisotropy. This results in a change in the relative numbers of 180° and non-180° domain walls. Since 180° domain walls do not contribute to MAE, the amplitude of emissions and the total number of emissions will change with stress.

Despite its close relation to the magnetic Barkhausen effect, MAE has a much shorter history. It was first reported by Lord [12] during magnetization of nickel. Its significance for NDE was realized by Kusanagi *et al.* [13] who were first to demonstrate the effect of stress on MAE. Shortly afterwards Ono and Shibata [14] reported MAE results on a number of steels. Their results indicated that the method could be used to determine the amount of prior cold work and differences in heat treatment.

Burkhardt *et al.* [15] have also investigated the dependence on MAE on the mechanical and thermal treatment of steels. They found that MAE was very sensitive to the amount of plastic deformation. Theiner and Willems [16] used MAE in conjunction with other independent measurements such as incremental permeability, MBE and magnetostriction. Their results showed that the MAE amplitude decreased with the mechanical hardness of steels but increased with tempering.

Edwards and Palmer [17] have recently shown that MAE signals are affected not only by stress and frequency of field but also by factors such as sample shape. Ranjan *et al.* [18] have used MAE and MBE for the determination of grain size in decarburized steels. They used two types of measurement, the MAE peak height and the total number of emissions, both of which were found to increase with grain size.

A related phenomenon has also been reported by Higgins and Carpenter [19]. Acoustic and magnetic Barkhausen emissions due to domain-wall motion were observed in ferromagnetic materials when the applied stress was changed without changing the magnetic field. This can easily be understood in terms of the domain-wall pinning model. The magnetic Barkhausen emission were also observed under dynamic stress by Jiles and Atherton during investigations of magnetomechanical effects, although they were not reported in the paper [20]. This phenomenon of magnetomechanical emissions has received little attention but would appear to have significant implications for the detection of dynamic stresses in steels.

16.1.3 Magnetic hysteresis

All ferromagnetic materials exhibit hysteresis in the variation of flux density \mathbf{B} with magnetic field \mathbf{H} (Fig. 16.5). The hysteretic properties such as permeability, coercivity, remanence and hysteresis loss are known to be sensitive to such factors as stress, strain, grain size, heat treatment and the presence of precipitates of a second phase, such as iron carbide in steels. In addition, the measurement of

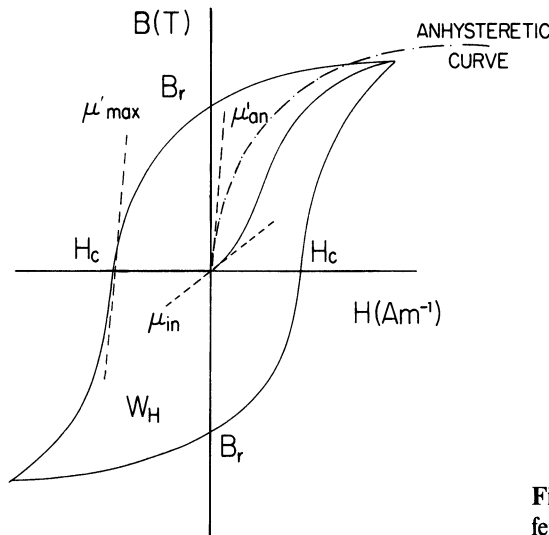


Fig. 16.5 Typical hysteresis loop of a ferromagnetic material.

hysteresis yields a number of independent parameters, each of which changes to some degree with stress, strain and microstructure. Since it has been remarked earlier that several independent parameters are needed in general to separate effects of mechanical treatment from microstructure, hysteresis measurement would seem to be ideally suited for the determination of intrinsic properties of steels because the several independent parameters can be obtained from one measurement.

Despite this economy of means, there are certain difficulties that need to be overcome with the magnetic hysteresis method. Firstly, the problem of demagnetizing effects due to finite geometries needs to be addressed, since results which may appear to be due to changes in sample properties can be caused by geometrical effects. Second, until recently it has proved impossible adequately to model hysteresis in ferromagnets so that it has been difficult to interpret changes in the hysteresis characteristics in terms of fundamental changes in sample properties. Of course this has also been true of other magnetic methods, such as the Barkhausen effect, and has not prevented their use for NDE.

Evaluation of the condition of magnetic steel components has been one area where NDE via hysteresis has had great success. Numerous applications have been reported in the literature. Mikheev and co-workers at the Urals Science Centre have made many investigations of the quality of heat treatment of steels from magnetic parameters [21], particularly the evaluation of hardness of various steels. In most cases the magnetic properties were determined using a coercimeter and correlations made between chemical composition, microstructure, heat treatment and hardness and the principal magnetic parameter of interest, the coercivity. Mikheev has written a review on the subject which may be used as an introduction to his work [22].

Kuznetsov and co-workers have also looked at the effects of heat treatments such as quenching, hardening and tempering on the magnetic properties of steels [23]. They have devised a method for determining the depth of case hardening. Similar work on determination of quality of steel component heat treatment has been carried out by Fridman *et al.*, Konovalov *et al.*, Melgui *et al.*, Katsevman and Sandorskii and Gorkunov. Specific applications to sorting of components have been described by Sandorskii and to determination of composition and microstructure by Khavatov. Zatsepin *et al.* [24] investigated the variation of coercivity with heat treatment and mechanical properties, while Rodigin and Syrochkin were able to use the effect of stress on coercivity to check mechanical hardness, thereby using hysteresis parameters as an accept-reject criterion for steel components [25].

The effects of stress on the magnetic hysteresis properties of steels are of interest because they have applications to nondestructive evaluation of structures such as railroad lines and pipelines. Typically the hysteresis ‘signature’ is changed by stress as shown in Fig. 16.6. Vekser *et al.* showed that it was possible to measure the stress in rail steel from the permeability. Schcherbinin *et al.* were able to detect defects in in-service railroad rails from inspection by fluxgate magnetometers [26]. Pyatunin and Slavov investigated the effects of microstresses and texture in steel on the bulk

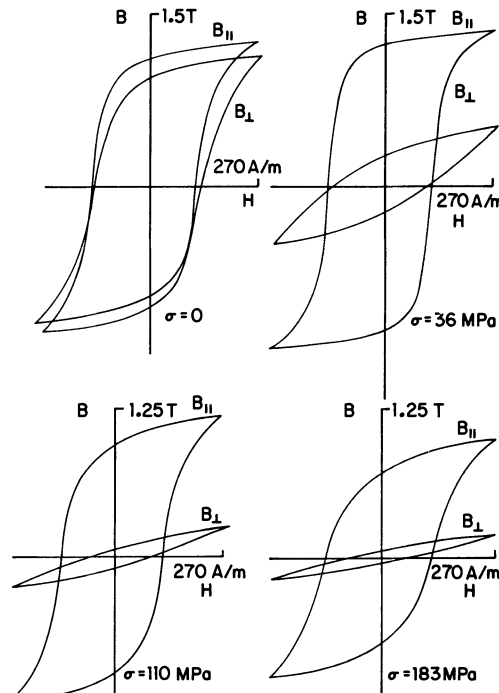


Fig. 16.6 Changes in magnetic hysteresis ‘signatures’ of mild steel with stress, after Langman [27]

magnetic properties and showed correlations between mechanical and magnetic properties for specimens of similar texture.

The dependence of magnetic properties on static and dynamic stresses was the subject of a study by Novikov and Fateev [28]. Similar work was performed by Pravdin who drew distinctions between the effects of static and dynamic stresses. The results revealed that dynamic loading changed the flux density B by different amounts depending on the applied field H . This was very similar to the findings of Jiles and Atherton described below.

The effects of elastic stress on hysteresis have been reported by a number of investigators, including Jiles and Atherton [29], Burkhardt and Kwun [30] and Polanschutz. The interpretation of results is difficult without a working mathematical model of hysteresis, since none of the direct hysteresis parameters such as coercivity, remanence, initial permeability or hysteresis loss is uniquely related to a single physical property. This was realized by Davis who had NDE applications of hysteresis for evaluation of steel quality in mind. Subsequent attempts were made to utilize Davis's harmonic model by Willcock and Tanner [31].

It is clear that any model which has a hope of being used for interpretation of NDE results such as effects of stress, elastic and plastic strain, creep and fatigue should have as few parameters as is reasonably possible. The stress or strain dependence of these parameters can then be determined. Such a criterion immediately excludes the Preisach model. Some success has been achieved recently with the model of Jiles and Atherton [32]. Changes in the magnetic parameters with stress have been determined empirically by Szpunar and Szpunar [33] and from first principles by Sablik *et al.* and these have been used to model the magnetic hysteresis properties under stress.

Hysteresis measurements have also been used by Abuku for evaluation of residual strain in steel rods. Changes in magnetic properties with stress cycling have been used to predict fatigue life of specimens by Sanford-Francis, and by Shah and Bose [34]. It was found that the hardness of the specimens, which can be inferred from coercivity measurements, began to change long before any crack failure appeared. Coercivity measurements have been used by Jakel for evaluation of quality control of steel components.

A brief review of several NDE techniques including hysteresis measurements for on-line measurement of microstructure and mechanical properties of steel has recently been given by Bussiere [35].

16.1.4 Residual field and remanent magnetization

This technique is closely related to the flux leakage method (see section 16.2.3). However, whereas the flux leakage method is used to detect flaws from anomalies in magnetic flux, the residual field method is usually aimed at detecting changes in intrinsic properties such as strain, microstructure or heat treatment from variations in the magnetic field close to the surface of a ferromagnetic structure or

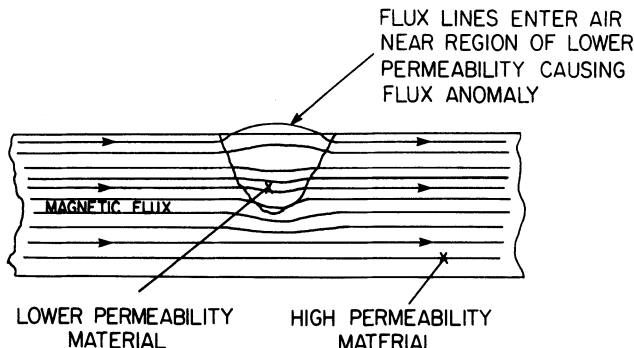


Fig. 16.7 Flux leakage into the air caused by a region of lower permeability within a piece of steel.

component (Fig. 16.7). The magnetometers used with the technique are often fluxgates (also known as ferroprobes), but Hall probes and induction coils are also used and in cases where the coercivity needs to be measured, a coercimeter is used.

The measurement of field intensity was used by Lees *et al.* for detecting the accumulation of oxides within steel boiler tubing. Atherton and co-workers used the same technique for detecting stresses in pipelines due to large-scale bending, while Konovalov *et al.* determined the mechanical properties of steel pipes from a combination of coercivity and remanence obtained from measurements of field intensity close to the surface of pipes [36].

Suzuki *et al.* [37] used measurements of remanent magnetization for detection of stresses in pressure vessels, Langman detected and measured stress levels in steel plates by a novel method of rotating the magnetic field H and noting any differences caused by stress-induced anisotropy [38]. A detailed discussion of the variation of magnetic field and flux density with stress has been given by Langman in a subsequent paper [27]. A number of techniques for sorting steel components on the basis of magnetic field measurements, usually from the determination of coercivity, have been reported by Mikheev *et al.* [39] and by Tabachnik *et al.*

No extensive reviews of the method have appeared in the literature. In general it is very similar in nature to the magnetic flux leakage method. The only differences lie in the interpretation of results, since the effect of stress on magnetic properties is complicated. Another additional feature is the use of the coercimeter in a number of instances. This device magnetizes the specimens to saturation in one direction, using an electromagnet, and then determines H_c by reversing the field until the flux density in the specimen is reduced to zero.

16.1.5 Magnetoelastic methods (magnetically induced velocity changes)

This method relies on the measurement of acoustic velocity in the presence of a magnetic field to determine stress. Both magnetic field and applied stress change

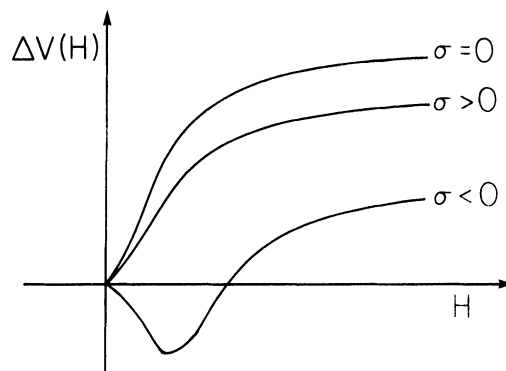


Fig. 16.8 Schematic diagram showing the change in ultrasonic velocity ΔV in steels with magnetic field H under various stress levels.

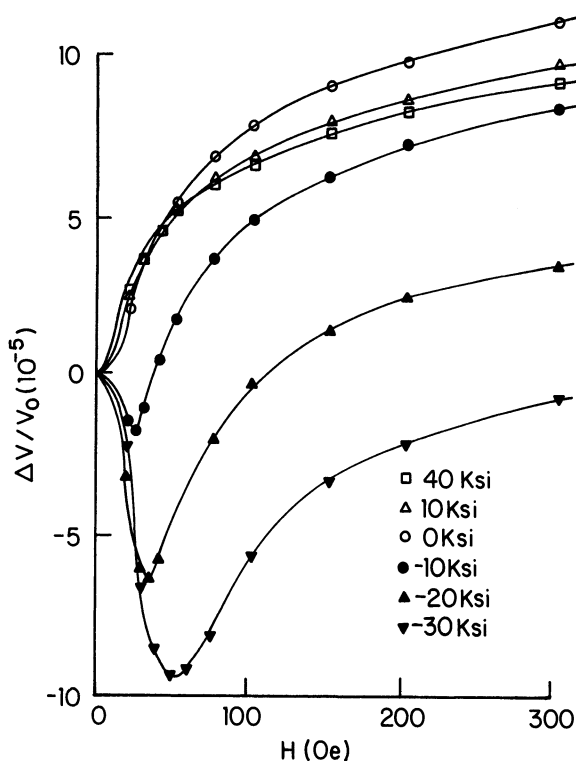


Fig. 16.9 Variation of acoustic velocity with magnetic field strength H for various stress levels applied parallel to the field, after Kwun [43].

the velocity of sound in ferromagnetic materials such as steel (Fig. 16.8). However until quite recently few investigations of the effect of stress on the rate of change of acoustic velocity with field (dV/dH), had been reported.

The first application of this method to NDE of stress in steels was by Kwun and Teller [40] who investigated the stress dependence of the velocity of ultrasonic shear waves. The method has also been used by Namkung, Utrata and co-workers [41, 42]. One of the great advantages of this technique for NDE of stress is that it is possible to detect residual uniaxial stress without reference to calibration data. The results of Namkung and Utrata, who measured the slightly different parameter (dV/dB), have shown that this is negative under coaxial compression but positive under coaxial tension. The work has recently been extended to an investigation of grain size and heat treatment of 4140 steel.

The most recent review of this technique has been given by Kwun [43]. Typical variations of the acoustic velocity in steel with stress and magnetic field parallel are shown in Fig. 16.9 and with stress and magnetic field perpendicular are shown in Fig. 16.10.

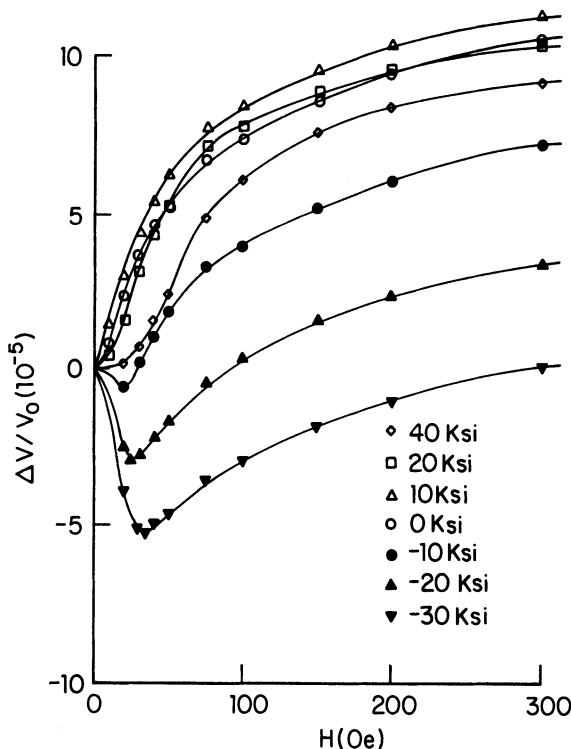


Fig. 16.10 Variation of acoustic velocity with magnetic field strength H for various stress levels applied perpendicular to the field, after Kwun [43].

16.2 METHODS FOR DETECTION OF FLAWS AND OTHER INHOMOGENEITIES

This section reviews nondestructive evaluation of defects or flaws in ferromagnetic steels. As in the first part of the chapter the objective is to provide a broad survey of the existing techniques giving a comprehensive summary of earlier work but without going into fine details, which have been covered in most cases by more specialized reviews of the particular techniques.

The subject of flaw detection in materials using magnetic methods has a long history, going back as far as the work of Saxby (1868). Systematic development of testing techniques based on perturbations of the magnetic flux in iron and steel due to the presence of defects did not begin however until after the chance discovery by Hoke, that iron filings accumulated close to defects in hard steels while in the process of being ground. The technique of magnetic particle inspection, which was based on this discovery, was then developed by DeForest and Doane.

Later as the subject of flaw detection became more quantitative additional methods were developed in which the leakage field in the vicinity of the flaw was measured with a magnetometer. Once the field strengths of the leakage fields were being measured on a routine basis it became desirable to relate these to flaw size and shape, and therefore there arose the need for modelling the leakage fields from different crack geometries.

16.2.1 Magnetic particle inspection

The technique of magnetic particle inspection (MPI) was the first magnetic NDE method in widespread use. It was discovered accidentally by Hoke in 1918, but it was left to DeForest to develop the method further for practical use. DeForest's work involved devising methods of generating a magnetic field of sufficient strength in any direction in a specimen. This was solved by using electrical contact prods with heavy duty cables being used to pass large currents through test specimens in desired directions. Furthermore it became apparent that better results were obtained by using magnetic powders with uniform properties such as particle shape, size and saturation magnetization in order to obtain more reliable results. Particle sizes with diameters ranging from 0.3 micrometres up to 300 micrometres are now used. DeForest and Doane formed the Magnaflux Corporation to exploit the MPI method in 1934. This company remains one of the principal suppliers of equipment for MPI in North America. In Europe the German company Tiede GmbH holds a comparable position.

The MPI method is very simple in principle. It depends on the leakage of magnetic flux at the surface of a ferromagnetic material in the vicinity of surface-breaking, or near-surface flaws, Fig. 16.11. There are now five main methods for generating a magnetic field in a material. Three of these depend on the generation of a magnetic field in the test specimen without necessarily inducing a current, and

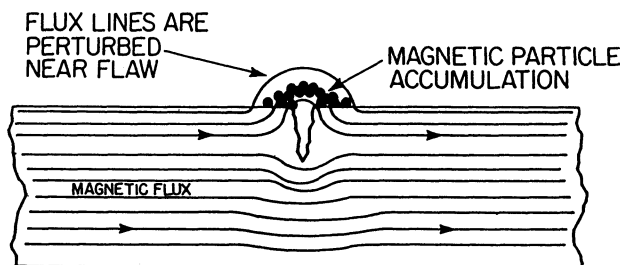


Fig. 16.11 Schematic diagram of leakage flux in the vicinity of a surface-breaking flaw with accumulation of magnetic particles. In the presence of narrow cracks the particles can form a 'bridge' across the crack. In the presence of wide cracks the particles accumulate on both sides of the crack.

these are the yoke method, the encircling coil method and the internal conductor method (also known as the 'threading bar' method). Two other methods depend exclusively on the generation of high current densities in the test specimen, and these are the 'prod' method, and the current induction method. These five methods are depicted in Figs 16.12 and 16.13. In each case the best indication is given when the magnetic field is perpendicular to the largest dimension of the flaw or crack.

Magnetic particle inspection is a very reliable method, when used correctly, for finding surface flaws and gives a direct indication of the location and length of the flaw. There is little or no limitation on the size or shape of component being tested, although more care is needed in the application of the method to complex geometries. Nevertheless the method does have some distinct limitations. It can of course only be used on ferromagnetic materials, and in addition the magnetic field must lie at a large angle to the direction of the flaw to give the best indication. An angle of 90° gives optimum performance, but good indications can be obtained with angles as low as 30°. Flaws can be overlooked if the angle is smaller. Finally although the length of the flaw is easily found the depth is difficult, if not impossible, to ascertain.

Various enhancements have been made to the original 'dry powder method'. These include the use of water-borne and oil-borne suspensions or magnetic inks, known as the 'wet method', and especially fluorescent powders or suspensions which often give a clearer indication of small flaws when viewed under ultra-violet light. Among these the water based suspensions of fluorescent particles are used predominantly.

Another related method that has found use in detection of flaws in structural components is the 'replica' or magnetographic method in which a magnetic tape is placed over the area to be inspected. The tape is magnetized by the strong surface field, and is then removed and inspected for magnetic anomalies. The magnetic tape, which records an imprint of the flux leakage from the surfaces of components can be inspected afterwards using magnetometers such as Hall probes or fluxgates. The advantage of this method over the magnetic particle inspection technique is

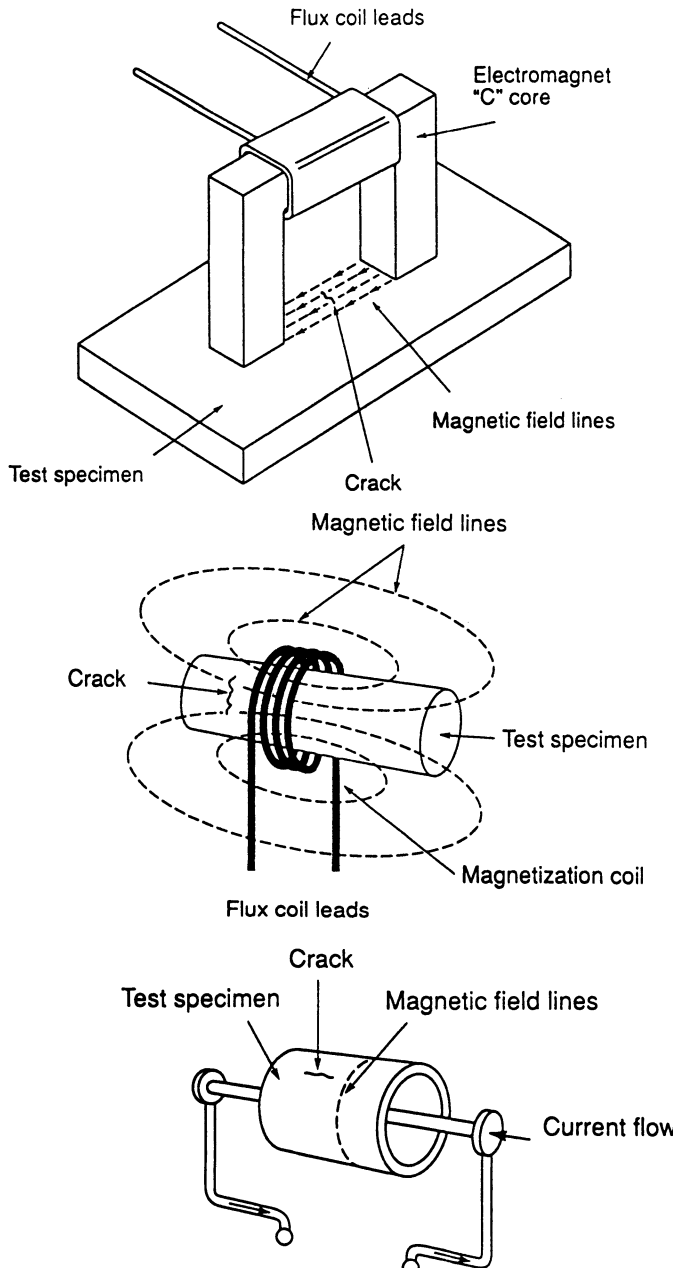


Fig. 16.12 Magnetization methods used in magnetic particle inspection based on generation of fields in the specimen with (e.g. a.c. fields) or without (e.g. d.c. fields) generation of associated currents in the specimen. (a) The magnetic yoke method; (b) the coil magnetization method; (c) the internal conductor method.

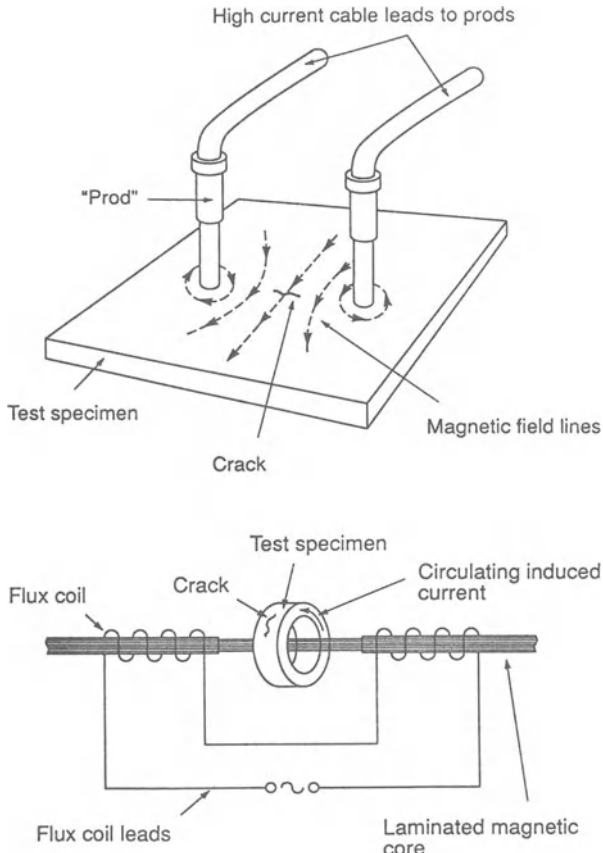


Fig. 16.13 Magnetization methods used in magnetic particle inspection based on generation of fields in the specimen via generation of associated currents in the specimen. *Top:* The current flow or 'prod' method. *Below:* The current induction method.

that the magnetograph (usually a magnetic tape) can be read using a magnetometer to obtain a quantitative measure of flux leakage from regions where it would be difficult to use a magnetometer, for example inside pipelines, or for underwater applications.

16.2.2 Applications of the magnetic particle method

A particular application has been found for magnetic particle inspection in the automotive industry where large numbers of parts (typically billions per year) have to be inspected on a routine basis. In these cases multicircuit magnetization using several of the principal techniques simultaneously has been found to be a reliable method of defect detection for any orientation of flaw on parts of complex shape, such as steering knuckles for cars.

Although it is possible to apply the MPI technique successfully to magnetically harder materials using solely the remanent magnetization of a specimen and its accompanying field, it is no longer possible to control the relative orientation of field and flaw. Therefore it is preferable to apply a controlled magnetic field to the specimen, using one of the five methods discussed above.

Research efforts in MPI have been directed towards establishing standard procedures and conditions for applying the method. Gregory [44] showed that for complex geometries the magnetic particle method is more difficult to apply and has sometimes failed to reveal structural faults in aerospace components because of low magnetization in some regions of those components. More recent developments using multicircuit magnetization methods described above have now overcome this problem.

Optimum conditions for the application of MPI to inspection of welds were described by Massa [45]. Once again the critical factor was to determine adequate levels of magnetization in order to reveal the presence of defects. No simple solution was found in that case but tables of values of critical field strength H for various geometries were given.

Recent research efforts in magnetic particle inspection have been directed towards modelling of the magnetic field throughout the whole of an object including the leakage fields in the vicinity of flaws. These calculations use Maxwell's equations and finite element methods of computation [46, 47, 48] which will be discussed in detail in section 16.2.5. The computer aided design of magnetic particle inspection systems, especially multicircuit units for inspection of automotive parts is now very much state of the art.

Some standard procedures have been recommended in the UK where a field strength of at least 2400 A/m (30 Oe) (British Standard 6072) was suggested for using MPI on steels. However, opinions seem to differ over the necessity of the recommendation. Work on MPI applications to pressure vessels and pipelines by Raine, Robinson and Nolan has shown that the recommendations of BS 6072 do not seem to be generally applicable. Their work indicated that lower field strengths than 2400 A/m were quite adequate for satisfactory MPI indications. Edwards and Palmer [49] have investigated procedures for applying the method to tubular specimens threaded on a current carrying conductor and for a cylindrical bar using prod magnetization. It was shown that care is needed to generate sufficient field strength for adequate magnetization of the specimen in these cases.

It is sometimes assumed that the optimum magnetizing condition corresponds to the maximum permeability, however this was not found to be true in the work of Oehl and Swartzendruber [50]. They found that for cylindrical defects with square cross sections the ratio of leakage field to applied field reached a maximum at an applied field of between 800 and 2400 A/m in steels, depending on the lift off. This was well removed from the maximum permeability of the material which occurred at $H = 120$ A/m.

Recent enhancements of the MPI method include fully automated scanning of steel components for crack indications using optoelectronic devices, followed by

computer operated digital image processing techniques to enhance the results [51, 52]. The automation of the inspection method has the advantage of eliminating subjective evaluation of results and is therefore desirable.

The 'wet method' in which a magnetic colloid (e.g. ferrofluid), or a suspension of larger magnetic particles in a carrier fluid, is used has many similarities with the Bitter pattern technique for magnetic domain observations. Because of the finer particles used in the wet method it has some advantages in spatial resolution over the dry powder method, and therefore it can be successfully used for detection of smaller flaws. However in the case of larger castings with relatively wide cracks the coarse grained dry powder method remains the appropriate technique.

Present developments in the MPI technique are concentrated on improving measurement techniques and control procedures for current, field strength and light intensity in order to enhance the capabilities of fully automated inspection systems. The next stage of the evolution of MPI should be the further development of expert systems to improve further automated measurements and to develop evaluation algorithms.

In conclusion therefore MPI is a well established technique and most of the problems associated with its use appear to have been solved. The remaining research effort is directed towards optimizing conditions for its use and increasing automation. The standard reference work on MPI is *Principles of Magnetic Particle Testing* by Betz [53], which contains much information on the subject, including the history of its development, the underlying principles, methods of generating fields in the materials and descriptions of the dry powder methods, the wet, or magnetic ink, method and the fluorescent powder method. A more recent reference work on MPI is to be found in volume six of the *NDT Handbook* [54].

16.2.3 Magnetic flux leakage

The magnetic flux leakage method is derived from the magnetic particle inspection method. Both depend on the perturbation of magnetic flux in a ferromagnetic material caused by surface or near-surface flaws. Whereas in the MPI method detection relies on the accumulation of magnetic powder, or sometimes the use of a magnetic recording tape, to indicate the presence of a defect, the flux leakage technique utilizes a magnetometer. The use of a magnetometer for detecting leakage fields was first suggested by Zuschlag. The magnetometer allows a quantitative measurement of the leakage field in the vicinity of a flaw to be obtained.

The field components in three directions, perpendicular and parallel to the flaw and normal to the surface can be measured although in practice only components parallel to the surface are usually measured. However the method only began to gain wide acceptance after the design of a practical flux leakage measuring system by Hastings [55]. This was capable of detecting surface and subsurface flaws on the inner diameter of steel tubes, a location that was quite unsuitable for the MPI

method. The flux leakage technique has now been further developed so that it can be used not only for flaw detection but also for their characterization. The magnetometer probe is most often a Hall probe or induction coil. It is scanned across the surface of the component looking for anomalies in the flux density which indicate the location of a flaw, as in Fig. 16.14. The leakage flux as a function of distance across a crack is shown in Fig. 16.15, together with a typical search coil output as it is moved across the crack.

A drawback of this compared with the particle method is that while large areas of material can be tested quickly using MPI, the scanning of a magnetometer over the surface can be time consuming. Therefore the flux leakage method has advantages in situations where the location of flaws is known or where the location can be predicted with a reasonable chance of success. Under those circumstances a careful magnetic inspection can be conducted over a confined area.

Another situation when flux leakage magnetometry has advantages over the particle method is where the part to be tested is not easily accessible for a visual inspection. An example is the inside surfaces of long tubes and pipelines. Once

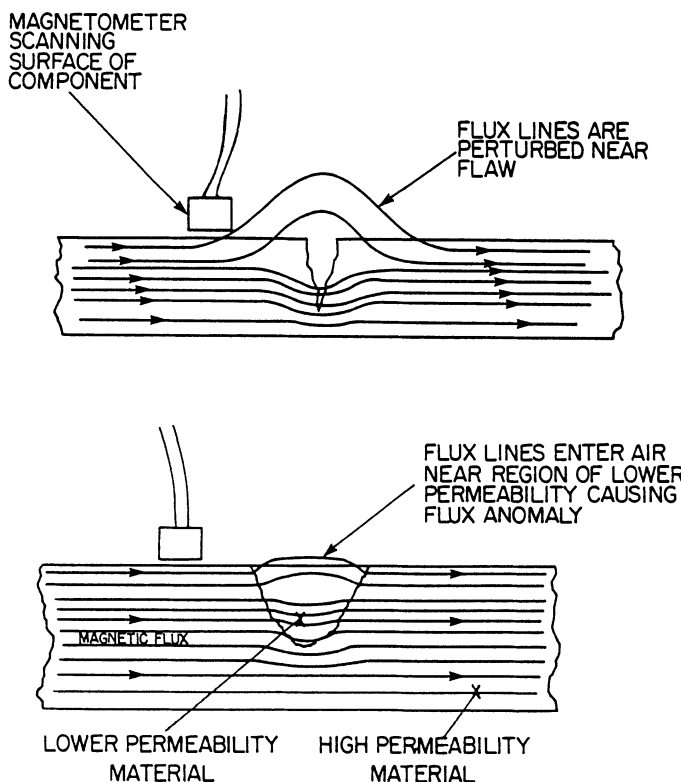


Fig. 16.14 Scanning the surface of a specimen with a magnetometer (a) to detect flaws and (b) to detect regions of low permeability by the magnetic flux leakage method.

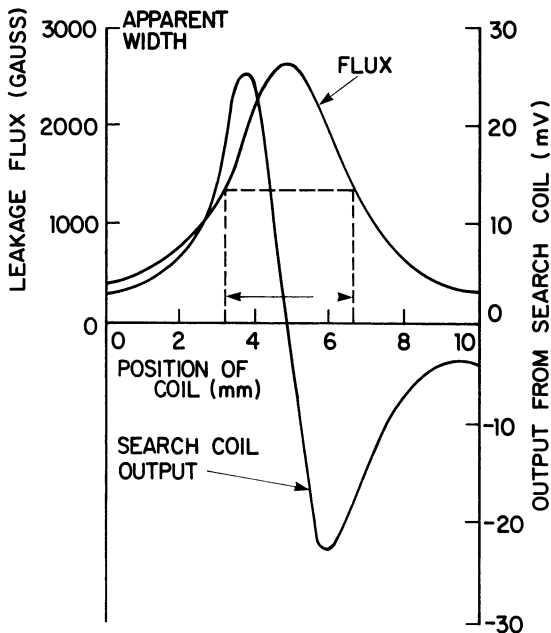


Fig. 16.15 Variation of flux leakage with distance across a crack.

again under these circumstances magnetic flux leakage magnetometry has been an important and highly successful technique, both for detection of flaws and for stresses. Subsequent work on detection of flux anomalies in pipelines indicated that these could be related to stresses within the pipe wall. The method has been particularly useful for the inspection of defects in underground pipelines as in the work of Atherton [56] and Khalileev, Fridman and Grigorev [57].

As with the MPI method the flux leakage signal depends on the level of magnetization within the material. Pashagin *et al.* have also shown that it depends on the method magnetization, such as magnetizing by current flow or via an electromagnet.

Introductory reviews of the flux leakage method and also a more advanced review have been given by Forster [58]. These discuss both the experimental and theoretical foundations of the method. The demagnetizing fields H_d of defects were calculated for ellipsoidal flaws inside the material, and consequently the true internal field in the defect H_i was calculated from the measured applied field H_a using the equation

$$H_i = H_a - H_d.$$

Once again this procedure is equivalent to assuming that the defect behaves like a simple magnetic dipole. Such an assumption is only valid as a first approximation. If the permeability of the material is μ_{iron} and the permeability of the flaw is μ_{flaw} and the demagnetizing factor which depends on the shape of the

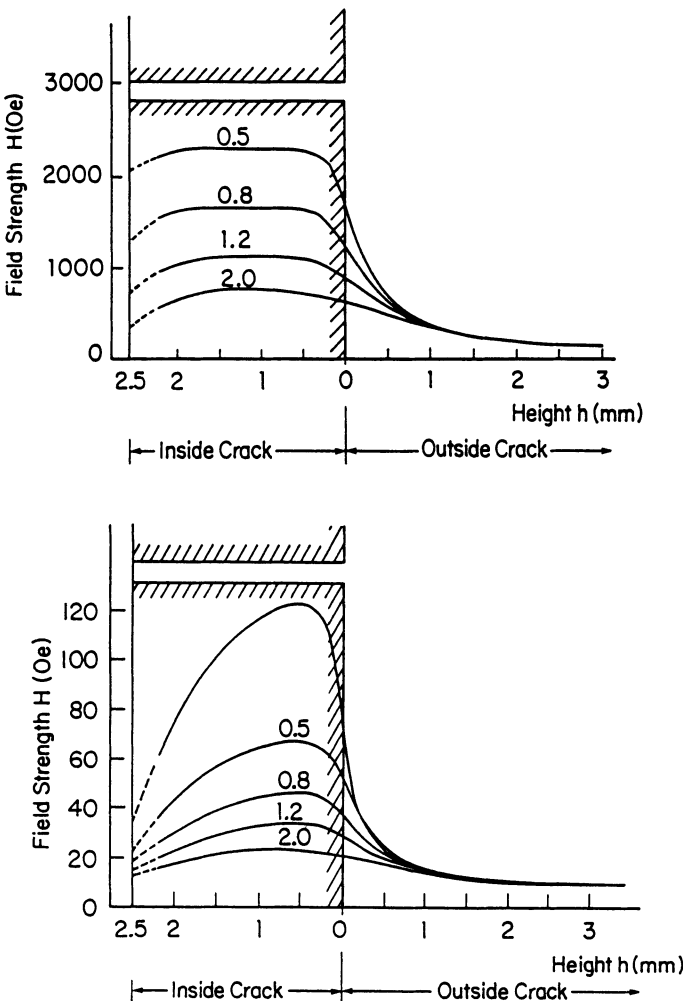


Fig. 16.16 Variation of leakage flux with position within and above a crack for various crack widths, after Forster (1985). Upper diagram is for a carbon steel. Lower diagram is for a chromium steel.

flaw is N_d , then the internal field is

$$H_i = H_a \left\{ \frac{\mu_{\text{iron}}}{\mu_{\text{iron}} + N_0(\mu_{\text{iron}} + \mu_{\text{flaw}})} \right\}.$$

One of the difficulties here is that of course in general the magnetic induction in a ferromagnet is not known as a function of field H , and hence μ_{iron} is not known as a function of H . These reviews were completed with experimental results on the variation of leakage flux with lift-off position above the crack and also as a function of depth within the crack as shown in Fig. 16.16. These showed that as the lift-off distance increased the leakage field became insensitive to crack depths at lift-off

distances above 1 mm for crack depths of 2.5 mm with varying widths of 0.2 to 2 mm.

16.2.4 Applications of the flux leakage method

Stumm [59] has described several devices based on the flux leakage technique which can be used for testing of ferromagnetic tubes for flaws. One of the problems identified with these instruments was the difference in defect signal between an external (near side) flaw and an internal (far side flaw). The signal from an internal flaw was much smaller than the signal from a comparable external flaw, as expected. The difficulty arises in deciding whether a given signal is due to a small external flaw or a much larger internal flaw.

One device called the 'rotomat' enabled the tube to be passed through a rotating magnetizing yoke which generated a circumferential magnetic field for detecting longitudinal defects in the tube wall. The leakage flux was measured using a array of Hall probes. Tube diameters of 20–450 mm could be inspected.

A second instrument, the 'tubomat' rotated the tube while maintaining the detection system stationary. The detection and field generation systems were identical to those used in the rotomat system. The method of magnetization was however dependent upon the size of the pipe. For large pipes the pipe was threaded with a central conductor which carried the high current required to obtain the optimum field strength in the pipe wall. For smaller pipes the magnetic yoke method was employed.

A third and somewhat different system described was the 'discomat' which was used primarily for weld inspection. The detection system containing five Hall probes was rotated on a disk at typically 50 rev/s and the tube was magnetized transversely to the direction of the weld using a magnetizing yoke.

Owston [60] has reported on measurement of leakage flux from fatigue cracks and artificial flaws such as saw slots in mild steel. These he attempted to interpret in terms of a simple dipole model of the type described by Zatsepin and Schcherbinin. The magnetic leakage field parallel to the surface and perpendicular to the cracks was measured as a function of lift-off (i.e. distance from the field detector to the surface of the test material). Results indicated that the leakage field increased linearly with slot depths of up to 0.2", while the derivative d^2H/dz^2 , where H is the magnetic field and z is the distance from the centre of the slot measured in the surface of the specimen, was found to be proportional to $1/l^4$ where l was the lift-off distance.

Barton, Lankford and Hampton [61] investigated the flux leakage method for testing of bearings, which revealed that magnetic signatures associated with pits, voids and inclusions could be identified in the leakage fields of bearing races.

Forster has written a number of papers on the subject of flux leakage at a fairly elementary level. The testing of round billets for cracks using leakage flux probes has been reported using both the 'tubomat' and the 'rotomat' devices. The locations of defects identified by these automated flux leakage detectors are

automatically marked with a paint spray for ease of identification. These systems were capable of inspecting 12 metre long billets of diameter 90–230 mm in 16 s.

The most extensive review of the subject of magnetic flux leakage as an NDE tool presently available is *NDE Applications of Magnetic Leakage Field Methods* by Beissner, Matzkanin and Teller [62] and it must be considered to be the standard reference on magnetic flux leakage at this time. It contains a history of the development of the method, discusses the underlying theory, including the analysis of leakage field results and defect characterization and finally a description of a number of applications.

16.2.5 Leakage field calculations

Once quantitative measurements of leakage fields became a routine technique it was natural to want to interpret the signals in terms of flaw size and shape. Therefore leakage field calculations for specific flaw shapes began to be made, so that the theoretical profiles could be compared with experimental observations with the objective of characterizing flaws from their leakage fields. Two of the most significant papers in the early development of this subject were by Schcherbinin and Zatsepин [63, 64], which were based on approximating surface defects by linear magnetic dipoles and calculating the dipole magnetic field. In this way, expressions were obtained for the normal and tangential components of the magnetic leakage field due to a defect.

Zatsepин and Schcherbinin realized that the exact calculation of leakage fields arising from real defects presented an extremely complicated problem, which was intractable given the numerical methods and state of computer technology at that time. They therefore looked for a relatively simple problem, the leakage field of flaws which could be approximated as a point, line or strip dipole and calculated the fields using analytical expressions. The results were then compared with observations of leakage fields due to defects as shown in Fig. 16.17. Notice that the horizontal component of field across the flaw leads to a unipolar response, while the normal component leads to a bipolar response. However these early papers did not relate the leakage field to the internal field in the material, and therefore there were limitations on its applicability to actual measured leakage fields.

Subsequent papers on leakage field calculations by Schcherbinin and Pashagin were based on the same model. Experimental measurements were made on specimens of carbon steel which had artificial flaws machined in the surfaces. These defects were typically $h = 0.2\text{--}3.0\text{ mm}$ deep, $2b = 1.0\text{ mm}$ wide and $2l = 1.0\text{--}30.0\text{ mm}$ long. The magnetic fields were generated using the magnetic yoke method, with a maximum magnetic field of 12 kA/m . Measurements of the leakage fields were made using a fluxgate (or ‘ferroprobe’) magnetometer. Field components tangential to the surface of the specimen normal to the flaw, H_x , and normal to the surface of the specimen, H_y , were measured.

It was found, for example, that the relationship between the field H_y and the magnetizing field H_0 remained almost linear, for any given length of flaw,

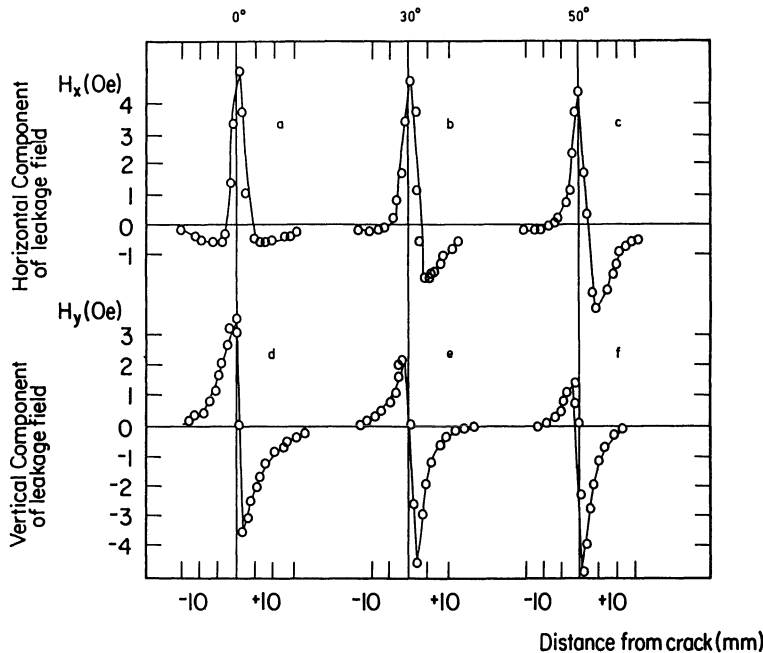


Fig. 16.17 Calculated leakage field due to a flat-bottomed flaw using the dipole model; (a), (b) and (c) are horizontal field components, (d), (e) and (f) are vertical field components. The spot is of length of length 4 mm, width 0.4 mm and depth 2 mm, after Zatsepin and Schcherbinin (1966).

although the actual ratio H_y/H_0 increased as the flaw length increased, and in fact appeared to reach a saturation level as the length tended to infinity. The tangential field H_x perpendicular to the flaw was also measured. For a given flaw it was found to decay with displacement z from the centre of the flaw. H_x was also found to increase with flaw length, although this variation was dependent upon the magnetizing field H_0 . The calculations of the leakage fields by Schcherbinin *et al.* were analogous to the fringing field calculations for idealized magnetic recording heads by Karlquist.

Significant progress in the calculation of leakage fields was made subsequently by Hwang and Lord [65] using finite-element methods. This was the first attempt to use numerical methods to find exact solutions for the field caused by defects and represented a real breakthrough in the development of the subject because it enabled the leakage fields to be calculated from the existing field and permeability in the bulk of the material. This represents a landmark in the calculation of leakage fields. Some results of their calculations are shown in Fig. 16.18. The earlier work of Zatsepin and Schcherbinin while commendable was not easily adaptable to the range of shapes of defects encountered in practice. The leakage field profiles obtained by Hwang and Lord for the case of a simple rectangular slot were in excellent agreement with observation. This paper was therefore instrumental in

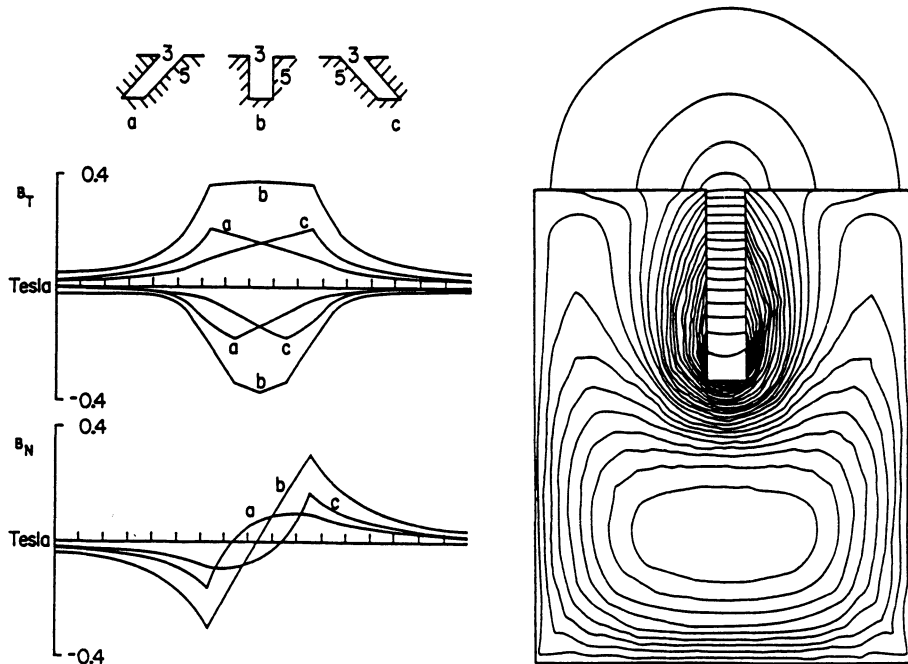


Fig. 16.18 Calculated leakage field due to a flaw using finite-element techniques, after Hwang and Lord [66].

demonstrating how the finite-element technique could be used for modelling fields of defects. It was clear from the work that the finite element method was sufficiently flexible, so that its successful application in the case of a simple slot defect indicated its likely successful application in the case of more complex defects, an extension to which the Schcherbinin model was not capable.

This was followed by a series of papers of which the most significant were by Lord and Hwang [66] and Lord *et al.* [67]. Lord and Hwang extended the application of the finite-element method to a variety of more complicated flaw shapes. It was deduced from this that the finite-element method provided the possibility of defect characterization from the leakage field profile. It was found, for example, that the peak-to-peak value of the leakage flux B_N increased with increasing flaw depth, while the separation between the peaks depended on flaw width. These results were in agreement with experimental observation and indicated the potential benefits of finite-element techniques for interpreting leakage flux measurements with the objective of characterizing the defects.

Lord, Bridges, Yen and Palanisamy [67] have remarked that the cornerstone of an approach to the application of magnetic flux leakage techniques to NDT is the development of an adequate mathematical model for magnetic field-defect interactions. It might also be added that the modelling of the B , H or hysteresis characteristics in ferromagnetic materials adds another dimension to this problem,

since even if the internal magnetic field is known there are a range of possible values of the flux density inside the material. These different possible values of \mathbf{B} will certainly affect the leakage flux for a given type of defect with a given magnetizing field \mathbf{H}_0 inside the material. Lord concluded that the complex defect geometries, together with the nonlinear magnetization characteristics of ferromagnetic steels, made closed form or analytical solutions of magnetic field defect interactions virtually impossible. However, they were able to show a number of examples of successful application of finite-element modelling and to conclude optimistically about the potential for defect characterization for nondestructive testing.

Lord [68] has given a review of the application of the finite-element numerical method for calculation of leakage fields arising from magnetic field-defect interactions. In this he had indicated that much progress has been made in theoretical modelling of leakage field signatures using numerical methods, but that there are many complex problems still to be solved. Perhaps the most significant of these is taking into account the hysteresis in \mathbf{B}, \mathbf{H} characteristics of ferromagnetic materials before applying the finite-element, or other numerical calculation of the leakage field.

The work of Lord and co-workers has firmly established the use of numerical methods such as finite-element calculations, as the technique with the most promise for characterization of defects from leakage flux measurements. This has lead to much interest in the area of numerical modelling of leakage fields, for example the recent work of Atherton [69] and Brudar [70]. However it is realized that three-dimensional finite-element calculations are ultimately desirable for more precise characterization of real defects.

An analytical solution for the leakage field of surface breaking cracks has recently been presented by Edwards and Palmer [71], in which the crack is approximated as a semi-elliptic slot in the material. The advantages of an analytical expression are that the fields due to defects can be rapidly calculated, and in addition the equations can be differentiated to find the forces on magnetic particles. From these results Edwards and Palmer calculated the magnetic field strength \mathbf{H} needed to detect 1 μm and 10 μm wide slots for a range of slot depths and permeabilities. They concluded that fields in the range 10^2 – 10^3 A/m are required for crack detection, and these are in agreement with those used in practice, for example BS 6072 which recommends a magnetic induction of 0.72 T, corresponding to fields of 5700 A/m in a steel of relative permeability 100.

Reviews of the subject of magnetic leakage field calculations and the interpretation of experimental measurements have been given by Holler and Dobmann [72]. Dobmann [73] has discussed the problems of both detection and sizing of defects and has attempted to relate these to theoretical model predictions. Theoretical work on flux leakage has lagged considerably behind experimental development. Dobmann and Holler have reviewed the theoretical modelling of the effects of various flaws on the leakage flux, and Forster has attempted to correlate observed magnetic flux leakage measurements with expectations based on finite-

element model calculations. His results showed serious discrepancies. This has made it difficult to quantitatively characterize flaws in some cases, although qualitatively the explanations are relatively simple and have been successful.

16.2.6 Eddy current inspection

Eddy current methods for nondestructive evaluation are not strictly magnetic methods as such. That is they do not depend for their validity on any inherent magnetic properties of the material under test. In fact they can be applied to any conducting material. Furthermore the literature for eddy current techniques is more extensive than that of all the other magnetic methods combined, and so it would not be possible to give a comprehensive review of the subject in this paper. Nevertheless in the interests of completeness eddy currents do deserve mention since they are used on magnetic materials.

The eddy current inspection method depends on the change in impedance of a search coil caused by the generation of electrical currents in the test specimen when it is subjected to a time-varying magnetic field, Fig. 16.19. The response is usually monitored in the form of a complex impedance plane map. Eddy currents can be used for the detection of cracks and other defects, because the defects interrupt the flow of the eddy currents generated in the material. This results in a different complex impedance of the eddy current pick-up coil when it is positioned over the flaw compared with when it is positioned over an undamaged region of the material. Eddy currents can also be used for checking thickness of coatings, determining permeability and conductivity, evaluating changes in heat treatment and microstructure, estimating tensile strength, chemical composition and ductility. However, whereas the interpretation of results in nonmagnetic materials is relatively straightforward, in ferromagnetic materials it is more difficult because

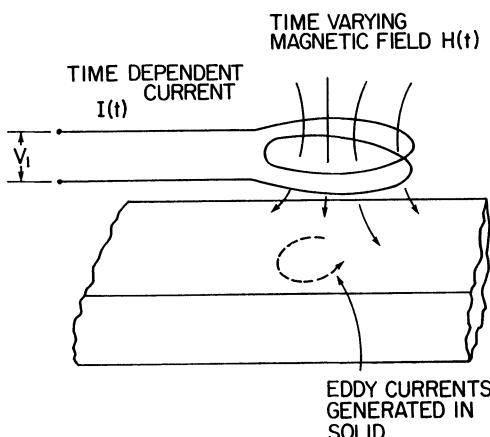


Fig. 16.19 Generation of eddy currents in a conducting material by a time-varying field.

the eddy current response depends on the permeability. In ferromagnetic materials such as steels the permeability varies in a complicated way with the generating field.

Much of the early work on development of eddy current techniques was due to Forster [74]. A survey of the field until 1970 was given by Libby [75].

16.2.7 Applications of eddy currents inspection

Application of eddy current techniques to magnetic materials by Vroman [76] has shown that the results are easier to interpret if the material is subjected to a saturating dc field at the same time as the ac field which generates the eddy currents. This insures that the prior state of magnetization of the material no longer affects the observed results, while also preventing large changes in permeability.

Cocco and Bax therefore saturated the magnetization within their steam generator tubing while scanning for defects. In this way they reported that they obtained improved sensitivity over earlier attempts to use eddy currents for ferromagnetic tubes which had been hampered by inherent 'magnetic noise'. Deeds and Dodd [77] have reported on detection of defects such as cracks, wall thinning or holes in steam generator tubing using eddy currents. Dodd and Simpson developed a low frequency eddy current system for accurate determination of small changes in permeability of weakly magnetic materials, which was used to evaluate the fabrication of austenitic stainless steels. This was able to determine the amount of cold working in components and to determine the amount of delta ferrite in welds, which reduces the incidence of hot cracking in the welds.

Detection of the depth of case hardening in steels by eddy current inspection has been reported by Kuznetsov and Skripova. Clark and Junker [78] have established the feasibility of an eddy current NDT approach for the detection of temper embrittlement in low alloy steels, which was known to be difficult to detect using other techniques. Eddy currents have also been used for mapping localized changes in residual stress using automated scanning equipment by Clark and Taszarek. However they concluded that the method was unable to discriminate between tensile and compressive residual stresses, only the absolute magnitude of stress could be ascertained. Lord and Palanisamy have also used eddy currents for inspection of steam generator tubing and modelled the results using finite-element techniques.

16.2.8 The remote field electromagnetic technique

The remote field electromagnetic technique is based on the diffusion of electromagnetic energy through a pipe wall. This can be used for the detection of corrosion or other forms of wall thinning in pipes and oil well castings. The method was developed in the 1950s and early 1960s, but it is only in recent years that it has suddenly received great attention as an NDE technique.

One of the earliest descriptions of the method was by Schmidt [79] who used it for *in situ* detection of external casing corrosion in down hole inspection in oil wells. This was an important breakthrough because there were no other techniques available for detection of external corrosion. The advantages of the method over conventional eddy current and ultrasonics inspection, which can also be used for measuring wall thickness, include full 360° scanning of the pipe, rapid logging speeds and its insensitivity to dirt or scale on the pipe.

Schmidt [80] has recently reviewed the remote field eddy current inspection technique. In this he has shown that the development of improved spatial resolution of these instruments has allowed isolated pits and cracks in the pipe wall to be resolved, a result not possible with alternative techniques under the conditions encountered in down hole inspection. The method has been used for detection and classification of stress corrosion cracking.

The advantage of the remote field technique is that it detects only a flux which has penetrated and been transmitted through the pipe wall. Even though both the transmitter and receiver coils are located within the pipe there is very little direct coupling between them. Therefore the detected signal contains information about the pipe wall thickness. The variation of the detected signal with distance between exciter and receiver coils is shown in Fig. 16.20.

The technique is equally sensitive to both interior and exterior metal loss, and the observed phase lag was found to be linear with wall thickness, which is a convenient property. Finally the problems that are normally encountered

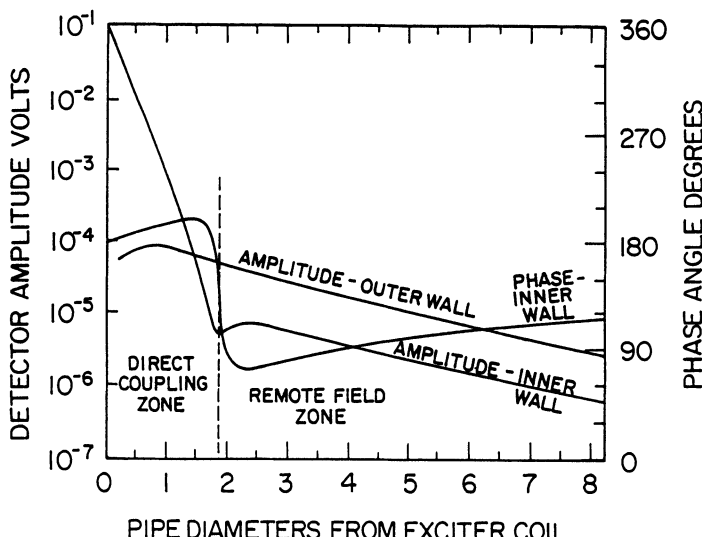


Fig. 16.20 Variation of phase and amplitude of a detected signal as a function of distance between exciter and receiver coils within the pipeline.

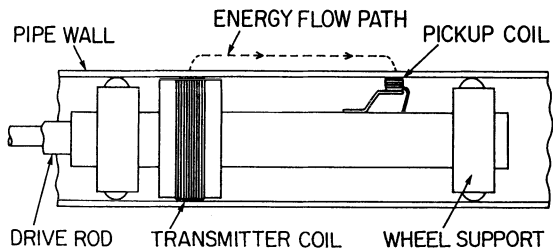


Fig. 16.21 Arrangement for the remote-field electromagnetic inspection of pipes as described by Atherton and Sullivan [81]

with lift-off in eddy current inspection are less evident in the remote field technique.

This method has recently been investigated by Atherton and Sullivan [81] for inspecting zirconium-2.5% niobium nuclear reactor pressure tubes, which are non-ferromagnetic, for the presence of defects. In this they operated the detection coil at a distance of one pipe diameter from the transmitter coil as shown in Fig. 16.21. They also have indicated that their results are consistent with Schmid's original suggestion that the signals are caused by a diffusion process through the wall close to the transmitter coil, followed by propagation along the outside of the tube, and then diffusion back through the pipe wall. Subsequently finite-element calculations were used to model the propagation of the electromagnetic signals in the remote field eddy current technique. The results of these calculations confirmed the mode of propagation originally suggested.

16.3 CONCLUSIONS

A variety of magnetic methods for NDE are available and these have been critically reviewed here. With the upsurge of interest in this field there must certainly be new magnetic methods awaiting development in the near future. One of these may be the use of magnetomechanical emissions of the type observed by Higgins and Carpenter which would seem to be ideal for the detection of dynamic stresses in steel, but which has not even begun to be exploited. Compared with ultrasound, most of the magnetic methods are in their infancy and so offer wide scope for future development and growth. But, also in comparison with ultrasound, the instrumentation required for magnetic inspection is far simpler and therefore in many cases easier to adapt to applications.

Three major classes of techniques for detection and characterization of flaws and defects in ferromagnetic materials have been discussed. These are magnetic particle inspection, magnetic flux leakage and eddy current inspection. The relative advantages and disadvantages of each technique have been discussed, and a survey of existing literature has been given. It is not possible to discuss each method in detail here, nor is it even desirable. The references given however do provide access to the specialized literature of each method and further details can be obtained from them.

REFERENCES

1. Barkhausen, H. (1919) *Phys. Z.*, **29**, 401.
2. Tebble R. S., Skidmore, I. C. and Corner, W. D. (1950) *Proc. Phys. Soc.*, **A63**, 739.
3. Tiiitto, S. (1977) *Acta Polytechnica Scand.*, **119**, 1.
4. Sundstrom, O. and Torronen, K. (1979) *Mater. Eval.*, **37**, 51.
5. Karjalainen, L. P., Moilanen, M. and Rautioaho, R. (1979) *Mater. Eval.*, **37**, 45.
6. Lomaev, G. V., Malyshev, V. S. and Degterev, A. P. (1984) *Sov. J. NDT.*, **20**, 189.
7. Mayos, M., Segalini, S. and Putignani, M. (1987) in *Review of Progress in Quantitative NDE*, (ed. D. O. Thompson and D. E. Chimenti), Plenum, New York.
8. Theiner, W. A. and Altpeter, I. (1983) in *New Procedures in NDT* (ed. P. Holler), Springer-Verlag Berlin.
9. Schneider, E., Theiner, W. A. and Altpeter, I. (1984) in *Nondestructive Methods for Materials Property Determination* (ed. C. O. Ruud and R. E. Green), Plenum, New York.
10. Matzkanin, G. A., Beissner, R. E. and Teller, C. M. (1979) *SWRI Report No. NTIAC-79-2*.
11. McClure, J. C. and Schroeder, K. (1976) *CRC Solid State Science*, **6**, 45.
12. Lord, A. E. (1975) in *Physical Acoustics XI* (ed. W. P. Mason and R. N. Thurston), Academic Press.
13. Kusanagi, H., Kimura, H. and Sasaki, H. (1979) *J. Appl. Phys.*, **50**, 1989.
14. Ono, K. and Shibata, M. (1980) *Mater. Eval.*, **38**, 55.
15. Burkhardt, G. L., Beissner, R. E., Matzkanin, G. A. and King, J. D. (1981) *Mater. Eval.*, **40**, 669.
16. Theiner, W. A. and Willems, H. H. (1984) in *Nondestructive Methods for Materials Property Determination* (ed. C. O. Ruud and R. E. Green), Plenum.
17. Edwards, C. and Palmer, S. B. (1987) *J. Acoust. Soc. Am.*, **82**, 534.
18. Ranjan, R., Jiles, D. C. and Rastogi, P. K. (1987) *IEEE Trans. Mag.*, **23**, 1869.
19. Higgins, F. P. and Carpenter, S. H. (1978) *Acta Metall.*, **26**, 133.
20. Jiles, D. C. and Atherton, D. L. (1984) *J. Phys. D: Appl. Phys.*, **17**, 1265.
21. Mikheev, M. N., Morozova, V. M., Morozov, A. P., Neizvestnov, B. M., Surin, G. V. and Zakharova, G. N. (1978) *Sov. J. NDT*, **14**, 9.
22. Mikheev, M. N. (1983) *Sov. J. NDT*, **19**, 1.
23. Kuznetsov, I. A., Somova, V. M. and Bashkirov, Y. P. (1982) *Sov. J. NDT*, **8**, 506.
24. Zatsepin, N. N., Ashtashenko, P. P., Potapova, N. A., Kaverin, V. D. and Smirnova, T. M. (1983) *Sov. J. NDT*, **19**, 158.
25. Rodigin, N. M. and Syrochkin, V. P. (1983) *Sov. J. NDT*, **9**, 453.
26. Schcherbinin, V. E., Vlasov, V. V. and Dovnar, D. P. (1972) *Sov. J. NDT*, **8**, 641.
27. Langman, R. (1985) *IEEE Trans. Mag.*, **21**, 1314.
28. Novikov, V. F. and Fateev, I. G. (1982) *Sov. J. NDT*, **18**, 489.
29. Atherton, D. L. and Jiles, D. C. (1983) *IEEE Trans. Mag.*, **19**, 2021.
30. Burkhardt, G. L. and Kwun, H. (1987) *J. Appl. Phys.*, **61**, 1576.
31. Willcock, S. N. M. and Tanner, B. K. (1983) *IEEE Trans. Mag.*, **19**, 2145.
32. Jiles, D. C. and Atherton, D. L. (1986) *J. Mag. Mag. Mater.*, **61**, 48.
33. Szpunar, B. and Szpunar, J. A. (1984) *IEEE Trans. Mag.*, **20**, 1882.
34. Shah, M. B. and Bose, M. S. C. (1984) *Phys. Stat. Solidi.*, **86**, 275.
35. Bussiere, J. F. (1986) *Mater. Eval.*, **44**, 560.
36. Konovalov, O. S., Golovko, A. S. and Roitman, V. I. (1982) *Sov. J. NDT*, **18**, 554.
37. Suzuki, M., Komura, I. and Takahashi, H. (1981) *Int. J. Press. Vessel Piping* **6**, 255.
38. Langman, R. (1981) *NDT International* **14**, 255.
39. Mikheev, M. N., Bida, G. V., Tsarkova, T. P. and Kastin, V. N. (1982) *Sov. J. NDT*, **18**, 641.

40. Kwun, H. and Teller, C. M. (1982) *Appl. Phys. Letts.*, **41**, 144.
41. Namkung, M., Utrata, D., Allison, S. G. and Heyman, J. S. (1986) *Review of Progress in Quantitative NDE*, (eds. D. O. Thompson and D. E. Chimenti), Plenum Press, New York.
42. Utrata, D. and Namkung, M. (1986) *Proceeding of the Second International Symposium for Nondestructive Characterization of Materials*, Montreal
43. Kwun, H. (1986) *Mater. Eval.*, **44**, 1560.
44. Gregory, C. A., Holmes, V. L. and Roehrs, R. J. (1972) *Mater. Eval.*, **30**, 219.
45. Massa, G. M. (1976) *NDT International*, **9**, 16.
46. Goebbel, K. and Simkin, J. (1990) *Review of Progress in Quantitative NDE* (eds D. O. Thompson and D. E. Chimenti), Plenum Press, New York.
47. Goebbel, K. (1989) *Proceedings of the Twelfth World Conference on NDT*, Amsterdam, April 1989, p. 719 (eds J. Boogaard and G. M. VanDijk) Elsevier Science Publishers.
48. Goebbel, K. (1988) *Materialprufung*, **30**, 327.
49. Edwards, C. and Palmer, S. B. (1981) *NDT International*, **14**, 177.
50. Oehl, C. L. and Swartzendruber, L. J. (1982) *J. NDE*, **3**, 125.
51. Chen, Y. F. (1984) *Mater. Eval.*, **42**, 1506.
52. Goebbel, K. and Ferrano, G. (1988) *Proceedings of the Fourth European Conference on NDT*, London, September 1987, p. 2762 (eds J. M. Farley and R. W. Nichols), Pergamon Press, Oxford.
53. Betz, C. E. (1966) *Principles of Magnetic Particle Testing*, Magnaflux Corporation.
54. Schmidt, J. T. and Skeie, K. (1989) *NDT Handbook, Volume 6: Magnetic Particle Testing* (ed. P. McIntire) American Society for Nondestructive Testing.
55. Hastings, C. H. (1947) *ASTM Proc.*, **47**, 651.
56. Atherton, D. L. (1983) *NDT International*, **16**, 145.
57. Grigorev, P. A., Fridman, L. A. and Khalilev, P. A. (1976) *Sov. J. NDT*, **12**, 351.
58. Forster, F. (1982) *Sov. J. NDT*, **18**, 841.
59. Stumm, W. (1974) *Non-destructive testing*, **7**, 251.
60. Owston, C. N. (1974) *Brit. J. NDT*, **16**, 162.
61. Barton, J. R., Lankford, J. and Hampton, P. L. (1972) *Trans. Soc. Auto. Eng.*, **81**, 681.
62. Beissner, R. E., Matzkanin, G. A. and Teller, C. M. (1980) *SWRI Report Number NTIAC-80-1*.
63. Zatsepin, N. N. and Schcherbinin, V. E. (1966) *Sov. J. NDT*, **2**, 50.
64. Schcherbinin, V. E. and Zatsepin, N. N. (1966) *Sov. J. NDT*, **2**, 59.
65. Hwang, J. H. and Lord, W. (1975) *J. Test. and Eval.*, **3**, 21.
66. Lord, W. and Hwang, J. H. (1977) *Brit. J. NDT*, **19**, 14.
67. Lord, W., Bridges, J. M., Yen, W. and Palanisamy, S. (1978) *Mater. Eval.*, **36**, 47.
68. Lord, W. (1983) *IEEE Trans. Mag.*, **19**, 2437.
69. Atherton, D. L. (1988) *Brit. J. NDT*, **30**, 159.
70. Brudar, B. (1985) *NDT International*, **18**, 353.
71. Edwards, C. and Palmer, S. B. (1986) *J. Phys. D. (Appl. Phys.)*, **19**, 657.
72. Holler, P. and Dobmann, G. (1980) in *Research Techniques in NDT*, Vol. IV (ed. R. S. Sharpe), Academic Press London.
73. Dobmann, G. (1985) in *Electromagnetic Methods of NDT*, (ed. W. Lord), Gordon and Breach.
74. Forster, F. (1954) *Z. Metallk.*, **45**, 221.
75. Libby, H. L. (1971) *Introduction to Electromagnetic Nondestructive Test Methods*, Wiley.
76. Vroman, J. (1981) *Brit. J. NDT*, **23**, 307.
77. Deeds, W. E. and Dodd, C. V. (1985) in *Electromagnetic Methods of NDT* (ed. W. Lord), Gordon and Breach.
78. Clark, W. G. and Junker, W. R. (1985) *Mater. Eval.*, **43**, 1546.
79. Schmidt, T. R. (1961) *Corrosion*, **17**, 81.

80. Schmidt, T. R. (1984) *Mater Eval.*, **42**, 225.
81. Atherton, D. L. and Sullivan, S. (1986) *Mater. Eval.*, **44**, 1544.

FURTHER READING

- Bezer, H. J. (1964) Magnetic methods for NDT, *Brit. J. NDT*, **6**, 85; and **6**, 109.
- Betz, C. E. (1966) *Principles of Magnetic Particle Testing*, Magnaflux Corporation.
- Halmshaw, R. (1987) *Non Destructive Testing*, Edward Arnold Publishers, Ch. 5.
- Jiles, D. C. (1988) Magnetic methods for non destructive evaluation, *NDT International*, **21**, 311.
- Jiles, D. C. (1990) Magnetic methods for non-destructive evaluation (Part 2), *NDT International*, **23**, 83.

Journals

Non-destructive Testing and Evaluation (formerly *NDT Communications*)

Journal of NDE

NDT International

Materials Evaluation (The official journal of the American Society of Non-destructive Testing)

British Journal of NDT (The official journal of the British Institute of NDT)

Solutions

Example 1.4 Magnetic field at the centre of a long solenoid. Using the result for the field on the axis of a single turn obtained in example 1.1 consider the field due to an elemental length of solenoid dx with n turns per unit length, each carrying a current i

$$d\mathbf{H} = \frac{ni}{2a} \sin^3 \alpha dx.$$

We now need to express either α in terms of x and integrate over the range $x = -\infty$ to $x = \infty$, or to express x in terms of α and integrate from $\alpha = -\pi$ to $\alpha = \pi$.

$$\tan \alpha = \frac{a}{x}$$

$$x = a \cot \alpha.$$

Therefore

$$dx = -a \operatorname{cosec}^2 \alpha d\alpha$$

$$\begin{aligned} d\mathbf{H} &= -\left(\frac{ni}{2}\right) \sin^3 \alpha \operatorname{cosec}^2 \alpha d\alpha \\ &= -\left(\frac{ni}{2}\right) \sin \alpha d\alpha. \end{aligned}$$

Now integrating from $\alpha = -\pi$ to $\alpha = +\pi$

$$\mathbf{H} = -\left(\frac{ni}{2}\right) \int_{-\pi}^{\pi} \sin \alpha d\alpha$$

$$\mathbf{H} = ni \text{ amps per metre.}$$

Example 1.5 Force on a current-carrying conductor. (a) The magnetic field at a distance a from a long conductor carrying a current i is

$$\mathbf{H} = \frac{i}{2\pi a}.$$

The force per metre exerted on a current carrying conductor by a field \mathbf{H} is

$$\mathbf{F} = \mu_0 i d\mathbf{l} \times \mathbf{H}.$$

In this case \mathbf{H} and $d\mathbf{l}$ are perpendicular so that the force per unit length is

$$F = \frac{\mu_0 i^2}{2\pi a}.$$

When the conductors both carry 1 amp and are 1 metre apart

$$\begin{aligned} F &= \frac{(4\pi \times 10^{-7})(1)(1)}{2\pi} \\ &= 2 \times 10^{-7} \text{ newtons per metre.} \end{aligned}$$

This is a surprisingly small force given that the currents seem so large.

(b) The force exerted, as given by the above equation, is

$$\mathbf{F} = \mu_0 i d\mathbf{l} \times \mathbf{H}$$

and in this case the current is perpendicular to the field, so

$$\begin{aligned} F &= \mu_0 i l H \\ &= (4\pi \times 10^{-7})(5)(0.035)(160 \times 10^3) \\ f &= 0.0352 \text{ newton.} \end{aligned}$$

Example 1.6 Torque on a current-loop dipole.

$$\begin{aligned} \tau &= \mu_0 \mathbf{m} \times \mathbf{H} \\ &= \mathbf{m} \times \mathbf{B} \end{aligned}$$

and if the \mathbf{m} and \mathbf{B} vectors are perpendicular and since $\mathbf{m} = ANi$

$$\begin{aligned} \tau &= ANiB \\ &= (4 \times 10^{-4})(100)(1 \times 10^{-3})(0.2) \\ &= 8 \times 10^{-6} \text{ newton metre.} \end{aligned}$$

Example 2.3 Demagnetizing field calculation.

$$\mathbf{H}_{\text{in}} = \mathbf{H}_{\text{app}} - N_d \mathbf{M}$$

and for a sphere $N_d = 1/3$. Since $\mathbf{M}_s = 1.69 \times 10^6$ amp/metre

$$\mathbf{H}_{\text{app}} = \mathbf{H}_{\text{in}} + (1/3)(1.69 \times 10^6) \text{ amp/metre}$$

and since we are assuming $N_d \mathbf{M} \gg \mathbf{H}_{\text{in}}$ this gives

$$\mathbf{H}_{\text{app}} = 5.62 \times 10^5 \text{ amps/metre.}$$

Example 2.4 Demagnetizing effects at different field strengths.

$$\mathbf{M} = \mathbf{B}/\mu_0 - \mathbf{H}.$$

At $H = 80 \text{ kA/m}$

$$\begin{aligned}\mathbf{M} &= 7.16 \times 10^5 - 0.8 \times 10^5 \text{ A/m} \\ &= 6.36 \times 10^5 \text{ A/m}\end{aligned}$$

The internal field is given by

$$\begin{aligned}\mathbf{H}_{\text{in}} &= \mathbf{H}_{\text{app}} - N_d \mathbf{M} \\ &= 8 \times 10^4 - (0.02)(6.36) \times 10^5 \\ &= 6.73 \times 10^4 \text{ A/m.}\end{aligned}$$

At 160 kA/m

$$\begin{aligned}\mathbf{M} &= 8.75 \times 10^5 - 1.6 \times 10^5 \text{ A/m} \\ &= 7.15 \times 10^5 \text{ A/m}\end{aligned}$$

and

$$\begin{aligned}\mathbf{H}_{\text{in}} &= 16.0 \times 10^4 - (0.02)(7.15) \times 10^5 \\ &= 14.57 \times 10^4 \text{ A/m.}\end{aligned}$$

Fractional errors obtained if fields are not corrected for demagnetizing effects are at 80 kA/m

$$\frac{(\mathbf{H}_{\text{app}} - \mathbf{H}_{\text{in}})}{\mathbf{H}_{\text{app}}} = 0.159$$

at 160 kA/m

$$\frac{(\mathbf{H}_{\text{app}} - \mathbf{H}_{\text{in}})}{\mathbf{H}_{\text{app}}} = 0.089.$$

Therefore demagnetizing effects become proportionally less of a problem at higher field strengths.

Example 2.5 Flux density in an iron ring with and without an air gap. In the continuous ring the flux density is given by

$$\begin{aligned}\Phi &= Ni/(l/\mu A) \\ &= 6.0 \times 10^{-4} \text{ weber.}\end{aligned}$$

When there is a saw cut in the ring the total reluctance is the sum of reluctance of the iron and the air, so the relation becomes

$$Ni = \Phi \left[\frac{l_a}{\mu_a A_a} + \frac{l_i}{\mu_i A_i} \right],$$

where $l_i = 0.4995 \text{ m}$, $l_a = 0.0005 \text{ m}$, $A_i = 2 \times 10^{-4} \text{ m}^2$, $\mu_i = 0.001885 \text{ H/m}$, $\mu_a = 12.57 \times 10^{-7} \text{ H/m}$.

Under these conditions the flux will be,

$$\begin{aligned}\Phi &= \frac{(800)(2 \times 10^{-4})}{(397.77 + 264.98)} \\ &= 2.4 \times 10^{-4} \text{ weber.}\end{aligned}$$

The additional current required to restore the flux to its original value is

$$\begin{aligned}N\delta i &= \frac{\Phi l_a}{\mu_a A_a} \\ \delta i &= \frac{(6.0 \times 10^{-4})(0.0005)}{(0.0002 \times 4\pi \times 10^{-7})} \\ &= 1.5 \text{ amps.}\end{aligned}$$

The total current needed to restore the flux density is therefore $i + \delta i = 2.5$ amps.

Example 3.1 Torque magnetometer.

$$\begin{aligned}\tau &= \mu_0 \mathbf{m} \times \mathbf{H} \\ &= \mu_0 \mathbf{m} \mathbf{H} \sin \theta.\end{aligned}$$

At 90°

$$\begin{aligned}\tau &= (4\pi \times 10^{-7})(0.318)(14) \text{ newton metre} \\ &= 5.6 \times 10^{-6} \text{ newton metre}\end{aligned}$$

At 30°

$$\begin{aligned}\tau &= (5.6 \times 10^{-6}) \sin 30^\circ \\ &= 2.8 \times 10^{-6} \text{ newton metre.}\end{aligned}$$

Example 3.2 Magnetic resonance. A paramagnet with $S = \frac{1}{2}$ is a system with one unpaired electron. Since this is a dilute paramagnet then we may consider the electrons on neighbouring ionic sites as non-interacting. The magnetic moment of a single electron is $\mathbf{m} = 9.27 \times 10^{-24} \text{ A m}^2$, therefore since the gyromagnetic ratio γ is

$$\gamma = -\mu_B g \left(\frac{2\pi}{h} \right).$$

For an electron $g = 2$

$$\begin{aligned}\gamma &= \frac{(9.27 \times 10^{-24})(2)(6.284)}{(6.63 \times 10^{-34})} \\ &= 1.76 \times 10^{11} \text{ Hz/T.}\end{aligned}$$

Therefore the using the expression for the resonant frequency v_0

$$\begin{aligned}v_0 &= \gamma B \\ &= (1.76 \times 10^{11})(0.1) \text{ Hz}\end{aligned}$$

$$= 1.76 \times 10^{10} \text{ Hz}$$

$$= 17600 \text{ MHz.}$$

Example 3.3 Induction coil method. The applied field in amps per metre can be found simply by multiplying the current in the windings by 400.

Reversing the current in the solenoid causes the flux density to reverse completely, so if the prevailing value is B_0 tesla the change in flux density caused by reversing the field is $2B_0$.

The flux density change is found by multiplying the deflection d (in mm) 0.17×10^{-4} Wb/mm, and then dividing by the result by the product of the number of turns, 40, and the cross-sectional area 0.196×10^{-4} m².

$$\mathbf{H} = 400i \text{ A/m}$$

$$\Delta\mathbf{B} = 2\mathbf{B} = 0.0217d \text{ tesla}$$

i_r (A)	H_a (A/m)	d (mm)	B (A/m)
1.5	600	24.0	0.26
3.1	1240	49.2	0.53
4.9	1960	77.6	0.84
8.5	3400	103.7	1.12
11.0	4400	107.5	1.17
12.7	5080	109.1	1.18

From this table a plot of \mathbf{B} against H_a gives the apparent magnetization curve.

From charts of demagnetizing factors given in Chapter 2, we find that $N_d = 0.0015$ for a cylinder with length to diameter ratio 40:1 and relative permeability greater than 150.

The demagnetizing field H_d is given by

$$\mathbf{H}_d = N_d(\mathbf{B}/\mu_0 - \mathbf{H}_a)$$

and hence the true internal field \mathbf{H}_i is given by

$$\begin{aligned}\mathbf{H}_i &= \mathbf{H}_a - \mathbf{H}_d \\ &= \mathbf{H}_a - N_d(\mathbf{B}/\mu_0 - \mathbf{H}_a).\end{aligned}$$

B (T)	H_a (A/m)	H_i (A/m)
0.26	600	291
0.53	1240	609
0.84	1960	960
1.12	3400	2068
1.17	4400	3009
1.18	5080	3678

At $B = 1$ tesla, by linear interpolation, the permeability is $6.276 \times 10^{-4} \text{ H m}^{-1}$. This corresponds to a relative permeability of 499.7.

Example 4.2 Use of initial magnetization curve to find flux in core. If the material is in the form of a toroid with mean circumference 40 cm and cross-sectional area 4 cm^2 , with a coil of 400 turns, then the magnetic field generated by a current i in the coils will be

$$\begin{aligned} H &= Ni/l \\ &= 400i/0.4 \\ &= 1000i \text{ A/m.} \end{aligned}$$

This will correspond to a certain magnetic induction at each field strength. The magnetic inductions B (in Wb/m^2 or equivalently tesla) can be read from the graph of B against H for the calculated values of H

i (A)	H (A/m)	B (T)
0.1	100	0.52
0.2	200	1.10
0.3	300	1.24
0.4	400	1.33
0.5	500	1.40

and since the flux Φ is given by

$$\Phi = BA,$$

where $A = 4 \times 10^{-4} \text{ m}^2$ we arrive at the following values

i (A)	B (T)	Φ ($\times 10^{-3}$ Wb)
0.1	0.52	0.208
0.2	1.10	0.440
0.3	1.24	0.496
0.4	1.33	0.532
0.5	1.40	0.560

Example 4.3 Calculation of atomic magnetic moment.

1 m³ of iron at saturation will have a magnetic moment of $1.7 \times 10^6 \text{ A m}^2$. This 1 m³ will have a mass of 7970 kg and therefore will contain N atoms

$$N = \frac{7970 \times 6.025 \times 10^{26}}{56}$$

$$= 8.58 \times 10^{28} \text{ atoms.}$$

Therefore the magnetic moment per atom is m_A given by

$$m_A = \frac{(1.7 \times 10^6)}{(8.58 \times 10^{28})} \text{ A m}^2$$

$$= 1.98 \times 10^{-23} \text{ A m}^2$$

$$= 2.49 \times 10^{-29} \text{ J A/m}$$

$$= 2.14 \mu_B.$$

Example 5.1 Determination of Rayleigh coefficients at low fields. Use the Rayleigh equation to determine the coefficients from the first two data points

$$B = \mu H + v H^2.$$

At $H = 5 \text{ A/m}$, $B = 0.0019$ tesla

$$0.0019 = 5\mu + 25v.$$

At $H = 10 \text{ A/m}$, $B = 0.0042$ tesla

$$0.0042 = 10\mu + 100v.$$

From these two equations we find $\mu = 3.4 \times 10^{-4} \text{ H m}^{-1}$ and $v = 8 \times 10^{-6} \text{ H A}^{-1}$. Substituting these into the equation and using the data points from the table it is apparent that the Rayleigh region does not extend to 40 A/m, but that the Rayleigh approximation is valid at 20 A/m.

The remanence B_R in the Rayleigh region is given by

$$B_R = \frac{1}{2}v H_m^2$$

therefore at $H_m = 10 \text{ A/m}$

$$B_R = 0.0004 \text{ T}$$

and at $H_m = 20 \text{ A/m}$

$$B_R = 0.0016 \text{ tesla.}$$

The hysteresis loss in the Rayleigh region is given by

$$W_H = \frac{4}{3}v H_m^2.$$

So at $H_m = 20 \text{ A/m}$

$$W_H = 85.3 \times 10^{-3} \text{ J m}^{-3}.$$

Example 5.2 Magnetostriiction of terfenol without stress. Since the specimen of terfenol does not have a preferred orientation and is not subject to stress we can use the equation for the averaged magnetostriiction of a randomly oriented polycrystal

$$\lambda_s = (2/5)\lambda_{100} + (3/5)\lambda_{111}.$$

Consequently for the values given for this particular piece of terfenol

$$\begin{aligned}\lambda_s &= 36 \times 10^{-6} + 960 \times 10^{-6} \\ &= 996 \times 10^{-6}.\end{aligned}$$

Now considering the observed magnetostriiction when the field is changed from perpendicular to parallel to a given direction,

$$\begin{aligned}\lambda_{s\parallel} - \lambda_{s\perp} &= \lambda_s + \frac{1}{2}\lambda_s = \frac{3}{2}\lambda_s \\ &= 1494 \times 10^{-6}.\end{aligned}$$

Example 5.3 Magnetostriiction of terfenol under compressive load. In this case the uniaxial compressive stress causes all domain magnetic moments to align perpendicular to the stress axis and hence to the field axis.

The magnetization will take place entirely by rotation and hence

$$\mathbf{M} = M_s \cos \theta$$

and therefore

$$\begin{aligned}\lambda &= \frac{3}{2}\lambda_s \cos^2 \theta \\ \lambda(\mathbf{M}) &= \frac{3}{2}\lambda_s (\mathbf{M}/M_s)^2 \\ &= (1494 \times 10^{-6})(\mathbf{M}/M_s)^2.\end{aligned}$$

Consequently, when $\mathbf{M} = M_s/2$

$$\lambda = 373.5 \times 10^{-6}$$

and when $\mathbf{M} = \mathbf{M}_s$

$$\lambda = 1494 \times 10^{-6}.$$

Example 6.3 Effects of anisotropy on rotation of magnetization. If the anisotropy is such that the (100) directions are the magnetically easy axes, then the anisotropy constant K will be positive. The anisotropy energy E_a can then be written

$$E_a = \frac{1}{4}K_1 \sin^2 2\phi$$

where ϕ is the angle of the magnetization away from the nearest $\langle 100 \rangle$ direction.

The field energy is E_H

$$\begin{aligned} E_H &= -\mu_0 \mathbf{M}_0 \mathbf{H} \cos \theta \\ &= -\mu_0 \mathbf{M}_s \mathbf{H} \cos \theta, \end{aligned}$$

where θ is the direction of the magnetization in any given domain away from the (110) direction of the field.

Clearly as θ becomes larger the anisotropy energy increases while the field energy decreases.

After all domain-wall processes have been completed the magnetization in any domain will lie along the (010) and (100) directions closest to the field direction (110). Under these conditions we must have,

$$\theta = \pi/4 - \phi$$

and

$$\begin{aligned} E_{\text{tot}} &= E_a + E_H \\ &= \left(\frac{K_1}{4} \right) \sin^2 2\phi - \mu_0 \mathbf{M}_s \mathbf{H} \sin \left(\frac{\pi}{4} - \phi \right). \end{aligned}$$

The magnetization will take up a direction such that $dE_{\text{tot}}/d\phi = 0$

$$\begin{aligned} \frac{dE_{\text{tot}}}{d\phi} &= K_1 \sin 2\phi \cos 2\phi - \mu_0 \mathbf{M}_s \mathbf{H} \cos \left(\frac{\pi}{4} - \phi \right) \\ &= 0. \end{aligned}$$

The component of magnetization in the field direction is of course

$$\mathbf{M} = \mathbf{M}_s \cos \left(\frac{\pi}{4} - \phi \right)$$

Consequently, we arrive at the following relation between magnetization \mathbf{M} and field \mathbf{H}

$$\mathbf{H} = \left(\frac{K_1}{\mu_0 \mathbf{M}_s} \right) \left[\frac{\sin 2\phi \cos 2\phi}{\sin \left(\frac{\pi}{4} - \phi \right)} \right]$$

$$= \left(\frac{K_1}{\mu_0 M_s} \right) \left(\frac{\mathbf{M}}{M_s} \right) \sin 2\phi \left[\frac{2 \cos 2\phi}{\sin \left(\frac{\pi}{2} - 2\phi \right)} \right]$$

and since $\cos 2\phi = \sin(\pi/2 - 2\phi)$

$$\mathbf{H} = \left(\frac{K_1}{\mu_0 M_s} \right) \left(\frac{\mathbf{M}}{M_s} \right) 2 \sin 2\phi$$

$$\sin 2\phi = 2(M/M_s)^2 - 1 = 2\cos^2(\pi/4 - \phi) - 1$$

$$\mathbf{H} = \left(\frac{4K_1}{\mu_0 M_s} \right) \left(\frac{\mathbf{M}}{M_s} \right) \left[\left(\frac{\mathbf{M}}{M_s} \right)^2 - \frac{1}{2} \right].$$

The field needed to saturate the magnetization under these conditions is therefore

$$\mathbf{H} = \frac{2K_1}{\mu_0 M_s}.$$

Example 6.4 Critical fields as determined by anisotropy.

The anisotropy energy in the case of uniaxial materials like cobalt is given by

$$E_a = K_{u1} \sin^2 \theta$$

while the field energy is

$$E_H = -\mu_0 M_s \mathbf{H} \cos \phi,$$

where ϕ is the direction of moments from the field direction. Given the situation we have chosen $\theta + \phi = \pi/2$ and therefore

$$\begin{aligned} E_{tot} &= K_{u1} \sin^2 \theta - \mu_0 M_s \mathbf{H} \cos \phi \\ &= K_{u1} \sin^2 \theta - \mu_0 M_s \mathbf{H} \sin \theta. \end{aligned}$$

The moments will reach equilibrium when $dE_{tot}/d\theta = 0$ so that

$$\frac{dE_{tot}}{d\theta} = 2K_{u1} \sin \theta \cos \theta - \mu_0 M_s \mathbf{H} \cos \theta = 0$$

$$0 = (2K_{u1} \sin \theta - \mu_0 M_s \mathbf{H}) \cos \theta$$

so either $\cos \theta = 0$, meaning $\theta = \pi/2$, or

$$2K_{u1} \sin \theta = \mu_0 M_s \mathbf{H}$$

and hence

$$\mathbf{H} = \left(\frac{2K_{u1}}{\mu_0 M_s} \right) \sin \theta.$$

So when $\theta = \pi/2$, meaning the magnetization is deflected into the base plane

$$\mathbf{H} = \frac{2K_{u1}}{\mu_0 M_s} = 4.58 \times 10^5 \text{ A/m},$$

and when $\theta = \pi/4$, meaning the moments are at 45° to the unique axis, we have

$$\mathbf{H} = \frac{K_{u1}\sqrt{2}}{\mu_0 M_s} = 3.24 \times 10^5 \text{ A/m}.$$

Example 6.5 Stress-induced anisotropy.

The stress anisotropy E_σ generated by a stress σ will be

$$E_\sigma = -\frac{3}{2}\lambda_s \sigma \cos^2 \phi,$$

where ϕ is the angle between the magnetization vector and the stress direction.

The anisotropy energy E_a is given by

$$E_a = K_1(\cos^2 \theta_1 \cos^2 \theta_2 + \cos^2 \theta_2 \cos^2 \theta_3 + \cos^2 \theta_3 \cos^2 \theta_1),$$

where the θ_i are the angles that the magnetization vector makes relative to the crystal axes. We note that the anisotropy energies along certain axes are

$$\begin{aligned} E_{a(111)} &= \frac{1}{3}K_1 \\ E_{a(110)} &= \frac{1}{4}K_1 \\ E_{a(100)} &= 0, \end{aligned}$$

and remember, K_1 is negative.

In order to rotate all the magnetization vectors into the plane perpendicular to the stress axis, consider the case which requires the most energy. This will be when the magnetization begins along an easy axis aligned coaxially with the stress.

To rotate this magnetization vector we must simply find the path of rotation, between the easy axis along the stress direction and an easy axis perpendicular to this axis, which has the smallest maximum anisotropy energy.

Clearly this energy maximum can not be any larger than $K_1/3$ which is the anisotropy energy along the hard axis. In fact if the rotation of magnetization is restricted to one of the (100) planes the maximum anisotropy energy experienced will be $\frac{1}{4}K_1$

$$E_{a\max} = \frac{1}{4}K_1$$

and we can write the anisotropy in this plane as a function of the angle θ from the (100) axes or the angle ϕ from the stress axis which is coincident with the (111) axis in this case

$$\begin{aligned} E_a &= \frac{1}{4}K_1(\sin^2 \theta - 1) \\ &= \frac{1}{4}K_1[\sin^2(\pi/2 - \phi) - 1] \\ &= \frac{1}{4}K_1(\cos^2 \phi - 1), \end{aligned}$$

where the additional constant term $K_1/4$ has been included for convenience only to ensure that the anisotropy along the (111) direction is zero. The moments must be rotated to overcome the maximum anisotropy in this plane of rotation. Therefore the stress anisotropy at the angle ϕ corresponding to $E_{\text{a max}}$ must equal $K_1/4$

$$E_\sigma(\phi) = E_{\text{a max}} \\ - \frac{3}{2} \lambda_s \sigma \cos^2 \left(\frac{\pi}{4} \right) \geq - \frac{1}{4} K_1$$

or

$$\sigma \leq \frac{K_1}{3 \lambda_s}$$

remembering that this is a compressive stress, and hence σ is negative.

Now substituting in the values of the saturation magnetostriction and the anisotropy constant

$$\sigma = \frac{-(2 \times 10^4)}{(3)(1067 \times 10^{-6})} \\ = -6.25 \times 10^6 \text{ Pa.}$$

So σ must be compressive with magnitude greater than 6.25 MPa, which is equivalent to 899 p.s.i.

Example 7.3 Critical dimensions for single-domain particles in nickel.

The magnetostatic energy per unit volume is E_{ms}/V

$$E_{\text{ms}}/V = \int \mu_0 \mathbf{H}_d dM$$

and for a sphere magnetized to saturation

$$\mathbf{H}_d = \frac{1}{3} \mathbf{M}_s$$

Therefore

$$E_{\text{ms}}/V = \frac{\mu_0 M_s^2}{6}$$

and $V = 4\pi r^3/3$, therefore

$$E_{\text{ms}} = \frac{2\pi \mu_0 M_s^2 r^3}{9}$$

The reduction of magnetostatic energy caused by dividing the particle into two domains is

$$\Delta E_{\text{ms}} = \frac{\pi \mu_0 M_s^2 r^3}{9}.$$

A Bloch wall through the centre of the particle will have an area of πr^2 , so the wall energy will be,

$$E_{\text{wall}} = \gamma \pi r^2,$$

where γ is the wall energy per unit area. The energy reduction caused by the splitting of such a particle into two domains will be

$$\Delta E = \gamma \pi r^2 - \frac{\pi \mu_0 M_s^2 r^3}{9}.$$

We therefore need to find the critical condition under which we just fail to save energy by dividing into two domains. Let r_c be the critical radius under this condition

$$\Delta E = \gamma \pi r_c^2 - \frac{\pi \mu_0 M_s^2 r_c^3}{9} = 0$$

$$r_c = \frac{9\gamma}{\mu_0 M_s^2}$$

$$= 1.92 \times 10^{-8} \text{ m.}$$

Example 7.4 Calculation of wall energy and thickness from anisotropy energy, saturation magnetization and exchange energy.

The material is barium ferrite. Following the equations given in the text we know that

$$\gamma = \frac{\mu_0 J m^2 \pi^2}{al} + Kl$$

$$= \frac{JS^2 \pi^2}{al} + Kl.$$

At equilibrium we must have $d\gamma/dl = 0$, and consequently,

$$l = \left(\frac{JS^2 \pi^2}{Ka} \right)^{1/2}$$

$$= 86.5 \times 10^{-10} \text{ m.}$$

The wall energy is

$$\gamma = \frac{JS^2 \pi^2}{al} + Kl$$

$$= 5.69 \times 10^{-3} \text{ J/m}^2.$$

The critical radius for a spherical single-domain particle is then

$$\begin{aligned} r_c &= \frac{9\gamma}{2\mu_0 M_s^2} \\ &= 14.1 \times 10^{-8} \text{ m.} \end{aligned}$$

Example 7.5 Estimation of domain spacing in cobalt.

The magnetostatic energy per unit area of the surface is given as

$$E_{\text{ms}} = 1.7 \times 10^{-7} M_s^2 d.$$

Suppose the other dimensions of the sample are x and y metres respectively, the total magnetostatic energy will be

$$E_{\text{ms}} = 1.7 \times 10^{-7} M_s^2 x y d$$

The total number of walls N in a cuboid of sides x , y and d with domains perpendicular to the xy plane and lying in the ly plane, is given by

$$N = \frac{x}{d}.$$

Total wall energy is then

$$\begin{aligned} E_{\text{wall}} &= N l y \gamma \\ &= \frac{l \gamma x y}{d}. \end{aligned}$$

The total energy is the sum of wall energy and magnetostatic energy

$$\begin{aligned} E_{\text{tot}} &= (1.7 \times 10^{-7} M_s^2 d + l \gamma / d) x y \\ \frac{dE_{\text{tot}}}{dd} &= [1.7 \times 10^{-7} M_s^2 - l \gamma / d^2] x y. \end{aligned}$$

At equilibrium

$$\frac{dE_{\text{tot}}}{dd} = 0$$

and so

$$1.7 \times 10^{-7} M_s^2 - l \gamma / d^2 = 0$$

The equilibrium spacing of the domains therefore does not depend on x and y , and is given by,

$$\begin{aligned} d &= \left[\frac{l \gamma}{1.7 \times 10^{-7} M_s^2} \right]^{1/2} \\ &= 1.49 \times 10^{-4} (l)^{1/2}. \end{aligned}$$

And if $l = 1 \text{ cm}, (0.01 \text{ m})$ then

$$d = 1.49 \times 10^{-5} \text{ m.}$$

Example 8.2 Magnetostatic energy associated with a void.

The magnetostatic energy per unit volume is given by

$$E_{\text{ms}} = -\mu_0 \int \mathbf{H} d\mathbf{M}.$$

In this case we have the demagnetizing field for a sphere, $\mathbf{H}_d = -(1/3) \mathbf{M}$

$$\begin{aligned} E_{\text{ms}} &= \left(\frac{2\pi}{9} \right) \mu_0 M_s^2 r^3. \\ &= \frac{\mu_0 M_s^2}{6}. \end{aligned}$$

The volume of the sphere is $(4/3)\pi r^3$, so the magnetostatic energy is

$$E_{\text{ms}} = \left(\frac{2\pi}{9} \right) \mu_0 M_s^2 r^3.$$

We assume that the reduction in magnetostatic energy caused when a domain wall intersects the void is $\Delta E_{\text{ms}} = (\pi/9) \mu_0 M_s^2 r^3$.

For iron with a spherical void of $r = 5 \times 10^{-8} \text{ m}$

$$\begin{aligned} \Delta E_{\text{ms}} &= \left(\frac{\pi}{9} \right) \mu_0 M_s^2 r^3 \\ &= 15.87 \times 10^{-17} \text{ joules.} \end{aligned}$$

The reduction in wall area is πr^2

$$\Delta A = 7.8 \times 10^{-15} \text{ m}^2$$

and hence the reduction in wall energy is

$$\Delta E_{\text{wall}} = (7.8 \times 10^{-15}) \gamma$$

where γ is the wall energy per unit area

$$\Delta E_{\text{wall}} = 1.57 \times 10^{-17} \text{ joules.}$$

For a spherical void of radius 10^{-6} m

$$\begin{aligned} \Delta E_{\text{ms}} &= \left(\frac{\pi}{9} \right) \mu_0 M_s^2 r^3 \\ &= 1.27 \times 10^{-12} \text{ joules.} \end{aligned}$$

The reduction in wall area is

$$\begin{aligned}\Delta A &= \pi r^2 \\ &= 3.14 \times 10^{-12} \text{ m}^2.\end{aligned}$$

The reduction in wall energy is

$$\begin{aligned}\Delta E_{\text{wall}} &= (2 \times 10^{-3})(3.12 \times 10^{-12}) \text{ m}^2 \\ &= 6.28 \times 10^{-15} \text{ joules.}\end{aligned}$$

In both cases the reduction in magnetostatic energy is more significant.

Example 8.3 Reduction of domain wall energy by voids.

Let ΔE_{ms} be the reduction in magnetostatic energy when a domain wall intersects a void of radius r .

$$\Delta E_{\text{ms}} = \left(\frac{\pi}{9}\right) \mu_0 M_s^2 r^3.$$

If there are N such voids and the separation between the planar walls is d then each domain wall will intersect n_w voids

$$n_w = N^{2/3}$$

and since the wall separation is d , there will be $1/d$ walls per unit volume. Therefore the total number of voids intersected by domain walls throughout the volume will be n

$$n = \frac{N^{2/3}}{d}.$$

The total decrease in magnetostatic energy is therefore

$$\Delta E_{\text{ms}} = \left(\frac{\pi}{9}\right) \mu_0 M_s^2 r^3 \left(\frac{N^{2/3}}{d}\right).$$

The total energy associated with domain walls in this unit volume is

$$\Delta E_{\text{wall}} = \frac{\gamma}{d}.$$

If the total reduction in magnetoelastic energy due to the voids is equal to the increase in wall energy, we must have,

$$\begin{aligned}\Delta E_{\text{ms}} &= \Delta E_{\text{wall}} \\ \left(\frac{\pi}{9}\right) \mu_0 M_s^2 r^3 \frac{N^{2/3}}{d} &= \frac{\gamma}{d} \\ N^{2/3} &= \frac{9\gamma}{(\pi\mu_0 M_s^2 r^3)}\end{aligned}$$

which gives

$$N = 1.98 \times 10^9 \text{ m}^{-3}.$$

Example 8.4 Effect of stress on anhysteretic susceptibility.

If a 180° wall is moved through a distance dx the change in field energy will be

$$dE_H = -2\mu_0 M_s H dx.$$

The change in magnetoelastic energy will be

$$dE_{me} = \frac{3}{2}\lambda_s d\sigma = 3\lambda_s a x dx.$$

At equilibrium we must have $dE_{\text{Tot}}/dx = 0$

$$\begin{aligned} \frac{dE_{\text{tot}}}{dx} &= \frac{dE_H}{dx} + \frac{dE_{me}}{dx} = 0 \\ &= -2\mu_0 M_s H + 3\lambda_s a x. \end{aligned}$$

Consequently

$$x = \frac{2\mu_0 M_s H}{3\lambda_s a}.$$

The magnetization will be

$$\mathbf{M} = 2AM_s x$$

where A is the wall area

$$\mathbf{M} = \frac{4A\mu_0 M_s^2 H}{3\lambda_s a}$$

and the initial susceptibility will therefore be

$$\frac{d\mathbf{M}}{dH} = \frac{4A\mu_0 M_s^2}{3\lambda_s a}.$$

In determining the anhysteretic we will use the Frohlich–Kennelly equation modified for the inclusion of the effects of stress. The original unstressed anhysteretic magnetization can be modelled using the equation

$$\mathbf{M}_{an} = \frac{\alpha H}{1 + \beta H}.$$

Since we know that $M_s = 0.9 \times 10^6 = \alpha/\beta$, and that the limit as H tends to zero of $dM_{an}/dH = 1000$ is equal to α , we can determine the two coefficients α, β

$$\alpha = 1000$$

$$\beta = 1.1 \times 10^{-3}.$$

Now turning to the anhysteretic magnetization under stress we replace H by

the effective field, giving

$$\mathbf{M}_{\text{an}} = \frac{\alpha \left[\mathbf{H} + \frac{3}{2}\sigma \frac{d\lambda}{d\mathbf{M}} \right]}{\left\{ 1 + \beta \left[\mathbf{H} + \frac{3}{2}\sigma \frac{d\lambda}{d\mathbf{M}} \right] \right\}}$$

If we make the approximation $\lambda = b\mathbf{M}^2$, then

$$\frac{d\lambda}{d\mathbf{M}} = 2b\mathbf{M}$$

$$\mathbf{M}_{\text{an}} = \frac{\alpha(\mathbf{H} + 3b\sigma\mathbf{M}_{\text{an}})}{\left[1 + \beta(\mathbf{H} + 3b\sigma\mathbf{M}_{\text{an}}) \right]}$$

$$\frac{d\mathbf{M}_{\text{an}}}{d\mathbf{H}} = \frac{\alpha - \beta\mathbf{M}_{\text{an}}}{\left[1 + \beta\mathbf{H} - 3\alpha b\sigma + 6\beta b\sigma\mathbf{M}_{\text{an}} \right]},$$

so that in the limit as \mathbf{H} approaches zero and \mathbf{M}_{an} approaches zero

$$\frac{d\mathbf{M}_{\text{an}}}{d\mathbf{H}} = \frac{\alpha}{1 - 3\alpha b\sigma}.$$

When $\sigma = 0$,

$$\frac{d\mathbf{M}_{\text{an}}}{d\mathbf{H}} = \chi_{\text{an}}(0) = 1000.$$

When $\sigma = -20 \text{ MPa}$

$$\frac{d\mathbf{M}_{\text{an}}}{d\mathbf{H}} = \frac{1000}{1 + 0.108}$$

$$\chi_{\text{an}}(\sigma) = 902.$$

Therefore the compressive stress reduces the susceptibility along the direction of the stress of a ferromagnet with positive magnetostriction coefficient provided $d\lambda/d\mathbf{M}$ is positive.

Example 9.1 Paramagnetic susceptibility of oxygen.

Since the substance is a gas we can assume no interactions between the electrons and neighbouring atoms, and hence no exchange interaction. According to the classical Langevin theory of paramagnetism the magnetization \mathbf{M} is given by

$$\mathbf{M} = N\mathbf{m} \left[\coth \left(\frac{\mu_0 \mathbf{mH}}{k_B T} \right) - \frac{k_B T}{\mu_0 \mathbf{mH}} \right].$$

At 0 °C or 273 K we know that for the realistic values of \mathbf{H}

$$\mu_0 \mathbf{m} \mathbf{H} \ll k_B T$$

and hence that

$$\mathbf{M} = \frac{N\mu_0 \mathbf{m}^2 \mathbf{H}}{3k_B T}.$$

Consequently

$$\begin{aligned}\chi &= \frac{N\mu_0 \mathbf{m}^2}{3k_B T} \\ \chi &= \frac{(4\pi \times 10^{-7})(2.69 \times 10^{25})(2.78 \times 10^{-23})^2}{(3)(273)(1.38 \times 10^{-23})} \\ &= 2.31 \times 10^{-6} \text{ (dimensionless).}\end{aligned}$$

Example 9.2 Magnetic mean interaction field for iron.

In the Curie–Weiss law we have

$$\begin{aligned}\chi &= \frac{\mathbf{M}}{\mathbf{H} + \alpha \mathbf{M}} \\ &= \frac{C}{T - T_c} \\ T_c &= \alpha C\end{aligned}$$

and using the Langevin equation the Curie constant is given by

$$\begin{aligned}C &= \frac{N\mu_0 \mathbf{m}^2}{3k_B} \\ T_c &= \frac{\alpha N\mu_0 \mathbf{m}^2}{3k_B}.\end{aligned}$$

So the value of α is given by

$$\begin{aligned}\alpha &= \frac{3k_B T_c}{N\mu_0 \mathbf{m}^2} \\ \alpha &= \frac{(3)(1.38 \times 10^{-23})(1043)}{(8.57 \times 10^{28})(4\pi \times 10^{-7})(2.2)^2(9.27 \times 10^{-23})^2} \\ \alpha &= 964\end{aligned}$$

and since $\mathbf{H}_e = \alpha \mathbf{M}_s$

$$\mathbf{H}_e = 1.64 \times 10^9 \text{ A/m.}$$

Example 9.3 Critical behaviour of spontaneous magnetization.

The classical Weiss-type ferromagnet for a system with two possible microstates leads to the following expression for magnetization.

$$\mathbf{M} = \mathbf{M}_0 \tanh\left(\frac{\mu_0 m \alpha \mathbf{M}_s}{k_B T}\right).$$

Close to the Curie point $T \simeq T_c$, and so

$$\frac{\mu_0 m \alpha \mathbf{M}_s}{k_B T} \ll 1.$$

The series expansion for $\tanh(x)$ is

$$\tanh(x) = x - \frac{x^3}{3} + \dots$$

Therefore using the first few terms of this series as the value of $\tanh(x)$ when x is small

$$\mathbf{M}_s = N \mathbf{m} \left[\frac{\mu_0 m \alpha \mathbf{M}_s}{k_B T} - \frac{1}{3} \left(\frac{\mu_0 m \alpha \mathbf{M}_s}{k_B T} \right)^3 \right].$$

For the $\tanh(x)$ expression the Curie temperature is given by

$$T_c = \frac{N \mu_0 m^2 \alpha}{k_B}.$$

Substituting these values into the above equation leads to,

$$\mathbf{M}_s = \left(\frac{T_c}{T} \right) \mathbf{M}_s - \left(\frac{T_c}{3T} \right) \left(\frac{\mu_0 m \alpha}{k_B T} \right)^2 \mathbf{M}_s^3.$$

Therefore

$$1 = \left(\frac{T_c}{T} \right) - \left(\frac{T_c}{3T} \right) \mathbf{M}_s^2 \left(\frac{\mu_0 m \alpha}{k_B T} \right)^2$$

$$T = T_c - \left(\frac{T_c}{3} \right) \mathbf{M}_s^2 \left(\frac{\mu_0 m \alpha}{k_B T} \right)^2$$

$$\mathbf{M}_s^2 = \frac{3(T_c - T)}{T_c} \left(\frac{k_B T}{\mu_0 m \alpha} \right)^2$$

$$\mathbf{M}_s = \left(\frac{k_B T}{\mu_0 m \alpha} \right) \frac{\sqrt{3} \cdot \sqrt{(T_c - T)}}{\sqrt{T_c}}$$

Example 10.4 Orbital and spin angular momentum of an electron. (a) The principal

quantum number n determines the shell of the electron, and hence its energy. Its allowed values are $n = 1, 2, 3, \dots$

The orbital angular momentum l defines the orbital angular momentum p_0 of the electron when multiplied by $(\hbar/2\pi)$. It can have values of $l = 0, 1, 2, 3, \dots, (n - 1)$, where n is the principal quantum number.

The magnetic quantum number m_l gives the component of the orbital angular momentum l along the z -axis when a magnetic field is applied along that axis. Its values are restricted to $m_l = -l, \dots, -2, -1, 0, 1, 2, \dots, +l$.

The spin quantum number s defines the spin angular momentum of an electron. The value of the spin quantum number is always $1/2$ for an electron. The angular momentum due to spin $sh/2\pi$ is therefore always an integer multiple of $\hbar/4\pi$. The component or resultant of s in a magnetic field is represented by m_s and is restricted to $m_s = \pm 1/2$.

The various angular momenta of an electron can be calculated from the two quantum numbers l and s

$$p_0 = l(\hbar/2\pi)$$

$$p_s = s(\hbar/2\pi).$$

The total angular momentum j can then be calculated from the vector sum of l and s , remembering that for a single electron the magnitude of j must be half integral.

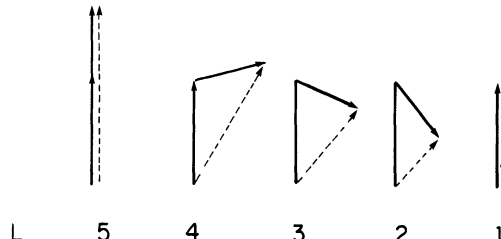
$$p_j = j(\hbar/2\pi).$$

The values of l, s and j differ from the classically expected values in practice and this can be explained by quantum mechanics. The solution of the Schroedinger equation in the simple case of a single electron orbiting a nucleus only permits solution (states) for which the angular momentum is $\langle \vec{l} \rangle = \sqrt{[l(l+1)]}$. A similar argument holds for s and hence j .

(b) The allowed solutions for the resultant orbital angular momentum L of the vector sum of two orbital angular momentum vectors of length 2 and 3 are

$$L = 5, 4, 3, 2, 1$$

The vector diagrams are shown in the accompanying figure.



(c) The Co^{2+} ion in a $3d^7$ state has its electrons in the following state, $l = 2$ for $3d$

electrons

m_l	2	1	0	-1	-2	2	1	0	1	2
m_s	$\frac{1}{2}$	$\frac{1}{2}$	$\frac{1}{2}$	$\frac{1}{2}$	$\frac{1}{2}$	$-\frac{1}{2}$	$-\frac{1}{2}$			
occupancy	s	\uparrow	\uparrow	\uparrow	\uparrow	\uparrow	\downarrow	\downarrow	\downarrow	

So by summing the spins $S = \sum m_s = \frac{3}{2}$ and summing the components of orbital angular momentum $L = \sum m_l = 3$. The shell is more than half full so $J = |L + S| = 9/2$.

Example 10.5 The Zeeman effect. The cadmium singlet observed at $\lambda = 643.8$ nm is a result of an electronic transition from 6^1D_2 ($L = 2, S = 0$) to 5^1P_1 ($L = 1, S = 0$). On application of a magnetic field this will exhibit the normal Zeeman effect since the net spin of the state is zero.

The shift in energy upon application of a magnetic field \mathbf{H} is

$$\begin{aligned}\Delta E &= \left(\frac{e\hbar}{4\pi m_e} \right) \mu_0 \mathbf{H} \\ &= \mu_B \mu_0 \mathbf{H} \\ &= 5.8 \times 10^{-5} \text{ eV/T} \\ &= 0.9273 \times 10^{-23} \text{ J/T} \\ &= 1.165 \times 10^{-29} \text{ J(A/m)}^{-1}\end{aligned}$$

The equation for the energy shift with field is

$$\begin{aligned}\Delta E &= 1.165 \times 10^{-29} \mathbf{H} \cdot \mathbf{J} \\ &= 0.9273 \times 10^{-23} \mu_0 \mathbf{H} \cdot \mathbf{J}.\end{aligned}$$

When $\mu_0 \mathbf{H} = 0.5$ T, this gives

$$\Delta E = 0.464 \times 10^{-23} \text{ J.}$$

When $\mu_0 \mathbf{H} = 1.0$ T

$$\Delta E = 0.927 \times 10^{-23} \text{ J.}$$

When $\mu_0 \mathbf{H} = 2.0$ T

$$\Delta E = 1.85 \times 10^{-23} \text{ J.}$$

The shift in frequency can be calculated from the relation

$$\Delta E = h(v - v_0)$$

$$\Delta v = \frac{\Delta E}{h}$$

$$\begin{aligned}
 &= \frac{(0.9273 \times 10^{-23})}{(6.626 \times 10^{-34})} \text{s}^{-1} \text{T}^{-1} \\
 &= 1.399 \times 10^{10} \text{s}^{-1} \text{T}^{-1}
 \end{aligned}$$

and using the relation

$$\lambda v = c,$$

where c is the speed of light

$$\begin{aligned}
 \frac{\Delta v}{\Delta \lambda} &= -\frac{c}{\lambda^2} \\
 \Delta \lambda &= -\frac{\lambda^2}{c} \Delta v.
 \end{aligned}$$

Substituting in the values for the shift in frequency at an induction of 1 T

$$\begin{aligned}
 \Delta \lambda &= -\frac{(643.8 \times 10^{-9})^2 (1.399 \times 10^{10})}{2.98 \times 10^8} \\
 &= -1.946 \times 10^{-11} \text{ m.}
 \end{aligned}$$

At 1 T

$$\Delta \lambda = -0.01946 \text{ nm.}$$

At 0.5 T

$$\Delta \lambda = -0.009730 \text{ nm.}$$

At 2.0 T

$$\Delta \lambda = -0.03892 \text{ nm.}$$

Example 10.6 Determination of atomic angular momentum. The values of J can be obtained by vector addition of L and S , remembering that if S is an integer then J is an integer and if S is half integer then J is half integer.

- (a) $L = 2, S = 3$. Possible values of J are 5, 4, 3, 2, 1.
- (b) $L = 3, S = 2$. Possible values of J are 5, 4, 3, 2, 1.
- (c) $L = 3, S = 5/2$. Possible values of J span the range from $|L + S|$ to $|L - S|$, that is 11/2, 9/2, 7/2, 5/2, 3/2, 1/2.
- (d) $L = 2, S = 5/2$. Possible values of J are 9/2, 7/2, 5/2, 3/2, 1/2.

The ground state of the carbon atom can be determined from Hund's rules. Carbon has four electrons in the $n = 2$ shell. The s subshell is full with two electrons, the p subshell, which has $l = 1$ has two electrons. The occupancy of available states must be such as to maximize S by Hund's rules.

m_l	1	0	-1	1	0	-1
m_s	$\frac{1}{2}$	$\frac{1}{2}$	$\frac{1}{2}$	$-\frac{1}{2}$	$-\frac{1}{2}$	$-\frac{1}{2}$
occupancy	s	↑	↑			

Therefore $S = \sum m_s = 1$ and $L = \sum m_l = 1$ and since the subshell is less than half full $J = |L - S|$

$$J = 0.$$

Example 11.1 The exchange interaction. The exchange interaction J arises from the determination of the total energy of a two electron system in which the electrons can never have the same set of quantum numbers by virtue of the Pauli exclusion principle. (This means that the two electron wavefunction must be antisymmetric).

Under these circumstances there arises an energy term which results from the electrons ‘exchanging’ places. Classically this would not alter the energy of the system (since the particles could occupy the same states in classical physics) but in quantum mechanics the situation is different and the electrons therefore have an additional energy which acts in many respects like a strong magnetic field.

Example 11.2 Magnetic moment of dysprosium ions. The dysprosium ion Dy^{3+} has 9 electrons in its 4f shell. For this shell $n = 4$ and $l = 3$ so the electron distribution is

m_{el}	3	2	1	0	-1	-2	-3	3	2	1	0	-1	-2	-3
s	↑	↑	↑	↑	↑	↑	↑	↓	↓					
m_s	$\frac{1}{2}$	$-\frac{1}{2}$	$-\frac{1}{2}$											

Summing these leads to $S = \sum m_s = 5/2$ and $L = \sum m_l = 5$. Since the shell is more than half full $J = |L + S| = 15/2$. To calculate the susceptibility of a salt containing 1 g mole of Dy^{3+} at 4 K first calculate the magnetic moment per ion

$$\begin{aligned} m &= -g\mu_B J \\ &= -g\mu_B \sqrt{[J(J+1)]} \\ g &= 1 + \frac{J(J+1) + S(S+1) - L(L+1)}{2J(J+1)} \end{aligned}$$

and in this case, when the values of L , S and J are substituted in we obtain $g = 4/3$.

$$\begin{aligned} m &= -\frac{4}{3}(9.27 \times 10^{-24}) \sqrt{\frac{255}{4}} \\ &= -9.87 \times 10^{-23} \text{ A m}^2 \end{aligned}$$

and

$$\begin{aligned} \chi &= \frac{M}{H} \\ &= \frac{N\mu_0 m^2}{3k_B T} \end{aligned}$$

$$\begin{aligned}
&= \frac{(6.02 \times 10^{23})(4\pi \times 10^{-7})(9.87 \times 10^{-23})^2}{3(1.38 \times 10^{-23})4} \\
&= 4.45 \times 10^{-5}.
\end{aligned}$$

Example 11.3 Paramagnetism of $S = 1$ system. The magnetization can be expressed as a function of temperature and magnetic field using the Brillouin function $B_J(x)$ where the argument of the function x is $\mu_0 \mathbf{mH}/k_B T$

$$\mathbf{M} = N \mathbf{m} B_J \left(\frac{\mu_0 \mathbf{mH}}{k_B T} \right),$$

where N is the number of atoms per unit volume and \mathbf{m} is the magnetic moment per atom.

For a system with spin only we have $g = 2$ and $J = S$. In this case therefore $J = 1$. Substituting these values into the Brillouin function

$$\begin{aligned}
B_J(x) &= \left[\frac{(2J+1)}{2J} \right] \coth \left[\frac{x(2J+1)}{2J} \right] - \left(\frac{1}{2J} \right) / \coth \left(\frac{x}{2J} \right) \\
&= \frac{3}{2} \coth \left(\frac{3x}{2} \right) - \frac{1}{2} \coth \left(\frac{x}{2} \right)
\end{aligned}$$

and $\coth(x) = 1/x + x/3$ for small x . If we make this approximation then, in this case

$$B_J(x) = \frac{2x}{3}.$$

So if $\mu_0 \mathbf{mH}/k_B T \ll 1$ we can make this approximation and consequently

$$B_J \left(\frac{\mu_0 \mathbf{mH}}{k_B T} \right) = \frac{2\mu_0 \mathbf{mH}}{3k_B T}$$

and the magnetization \mathbf{M} is given by

$$\begin{aligned}
\mathbf{M} &= N \mathbf{m} B_J \left(\frac{\mu_0 \mathbf{mH}}{k_B T} \right) \\
&= \frac{N \mathbf{m} 2\mu_0 \mathbf{mH}}{3k_B T} \\
&= \frac{2N\mu_0 \mathbf{m}^2 \mathbf{H}}{3k_B T}.
\end{aligned}$$

Author Index

- Abbundi, R., 56
Abrikosov, A. A., 350
Adey, R. A., 24
Allison, S. G., 376
Altpeter, I., 368
Ampère, A.M. (1785–1836), 4, 108, 109
Argyle, B., 116
Artman, J. O., 116
Asano, T., 359
Ashburn, J. R., 348, 358
Ashtashenko, P. P., 372
Astie, B., 159, 161, 162
Atherton, D. L., 158, 165, 169, 370, 373,
 382, 388, 392

Back, E., 244
Bacon, D. J., 149
Bacon, G. E., 197, 198, 201, 202
Bader, C. J., 58–59
Bardeen, J., 356
Barkhausen, H., 97, 113, 366
Barnier, Y., 134
Barton, J. R., 385
Baruchel, J., 117, 137
Bashkirov, Y. P., 372
Bate, G., 77
Becker, J. J., 79, 309, 311, 316–317
Becker, R., 94, 96, 138, 149
Bednorz, J. G., 348, 358
Behrendt, D. R., 210
Beissner, R. E., 98, 369, 370, 385
Bernards, J. P. C., 78, 325
Bertram, H. N., 334, 342, 343
Bertraut, F., 289
Bethe, H., 253
Betz, C. E., 114, 380

Bezer, H. J., 380
Bida, G. V., 374
Biot, J. B., 2
Bitter, F., 114
Bixio, A., 310
Blackie, G. N., 212
Bloch, F., 128, 199, 211
Bly, P. H., 207
Bobrov, E. S., 310
Bohr, N. (1881–1964), 221
Boll, R., 270
Bonnebat, C., 329
Bose, M. S. C., 373
Bozorth, R. M., 96, 114, 212, 213
Bradbury, A., 344
Bradley, F. N., 309
Brebbia, C. A., 24, 25
Bridges, J. M., 387, 388
Briggs, G. A. D., 98
Brillouin, L., 256
Brown, G. V., 22
Brown, R. E., 48, 52
Brown, W. F., 31
Brudar, B., 388
Bull, S. A., 325
Burkhardt, G. L., 171, 370, 373
Buschow, K. H. J., 311
Bussiere, J. F., 373
Buttle, D. J., 98

Cable, J. W., 207, 208
Camras, M., 324, 327, 328
Carey, R., 115
Carlson, W. L., 324
Carpenter, G. W., 324
Carpenter, S. H., 370

- Carrigan, R. A., 29
 Casimir, H. B. G., 345
 Celiotta, R. J., 117
 Chandrasekar, B. S., 134
 Chang, T. T., 73, 162
 Chantrell, R. W., 344
 Chari, M. V. K., 24
 Charles, S. W., 344
 Chen, C. W., 72, 130, 134, 380
 Chen, Y. F., 275
 Chikazumi, S., 134, 140, 158, 309
 Child, H. R., 207
 Chin, G. Y., 75, 290
 Chu, C. W., 348, 358
 Clark, A. E., 56, 57
 Clark, D. L., 324
 Clark, W. G., 390
 Clegg, A. G., 319
 Cockcroft, J. D., 21
 Coleman, R. V., 119
 Comstock, R. L., 338
 Cooper, L. N., 356
 Corliss, L. M., 207
 Corner, W. D., 207
 Craik, D. J., 57
 Crangle, J., 31, 200, 342
 Cribier, D., 203, 204
 Croat, J. J., 79, 318
 Cullity, B. D., 28, 56, 132, 134, 276, 300,
 303
 Curie, P. (1859–1906), 182, 185
- Davis, M. E., 360
 de Bie, R. W., 78, 325
 De Mott, E. G., 48
 Debye, P., 84
 Decker, S. K., 114
 Deeds, W. E., 390
 DeForest, A. V., 114, 377
 Degauque, J., 159, 161, 162
 Degterev, A. P., 368
 Del Mut, G., 310
 Della Torre, E., 343
 Demerdash, N. A., 25
 Dietze, H. D., 158
 Dijkstra, L. J., 154
 Dirac, P. A. M., 29, 251, 358
 Dobmann, G., 389
- Doclo, R., 208
 Dodd, C. V., 390
 Doring, W., 94, 96, 149
 Dovnar, D. P., 372
 Drillat, A., 137
 Dunn, F. W., 380
 Duplex, P., 162, 163, 164
 Durst, K. D., 309
- Edwards, C., 370, 379, 388
 Elmen, G. W., 269
 English, A. T., 171, 291
 Enz, U., 74, 196
 Erdelyi, E. A., 24
 Ewing, J. A. (1855–1935) 70, 108, 109
- Fabry, M. P. A. (1867–1945), 21
 Faraday, M., (1791–1867) 115
 Fastnacht, R. A., 360
 Fateev, I. G., 373
 Ferrari, R. L., 24
 Fert, C., 50–51
 Flax, L., 22
 Fleischer, R. L., 29
 Foner, S., 52, 208
 Forrer, R., 191, 294
 Forret, F., 289
 Forster, F., 378, 382, 390
 Fort, D., 137
 Freeman, A. J., 252
 Freese, R. P., 331
 Fridman, L. A., 382
 Frohlich, O., 94, 247
 Fuchs, E. F., 24, 291, 292, 293
 Fujimura, S., 318, 319
 Fukutomi, M., 359
 Fuller, H. W., 116
 Fussel, R. L., 58–59
- Galt, J. K., 130
 Gao, L., 348, 358
 Garcia, N., 117
 Garikepati, P., 73
 Gautier, P., 50–51
 Gerlach, W., 236
 Gerstein, B. C., 210
 Giacolletto, L. J., 31
 Giauque, W. F., 84

- Gilbert, W. (1540–1603), 73
 Ginzburg, W. L., 350, 355
 Globus, A., 162, 163, 164
 Golovko, A. S., 374
 Gordon, D. I., 48, 52
 Gorkov, L. P., 350
 Gorter, C. J., 345
 Goudsmit, S., 234
 Graham, C. D., Jr., 31, 132, 134, 207, 301
 Green, H. S., 215
 Green, R. W., 210
 Greenough, R. D., 213
 Gregory, C. A., 379
 Griffel, M., 210
 Grigorev, P. A., 382
 Grossinger, R., 300
 Guyot, M., 164
 Haben, J. F., 48
 Hadjipanayis, G. C., 309
 Halé, M. E., 116
 Hall, R. C., 295
 Halpern, O., 200
 Hampton, P. L., 385
 Harker, J. M., 325
 Harle, M. E., 169
 Hart, H. R., 29
 Hart, P. J., 22
 Hartman, F., 60
 Hartmann, U., 116
 Hastings, C. H., 381
 Hastings, J. M., 207
 Hayakawa, K., 117
 Heck, C., 69, 81, 278
 Hegland, D. E., 210
 Heisenberg, W., 251, 267
 Heisz, S., 300
 Heitler, W., 248, 249
 Hembree, G., 117
 Henry, W. E., 258
 Herbst, J. F., 79, 318
 Herman, A. M., 359
 Herman, D., 116
 Herring, C., 254
 Hertzberg, G., 58–59, 232
 Heyman, J. S., 376
 Higgins, F. P., 370
 Hilscher, G., 300
 Hilzinger, H. R., 73, 157, 158, 159
 Hinton, E., 24
 Hiroswa, S. 318
 Hoffer, G., 111, 316–317
 Hofman, J. A., 132, 134, 210, 252
 Hoke, 114
 Holler, P., 389
 Holmes, L. C., 324
 Holmes, V. L., 379
 Honda, K., 204
 Hoole, S. R. H., 25
 Hopkins, N., 344
 Hopkins, R. A., 31
 Hor, P. H., 348, 358
 Hoselitz, K., 140, 149
 Hougen, D. R., 162
 Huang, Z. J., 348, 358
 Hubert, A., 115
 Hull, D., 149
 Hummel, R., 300
 Hund, F., 239
 Hurst, C. A., 215
 Hwang, C., 116
 Hwang, J. H., 24, 387
 Ingersoll, L. P., 115
 Irons, H. R., 58–59
 Isaac, E. E., 115
 Isci, C., 212, 213
 Isin, A., 119
 Ising, E., 110, 214
 Islam, M. N., 212
 Itozaki, H., 360
 Iwasaki, S., 329
 Jacobs, I. S., 29
 Jacrot, B., 203, 204
 Jakubovics, J. P., 98, 270
 Jeanniot, D., 325
 Jennings, L. D., 210
 Jiles, D. C., 73, 158, 162, 165, 169, 170, 171, 212, 370, 373
 Jin, S., 360
 Johnson, M. H., 200
 Jones, G. A., 115
 Josephson, B. D., 361
 Joule, J. P. (1818–89), 99

- Junker, W. R., 390
- Kadar, G., 343
- Kamerlingh Onnes, H., 345
- Kammlott, G. W., 360
- Karjalainen, L. P., 368
- Karlqvist O., 338
- Kastin, V. N., 374
- Kaverin, V. D., 372
- Kaya, A., 204
- Keith, H. D., 360
- Kennelly, A. E., 94
- Kerr, J., 115
- Kersten, M., 138, 139, 141, 149, 154, 158
- Khalileev, P. A., 382
- Kimura, H., 98, 370
- King, J. D., 370
- Kittel, C., 101, 130, 131, 134, 138, 242
- Koehler, W. C., 197, 199, 207, 208
- Koike, K., 117
- Kojima, H., 316–317
- Komura, I., 374
- Kondorsky, E., 138, 149
- Konovalov, O. S., 374
- Kronmuller, H., 72, 157, 158, 159, 309
- Kusanagi, H., 98, 370
- Kuznetsov, I. A., 372
- Kwun, H., 171, 373, 375, 376
- Labusch, R., 158
- Lamont, 96
- Landau, L. D., 118, 350, 355
- Landry, P. C., 207
- Lang, A. R., 117
- Langevin, P. (1872–1946), 110, 178, 182, 183, 258
- Langman, R., 372, 374
- Lankford, J., 385
- Larmor, J. (1857–1942), 223
- Laughlin, D. E., 116
- Layadi, A., 116
- Lean, M. H., 25
- Lee, E. W., 102, 103, 212
- Lee, R. W., 79, 318
- Legvold, S., 210
- Leslie, W. C., 171
- Libby, H. L., 390
- Lifschitz, E. M., 118
- Lilley, B. A., 131, 134
- Littmann, M. F., 274
- Lodder, J. C., 116
- Lomaev, G. V., 368
- London, F., 248, 249, 354
- London, H., 354
- Lord, A. E., 98, 370
- Lord, W., 24, 387, 388
- Lorentz, H. A. (1853–1928), 234
- Lovesey, S. W., 197, 204
- Luborsky, F. E., 76, 284, 311
- Luitjens, S. B., 78, 325
- Luthi, B., 212
- McCaig, M., 79, 309, 311, 319
- McClure, J. C., 97, 369
- McCurrie, R. A., 312
- McNiff, E. J., 208
- Maeda, M., 359
- Maekawa, S., 212
- Mallinson, J. C., 324, 327
- Malyshев, V. S., 368
- Marabotto, R., 319
- Marshall, W., 252, 253
- Martin, D. H., 247
- Martin, D. L., 311
- Martin, Y., 117
- Massa, G. M., 379
- Matsuura, Y., 318, 319
- Matsuyama, H., 117
- Matzkanin, G. A., 98, 369, 370, 385
- Maxwell, E., 356
- Mayer, L., 117
- Mayos, M., 368
- Mee, C. D., 94
- Meissner, W., 349, 352
- Meng, R. L., 348, 358
- Mikheev, M. N., 371, 374
- Miller, R. E., 210
- Mitchell, P. V., 116
- Moilanen, M., 368
- Molfino, P., 310
- Montgomery, D. B., 20
- Moran, T. J., 212
- Morozov, A. P., 371
- Morozova, V. M., 371
- Morrish, A. H., 242
- Moskowitz, L. R., 79, 300

- Mountfield, K., 116
 Muller, A., 348, 358
- Namkung, M., 376
 Neel, L., 136, 138, 141, 154, 194, 195
 Nehl, T. W., 25
 Neizvestnov, B. M., 371
 Nesbitt, E. A., 300, 316–317
 Nicklow, R. M., 196
 Nicolas, J., 289
 Nigh, H. E., 210
 Nolan, P., 379
 Novikov, V. F., 373
- O’Grady, K., 344
 Ochsenfeld, R., 349, 352
 Oehl, C. L., 380
 Oersted, H. C., (1777–1851) 1, 6
 Olson, J., 79, 316–317
 Ono, K., 98, 370
 Orowan, E., 149
 Osborne, J. A., 38
 Ostertag, W., 79, 316–317
 Ouchi, K., 329
 Owen, D. R. J., 24
 Owston, C. N., 384
- Palanisamy, S., 387, 388
 Palmer, S. B., 117, 137, 212, 213, 370,
 379, 388
 Parette, G., 203, 204
 Parker, R. J., 311, 313
 Paschen, F., (1865–1947) 244
 Paskin, A., 132, 210, 245, 252
 Patterson, C., 137
 Pauli, W., 182, 251, 262, 263
 Pauling, L., 265, 266
 Pauthenet, R., 134
 Pierce, D. T., 117
 Pinkerton, F. E., 79, 309, 318
 Pippard, A. B., 355
 Poisson, S. D., (1781–1840), 107
 Polanyi, M., 149
 Polcarova, M., 117
 Pollina, R. J., 212
 Porteseil, J. L., 159, 161, 162
 Potapova, N. A., 372
 Poulsen, V., 324
- Preis, K., 43
 Preisach, F., 165, 343
 Price, P. B., 29
 Primdahl, H., 52
 Puchalska, I., 115
 Punchard, W. F. B., 310
 Putignani, M., 368
- Raine, G. A., 379
 Ranjan, R., 162, 370
 Rastogi, P. K., 370
 Rautioaho, R., 368
 Rave, W., 115
 Rayleigh, L. (1842–1919), 95
 Read, R. E., 196
 Repetto, M., 310
 Rhyne, J. J., 208
 Richter, K. R., 43
 Rieger, H., 157
 Rimet, G., 134
 Robinson, A. N., 379
 Rodigin, N. M., 372
 Roe, W. C., 207
 Roehrs, R. J., 379
 Roitman, V. I., 374
 Rubinstein, H., 116
 Russell, H. N., 240
- Sablik, M. J., 171
 Saenz, J. J., 117
 Sagawa, M., 318, 319
 Saito, Y., 44
 Sasaki, H., 98, 370
 Sassik, H., 300
 Sato, H., 134
 Saunders, F. A., 240
 Savage, H. T., 57
 Savart, F., 3–4
 Schafer, R., 115
 Schcherbinin, V. E., 372, 385
 Schlenker, M., 117
 Schmidt, T. R., 391
 Schneider, E., 368
 Schrauwen, C. P. G., 78, 325
 Schrieffer, J. R., 356
 Schroeder, K., 97, 369
 Schwall, R. E., 363
 Schwarz, W. M., 29

- Schwee, H. R., 58–59
Scott, C., 119
Scruby, C. B., 98
Seeger, A., 157
Segalini, S., 368
Seiden, P. E., 58–59
Sells, R. L., 233
Shah, M. D., 373
Sheng, Z. Z., 359
Sherwin, C. W., 228
Sherwood, R. C., 360
Shibata, M., 98, 370
Shiozaki, M., 76
Shockley, W., 114
Shull, C. G., 199, 207
Silsbee, F. B., 352
Silvester, P. P., 24
Simkin, J., 25
Sixtus, K. J., 149
Skochdopole, R. E., 210
Slater, J. C., 253, 264, 265
Slick, P. I., 289
Smirnova, R. M., 372
Smith, D. O., 50–51
Snyder, J. E., 116
Sommerfeld, A., 222
Somova, V. M., 372
Spedding, F. H., 210
Squires, G. L., 203
Stablein, H., 316–317
Stanley, H. E., 215
Stanton, R. M., 210
Steinmetz, C., 271
Stephenson, E. T., 271
Stern, O., 236
Stevens, D. W., 171
Stoffers, R. C., 291
Stogner, H., 43
Stoner, E. C., 165, 264, 305, 344
Strandburg, D. L., 210
Strnat, K., 79, 316–317, 319
Stuart, R., 252, 253
Studders, R. J., 311, 313
Stumm, W., 384
Sullivan, S., 392
Sundstrom, O., 367
Surin, G. V., 371
Suzuki, M., 374
Swartzendruber, L. J., 380
Swisher, J. H., 291, 292, 293
Syrochkin, V. P., 372
Szpunar, B., 373
Szpunar, J. A., 373
Tachiki, M., 212
Takahashi, H., 374
Tanaka, S., 360
Tanaka, Y., 359
Tanner, B. K., 207, 373
Tauer, K. J., 132, 210, 252
Taylor, G. I., 149
Taylor, K. N. R., 207
Tebble, R. S., 57, 367
Teller, C. M., 98, 393, 376, 385
Theiner, W. A., 368, 370
Thoelke, J. B., 170
Thomson, J. J., 158
Tiefel, T. H., 360
Tiiitto, S., 367
Todokoro, H., 117
Togawa, N., 318
Tonks, L., 149
Torng, C. J., 348, 358
Torronen, K., 367
Trauble, H., 157
Trowbridge, C. W., 24
Trower, W. P., 29
Tsang, C., 114
Tsarkova, T. P., 374
Uhlenbeck, G. E., 234
Unguris, J., 117
Utrata, D., 376
Van Dover, R. B., 360
Van Vleck, J. H., 182
Van Wingerden, D. J., 309
Vergne, R., 159, 161, 162
Vicena, F., 157
Vigoureux, P., 31
Vlasov, V. V., 372
Vroman, J., 390
Wakabayashi, N., 196
Wakiyama, T., 213
Walker, S., 25

- Wang, Y. Q., 348, 358
Warburg, E., 70
Watson, R. E., 252
Webb, W., 64
Weber, W., (1804–1890) 107, 109
Weidner, R., 233
Weiss, P. (1865–1940), 94, 109, 185, 186,
191, 192, 193, 251, 252, 267, 294
Weiss, R. J., 132, 197, 207, 210, 354
Wernick, J. H., 75, 290, 300, 316–317
Wert, C., 154
Wexler, A., 25
White, R. M., 331
Wickramsinghe, H. K., 117
Wiesinger, G., 300
Wilkinson, M. K., 196, 207, 208
Willcock, S. N. M., 373
Willems, H. H., 370
Williams, H. J., 114
Williams, M. L., 338
Winslow, A. M., 24
Wohlfarth, E. P., 69, 165, 252, 305, 344,
357
Wollan, E. O., 199, 207, 208
Woods, R. T., 29
Wu, M. K., 348, 358
Wun Fogle, M., 57
Yamamoto, H., 318, 319
Yen, W., 387, 388
Zakharova, G. N., 371
Zatsepin, N. N., 372, 385
Zeeman, P. (1865–1943), 58–59, 232
Zieren, V., 78, 325
Zijlstra, H., 301

Subject Index

- a.c. applications, materials for, 272
- a.c. bias recording, 341
- a.c. losses in transformers, 270
- acoustic velocity, field dependence in ferromagnets, 374
- adiabatic demagnetization of paramagnets, 84
- alignment of magnetic moments, 113
- alnico, 312
- aluminum–iron alloys, 277
- amorphous metals, 76, 284
- Ampère's circuital law, 4
- Ampère's hypothesis, 108
- analytical balance, 62
- angular momentum of electrons, 222, 223, 225
 - wave mechanical corrections to, 228
- anhysteretic magnetization, 92
 - measurement of, 94
- anisotropic materials, 102
- anisotropy, 92, 122
 - constants, 124
 - cubic, 123
 - and domain rotation, 122, 305
 - energy of domain wall, 128
 - hexagonal, 122
- antiferromagnetism, 136, 194
- atomic force microscopy, 115
- atomic magnetic moment, 70, 107, 237
- atomic orbital angular momentum, 238
- atomic spin angular momentum, 239
- atomic total angular momentum, 240

- band theory of ferromagnetism, 263
- band theory of magnetism, 261
- band theory of paramagnetism, 262

- Bardeen–Cooper–Schrieffer theory, 356
- Barkhausen effect, 97, 113, 164, 366
 - for detection of stress, 366
 - for evaluation of microstructure, 366
- BCS theory, 356
- bending of domain walls, 141
- Bethe–Slater curve, 253
- Biot–Savart law, 2
- bismuth–strontium–calcium–copper oxide, 347
- Bitter patterns, 114
- Bloch walls, 128
- boundary element technique, 23
- Brillouin function, 256
- bubble domain devices, 329

- ceramic magnets, 81
- chromium dioxide, 327
 - tapes, 77
- circuits, 303
- classical theory of diamagnetism, 179
- classical theory of ferromagnetism, 189
- classical theory of paramagnetism, 182
- closure domains, 135
- cobalt–chromium recording media, 325
- cobalt–iron alloys, 296
- cobalt–platinum, 415
- cobalt–samarium, 318
- cobalt surface-modified gamma iron oxide, 327
- coercimeter, 370, 373
- coercivity, 72, 91, 269, 300
- coherence length, 354
- core losses, 76
- Cotton–Mouton effect, 57
- critical behaviour at the ordering temperature, 209

- critical current density, 352
- critical field of superconductor, 348
- critical magnetic field
 - under strong pinning, 154
 - under weak pinning, 155
- critical temperature of superconductor, 346
- cubic anisotropy, 123
- Curie temperature, 73
 - and the mean field interaction, 193
- Curie's law, 82, 182, 258
- Curie–Weiss law, 185, 259
- d.c. applications of soft magnetic materials, 290
- demagnetization curve, of permanent magnet, 302
- demagnetizing factors, 38
- demagnetizing fields, 36, 38
- density of magnetic recording, 340
- diamagnetism, theory of, 177
- diamagnets, 33, 81, 85
 - susceptibility of, 33
- Dipole, model for leakage field calculation, 385
- discontinuous magnetization, 97, 164
- disks, magnetic recording, 325
- domain
 - patterns and energy minimization, 118
 - processes, reversible and irreversible, 147
 - rotation, 120, 147
 - and anisotropy, 122
 - wall motion, 120, 137, 366
- domain wall
 - bowing of, 141
 - defect interactions, 159
 - forces on, 138
 - motion
 - and the Barkhausen effect, 164, 366
 - and magnetoacoustic emission, 369
 - and magnetostriction, 165
- pinning
 - by inclusions, 152
 - by strains, 149
- planar displacement of, 139
- strong pinning, 154
- surface energy, 138
- weak pinning, 155
- domain walls, 127
 - 180°, 134
 - anisotropy and exchange energies, 131
 - effects of stress on, 135
 - effects of weak fields on, 137
 - energy, 128
 - energy balance in, 137
 - Neel walls, 136
 - non-180°, 134
 - thickness, 128, 130
- domains, 107
 - and the magnetizing process, 120
 - nucleation, 119
 - observation of, 113, 115
 - single, 118
 - Weiss domain theory, 109
- eddy current inspection methods
 - applications of, 390
 - for magnetic materials, 389
- elastic constant anomalies at critical temperatures, 212
- electric motors, 272
- electrical losses, 76
 - in transformers, 270
- electromagnetic induction, 9
- electromagnetic inspection, remote field monitoring, 391
- electromagnetic relays, 77
- electromagnets, 74, 271
- electron–electron interactions, 247
- electron band theory of magnetism, 261
- Electron microscopy
 - SEM, 117
 - TEM, 116
- Electron spin
 - and exchange energy, 251
 - resonance, 79
- electron states, occupancy according to Hund's rules, 239
- electronic energy levels, splitting by magnetic field, 232
- electronic magnetic moment, quantum theory of, 221
- electronic magnetic moments, 219
- electronic orbital magnetic moment, 219

- electronic spin magnetic moment, 220
- electronic total magnetic moment, 221
- energy gap in superconductors, 357
- energy loss through wall pinning, 166
- energy minimization and domain structure, 118
- energy product, 111, 301
 - typical values for permanent magnets, 78
- energy states of magnetic moment configurations, 112
- exchange energy, 128
 - dependence on interatomic spacing, 253
 - and electron spin, 251
 - between electrons in filled shells, 252
 - values for various solids, 252
- exchange integral, 249
- exchange interaction, 249
- excited states and spin waves, 208
- Faraday effect, 57, 116
- Faraday's law of induction, 9, 47
- fatigue, effects of, on magnetic properties, 370
- ferrimagnetism, 195
- ferrites, 80, 81, 288, 315
 - hard, 81, 315
 - soft, 80, 288
- ferrofluids, 114
- ferromagnetism, 188
- ferromagnets, 33, 69, 108
 - applications of, 74
- ferroprobes (fluxgates), 374
- field lines, 37
- finite element techniques, 23
- flaw detection using magnetic methods, 377
- flux
 - coil
 - moving, 48
 - stationary, 48
 - leakage, 380
 - application of flux leakage method to NDE, 380
 - lines, 36
 - pinning, in type II superconductor, 350
 - quantization, 64
- quantum, 349
- rate of change of, 47
- trapping by toroid of superconductors, 353
- fluxgate magnetometer, 52
- fluxgates (ferroprobes), 373
- fluxmeter, 48
- force on current-carrying conductor in a field \mathbf{H} , 8
- free atoms, 237
- Frohlich–Kennelly equation, 93
- gamma iron oxide, 77, 324, 327
- generators, 272
- Ginzburg–London theory of superconductivity, 355
- Globus–Guyot model, 162
- Hall coefficient, 53
- Hall effect, 53
 - magnetometers, 53
- hard magnetic materials, 74, 299
- Heisenberg model of ferromagnetism, 251
- Heitler–London approximation, 249
- helimagnetism, 196
- Helmholz coils, 16
- hexagonal anisotropy, 122
- hexagonal ferrites, 328
- high-frequency applications, 288
- Hund's rules, 239
- hysteresis, 70, 89
 - coefficients and magnetic properties, 170
 - effects of microstructure and deformation on, 171
 - loss, 91
 - macroscopic mean field theory of, 165
 - parameters, 90
 - stress dependence of, 370
- hysteresisgraphs, 48
- inclusion theory of domain-wall pinning, 152
- inductance cores, 80
- induction coil methods, 47
- initial permeability, 90
- initial susceptibility
 - in the planar wall approximation, 141

- in the wall bending approximation, 143
- intensity of magnetization, 30
- interatomic spacing, effect on exchange energy, 253
- iron–aluminum alloys, 277
- iron–cobalt alloys, 296
- iron and low-carbon steels, 290
- iron–neodymium–boron, 319
- iron–nickel alloys, 278, 292
- iron oxide, 327
- iron–silicon alloys, 272
- irreversible magnetization changes, 166
- Ising model, 161, 214
- isotope effect, 356
- itinerant electron model, 261
 - criticism of, 266
- J–J* coupling, 242
- Josephson junction, 64
 - devices, 361
- Kerr effect, 57, 115
- Kundt's constant, 57
- Langevin function, 84
- Langevin theory
 - of diamagnetism, 178
 - of paramagnetism, 182
- Langevin–Weiss theory, critique of, 187
- laser magneto-optic microscope, 115
- Law of approach to saturation, 96
- Leakage fields, 377
 - calculation and modelling of, 385
 - finite element calculation of, 387
- Lenz's law of induction, 9
- localized atomic moments, 254
- localized electron model, criticism of, 261
- localized electron theory, 254
- localized theory of electronic magnetic moments, 254
- London equations, 354
- Lorentz microscopy, 116
- magnetic bubble domain devices, 329
- magnetic circuits, 36, 40, 303
- magnetic dipole, 10
- magnetic field
 - of circular coil, 13
 - definition, 1, 2
 - due to long conductor, 3
 - generation, 1
 - of long thin solenoid, 12
 - in magnetic materials, 43
 - numerical methods for calculation of, 23
 - patterns around conductor, 4
 - of a short thick solenoid, 19
 - of short thin solenoid, 19
 - of two coaxial coils, 16
- magnetic flux leakage, 380
 - applications of, 384
 - instruments for automation of, 384
 - models for, 385
- magnetic hysteresis, 370
 - applications in NDE, 371
- magnetic induction, 6
 - definition of tesla, 7
 - lines of, 9
- magnetic moment, 27, 107, 219
 - of closed shell of electrons, 237
 - of electron, 219
 - due to orbital angular momentum, 219
 - due to spin angular momentum, 220
 - total, 221
- magnetic order, 108, 204
- magnetic properties
 - of free atoms, 237
 - microscopic, typical values of, 134
- magnetic quantum numbers, 223
- magnetic recording
 - history, 324
 - materials, 77
 - media, 323
 - materials for, 327
 - tapes, 324
- magnetic particle inspection, 377
 - applications of, 379
 - 'dry' method, 378
 - fluorescent particles, 379
 - optimum conditions for, 379
 - 'wet' method, 379
- magnetic resonance imaging, 363
- magnetic structure, 197, 204
- magnetic units, 11

- magnetite (lodestone), 311
 magnetization, 29
 in materials with few defects, 162
 microstructural effects, 157
 relation to B and H , 30
 relation to magnetic moment, 10
 saturation, 31, 71
 strain effects, 157
 technical saturation, 101, 121
 magneto-acoustic emission, 98, 369
 stress dependence of, 369
 magnetoelastic method for NDE, 374
 magnetographic method of leakage flux detection, 377
 magnetometers, 47
 magnetomotive force, 56
 magneto-optic recording devices, 331
 magnetoresistors, 56
 magnetostatic energy, 40
 magnetostriction, 98
 at an angle θ to the magnetic field, 101
 field induced, 103
 forced, 101
 polycrystalline, 103
 saturation, 100
 single-crystal magnetostriction
 constant, cubic, 102
 spontaneous, 99
 in terms of single crystal
 magnetostriction constants, 102
 transverse, 104
 magnetostrictive devices, 56
 maximum energy product, 78
 mean field, 109, 190
 Meissner effect, 352
 metallic glasses, 284
 metglas, 284
 modelling of magnetization curves based on pinning, 156
 molecular field, 109
 motors, 272
 moving coil, 48
 galvanometer, 48
 MRI, 363
 mumetal, 281

 NDE, magnetic methods for, 365
 nearest neighbour interactions, 192

 Neel temperature, 195
 Neel walls, 136
 neodymium–iron–boron, 78, 319, 363
 Neutron diffraction, 197
 antiferromagnetic scattering, 201
 Bragg diffraction peaks, 199
 elastic scattering, 199
 ferromagnetic scattering, 201
 inelastic scattering, 203
 magnetic diffraction peaks, 201
 paramagnetic scattering, 201
 topography, 115
 nickel–iron alloys, 278, 292
 ninety degree (90°) domain-wall motion, 369
 niobium–tin, 359, 361
 niobium–titanium, 361
 niobium–zirconium, 361
 non-integral atomic magnetic moments, 264
 nuclear magnetic resonance (NMR) (see magnetic resonance imaging), 60, 363
 numerical methods for calculation of magnetic fields, 123

 orbital magnetic moment
 of atom, 238
 of electron, 219
 orbital momentum quantum number, 222
 orbital wave functions, two electron system, Heitler–London model, 249
 order in rare earth solids, 205
 ordered magnetism, theories of, 188
 ordering temperature, 73, 209

 paramagnetism, 181
 classical (Langevin) theory, 182
 classical (Weiss) theory, 186
 of ‘free’ electrons, Pauli theory, 262
 theory of, 177, 182, 186
 paramagnets, 33, 81
 applications of, 84
 field dependence of susceptibility, 83
 properties of, 81
 susceptibility of, 33
 temperature dependence of susceptibility, 82

- Paschen–Back effect, 244
 Pauli paramagnetism, 262
 permalloy, 278, 292
 permanent magnet steels, 311
 permanent magnets, 79
 applications, 309
 materials, 311
 properties, 299
 stability, 310
 permeability, 8, 32, 69, 108
 differential, 32, 73
 initial, 90
 relative, 32
 permeance coefficient, 303
 permendur, 296
 perpendicular recording media, 77, 329
 pinning models, 156
 pinning of domain walls
 critical field, 154, 155
 by inclusions, 152
 by strains, 149
 platinum–cobalt, 415
 pole strength, 10
 potential approximation for domain-wall motion, 139
 Preisach model, 343
 use in magnetic recording industry, 343
 principal quantum number, 221
 proton precession magnetometers, 60
- quantization
 of angular momentum, 225
 of electron spin, 232
 of flux, 350
 quantum mechanical exchange interaction, 249
 quantum number
 l , 222
 m_l , 223
 m_s , 225
 n , 221
 s , 223
 quantum of flux, 349, 357
 quantum theory of
 electron–electron interactions, 247
 electronic magnetic moments, 221
 ferromagnetism, 259
 paramagnetism, 255
- quenching of orbital angular momentum, 242
 Rayleigh's law, 95
 recording density, 340
 recording devices, 322
 recording heads, 334
 recording materials, 77
 recording media, 77
 recording process, 334
 reading, 341
 writing, 336, 338
 relative permeability, 32
 relays, 77, 271
 reluctance, 40
 remanence, 72, 90, 300, 373
 remote field electromagnetic inspection
 for NDE, 391
 residual field, 373
 resistance magnetometers, 56
 resonance magnetometers, 60
 retentivity, 70
 reversible magnetization changes, 167
 rigid band model of ferromagnetism
 (Slater–Pauling), 265
 rigid domain-wall motion, 139
 initial susceptibility of, 141
 rotating coil, 49
 Russell–Saunders coupling, 241
- samarium–cobalt, 78, 318
 saturable coil magnetometers, 52
 saturation, law of approach to, 96
 saturation magnetization, 31, 71, 300
 technical, 101, 121
 search coil, 48
 silicon–iron alloys, 272
 Slater–Pauling curve, 265
 soft ferrites, 288
 soft iron, 290
 soft magnetic materials, 74, 269
 a.c. losses, 270
 coercivity, 269
 hysteresis loss, 270
 permeability, 269
 saturation magnetization, 270
 solenoid
 general formula for field of, 21

- magnetic field
 - of a long thin, 12
 - of a short thick, 19
 - of a short thin, 19
- optimization of geometry, 20
- power considerations, 20
- specific heat anomalies at critical temperatures, 210
- spin magnetic moment, 220
 - of atom, 239
- spin quantum number, 223
- spin waves, 208
- spontaneous magnetization, 260
 - temperature dependence of, 260
- SQUIDS, 64, 361
- stability of permanent magnets, 310
- steel, production, 365
- Stern–Gerlach experiment, 236
- Stoner–Slater (electron band) theory of ferromagnetism, 263
- Stoner–Wohlfarth model, 305, 344
- strain theory of domain-wall pinning, 149
- stress, effects of, on bulk magnetization, 171
- strong magnetic fields, effect on electron coupling, 244
- superconducting
 - magnets, 360
 - solenoids, 360
- superconductors, 85
 - applications, 358
 - conduction mechanism in, 359
 - development of improved materials, 358
 - basic properties, 345
- supermalloy, 278
- surface currents in superconductors, 354
- susceptibility, 32, 108
 - anomalies at critical temperatures, 210
 - balance, 62
 - differential, 32
- tapes, magnetic recording, 324
- technical saturation magnetization, 31, 121
- temperature dependent paramagnetic susceptibility (Curie), 82, 258
- temperature independent paramagnetic susceptibility (Pauli), 262
- thallium–barium–calcium–copper oxide, 360
- theories of magnetic ordering, 188
- thermal conductivity of superconductors, 357
- thermal expansion anomalies at critical temperature, 212
- thin-film magnetometers, 57
- three-d (3d) band electrons, magnetic properties, 264
- torque, 10
 - magnetometer, 60
- torsion balance, 62
- total atomic orbital angular momentum, 240
- transformers, 76, 272
- transverse magnetostriction, 104
- type I superconductor, 349
- type II superconductor, 349
- ultrasonic velocity, field dependence in steels, 374
- units in magnetism, 11
- vector model of the atom, 226
- Verdet's constant, 57
- vibrating coil, 49
 - magnetometer, 50
- vibrating-sample magnetometer, 52
- vortices in superconductor, 349
- wall bowing approximation, 141
- wave function of two-electron system, 247
 - including spin, 250
- wave mechanical corrections to angular momentum of electrons, 228
- Weiss domain theory, 109
- Weiss mean field theory, 109
 - consequences of, 187
 - critique of, 187
 - of ferromagnetism, 189
 - of paramagnetism, 186
- Wiedemann–Franz ratio, 451

440 *Subject Index*

Winchester disk drive, 325

critical temperatures, 358

X-ray topography, 115

Zeeman effect

anomalous, 234

normal, 232

yttrium-barium-copper oxide, 358

zero resistivity, 345

critical current density, 358

critical fields, 358